VI International Conference

CONDENSED MATTER & LOW TEMPERATURE PHYSICS 2026

Book of Abstracts

June 1–5, 2026

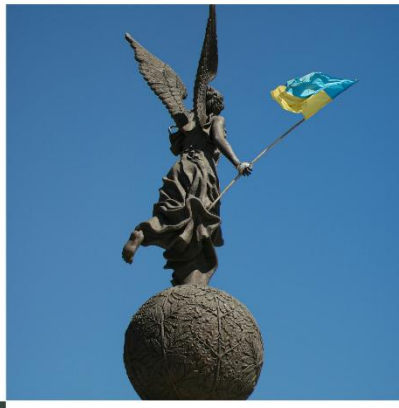

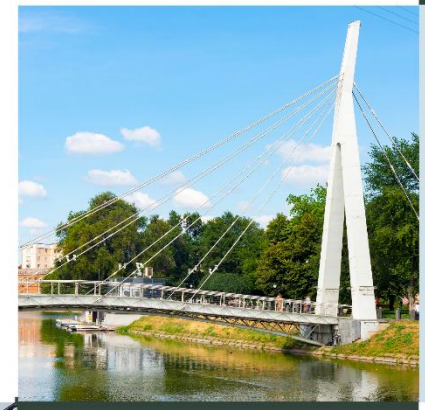

Kharkiv
Ukraine

CM&LTP 2026 | Kharkiv, Ukraine

VI International Conference
Condensed Matter and Low Temperature Physics
CM&LTP 2026

Book of abstracts

Kharkiv, B. Verkin ILTPE of NASU, 2026

https://doi.org/10.35668/cmltp2026boa
UDK 538.9
H 88

Hurova D.E., Dolbin A.V., Konotop O.P. (editors) VI International Conference "Condensed Matter and Low Temperature Physics" 2026. Book of abstracts. – Kharkiv: B. Verkin ILTPE of NASU, 2026. – 297 p.

ISBN 978-617-95630-0-3

This book collects 245 peer-reviewed reports presented at the VI International Conference "Condensed Matter and Low Temperature Physics" 2026. These materials present the studies of modern aspects of condensed matter and low temperature physics including electronic properties of conducting and superconducting systems, magnetism and magnetic materials, optics, photonics and optical spectroscopy, quantum liquids and quantum crystals, cryocrystals, nanophysics and nanotechnologies, biophysics and physics of macromolecules, materials science, theory of condensed matter physics, technological peculiarities of the instrumentation for physical experiments, and related fields.

The book will be useful to undergraduate, postgraduate students, and researchers in the field of Physics and Condensed matter physics.

Ця книга зібрала 245 доповідей, представлених на VI Міжнародній конференції "Condensed Matter and Low Temperature Physics" 2026 року. Дані матеріали представляють дослідження у галузі сучасних аспектів фізики конденсованого стану та низьких температур, у тому числі електронні властивості провідних та надпровідних систем, магнетизм, оптику, фотоніку та оптичну спектроскопію, квантові рідини та квантові кристали, кріокристали, нанофізику та нанотехнології, біофізику та фізику макромолекул, матеріалознавство, теорію фізики конденсованого стану, технологічні особливості обладнання для фізичних експериментів та суміжні галузі.

Книга призначена для студентів, аспірантів та дослідників у галузі загальної фізики та фізики конденсованого стану.

Recommended to publish by Scientific Council of B. Verkin Institute for Low Temperature Physics and Engineering of the National Academy of Sciences of Ukraine (protocol № 4, 13.05.2026)

Published by B. Verkin ILTPE of NASU
ISBN 978-617-95630-0-3

PROGRAM COMMITTEE

Chair: Prof. Alexander Dolbin, ILTPE NASU (Kharkiv, Ukraine)
Vice-chair: Prof. Sergey Shevchenko, ILTPE NASU (Kharkiv, Ukraine)
Prof. Yurii Naidyuk, Corr. Member NASU, ILTPE NASU (Kharkiv, Ukraine)
Prof. Oleksandr Kordyuk, Full Member NASU, IMP NASU (Kyiv, Ukraine)
Prof. Leonid Pastur, Full Member NASU, ILTPE NASU (Kharkiv, Ukraine)
Prof. Viktor Chabanenko, DonFTI NASU (Kyiv, Ukraine)
Dr. Alexey Fedorchenko, ILTPE NASU (Kharkiv, Ukraine)
Dr. Alexander Yu. Glamazda, ILTPE NASU (Kharkiv, Ukraine)
Dr. Mykola Glushchuk, ILTPE NASU (Kharkiv, Ukraine)
Dr. Volodymyr P. Gnezdilov, ILTPE NASU (Kharkiv, Ukraine)
Prof. Andrzej Jezowski, INTiBS PAN (Wroclaw, Poland)
Dr. Oleksandr Kalinenko, ILTPE NASU (Kharkiv, Ukraine)
Prof. Gennadii Kamarchuk, ILTPE NASU (Kharkiv, Ukraine)
Prof. Yuriy Kolesnichenko, ILTPE NASU (Kharkiv, Ukraine)
Prof. Konstantin Nemchenko, V.N.Karazin KNU (Kharkiv, Ukraine)
Prof. Pavel Pal-Val, ILTPE NASU (Kharkiv, Ukraine)
Prof. Elena Savchenko, ILTPE NASU (Kharkiv, Ukraine)
Dr. Victor Slavin, ILTPE NASU (Kharkiv, Ukraine)
Prof. Svyatoslav Sokolov, ILTPE NASU (Kharkiv, Ukraine)
Dr. Stepan Stepanian, ILTPE NASU (Kharkiv, Ukraine)
Prof. Andrzej Szewczyk, IF PAN (Warsaw, Poland)
Prof. Yevgen Syrkin, ILTPE NASU (Kharkiv, Ukraine)
Dr. Andrii Terekhov, ILTPE NASU (Kharkiv, Ukraine)

ORGANIZING COMMITTEE

Chair: Dr. Diana Hurova
Vice-chair: Dr. Oleksii Konotop
Vice-chair (treasurer): Dr. Vusal Geidarov
Secretary: Dr. Yuliya Savina

Dr. Razet Basnukaeva
Dr. Ivan Bondar
Dr. Valentin Koverya
Dr. Oleksandr Leha
Dr. Yevhen Petrenko
PhD St. Tymofii Piddubnyi
Dr. Sergii Poperezhai

https://www.ilt.kharkiv.ua/cmltp2026/

CONFERENCE PROGRAM

**Time is specified for the Time Zone UTC/GMT+3,
Eastern European Summer Time (EEST)**

MONDAY, 1st of JUNE

9:50-10:00 **Opening Remarks**
Acting Director of the B. Verkin ILTPE of NAS of Ukraine
Corresponding Member of NAS of Ukraine
Prof. Alexander Dolbin
and
Chair of Organizing Committee Dr. Diana Hurova

PLENARY LECTURES OF INVITED SPEAKERS

Chairs *Dr. Valentin Koverya, Dr. Andrii Terekhov*

10:00-10:30 **Thermal transport properties and phonon glass features in dimer-Mott quantum spin-liquid compounds** **49**
(16:00 UTC+9) Y. Nakazawa[1], L. Zhang[1], T. Nomoto[2], S. Yamashita[1], and H. Akutsu[1]
[1]Dept. of Chemistry, Graduate School of Science, the University of Osaka, Osaka, Japan
[2]RIKEN Center for Emergent Matter Science (CEMS), Wako, Saitama, Japan

10:30-11:00 **The Role of A in ARPES** **39**
S. Borisenko
IFW-Dresden, Dresden, Germany

ELECTRONIC PROPERTIES OF CONDUCTING AND SUPERCONDUCTING SYSTEMS

Chair *Dr. Valentin Koverya, Dr. Andrii Terekhov*

11:00-11:12 **Pinning and dynamics of Abrikosov vortices in S-F bilayer films** **57**
A. L. Kasatkin, V. P. Tsvitkovskyi
G.V.Kurdyumov Institute for Metal Physics of NASU, Kyiv, Ukraine

11:12-11:24 **Excitation of eigenmodes in cylindrical layered superconductors by non-relativistic electron flows** **58**
Yu. O. Averkov, O. Yu. Averkov, Yu. V. Prokopenko, V. A. Yampol'skii
O.Ya.Usikov Institute for Radiophysics and Electronics of NASU, Kharkiv, Ukraine

11:24-11:36 **Enhancing electronic dispersion determination by employing an ensemble learning approach** **59**
Yu. V. Pustovit, M. O. Ohloblia, Ya. B. Yanenko
Taras Shevchenko National University of Kyiv, Kyiv, Ukraine

11:36-11:48 **Comparative analysis of the effects of low-energy helium-ion (He^+) and high-energy electron irradiation on fluctuation conductivity and pseudogap in $YBa_2Cu_3O_{7-\delta}$ compounds** **60**

A. L. Solovjov[1,2,3], M. V. Shytov[1], L. V. Bludova[1], A. S. Kolisnyk[1], A. Sedda[3], E. Lähderanta[3], W. Lang[4]

[1]*B.Verkin Institute for Low Temperature Physics and Engineering of NASU, Kharkiv, Ukraine*
[2]*Institute of Low Temperatures and Structure Research of PAS, Wroclaw, Poland*
[3]*Department of Physics, LUT University, Lappeenranta, Finland*
[4]*Faculty of Physics, University of Vienna, Vienna, Austria*

11:48-12:00 **Non-stationary longitudinal Josephson effect in electron-hole bilayers** **61**

O. M. Konstantynov, S. I. Shevchenko

B.Verkin Institute for Low Temperature Physics and Engineering of NASU, Kharkiv, Ukraine

12:00-12:12 **Charge transport and dielectric properties of the $BaTiO_3$ ceramics** **62**

O. V. Bereznykov[1], D. O. Stetsenko[1], T. O. Kuzmenko[1,2], O. S. Pylypchuk[1], S. E. Ivanchenko[3], V. I. Styopkin[1], A. N. Morozovska[1], V. N. Poroshin[1], V. V. Vainberg[1]

[1]*Institute of Physics, NAS of Ukraine, Kyiv, Ukraine*
[2]*Taras Shevchenko National University of Kyiv, Kyiv, Ukraine*
[3]*Frantsevich Institute for Problems in Materials Science, NAS of Ukraine, Kyiv, Ukraine*

12:12-12:24 **Balance between optical and superconducting properties in oxygen-deficient ITO films** **63**

D. Menesenko[1,2], O. Feia[1, 2, 3], A. Shapovalov[1,2]

[1]*Kyiv Academic University, Kyiv, Ukraine*
[2]*G.V.Kurdyumov Institute for Metal Physics of NASU, Kyiv, Ukraine*
[3]*Leibniz Institute for Solid State and Materials Research, Dresden, Germany*

12:24-12:36 **Enhancement of superconductivity in twisted metallic materials** **64**

V. Tarenkov[1,2], D. Mindich[3], V. Dmytrenko[1], E. Zhitlukhina[1], V. Krivoruchko[1], I. Gavrysh[2], A. Shapovalov[2,3], O. Kalenyuk[2,3], M. Belogolovskii[3]

[1]*O.O.Galkin Donetsk Institute for Physics and Engineering of NASU, Kyiv, Ukraine*
[2]*G.V.Kurdyumov Institute for Metal Physics of NASU, Kyiv, Ukraine*
[3]*Kyiv Academic University, Kyiv, Ukraine*

12:36-12:48 **Spin-paramagnetic effects and possible singlet–triplet transition in $Dy_{1-x}Er_xRh_{3.8}Ru_{0.2}B_4$** **65**

P. M. Fesenko[1], A. V. Terekhov[2], K. O. Minakova[1], A. P. Kazakov[3], I. V. Zolochevskii[2]

[1]*National Technical University "Kharkiv Polytechnic Institute", Kharkiv, Ukraine*
[2]*B.Verkin Institute for Low Temperature Physics and Engineering of NASU, Kharkiv, Ukraine*
[3]*International Research Centre MagTop, Institute of Physics of PAS, Warsaw, Poland*

12:48-13:00 **Anomalous magnetoresistance in $Bi_{95.69}Mn_{3.69}Fe_{0.62}$ and $Bi_{88.08}Mn_{11.92}$ solid solutions** **66**

V. M. Yarovyi[1], A. V. Terekhov[1], K. Rogacki[2], E. Lähderanta[3], A. L. Solovjov[1,2,3]

[1]*B.Verkin Institute for Low Temperature Physics and Engineering of NASU, Kharkiv, Ukraine*
[2]*Institute of Low Temperatures and Structure Research of PAS, Wroclaw, Poland*
[3]*Lappeenranta University of Technology, Lappeenranta, Finland*

13:00-13:15 **Quantum reflectometry meets quantum averaging theory** **67**

O. Yu. Kitsenko[1,2], S. N. Shevchenko[1,3], L. Peri[4,5], F. Nori[6,7]

[1]*B.Verkin Institute for Low Temperature Physics and Engineering of NASU, Kharkiv, Ukraine*
[2]*V.N.Karazin Kharkiv National University, Kharkiv, Ukraine*
[3]*Department of Mathematics, Kyiv School of Economics, Kyiv, Ukraine*
[4]*Quantum Motion, London, United Kingdom*
[5]*Cavendish Laboratory, University of Cambridge, Cambridge, UK*
[6]*Quantum Computing Center, RIKEN, Saitama, Japan*
[7]*Physics Department, The University of Michigan, Ann Arbor, MI, USA*

13:15-14:00 **BREAK**

PLENARY LECTURES OF INVITED SPEAKERS

Chair *Dr. Sergii Poperezhai*

14:00-14:30 **Structural defects as crucial factors for persistent luminescence in Cr-doped $ZnGa_2O_4$ spinels** **38**
V. Boiko
Institute of Low Temperatures and Structure Research of PAS, Wroclaw, Poland

14:30-15:00 **From near-infrared silicon photonics to magnetic control of matter: extending design principles across scales** **50**
M. F. Pereira[1,2], H. Zafar[1], A. Al-Ateqi[1] and Y. Tawalbeh[1,2]
[1]*Department of Physics, Khalifa University, Abu Dhabi, UAE*
[2]*Institute of of Physics, Czech Academy of Sciences, Prague, Czech Republic*

OPTICS, PHOTONICS AND OPTICAL SPECTROSCOPY

Chair *Dr. Sergii Poperezhai*

15:00-15:12 **High-speed photonic VQE: overcoming optimization latency with liquid crystals** **113**
B. Bilash[1,2*], I. Ali[1,2], J. Lee[1,2], D. Parvatharajan[1], H.-T. Lim[1,2], and Y.-S. Kim[1,2†]
[1]*Center for Quantum Technology, KIST, Seoul, Republic of Korea*
[2]*Division of Quantum Information, KIST School, UST, Seoul, Republic of Korea*

15:12-15:24 **Features of surface waves in extremely anisotropic media** **114**
A. F. Bukhanko
O.O.Galkin Donetsk Institute for Physics and Engineering of NASU, Kyiv, Ukraine

15:24-15:36 **Influence of the distribution of energies of monomers on dynamical characteristics of molecular aggregates** **115**
I. Yu. Ropakova[1], A. A. Zvyagin[2]
[1]*Institute for Scintillation Materials of the NASU, Kharkiv, Ukraine*
[2]*B.Verkin Institute for Low Temperature Physics and Engineering of NASU, Kharkiv, Ukraine*

15:36-15:50 **Using an optimization algorithm to improve the metrological performance of a surface plasmon resonance biosensor** **116**
R. S. Terekhov[1], Z. E. Eremenko[1,2], S. M. Kulish[1,3]
[1]*O.Ya.Usikov Institute for Radiophysics and Electronics of NASU, Kharkiv, Ukraine*
[2]*Leibniz Institute for Solid State and Materials Research, Dresden, Germany*
[3]*National Aerospace University "Kharkiv Aviation Institute", Kharkiv, Ukraine*

15:50-16:30 **BREAK**

16:30-18:10 POSTER SESSION (1, 2, 3, 4, AND 5 SECTIONS)

Chairs *Dr. Sergii Poperezhai, Dr. Diana Hurova*

16:30-17:20 Stage 1 (P1-P39)

17:20-18:10 Stage 2 (P40-P78)

ELECTRONIC PROPERTIES OF CONDUCTING AND SUPERCONDUCTING SYSTEMS

MAGNETISM AND MAGNETIC MATERIALS

QUANTUM LIQUIDS AND QUANTUM CRYSTALS, CRYOCRYSTALS

OPTICS, PHOTONICS AND OPTICAL SPECTROSCOPY

NANOPHYSICS AND NANOTECHNOLOGIES

P77 **Kinetics of electrophysical properties of diluted aqueous colloidal solutions of fullerene $C_{60}@\{H_2O\}_n$** **179**
M. A. Vinnikov, M. T. Pohribnyi, O. V. Dolbyn, R. M. Basnukaeva, L. M. Buravtseva, S. V. Cherednychenko
B.Verkin Institute for Low Temperature Physics and Engineering of NASU, Kharkiv, Ukraine

P78 **Study of early stages of clustering in a supersonic nitrogen jet** **180**
Yu. S. Doronin, A. A. Tkachenko, V. L. Vakula, G. V. Kamarchuk
B.Verkin Institute for Low Temperature Physics and Engineering of NASU, Kharkiv, Ukraine

TUESDAY, 2nd of JUNE

PLENARY LECTURES OF INVITED SPEAKERS

Chair *Dr. Maksym Barabashko*

10:00-10:30 **The CISS effect as a unsolved problem** **51**
J. M. van Ruitenbeek
Huygens-Kamerlinhgh Onnes Laboratory, Leiden University, Leiden, Netherlands

10:30-11:00 **Sagnac and Mashhoon effects in graphene** **52**
Y. V. Shtanov[1], T.-H. O. Pokalchuk[2], S. G. Sharapov[1,2]
[1]*Bogolyubov Institute for Theoretical Physics of NASU, Kyiv, Ukraine*
[2]*Kyiv Academic University, Kyiv, Ukraine*

NANOPHYSICS AND NANOTECHNOLOGIES

Chair *Dr. Maksym Barabashko*

11:00-11:12 **The effect of $BaTiO_3$ nanoparticles on the dielectric properties of the 5CB nematic liquid crystal** **151**
J. M. Gudenko[1], V. V. Vainberg[1], O. S. Pylypchuk[1], S. E. Ivanchenko[2], V. N. Poroshin[1], D. O. Stetsenko[1], I. A. Gvozdovskyy[1], A. N. Morozovska[1]
[1]*Institute of Physics, NAS of Ukraine, Kyiv, Ukraine*
[2]*Frantsevich Institute for Problems in Materials Science, NAS of Ukraine, Kyiv, Ukraine*

11:12-11:24 **Universal method of selective detection of a wide range of pollutants in liquids using conductance quantization** **152**
A. Herus[1], O. Pospelov[2], A. Savytskyi[1], V. Vakula[1], M. Sakhnenko[2], N. Kalashnyk[3], E. Faulques[3], G. Kamarchuk[1]
[1]*B.Verkin Institute for Low Temperature Physics and Engineering of NASU, Kharkiv, Ukraine*
[2]*National Technical University "Kharkiv Polytechnic Institute", Kharkiv, Ukraine*
[3]*Univ. Lille, CNRS, Centrale Lille, Yncréa ISEN, Univ. Polytechnique Hauts -de -France, Lille, France*

11:24-11:36 **Correlations between the dielectric properties and phase diagrams of $Bi_{1-x}Sm_xFeO_3$ nanopowders** **153**
V. O. Kolupaiev[1], O. S. Pylypchuk[1], V. V. Vainberg[1], V. N. Poroshin[1], I. V. Fesych[2], L. D. Demchenko[3,4], E. A. Eliseev[5], A. N. Morozovska[1]
[1]*Institute of Physics, NAS of Ukraine, Kyiv, Ukraine*
[2]*Taras Shevchenko National University of Kyiv, Kyiv, Ukraine*
[3]*Stockholm University, Department of Chemistry, Stockholm, Sweden*
[4]*University of Ukraine "Igor Sikorsky Kyiv Polytechnic Institute", Kyiv, Ukraine*
[5]*Frantsevich Institute for Problems in Materials Science, NAS of Ukraine, Kyiv, Ukraine*

11:36-11:48 **Optimization of thermal transport properties in silicon structures with inhomogeneous porosity: experiment and machine learning** **154**
P. O. Lishchuk, L.I. Chepela, V. B. Shevchenko, M. O. Borovoy, V. V. Kuryliuk, O. Ya. Olikh
Taras Shevchenko National University of Kyiv, Kyiv, Ukraine

11:48-12:00 **Controlling the pro-oxidant properties of cerium oxide nanocrystals by Fe^{3+} doping and morphology modification** **155**
M. I. Lupan, G. V. Grygorova, V. V. Seminko, P. O. Maksimchuk, S. L. Yefimova
Institute for Scintillation Materials of the NASU, Kharkiv, Ukraine

12:00-12:12 **Defect evolution in irradiated multilayer graphene** **156**
S. I. Menshykova*, S. I. Khaldeev[1], A. Ruhtinas[2], S. Moulick[1], J. T. Mäkinen[1], P. Hakonen[1]
[1]*Department of Applied Physics, Aalto University, Aalto, Finland*
[2]*Nanoscience Center, University of Jyväskylä, Jyväskylä, Finland*

12:12-12:24 **Nanoceria-based complexes for improved sensing of redox-active molecules in biological media** **157**
V. V. Seminko, Ye. I. Neuhodov, P. O. Maksimchuk, G. V. Grygorova, S. L. Yefimova
Institute for Scintillation Materials of the NASU, Kharkiv, Ukraine

12:24-12:36 **Dimensional effect on relaxation processes of polypropylene glycol 1000 confined in silica-gel nanopores** **158**
A. O. Sobchuk[1], D. A. Andrusenko[1], V. B. Shevchenko[1], S. A. Alekseev[1], K. S. Yablochkova[1], R. V. Dinzhos[2,3]
[1]*Taras Shevchenko National University of Kyiv, Kyiv, Ukraine*
[2]*Petro Mohyla Black Sea National University, Mykolaiv, Ukraine*
[3]*Institute of Polymers, Bulgarian Academy of Sciences, Sofia, Bulgaria*

12:36-12:48 **Analytical approaches to describe phonon heat transfer in two-dimensional nanoconductors** **159**
J. Amrit[1], I. Kudriavtsev[2], K. Nemchenko[2], Y. Niemchenko[2], M. Spotar[2], T. Vikhtynska[2]
[1]*LISN, Université Paris-Saclay, CNRS, Orsay, France*
[2]*V.N.Karazin Kharkiv National University, Kharkiv, Ukraine*

12:48-13:00 **Long-range tunneling of magnons between nanomagnets connected by a ferromagnetic chain** **160**
S. M. Tunyk, E. G. Petrov
Bogolyubov Institute for Theoretical Physics of NASU, Kyiv, Ukraine

13:00-13:12 **Influence of post annealing temperature and aging effect on electrical properties of chromium nanofilms** **161**
S. Udachan[1], S. B. Kolavekar[1], N. H. Ayachit[1], L. A. Udachan[2], S. S. Kolkundi[3], S. Ramya[4], S. Veeresh[4]
[1]*School of Advanced Sciences, KLE Technological University, Hubballi, India*
[2]*S.S.Tegnoor Degree College, Kalaburagi, India*
[3]*Government First Grade College, Shahapur, Yadgir, India*
[4]*Shree Sangam Vidya Mandir, Kalburagi, India*

MATERIALS SCIENCE

Chair *Dr. Maksym Barabashko*

13:12-13:25 **Thermal behaviour and evaluation of individual kinetic analysis approaches in the Al_2O_3-Yb_2O_3-Er_2O_3 glass systems** **207**
L. Šedivá[1,2], K. Faturíková[3], B. Pecušová[3], P. Švančárek[2], J. Valúchová[2], A. Prnová[2], D. Galusek[2,3]
[1]Faculty of Chemical and Food Technology STU, Bratislava. Slovakia
[2]Joint Glass Centre of the IIC SAS, TnUAD, and FCHPT STU, Trenčín. Slovakia
[3]Alexander Dubček University of Trenčín, Trenčín. Slovakia

13:25-14:00 **BREAK**

PLENARY LECTURES OF INVITED SPEAKERS

Chairs *Dr. Sergii Poperezhai, Dr. Yuliya Savina*

14:00-14:30 **Optical coherence tomography versus scanning electron microscopy for investigations of metallic fractures** **42**
G. Hutiu[1], V.-F. Duma[2], D. Demian[1], A. Bradu[3], A. Podoleanu[3]
[1]Aurel Vlaicu" University of Arad, Arad, Romania
[2]Polytechnic University of Timisoara, Timisoara, Romania
[3]School of Physical Sciences, University of Kent, Canterbury, UK

14:30-15:00 **THz-driven nonlinear magnetization dynamics and the magnetic Jahn-Teller effect in rare-earth orthoferrites with Kramers and non-Kramers ions** **53**
N. R. Vovk[1], O. Y. Kovalenko[2], E. V. Ezerskaya[3], R. V. Mikhaylovskiy[2]
[1]James Watt School of Engineering, University of Glasgow, Glasgow, UK
[2]Lancaster University, Bailrigg, Lancaster, United Kingdom
[3]V.N.Karazin Kharkiv National University, Kharkiv, Ukraine

MAGNETISM AND MAGNETIC MATERIALS

Chairs *Dr. Sergii Poperezhai, Dr. Yuliya Savina*

15:00-15:12 **Comprehensive Law of approach to saturation for the determination of magnetic anisotropy in Co/SiO2 granular films** **85**
O. E. Baibara[1], Y. A. Stelmakh[2], L. A. Krushinskaya[2], A. I. Ievtushenko[1]
[1]Frantsevich Institute for Problems in Materials Science, NAS of Ukraine, Kyiv, Ukraine
[2]E.O.Paton Electric Welding Institute, NAS of Ukraine, Kyiv, Ukraine

15:12-15:24 **Electric-field control of spin-wave propagation: the Aharonov-Casher effect** **86**
O. O. Boliasova[1,2], V. N. Krivoruchko[3]
[1]Kyiv Academic University, Kyiv, Ukraine
[2]G.V.Kurdyumov Institute for Metal Physics of NASU, Kyiv, Ukraine
[3]O.O.Galkin Donetsk Institute for Physics and Engineering of NASU, Kyiv, Ukraine

15:24-15:36 **Eigenoscillations of the topological spin texture in an antiferromagnet with the Dzyaloshinskii–Moriya interaction** **87**
V. S. Gerasimchuk[1], I. V. Gerasimchuk[1,2]
[1]National Technical University of Ukraine "Igor Sikorsky Kyiv Polytechnic Institute", Kyiv, Ukraine
[2]V.G.Baryakhtar Institute of Magnetism of the NASU, Kyiv, Ukraine

15:36-15:48 **Ab initio calculations of altermagnetic materials** **88**
O. Hrechykha, O. Feia
Kyiv Academic University, Kyiv, Ukraine

15:48-16:00 **From a quasi-2D isotropic square-lattice ferromagnet to ferromagnetic chains: refined spin Hamiltonian of Cu(*en*)(*sal*)Cl** **89**
I. Kozin[1], R. Tarasenko[1], J. Šebesta[2], D. Legut[2, 3], J. Strečka[1], E. Čižmár[1], A. Orendáčová[1], V. Tkáč[1], and M. Orendáč[1]
[1]*Institute of Physics, P.J. Šafárik University in Košice, Košice, Slovakia*
[2]*IT4Innovations, VŠB-Technical University of Ostrava, Ostrava-Poruba, Czech Republic*
[3]*Charles University, Prague, Czech Republic*

16:00-16:12 **Magnetic-field-driven release of strain in FeRh films** **90**
I. Lukiienko[1,2], V. Uhlíř[1]
[1]*Central European Institute of Technology, Brno, Czechia*
[2]*B.Verkin Institute for Low Temperature Physics and Engineering of NASU, Kharkiv, Ukraine*

16:12-16:24 **Impact of ferroelastic phase transition on magnetic susceptibility of ferromagnet and magnetocaloric effect** **91**
V. A. L'vov[1], A. Kosogor[1,2]
[1]*V.G.Baryakhtar Institute of Magnetism of the NASU, Kyiv, Ukraine*
[2]*University of Vienna, Faculty of Physics, Vienna, Austria*

16:24-16:36 **Propagation of spin excitations along domain walls in d-wave altermagnets** **92**
O. Peschanska[1], V. Kravchuk[1,2]
[1]*Bogolyubov Institute for Theoretical Physics of NASU, Kyiv, Ukraine*
[2]*Leibniz Institute for Solid State and Materials Research, Dresden, Germany*

16:36-16:50 **Rotational symmetry in s = 1/2 dimers and tetramers with non-collinear local ion axes** **93**
O. V. Zhuravlev
O.O.Galkin Donetsk Institute for Physics and Engineering of NASU, Kyiv, Ukraine

16:50-17:30 **BREAK**

17:30-19:10 **POSTER SESSION (6, 7, 8, AND 9 SECTIONS)**

Chairs *Dr. Diana Hurova, Dr. Oleksii Konotop*

17:30-18:20 **Stage 1 (P79-P112)**

18:20-19:10 **Stage 2 (P113-P145)**

BIOPHYSICS AND PHYSICS OF MACROMOLECULES

P79 **Ions binding to model lipid membranes: obtaining the adsorption value from indirect measurements** **188**
R. Ye. Brodskii[1], O. V. Vashchenko[2]
[1]*Institute for Single Crystals of NAS of Ukraine, Kharkiv, Ukraine*
[2]*Institute for Scintillation Materials of the NAS of Ukraine, Kharkiv, Ukraine*

P80 **Virtual screening and molecular dynamics simulation of phytochemicals as potential inhibitors of extended-spectrum beta-lactamases** **189**
N. V. Khmil[1,2], M. O. Kryvobok[2], A. V. Shestopalova[1]
[1]*O.Ya.Usikov Institute for Radiophysics and Electronics of NASU, Kharkiv, Ukraine*
[2]*Kharkiv National University of Radio Electronics, Kharkiv, Ukraine*

MATERIALS SCIENCE

THEORY OF CONDENSED MATTER PHYSICS

TECHNOLOGIES AND INSTRUMENTATION FOR PHYSICAL EXPERIMENTS

WEDNESDAY, 3rd of JUNE

PLENARY LECTURES OF INVITED SPEAKERS

Chair *Dr. Nikita Kurnosov*

10:00-10:30 **Biophysical processes in the Universe as viewed by mass spectrometry** **46**
M. V. Kosevich
B.Verkin Institute for Low Temperature Physics and Engineering of NASU, Kharkiv, Ukraine

10:30-11:00 **CARS, SHG, Raman spectroscopy and imaging for analysis of biological molecules and cells** **41**
G. I. Dovbeshko[1], A. Dementjev[2], O. P. Gnatyuk[1]
[1]*Institute of Physics, NAS of Ukraine, Kyiv, Ukraine*
[2]*Center for Physical Sciences and Technology, Vilnius, Lithuania*

BIOPHYSICS AND PHYSICS OF MACROMOLECULES

Chair *Dr. Nikita Kurnosov*

11:00-11:12 **Enzyme adsorption on single-walled carbon nanotubes: Raman spectroscopy analysis** **182**
A. Glamazda and V. Karachevtsev
B.Verkin Institute for Low Temperature Physics and Engineering of NASU, Kharkiv, Ukraine

11:12-11:24 **Quantitative assessment of tryptophan content in the blood plasma of oropharyngeal cancer patients after COVID-19** **183**
I. Gnatyuk[1], D. Doni[2], S. Verevka[2], A. Tarasenko[3], O. Gnatyuk[1], T. Isokov[1], G. Dovbeshko[1]
[1]*Institute of Physics, NAS of Ukraine, Kyiv, Ukraine*
[2]*O.S.Kolomiychenko Institute of Otolaryngology, NAMS of Ukraine, Kyiv, Ukraine*
[3]*A.V.Palladin Institute of Biochemistry, NAS of Ukraine, Kyiv, Ukraine*

11:24-11:36 **Machine learning–based conformational sampling does not improve rigid protein–protein docking performance** **184**
I. Koleiev[1,2], T. Voitsitskyi[1,2], I. Savchenko[1,2], S. Starosyla[2], S. Yesylevskyy[1,2]
[1]*Institute of Physics, NAS of Ukraine, Kyiv, Ukraine*
[2]*Receptor.AI Inc., London, United Kingdom*

11:36-11:48 **Composite film of N-doped reduced graphene oxide with MoS_2: spectroscopy characterization and analysis of low-temperature electron transport** **185**
N. V. Kurnosov, A. Yu. Glamazda, A. M. Plokhotnichenko, V. A. Karachevtsev
B.Verkin Institute for Low Temperature Physics and Engineering of NASU, Kharkiv, Ukraine

11:48-12:00 **Correlative nanoscale imaging of adherent Lewis lung carcinoma cells** **186**
G. Monastyrskyi[1], O. Gnatyuk[1], M. Olenchuk[1], D. Kolesnik[2], A. Boisen[3], Z. Zhang[3], S. Karakhim[4], G. Solyanik[2], G. Dovbeshko[1]
[1]*Institute of Physics, NAS of Ukraine, Kyiv, Ukraine*
[2]*R.E.Kavetsky Institute of Experimental Pathology, Oncology and Radiobiology of the NAS of Ukraine, Kyiv, Ukraine*
[3]*Technical University of Denmark, Lyngby, Denmark*
[4]*O.V.Palladin Institute of Biochemistry of the NAS of Ukraine, Kyiv, Ukraine*

12:00-12:15 **Protein-ligand molecular docking with unbound protein conformations using machine learning** **187**
T. Voitsitskyi[1,2], I. Koleiev[1,2], I. Savchenko[1,2], S. Starosyla[2], S. Yesylevskyy[1,2]
[1]*Institute of Physics, NAS of Ukraine, Kyiv, Ukraine*
[2]*Receptor.AI Inc., London, United Kingdom*

12:15-13:20 **BREAK**

PLENARY LECTURES OF INVITED SPEAKERS

Chair *Dr. Oleksii Konotop*

13:20-13:50 **^{4}He and ^{3}He – ^{4}He mixture films studied by neutron reflectometry** **45**
O. Kirichek[1], A. T. Jones[1], C. J. Kinane[1], C. R. Lawson[1], S. Langridge[1], and P. V. E. McClintock[2]
[1]*ISIS Neutron and Muon Source, Rutherford Appleton Laboratory, Harwell Science and Innovation Campus, Oxon, UK*
[2]*Department of Physics, Lancaster University, Lancaster, UK*

QUANTUM LIQUIDS AND QUANTUM CRYSTALS, CRYOCRYSTALS

Chair *Dr. Oleksii Konotop*

13:50-14:02 **Photon-driven relaxation in cryogenic solids and the role of charged particles** **138**
E. V. Savchenko, I. V. Khyzhniy, M. A. Bludov, S. A. Uyutnov
B.Verkin Institute for Low Temperature Physics and Engineering of NASU, Kharkiv, Ukraine

14:02-14:14 **Molecular-shape control of Boson-peak-like heat-capacity anomalies in polycyclic aromatic hydrocarbon crystals** **139**
V. Sokolenko[1], D. Szewczyk[1], A. I. Krivchikov[1,2], A. Jeżowski[1]
[1]*Institute of Low Temperatures and Structure Research of PAS, Wroclaw, Poland*
[2]*B.Verkin Institute for Low Temperature Physics and Engineering of NASU, Kharkiv, Ukraine*

14:14-14:26 **Low-temperature heat capacity scaling patterns in cryocrystals** **140**
M. Barabashko[1], A. Jeźowski[2], A. Krivchikov[1,2]
[1]*B.Verkin Institute for Low Temperature Physics and Engineering of NASU, Kharkiv, Ukraine*
[2]*Institute of Low Temperatures and Structure Research of PAS, Wroclaw, Poland*

14:26-14:38 **Rotation of chains of vortices and dipoles in circular cylinders** **141**
T. I. Zueva
B.Verkin Institute for Low Temperature Physics and Engineering of NASU, Kharkiv, Ukraine

14:38-14:50 **Condensed-state rearrangements in N_2O-CO_2 alloys according to THEED data** **142**
O. P. Konotop, A. A. Solodovnik
B.Verkin Institute for Low Temperature Physics and Engineering of NASU, Kharkiv, Ukraine

14:50-15:02 **Persistent current oscillation in double-ring quantum gas** **143**
A. A. Chaika[1], A. O. Oliinyk[1], I. V. Yatsuta[2], Y. O. Nikolaieva[1], M. Edwards[3], N. P. Proukakis[4], T. Bland[5], A. I. Yakimenko[1,6]
[1]*Taras Shevchenko National University of Kyiv, Kyiv, Ukraine*
[2]*Weizmann Institute of Science, Rehovot, Israel*
[3]*Georgia Southern University, Statesboro, Georgia, USA*
[4]*Newcastle University, Newcastle upon Tyne, United Kingdom*
[5]*LTH, Lund University, Lund, Sweden*
[6]*Universit´a di Padova, Padova, Italy*

15:02-15:15 **Optimization of phonon transmission through the interface between superfluid ^{4}He and bilayer solid structures** **144**
J. Amrit[1], V. Luzik[2], K. Niemchenko[2], Ye. Niemchenko[2], T. Vikhtynska[2]
[1]LISN, Université Paris-Saclay, CNRS, Orsay, France
[2]V.N.Karazin Kharkiv National University, Kharkiv, Ukraine

15:15-16:00 **BREAK**

PLENARY LECTURES OF INVITED SPEAKERS

Chair *Dr. Diana Hurova*

16:00-16:20 **On the 125th anniversary of the birth of Lev V. Shubnikov** **36**
Yu. G. Naidyuk
B.Verkin Institute for Low Temperature Physics and Engineering of NASU, Kharkiv, Ukraine

WORKSHOP: OPPORTUNITIES AND TECHNOLOGIES FOR RESEARCHERS

Chair *Dr. Diana Hurova*

16:20-17:20 **Modern scientific computing and data visualisation in Python** **55**
P. Jaeger
Pexon Consulting GmbH, Munich, Germany

THURSDAY, 4th of JUNE

PLENARY LECTURES OF INVITED SPEAKERS

Chair *Dr. Yevhen Petrenko*

10:00-10:30 **Formation of bio-oligomers in space through low-temperature radiation chemistry** **48**
(00:00 UTC-7) D. V. Mifsud[1,2,3], A. T. Hopkinson[4], P. Herczku[3], R. Rácz[3], A. M. Wilson[4], J. Pitfield[4], A. Traspas Muiña[5], G. Lakatos[3,6], B. Sulik[3], Z. Juhász[3], S. Biri[3], R. W. McCullough[7], N. J. Mason[3,8], C. Scavenius[4], L. Hornekær[4], S. Ioppolo[4]
[1]NASA Ames Research Center, Moffett Field CA, United States
[2]Bay Area Environmental Research Institute, Moffett Field CA, United States
[3]HUN-REN Institute for Nuclear Research (ATOMKI), Debrecen, Hungary
[4]University of Aarhus, Aarhus DK, Denmark
[5]Queen Mary University of London, London, United Kingdom
[6]University of Debrecen, Debrecen, Hungary
[7]Queen's University Belfast, Belfast, United Kingdom
[8]University of Kent, Canterbury, United Kingdom

10:30-11:00 **Applied aspects of pulsed and continuous wave laser microstructuring of materials for sensors and optoelectronics** **43**
P. Lytvyn, A. Korchovyii, A. Rusavsky, A. Vasin, S. Serhiichuk, I. Minailova, K. Svezhentsova, V. Dzhagan
V.Ye.Lashkaryov Institute of Semiconductor Physics, NAS of Ukraine, Kyiv, Ukraine

MATERIALS SCIENCE

Chair *Dr. Yevhen Petrenko*

11:00-11:12 **Crystallization of amorphous films of ytterbium oxide sulfide at thermal and electron beam influence** **198**
A. G. Bagmut
National Technical University "Kharkiv Polytechnic Institute", Kharkiv, Ukraine

11:12-11:24 **UVC up-conversion and vis-luminescence of $CaF_2:Pr^{3+}$ crystallites** **199**
O. Bezkrovna[1,2], R. Lisiecki[1], P.J. Dereń[1]
[1]Institute of Low Temperatures and Structure Research of PAS, Wroclaw, Poland
[2]Institute for Single Crystals of NAS of Ukraine, Kharkiv, Ukraine

11:24-11:36 **Quantum tunneling and above-barrier reflection of high-energy positively charged particles in oriented crystals** **200**
M. V. Bondarenco[1,2]
[1]National Science Center "Kharkiv Institute of Physics and Technology" of NASU, Kharkiv, Ukraine
[2]V.N.Karazin Kharkov National University, Kharkiv, Ukraine

11:36-11:48 **DFT investigation of native and carbon defects in oxides grown under a CO atmosphere: a case study of YAG** **201**
K. V. Hermash[1], D. V. Fil[1,2]
[1]Institute for Single Crystals of NAS of Ukraine, Kharkiv, Ukraine
[2]V.N.Karazin Kharkov National University, Kharkiv, Ukraine

11:48-12:00 **Crystal growth and properties of co-doped (Cr, Co, Fe):ZnSe** **202**
O. K. Kapustnyk, S. V. Naydenov, O. K. Kosteniukova, D. S. Sofronov, and I. M. Pritula
Institute for Single Crystals of NAS of Ukraine, Kharkiv, Ukraine

12:00-12:12 **Low-temperature ultrasonic studies of $CoCrFeMnNiV_{0.85}$ high-entropy alloy in different structural states** **203**
V. S. Klochko, A. V. Korniiets, V. I. Sokolenko, I. V. Kolodiy, O. O. Kondratov, I. F. Kislyak, Yu. S. Lypovska, T. M. Tykhonovska
National Science Center "Kharkiv Institute of Physics and Technology" of NASU, Kharkiv, Ukraine

12:12-12:24 **Effect of iodine pentoxide evaporation on the synthesis and superconducting properties of Tl-1223** **204**
I. R. Metskhvarishvili[1,2], M. Menelaou[3], D. L. Surmanidze[1,4], T. E. Lobzhanidze[4], A. D. Tchankvetadze[1,4], B. G. Bendeliani[1], G. N. Dgebuadze[1], V. M. Gabunia[1,5], M. R. Metskhvarishvili[6]
[1]Ilia Vekua Sukhumi Institute of Physics and Technology, Tbilisi, Georgia
[2]Georgian Technical University, Tbilisi, Georgia
[3]Cyprus University of Technology, Limassol, Cyprus
[4]Ivane Javakhishvili Tbilisi State University, Tbilisi, Georgia
[5]Petre Melikishvili Institute of Physical and Organic Chemistry of the Ivane Javakhishvili Tbilisi State University, Tbilisi, Georgia
[6]"Talga" Institute of Georgian Technical University, Tbilisi, Georgia

12:24-12:36 **Intrinsic and radiation defects in ZrO_2 powders** **205**
V. V. Nosenko, I. P. Vorona, T. L. Petrenko, L. Yu. Khomenkova
V.Ye.Lashkaryov Institute of Semiconductor Physics, NAS of Ukraine, Kyiv, Ukraine

12:36-12:48 **DFT study of point defects in Y_2O_3 doped with fluorine** **206**
D. O. Puhachev[1] and D. V. Fil[1,2]
[1]Institute for Single Crystals of NAS of Ukraine, Kharkiv, Ukraine
[2]V.N.Karazin Kharkov National University, Kharkiv, Ukraine

12:48-13:00 **Implementation of a methodology for crystal structure prediction using genetic algorithms integrated into the Python ASE library** **208**
B. Y. Semeniuk, O. D. Feia
Kyiv Academic University, Kyiv, Ukraine

13:00-13:12 **Formation and characterization of TBCCO superconductor coated lanthanum aluminate films via organometalic routes** **209**
A. D. Tchankvetadze[1,2], T. E. Lobzhanidze[2], M. Menelaou[3], I. R. Metskhvarishvili[1,4], D. L. Surmanidze[2], V. M. Gabunia[1,5], G. N. Dgebuadze[1], B. G. Bendeliani[1]
[1]Ilia Vekua Sukhumi Institute of Physics and Technology, Tbilisi, Georgia
[4]Ivane Javakhishvili Tbilisi State University, Tbilisi, Georgia
[3]Cyprus University of Technology, Limassol, Cyprus
[4]Georgian Technical University, Tbilisi, Georgia
[5]Petre Melikishvili Institute of Physical and Organic Chemistry of the Ivane Javakhishvili Tbilisi State University, Tbilisi, Georgia

13:12-13:25 **Effect of pressure on electrical resistivity of tin films** **210**
S. L. Udachan[1], S. B. Kolavekar[1], N. H. Ayachit[1], L. A. Udachan[2], S. S. Kolkundi[3], S. Ramya[4], S. Veeresh[4]
[1]School of Advanced Sciences, KLE Technological University, Hubballi, India
[2]S.S.Tegnoor Degree College, Kalaburagi, India
[3]Government First Grade College, Shahapur, Yadgir, India
[4]Shree Sangam Vidya Mandir, Kalaburagi, India

13:25-14:30 **BREAK**

PLENARY LECTURES OF INVITED SPEAKERS

Chair *Dr. Denys Laptiev*

14:30-15:00 **Superconducting quantum & classical thermoelectricity** **40**
A. Braggio
CNR-NANO & NEST, Scuola Normale Superiore Pisa, Pisa, Italy

THEORY OF CONDENSED MATTER PHYSICS

Chair *Dr. Denys Laptiev*

15:00-15:12 **Polaron dynamics in external magnetic field** **251**
L. S. Brizhik[1], B. M. A. G. Piette[2]
[1]Bogolyubov Institute for Theoretical Physics of NASU, Kyiv, Ukraine
[2]University of Durham, Durham, UK

15:12-15:24 **The Lindblad equation in different bases: application to two- and multilevel systems** **252**
O. A. Ilinskaya[1], O. V. Ivakhnenko[1,2], A. I. Ryzhov[1], S. N. Shevchenko[1,3]
[1]B.Verkin Institute for Low Temperature Physics and Engineering of NASU, Kharkiv, Ukraine
[2]RIKEN Center for Quantum Computing (RQC), Wakoshi, Saitama, Japan
[3]Kyiv School of Economics, Kyiv, Ukraine

15:24-15:36 **Fast GPU-based quantum interferometry solver** **253**
O. V. Ivakhnenko[1,2], S. N. Shevchenko[1,3], and F. Nori[2,4]
[1]*B.Verkin Institute for Low Temperature Physics and Engineering of NASU, Kharkiv, Ukraine*
[2]*RIKEN Center for Quantum Computing (RQC), Wakoshi, Saitama, Japan*
[3]*Kyiv School of Economics, Kyiv, Ukraine*
[4]*University of Michigan, Ann Arbor, MI, USA*

15:36-15:48 **Hydrodynamics of polarons in semiconductors** **254**
S. O. Sokolovsky[1,2], A. I. Sokolovsky[3]
[1]*Dnipro polylingual lyceum №23 of Dnipro city council, Dnipro, Ukraine*
[2]*Dnipro Academy of Continuing Education, Dnipro, Ukraine*
[3]*Oles Honchar Dnipro National University, Dnipro, Ukraine*

15:48-16:00 **Comprehensive investigation of the structural, mechanical, electronic, phonon, thermodynamic and hydrogen storage properties of the hydride perovskite Mg_2IrH_6** **255**
C. Aksu[1], N. Arikan[1], A. İyigör[2] and E. Tel[1]
[1]*Osmaniye Korkut Ata University, Osmaniye, Türkiye*
[2]*Kırşehir Ahi Evran University, Kırşehir, Türkiye*

16:00-16:30 **BREAK**

PLENARY LECTURES OF INVITED SPEAKERS

Chair *Dr. Denys Laptiev*

16:30-17:00 **Soft point-contact spectroscopy of PdTe at ultralow temperatures** **47**
(09:30 UTC-4)
S. Lee[1], D. Duong[2], A. M. Donald[1], S. Hauang[2], R. Gazizulin[1], M. W. Meisel[1], and R. Jin[2]
[1]*Department of Physics and MagLab High B/T Facility, University of Florida, Gainesville, FL, USA*
[2]*SmartState Center for Experimental Nanoscale Physics, University of South Carolina, Columbia, USA*

THEORY OF CONDENSED MATTER PHYSICS

Chair *Dr. Denys Laptiev*

17:00-17:12 **Algorithm for unitary evolution of quantum systems with tridiagonal Hamiltonians** **256**
D. Bondar[1], R. T. Ovsiannikov[2], K. Jacobs[3, 4], A. G. Sotnikov[2]
[1]*Tulane University, New Orleans, Louisiana, United States*
[2]*National Science Center "Kharkiv Institute of Physics and Technology" of NASU, Kharkiv, Ukraine*
[3]*United States Army Research Laboratory, Adelphi, Maryland, USA*
[4]*University of Massachusetts at Boston, Boston, Massachusetts, USA*

17:12-17:24 **Heisenberg model on the face-centered cubic lattice: iPEPS study** **257**
I. V. Lukin[1,2], A. G. Sotnikov[2,3]
[1]*Haiqu, Inc., San Francisco, California, United States*
[2]*Akhiezer Institute for Theoretical Physics, NSC KIPT, Kharkiv, Ukraine*
[3]*V.N.Karazin Kharkiv National University, Kharkiv, Ukraine*

17:24-17:36 **Tensor network study of quasi-one-dimensional Hubbard models** **258**
O. R. Hryniv[1,2], I. V. Lukin[1,2], A. G. Sotnikov[2,3]
[1]*Haiqu, Inc., San Francisco, California, United States*
[2]*Akhiezer Institute for Theoretical Physics, NSC KIPT, Kharkiv, Ukraine*
[3]*V.N.Karazin Kharkiv National University, Kharkiv, Ukraine*

17:36-17:48 **Spin-dependent atomtronic current induced by asymmetric potential barriers in the Fermi-Hubbard lattice model** **259**
S. S. Litvinova[1], A. G. Sotnikov[1,2]
[1]*V.N.Karazin Kharkiv National University, Kharkiv, Ukraine*
[2]*Akhiezer Institute for Theoretical Physics, NSC KIPT, Kharkiv, Ukraine*

17:48-18:00 **Inhomogeneous equilibrium structures in s=3/2 magnets under spontaneously broken SO(3)×U(1) symmetry** **260**
M. Yu. Kovalevsky, M. G. Shatnev
National Science Center "Kharkiv Institute of Physics and Technology" of NASU, Kharkiv, Ukraine

FRIDAY, 5th of JUNE

PLENARY LECTURES OF INVITED SPEAKERS

Chair *Dr. Denys Laptiev*

10:00-10:30 **Fractional charges and conductances in the strongly interacting wires** **44**
V. Kagalovsky
Shamoon College of Engineering, Beer-Sheva, Israel

THEORY OF CONDENSED MATTER PHYSICS

Chair *Dr. Denys Laptiev*

10:30-10:42 **Statistical ensembles for non-Boltzmann-Gibbs distributions of Ising-Markov sequences** **261**
O. V. Usatenko[1,2]
[1]*O.Ya.Usikov Institute for Radiophysics and Electronics of NASU, Kharkiv, Ukraine*
[2]*Center for Theoretical Physics, Polish Academy of Sciences, Warsaw, Poland*

10:42-10:54 **Resonant transmission of nonlinear terahertz waves through layered superconductors** **262**
T. Rokhmanova[1], Z. Maizelis[1,2], V. Yampol'skii[2]
[1]*O.Ya.Usikov Institute for Radiophysics and Electronics of NASU, Kharkiv, Ukraine*
[2]*V.N.Karazin Kharkiv National University, Kharkiv, Ukraine*

10:54-11:06 **Impact of frequency noise statistics on measurement-assisted entanglement** **263**
A. O. Guzenko[1], O. M. Konovalenko[1] and Z. A. Maizelis[1,2]
[1]*O.Ya.Usikov Institute for Radiophysics and Electronics of NASU, Kharkiv, Ukraine*
[2]*V.N.Karazin Kharkiv National University, Kharkiv, Ukraine*

11:06-11:18 **Sensitivity of two qubit Werner state entanglement preservation to decoherence parameters in measurement based protocol** **264**
O. Konovalenko[1], Z. Maizelis[1,2]
[1]*O.Ya.Usikov Institute for Radiophysics and Electronics of NASU, Kharkiv, Ukraine*
[2]*V.N.Karazin Kharkiv National University, Kharkiv, Ukraine*

11:18-11:30 **Exceptional-point control of reset-induced quantum Zeno and anti-Zeno transport** **265**
J. Kumar
Aalto University, Aalto, Espoo, Finland

11:30-11:42 **First-principles investigation of Mg_3XH_4 (X = Sc, Ti) hydrides: structural, electronic, elastic, thermodynamic, and hydrogen storage properties** **266**
C. Aksu[1], N. Arikan[1], A. İyigör[2] and E. Tel[1]
[1]Osmaniye Korkut Ata University, Osmaniye, Türkiye
[2]Kırşehir Ahi Evran University, Kırşehir, Türkiye

11:42-11:54 **Predicting magnetic properties of one-dimensional Ising systems with arbitrary lattice geometry** **267**
O. O. Kryvchikov, D. V. Laptiev
B.Verkin Institute for Low Temperature Physics and Engineering of NASU, Kharkiv, Ukraine

11:54-12:06 **Zero-temperature phase diagrams and thermodynamic properties of the armchair-type and zigzag-type decorated honeycomb Ising spin chains** **268**
D. V. Laptiev, O. O. Kryvchikov
B.Verkin Institute for Low Temperature Physics and Engineering of NASU, Kharkiv, Ukraine

12:06-12:18 **Influence of magnetic quantization and exchange interaction on the seebeck coefficient in diluted magnetic semiconductor superlattices** **269**
M. M. Mahmudov, R. Y. Damirov
Baku State University, Baku, Azerbaijan

12:18-12:30 **Current-Voltage & Current ? Phase of superconducting order parameter scattering matrix for semiconducting & superconducting structures** **270**
K. Pomorski[1,2], D. Khadka[1], M. Osinski[1]
[1]University of New Mexico, Center for High Technology Materials, Albuquerque, USA
[2]Quantum Hardware Systems, Lodz, Poland

PLENARY LECTURES OF INVITED SPEAKERS

Chair *Dr. Diana Hurova*

13:30-14:00 **A high-temperature limit penalizing high-frequency quantum fluctuations** **37**
E. Aurell
KTH Royal Institute of Technology, Stockholm, Sweden

14:00-14:30 **Closing Remarks**
Acting Director of the B. Verkin ILTPE of NAS of Ukraine
Corresponding Member of NAS of Ukraine
Prof. Alexander Dolbin
and
Chair of Organizing Committee Dr. Diana Hurova

PLENARY LECTURES OF INVITED SPEAKERS

On the 125th anniversary of the birth of Lev V. Shubnikov

Yu. G. Naidyuk

B.Verkin Institute for Low Temperature Physics and Engineering of the NAS of Ukraine,
47 Nauky Ave., Kharkiv, 61103, Ukraine
e-mail: naidyuk@ilt.kharkov.ua

Lev V. Shubnikov was an outstanding experimental physicist who laid the foundations of the Ukrainian school of low-temperature physics and cryogenics. His groundbreaking experiments at the Ukrainian Institute of Physics and Technology (UPTI) in Kharkiv were decades ahead of world science in the 1930s. In my talk, I briefly share some facts from his life before he started his work at UPTI that may be less well-known. Also, chronicles of Shubnikov's brilliant career, from his education in Leningrad to his groundbreaking discoveries in Leiden and Kharkiv—most notably the Shubnikov–De Haas effect and the discovery of type-II superconductivity —will be referred. Most of the events and information reported are taken from the book edited by L. J. Reinders "The Life, Science and Times of Lev Vasilevich Shubnikov, Pioneer of Soviet Cryogenics" Springer International Publishing AG, 2018.

A high-temperature limit penalizing high-frequency quantum fluctuations

E. Aurell

KTH Royal Institute of Technology, Stockholm, Sweden
e-mail: eaurell@kth.se

The time evolution of a quantum system interacting with an Ohmic bath of harmonic oscillators is one of the most widely studied models of open quantum systems theory. It is applicable in numerous physical situations where the damping becomes frictionlike (frequency independent) in the semiclassical limit, such as for photon and phonon baths, as well as superconducting qubits coupled to resistive elements in quantum circuits. Caldeira and Leggett famously used this model to investigate the classical limit of quantum Brownian motion and macroscopic tunnelling. An important conceptual problem with this model is that a straightforward high-temperature limit leads to a quantum Markov evolution which is not a CPTP map. In the language of Lindblad equations one of the jump rates is slightly negative, hence, in fact, the evolution is not governed by a proper Lindblad equation. The problem has been known for a long time and addressed e.g. by adding a phenomenological term which can be shown to vanish in the high temperature limit (Breuer, H.-P., & Petruccione, F. (2002). "The theory of open quantum systems". Oxford University Press), more recent contributions include L. Ferialdi (2017) "Dissipation in the Caldeira-Leggett model", Phys. Rev. A, 95: 052109.

In this lecture I will revisit the model, and derive an additional contribution to the decoherence kernel in a new high-temperature limit at arbitrarily large cut-off frequency. The resulting evolution is that of Lindblad equation with only positive jump rates, which hence solves the problem. The new contribution reveals a new mechanism for classicalization of high-frequency quantum fluctuations, as they are damped.

I will also discuss end contributions to the Feynman-Vernon kernel, earlier considered by Hänggi and others, but which can be discussed a little differently taking into account also the new contribution to the high-temperature limit. Finally, I will discuss the opposite low-temperature limit and Feynman-Vernon kernel with long-time memory.

The talk is based on joint work with Graeme Pleasance and Francesco Petruccione [under review, available as arXiv:2508.14262].

Structural defects as crucial factors for persistent luminescence in Cr-doped $ZnGa_2O_4$ spinels

V. Boiko

Institute for Low Temperatures and Structure Research, Polish Academy of Sciences, Okólna 2, PL-50-422 Wroclaw, Poland
e-mail: v.boiko@intibs.pl

Persistent luminescence (PersL) materials that emit in the near-infrared (NIR) region have attracted considerable attention for their potential applications in bioimaging, sensing, and photonic technologies. Among these, Cr^{3+}-doped $ZnGa_2O_4$ (ZGO:Cr) spinels represent a vital class of materials exhibiting long-lasting emission within the NIR-I biological window (650–750 nm), making them suitable candidates for optical tagging and bio-visualisation [1,2].

The efficiency and duration of persistent luminescence in these materials are strongly influenced by structural defects that serve as charge-trapping centres [3]. This work examines the role of defect formation in ZGO:Cr nanoparticles, focusing on antisite defects and lattice distortions that arise from non-ideal cation distributions within the spinel lattice. Previous studies have shown that hydrothermal synthesis parameters can regulate the degree of spinel inversion, thereby modifying the trap landscape responsible for charge storage [4].

New experimental results from temperature-dependent optical spectroscopy have provided more details on defect-related excitation pathways and trap-assisted recombination processes. Additionally, photoluminescence excitation and emission spectra recorded in the deep-ultraviolet (UV) region, up to 12 eV, allow for the direct probing of high-energy electronic transitions associated with charge-transfer processes and defect states in the host lattice.

The combined spectroscopic analysis emphasises the critical role of structural disorder in controlling charge trapping, energy transfer to Cr emission centres, and the resulting persistent luminescence behaviour. These findings enhance our understanding of the defect-mediated mechanisms governing afterglow in ZGO spinels and lay the foundation for rational defect engineering to improve the performance of NIR persistent luminescent phosphors.

This work was supported by NSC grant No. DEC-2024/08/X/ST5/00392 and the NEPHEWS programme under Grant Agreement No. 101131414 from the EU Framework Programme for Research and Innovation Horizon Europe. Parts of this research were conducted at PETRA III, P66 Superlumi, proposal ID: I-20250937 EC.

[1] A. Bessière, S. Jacquart, K. Priolkar, A. Lecointre, B. Viana, and D. Gourier, Opt. Express. 19, 10131-10137 (2011) https://doi.org/10.1364/OE.19.010131.
[2] M.S. Relvas, M.R.N. Soares, S.O. Pereira, A.V. Girão, F.M. Costa, T. Monteiro, J. Phys. Chem. Solids, 129, 413-423, (2019) https://doi.org/10.1016/j.jpcs.2019.01.022.
[3] A. De Vos, K. Lejaeghere, D. E. P. Vanpoucke, J. J. Joos, P. F. Smet, and K. Hemelsoet, Inorg. Chem. 55, 2402-2412 (2016) https://pubs.acs.org/doi/10.1021/acs.inorgchem.5b02805
[4] A. Gerus, V. Boiko, V. C. Ciaramitaro, M. L. Saladino, D. Hreniak, Mater. Res. Bull. 168, 112473 (2023) https://doi.org/10.1016/j.materresbull.2023.112473

The Role of A in ARPES

S. Borisenko

IFW-Dresden, Helmholtzstrasse 20, 01069 Dresden, Germany
e-mail: S.Borisenko@ifw-dresden.de

Angle-resolved photoemission spectroscopy (ARPES) was developed in the 1970s–1990s as a momentum-resolved probe of the electronic structure of solids, with its basic principles summarized in early seminal works and classic reviews. The basic ARPES result is currently almost exclusively associated with the two-dimensional intensity distribution with coordinate axes labeled as Binding Energy and Momentum. Such datasets are usually directly compared to the bandstructure calculations along high symmetry directions of the Brillouin zone. Here we show that this is the result of an oversimplified treatment of the ARPES data leading to incorrect interpretations of the experimental results. We suggest practical ways of how to avoid it in both data collection and analysis.

Superconducting quantum & classical thermoelectricity

A. Braggio

CNR-NANO & NEST, Scuola Normale Superiore Pisa,
Piazza San Silvestro 12, I-56127 Pisa, Italy
e-mail: alessandro.braggio@nano.cnr.it

Superconducting devices are generally assumed to present weak thermoelectric effects[1]. However since the inspiring works of Ginzburg[2] this has been progressively questioned with important experimental confirmations[3]. In recent years many examples in mesoscopic superconductivity have been reported of systems with strong thermoelectrical effects.

Finally more recently have been clearly identified a novel mechanism, the bipolar thermoelectric effect, to get the thermoelectricity from spontaneous particle-hole symmetry breaking in asymmetric superconducting tunnel junctions SIS' under strong temperature gradients[4,5]. This mechanism in some measure anticipated years ago by Aronov & Spivak[6], is a combination of a non-equilibrium effect over an interacting system, as essentially is the superconducting instability.[4,5,7] In recent years we have demonstrated a long list of application for quantum technologies of this effect.[8]

More recently we have demonstrated that the same system can be used to develop a purely *quantum* thermoelectric mechanism.[9] Essentially, we showed that in a hot SIS' junction with different gaps coupled electromagnetically with a resistive cold environment, the interplay between photon emission-absorption asymmetry and the dynamical Coulomb blockade of the junction could generate a finite thermoelectrical power revealing a Seebeck coefficient up to 100 microV/K. This mechanism is purely quantum since, in the classical regime, where photon emission-absorption asymmetry disappear no thermoelectricity is developed.

Finally, we will present an example where a hybrid quantum Hall system which is not thermoelectric in the normal state but become thermoelectric in the subgap if proximixed with a superconductor containing triplet components.[10]

[1] W. Z. Meissner, Das elektrische verhalten der metalle im temperaturgebiet des flüssigen heliums. Z. Ges. Kälte Industrie 34, 197 (1927).
[2] Ginzburg, V. On the thermoelectric phenomena in superconductors. Zh. Eksp. Teor. Fiz. 14, 134 (1944)
[3] C. D. Shelly, E.A. Matrozova, and V. T. Petrashov, Resolving thermoelectric "paradox" in superconductors. Science adv., *2*, e1501250 (2016)
[4] G. Marchegiani, A. Braggio, and F. Giazotto Nonlinear Thermoelectricity with Electron-Hole Symmetric Systems Phys. Rev. Lett. 124, 106801 (2020)
[5] G. Germanese, F. Paolucci, G. Marchegiani, A. Braggio, and F. Giazotto, Bipolar thermoelectric Josephson engine. Nature Nanotech., 17, 1084 (2022).
[6] A.G Aronov and B. Z. Spivak, Photoeffect in a Josephson junction. JETP Lett. 22, 101 (1975).
[7] S. Battisti, G. De Simoni, L. Chirolli, A. Braggio, and F. Giazotto, Bipolar thermoelectric superconducting single-electron transistor. Phys. Rev. Research, 6, L012022 (2024).
[8] F. Antola, G. Marchegiani, A. Braggio and F. Giazotto, in preparation
[9] F. Antola, G. De Simoni, F. Giazotto, and A. Braggio, Quantum Bipolar Thermoelectricity. arXiv preprint arXiv:2508.03219
[10] L. Pierattelli, F. Taddei, A. Romito and A. Braggio in preparation.

CARS, SHG, Raman spectroscopy and imaging for analysis of biological molecules and cells

G. I. Dovbeshko[1], A. Dementjev[2], O. P. Gnatyuk[1]

[1]Institute of Physics of NAS of Ukraine, 46 Nauky Ave., 03028, Kyiv, Ukraine
[2]Center for Physical Sciences and Technology, Saulėtekio al. 3, LT-10257 Vilnius, Lithuania
e-mail: matinelli@gmail.com

Methods of vibrational spectroscopy- coherent anti-Stokes Raman scattering (CARS), second harmonic generation (SHG), Raman scattering (RS) are successfully used in biology and medicine. For last decades, CARS is a third-order process, often considered as a nonlinear four-wave mixing process, allows vibrational imaging with high sensitivity, high spectral resolution and three-dimensional sectioning capabilities. SHG, second-order nonlinear optical process occurs in non-centrosymmetric crystals and molecules, as a label-free microscopy method has been applied recently for medical diagnostics of cancer, fibrosis, connective tissue disorders RS method along with IR spectroscopy provides a unique "molecular fingerprint" of biological samples without the use of labels, making it an effective non-invasive tool also.

Despite numerous discussions, a few biological molecules or structures have well-known non-linear properties. Among them are thymine [1], one of the bases of nucleic acids and collagen.

Here we present data on CARS and SHG of thymine (Thy) and adenine (Ade, another DNA base), collagens (Sigma-Aldrich 5162-1G) and cancer cells. Thy is one of the four essential components of DNA molecule and has monoclinic symmetry with the space group P21/c. Ade is a purine type molecule with monoclinic symmetry of space group P21/n. So, the symmetry of both crystals is the similar– monoclinic and non-centrosymmetric, however, we found the SHG signal only in the Thy crystal. Similarly, some of collagen molecules do not show SHG either. The spectra, images, physical property and possible reasons of SHG missing are discussed in the report. CARS spectra of DNA and cell components which is difficult task for modern industrial CARS microscope are obtained and compared with RS spectra. Different application of non-linear CARS and SHG imaging for cells are discussed.

Acknowledgement

Authors acknowledge the the project №1.4. B/218 "Physical effects and molecular mechanisms of interaction of biological molecules and biological systems of different levels of structural organization with small molecules, nanoscale and supramolecular complexes".

[1] Dementjev A., Rutkauskas D., Polovy I, Macernis M., Abramavicius D., Valkunas L., Dovbeshko G. Characterization of thymine microcrystals by CARS and SHG microscopy // Sci Rep.-2020.-10.-P. 17097.

Optical coherence tomography versus scanning electron microscopy for investigations of metallic fractures

G. Hutiu[1], V.-F. Duma[2], D. Demian[1], A. Bradu[3], A. Podoleanu[3]

[1]Faculty of Engineering, „Aurel Vlaicu" University of Arad, 77 Revolutiei Ave., 310130 Arad, Romania
[2]3OM Optomechatronics Group, Department of Measurements and Electro-Optics, Faculty of Electronics, Telecommunications, and Information Technology, Polytechnic University of Timisoara, 2 Vasile Parvan Ave., 300223 Timisoara, Romania
[3]Applied Optics Group, School of Physical Sciences, University of Kent, Canterbury, CT2 7NH, United Kingdom
e-mail: virgil.duma@upt.ro

Depending on how a static or dynamic load is applied to a certain material, metallic breaks can be either *ductile* or *brittle*. The variety of factors that must be considered include the way in which the load is applied, the shape of the mechanical sample/part, its nature and structure, the operating conditions, and the working temperature. Also, when subjected to variable loads, metals break due to what is called *fatigue*. The gold standard in the study of the fractures of metallic materials is scanning electron microscopy (SEM). The area of application of microscopic analysis of metallic surfaces targets especially forensic investigations, for plane or rails accidents, for pipes or turbines ruptures, etc. We have proposed for the first time to our knowledge [1], the use of Optical Coherence Tomography (OCT) for analyzing fracture surfaces of metals [2]. Our first study in this respect demonstrated that this low coherence interferometry technique, OCT can replace SEM for investigating and validating ductile or brittle fractures, although the former imaging technique has an axial resolution that is three orders of magnitude lower than the latter [1]. A second study has explored and demonstrated the threshold of the OCT resolution for achieving optimally the profilometry of metallic fractures [3]. Also, it has shown how OCT can assess fatigue fractures, as well. We present OCT versus SEM investigations of ductile, brittle, or fatigue fractures, for a range of metallic alloys tested under different conditions. Applications for such assessments are pointed out, as well. Advantages of OCT versus SEM are discussed. This development opens the way for *in situ* investigations, as is necessary in forensic sciences, for example, where OCT can be applied, including with our developed handheld scanning probes. In contrast, SEM, TEM, and AFM are lab-based techniques that require large and more expensive equipment, while OCT systems can be portable and their cost is with an order of magnitude lower.

Acknowledgement: This work is supported by the European Union – NextGenerationEU, through the National Recovery and Resilience Plan (PNRR) of Romania, Component 9, Investment 4, under the Important Project of Common European Interest (IPCEI ME/CT), project ASSET-IxC - UPT (Contract No. 5.PI/I4/C9), implemented by the Polytechnic University of Timisoara in collaboration with Aumovio Technologies Romania (formerly Continental Automotive Romania). The content of this material does not necessarily represent the official position of the European Union or of the Government of Romania.

[1] Gh. Hutiu, V.-F. Duma, D. Demian, A. Bradu, A. Podoleanu, Surface imaging of metallic material fractures using optical coherence tomography, Appl. Opt. 53(26), 5912-5916 (2014); http://dx.doi.org/10.1364/AO.53.005912.
[2] W. Drexler, M. Liu, A. Kumar, T. Kamali, A. Unterhuber, et al. Optical coherence tomography today: speed, contrast, and multimodality, J. Biomed. Opt. 19, 071412 (2014).
[3] Gh. Hutiu, V.-F. Duma, D. Demian, A. Bradu, A. Podoleanu, Assessment of ductile, brittle, and fatigue fractures of metals using optical coherence tomography, Metals 8(2), 117 (2018); doi: https://doi.org/10.3390/met8020117.

Applied aspects of pulsed and continuous wave laser microstructuring of materials for sensors and optoelectronics

P. Lytvyn, A. Korchovyii, A. Rusavsky, A. Vasin, S. Serhiichuk, I. Minailova, K. Svezhentsova, V. Dzhagan

V. Lashkaryov Institute of Semiconductor Physics, NAS of Ukraine,
41 Nauky Ave., 03028 Kyiv, Ukraine.
e-mail: dzhagan@isp.kiev.ua

Laser micro- and nano-structuring represents a transformative approach in advanced manufacturing, offering exceptional precision for material processing in the semiconductor sector for next-generation electronic systems [1]. This study presents a comparative analysis of light-matter interactions utilizing three distinct laser sources: a nanosecond pulsed IR fiber laser (1064 nm), a UV DPSS laser (355 nm), and a PWM-modulated CW semiconductor laser (455 nm). We investigate the wavelength-dependent mechanisms—ranging from multiphoton absorption to photothermal and photochemical effects—governing the modification of diverse materials.

The practical applications demonstrated range from the high-aspect-ratio cutting and drilling of refractory dielectrics (fused silica, sapphire) and metal foils to the delicate functionalization of soft matter. Specifically, we report on the direct prototyping of sensor devices utilizing polymers, 2D material suspensions, and nanometer-thick metal films. Significant attention is paid to carbon-based electronics, including the precisely controlled reduction of graphene oxide (GO) and the conversion of polyimide into porous graphene-like materials (LIG) via short-pulse thermal and photoelectric exploitation. Furthermore, processing in controlled gas and liquid media allowed for fine-tuning of surface chemistry and thermal influence.

In the semiconductor domain, results extend beyond morphological structuring to electronic structure modification, ranging from structural changes in classical silicon to direct band-gap engineering in GeSn alloys. To validate these complex modifications, a comprehensive diagnostic suite was employed. Advanced scanning probe microscopy (SPM) enabled simultaneous nanomechanical and electrophysical characterization at the nanoscale, utilizing Kelvin probe force microscopy (KPFM), scanning spreading resistance microscopy (SSRM), and scanning capacitance microscopy (SCM). These local analyses were complemented by High-Resolution X-Ray Diffraction (HRXRD) and vibrational spectroscopy (confocal Raman and FTIR). Furthermore, the physical processes of laser power absorption and material phase transformations were simulated through numerical modeling to correlate experimental data with theoretical predictions.

By tailoring pulse duration, power density, and wavelength, this work establishes optimized protocols for maskless rapid prototyping, bridging the gap between fundamental laser physics and functional device fabrication.

This work was supported by NRFU project #2023.05/0022

[1] V.M. Dzhagan, P.M. Lytvyn, A.A. Korchovyi, V.O. Yukhymchuk, V.V. Strelchuk, K.V. Svezhentsova, G.M. Androsyuk, O.V. Dubikovsky, V.V. Dzhahan, S.V. Kondratenko. Raman study of structural changes in Si-based materials induced by scanning with IR ns-pulsed laser. Semicond. Phys., Quantum Electronics & Optoelectronics 28 (2025) 456-463, https://doi.org/10.15407/spqeo28.04.456.

Fractional charges and conductances in the strongly interacting wires

V. Kagalovsky

Shamoon College of Engineering, Beer-Sheva, 8410802 Israel.
e-mail: victork@sce.ac.il

This research considers a strongly interacting one-dimensional system with N channels and explains the variety of experimentally observed fractional conductances in GaAs/AlGaAs heterostructures [1-3]. We study relevant backscattering perturbations that create gaps in the corresponding fields, thereby altering the system's properties. We model these gapped fields by introducing masses for the bosonic fields and sending them to infinity to compute the correlator of the two fields that describe the original channels. The exact solution of the corresponding Green function in the low-frequency limit enables us to apply the Kubo formula to calculate the system's dc conductance [4], which accounts for all the seminal experimental results [1-3]. We construct a pseudo-orthogonal transformation that reduces each backscattering term to a single-channel field [5] and derive the expression for the fractional charge transferred during the tunneling of the gapped mode, which dominates the dc shot noise. The coexistence of two gapped modes (two relevant perturbations) affects the tunneling of fractional charges in each of the modes.

[1] Y. Gul, S. N. Holmes, M. Myronov, S. Kumar, M. Pepper, J. Phys. Condens. Matter 30, 09LT01 (2018)
[2] S. Kumar, M. Pepper, S. N. Holmes, H. Montagu, Y. Gul, D. A. Ritchie, I. Farrer, Phys.Rev. Lett. 122, 086803 (2019)
[3] S. Kumar, M. Pepper, Appl. Phys. Lett. 119, 110502 (2019).
[4] R. Davies, V. Kagalovsky, and Igor. V. Yurkevich, Low Temperature Physics 52, (2026).
[5] R. Davies, V. Kagalovsky, and Igor. V. Yurkevich, Crystals 15, 818 (2025).

^{4}He and ^{3}He – ^{4}He mixture films studied by neutron reflectometry

O. Kirichek[1], A. T. Jones[1], C. J. Kinane[1], C. R. Lawson[1], S. Langridge[1], and P. V. E. McClintock[2]

[1]ISIS Neutron and Muon Source, Rutherford Appleton Laboratory, Harwell Science and Innovation Campus, Oxon, OX11 0QX, UK
[2]Department of Physics, Lancaster University, Lancaster, LA1 4YB, UK
e-mail: oleg.kirichek@stfc.ac.uk

In the quantum world superfluid helium ^{4}He can defy gravity and is able to climb out of any container in a thin film that moves with such a pace that the container is drained in minutes. However, of the many quantum fluid systems superfluid helium films remain one of the most elusive for experimental investigation.

Here we present a study of pure ^{4}He and ^{3}He/^{4}He mixture films using specular neutron reflection, in the temperature range of 150 mK to 1.5 K [1]. Thanks to the exceptional sensitivity and precision of this technique, we have observed a phase-separated ^{3}He/^{4}He mixture film at 170 mK. The neutron scattering density profile of the 165 Å thick helium mixture film presented in Figure 1 clearly demonstrates a thin ^{3}He layer on a top of the helium film. Then we have been able to watch the gradual dissolution of its ^{3}He top layer into ^{4}He with increasing temperature, in agreement with current theories. Furthermore, the surprising behavior of the helium mixture at 300 mK hints at the possibility of an as-yet unstudied geometrically restricted phase transition. The subsequent restoration of the layered structure at 1.5 K was equally unexpected.

We also developed a sample environment application based on the surprising behavior of the helium mixture at 300 mK. In neutron scattering powder diffraction experiments the helium exchange gas is often loaded into the experimental cell to thermalize the sample. We have used destruction of ^{3}He/^{4}He mixture film at 300 mK to reduce the heat flow through the filling capillary.

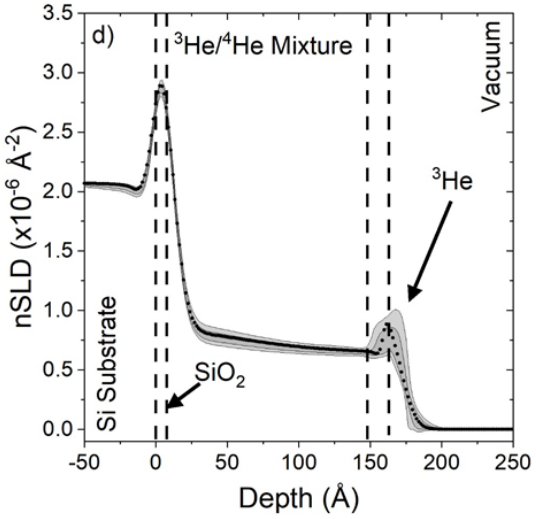

Figure 1: The neutron scattering density profiles of the helium mixture film.

[1] O. Kirichek, et al. Commun. Phys. **7**, 181 (2024).

Biophysical processes in the Universe as viewed by mass spectrometry

M. V. Kosevich

B.Verkin Institute for Low Temperature Physics and Engineering of the NAS of Ukraine,
47 Nauky Ave., Kharkiv, 61103, Ukraine
e-mail: mvkosevich@gmail.com

In our material world, measuring the mass of atoms and molecules is an important tool of scientific research. The main contributions of mass spectrometry to our basic knowledge about the Universe and Nature are establishing the exact masses of chemical elements, the discovery of isotopes and mass defect (eventually resulting in atomic energy and weapons), establishing the age of the Earth and geochronology, discovery of new compounds (such as fullerenes). The Nobel-prize-worthy (2002) achievement of mass spectrometry was the development of soft ionization techniques for measuring the masses of biomacromolecules, which advanced a series of "omics" sciences, particularly proteomics.

Currently, space missions are equipped with mass spectrometers intended for the detection of atoms, molecules, and interstellar dust in outer space and the disclosure of the composition of other planets' atmospheres [1]. The ILTPE NASU had contributed to this field since the development of portable mass spectrometers for spacecraft in the 80-ies of the XXth century. Several hundred molecules have been discovered in space so far. In laboratory experiments, conditions in cosmic space, such as vacuum, low temperatures, and particle and beam irradiation, can be created to simulate the processes leading to primary molecules formation. Mass spectrometry measurements contributed to the problem of early prebiological chemical evolution and the origin of life.

Two of our recent achievements related to the application of mass spectrometry to elucidate the origin of biomolecules will be discussed in this presentation. While mass spectrometry is used to model space conditions, some effects observed in mass spectrometric experiments can, in turn, be extrapolated to possible processes in space. Namely, we have shown that under the conditions of low temperature secondary emission mass spectrometry, efficient sputtering of a variety of species – positively and negatively charged molecules, radicals, clusters – occurs from water-alcohol mixtures which can preserve a liquid state down to approximately -120 °C [2, 3]. The occurrence of similar processes with interstellar dust irradiated by cosmic rays may make a noticeable contribution to the population of organic molecules and reactive species in outer space. Another effect relates to the stage of prebiological biochemical evolution consisting in the interaction of primary organic molecules with Earth's minerals. The catalytic activity of minerals containing transition-metal dichalcogenides (TMD) promoted the formation of new molecules, which can be modeled under conditions of laser desorption/ionization mass spectrometry [4]. In the course of these studies, an unexpected result was obtained, which demonstrated the possibility of trapping a molybdenum atom from the TMD MoS_2 by thio-derivatives of nitrogen bases. The observed process may explain the mechanism by which metals were incorporated into metal-containing coenzymes.

This work was supported by the grant 0126U001857 of the NAS of Ukraine.

[1] R. Arevalo, Z. Ni, and R. M. Danell, J. Mass Spectrom. 55(1), e4454 (2020). http://dx.doi.org/10.1002/jms.4454.
[2] M. V. Kosevich, V. S. Shelkovsky, O. A. Boryak, and V. V. Orlov, Rapid Commun. Mass Spectrom. 17(15) 1781 (2003). https://doi.org/10.1002/rcm.1121.
[3] M. V. Kosevich, O. A. Boryak, and V. S. Shelkovsky, Low Temp. Phys. 47(4), 335 (2021). https://doi.org/10.1063/10.0003746.
[4] M. V. Kosevich, V. A. Psahynska, V. S. Shelkovsky, O. A. Boryak, P. O. Kuzema, and V. A. Karachevtsev, J. Mass Spectrom. 60(12) e5191 (2025). https://doi.org/10.1002/jms.5191.

Soft point-contact spectroscopy of PdTe at ultralow temperatures

S. Lee[1], D. Duong[2], A. M. Donald[1], S. Hauang[2], R. Gazizulin[1], M. W. Meisel[1], and R. Jin[2]

[1]Department of Physics and MagLab High B/T Facility, University of Florida, Gainesville, FL 32611-8440, USA
[2]SmartState Center for Experimental Nanoscale Physics, Department of Physics and Astronomy, University of South Carolina, Columbia, SC 29208, USA
e-mail: sangyun.lee@ufl.edu

Topological semimetals have emerged as fertile ground for exploring the interplay between non-trivial topology and superconductivity. Among these, PdTe is of particular interest due to its unique band structure and potential for hosting unconventional pairing states [1-3]. The present study provides compelling evidence for the existence of multiple superconducting gaps in PdTe.

The experimental challenge of measuring the superconducting gap in PdTe lies in its low transition temperature and the sensitivity of the point-contact interface. To address this challenge, pure ^{3}He immersion cooling of the sample and the contact leads was employed. This setup effectively provided the ultralow temperature stability required for millikelvin spectroscopy. The "soft" contact was established using silver paint (Panels (a) and (b)) to minimize local strain and preserve the intrinsic properties of the possible surface states [4].

The measured differential conductance spectra exhibited characteristic Andreev reflection features (Panel (c)). However, the differential conductance spectra, specifically the width of the conductance peaks and the sub-gap structure, could not be adequately described by the standard single-gap Blonder-Tinkham-Klapwijk (BTK) theory [5]. Instead, a two-gap BTK model was employed [4], which yielded two distinct superconducting gaps, $\Delta_{small} = 0.6$ meV and $\Delta_{large} = 1.2$ meV. The agreement between the two-gap BTK model and the experimental data indicates PdTe is a multiband superconductor. These results suggest the pairing symmetry in PdTe is more complex than a simple isotropic *s*-wave, potentially hinting at the presence of topological superconductivity.

Acknowledgements. Aspects of this work were supported by the Grant No. DE-SC0024501 funded by the U.S. Department of Energy, Office of Science. The work performed at the National High Magnetic Field Laboratory (MagLab) High B/T Facility was supported by the National Science Foundation (NSF) through cooperative agreement DMR-2128556 and the state of Florida.

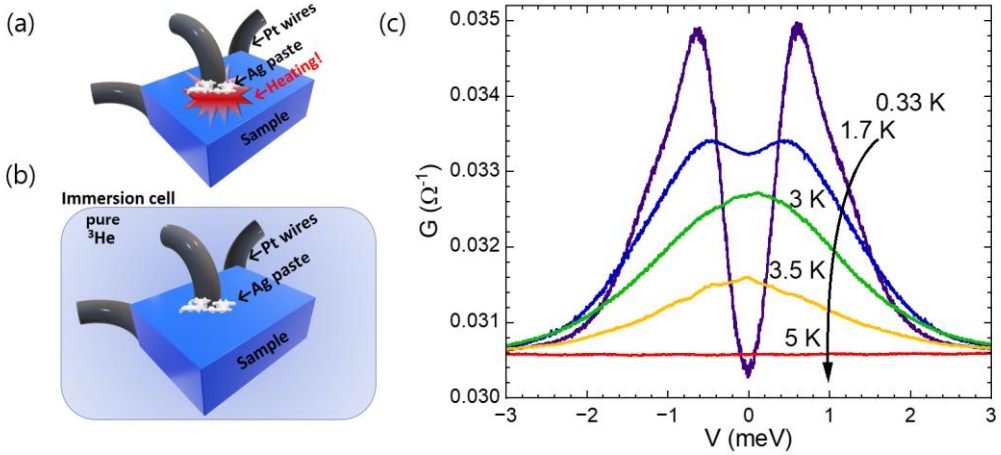

[1] R. Chapai et al., Sci. Rep. 13, 6824 (2023), doi:41598-023-33237-5.
[2] C. Zhao et al., Phys. Rev. B 109, 174502 (2024), doi:10.1103/PhysRevB.109.174502.
[3] D. Duong et al., Supercond. Sci. Technol. 39, 015007 (2024), doi:10.1088/1361-6668/ae34ef.
[4] E. Park et al., J. Phys.: Condens. Matter 30, 165401 (2018), doi:10.1088/1361-648X/aab5e5/meta.
[5] G.E. Blonder, M. Tinkham, and T.M. Klapwijk, Phys. Rev. B 25, 4515 (1982), doi:10.1103/PhysRevB.25.4515.

Formation of bio-oligomers in space through low-temperature radiation chemistry

D. V. Mifsud[1,2,3], A. T. Hopkinson[4], P. Herczku[3], R. Rácz[3], A. M. Wilson[4], J. Pitfield[4], A. Traspas Muiña[5], G. Lakatos[3,6], B. Sulik[3], Z. Juhász[3], S. Biri[3], R. W. McCullough[7], N. J. Mason[3,8], C. Scavenius[4], L. Hornekær[4], S. Ioppolo[4]

[1]NASA Ames Research Center, Moffett Field CA 94035, United States
[2]Bay Area Environmental Research Institute, Moffett Field CA 94035, United States
[3]HUN-REN Institute for Nuclear Research (ATOMKI), Debrecen H-4026, Hungary
[4]University of Aarhus, Aarhus DK-8000, Denmark
[5]Queen Mary University of London, London E1 4NS, United Kingdom
[6]University of Debrecen, Debrecen H-4032, Hungary
[7]Queen's University Belfast, Belfast BT7 1NN, United Kingdom
[8]University of Kent, Canterbury CT2 7NH, United Kingdom
e-mail: duncan.mifsud@nasa.gov, mifsud@baeri.org, mifsud.duncan@atomki.hu

Laboratory experiments over the past two decades or so have demonstrated that the synthesis of biomolecular monomers (e.g., amino acids, nucleobases, sugars) in nano- to microscale ices adsorbed on interstellar dust particles can occur *via* photolytic and radiolytic mechanisms even at temperatures as low as 10-20 K [1,2]. Such results carry important implications for astrobiology and the origins of life on Earth and (potentially) elsewhere in the cosmos. To date, however, there has been little firm evidence for the abiotic, low-temperature synthesis of more complex molecular bio-structures (e.g., peptides, nucleic acids, polysaccharides) in interstellar ices. In this presentation, I discuss the results of our experiments that demonstrated the radiolytic synthesis of glycylglycine, the simplest peptide, in an interstellar ice analogue as a result of its irradiation by keV and MeV protons mimicking space radiation at 20 K [3]. Our results demonstrate that the prebiotic chemistry leading to relatively complex bio-molecular structures may occur efficiently in an extra-terrestrial environment. The seeding of peptides (rather than simpler amino acids) to the early Earth may have provided an important chemical feedstock to facilitate the emergence of life.

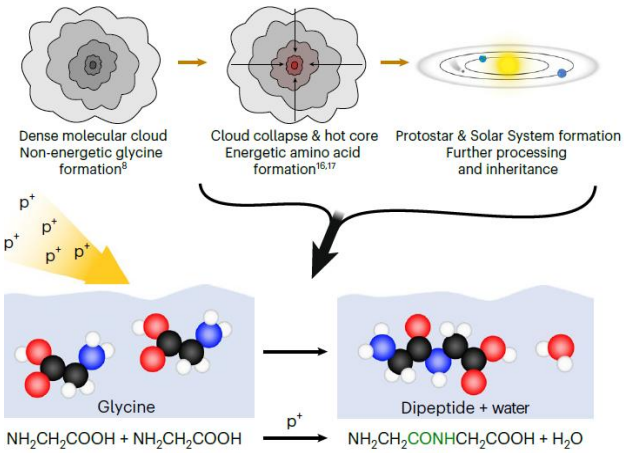

Figure 1. Schematic diagram depicting peptide formation as a result of the irradiation of amino acids in interstellar ices by energetic protons mimicking space radiation [3].

[1] S. A. Sandford, M. Nuevo, P. P. Bera, and T. J. Lee (2020). Chem. Rev. 120, 4616-4659. https://doi.org/10.1021/acs.chemrev.9b00560
[2] L. M. Ziurys (2024). Annu. Rev. Phys. Chem. 75, 307-327. https://doi.org/10.1146/annurev-physchem-090722-010849
[3] A. T. Hopkinson, A. M. Wilson, J. Pitfield, A. Traspas Muiña, R. Rácz, D.V. Mifsud et al. (2026). Nature Astron. https://doi.org/10.1038/s41550-025-02765-7

Thermal transport properties and phonon glass features in dimer-Mott quantum spin-liquid compounds

Y. Nakazawa[1], L. Zhang[1], T. Nomoto[2], S. Yamashita[1], and H. Akutsu[1]

[1]Dept. of Chemistry, Graduate School of Science, the University of Osaka, Machikaneyama 1-1, Toyonaka, Osaka 560-0043 Japan
[2]RIKEN Center for Emergent Matter Science (CEMS), Wako, Saitama 351-0198, Japan
e-mail: nakazawa@chem.sci.osaka-u.ac.jp

Quantum spin liquid (QSL) state in charge transfer complexes of organic molecules having κ–type and β'–type structures is considered as an intrinsic ground state emerges in these structure. This state emerging in frustrated dimer lattices, is considered as a strongly correlated electronic states of π–electrons/holes. The electronic states of these dimer-based materials have been understood systematically using a parameter of U/W and t'/t, where the former denotes the magnitude of electron correlations in the dimer lattices and the latter is a frustration parameter determined by a ratio of transfer integrals between neighboring dimers. QSL ground state is realized in the larger U/W case and it is considered as a kind of Mott insulator. If the frustration parameter is smaller, the system is recognized as a square lattice and antiferromagnetic ordering is possible, while in the specific situation with $t'/t \sim 1$ corresponding to an ideal triangle lattice, QSL state emerges at low temperatures. The physical properties especially thermal properties of this state have been extensively studied and continuous or extremely tiny-gapped thermal excitations have been reported by the heat capacity and the thermal conductivity measurements [1]. However, concerning the thermal transport property, temperature dependence of thermal conductivity in a wide temperature region demonstrates that unique features peculiar for dime-Mott triangle lattice should exit as was predicted by Nomoto *et al.* [2]. Intrinsic features dominating the heat transport properties have not been clarified in them since the sample dependences as well as cooling rate dependences have been reported up to now.

In this presentation, in order to obtain information of the temperature dependence of thermal conductivity mainly due to phonons for dime-Mott type spin liquid compounds, we performed systematic measurements for $EtMe_3Sb[Pd(dmit)_2]_2$ and κ–$(BEDT\text{-}TTF)_2Cu_2(CN)_3$ from extremely low temperature region near 1 K up to near room temperature by using our recently constructed apparatus [3,4]. For the former compound, we focus on the cooling rate dependence of the thermal conductivity obtained without changing sample set-up in a wide temperature between 1 K and 300 K. We also examined the extremely slow cooling case with a rate of 0.015 K/min and rapidly cooled cases and found that the phonon state of these QSL compound tends to show charge-glass type thermal transport properties. Furthermore, we compare the temperature dependence of the thermal conductivity of κ–$(BEDT\text{-}TTF)_4Hg_{2.89}Br_8$ that is considered as a doped spin liquid system where mobile carriers also conduct heat in the measurements. Almost similar behavior has been observed by our thermal conductivity measurements. The common features in these QSL compounds demonstrate that the hindered charge fluctuations inherent in these dimer-Mott materials are important and it affects the phonon structure that dominates the thermal conductivity of these compounds.

[1] S. Yamashita et al. Nature Communications 2, 275 (2011).
[2] T. Nomoto et al. Phys. Rev. B 105, 245133 (2022).
[3] L. Zhang et al. Low Temp. Phys. 49.5 (2023).
[4] L. Zhang et al. submitted to Thermochimica Acta (2026).

From near-infrared silicon photonics to magnetic control of matter: extending design principles across scales

M. F. Pereira[1,2], H. Zafar[1], A. Al-Ateqi[1] and Y. Tawalbeh[1,2]

[1]Department of Physics, Khalifa University, Abu Dhabi, UAE.
[2]Institute of of Physics, Czech Academy of Sciences, Prague, Czech Republic.
e-mail: mauro.pereira@ku.ac.ae

Silicon photonics has achieved remarkable maturity in the near-infrared (NIR), where waveguide engineering, polarization handling, and directional coupling are optimised for large-scale telecommunications. A critical assessment of state-of-the-art silicon-on-insulator (SOI) component including polarizers, polarization splitters and rotators, and asymmetric directional couplers reveals both their strengths and intrinsic limitations. Finite extinction ratios, Bragg back-reflections in subwavelength grating geometries, and wavelength sensitivity define clear performance ceilings. Importantly, understanding these constraints provides a roadmap for progress [1].

In this talk, we explore how these established NIR design principles can be systematically translated into the technologically demanding mid-infrared (MIR) spectral window (3.1–3.6 μm), where applications in chemical, environmental, and biomedical sensing are rapidly expanding. We present compact TM-pass polarizers based on periodic SOI waveguides that combine ultra-low insertion loss with strong suppression of unwanted modes. Building on this foundation, we introduce polarization splitter/rotators enabling efficient TM-to-TE conversion, an essential function for integrating quantum cascade laser sources with TE-optimised photonic circuitry.

Complementary asymmetric Euler bends allow dense, low-crosstalk waveguide arrays, while wavelength-stable directional couplers are engineered specifically for MIR operation, revealing both parallels and critical differences relative to their NIR counterparts. Together, these elements form a coherent MIR device ecosystem that preserves CMOS compatibility while addressing the distinct modal and material realities of longer wavelengths [2-4].

Complementing these photonic advances, we present an analytical thermodynamic framework for controlling nanoparticle formation through externally applied magnetic fields. By uniting classical nucleation theory with a sphere-packing description, we derive a closed-form relation linking magnetic field strength to most-probable particle radius. Calibrated against experimental observations in silver nanoparticles, the model captures the field-induced reduction in nucleation barrier and the shift toward smaller particle sizes. The framework remains robust above a few nanometers, while delineating the limits where non-extensive and collective effects emerge [5]. This approach offers a pathway toward inexpensive, field-engineered nanomaterials with direct relevance to photonic media.

Across both themes, the unifying idea is clear: by combining rigorous theory with careful device design, we can control light and matter across scales: from integrated waveguides to nanoscale particles: transforming physical insight into technological resilience.

[1] H Zafar, M. F. Pereira, Laser Photonics Rev 2024, 2301025.
[2] H. Zafar, M.F. Pereira, Sci Rep 15, 44122 (2025).
[3] H. Zafar, M.F. Pereira, Sci Rep 15, 5160 (2025).
[4] H. Zafar and M. F. Pereira, IEEE Access, vol. 12, pp. 48294-48300, 2024.
[5] Y. Tawalbeh, M. Ghazi, M.F. Pereira, Sci Rep 15, 41725 (2025).

The CISS effect as a unsolved problem

J. M. van Ruitenbeek

Huygens-Kamerlinhgh Onnes Laboratory, Leiden University,
Niels Bohrweg 2, Leiden, Netherlands
e-mail: ruitenbeek@physics.leidenuniv.nl

The effect known as Chiral Induced Spin Selectivity (CISS) was first discovered in 1999 [1], and has since been extensively investigated in many experiments [2]. In fact, there is not one CISS effect, but it is a collection of effects. They have in common that there is apparently a mutual influence of the chirality of a (molecular) conductor and the spin state of conduction electrons.

Although there have been many attempts at a theoretical explanation of the effects [4-5], there is still no generally accepted theory available. The situation is even worse, because several of the theoretical proposals violate basic principles of physics. This probably expresses the desperate state that the field finds itself in.

Initially, the CISS effect was observed in the form of spin polarization of electrons detected in photoemission experiments, for a self-assembled monolayer of homochiral molecules on the surface of a Au film. While this observation does not violate any basic principles, the size of the reported effect is much larger than can be expected for the modest spin-orbit coupling for organic molecules. Soon, this was followed by experiments measuring a difference in two-terminal magnetoresistance for the tow directions of magnetization, for a layer of chiral molecules connected by a normal metal on one side, and a ferromagnet on the other side. This result is in apparent contradiction to the famous Onsager relations. Even more striking are those results which appear to show that the direction of the magnetization of a thin magnetic film is dictated by the handedness of a monolayer of chiral molecules on its surface. This result appears to violate the time reversal symmetry of the Schrödinger equation.

Given this precarious state of affairs, it is useful to critically review the experimental evidence. I will briefly review the experiments and discuss the open questions and ambiguities that need to be resolved. The presentation is based upon a critical review paper that is in progress [6].

[1] K. Ray, S. P. Ananthavel, D. H. Waldeck, R. Naaman, Asymmetric scattering of polarized electrons by organized organic films of chiral molecules, Science 283, 814-816 (1999).
[2] B.P. Bloom, Y. Paltiel, R. Naaman, and D.H. Waldeck, Chiral Induced Spin Selectivity, Chemical Reviews 124, 1950-1991 (2024).
[3] F. Evers *et al.*, Theory of Chirality Induced Spin Selectivity: Progress and Challenges, Advanced Materials 2022, 2106629 (2022).
[6] S. Tirion, B van Wees, P. Hedegård, J.M. van Ruitenbeek, to be published.

Sagnac and Mashhoon effects in graphene

Y. V. Shtanov[1], T.-H. O. Pokalchuk[2], S. G. Sharapov[1,2]

[1]Bogolyubov Institute for Theoretical Physics,
14-b Metrologichna st., Kyiv 03143, Ukraine
[2]Kyiv Academic University, 36 Vernadsky blvd., Kyiv 03142, Ukraine
e-mail: sharapov@bitp.kyiv.ua

The Sagnac effect refers to the phase shift between two coherent waves, such as light, traveling in opposite directions within an interferometer mounted on a rotating disk. The magnitude of the phase shift is directly proportional to the area enclosed by the light rays, the frequency of the light, and the angular velocity of the interferometer's rotation. Given that material particles also exhibit wave-like properties, the Sagnac effect has been experimentally observed in free electrons in vacuum, neutrons, and even atoms. Moreover, when the Sagnac effect is realized on electrons, the resulting phase shift in the interference pattern is roughly a million times larger than that for light. This prompted a theoretical question: how would the Sagnac effect manifest in solid-state interferometers using free electrons in monolayer graphene? Graphene is known for its zero effective carrier mass and linear electron dispersion, properties that closely resemble those of light.

We investigate the Sagnac and Mashhoon effects in graphene, taking into account both the pseudospin and intrinsic spin of electrons, within a simplified model of a rotating nanotube or infinitesimally narrow ring. Based on considerations of the relativistic phase of the wave function and employing the effective Larmor theorem, we demonstrate that the Sagnac fringe shift retains a form analogous to that for free electrons, governed by the electron's vacuum mass. As a result, the effect in graphene remains approximately a million times stronger than in light-based interferometers. In the case of a narrow ring, an additional π-phase shift arises due to the Berry phase associated with the honeycomb graphene lattice. The Mashhoon fringe shift, which characterizes the dynamics of intrinsic spin, retains its conventional form in graphene, with its dependence on the Fermi velocity. Our analysis highlights both the similarities and differences between spin and pseudospin degrees of freedom in graphene.

[1]. A. Fesh, Yu.V. Shtanov, and S.G. Sharapov, Phys. Rev. B 110, L121402 (2024). https://doi.org/10.1103/PhysRevB.110.L121402.
[2] Yu.V. Shtanov T.-H.O. Pokalchuk, and S.G. Sharapov, SciPost Phys. 20, 053 (2026). https://doi.org/10.21468/SciPostPhys.20.2.053.

THz-driven nonlinear magnetization dynamics and the magnetic Jahn-Teller effect in rare-earth orthoferrites with Kramers and non-Kramers ions

N. R. Vovk[1], O. Y. Kovalenko[2], E. V. Ezerskaya[3], R. V. Mikhaylovskiy[2]

[1]James Watt School of Engineering, Electronics & Nanoscale Engineering Division, University of Glasgow, Glasgow G12 8QQ, United Kingdom
[2]Department of Physics, Lancaster University, Bailrigg, Lancaster, United Kingdom
[3]Department of Physics, V. N. Karazin Kharkiv National University, Kharkiv 61022, Ukraine
e-mail: Nikolay.Vovk@glasgow.ac.uk

In recent years, rare-earth orthoferrites have emerged as a prominent platform for the fully coherent terahertz (THz) control of ultrafast spin dynamics on picosecond timescales. In these altermagnets, intense THz pulses can resonantly drive rare-earth 4f crystal-field transitions, which in turn renormalize the effective magnetic anisotropy of the Fe sublattice via strong 4f–3d exchange. This mechanism enables strongly nonlinear excitation of Fe spins and, in suitable regimes, their coherent switching. Following the first demonstration of THz-driven magnetization dynamics in orthoferrites via anisotropy control [1], antenna-enhanced near fields were shown to induce fully coherent Fe-spin switching in $TmFeO_3$ [2]. More recently, room-temperature switching was achieved in the mixed orthoferrite $Sm_{0.7}Er_{0.3}FeO_3$, where the process is triggered by the magnetic-field component of the THz pulse, revealing a Zeeman-driven inertial pathway [3].

To describe these phenomena, we developed a theoretical framework for THz-driven spin dynamics in orthoferrites with non-Kramers rare-earth ions, using $TmFeO_3$ as a model system [4]. The model combines the crystal-field structure of the rare-earth subsystem with 4f–3d exchange and THz-driven Zeeman and Stark interactions, and couples these degrees of freedom to the Fe sublattice. It reproduces the temperature dependence of the effective anisotropies across the spin-reorientation phase transition, yields analytical expressions for the Fe and rare-earth mode frequencies in agreement with experiment [1], and captures the threshold behaviour of coherent spin switching observed in $TmFeO_3$ [2]. The next important step is to generalize this approach to orthoferrites with Kramers ions, such as $Sm_{0.7}Er_{0.3}FeO_3$ [3] and $ErFeO_3$ [5]. In these compounds, the rare-earth 4f states form Kramers doublets, leading to a richer exchange-split spectrum and potentially stronger dynamical back-action on the Fe subsystem. At the same time, our previous analysis identified a regime in which the commonly used adiabatic approximation for the coupled Fe and rare-earth dynamics breaks down. Most recently, using THz pump–optical probe spectroscopy, we obtained experimental results for the related altermagnets $TbFeO_3$ and $YbFeO_3$. In these compounds, we investigated the interaction between ensembles of two-level Tb/Yb ions and Fe spins, which manifests itself as ultrastrong coupling, leading to an avoided-crossing regime and revealing signatures of a magnetic analogue of the Jahn–Teller effect, which we also explain within our theoretical framework.

Here we outline a unified theoretical approach combined with our recent experimental findings at describing THz-driven nonlinear magnetization dynamics in rare-earth orthoferrites with Kramers and non-Kramers ions. The goal is to establish a predictive framework that explains THz-driven magnetization dynamics in altermagnets such as orthoferrites with and without coupling regimes between the modes, identifies the dominant switching pathways driven by the electric and magnetic components of the THz pulse, and determines the threshold fields, optimal temperature windows across the phase transitions, required for low-dissipation ultrafast spin switching. Such a framework is essential for understanding coherent spin control in complex rare-earth altermagnets and for guiding the development of the next generation energy-efficient THz spintronic memory elements.

[1] S. Baierl, M. Hohenleutner, T. Kampfrath, et al., Nat. Photonics 10, 715 (2016).
[2] S. Schlauderer, C. Lange, S. Baierl, et al., Nature 569, 383 (2019).
[3] Z. Zhang et al., Nat. Mater. 24, 219–225 (2025).

WORKSHOP:
OPPORTUNITIES AND TECHNOLOGIES FOR RESEARCHERS

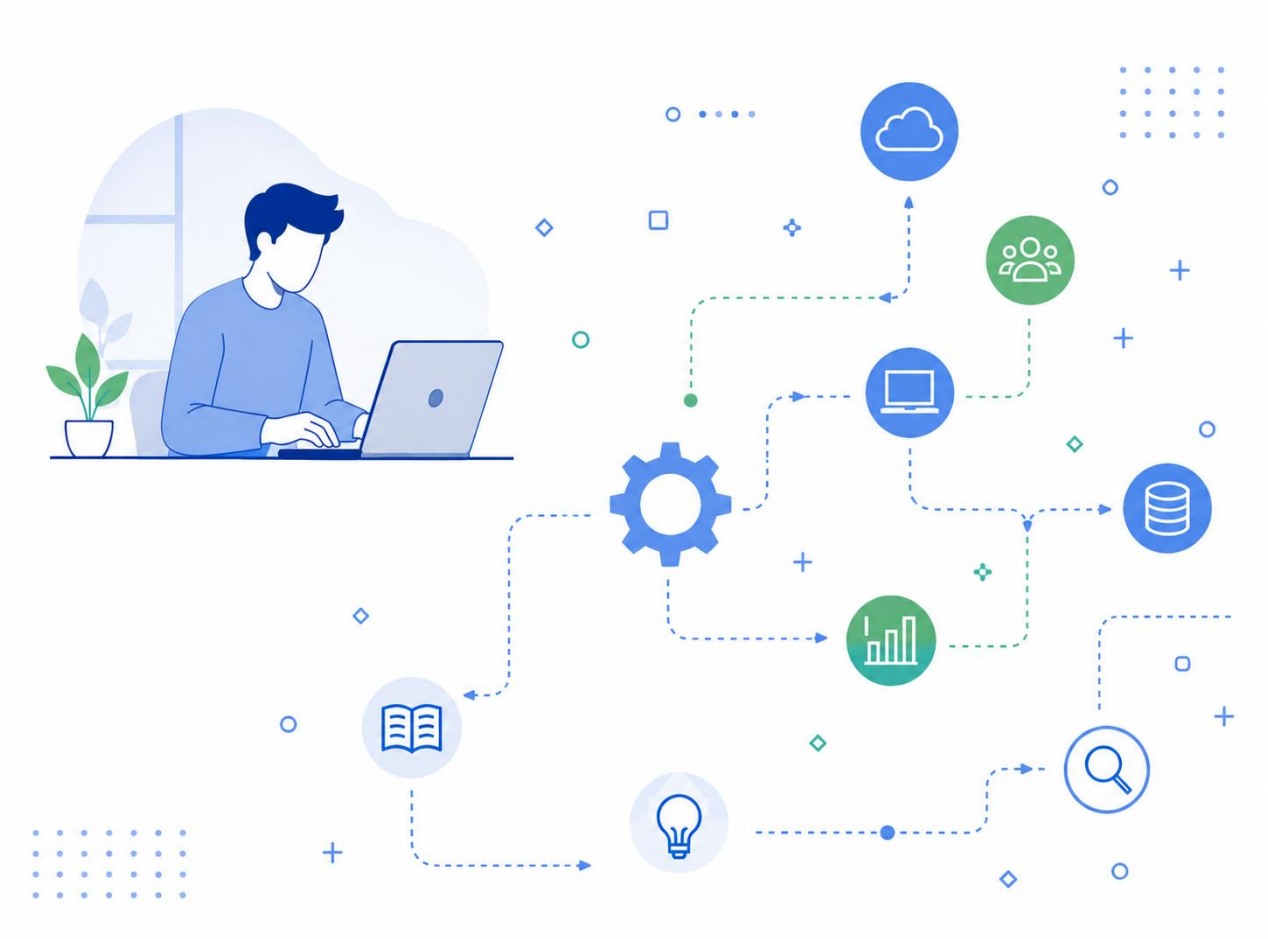

Modern scientific computing and data visualisation in Python

P. Jaeger

Pexon Consulting GmbH, Munich, Germany
e-mail: philipp.jaeger@pexon-consulting.de

Python has become a central platform for modern scientific research, combining rapid interactive development with powerful tools for numerical computation, data analysis, visualisation, and scalable computing. This workshop introduces practical Python-based workflows for scientific and data-intensive research, with a focus on techniques that are immediately useful in academic computing environments. Topics include exploratory analysis in notebook-based workflows, handling and visualising scientific datasets, creating publication-quality and interactive figures, and approaches to scaling computations from local systems to HPC environments. Practical aspects of research computing—such as software environments, optimized numerical libraries, compiler toolchains, and distributed execution—will also be discussed. Drawing on examples from computational and data-driven research, the workshop emphasizes reproducibility, performance awareness, and effective scientific workflows, while also briefly exploring the emerging role of AI-assisted tools in scientific computing.

ELECTRONIC PROPERTIES OF CONDUCTING AND SUPERCONDUCTING SYSTEMS

Pinning and dynamics of Abrikosov vortices in S-F bilayer films

A. L. Kasatkin, V. P. Tsvitkovskyi

G.V. Kurdyumov Institute for Metal Physics of NAS of Ukraine,
36 Vernadsky blvd., Kyiv, 03142, Ukraine
e-mail: alkas1951@gmail.com

Increasing the critical current in superconducting materials used in modern electrical engineering and electronics is one of the main objectives of applied superconductivity. Along with the creation of effective defect nanostructures that pin vortices in superconducting materials, an alternative approach is to use vortex pinning on localized magnetic moments within the superconducting material or in layered superconductor-magnet (S-F) structures [1]. Effective vortex pinning can be created, for example, on domain walls within a ferromagnet in a layered S-F structure [2]. A number of experiments have indeed observed a significant increase in the critical current density upon transition from isolated superconductor films to hybrid S-F film structures [3].

In this paper, the possibility of achieving high critical current values using the polaron mechanism of vortex pinning in S-F hybrid film structures is considered [4]. It is assumed that the magnetic layers are characterized by high values of magnetic polarizability and slow magnetization relaxation, which is necessary to ensure strong coupling of vortices in the S-layer and local magnetization in the F-layer induced by the magnetic field of the vortex. At low velocities, vortices in the S-layer are dressed in a cloud of inhomogeneous magnetization of the F-layer and move as a single unit – magnetic polaron. In this case, the viscosity of such polarons is determined by the magnetic relaxation time in the F-layer and significantly exceeds the viscosity of conventional vortices in superconductors determined by the Bardeen–Stephen law. With an increase in the velocity of motion at high currents, the polaron can decay (dissociate). In this case, the viscosity will drop abruptly to the Bardeen-Stephen value for a normal vortex, which will be reflected as a voltage jump on the current-voltage characteristic. Thus, the polaron instability (dissociation) current will be similar to the vortex depinning current, as shown in Fig. 1.

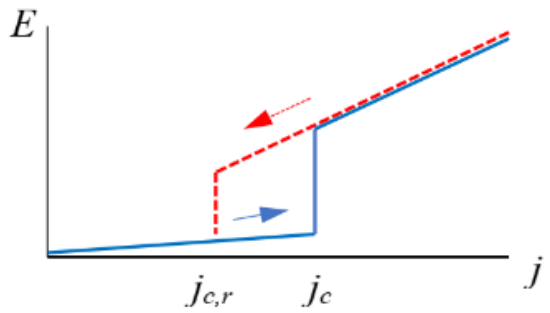

Fig.1. An expected CVC of the S/F bilayer narrow bridge in the magnetic polaron model.

[1] J. Huang and H. Wang, Supercond. Sci. Technol. 30, 114004 (2017). https://doi.org/10.1088/1361-6668/aa8d32.
[2] L. N. Bulaevskii, E. M. Chudnovsky, and M. P. Maley, Appl. Phys. Lett. 76, 2594 (2000). https://doi.org/10.1063/1.126419.
[3] E. Zhitlukhina, M. Poláčková, S. Volkov, B. Grančič, M. Gregor, T. Plecenik, M. Belogolovskii Appl Nanosci 13, 4771 (2023). https://doi.org/10.1007/s13204-022-02614-3.
[4] L. N. Bulaevskii and S.-Z. Lin, Phys. Rev. B 86, 064523 (2012). https://doi.org/10.1103/PhysRevB.86.064523.

Excitation of eigenmodes in cylindrical layered superconductors by non-relativistic electron flows

Yu. O. Averkov, O. Yu. Averkov, Yu. V. Prokopenko, V. A. Yampol'skii

O. Ya. Usikov Institute for Radiophysics and Electronics of NAS of Ukraine,
12 Acad. Proskury St., Kharkiv, 61085, Ukraine
e-mail: yuriyaverkov@gmail.com

Layered high-temperature superconductors (e.g., $Bi_2Sr_2CaCu_2O_{8+\delta}$) are considered promising candidates for bridging the "terahertz gap" due to their ability to support Josephson plasma waves (JPWs). While planar geometries have been extensively studied, cylindrical configurations offer distinct advantages for coupling with particle flows. This work presents a theoretical study of flow-wave interaction in a coaxial waveguide structure where an external hollow (tubular) non-relativistic electron beam (flow) propagates in the region $r_2 < r < r_3$ along a cylindrical shell made of a layered superconductor (region $r_1 < r < r_2$). The **c**-axis of superconductor is parallel to the z-axis of the waveguide. The inner region, $0 < r < r_1$, is occupied by a refrigerant, e.g. liquid nitrogen (see fig. 1).

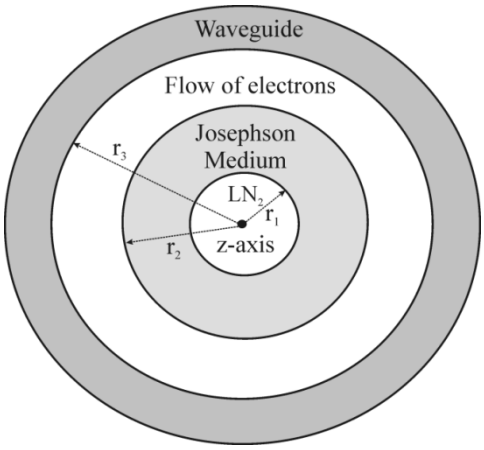

Fig. 1. Geometry of the problem.

A key feature of the proposed model is the utilization of a charge-compensated electron flow (ion-focused regime). This approach eliminates the necessity for a strong external guiding magnetic field, thereby preserving the superconductor in the Meissner state and preventing vortex penetration. Using a rigorous electrodynamic approach based on the matching of fields at the interfaces, we derived the dispersion relation for the hybrid modes in the electrostatic limit.

Our analysis reveals that the eigenmodes of the system—specifically the bulk-surface Josephson plasma waves—exhibit anomalous dispersion characteristics ($d\omega/dk < 0$, where ω is the wave frequency, k is the longitudinal wave vector). Such "backward-wave" behavior is critical for the development of instabilities. We demonstrate that the interaction between the forward-moving electron flow and these backward electromagnetic modes leads to the development of an absolute instability. Unlike convective instability, which amplifies signals as they propagate, the absolute instability provides an intrinsic distributed feedback mechanism. This allows the system to function as a compact oscillator without the need for external mirrors or cavities. The oscillation frequency is shown to be tunable and asymptotically approaches the Josephson plasma frequency. The proposed configuration suggests a robust pathway for designing efficient, tunable THz sources.

The research was conducted under the support of National Research Foundation of Ukraine, Project No. 2025.07/0256 "Electrodynamic linear and nonlinear phenomena in layered superconductors".

Enhancing electronic dispersion determination by employing an ensemble learning approach

Yu. V. Pustovit, M. O. Ohloblia, Ya. B. Yanenko

Faculty of Radiophysics, Electronics and Computer Systems of Taras Shevchenko National University of Kyiv, Hlushkova Avenue, 4g, Kyiv, Ukraine, 03127
e-mail: jura.pustvit@gmail.com

In Ref. [1], DeepLabV3 and U-Net models were applied to treat electronic dispersion extraction from ARPES spectra as a semantic segmentation problem. Even though both networks were trained on the same generated dataset, each model has its own peculiarities. While U-Net provides precise electronic dispersion extraction with high confidence level, it tends to overlook low-intensity bands, DeepLabV3 captures these weak zones but suffers from lower accuracy and the introduction of artifacts.

To leverage the high precision of U-Net alongside DeepLabV3's sensitivity to low-intensity features, a stacking ensemble approach was implemented. In this configuration, a meta-model integrates predictions from multiple base learners (level-0 models). Here, DeepLabV3, U-Net, and LinkNet served as base learners, each trained on a synthetic dataset of 10,000 examples. The optimization utilized binary focal loss, with hyperparameters set to $\alpha=1$ and $\gamma=2$ for U-Net and LinkNet, and $\gamma=1.5$ for DeepLabV3.

The predictions from all base models were concatenated to serve as input for the meta-model. Several architectures were evaluated: simple and weighted averaging were used as baselines, while an autoencoder and a convolutional neural network (CNN) were employed as more advanced alternatives. For the parameterized meta-models, a training set of 2,000 examples was used, with binary focal loss ($\alpha=1$, $\gamma=2$) as the objective function.

Model performance was evaluated using the Dice coefficient and Intersection over Union (IoU) metrics. Among the base learners, DeepLabV3 achieved the highest scores (Dice=0.76, IoU=0.85). While simple and weighted averaging baselines underperformed— reducing the overall ensemble accuracy (Dice=0.71, IoU=0.82)—the CNN and autoencoder meta-models enhanced performance (Dice=0.85, IoU=0.92). These results demonstrate that advanced meta-models successfully learn to combine the specific strengths of each base learner, leading to more robust and accurate predictions.

Also, the meta-models were evaluated on experimental ARPES spectra of *Fe(Se,Te)* collected across a wide temperature range (20–220 K), which were representative of the training data. To assess generalization, the models were tested on a diverse collection of ARPES spectra from a 3D angle scan database [2], including *CrSBr*, single-layer WS_2 films on *Ag(111)* and *Au(111)*, and *Rb*-intercalated Bi_2Se_3.

Analysis of the processed experimental spectra leads to the following conclusions: the use of meta-models facilitates significant artifact reduction and enables the identification of weak features even against a high-intensity background. Furthermore, this approach preserves the integrity of the band structure in high-noise environments while maintaining high classification confidence for electronic dispersion pixels.

[1] Yu. V. Pustovit and M. O. Ohloblia, Low Temp. Phys. 52, 145 (2026). https://doi.org/10.1063/10.0042266.
[2] S. M. Agústsson, M. A. Haque, T. T. Truong, M. Bianchi, N. Klyuchnikov, D. Mottin, P. Karras, and P. Hofmann, Mach. Learn.: Sci. Technol. 6, 015019 (2025). https://doi.org/10.1088/2632-2153/ada8f2.

Comparative analysis of the effects of low-energy helium-ion (He^+) and high-energy electron irradiation on fluctuation conductivity and pseudogap in $YBa_2Cu_3O_{7-\delta}$ compounds

A. L. Solovjov[1,2,3], M. V. Shytov[1], L. V. Bludova[1], A. S. Kolisnyk[1], A. Sedda[3], E. Lähderanta[3], W. Lang[4]

[1]B. Verkin Institute for Low Temperature Physics and Engineering of NAS of Ukraine, Kharkiv 61103, Ukraine
[2]Institute of Low Temperatures and Structure Research, of PAS, Wroclaw 50-422, Poland
[3]Department of Physics, LUT University, Lappeenranta 53850, Finland
[4]Faculty of Physics, University of Vienna, 1090 Vienna, Austria
e-mail: shytovnikita@gmail.com

In this work, the effect of irradiation with low-energy (75 keV) helium ions (He^+) on the resistivity, fluctuation conductivity (FLC), and pseudogap (PG) of $YBa_2Cu_3O_{7-\delta}$ films was studied. He^+ ion irradiation allows controlled defect generation in the crystal structure of $YBa_2Cu_3O_{7-\delta}$ [1], making it possible to study the evolution of FLC and PG over the irradiation fluence range from $\varphi_1=0$ to $\varphi_4 = 1.5 \times 10^{15}$ ions/cm^2.

It was established that with increasing irradiation fluence the critical temperature T_c gradually decreases from 89.6 K to 61.0 K. At the same time, a significant increase in resistivity is observed: the value of ρ(300 K) rises from 278.2 to 547.8 $\mu\Omega\cdot$cm. The analysis of the temperature dependences of ρ showed that Matthiessen's rule holds for all irradiation fluences: the slope $d\rho/dT$ of the linear regions of $\rho(T)$ remains nearly unchanged regardless of the irradiation fluence. The change from $d\rho/dT$=0.9 for the unirradiated sample to $d\rho/dT$=0.99–1.0 for the irradiated samples indicates that the introduction of radiation-induced disorder leads to a qualitative modification of the contributions of different scattering mechanisms and stabilizes the normal-state conductivity regime of the system.

Analysis of FLC conducted within the local pair model revealed that radiation defects generated by He^+ ion irradiation noticeably affect the parameters of three-dimensional and two-dimensional fluctuations. All characteristic temperatures shift toward the low-temperature region as the fluence increases. The fluctuation region width, ΔT_{fl}, decreases from 11 K to 6 K, indicating a substantial narrowing of the temperature range where FLC exists. The transverse coherence length, $\xi_c(0)$ decreases from 2.80 Å to 2.57 Å at the maximum fluence.

The pseudogap parameters at different irradiation fluences also demonstrate high sensitivity to He^+ ion irradiation. In contrast to electron irradiation described in the literature [2], when exposed to He^+ ions in this fluences range, no anomalous effect of "restoration" of the parameters of the PG is observed, but on the contrary, their monotonous degradation is recorded. With increasing radiation intensity, a stable suppression of superconducting fluctuations occurs. The characteristic temperatures T^* and T_{pair} decrease linearly, which indicates the destructive influence of defects on the process of formation of local pairs in the CuO_2 planes. A significant decrease in the energy gap $\Delta(T_G)$ and the parameter $D^*=2\Delta^*(T_G)/k_BT_c$ was also recorded, which is most likely characteristic of samples with T~60K.

[1] W. Lang, M. Dineva, M. Marksteiner, T. Enzenhofer, K. Siraj et al., Microelectronic Engineering 83, 1495 (2006). https://doi.org/10.1016/j.mee.2006.01.091.
[2] A. L. Solovjov, K. Rogacki, N. V. Shytov, E. V. Petrenko, L. V. Bludova, A. Chroneos, and R. V. Vovk, Phys.Rev. B 111, 174508 (2025). https://doi.org/10.1103/PhysRevB.111.174508.

Non-stationary longitudinal Josephson effect in electron-hole bilayers

O. M. Konstantynov, S. I. Shevchenko

B. Verkin Institute for Low Temperature Physics and Engineering of NAS of Ukraine,
47 Nauky Ave., Kharkiv, 61103, Ukraine
e-mail: akonstantinov@ilt.kharkov.ua

The counterflow superconductivity in electron-hole bilayers continues to be a subject of active theoretical and experimental studies (see, for example, review [1], recent works [2-5], and the literature cited therein). In particular, in our previous work [4] the features of the longitudinal stationary Josephson effect (which arises in a system where the right and left regions with electron-hole pairing are weakly coupled to each other) in such systems were considered and it was shown that the results depend significantly on the carrier density. In the present work, we consider the non-stationary longitudinal Josephson effect in bilayer systems with pairing of spatially separated electrons and holes in the presence of an external voltage applied between the left and right sides of the system. The analysis is performed both in the low-density limit corresponding to an excitonic Bose condensate and in the high-density limit where electron-hole pairing is realized in momentum space.

In the high-density limit, it is shown that the total current, for example, in the electron layer, consists of quasiparticle, superconducting and interference components (similar to a traditional superconductor), which are proportional to the second order of the transparency of the barriers in the electron and hole layers. In the case of a constant (time-independent) external voltage, it is established that the quasiparticle current is determined by the voltage across the barrier in the electron layer, while the amplitudes of the superconducting and interference currents are determined by voltage across the barrier in the hole layer. It is shown that at zero temperature, the quasiparticle and interference currents are generally characterized by different threshold voltages and, in particular, a situation is possible when the interference current is non-zero, while the quasiparticle current is zero. For voltages below the threshold, only a non-dissipative supercurrent flows in the system.

In the low-density limit, it was established that a characteristic feature of the supercurrent is its non-zero value already in the first order in the total transparency of the barriers. In the second order of perturbation theory, terms related to quasiparticle and interference currents are obtained, and it is shown that even at zero temperature they are non-zero at arbitrarily small voltages and lead to the damping of Josephson oscillations. Finally, it was shown, in the case where the distance between the barriers in the longitudinal direction is much greater than the coherence length, the phase of the order parameter undergoes a jump at each of the barriers and at constant voltage, in the general case, oscillations of voltages on the electron and hole barriers are obtained. At the same time, the dependence of the supercurrent on the total phase difference φ in the quasistatic case is determined by the relation $I(t) = I_{c1} I_{c2} \sin\varphi(t) / \sqrt{I_{c1}^2 + I_{c2}^2 + 2 I_{c1} I_{c2} \cos\varphi(t)}$, where $I_{c1,2}$ are the critical currents at each of the barriers.

[1] D. V. Fil and S. I. Shevchenko, Low Temp. Phys. 44, 867 (2018). https://doi.org/10.1063/1.5052674
[2] Bo Zou and A. H. MacDonald, Phys. Rev. Lett. 135, 086002 (2025). https://doi.org/10.1103/83f9-pln9
[3] J. Zhu and S. Das Sarma, Phys. Rev. B 112, 214521 (2025). https://doi.org/10.1103/bf1f-byy3
[4] S. I. Shevchenko and O. M. Konstantynov, Low Temp. Phys. 51, 1245 (2025). https://doi.org/10.1063/10.0039420
[5] Y. Zeng, D. Sun, N. J. Zhang et al., Nature 650, 86 (2026). https://doi.org/10.1038/s41586-025-09986-w.

Charge transport and dielectric properties of the $BaTiO_3$ ceramics

O. V. Bereznykov[1], D. O. Stetsenko[1], T. O. Kuzmenko[1,2], O. S. Pylypchuk[1], S. E. Ivanchenko[3], V. I. Styopkin[1], A. N. Morozovska[1], V. N. Poroshin[1], V. V. Vainberg[1]

[1]Institute of Physics, NAS of Ukraine, 46 Nauky Avenue, 03028 Kyiv, Ukraine
[2]Educational Scientific Institute of High Technologies, Taras Shevchenko National University of Kyiv, 4-g Hlushkova Avenue, 03022 Kyiv, Ukraine
[3]Frantsevich Institute for Problems in Materials Science, National Academy of Sciences of Ukraine Omeliana Pritsaka str., 3, Kyiv, 03142, Ukraine
e-mail: alexber36@gmail.com

The electric charge transport and dielectric properties of the $BaTiO_3$ ceramics doped with carbon fraction within 0 to 1 vol. % have been investigated in the range of 77 through 410 K. The samples were fabricated by spark-plasma sintering (SPS) in a graphite press at 1100°C in vacuum under a pressure of 50 MPa. It is established that the DC conduction of samples at temperatures below 150 – 200 K down to 77 K is a variable range hopping (VRH) kind and in non-heating electric fields it obeys the Mott law $\sigma(T)\sim\exp\left(-\frac{T_0}{T}\right)^{1/4}$ with $T_0=6\cdot10^7\div3.5\cdot10^8$ K depending on the carbon content. The conductivity magnitude in each sample varies in the whole VRH temperature range approximately by 3 orders of magnitude. The effective dielectric permittivity in the VRH range varies for the samples with different carbon content from 10^4 to $3\cdot10^5$. Though for each sample it quite slowly varies with temperature in the whole VRH range. At that its magnitude strongly depends both on the frequency and carbon concentration and it behaves synchronously in regard to conductivity at equal temperature. The more carbon concentration, the more dielectric permittivity and conductivity. At higher temperatures T > 200 K the dielectric permittivity strongly increases, shaping a sharp maximum while the resistivity sharply decreases. In the AC regime both the dielectric permittivity and resistivity at all temperatures manifest strong falling with the frequency increase from 10 Hz up to 500 kHz. The studied SPS samples possess in general a colossal dielectric permittivity which at low frequency and at higher temperatures reaches in the maximum almost 10^7. In the VRH range at $T\leq150$ K and E > 1 kV/cm the DC conductivity measured in the pulsed regime, to avoid the Joule heating, behaves as $ln[\sigma(E)]\sim AE$ with the slope A increasing with lowering temperature. The observed low temperature DC conduction features, including non-ohmic field one, are explained based on the model from Ref. [1, 2] which predicts similar conduction behavior in the case of moderately strong electric fields ($eE_a/k_BT\leq1$). Also, we account for the localization radius enlargement due to a large dielectric permittivity and impact of percolation in inhomogeneous sample [3]. Based on obtained results, one may estimate the localized states density at the Fermi level to be of order of 10^{17} eV^{-1} cm^{-3}, the charge carrier localization radius in average of several nm. A possible role of oxygen vacancies is discussed. The work of D.O.S., O.S.P. and A.N.M. are funded by the National Research Foundation of Ukraine (project “Manyfold-degenerated metastable states of spontaneous polarization in nanoferroics: theory, experiment and perspectives for digital nanoelectronics”, grant application 2023.03/0132). The work of O.V.B. is funded by the NAS of Ukraine, grant No. 07/01-2026(6) “Nano-sized multiferroics with improved magnetocaloric properties.” The work of V.V.V. and V.N.P. are funded by the Target Program of the National Academy of Sciences of Ukraine, Project No. 5.8/26-П “Energy-saving and environmentally friendly nanoscale ferroics for the development of sensorics, nanoelectronics and spintronics”.

[1] R. M. Hill, The Philosophical Magazine: A Journal of Theoretical Experimental and Applied Physics 24, 1307 (1971). https://doi.org/10.1080/14786437108217414.
[2] M. Pollak, I. Riess, J. Phys. C: Solid State Phys. 9, 2339 (1976). https://doi.org/10.1088/0022-3719/9/12/017.
[3] Yi Huang, Y. Ayino, and B. I. Shklovskii. Phys. Rev. Materials 5, 044606 (2021).

Balance between optical and superconducting properties in oxygen-deficient ITO films

D. Menesenko[1,2], O. Feia[1, 2, 3], A. Shapovalov[1,2]

[1]Kyiv Academic University, 36 Academician Vernadsky Blvd., UA-03142 Kyiv, Ukraine
[2]G. V. Kurdyumov Institute for Metal Physics, NAS of Ukraine, Kyiv, Ukraine
[3]Leibniz Institute for Solid State and Materials Research, Dresden, Germany
e-mail: d.menesenko@kau.edu.ua

Materials that simultaneously combine superconductivity and optical transparency are highly desirable for integrated superconducting–photonic technologies [1]. However, these properties are intrinsically difficult to reconcile because superconductivity requires favorable electronic conditions, including sufficient carrier density and electron–phonon coupling, while optical transparency requires a low plasma frequency. Transparent conducting oxides such as indium tin oxide (ITO) provide a promising platform to investigate this fundamental trade-off [2]. In these materials, both properties are governed by the carrier density n. Increasing oxygen vacancy concentration enhances superconductivity by increasing the density of states [3] at the Fermi level $N(0)$, but simultaneously shifts the plasma frequency toward the visible spectral range, thereby reducing transparency.

$$\omega_p^2 = \frac{ne^2}{\varepsilon_0 m^*}$$

Here we study oxygen-deficient ITO films as a model system. Pristine ITO films are non-superconducting down to 0.3 K. Oxygen vacancies were introduced via electrochemical reduction [3], enabling controlled removal of oxygen anions at the ITO surface and systematic tuning of the electronic structure. The degree of reduction is quantified by the injected charge density (C/cm^2), which is directly related to the concentration of oxygen vacancies.

Superconductivity was achieved in films ~360 nm thick. At low injected charge density (0.025 C/cm^2), superconductivity emerges below 3.5 K with a sharp transition width ΔT_c ~0.7 K while optical transparency at 500 nm decreases from ~85% to ~70%. Further increase of injected charge density (0.05 C/cm^2) raises T_c to 4 K with a sharp transition width ΔT_c ~0.1–0.2 K but reduces transparency to ~35%. Density functional theory calculations reveal band flattening near the Γ point and an increase of the density of states from ~3 to ~9 states/eV with increasing vacancy concentration.

These results demonstrate that superconductivity and optical transparency coexist only within a narrow range of oxygen vacancy concentration, highlighting the fundamental trade-off between electronic and optical properties in ITO.

This work was supported by NATO SPS Project G6082 and the German Federal Ministry of Research, Technology and Space (BMFTR) through the GU-QuMat project (01DK24008).

[1] X.-B. Xu, W.-T. Wang, L.-Y. Sun, and C.-L. Zou, Chip 1, 100016 (2022). https://doi.org/10.1016/j.chip.2022.100016.
[2] A. Aliev and M. Belogolovskii, Nat. Rev. Electr. Eng. 1, 563 (2024). https://doi.org/10.1038/s44287-024-00092-z.
[3] A. Parra et al., IEEE Trans. Appl. Supercond. 35, 7000105 (2025). https://doi.org/10.1109/TASC.2025.3530326.

Enhancement of superconductivity in twisted metallic materials

V. Tarenkov[1,2], D. Mindich[3], V. Dmytrenko[1], E. Zhitlukhina[1], V. Krivoruchko[1], I. Gavrysh[2], A. Shapovalov[2,3], O. Kalenyuk[2,3], M. Belogolovskii[3]

[1]O.O. Galkin Donetsk Institute for Physics and Engineering of NAS of Ukraine, 46 Nauky Ave., Kyiv, 03028, Ukraine
[2]G.V. Kurdyumov Institute for Metal Physics, National Academy of Sciences of Ukraine, Academician Vernadsky Blvd. 36, Kyiv, 03142, Ukraine
[3]Kyiv Academic University, Academician Vernadsky Blvd. 36, Kyiv, 03142, Ukraine
e-mail: dennis.mindich.official@gmail.com

Twistronics is a rapidly evolving field in condensed matter physics that explores how the electronic properties of layered materials change when the layers are rotated relative to one another. In this work, we expand the range of studied materials by applying this approach to two superconducting materials, a MoRe alloy and Ta foils, torsionally strained under high pressure. Below we compare the evolution of their superconducting properties subjected to the strong deformation and argue that this is a versatile way to design novel quantum materials by mechanical means. In our experiments, the superconducting plates were placed between two 45 mm diameter high carbon steel anvils with a Brinell hardness of 68 and working surfaces polished to a mirror shine. To exclude possible distortions during pressure loading, a steel casing with a sliding fit was used. A force of two tons was applied to the anvils, resulting in a pressure of 60 kbar on the samples. Under this uniaxial pressure, the upper anvil rotated making five revolutions. The rotation and the friction of the upper surface of the samples under pressure led to shear deformation of the upper surface becoming mirror-smooth like the surface of the upper anvil, while that in contact with the lower anvil remained unchanged. The superconducting characteristics of MoRe alloys and Ta differ significantly, making them suitable for distinct applications in research and industry. MoRe is a high-performance refractory alloy, known for its exceptional critical magnetic field and mechanical hardness, with T_c reaching 10–12 K around 40–50 at.% Re. Ta is a conventional elemental superconductor valued for its chemical stability and high-quality native oxides, with T_c about 5 K. In addition to traditional measurements of resistive characteristics near the transition from the normal to the superconducting state, we measured the differential conductance $dI(V)/dV$ of a point contact between an Ag tip and the surface superconductivity in deformed and control samples as a function of the voltage bias V at T = 4.2 K. Due to the significant differences in superconducting properties of MoRe and Ta, such measurements made it possible to establish fundamental aspects of the changes introduced into the samples. In particular, it relates the extraction of the superconductor's energy gap Δ far below T_c and in close proximity to it. Principally, the obtained results have been in qualitative agreement. In the as-prepared samples, the ratio $2\Delta/kT_c$ was significantly smaller than the BCS value 3.528 and was in the range of 2.1–2.4, which may be due to the corresponding depletion of the superconducting density of states directly on the untreated surface. After the high-pressure torsion, the ratio increased to values $2\Delta/kT_c$ near 4.0, thereby indicating the presence of a strong electron-phonon coupling. We attribute this increase to the loss of crystallinity in the studied samples with their subsequent amorphization and discuss the advantages of the extremely high deformation at low temperatures compared to other methods for inducing amorphous phase formation in superconducting materials. These results show that twistronics as an experimental technique expands beyond graphene and can include other materials, offering a highly tunable platform for studying correlated electron physics and providing valuable insights into unconventional superconductivity mechanisms. This approach has potential for advancing quantum technologies, enabling significant changes in electronic behavior, and engineering systems with higher critical temperatures T_c.

This work was partially supported by the National Academy of Sciences of Ukraine through the research program No. 0125U000295 (G.V. Kurdyumov Institute for Metal Physics).

Spin-paramagnetic effects and possible singlet–triplet transition in $Dy_{1-x}Er_xRh_{3.8}Ru_{0.2}B_4$

P. M. Fesenko[1], A. V. Terekhov[2], K. A. Minakova[1], A. P. Kazakov[3], I. V. Zolochevskii[2]

[1]National Technical University "Kharkiv Polytechnic Institute", 2 Kyrpychova str., Kharkiv, 61002, Ukraine
[2]B. Verkin Institute for Low Temperature Physics and Engineering of NAS of Ukraine, 47 Nauky Ave., Kharkiv, 61103, Ukraine
[3]International Research Centre MagTop, Institute of Physics, Polish Academy of Sciences, PL-02-668 Warsaw, Poland
e-mail: Pavlo.Fesenko@infiz.khpi.edu.ua

Triplet superconductivity is an unconventional superconducting state that has attracted considerable attention from researchers amid the rapid development of quantum computing and spintronics. In many cases, the pairing interaction is believed to originate from spin fluctuations rather than phonon-mediated mechanisms, suggesting that magnetic materials in which superconductivity coexists with magnetism may represent promising candidates for triplet superconductivity.

Rare-earth rhodium borides represent a convenient class of materials for investigating the interplay between superconductivity and long-range magnetic ordering. In our previous studies, we examined the superconducting compounds $Dy_{1-x}Y_x(Rh,Ru)_4B_4$, during which several unusual phenomena were observed. These include the Wohlleben effect [1], the coexistence of superconductivity with ferri- or ferromagnetism [2], and, most importantly, indications of triplet superconductivity [2–3].

This work aims to provide a systematic analysis of the temperature dependence of the upper critical field in $Dy_{1-x}Er_xRh_{3.8}Ru_{0.2}B_4$ compounds (x = 0, 0.2, 0.4) and to discuss the observed anomalies, which may, in particular, indicate the presence of unconventional superconductivity.

A detailed analysis of the temperature dependence of the upper critical field $H_{c2}(T)$ in the compounds $Dy_{1-x}Er_xRh_{3.8}Ru_{0.2}B_4$ (x = 0, 0.2, 0.4) has been performed. It was found that the $H_{c2}(T)$ curve for $Dy_{0.8}Er_{0.2}Rh_{3.8}Ru_{0.2}B_4$ exhibits an inflection point at approximately 3 kOe, which may be associated with low-temperature magnetic ordering. At the same time, a more unconventional mechanism related to a possible transition from conventional singlet to triplet superconductivity cannot be ruled out. The experimental $H_{c2}(T)$ dependences for $Dy_{1-x}Er_xRh_{3.8}Ru_{0.2}B_4$ (x = 0, 0.2, 0.4) have been successfully described within the framework of the Werthamer–Helfand–Hohenberg (WHH) theory using a nonzero Maki parameter $\alpha > 0$. This result indicates that spin-paramagnetic effects arising from magnetic exchange interactions play an important role in suppressing superconductivity in these compounds.

[1] V.M. Dmitriev, A.V. Terekhov, A. Zaleski, E.N. Khatsko, P.S. Kalinin, A.I. Rykova, A.M. Gurevich, S.A. Glagolev, E.P. Khlybov, I.E. Kostyleva, and S.A. Lachenkov, Low Temp. Phys. 38, 154 (2012). https://doi.org/10.1063/1.3681903.
[2] A.V. Terekhov, I.V. Zolochevskii, L.A. Ischenko, A.N. Bludov, A. Zaleski, E.P. Khlybov, and S.A. Lachenkov, Low Temp. Phys. 45, 1241 (2019). https://doi.org/10.1063/10.0000202.
[3] L.F. Rybaltchenko, E.V. Khristenko, L.A. Ishchenko, A.V. Terekhov, I.V. Zolochevskii, T.V. Salenkova, E.P. Khlybov, and A.J. Zaleski, Low Temp. Phys. 38, 1106 (2012). https://doi.org/10.1063/1.4769209.

Anomalous magnetoresistance in $Bi_{95.69}Mn_{3.69}Fe_{0.62}$ and $Bi_{88.08}Mn_{11.92}$ solid solutions

V. M. Yarovyi[1], A. V. Terekhov[1], K. Rogacki[2], E. Lähderanta[3], A. L. Solovjov[1,2,3]

[1]B. Verkin Institute for Low Temperature Physics and Engineering of NAS of Ukraine, 47 Nauky Ave., Kharkiv, 61103, Ukraine
[2]Institute for Low Temperatures and Structure Research, Polish Academy of Sciences, Wroclaw, Poland
[3]Lappeenranta University of Technology, School of Engineering Science, Lappeenranta, Finland
e-mail: yarovyi@ilt.kharkov.ua

Bismuth has unique electronic properties that make it important for research in quantum and condensed-matter physics. Certain electronic states in bismuth can be described as massive Dirac fermions. In addition, bismuth is regarded as a promising material for valleytronics, where the valley degree of freedom is used to encode quantum information in multivalley semiconductors and semimetals, potentially enabling valley-based quantum qubits.

Our investigations have demonstrated that Bi–Mn solid solutions containing 3.69 at.% Mn exhibit large positive magnetoresistance with pronounced anisotropy and unusual temperature and magnetic-field dependences [1, 2].

In this work, the magnetic-field dependence of magnetoresistance $MR = ([R(H) - R(0)]/R(0))*100$ % in $Bi_{88.08}Mn_{11.92}$ was studied at different temperatures for two field orientations ($H \perp I$ and $H \parallel I$). The results are compared with those for $Bi_{95.69}Mn_{3.69}Fe_{0.62}$ containing a smaller fraction of the magnetic α-BiMn phase.

It was shown that the field dependences of magnetoresistance for $Bi_{88.08}Mn_{11.92}$ differ markedly from those of $Bi_{95.69}Mn_{3.69}Fe_{0.62}$ below 100 K, but become nearly identical as the temperature approaches room temperature. The maximum relative magnetoresistance for $Bi_{88.08}Mn_{11.92}$ is observed at 100 K in a magnetic field of 90 kOe for both configurations ($H \perp I$ and $H \parallel I$), reaching 3170% and 380%, respectively. These values are significantly lower than the previously reported ones for the solid solution with lower Mn content ($Bi_{95.69}Mn_{3.69}Fe_{0.62}$), which reached 3877% and 742%, respectively. The observed differences in field dependences are attributed to different amounts of the magnetic α-BiMn phase in the studied materials. The anomalous magnetoresistance, compared with pure bismuth, is attributed to the effect of internal magnetism on charge transport in the bismuth matrix of the studied solid solutions.

The work was supported by the National Academy of Sciences of Ukraine within the F19-5 project. Work was also funded by Office of Naval Research (ONRG) and US National Academy of Sciences (NAS) IMPRESS-U grant via STCU project #7120.

[1] A. V. Terekhov, K. Rogacki, A. L. Solovjov, A. N. Bludov, A. I. Prokhvatilov, V. V. Meleshko, I. V. Zolochevskii, E. V. Khristenko, J. Cwik, A. Los, A. D. Shevchenko, Z. D. Kovalyuk, and O. M. Ivasishin, Low Temp. Phys. 44, 1153 (2018). https://doi.org/10.1063/1.5060969.
[2] A. V. Terekhov, K. Rogacki, V. M. Yarovyi, V. B. Stepanov, Yu. A. Kolesnichenko, A. D. Shevchenko, Z. D. Kovalyuk, E. Lähderanta, A. L. Solovjov, Low Temp. Phys. 49, 998 (2023). https://doi.org/10.1063/10.0020170.

Quantum reflectometry meets quantum averaging theory

O. Yu. Kitsenko[1,2], S. N. Shevchenko[1,3], L. Peri[4,5], F. Nori[6,7]

[1]B. Verkin Institute for Low Temperature Physics and Engineering of NAS of Ukraine, 47 Nauky Ave., Kharkiv, 61103, Ukraine
[2]V. N. Karazin Kharkiv National University, Kharkiv 61022, Ukraine
[3]Department of Mathematics, Kyiv School of Economics, 03113 Kyiv, Ukraine
[4]Quantum Motion, London N7 9HJ, United Kingdom
[5]Cavendish Laboratory, University of Cambridge, Cambridge, UK
[6]Quantum Computing Center, RIKEN, Wako-shi, Saitama, 351-0198, Japan
[7]Physics Department, The University of Michigan, Ann Arbor, MI 48109-1040, USA
e-mail: kitsenko.sasha1212@gmail.com

Physical systems often involve multiple characteristic timescales, making their theoretical description challenging [1]. We investigate hybrid quantum-classical systems in which a "fast" quantum system is both resonantly excited by a microwave driving signal and weakly probed by a "slow" classical *RLC* circuit (Fig. 1a). Such driven-probed systems naturally evolve on three distinct timescales: the fastest timescale of the quantum system; the intermediate timescale of Rabi oscillations; and the slowest radio-frequency timescale of classical probing. We study the radio-frequency effective response of such isolated quantum systems — their effective capacitance [2] — using both a phenomenological approach [3] and the recently developed quantum averaging theory (QAT) [1], which, through the use of a renormalization technique, separates different timescales while restoring the total time evolution of the quantum system. We discuss how the effective capacitance can be decomposed into three components: geometric capacitance, corresponding to the classical limit without quantum effects; quantum capacitance, arising from the curvature of the energy levels; and tunneling capacitance, due to population redistribution between quantum states. We also identify the timescales on which these contributions emerge.

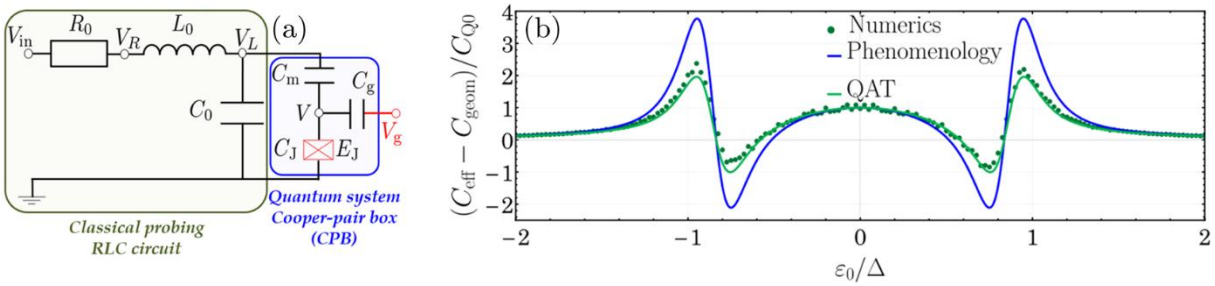

Fig.1 Hybrid quantum-classical system and its rf response. (a) Schematic of a classical probing circuit coupled to a quantum system, illustrated using a Cooper-pair box (CPB) as an example. The gate voltage V_g contains a DC component setting the working bias point ε_0 and an AC component $V_d \cos(\omega_d t)$ that excites the system. (b) Effective capacitance of the CPB in the two-level approximation, in the units of C_{Q0}, the maximum value of the quantum capacitance at $\varepsilon_0 = 0$, shown versus ε_0, comparing numerical solution of the Schrödinger equation, phenomenology, and QAT.

This work was supported by the ARO, ONR, IEEE, JST, NAS, NRFU (Grant No. 2025.07/0044).

[1] K. D. Barajas, W. C. Campbell, Phys. Rev. A 113, 032210 (2026). https://doi.org/10.1103/jjvf-dw3l.
[2] M. F. Gonzalez-Zalba, S. N. Shevchenko, S. Barraud, J. R. Johansson, A. J. Ferguson, F. Nori, and A. C. Betz, Nano Lett. 16, 1614 (2016). https://doi.org/10.1021/acs.nanolett.5b04356.
[3] F. Vigneau, F. Fedele, A. Chatterjee, D. Reilly, F. Kuemmeth, M. F. Gonzalez-Zalba, E. Laird, and N. Ares, Appl. Phys. Rev. 10, 021305 (2023). https://doi.org/10.1063/5.0088229.

Study of structural, mechanical and electronic properties of the 2H-$NbSe_2$ alloy using density functional theory approach

I. S. Bondar[1], V. A. Sirenko[1], K. A. Minakova[2]

[1]B. Verkin Institute for Low Temperature Physics and Engineering of NAS of Ukraine, 47 Nauky Ave., Kharkiv, 61103, Ukraine
[2]National Technical University "Kharkiv Polytechnic Institute", 2 Kyrpychova str., Kharkiv, 61002, Ukraine
e-mail: ibondar@ilt.kharkov.ua

The layered transition metal dichalcogenide 2H-$NbSe_2$ is of considerable interest due to its metallic conductivity, superconducting properties, and potential applications in nanoelectronics [1, 2]. Understanding the relationship between its mechanical and electronic properties is essential for strain-engineered functional materials.

In this work, the structural, mechanical, and electronic properties of 2H-$NbSe_2$ were investigated using density functional theory (DFT) as implemented in the Quantum Espresso package. The exchange–correlation effects were treated within the generalized gradient approximation (GGA). A plane-wave basis set and periodic boundary conditions were employed.

The optimized lattice parameter was found to be a = 3.445 Å, which is in good agreement with available experimental data [1]. The calculated elastic constants (C_{11}, C_{12}, C_{13}, C_{33}, C_{44}) satisfy the mechanical stability criteria for hexagonal crystals. The derived bulk, shear, and Young's moduli indicate moderate stiffness of the material. The Pugh ratio B/G = 1.18 suggests a brittle mechanical behavior under ambient conditions, consistent with the layered nature of the compound.

The effect of small symmetric displacements of Se atoms (±1%) was analyzed. These deformations lead to noticeable changes in the shear modulus and longitudinal stiffness, indicating a pronounced sensitivity of the mechanical response to local atomic distortions.

Electronic structure calculations confirm the metallic nature of 2H-$NbSe_2$. The density of states near the Fermi level is dominated by Nb *d*–states. Variations in the interlayer spacing affect the width and position of the Nb *d*–band near the Fermi level, demonstrating a coupling between mechanical deformation and electronic properties.

The obtained results highlight the interplay between structure, mechanical response, and electronic behavior in 2H-$NbSe_2$. This coupling suggests the possibility of tuning electronic properties by controlled strain, which is of interest for nanoelectronic and strain-engineered applications. The results are consistent with previously reported theoretical and experimental studies of layered transition metal dichalcogenides [1–4].

[1] J. A. Wilson, F. J. Di Salvo, S. Mahajan, Advances in Physics 24, 117 (1975). https://doi.org/10.1080/00018737500101391.
[2] X. Xi, L. Zhao, Z. Wang et al., Nature Nanotech 10, 765 (2015). https://doi.org/10.1038/nnano.2015.143.
[3] D. Wickramaratne, S. Khmelevskyi, D. F. Agterberg, I. I. Mazin, Phys. Rev. X 10, 041003 (2020). https://doi.org/10.1103/PhysRevX.10.041003.
[4] M. S. Dave et al., Next Materials 7, 100361 (2024). https://doi.org/10.1016/j.nxmate.2024.100361.

Spin Hall effect in aluminum and platinum

Yu. N. Chiang (Tszyan), M. O. Dzyuba

B. Verkin Institute for Low Temperature Physics and Engineering of NAS of Ukraine,
47 Nauky Ave., Kharkiv, 61103, Ukraine
e-mail: dzyuba@ilt.kharkov.ua

Spin-orbit interaction (SOI) is the interaction of the effective magnetic field $\boldsymbol{B_i}$, which arises in the rest frame of a moving electron, with its magnetic moment (spin). The Hamiltonian of this interaction, derived from the Dirac equation as a correction of order v^2/c^2 (c- being the speed of light), is relativistic. The effects described by such a relativistic Hamiltonian include the Rashba effect [1] — a phenomenon of spin splitting that arises due to spin-orbit interaction in electronic systems lacking out-of-plane inversion symmetry. The effective magnetic field, arising from the spin-orbit interaction, is determined by the electron momentum $\boldsymbol{p}$ and mass m. It characterizes a typical relativistic effect in a solid, induced by the spin splitting of energy bands at wave vector $\boldsymbol{k}$. If an electron is subject to an electric field **E** that breaks spatial inversion symmetry, the Rashba spin-orbit contribution leads to the lifting of the two-fold spin degeneracy of the energy bands. We consider effects in the conduction bands of aluminum and platinum, where spin-orbit coupling arises from $\boldsymbol{k}\cdot\boldsymbol{p}$ hybridization — specifically between s and p bands (or s and d bands in the case of Pt). According to our estimates, the intrinsic relativistic magnetic field in both metals is estimated to be approximately $\boldsymbol{B_i}\sim10^{-13}$G. In the absence of external magnetic fields and the presence of an electric field **E**, the $\boldsymbol{B_i}$ field mediates the spin Hall effect (SHE), as previously reported [for example, 2]. Furthermore, the estimated value of $\boldsymbol{B_i}$ suggests the possibility of controlling the spin polarization direction and, consequently, the spin currents using external magnetic fields of any magnitude. This is of significant importance for spintronics applications.

In this work, we rigorously justify the procedure for extracting the nanovolt-scale SHE contribution from the total signal U_y measured in an external magnetic field along the z-axis. With a constant current **I** applied along the x-axis, the measured signal is dominated by the conventional Hall effect (CHE), which is several orders of magnitude larger than the SHE component. Building on our previous study [3], we utilize an asymmetric sample geometry to ensure a non-equilibrium spin distribution at the edges, thereby facilitating the manifestation of the spin Hall effect.

We investigated the behavior of the relativistic spin Hall effect (SHE) in Al and Pt paramagnets under both intrinsic and external magnetic fields, providing evidence of spin polarization aligned with the external field. We only considered measurements where the conventional Hall effect (CHE) contribution during current reversal remained perfectly symmetric, with a precision exceeding the magnitude of the measured SHE signal. The obtained SHE values for both metals allow us to determine the actual ratio of the spin-orbit relativistic energy shifts. At $\boldsymbol{Bz}$=200 G, this ratio is estimated to be approximately 120. This pronounced difference in Rashba contributions directly indicates a stronger spin-orbit interaction in Pt compared to Al, resulting from the spin-orbit splitting of different bands: the p-band in Al and the d-band in Pt.

The work was supported by the National Academy of Sciences of Ukraine within the F19-5 project.

[1] Yu. Bychkov and E. I. Rashba, JETP Lett. 39, 78 (1984).
[2] S. O. Valenzuela, M. Tinkham, Nature 442, 176 (2006). https://doi.org/10.1038/nature04937.
[3] Yu. N. Chiang, M. O. Dzyuba, EPL 120, 17001 (2017). https://doi.org/10.1209/0295-5075/120/17001.

Violation of the Wiedemann-Franz law in $Al_{0.5}CoCuCrNiFe$ high entropy alloy and its correlation with thermopower anomaly

V. A. Frolov, N. A. Azarenkov, E. V. Karaseva, A. V. Korniiets, V. I. Sokolenko, V. S. Okovit

National Science Center "Kharkiv Institute of Physics and Technology", Kharkiv, Ukraine
e-mail: vsokol@kipt.kharkiv.ua

A number of low-temperature studies of the $Al_{0.5}CoCuCrNiFe$ high-entropy alloy have focused on the range of ~260-120 K, where its various properties exhibit correlated thermally activated anomalies. Specifically, the dynamic Young's modulus and some mechanical properties change here anomalous, the internal friction and ultrasound absorption have resonances and so on. These same studies also reveal the peculiarities in the absolute thermoelectric power S, indicating however the anomalies other nature, namely in the free charge carrier system. In [1], two peaks of internal friction Q^{-1} associated with the resonances of dislocation threads via a Hasiguti and Bordoni (Seeger) mechanisms. In [2], the S-anomaly is considered as possible result of a change in the ratio between the concentrations of electron-like and hole-like quasiparticles. The correlation of the ultrasonic and thermoelectric anomalies was demonstrated in [3], however their connection remains unclear.

The data presented in this report suggest the influence of the conversion transformation [2] on the temperature dependence of another transfer coefficient. This coefficient is the thermal conductivity χ, which has, in addition to the phonon component, a charge (q) component: $\chi=\chi_q+\chi_{ph}$. The same sample as in [3] was investigated, having the shape of a parallelepiped ~5.7×4×4 mm^3. Such form is far from usual one in measurements of χ. Therefore, a clone [4] of the uniaxial steady-state flow method was used. That makes it possible to determine the temperature dependence of the so-called "scaled" thermal conductivity coefficient χ^*, leaving the value of χ itself out of equation.

It was established that the $\chi^*(T)$-dependence has anomalies in the range of ~260-120 K, the sign of which conforms to the sign of the thermoelectric anomaly in [3] (in agreement with version [2]). One of hypothesis that could combine the "resonance" and "conversion" versions is the assumption of a significant role of lattice distortion due to the nonconformity of its temperature changes. Consequences of these distortions may include distortions of the Brillouin zones and the Fermi surface. On the other hand, the resulting lattice microdeformations should exacerbate the resonance phenomena.

The temperature dependence of the "scaled" Lorentz number $L^*=\chi^*/\sigma^*T$ indicates violations of the Wiedemann-Franz law (WF) of two levels. 1). The well-known one, associated with existence of the $\chi_{ph}(T)$ component, appears in the character itself of the temperature dependence $L^*(T)/L_0=f(T)\neq$const, where $L_0=\pi^2/3(k_B/e)$. 2). A violation of a higher level is recorded as anomaly in the $L^*(T)$ dependence in the range of ~260-120 K.

The research presented was financially supported by the Simons Foundation International Program: PD-Ukraine: President Directed – Ukraine Support Grants, Record ID: SFI-PD-Ukraine-00014584.

[1] Yu. O. Semerenko, V. D. Natsik. Low Temp. Phys., 46, 78, (2020) https://doi.org/10.10.63/10.0000367.
[2] V. N. Voyevodin, V. A. Frolov, E. V. Karaseva, E. S. Savchuk, V. I. Sokolenko, Func. Mat. 28, 683, (2021). https://doi.org/10.1540.
[3] V. A. Frolov, N. A. Azarenkov, E. V. Karaseva, V. S. Klochko, A. V. Korniets, V. I. Sokolenko, V. S. Okovit, A. V. Poida. V Int. Conf. "Cond. Mat. & Low-Temp. Phys.", June 2-6, 2025, Kharkiv, 85.
[4] V. I. Sokolenko, V. A. Frolov, E. S. Savchuk, Problems of Atomic Science and Technology. Series: «Vacuum, Pure metals, Superconductors» 137, 90, (2022). https://doi.org/10.46813/2022-137-90.

Microwave response of MoSi-based superconducting resonator under infrared excitation

O. A. Kalenyuk[1,2], S. I. Futimsky[1,2], A. P. Shapovalov[1,2], O. O. Leha[3], V. Yu. Lyakhno[1,3], O. V. Zraichenko[3]

[1]G. V. Kurdyumov Institute for Metal Physics, NAS of Ukraine, Kyiv, 03142, Ukraine
[2]Kyiv Academic University, Kyiv, 03142, Ukraine
[3]B. Verkin Institute for Low Temperature Physics and Engineering of the National Academy of Sciences of Ukraine, Kharkiv, 61103, Ukraine
e-mail: futimskysi@gmail.com

One of the most promising types of infrared (IR) radiation detectors for applications such as astronomy are Microwave Kinetic Inductance Detectors (MKIDs), whose operating principle is based on the change in kinetic inductance of a superconductor under irradiation. These detectors typically operate at millikelvin temperatures. However, for a wide range of applications, including security and medical diagnostics, it is essential to investigate the response of such detectors under conditions of significant background noise and at relatively elevated temperatures. For these purposes, thin films of the amorphous superconductor MoSi are considered particularly promising. Due to their high normal-state resistivity, MoSi films introduce an additional bolometric contribution to the detection mechanism. Figure (a) shows the topology of a fractal microstrip resonator fabricated from a 50 nm thick $Mo_{83}Si_{17}$ film. The resonator was irradiated with short 50 ms IR pulses emitted by an incandescent filament with different peak temperatures T_{pulse} (experimental details are provided in [1]). As a result of pulse absorption, the concentration of superconducting charge carriers changed, leading to variations in the resonance frequency and the quality factor of the resonator. Measurements performed at a fixed initial resonance frequency revealed an increase in insertion loss (IL) upon the arrival of the IR pulse (Fig. (b)). Since the power of the IR radiation depends on the temperature of the incandescent filament, the time response of the resonator $IL(t)$ to the IR pulses was synchronized with the temporal evolution of the filament temperature. This behavior indicates a fast response of the detector to incident IR radiation.

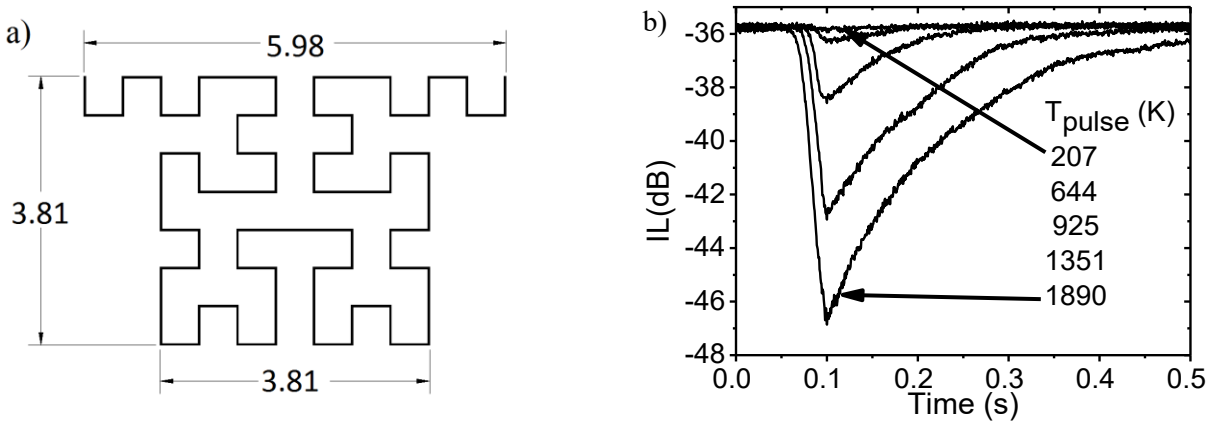

This work was supported by the NAS of Ukraine through the research program No. 0125U000295 (G. V. Kurdyumov Institute for Metal Physics). O.L., V.L., and O.Z. acknowledge support from the IEEE "Magnetism for Ukraine 2025-2026" program, project No. 9918.

[1] O. A. Kalenyuk, S. I. Futimsky, I. A. Martynenko, A. P. Shapovalov, O. O. Boliasova, V. I. Shnyrkov, A. L. Kasatkin, and A. A. Kordyuk, J. Appl. Phys. 139, 073905 (2026). https://doi.org/10.1063/5.0314771.

Deviations from variable-range hopping transport in LSCO

E. Beliayev[1], I. Mirzoiev[1], V. Horielyi[1], A. Terekhov[1], V. Andrievskii[1], I. Chichibaba[2]

[1]B. Verkin Institute for Low Temperature Physics and Engineering of NAS of Ukraine, 47 Nauky Ave., Kharkiv, 61103, Ukraine
[2]National Technical University "Kharkiv Polytechnic Institute", 2 Kyrpychova str., Kharkiv, Ukraine
e-mail: beliayev@ilt.kharkov.ua

The evolution of charge transport in lightly doped cuprate superconductors is strongly influenced by disorder, electronic inhomogeneity, and magnetic correlations. In $La_{2-x}Sr_xCuO_{4+\delta}$ (LSCO) the very low doping regime ($p \lesssim 0.02$), well below the superconducting threshold, represents a strongly localized electronic state where conventional metallic transport is absent and conduction proceeds via hopping processes. Understanding how this localized regime breaks down is important for clarifying the early stages of the insulator-superconductor transition.

Figure 1 shows that the temperature dependence of resistivity of LSCO with very low Sr concentrations (x = 0.001 and x = 0.01) follows the three-dimensional Mott variable-range hopping (VRH) law over an intermediate temperature range [1]. The figure also shows that transport becomes strongly nonlinear at low temperatures and high bias currents, and current-voltage measurements reveal pronounced nonequilibrium phenomena including negative differential resistance (NDR). These effects are attributed to percolative hopping transport combined with current-induced carrier overheating in a strongly disordered antiferromagnetic matrix. The most important feature of the data is the systematic deviation from the VRH dependence at low temperatures and under elevated bias currents [2]. These deviations manifest themselves as a downward curvature in the VRH plots and a strong reduction of resistivity relative to the linear VRH extrapolation. Such behavior points to the onset of nonequilibrium transport processes in a highly inhomogeneous electronic medium. Possible mechanisms include electric-field-assisted hopping, current-induced modification of the percolative conduction network, or local heating effects in strongly localized regions. In cuprates with nanoscale electronic inhomogeneity, such nonlinear transport phenomena may also reflect the formation of conductive filaments or weakly connected clusters within the insulating matrix.

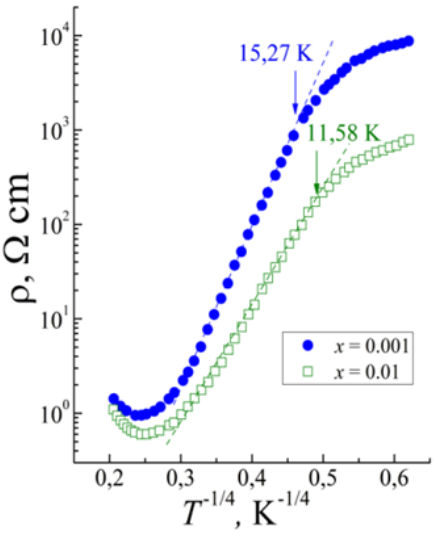

Fig. 1. Temperature dependence of the resistivity ρ(T) for lightly Sr-doped $La_{2-x}Sr_xCuO_4$ samples with x = 0.001 and x = 0.01.

These results demonstrate that lightly doped LSCO should not be viewed as a simple VRH insulator. Instead, the VRH regime represents only an intermediate transport behavior, while deviations from the Mott law reveal the emergence of nonlinear and nonequilibrium conduction processes characteristic of strongly disordered correlated systems. Understanding these deviations provides important insight into the role of disorder and electronic granularity in the early stages of doping in high-T_c cuprates.

[1] H. Takagi, B. Batlogg, H.L. Kao, J. Kwo, R.J. Cava, J.J. Krajewski, W.F. Peck, Phys. Rev. Lett. 69, 2975 (1992). https://doi.org/10.1103/PhysRevLett.69.2975.
[2] N. V. Dalakova, B.I. Belevtsev, E.Y. Belyaev, A.S. Panfilov, N.P. Bobrysheva, A.A. Selyutin, Low Temp. Phys. 40, 397 (2014). https://doi.org/10.1063/1.4881175.

Quantum-mechanical analysis of electron transport in a cylindrical crossed-field vacuum diode with a periodic boundary potential

D. V. Kadygrob

O. Ya. Usikov Institute for Radiophysics and Electronics of NAS of Ukraine,
12, Akademika Proskury street, Kharkiv, 61085, Ukraine
e-mail: dimakadygrob@gmail.com

This work presents a fully quantum-mechanical theoretical framework for describing electron dynamics and emission processes in a cylindrical vacuum diode operating in orthogonal static electric and magnetic fields, subject to a spatially periodic boundary potential. While classical models of such crossed-field devices typically rely on single-particle trajectory tracing or fluid approximations, a rigorous quantum description becomes essential when exploring nanoscale device scaling, or the fine energy structure of the confined electron cloud.

We analyze the behavior of an electron gas in crossed inhomogeneous radial electric and axial magnetic fields. By solving the Schrödinger equation with the corresponding gauge potentials in cylindrical coordinates, we determine the quantized energy spectrum and the spatial distribution of the electron wave functions [1]. A key focus is placed on the influence of an azimuthal periodic potential at the anode boundary, which fundamentally modifies the quantum states of the system.

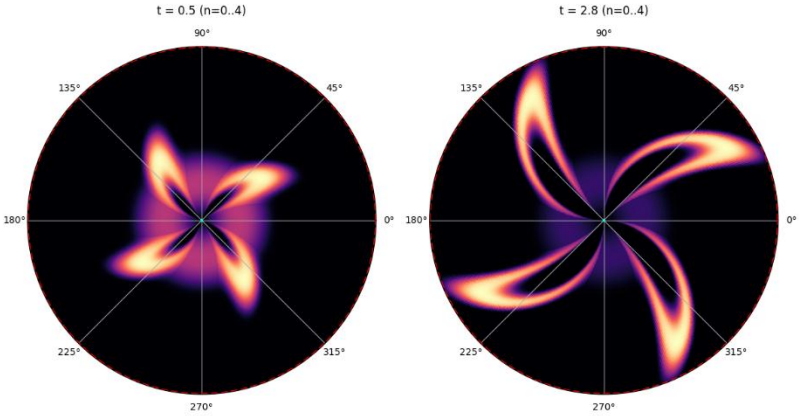

Fig.1. Space charge distribution for different moments of time

Our model demonstrates the quantization of azimuthal momentum and evaluates the conditions for resonant interaction between the confined electron space-charge and the periodic potential structure (see Fig. 1). We introduce a quantum perturbation approach to describe the phase-locking mechanism and the energy transfer dynamics governed by the spatial periodicity.

The results indicate that quantum tunneling and the discrete nature of the energy levels significantly modify the space-charge distribution compared to the classical Brillouin flow model. These quantum corrections provide a deeper understanding of crossed-field devices.

[1] L. D. Landau and E. M. Lifshitz, Quantum Mechanics: Non-Relativistic Theory (Pergamon Press, Oxford 1977).

Distinguishing transport characteristics of ferromagnetic metal–magnetic quantum dot–superconductor (F-mQD-SC) nanoscale structures

E. A. Koshina, V. N. Krivoruchko

O.O. Galkin Donetsk Institute for Physics and Engineering of NAS of Ukraine,
46 Nauky Ave., Kyiv, 03028, Ukraine
e-mail: elena.koshina1@gmail.com

Spin-dependent resonant tunneling through a quantum dot (QD), a small system characterized by discrete electronic states and coupled with a ferromagnetic normal metal (F) and an s-wave superconductor (S), in the F-QD-S system, has been a subject of significant experimental and theoretical interest. Beyond their fundamental importance, such hybrid meso-nanostructured systems offer potential applications in future electronic devices that exploit both the charge and spin degrees of freedom of electrons. This motivated us to investigate nonequilibrium electron tunneling through a ferromagnetic normal metal–magnetic quantum dot–s-wave superconductor (F-mQD-SC) Ref. [1]. Unlike Ref. [2], where the QD's discrete levels were spin-independent, we assumed that the QD has spin-split discrete levels (magnetic QD, mQD), with this splitting controllable by an external magnetic field. Special attention was given to analyzing how the spin splitting of the electron levels in the dot affects the tunneling process and the system's conductance properties. Using the Keldysh nonequilibrium Green's function method, we derived and analyzed expressions for the tunneling current, I, and the probability of Andreev reflection (AR) versus energy, $T_A(\omega)$, for the F-mQD-S structure. It was demonstrated that, in contrast to a system with a non-magnetic QD, $T_A(\omega)$ exhibits a series of additional peaks caused by the splitting of the mQD levels by an effective (external and proximity-induced) magnetic field.

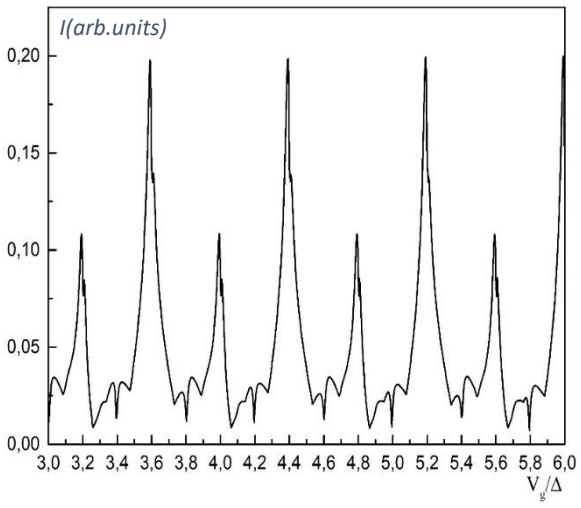

FIG.1. The current I *vs* the gate voltage v_g for $V>\Delta$. The mQD has ten states with equal level spacing $\Delta\epsilon = 0.8\Delta$, $\epsilon_0{}^0 = 0$, when the bias voltage $V=1.05\Delta$, F-lead current spin polarization is fixed $P=0.1$, the Zeeman energy $E_{Ze} = 0.1\Delta$ (1), the linewidths $\Gamma_{F0} = \Gamma_S = 0.02$.

In this work, we discuss the distinguishing transport characteristics of an F-mQD-SC nanoscale structure in a non-topological state. We investigate the behavior of Andreev, quasiparticle, and total currents. We found that resonant curves for tunnel current versus gate voltage of mQD have different kinds of peaks (see Fig. 1), depending on (i) the value of external magnetic field and spin-splitting under the effect of the Zeeman energy, (ii) bias voltage, (iii) F-lead current spin polarization, (iv) the F-lead linewidth, and (v) the level of mQD spacing. Also, the current I vs bias voltage V behavior at different values of external magnetic field, gate voltage, F-lead current spin polarization, the F-lead linewidth, and the level of mQD spacing was studied. The results open a way for exploring such systems in tunable spintronic devices.

[1] V. N. Krivoruchko and E. A. Koshina. Low Temp. Phys. 49, 1015 (2023). https://doi.org/10.1063/10.0020593.
[2] Q.-F. Sun, J. Wang, T. H. Lin, Phys. Rev. B 59, 3831 (1999). https://doi.org/10.1103/PhysRevB.59.3831.

Features of determining the superconducting properties of single-crystal FeSe using EPR-spectrometer

S. I. Bondarenko[1], A. A. Prokhorov[2], N. N. Galtsov[1], V. P. Timofeev[1], V. P. Koverya[1], A. V. Krevsun[1]

[1]B. Verkin Institute for Low Temperature Physics and Engineering of NAS of Ukraine, 47 Nauky Ave., Kharkiv, 61103, Ukraine
[2]Institute of Physics of the Czech Academy of Sciences, 18221, Prague, Czech Republic
e-mail: koverya@ilt.kharkov.ua

Iron-based superconductors (IBSCs) are "unconventional" and promising high-temperature superconductors (HTSCs). Their critical temperatures (T_c) at normal pressure approach the boiling point of liquid nitrogen, which will stimulate the development and widespread use of IBSC devices. FeSe and FeTeSe compounds have been actively studied since 2008, however, many details regarding the mechanism of superconductivity development and its dynamics remain unclear. Non-contact magnetometric studies of single-crystal FeTeSe, including those using EPR spectroscopy, have demonstrated the potential of doping with hydrogen from the gas phase to increase the critical current density (J_c) in it by more than an order of magnitude [1]. We continued this study in the related compound FeSe, which has the simplest quasi-two-dimensional crystalline structure among IBSCs. Using a Bruker E580 EPR- spectrometer, we studied the dependences of the spectrometer signal in undoped FeSe ($T_c \approx 8$K) on temperature ($3.5 < T < 25$ K) in steady magnetic fields (in the range of 0–6000 Oe). The most interesting picture was observed for the non-resonant spectrometer signals in low magnetic fields (LFMA) ($0 < H < 30$ Oe) and at temperatures in the region of the superconducting phase transition (Fig.1). The observed pattern of nonresonant LFMA signals is caused by the

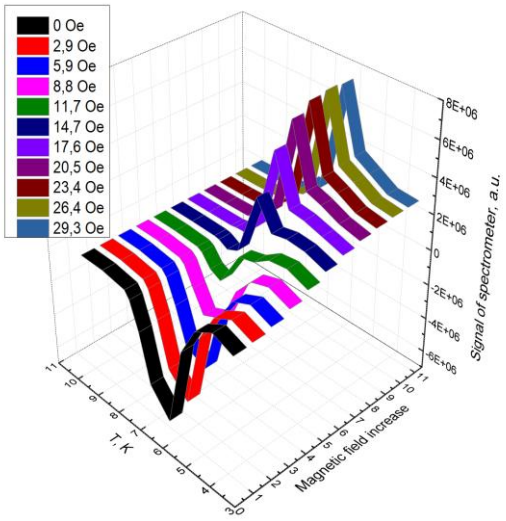

Fig.1. Temperature dependences of the spectrometer output signal in magnetic fields of 0 – 29.3 Oe.

application of a weak constant magnetic field and the influence of a microwave (MW) field. The dependences in Figure 1 allow us to determine the width of the superconducting transition ($\delta T \approx 3$K) and the first critical magnetic field of FeSe at the transition ($H_{c1} \approx 12$ Oe). In this magnetic field, the spectrometer signal changes from negative to positive, indicating the formation of Abrikosov vortices in the crystal and the absorption of MW radiation within it. This work was partially supported by grant of the IEEE Magnetic Society (project No. 9918) and National Research Foundation of Ukraine (Grant No. 2025.07/0044).

[1] S.I. Bondarenko, A.I. Prokhvatilov, R. Puzniak, J. Pietosa, A.A. Prokhorov, V.V. Meleshko, V.P. Timofeev, V.P. Koverya, D.J. Gawryluk, A. Wisniewski, Materials 14, 7900 (2021). https://doi.org/10.3390/ma14247900.

Structure and properties of the boundary between graphene-like and Lieb lattices

I. V. Kozlov, Yu. A. Kolesnichenko

B. Verkin Institute for Low Temperature Physics and Engineering of NAS of Ukraine,
47 Nauky Ave., Kharkiv, 61103, Ukraine
e-mail: kozlov@ilt.kharkov.ua

The boundary between two topological conductors can be characterized by a number of properties that arise due to the irremovable difference in the topological characteristics of the two media, and are therefore resistant to external influences. The boundary between graphene-like and Lieb lattices is a system of this kind. Both lattices are characterized by a linear electron energy spectrum, but differ in the Berry phase, which is absent in the Lieb lattice. As was shown previously for a simple model [1], specific local edge states arise in such a system, and the transmission coefficient is independent of the magnitude of the wave vector $|\mathbf{k}|$ or the energy E, retaining only the angular dependence. In this way, the effective barrier cannot be characterized by any dimensional parameters such as width or potential energy, which emphasizes its topological nature. Naturally, a number of properties characteristic of topological materials are sensitive to the structure of the boundary between topological conductors. For example, supertunneling is not realized within the model [1], which is a consequence of the limitations of the model used. However, in another related system with a changing Berry phase [2], supertunneling occurs even with a relatively simple structure of the boundary. Thus, it is important to distinguish between constraints imposed by the model used and unavoidable general constraints, such as the "no-go" theorem [3].

In the present research, the influence of the boundary structure between graphene-like and Lieb lattices on tunneling and effective boundary conditions is investigated. Different boundary configurations between two lattices are considered under the tight-binding approximation and under the condition of maximum similarity of the conical energy spectrum of charge carriers in both conductors in the choice of model parameters. The transmission coefficient in the absence of an external magnetic field is calculated. A matrix of effective boundary conditions is obtained that relates the electron wave function on both sides of the boundary and is necessary for the analytical description of edge states in a quantizing magnetic field. The research was carried out within the fundamental scientific program No. 0122U001501, NAS Ukraine.

[1] I. V. Kozlov, Yu. A. Kolesnichenko, arXiv:2507.17612 (2025). http://dx.doi.org/10.48550/arXiv.2507.17612.
[2] L. Mandhour, F. Bouhadida, F. Piéchon, Phys. Rev. B 112, 155402 (2025). https://doi.org/10.1103/9gt4-3pwl.
[3] H. B. Nielsen, M. Ninomiya, Phys. Lett. 105B, 219 (1981). https://doi.org 10.1016/0370-2693(81)91026-1.

Dissipative Landau-Zener-Stückelberg-Majorana gates

B. A. Kushnarov[1,2], A. I. Ryzhov[2], O. V. Ivakhnenko[2,3], S. N. Shevchenko[2,4]

[1]V.N. Karazin Kharkiv National University, 4 Svobody Sq., Kharkiv, 61022, Ukraine
[2]B. Verkin Institute for Low Temperature Physics and Engineering of NAS of Ukraine, 47 Nauky Ave., Kharkiv, 61103, Ukraine
[3]Center for Quantum Computing, RIKEN, Wako, Saitama, 351-0198, Japan
[4]Department of Mathematics, Kyiv School of Economics, Kyiv, 03113, Ukraine
e-mail: kushnaryov2021tya11@student.karazin.ua

Achieving high-precision quantum computing requires a variety of approaches, ranging from selecting the optimal physical form for the qubit to developing advanced error-correction methods. We are exploring a method for controlling the qubit state using non-adiabatic transitions, known as the Landau-Zener-Stückelberg-Majorana (LZSM) transitions. Experimental studies show that such gates allow implementing extremely fast operations [1] and also demonstrate sufficient robustness to low-frequency noise [2]. This method overcomes most of the drawbacks, such as the strict driving frequency limitations and the strong correlation between accuracy and speed, associated with commonly used Rabi oscillations-based gates. Numerical simulation results, shown in Fig. 1, also confirm the shorter duration and lower error rates of LZSM-based gates compared to Rabi oscillations-based gates (*cf.* difference between the Bloch vector components Z and Z_r). A method for finding the control parameters of a system for implementing a desired quantum gate is proposed in Ref. [3]. However, only ideal (isolated) qubits were considered in that study. We consider the LZSM transitions of real systems taking decoherence into account, analyze the resulting distribution of errors and look for ways to minimize them.

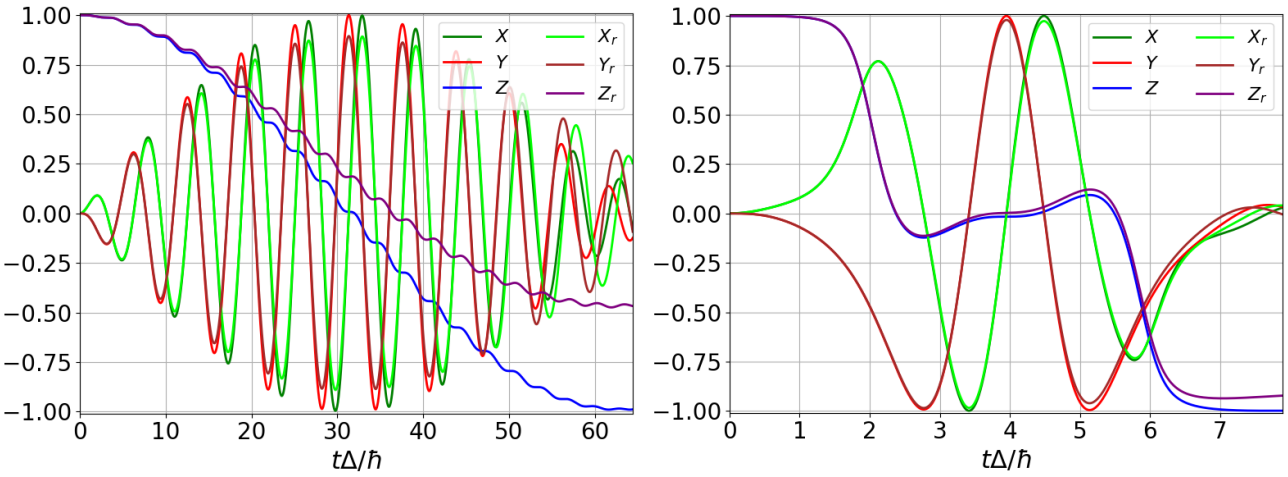

Fig.1 Dynamics in ideal (no relaxation; the components of the Bloch vector X, Y, Z) and real (with relaxation; the components of the Bloch vector $X_\mathrm{r}, Y_\mathrm{r}, Z_\mathrm{r}$) systems with $\frac{\Delta}{\hbar} T_{1,2} = 100$ for Rabi-based (left panel) and LZSM-based (right panel) X-gate.

This work was supported by grant of the IEEE Magnetic Society (project No.9918) and National Research Foundation of Ukraine (Grant No.2025.07/0044).

[1] Helin Zhang *et al.*, Phys. Rev. X 11, 011010 (2021). https://doi.org/10.1103/PhysRevX.11.011010.
[2] D. L. Campbell *et al.*, Phys. Rev. X 10, 041051 (2020). https://doi.org/10.1103/PhysRevX.10.041051.
[3] A. I. Ryzhov, O. V. Ivakhnenko, S. N. Shevchenko, M. F. Gonzalez-Zalba, Franco Nori, Phys. Rev. Research 6, 033340 (2024). https://doi.org/10.1103/PhysRevResearch.6.033340.

Point-contact exploration of the superconducting state in Te-doped $PtBi_2$

O. E. Kvitnitskaya[1,2], S. Ash[2], Yu. G. Naidyuk[1], B. Büchner[2,3]

[1]B. Verkin Institute for Low Temperature Physics and Engineering of NAS of Ukraine, 47 Nauky Ave., Kharkiv, 61103, Ukraine
[2]Leibniz Institute for Solid State and Materials Research, IFW Dresden, Dresden, Germany
[3]Würzburg-Dresden Cluster of Excellence ct.qmat, Dresden, Germany
e-mail: kvitnitskaya@yahoo.com

γ-$PtBi_2$ is a Weyl semimetal, exhibiting superconductivity with critical temperature $T_c \approx 0.6$–1.1 K [1,2]. Notably, surface-sensitive spectroscopic measurements [3,4] reveal an enhanced T_c, suggesting the realization of unconventional surface superconductivity. Bulk superconductivity with a much higher $T_c \approx 2.4$ K [5] was discovered in the partially tellurium-substituted compound $PtBi_{2-x}Te_x$.

We measured two types of Te-substituted $PtBi_2$ compounds with 2 and 10% of Te applying point-contact (PC) technique. For all PCs, differential resistance dV/dI showed typical zero-bias minimum due to the superconducting transition (Fig.1a,b). The average T_c for the all measured $PtBi_{1.96}Te_{0.04}$ PCs amounted to 3.1K, which exceeds the T_c value in the bulk. The reason for the increase in T_c may be the influence of pressure during the creation of PCs. PC studies of the doped compound $PtBi_{1.8}Te_{0.2}$ with a higher Te content showed almost no increase of T_c compared to the bulk (Fig.1d). Another reason for the enhanced T_c could be compositional variations in $PtBi_{1.96}Te_{0.04}$ system and the presence in the PC of some areas with stoichiometry close to pure $PtBi_2$, which, as measured [4], possesses surface superconductivity with increased T_c.

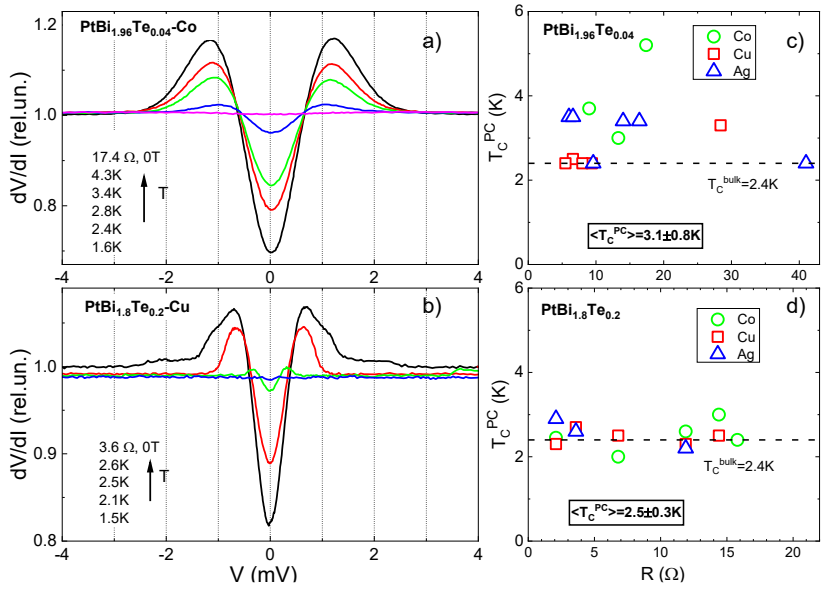

Fig.1. Temperature variation of dV/dI of $PtBi_{1.96}Te_{0.04}$- Co (a) and $PtBi_{1.8}Te_{0.2}$- Cu (b) PCs. T_c distribution for all $PtBi_{1.96}Te_{0.04}$ PCs (c) and $PtBi_{1.8}Te_{0.2}$ (d) PCs with normal (Ag, Cu) and ferromagnetic Co metal counterelectrodes.

[1] G. Shipunov *et al,* Phys. Rev. Mat. 4, 124202 (2020). https://doi.org/10.1103/PhysRevMaterials.4.124202.
[2] J. Zabala *et al*, Journal of Physics: Condensed Matter 36, 285701 (2024). https://doi.org/10.1088/1361-648X/ad3878.
[3] A. Kuibarov *et al,* Nature 626, 294 (2024). https://doi.org/10.1038/s41586-023-06977-7.
[4] D. Bashlakov *et al,* Low Temp. Phys. 48, 747 (2022). https://doi.org/10.1063/10.0014014.

Manifestation of the superconducting proximity effect in superconductor–magnet contacts

I. Martynenko[1,2], O. Kalenyuk[1,2], V. Tarenkov[1,3], A. Shapovalov[1,2]

[1]G.V. Kurdyumov Institute for Metal Physics, NAS of Ukraine, 03142, Kyiv, Ukraine
[2]Kyiv Academic University, 03142, Kyiv, Ukraine
[3]O.O. Galkin Donetsk Institute for Physics and Engineering, NAS of Ukraine, 03028, Kyiv, Ukraine
e-mail: i.martynenko@kau.edu.ua

The current–voltage characteristics and the corresponding differential conductance were investigated for MoRe–Ni (S–M) contacts exhibiting Andreev-type charge transport. The analysis of the conductance curves allows the observed behavior to be interpreted in terms of the induced superconducting proximity effect in the magnetic material, nickel.

It is known that the spin polarization of charge carriers in nickel is approximately $P \approx 30\%$. This polarization manifests itself in the conductance spectra as a suppression near zero bias voltage. The suppression is associated with spin-polarized carriers in nickel that cannot form Cooper pairs in the superconductor because the transport current lacks electrons with opposite spin projections required for electron–hole conversion via Andreev reflection. As a result, the current through the contact is partially blocked, leading to a reduction of conductance in the vicinity of zero bias. In the limiting case of 100% spin polarization, the current through the contact would be completely suppressed up to bias voltages exceeding the superconducting energy gap of the superconductor. Additional features are observed in the conductance spectra at a bias voltage of V=0.82 mV (Fig.1). These features may be associated with the manifestation of a superconducting energy gap induced in the magnetic material as a result of the proximity effect at the MoRe–Ni interface. The superconducting proximity effect at the MoRe–Ni interface leads to modifications of the density of states in the ferromagnet.

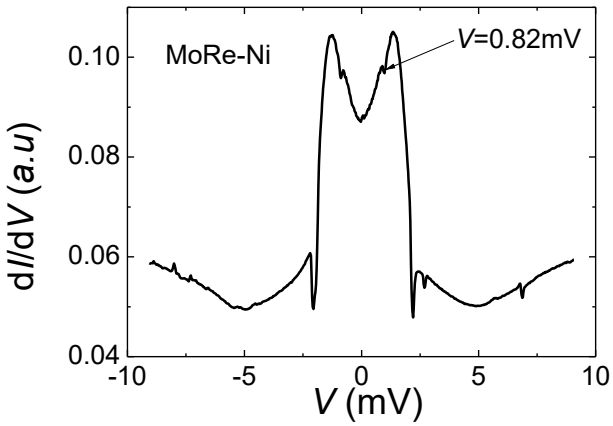

Fig. 1. Differential conductance dI/dV of the MoRe–Ni contact.

This work was supported by the National Academy of Sciences of Ukraine under research program No. 0125U000295 (G. V. Kurdyumov Institute for Metal Physics). I. Martynenko acknowledges support from the German Federal Ministry of Research, Technology and Space (BMFTR) through the GU-QuMat project (01DK24008).

[1] I. Martynenko, O Kalenyuk, A Shapovalov, H Kondakova, V Shamaev, O. Boliasova, O. Zhitlukhina, Metallofizika i Novejsie Tehnologii 45, 1141 (2023). https://doi.org/10.15407/mfint.45.10.1141.

The influence of hysteresis absorption locality in a microwave nonlinear HTS transmission line on its properties

S. I. Melnyk, S. S. Melnyk, N. T. Cherpak, A. A. Lavrinovich

O.Ya. Usikov Institute for Radiophysics and Electronics of NAS of Ukraine,
12, Ac. Proskury st., Kharkiv, 61085, Ukraine
e-mail: melnyksergiy72@gmail.com

In an experimental study of the properties of a microwave (MW) coplanar waveguide transmission line (TL) based on high-temperature superconductors (HTS) at specific values of input power Pin and direct current (DC) Idc, the effect of strong (tens of dBs) and abrupt changes in MW losses was observed at a certain waveguide temperature $T < T$c, where Tc is the critical temperature [1]. In this paper, we analyze the specifics of modeling and calculating losses in such a line. When calculating power losses for a nonlinear waveguide line based on HTS in a MW field, a standard electrical engineering approach is typically used: determining the area of the hysteresis loop arising in the waveguide cross-section when calculating the magnetization curve within the Bean model [2]. It turns out that taking into account the dependence of the critical current density on the magnetic field strength leads to significant distortions of the magnetization curve shape [3]. Furthermore, neglecting the fact that both the hysteresis loop shape and its initial phase are local—depending on the distance to the strip center—can lead to significant errors in describing the response dynamics and calculating losses. Therefore, previously [4], when calculating the Q-factor of such a line, we proposed first using a local calculation of the magnetization curve and then integrating the resulting power loss density values over the width of the waveguide TL.

Furthermore, local energy absorption leads to local heat generation in the waveguide cross-section, which is compensated primarily by heat dissipation into the dielectric substrate (for example, single-crystal MgO) via the phonon heat transfer mechanism. For such systems, the classical Fourier heat transfer equation is inapplicable due to ballistic heat transfer and boundary scattering effects. Therefore, the Boltzmann transfer equation (BTE) or modified equations are used to analyze heat transfer [5].

In general, locally dependent heat generation with a high-frequency time component and nanoscale heat transfer effects necessitate taking into account heat transfer between different sections of a waveguide line when analyzing the dynamics of the vortex structure and calculating the associated losses. To address this problem, we proposed a phenomenological model and investigated some of its properties. It is shown that both of these effects can have a significant impact on the results of calculating MW absorption of the microwave field by a waveguide TL and must be taken into account in the calculations.

[1] N. T. Cherpak, A. I Gubin, A. A. Lavrinovich, S. A. Vitusevich, IEEE Trans. on Appl. Supercond. 26, 1501204 (2016). https://doi.org/10.1109/TASC.2016.2537138.
[2] E. H. Brandt, arXiv:1008.2231 (2010). https://doi.org/10.48550/arXiv.1008.2231.
[3] E. H. Brandt, Physical Review B 55, 14513 (1997). https://doi.org/10.1103/PhysRevB.55.14513.
[4] S. I. Melnyk, Analysis of the influence of vortex dynamics on the possibility of an avalanche-like transition of a microwave nonlinear HTS transmission line into a dissipative state, https://www.ilt.kharkov.ua/cmltp2025/doc/Book_of_Abstracts_2025.pdf.
[5] E. V. Bezugly, A. V. Voychuk, Low Temperature Physics 22, 542 (1996). https://doi.org/10.1063/10.0034047.

Phenomenological model of the influence of Majorana states in the vortex structure of a nonconventional superconductor film on the microwave absorption features

S. I. Melnyk, S. S. Melnyk, N. T. Cherpak

O.Ya. Usikov Institute for Radiophysics and Electronics of NAS of Ukraine,
12, Ac. Proskury st., Kharkiv, 61085, Ukraine
e-mail: melnyksergiy72@gmail.com

In [1], an anomalous temperature dependence of losses was observed in a thin-film disk of nonconventional superconductor (SC) FeSe1-xTex when placed in a microwave field (MW) orthogonal to the disk, near the critical temperature. However, similar experiments with other types of SCs or with a magnetic field orientation parallel to the disk did not reveal this effect. In this connection, a hypothesis was put forward linking this effect to the emergence of 0-th Majorana modes, previously detected by other methods in this type of SC [2]. The aim of this study is to develop a phenomenological model of this effect based on general quantum mechanical concepts of the properties of entangled vortices forming a Majorana pair.

We previously demonstrated [3] that the energy dissipation mechanism in an SC thin disk exposed to a magnetic field perpendicular to the film can be described as a consequence of vortex reorientation within the framework of Bean's model. However, when -Majorana zero modes (MZM) arise, entangled quantum states arise, both between pairs of spatially separated vortices and between vortices and surface current states [4]. Such a quantum entanglement leads to a transition to another quantum state occurring in a coordinated manner for each Majorana pair of the current states. As a result, the fundamental approximation of Bean's model - the absence of changes in vortex structure in regions of subcritical surface current values, may be violated. In general, due to the entangled behavior of vortices, the probability of their joint transition to a new quantum state is determined by a pair of local surface current density values at their locations.

To account for this possibility, we proposed a phenomenological model that generalizes Bean's model by introducing a mechanism for nonlocal interaction of the vortex structure. Mathematically, this manifests itself in the fact that in Bean's model, instead of local values of surface current density and vortex density, their integrally weighted average values should be used. In this case, we use a Gaussian integral transform kernel with a variable half-width parameter.

The simulated effect of the nonlocal influence of surface current density on the dynamics of the vortex structure allows us to qualitatively explain the anomalies in the experimentally obtained temperature dependence of the MW loss. And comparing it with the results of numerical simulations allows us to estimate the values of the phenomenological parameters used in it: the characteristic half-width of the distribution of nonlocal couplings and the proportion of Majorana pairs in the total number of formed vortices.

[1] Y. Wu, A. A. Barannik, L. Sun, Y.-S. He, N. T. Cherpak, The unusual microwave response of chalcogenide $FeSe_{1-x}Te_x$ film compared to other superconductors, Condensed Matter & Low Temperature Physics: II Intern. Advanced Study Conference. June 6-12, 2021.
[2] N.T. Cherpak, A.A. Barannik, Y.-S. He, L. Sun, Y. Wu, S.I. Melnyk, arXiv:2312.11155 [cond-mat.supr-con] (2023). https://doi.org/10.48550/arXiv.2312.11155
[3] S. I. Melnyk, N. T. Cherpak, Features of vortex dynamics in the description of microwave absorption by a thin HTSC disk.
https://www.ilt.kharkov.ua/cmltp2025/doc/Book_of_Abstracts_2025.pdf
[4] M. Mandal, N.C. Drucker, P. Siriviboon, T. Nguyen, A. Boonkird, T. N. Lamichhane, M. Li, Chemistry of Materials 35, 6184 (2023). https://doi.org/10.1021/acs.chemmater.3c00713.

Hydrostatic pressure effect on the pseudogap in slightly doped $Y_{0.66}Pr_{0.34}Ba_2Cu_3O_{7-\delta}$ single crystals

Ye. V. Petrenko[1,2,3,4], L. V. Bludova[1], A. S. Kolisnyk[1], M. V. Shytov[1], A. Sedda[5], E. Lähderanta[5], R. V. Vovk[4], A. L. Solovjov[1,5,6]

[1]B. Verkin Institute for Low Temperature Physics and Engineering of NAS of Ukraine, 47 Nauky Ave., Kharkiv, 61103, Ukraine
[2]Centre of Low Temperature Physics, Institute of Experimental Physics, Slovak Academy of Sciences, Watsonova 47, 04001 Košice, Slovakia
[3]Centre of Low Temperature Physics, Faculty of Science, P. J. Šafárik University, Park Angelinum 9, 04001 Košice, Slovakia
[4]Physics Department, V. N. Karazin Kharkiv National University, Kharkiv 61022, Ukraine
[5]Department of Physics, LUT University, Lappeenranta 53850, Finland
[6]Institute of Low Temperatures and Structure Research, of PAS, Wroclaw 50-422, Poland
e-mail: petrenko@ilt.kharkov.ua

The pseudogap (PG) state, which is opened in cuprate high-temperature superconductors (HTSCs) below the characteristic temperature $T^* >> T_c$, is one of the most mysterious and simultaneously interesting phenomena in modern solid state physics [1]. It is well established that in HTSCs, the PG is observed when the charge carrier concentration, p, varies between slightly doped (SD) and optimally doped (OD) levels. Understanding the PG physics would definitely shed more light on the mechanism of superconducting pairing in HTSCs, which is also not fully clarified yet. Knowledge of this mechanism is of primary importance for the search for superconductors with an even higher, preferably room temperature of superconducting (SC) transition T_c. The temperature dependence of the resistivity of HTSC in the normal state above T^* is always linear. However, it deviates unexpectedly downwards from linearity at $T \leq T^*$ [1]. It has been convincingly shown that at $T = T^*$ not only does $\rho(T)$ deviate from linearity, but the density of states at the Fermi level (DOS) also begins to decrease noticeably, which is just called a pseudogap (PG) [1]. Perhaps, this is the only experimental result with which the entire superconducting community agrees. In our work, for the first time, we carried out the analysis of the influence of hydrostatic pressure up to 0.97 GPa on the temperature dependence of pseudogap $\Delta^*(T)$ of the SD $Y_{0.66}Pr_{0.34}Ba_2Cu_3O_{7-\delta}$ single crystals It is shown that the pressure effect on T_c and resistivity $\rho(T)$ is different. Under pressure $\rho(T)$ decreases linearly at a rate $d\ln\rho(100K)/dP = -14\%GPa^{-1}$, while T_c increases at a rate $dT_c/dP = +2.88\ KGPa^{-1}$, which is associated with the redistribution of charge carriers in the CuO_2 planes. Near T_c, independently on pressure, $\sigma'(T)$ is well described by the Aslamasov–Larkin and Hikami–Larkin fluctuation theories, demonstratinga 3D–2D crossover with increase of temperature [1]. The crossover temperature T_0 determines the coherence length along the c-axis $\xi_c(0) \simeq (3.36 \pm 0.01)$Å at P=0, which decreases to (3.05±0.01)Å, at P = 0.97 GPa. At the same time, $\Delta^*(T_G)$ increases with increasing hydrostatic pressure at a rate $d\ln\Delta^*(T_G)/dP = 0.10\ GPa^{-1}$, implying an increase of the coupling strength with increasing P, whereas the BCS ratio $2\Delta^*(T_G)/k_BT_c = 5$ remains constant. The dependence $\Delta^*(T)$ shows a narrow maximum at high temperatures, which is typical for magnetic superconductors [2] and is due to the presence of magnetic inclusions PrBCO in the sample. Note that the slope of the dependence $\Delta^*(T)$ below T_{pair} increases with increasing pressure and at P = 0.97 GPa coincides with the slope in the Fe-As base pnictide $SmFeAsO_{0.85}$ [2]. By analogy, it is assumed that below $T_{SDW} < T_{pair}$, the spin density wave regime is realized in the sample.

[1] A. L. Solovjov, K. Rogacki, Low Temp. Phys. 49, 345 (2023). https://doi.org/10.1063/10.0017238 (2023).
[2] A. L. Solovjov, L. V. Omelchenko, V. B. Stepanov et al., Phys. Rev. B 94, 224505 (2016). https://doi.org/10.1103/PhysRevB.94.224505.

Phase slip processes in $Bi_2Sr_2CaCu_2O_8$ single crystals

A. G. Sivakov, A. S. Pokhila, A. E. Kolinko

B. Verkin Institute for Low Temperature Physics and Engineering of NAS of Ukraine,
47 Nauky Ave., Kharkiv, 61103, Ukraine
e-mail: pokhila@ilt.kharkov.ua

The study examined superconducting bridges made from high-temperature superconductor (HTSC) single crystals. The samples were fabricated by Yuri Koval in Professor A. Ustinov's laboratory at the University of Erlangen-Nuremberg. 300-nm-thick layers were exfoliated from a massive single crystal. Then, using electron beam lithography and Ar ion etching, bridges 10 μm long and 2 and 10 μm wide were fabricated.

Superconducting transitions and current-voltage characteristics near T_c were studied. Special attention was paid to the analysis of heating effects in the region of normal gold current leads using LTLSM [1], which allowed for an adequate interpretation of the resistive state study results over a wide current range. It was shown that the resistive state in HTSC bridges is caused by phase slip processes and completely replicates the structure and characteristic features of the phase slip centers in narrow channels and the phase slip lines in wide films (namely, the destruction of superconductivity by current occurs due to an increase in the number of multiple discrete resistive sections with constant differential resistances and excess current). Since all the linear dimensions of our samples are much larger than the coherence length, by analogy with the phase slip centers and phase slip lines, the features we observed can be called phase slip surfaces (PSS).

Irradiation of samples with microwave power revealed that at low intensities and frequencies, adiabatic processes associated with the addition of the transport current to the microwave current are decisive. This is reflected in the collapse of the hysteresis in the I–V characteristics shown in Fig. 1. As the power increases, due to the suppression of the order parameter, the PSS s first transform into stationary discrete ohmic domains, and then superconductivity is completely suppressed.

In the first PSSs with low differential resistance, Shapiro steps were discovered (Fig. 2), similar to those observed in work [2], which indicates the Josephson behavior of the PSS and once again confirms the fundamental nature of the phase slip mechanism for any superconductors.

It should be noted that all measurements were carried out using liquid nitrogen.

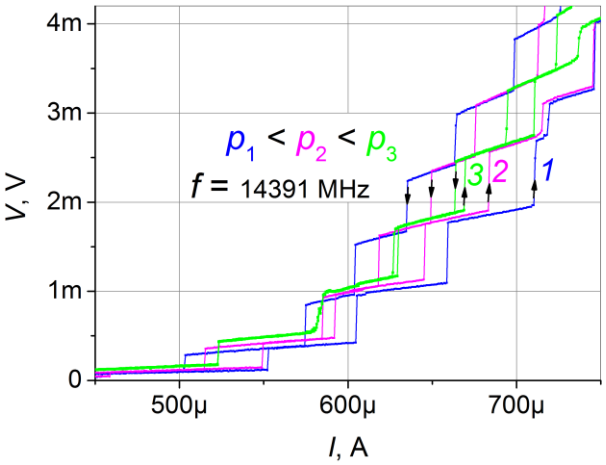

Fig. 1. Collapse of the I–V hysteresis

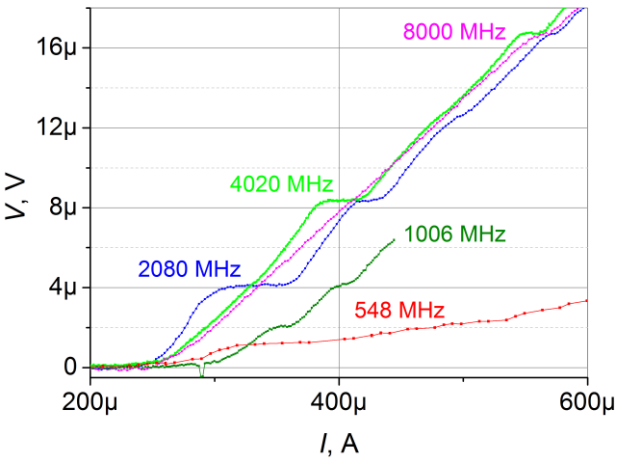

Fig. 2. Shapiro steps

[1] A. P. Zhuravel. A. G. Sivakov. O. G. Turutanov. A. N. Omelyanchouk. Steven M. Anlage, A. Lukashenko. A. V. Ustinov. D. Abraimov, Low Temp. Phys. 32, 592 (2006). https://doi.org/10.1063/1.2215376
[2] A. G. Sivakov, A. M. Glukhov, and A. N. Omelyanchouk, Y. Koval, P. Müller, A. V. Ustinov, Phys. Rev. Lett. 91, 267001 (2003). https://doi.org/10.1103/PhysRevLett.91.267001.

MAGNETISM AND MAGNETIC MATERIALS

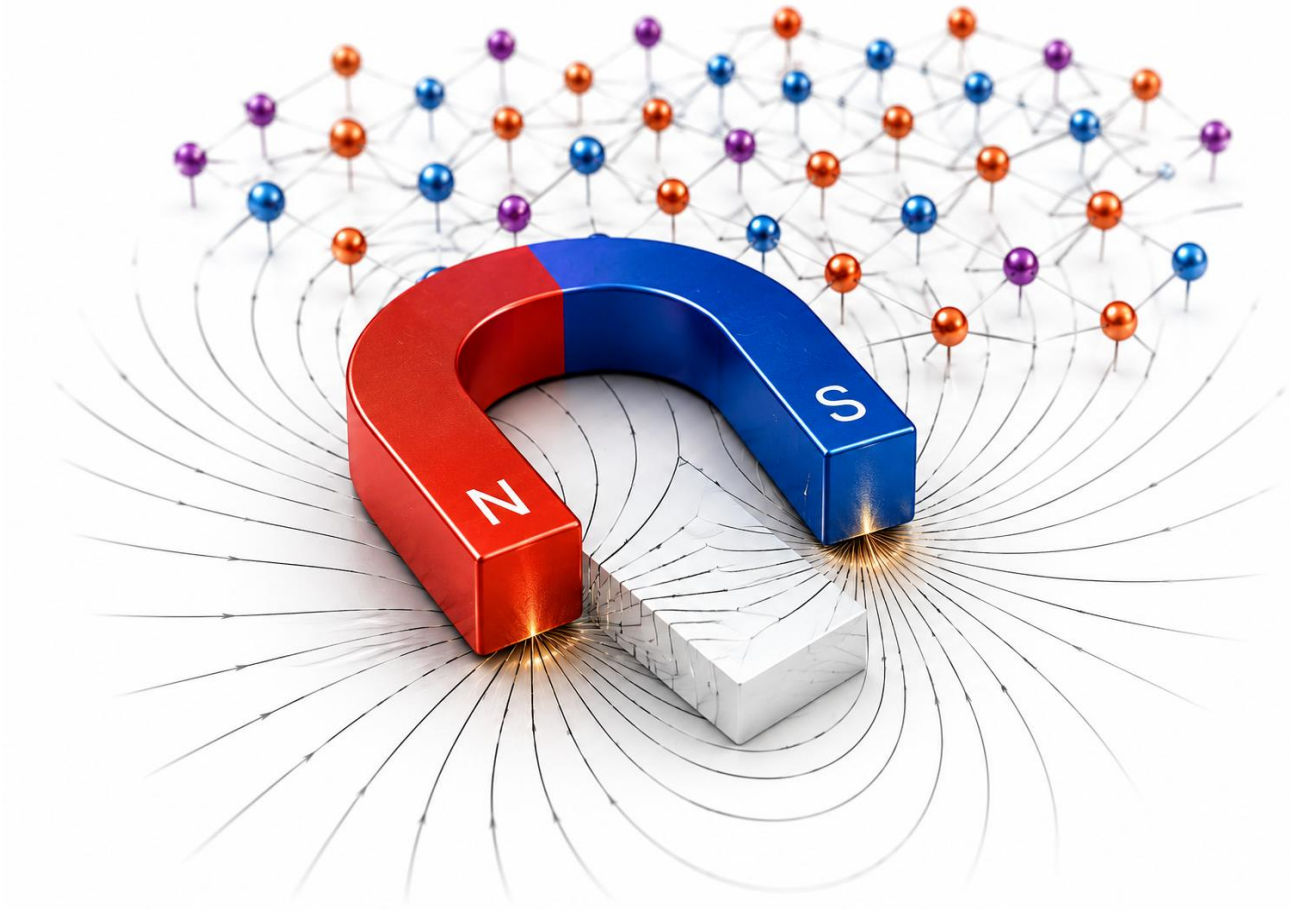

Comprehensive Law of approach to saturation for the determination of magnetic anisotropy in Co/SiO2 granular films

O. E. Baibara[1], Y. A. Stelmakh[2], L. A. Krushinskaya[2], A. I. Ievtushenko[1]

[1]Frantsevych Institute for Problems of Material Science, National Academy of Sciences of Ukraine, 3 Omeljana Pritsaka str., Kyiv 03142, Ukraine
[2]E.O. Paton Electric Welding Institute, National Academy of Sciences of Ukraine, 68 Antonowich str., Kyiv 03680, Ukraine
e-mail: o.baibara@ipms.kyiv.ua

Magnetocrystalline anisotropy is a key factor that defines the efficiency of magnetic materials in a wide range of applications. First-hand information about magnetization curves provides only basic information about the magnetic properties, such as saturation magnetization, coercive force; and the shape of the curves allows determining parameters such as hardness and loss factor. Research of anisotropy constant and information on magnetic microstructures requires a more complex approach. The method law of approach to saturation (LAS) allows effectively determines the internal magnetic parameters, namely anisotropy and saturation constants:

$$M = M_s\left(1 - \frac{a}{H} - \frac{b}{H^2}\right) + kH \quad (1)$$

where M_s is the saturation magnetization; a, b and k are constants.

It was found that the dependency of magnetization does not describe the experimental results satisfactorily using only one or all above 1/H, $1/H^2$, H terms and LAS seem to take different forms according to the kind of the materials, compositions, production methods and approaches. This leads to theoretical and practical difficulties with the law of approach to saturation, especially in the analysis of granular films. A distinctive feature of such materials is that by varying the concentration of the filler, the size of the magnetic nanoparticles changes, and at a certain critical concentration they reach the superparamagnetic limit [1].

Granular films with Co nanoparticles (NPs) distributed in SiO_2 amorphous matrix were grown by the EB-PVD method in the form of film with thickness from 1 to 5 μm on Al_2O_3 substrates (polycor). The Co concentration x varied in wide region from 10 to 70 at.%.

The obtained dependences of the magnetic moment on temperature and magnetic field in the temperature range of 5-300 K were analyzed. The transition of the NPs to the superparamagnetic state is associated with magnetocrystalline anisotropy energy and defined as $E_A = K_{eff} \cdot V$ that related to the effective anisotropy constant (K_{eff}) and the volume (V) of the NP. The values of the effective magnetic anisotropy constants have been determined by the Law of approach to saturation method. For this, parameters such as the combination of different LAS terms, proximity to unity M/M_s, high field region without coercive force, and goodness of fitting are considered.

The value of K_{eff} decreases from $6{,}1 \cdot 10^6$ erg/cm^3 for the Co concentration 65 at.% to $4{,}2 \cdot 10^6$ erg/cm^3 for Co concentration 32 at.%. For a more accurate determination of the K_{eff} values, surface anisotropy was taken into account.

Also, a comparative method for estimating the size of NPs from magnetic properties (by the LAS method and the inverse magnetization analysis) are presented.

[1] G.V. Lashkarev, M. V. Radchenko, O. E. Baibara, M. E. Bugaiova, L.I. Petrosian, Y. Dumond, T. Story, W. Knoff, N. Nedelko, A. Ślawska-Waniewska, M. Foltyn, Y. A. Stelmakh, and L. A. Krushynskaya, Nontrivial phenomena in magnetic nanocomposites Co/Al_2O_3 and Co/SiO_2, Low Temp. Phys. 45 (2019). https://doi.org/10.1063/1.5086418.

Electric-field control of spin-wave propagation: the Aharonov-Casher effect

O. O. Boliasova[1,2], V. N. Krivoruchko[3]

[1]State Research Institution «Kyiv Academic University»
36 Academician Vernadsky Boulevard, 03142, Kyiv, Ukraine,
[2]G. V. Kurdyumov Institute for Metal Physics of the N.A.S. of Ukraine
36 Academician Vernadsky Boulevard, Kyiv, 03142, Ukraine
[3]Donetsk Institute for Physics and Engineering named after O.O. Galkin of the NAS of Ukraine,
46 Nauki Avenue, Kyiv, 03028, Ukraine
e-mail: ol.boliasova@gmail.com

Magnons, quantum magnetization excitations, could be used as carriers of information in future computational devices. Magnetic devices have the potential to speed up and improve the energy efficiency of information transfer. Control of spin-wave propagation is one of the key requirements for practical applications. Among the different ways proposed for controlling spin-wave dynamics, an electric field is considered a promising mechanism. The effect of the external electric field on magnon dynamics in magnetic insulators manifested in the form of an additional phase - the Aharonov-Casher (AC) phase [1]. Within a linear approximation, the magnonic AC effect can be considered by adding a Dzyaloshinskii-Moriya-like interaction between neighboring spins, which is proportional to the magnitude and sign of the applied electric field. Due to this quantum effect, the spin-wave's spectrum, the splitting and distinguishing of right- and left-handed magnons, their propagation length and damping, etc., can be effectively manipulated by an external electric field [2-4].

In this work, we investigate spin-wave propagation in an antiferromagnetic insulator through the interface between two regions under different electric fields. The analysis is performed using the magnonic analogue of Snell's law. The results obtained demonstrate that the electric field can significantly modify the refraction and reflection angles of right- and left-handed spin-waves at the interface, and their dynamic characteristics in regions under different electric fields. Thus, an electric field provides an efficient way to manipulate magnon trajectories and opens new possibilities for the design of electrically controlled magnonic elements such as waveguides, lenses, and logic components for future spin-wave-based information technologies.

[1] Y. Aharonov and A. Casher, Topological quantum effects for neutral particles. Phys. Rev. Let. 53, 319 (1984). https://doi.org/10.1103/PhysRevLett.53.319.
[2] X. Zhang, T. Liu, M. E. Flatté, and H. X. Tang, Electric-field coupling to spin waves in a centrosymmetric ferrite, Phys. Rev. Lett. 113, 037202 (2014). https://doi.org/10.1103/PhysRevLett.113.037202.
[3] R. O. Serha, V. I. Vasyuchka, A. A. Serga, and B. Hillebrands, Towards an experimental proof of the magnonic Aharonov-Casher effect, Phys. Rev. B 108, L220404 (2023). https://doi.org/10.1103/PhysRevB.108.L220404.
[4] O. Boliasova and V. Krivoruchko, Magnonic Aharonov-Casher effect and electric field control of chirality-dependent spin-wave dynamics in antiferromagnets. Phys. Rev. B 111, 174440 (2025). https://doi.org/10.1103/PhysRevB.111.174440.

Eigenoscillations of the topological spin texture in an antiferromagnet with the Dzyaloshinskii–Moriya interaction

V. S. Gerasimchuk[1], I. V. Gerasimchuk[1,2]

[1]National Technical University of Ukraine "Igor Sikorsky Kyiv Polytechnic Institute", 37 Beresteisky Ave., Kyiv, 03056, Ukraine
[2]V.G. Baryakhtar Institute of Magnetism of the NAS of Ukraine, 36b Vernadsky Blvd., Kyiv, 03142, Ukraine
e-mail: igor.gera@gmail.com

Topological spin textures – spatially localized magnetization configurations – are of strong fundamental and applied interest, particularly as potential information carriers in magnonics and spintronics. Antiferromagnets (AFMs) with perpendicular magnetic anisotropy are especially promising, as they support stable spin textures at room temperature without external fields. A special role is played by the Dzyaloshinskii–Moriya interaction (DMI), which can induce long-period spiral textures in magnets devoid of inversion symmetry, forming chiral structures and magnetic skyrmions. In such systems, a wide range of topological states arises, including target skyrmions – axisymmetric multi-ring spin configurations. Although often modeled as 2D topological solitons, these textures are inherently 3D spatial configuration at the nanoscale.

Skyrmions exhibit various dynamical regimes, including breathing modes (radius oscillations) and rotational modes (core motion), as well as inertial effects. In collinear uniaxial AFMs, they possess a discrete spectrum of bound eigenmodes, and in confined geometries can display controllable oscillations. While oscillations of ring-like spin textures in a two-sublattice AFM in the absence of DMI have been studied [1], the dynamics of realistic non-uniform spin textures – especially with an inhomogeneous distribution of inertial mass – remain insufficiently explored.

In this work, we analytically study eigenoscillations of the topological spin texture in a two-sublattice AFM with DMI [2]. Using the solution of the Landau–Lifshitz equations, we calculate the surface energy and surface mass densities as functions of the spin isosurface radius and derive the *equation of free oscillations of the topological spin texture magnetization* that accounts for magnetization inhomogeneity. The problem is reduced to a wave-type equation with variable coefficients. We formulate a boundary value problem of eigenexcitations of the thin axisymmetric nanoscale spin configuration, allowing us to obtain key dynamical characteristics such as oscillation energy, frequency, relative amplitude, and both *topological* and *inertial masses*. It is shown that target skyrmion-type AFM spin textures support intrinsic spin excitation modes.

Comparing the studied axisymmetric radial oscillations with micromagnetic results for a skyrmion tube [3], we find close agreement: in both cases radial symmetry is preserved, rotational modes are suppressed, and only the breathing mode is allowed.

Our results can be useful for a deeper understanding of the fundamental principles of magnetism, in particular the nature of non-uniform spatial distributions of magnetization, their stability, and dynamical properties. The results are relevant for prospective applications in magnonics and spintronics, where controlled manipulation of spin texture dynamics, including their intrinsic oscillation modes, can be exploited for information processing and storage.

I.V.G. acknowledges support by the National Research Foundation of Ukraine, Grant No. 2025.07/0132.

[1] V. S. Gerasimchuk, Yu. I. Gorobets, O. Yu. Gorobets and I. V. Gerasimchuk, Sci. Rep. 13, 6613 (2023). https://doi.org/10.1038/s41598-023-33220-0.
[2] V. S. Gerasimchuk and I. V. Gerasimchuk, Low Temp. Phys. 51, 1023 (2025). https://doi.org/10.1063/10.0038649.
[3] X. Xing, Y. Zhou, and H. B. Braun, Phys. Rev. Applied 13, 034051 (2020). https://doi.org/10.1103/PhysRevApplied.13.034051.

Ab initio calculations of altermagnetic materials

O. Hrechykha, O. Feia

Kyiv Academic University, 36 Vernadsky blvd., Kyiv, 03142, Ukraine
e-mail: o.hrechykha@kau.edu.ua

Altermagnets present a new class of magnetic materials. Their main properties include alternating spin signs in *k*-space, absence of net magnetization, time-reversal symmetry breaking and spin-split *d,g,i*-wave Fermi surfaces [1, 2]. They represent a broad category of known crystal structures and compounds exhibiting a wide range of properties and magnetic responses, including metals, insulators, semiconductors, and possibly superconductors, making them a compelling subject of study due to the potential width of applications [3]. The main method used when searching for altermagnetic properties in known materials is ab initio (density functional theory, DFT) calculations.

Such calculations have been successfully performed on Mn-based materials. The research has predicted altermagnetism in MnF_2 [4,5] and MnTe [2]. In this work, we aim to use DFT methodology on a similar material – $MnTe_2$ – showcasing similarities and differences in relation to the materials listed above. We present the respective band structure, highlighting the effects of introducing spin-orbit coupling, magnetism and Hubbard potential in the Mn sublattice and compare them, when possible, with experimental results and calculations done by other researchers.

[1] Šmejkal L., Sinova K., Jungwirth T. Emerging Research Landscape of Altermagnetism, Phys. Rev. X 12, 040501 (2022). https://doi.org/10.1103/PhysRevX.12.040501.
[2] Šmejkal L., Sinova K., Jungwirth T. Beyond Conventional Ferromagnetism and Antiferromagnetism: A Phase with Nonrelativistic Spin and Crystal Rotation Symmetry, Phys. Rev. X 12, 031042. https://doi.org/10.1103/PhysRevX.12.031042.
[3] Song, C., Bai, H., Zhou, Z. et al. Altermagnets as a new class of functional materials. Nat Rev Mater 10, 473–485 (2025). https://doi.org/10.1038/s41578-025-00779-1.
[4] S. López-Moreno et. al. First-principles study of pressure-induced structural phase transitions in MnF2, Phys. Chem. Chem. Phys., 2016,18, 33250-33263, https://doi.org/10.1039/C6CP05467F.
[5] Lin-Ding Yuan et. al. Giant momentum-dependent spin splitting in centrosymmetric low-*Z* antiferromagnets, Phys. Rev. B 102, 014422. https://doi.org/10.1103/PhysRevB.102.014422.

From a quasi-2D isotropic square-lattice ferromagnet to ferromagnetic chains: refined spin Hamiltonian of Cu(*en*)(*sal*)Cl

I. Kozin[1], R. Tarasenko[1], J. Šebesta[2], D. Legut[2, 3], J. Strečka[1], E. Čižmár[1], A. Orendáčová[1], V. Tkáč[1], and M. Orendáč[1]

[1]Institute of Physics, Faculty of Science, P.J. Šafárik University in Košice, Park Angelinum 9, 040 01 Košice, Slovakia
[2]IT4Innovations, VŠB-Technical University of Ostrava, 17. listopadu 2172/15, 708 00 Ostrava-Poruba, Czech Republic
[3]Department of Condensed Matter Physics, Faculty of Mathematics and Physics, Charles University, Ke Karlovu 3,121 16 Prague 2, Czech Republic
e-mail: illia.kozin@student.upjs.sk

We report a refined analysis of the magnetic properties of the metal-organic complex Cu(*en*)(*sal*)Cl (*en* = ethylenediamine; *sal* = salicylic acid), focusing on the determination of the dominant magnetic exchange interactions and the effective magnetic model describing this compound. The previously determined crystal structure reveals a layered arrangement with a square-like framework of Cu^{2+} ions in the *bc* plane [1].

Preceding low-temperature heat-capacity measurements down to 0.38 K revealed a magnetic phase transition at T_C = 0.82 K, indicating the presence of long-range ferromagnetic order. Magnetization and susceptibility measurements supported this behavior, showing a divergence between zero-field-cooled and field-cooled magnetization curves as well as a ferromagnetic hysteresis at low temperature ($T<T_C$). Initial analysis of the susceptibility and heat capacity data suggested that Cu(*en*)(*sal*)Cl could be described as a quasi-two-dimensional spin-1/2 Heisenberg ferromagnet on an isotropic square lattice with an exchange interaction $J/k_B \approx 2$ K.

Subsequent first-principles *ab initio* calculations of the magnetic couplings, however, revealed a pronounced spatial anisotropy in exchange interaction within the magnetic layers. The dominant ferromagnetic exchange was found along the crystallographic *c* direction with $J_1/k_B \approx 5.69$ K, while a much weaker antiferromagnetic interaction $J_2/k_B \approx -0.24$ K was obtained along the *b* direction. Motivated by these results, the experimental data were reanalyzed using theoretical predictions based on a one-dimensional spin-1/2 Heisenberg ferromagnetic chain model, employing quantum Monte Carlo simulations for comparison with the experimental results.

The combined experimental and theoretical analysis indicates that Cu(*en*)(*sal*)Cl is best described as a system of ferromagnetic spin-1/2 chains with dominant intrachain exchange $J_1/k_B \approx 5.69$ K and weak antiferromagnetic interchain coupling $J_2/k_B \approx -0.24$ K. These results establish Cu(*en*)(*sal*)Cl as a rare realization of a quasi-one-dimensional ferromagnetic Heisenberg system with weak interchain interactions.

The financial support by projects vvgs-2026-3893, VEGA 1/0149/26, APVV-18-0197, APVV-23-0006, and APVV-22-0172 is highly acknowledged.

[1] S. S. Batool, S. R. Gilani, M. N. Tahir, A. Siddique and W. T. A. Harrison, Journal of Structural Chemistry 57 (6), 1176–1181 (2016). https://doi.org/10.1134/S0022476616060172.

Magnetic-field-driven release of strain in FeRh films

I. Lukiienko[1,2], V. Uhlíř[1]

[1]Central European Institute of Technology, Brno University of Technology, Czechia
[2]B.Verkin Institute for Low Temperature Physics and Engineering of NAS of Ukraine, 47 Nauky Ave., Kharkiv, 61103, Ukraine
e-mail: andrik1982@ukr.net

Antiferromagnets (AF) that undergo a first-order phase transition to a ferromagnetic (FM) state by the application of an external magnetic field are known as metamagnetic materials. Due to the phase transition sharpness, these materials are promising for applications in spintronics and magnetic field sensing [1]. The phase transition is accompanied by a magnetocaloric effect characterized by temperature changes during AF-FM-AF cycles, which makes these materials promising for magnetic refrigeration [2].

In this work, we demonstrate how to release strain induced by a substrate and improve the quality of metamagnetic films without thermal annealing, using high magnetic fields. We studied metamagnetic epitaxial FeRh films featuring the transition from AF to FM phase around 360 K. Typically, application of an external magnetic field lowers the phase transition by around 0.9 K/kOe. We found that application of 90 kOe, which is sufficient to trigger the phase transition at room temperature, causes a permanent 10 kOe shift in the magnetic-field-induced phase transition hysteresis. At the same time, the thermal hysteresis of the phase transition was also found to be shifted by around 10 K to lower temperatures. Moreover, X-ray diffractometry identified a shift of the FeRh (002) diffraction peak towards its positions for the bulk sample. This points to relaxation of internal compressive strain in the FeRh crystal lattice, formed during its growth on a MgO (001) substrate. We term this effect “quasiannealing”, as it relates to the process with a similar impact as thermal annealing, but without negative side effects, such as intermixing between the FeRh and a Pt cap layer. This effect is significant in the 300-nm-thick FeRh films, but not in the 30 nm films, where the net compressive strain from the MgO substrate is more prominent. A key ingredient of such prominent quasiannealing effect is the giant ~ 1% FeRh lattice expansion across the phase transition, which amplifies the common effect of strain release by magnetic field - magnetostriction.

CzechNanoLab Research Infrastructure (ID 90251), funded by MEYS CR, is gratefully acknowledged for the financial support of the measurements/sample fabrication.

[1] H. Chen et al., Antiferromagnets for Spintronics, Adv. Mater. 36, 2310379 (2024). https://doi.org/10.1002/adma.202310379.
[2] U. Lucia, and G. Grisolia. Magnetocaloric Refrigeration in the Context of Sustainability: A Review of Thermodynamic Bases, the State of the Art, and Future Prospects. Energies 17, 3585 (2024). https://doi.org/10.3390/en17143585.

Impact of ferroelastic phase transition on magnetic susceptibility of ferromagnet and magnetocaloric effect

V. A. L'vov[1], A. Kosogor[1,2]

[1]V.G. Baryakhtar Institute of Magnetism of NAS of Ukraine,
36-b Akad. Vernadskoho blvd., 03142, Kyiv, Ukraine
[2]University of Vienna, Faculty of Physics, Boltzmanngasse 5, 1090 Vienna, Austria
e-mail: victor.a.lvov@gmail.com

Experimental temperature dependence of magnetization, $M(T)$, in the strong magnetic field, H, is often used for evaluation of the field-induced temperature change, ΔT_H (see e.g. [1]). According to the common belief, the sharp change of $M(T)$ value observed for ferromagnets, which undergo structural phase transitions (PTs), provides large values of ΔT_H. The equation for quantitative description of experimental $M(T)$ values due to the proper account of the influence of PT on the spin-exchange energy was obtained recently and applied to Ni-Mn-Ga alloys [2, 3].

In this presentation we show that the above mentioned equation provides a precise fit of theoretical $M(T)$ curves to experimental values obtained in Ref. [4] for $Ni_{50}Mn_{17.5}Ga_{25}Cu_{7.5}$ alloy, which undergoes ferroelastic PTs on cooling and heating at T_{PT} of 329 K and 339 K, respectively (see Fig. 1 a)). Using theoretical $M(T)$ values the magnetic susceptibility caused by the paraprocess, $\chi_{pp}(T)$, and the temperature change, induced by the field H = 20 kOe, were evaluated (see Fig. 1 b) and Fig. 1 c), respectively). Comparing the values shown by the solid lines with those shown by the dashed ones, one can see that the ferroelastic phase transition from the high-symmetry paramagnetic to the low-symmetry ferromagnetic phase results in a sharp increase of $M(T)$ but reduces the $\chi_{pp}(T)$ and ΔT_H values. The interrelation between these values is discussed in the presentation.

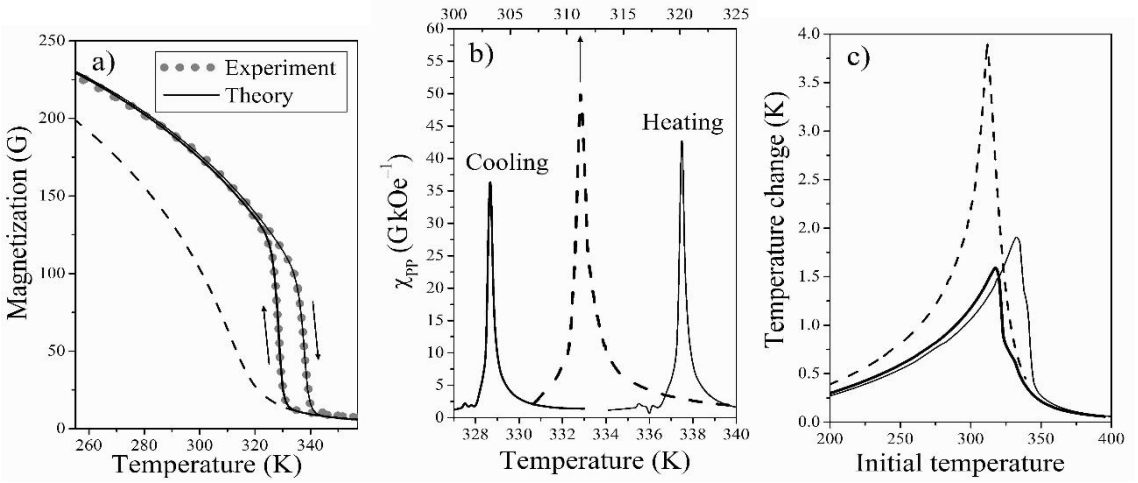

Fig. 1. The values computed for $Ni_{50}Mn_{17.5}Ga_{25}Cu_{7.5}$ (solid lines) and for the alloy, which does not undergo PT (dashed lines).

It can be concluded that, in spite of the common belief, the sharp temperature dependence of the magnetization value is not a universal indicator of the giant magnetocaloric effect.

[1] A. Biswas, R. K. Chouhan, A. Thayer, V. K. Pecharsky, Phys. Rev. Mater. 6, 114406 (2022). https://doi.org/10.1103/PhysRevMaterials.6.114406.
[2] V. A. L'vov, O. Salyuk, A. Kosogor, Sci. Rep. 15, 31002 (2025). https://doi.org/10.1038/s41598-025-15896-8.
[3] V. A. L'vov, Low Temp. Phys. 51, 928 (2025). https://doi.org/10.1063/10.0037097.
[4] A. Kosogor, V. A. L'vov, P. Lázpita, C. Seguí, E. Cesari, Metals 9, 11 (2019). https://doi.org/10.3390/met9010011.

Propagation of spin excitations along domain walls in d-wave altermagnets

O. Peschanska[1], V. Kravchuk[1,2]

[1]Bogolyubov Institute for Theoretical Physics of the NAS of Ukraine,
14-B Metrolohichna str., Kyiv 03143, Ukraine
[2]Leibniz-Institut für Festkörper- und Werkstoffforschung,
Helmholtzstraße 20, D-01069 Dresden, Germany
e-mail: sombercy@gmail.com

The study addresses properties of the bound states of altermagnetic domain wall (DW) in d-wave altermagnets with easy-axis anisotropy. As a case study, we consider rutiles, which cover a broad range of d-wave altermagnets (NiF2, MgF2, CoF2). We consider a Heisenberg model of a d-wave altermagnet [1,2], which accounts for altermagnetic properties via additional superexchange interactions that respect the positions of the nonmagnetic atoms. The DW bound states are studied in the framework of the continuous Lagrangian formulated for the Neel vector in the exchange approximation [1,3].

In the absence of the magnetic field, we consider two different orientations of the DW. For a DW oriented along the nodal directions, the dispersion of the bound state propagating along the DW is strongly nonlinear, in contrast to the antiferromagnetic limit, and the wavefront of the bound state tilts. For a DW, whose orientation differs from a nodal direction, the altermagnetism results in three additional effects: (i) appearance of new high-energy bound states; (ii) dependence of the localization region on the eigenenergy, and (iii) the degeneracy with respect to the eigenstate polarization (clockwise or counterclockwise precession of the Neel vector) is removed.

In the presence of an external magnetic field oriented along the easy axis, we consider the DW orientation along a nodal axis. In this case, the only effect of the field on the static DW is the increase in the DW width. We show that the magnetic field doesn't affect the number of bound states. However, it sets an upper limit on the absolute value of the wave vector of the bound eigenstate propagating along the DW, and altermagnetism further reduces this limit. The behaviour of the localization region has also changed. In contrast to the symmetric localization around DW when the magnetic field is turned off, in the magnetic field, the localization region becomes asymmetric, and the asymmetry increases with magnetic field strength. The sign of the asymmetry depends on the eigenstate polarization, the direction of the magnetic field, and the topological charge of the DW.

This work was supported by the German Federal Ministry of Research, Technology and Space (BMFTR) through the GU-QuMat project (01DK24008).

[1] O. Gomonay, V. Kravchuk, R. Jaeschke-Ubiergo, et al., npj Spintronics 2, 35 (2024). https://doi.org/10.1038/s44306-024-00042-3.
[2] K. Yershov, V. Kravchuk, M. Daghofer, J. van den Brink, Phys. Rev. B, 110, 144421 (2024). https://doi.org/10.1103/PhysRevB.110.144421.
[3] K. Yershov, O. Gomonay, J. Sinova, J. van den Brink, V. Kravchuk, Phys. Rev. Lett, 134, 116701 (2025). https://doi.org/10.1103/PhysRevLett.134.116701.

Rotational symmetry in s = 1/2 dimers and tetramers with non-collinear local ion axes

O. V. Zhuravlev

Donetsk Institute for Physics and Engineering named after O.O. Galkin of the NAS of Ukraine,
46 Nauki Avenue, Kyiv, 03028, Ukraine
e-mail: alexander.zhuravlev01@gmail.com

A wide variety of single-molecule magnets (SMMs) structures have been synthesized to date, ranging from fairly asymmetric to highly symmetric. In SMMs with a certain class of molecular symmetry, the electron shells of magnetic ions and their local coordinate systems (LCSs) are also oriented symmetrically, although a reduction in symmetry is possible. Therefore, an analytical model that accounts for the orientation of the ion LCSs relative to the molecular coordinate system (MCS) would be extremely useful and relevant in studies of SMMs and other spin clusters.

There are several systematic theoretical approaches that consider the symmetry of SMMs, based on the irreducible tensor operator technique and its extension considering the permutation symmetry, on the algebraic combinatorics, or on the present point-group and operator technique shift (see refs in [3]). None of these approaches allows one to describe the properties of spin clusters in terms of the LCSs orientations in the MCS.

The development of the "Redefined Pauli Matrix Spin Hamiltonian" (RPMSH) model, described previously [6, 7], utilizes the properties of the Pauli matrices, allowing spins to be represented not as abstract operators, but as matrices of a specific type. The basic principle of the model is based on permutation symmetry for spins $s^{(i)}$ and $s^{(j)}$, related by a certain operation O:

$$s^{(j)} = T\, O\, s^{(i)}\, O'\, T',$$

where T is the permutation operator required in the Pauli matrix formalism. Based on RPMSH, a model is constructed that takes into account the symmetry of the SMMs ("Symmetrized Pauli Matrix Spin Hamiltonian", SPMSH).

The SPMSH model was applied to the analysis of binuclear molecular complexes with C_2 symmetry [7], tetranuclear complexes with C_4 and S_4 symmetries [8], and to calculations with variations in the polar angle of deviation of LCSs from MCS ($\theta^{(i)}$, where i is the ion number). Symmetry restrictions redefine all LCSs in the cluster, starting from the second to the first coordinate system, with the polar angle assigned as θ.

The paper provides a brief overview of the results [7, 8] and presents the results for tetramers with C_2 symmetry. For all objects studied, common patterns were found in changes in the EPR spectra with variation in θ. All EPR lines for arbitrary angles θ can be conditionally divided into lines existing at θ = 0 (the unique coordinate system case) and lines appearing when the LCS axes diverge. The intensity of the former decreases, while that of the latter increases, with increasing θ.

The most general result of this study is the prediction of the appearance of additional EPR lines upon misorientation of the local coordinate systems of magnetic ions in a spin cluster.

[1] S. Hill, R. S. Edwards, N. Aliaga-Alcalde, G. Christou, Science 302, 1015 (2003).
DOI: 10.1126/science.1090082.
[2] D. Gatteschi, B.S. Tsukerblat, Mol. Phys. 79, 121 (1993).
https://doi.org/10.1080/00268979300101111.
[3] A. V. Zhuravlev, Low Temp. Phys. 47, 1053 (2021). https://doi.org/10.1063/10.0006578.

The study of piezomagnetism in MnF_2 single crystals

I. V. Bilych[1], K. R. Zhekov[1], G. A. Zvyagina[1], V. D. Fil, D. V. Fil[2,3]

[1]B.Verkin Institute for Low Temperature Physics and Engineering of NAS of Ukraine, 47 Nauky Avenue, Kharkiv, 61103, Ukraine
[2]Institute for Single Crystals, NAS of Ukraine, 60 Nauky Avenue, Kharkiv, 61072, Ukraine
[3]V.N. Karazin Kharkiv National University, 4 Svobody Square, Kharkiv, 61022, Ukraine
e-mail: bilich@ilt.kharkov.ua

This work is devoted to the research of the piezomagnetic phenomena in single crystals of MnF_2 using the acoustoelectric transformation (AET) method, which has previously been successfully used to study piezomagnetism in CoF_2 [1]. This method allows studying the quantitative and qualitative characteristics of magnetoelastic effects by measuring the phase and amplitude of the AET signal at different polarizations of the elastic mode, at different antenna orientations, and in the presence of an external magnetic field. A significant advantage of the AET method is its high information content in studying various mechanisms of magnetoelastic interaction in magnetoactive media, as well as flexibility in implementing various experimental geometries and the practical absence of a background signal.

All experiments were performed in the $\mathbf{q} \parallel C_4$ geometry ($\mathbf{q}$ is the sound wave vector; C_4 is the 4th order axis). Experiments have shown that in MnF_2 below the Neel temperature (T_N), a transverse acoustic wave propagating along the C_4 axis always generates a piezomagnetic response, and its orientation is determined by the polarization of the elastic field. The amplitude-phase polarization diagrams of rotation at different polarizations of the elastic field, observed in the absence and in the presence of an external magnetic field, were studied. The temperature dependence of the piezomagnetic response in the absence of an external magnetic field was obtained, measured when the antenna was tuned to the maximum signal.

The temperature behavior of the amplitude and phase of the piezomagnetic response $\mathbf{m}^H$ in the magnetic field was studied. The response $\mathbf{m}^H$ is the result of the interference of two contributions whose phases are different and are almost independent of the temperature. The first one, which is quite weak, exists at temperatures both above and below T_N, while the second one, with rapidly increasing intensity, appears only in the antiferromagnetic phase. One possible explanation for the origin of the response $\mathbf{m}^H$ is the so-called "wave" scenario. The deformation initiates the emergence of a non-diagonal component in the magnetic susceptibility tensor, i.e., a magnetization component orthogonal to $\mathbf{H}$ appears. This effect is possible because the field of shear displacement gradients (shear deformation) changes the symmetry of the lattice, making it more anisotropic.

Thus, the manifestations of piezomagnetism have been studied in MnF_2. The anisotropy of the effect and its temperature behavior have been determined. A phenomenological description of the experimental results is presented. It has been established that under shear deformations, the magnetic susceptibility of MnF_2 acquires a non-diagonal component of the magnetic susceptibility tensor, proportional to the square of the antiferromagnetism vector.

[1] T. N. Gaydamak, G. A. Zvyagina, K. R. Zhekov, I. V. Bilich, V. A. Desnenko, N. F. Kharchenko, and V. D. Fil, Acoustopiezomagnetism and the elastic moduli of CoF_2, Low Temp. Phys. 40, 524 (2014). https://doi.org/10.1063/1.4883897.

Magnetic properties of $EuCr_3(BO_3)_4$

O. Bludov[1], Yu. Savina[1], I. Lukiienko[1,2], V. Pashchenko[1], M. Kobets[1], O. Zaremba[3], Yu. Tyvanchuk[3]

[1]B.Verkin Institute for Low Temperature Physics and Engineering of the NAS of Ukraine, 47 Nauky Ave., Kharkiv, 61103, Ukraine
[2]Central European Institute of Technology, Brno University of Technology, Purkyňova 123, 62100 Brno, Czechia
[3]Department of Inorganic Chemistry, Ivan Franko National University of Lviv, 6 Kyryla and Mefodiya St., Lviv 79005, Ukraine
e-mail: bludov@ilt.kharkov.ua

Complex oxides with ions of transition (3d) and rare earth (4f) metals attract considerable attention of scientists. In such compounds 3d ions can provide comparative high temperature of magnetic ordering, while features of electronic properties of 4f ions can form electric polarization and elastic deformation. Magnetoelectric and magnetoelastic effects, giant magnetocaloric effect and exotic magnetic phases can be found in the mixed 3d-4f compounds due to interaction between 3d and 4f subsystems.

Europium chromium borate $EuCr_3(BO_3)_4$ belongs to the large family of compounds with a general chemical formula $RM_3(BO_3)_4$ (R = rare-earth element or Y; M = Al, Ga, Sc, Fe or Cr). Members of the family attract a considerable attention over the last two decades, primarily due to their optical [1,2], magnetoelectric and magnetoelastic properties [3,4]. Six structural polytypes (space groups $R32$, $P321$, $P3_121$, $C2/c$, $C2$ and Cc) are known for the family [5]. Majority of the members crystallize in the huntite-like rhombohedral structure ($R32$). All polytypes have common motif: spiral chains of CrO_6 octahedra with common edges that are interconnected into a 3D structure by means of BO_3 planar triangular groups and RO_6 trigonal prisms. The main differences between the polytypes are different topology of the chains, and slight variation of the Cr–Cr distances in the chains and between them.

Structure of the $EuCr_3(BO_3)_4$ powdered sample has been studied at ambient temperature by using the general purpose X-ray diffractometer. The temperature dependences of magnetic susceptibility $\chi(T)$, the field dependences of magnetization $M(H)$ of polycrystalline sample have been measured by using the vibration magnetometer (2-300 K, up to 10 T).

The rhombohedral ($R32$) structure with lattice parameters $a = 9.486$ Å, $c = 7.507$ Å was confirmed by X-ray diffraction. It was found that the sample orders antiferromagnetically at $T_{N1} = 9\pm1$ K that in agreement with [6]. Magnetic phase transition was observed at about 3 T for 4 K. It was shown that at $T > T_N$ the magnetic susceptibility $\chi(T)$ of $EuCr_3(BO_3)_4$ is described well by using an one-dimensional spin model for a system of the coupled chains of the Cr^{3+} ions with the antiferromagnetic intrachain exchange interaction $J/k = 4{,}5\pm0.5$ K and the ferromagnetic interchain one $J'/k = -0{,}6\pm0.2$ K.

[1] X. Chen, Z. Luo, D. Jaque et al., J. Phys.: Condens. Matter. 13, 1171, (2001).
[2] M. Huang, Y. Chen, X. Chen, Y. Huang, Z. Luo, Opt. Commun. 208, 163, (2002).
[3] K.-C. Liang, R.P. Chaudhury, B. Lorenz et al., J. of Phys.: Conf. Ser. 400, 032046, (2012).
[4] A.M. Kadomtseva, Yu.F. Popov, G.P. Vorob'ev et al., Low Temp. Phys. 36, 511, (2010).
[5] G.M. Kuz'micheva, I.A. Kaurova, V.B. Rybakov, V.V. Podbel'skiy, Crystals 9, 100 (2019).
[6] L. Gondek, A. Szytu, J. Przewonik et al., Journal of Solid State Chemistry 210(1), 30, (2014).

Ferromagnetic nanoparticles as a perspective tool for the investigations and the therapy of the oncological diseases

P. M. Boltovets[1], B. A. Snopok[1], V. V. Bondar[2], V. F. Chekhun[2]

[1]V.Ye. Lashkaryov Institute of Semiconductor Physics, NAS of Ukraine,
41 Nauky Ave., Kyiv, 03039, Ukraine
[2]R. E. Kavetsky Institute of Experimental Pathology NAS of Ukraine,
45 Vasylkivska str., Kyiv, 03022, Ukraine
e-mail: boltovets@isp.kiev.ua

Recently nanotechnologies have been widely used for the development of the new approaches in medicine. For direct delivery of the active composition to the target cells special vectors are used which must be conjugated with nano-object.

Practical delivery of the modified magnetic nanoparticles to the area of specific tissues etc. can be realized by the external magnetic field [1]. For example, moving of nanoparticles can be realized by the permanent magnets whereas their activity can be modulated by the alternating magnetic fields, - moderate heating induce the release an active substance from the surface whilst the higher temperatures allows locally damage cancer cells [2]. To be sure that the active composition will be directly delivered to the target cells special vectors are used. Drug-loaded materials may be conjugated by iron binding protein transferrin/apo-Transferrin for recognition and facilitating binding to cancer cells [3].

In the present study we discuss possibility to create stable conjugate containing various iron oxide nanoparticles and apo-Transferrin, the major carrier of iron in the body. The results of surface plasmon resonance study demonstrate that formation of conjugate depends on nanoparticle composition and presence of the shell whereas surface induced irreversible aggregation of nanoparticles controlled by a pH dependent mechanism. The stable aggregation-free conjugates were formed in pure water and in the presence of CO_3^{2-} anions at low alkaline pH for shell-free magnetite Fe_2O_3 nanoparticles. The obtained results strikingly demonstrate that before *in vivo* studies it is necessary to exclude *a fortiori* false compositions that are unstable under near physiological conditions by investigations *in vitro*.

[1] A. Pusta, M. Tertis, I. Crăciunescu, R. Turcu, S. Mirel, C. Cristea, Pharmaceutics. 2023 15(7):1872. https://doi.org/10.3390/pharmaceutics15071872.
[2] N.Rarokar, S.Yadav, S. Saoji, P.Bramhe, R.Agade, S. Gurav, P. Khedekar, V. Subramaniyan, L. S Wong, V. Kumarasamy, International Journal of Pharmaceutics: 2024 X, 7, Article 100231. https://doi.org/10.1016/j.ijpx.2024.100231.
[3] Chang Li, Liya Zhou, Xunzhe Yin, Front Pharmacol. 2024; 15:1342181 https://doi.org/10.3389/fphar.2024.1342181.

Magneto-dynamic response of YIG ceramics: influence of secondary phases

V. Borynskyi[1], D. Popadiuk[2], A. Kravets[2], S. Solopan[3], A. Belous[3], V. Korenivski[2], A. Tovstolytkin[1]

[1]V.G. Baryakhtar Institute of Magnetism of the NAS of Ukraine,
36-b, Akad. Vernadskogo blvd., Kyiv 03142, Ukraine
[2]Nanostructure Physics, Royal Institute of Technology,
Hannes Alfvénsväg 12, Stockholm 10691, Sweden
[3]V.I. Vernadsky Institute of General and Inorganic Chemistry of the NAS of Ukraine,
32/34, Palladina ave., Kyiv 03142, Ukraine
e-mail: vladislav.borinskiy@gmail.com

Doping garnet-based ceramics with magnetic and non-magnetic ions such as Co, Ni, Al, Sm, and Gd is a well-established strategy for tailoring their electromagnetic properties for microwave electronics and spintronic devices [1]. Previous studies demonstrated that substitution of Fe^{3+} with non-magnetic Al^{3+} cations not only enhances dielectric permittivity but also significantly reduces effective magnetic anisotropy, thereby shifting the critical single-domain size into a technologically attractive nanoscale range [2]. However, both Al-doped and undoped yttrium iron garnet (YIG) ceramics exhibited non-trivial resonance behavior, including additional signals and non-uniform broadening of the main mode. This suggests the possible formation of nano- and microscale clusters of secondary crystalline phases within the ceramic matrix. During sintering, intermediate phases such as hematite (α-Fe_2O_3), yttrium oxide (Y_2O_3), and orthoferrite ($YFeO_3$) may form and persist depending on stoichiometry and thermal conditions.

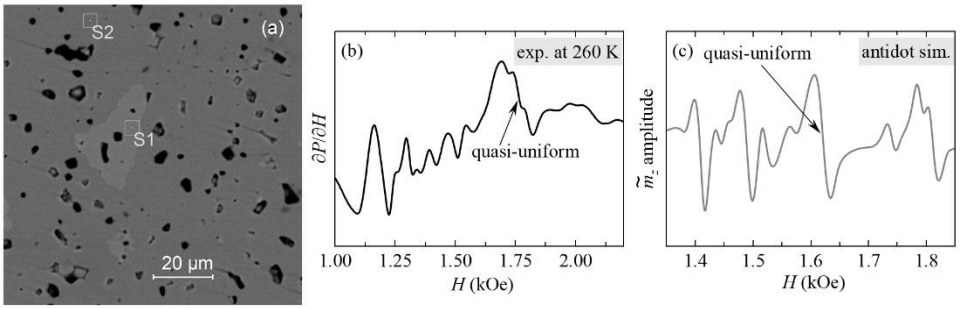

Fig. 1. (a) BSE image of the sample surface. (b) Ferromagnetic resonance spectrum of the synthesized YIG ceramics at 260 K. (c) Simulated spectrum of an antidot array in YIG matrix.

To clarify these anticipations, we investigated the magneto-dynamic response of undoped YIG ceramics synthesized under an artificial iron deficiency (~1 m.%). Back-scattered electron micrograph of the sample surface in Fig.1(a) revealed regions with varying chemical composition, implying the presence of secondary crystalline phases, which, however, were not detected by X-ray diffraction. Ferromagnetic resonance measurements showed multiple additional peaks, particularly pronounced at low temperatures, see Fig.1(b). Micromagnetic simulations of antidot arrays, shown in Fig.1(c), reproduced the multimode spectrum with the promising absolute position of the quasi-uniform mode and relative locations of the satellite peaks. Based on these results, we propose that residual micro- and nanoscale clusters of orthoferrite $YFeO_3$ are the most likely origin of the observed anomalies. The antiferromagnetic nature of $YFeO_3$ introduces magnetic inhomogeneities in the YIG ceramic matrix, thereby facilitating the excitation of spin waves.

[1] V. Harris, Modern Ferrites: Emerging Technologies and Applications (Wiley, 2022) ISBN 978-1-394-15613-9.
[2] V. Borynskyi, D. Popadiuk, A. Kravets, Y. Shlapa, S. Solopan, V. Korenivski, A. Belous and A. Tovstolytkin, J. Alloys Compd. 1010, 178320 (2025). https://doi.org/10.1016/j.jallcom.2024.178320.

Low-temperature magnetism of Co-Al-based LDH

A. V. Fedorchenko[1], E. L. Fertman[1], I. P. Kobzar[1], Yu. G. Pashkevich[2,3], V. Tkáč[4], R. Tarasenko[4], E. Čižmár[4], A. Feher[4], M. Holub[5], C. S. Neves[6], D. E. L. Vieira[6], A. N. Salak[6]

[1]B.Verkin Institute for Low Temperature Physics and Engineering of NAS of Ukraine, 47 Nauky Ave., Kharkiv, 61103, Ukraine
[2]O. Galkin Donetsk Institute for Physics and Engineering of NASU, 03028 Kyiv, Ukraine
[3]Department of Physics and Fribourg Center for Nanomaterials, University of Fribourg, CH-1700 Fribourg, Switzerland
[4]Institute of Physics, Faculty of Science, P.J. Šafárik University in Košice, 041 54 Košice, Slovakia
[5]AGH University of Krakow, al. Adama Mickiewicza 30, 30-059 Krakow, Poland
[6]Department of Materials and Ceramic Engineering, CICECO – Aveiro Institute of Materials, University of Aveiro, 3810-193 Aveiro, Portugal
e-mail: fedorchenko.alexey@gmail.com

Layered double hydroxides (LDH) Co(n)Al with cation ratios n = 2 and 3, intercalated with NO_3^-, CO_3^{2-}, and OH^- anions, were synthesized via co-precipitation and anion exchange, including preparations carried out in the presence and absence of an external magnetic field in order to assess its influence on the low-temperature magnetic properties of the resulting materials. The magnetic behavior of the synthesized compounds was characterized by both static and dynamic susceptibility measurements. Static (*dc*) magnetization and susceptibility were measured as a function of temperature and applied field at low temperatures. Complex *ac* susceptibility, $\chi = \chi' - i\chi''$, where χ' and χ'' denote the in-phase and out-of-phase components, respectively, was recorded at multiple fixed frequencies up to 1 kHz in an *ac* driving field of 1.5 Oe. Heat capacity measurements were performed over the temperature range of 2-100 K in applied magnetic fields up to 90 kOe; to isolate the magnetic contribution to the heat capacity, C_{mag}, the Co-containing LDH samples were compared against their isostructural non-magnetic Mg-Al analogs.

The low-temperature magnetic measurements reveal that Co-Al LDH materials exhibit cluster spin glass behavior rather than conventional long-range magnetic ordering. The frequency dependence of the ac susceptibility, combined with magnetic relaxation dynamics analyzed within the Vogel-Fulcher framework, consistently indicates the formation of interacting magnetic clusters within the hydroxide layers. The observed behavior is governed by both the cation distribution in layers and the nature of the interlayer anions, reflecting the strong sensitivity of the low-temperature magnetic properties to the structural and compositional characteristics of the LDH framework.

Analysis of the heat capacity data reveals that the lattice contribution in Mg-Al analogs bears signatures of both two-dimensional solids and structural glasses, with glassy disorder arising from the intercalated anions. Subtraction of this lattice background from the Co-Al LDH data yields the magnetic heat capacity contribution, C_{mag}, which dominates at low temperatures. In zero applied field, C_{mag} follows a power-law temperature dependence whose exponent is sensitive to the Co/Al ratio, while the application of sufficiently strong magnetic fields drives the behavior toward a conventional magnon-like regime, reflecting the suppression of magnetic correlations in these quasi-two-dimensional systems.

This work was supported by the EU H2020 project European Microkelvin Platform (EMP), grant agreement No. 824109. The research at the B. Verkin ILTPE of NASU was supported by the Department of Physics and Astronomy of the NASU under fundamental scientific programs 0122U001501, 0122U001502. The research at the P.J. Šafárik University was supported by the Slovak Research and Development Agency under grant Nos. APVV-22-0172 and APVV-SK-PT-18-0019 and by the Scientific Grant Agency of the Ministry of Education, Science, Research and Sport of the Slovak Republic under grant No. 1/0132/22.

Field-controlled thermal spin transport in rutile-type altermagnets

Y. I. Gusieva[1, 2], K. V. Yershov[3,4], V. P. Kravchuk[3,4]

[1]G.V. Kurdyumov Institute for Metal Physics of the NAS of Ukraine
[2]Kyiv Academic University of the NAS of Ukraine,
36 Academician Vernadsky Boulevard, Kyiv 03142, Ukraine
[3]Institute for Theoretical Solid State Physics, Leibniz Institute for Solid State and Materials Research, Dresden, D-01069 Dresden, Germany
[4]Bogolyubov Institute for Theoretical Physics of the NAS of Ukraine,
14-B Metrolohichna str., Kyiv 03143, Ukraine
e-mail: yuleva1313@gmail.com

The magnon-driven transport properties of a two-dimensional model of a d-wave altermagnet are investigated. As a case study, we consider a rutile with easy-planar anisotropy (e.g., NiF_2), where the sublattice magnetization vectors lie within the xy-plane in the equilibrium state. An external magnetic field is applied perpendicular to this plane, along the z-axis. The model Hamiltonian accounts for anisotropy, Zeeman interaction, and the complex structure of the Heisenberg exchange, including ferromagnetic, antiferromagnetic, and specific altermagnetic exchange contributions.

We computed the spectrum of spin waves and found that altermagnetism renders magnons chiral, as in the case of the easy-planar g-wave altermagnets [1]. The altermagnetically-induced magnon magnetic moment is k-dependent, and its distribution over the 1st Brillouin zone possesses d-wave symmetry for each magnon branch. The latter results in a magnon-driven spin current in response to an applied temperature gradient, similar to that in easy-axial d-wave altermagnets [2]. The corresponding tensor of the thermal spin conductivity σαβ was derived from the transport Boltzmann equation within the relaxation time approximation. The direction of the spin current is determined by the direction of the temperature gradient relative to the crystallographic axes (Fig. 1). An important finding of this research is the possibility of controlling the spin conductivity by the applied magnetic field. We observe that at low temperatures, the conductivity is governed by the lowest-energy magnon mode, and its temperature dependence follows a T^2-law. However, for high temperatures, σαβ is temperature-independent, and its value and sign are determined by the magnetic field. The field-controlled spin conductivity highlights the potential for tunable magnonic and spin-caloritronic devices, providing a robust mechanism for controlling spin and heat currents at the nanoscale.

This work was supported by the German Federal Ministry of Research, Technology and Space (BMFTR) through the GU-QuMat project (01DK24008).

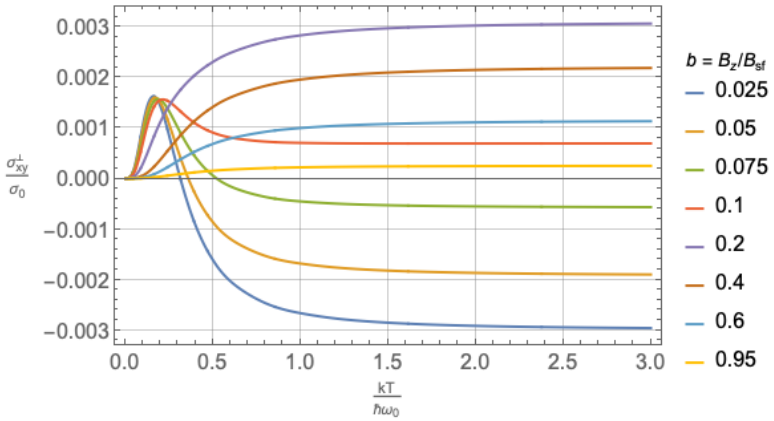

Fig.1 Temperature dependencies of σ_{xy} for different values of the reduced magnetic field $b=B_z/B_{sf}$, where B_{sf} is the critical spin-flip field.

[1] V.P. Kravchuk, et al., Phys. Rev. B, 112, 144421 (2025). https://doi.org/10.1103/zn8d-ft9b.
[2] K.V. Yershov, et al., Phys. Rev. B, 110, 144421 (2024). https://doi.org/10.1103/PhysRevB.110.144421.

Direct and indirect estimates of magnetocaloric response in Fe-Mn-Ga alloys

S. M. Konoplyuk[1], A. V. Kolomiets[2], E. Dzevin[3], V. E. Danilchenko[3]

[1]Institute of magnetism of NASU and MESU, Kyiv 03142, Ukraine
[2]Department of Physics, Lviv Polytechnic National University, Lviv 79005, Ukraine
[3]G.V. Kurdyumov Institute for Metal Physics of NASU, Kyiv 03142, Ukraine
e-mail: konoplyuk.s.m@nas.gov.ua

Fe–Mn–Ga alloys are multifunctional Heusler-family materials capable of shape change via martensitic transformation triggered by a magnetic field [1]. Beyond actuator applications, these alloys show promise for elastocaloric and magnetocaloric refrigeration. Maxwell relation estimates [2] yield a negative magnetic entropy change of approximately 60 J/kg·K at 5 T, associated with a field-induced ferromagnetic-to-antiferromagnetic transition.

In this work, the $Fe_{51.6}Mn_{17.8}Ga_{30.6}$ ferromagnetic shape memory alloy was investigated by magnetic, structural, and magnetocaloric measurements to assess its potential for magnetic refrigeration. The alloy adopts a b.c.c. crystal structure and undergoes a ferromagnetic-to-paramagnetic transition at approximately 200 K. The magnetocaloric effect (MCE) was evaluated over the temperature range of 100–350 K from temperature-dependent magnetization data using the Maxwell relation. The magnetization–temperature curves required for MCE evaluation were reconstructed by fitting experimental data, collected at 0.05, 1, and 7 T, with Brillouin functions. The MCE values derived from magnetization data show good agreement with those obtained from direct measurements at 4 T.

[1] T. Omori, K. Watanabe, R. Y. Umetsu, R. Kainuma, K. Ishida, Appl. Phys. Lett. 95 (2009) 082508. https://doi.org/10.1063/1.3213353.
[2] H. Yang, K. An, Z. H. Nie, Y. D. Wang, B. Tang, T. Peng, Intermetallics 127, 106975 (2020). https://doi.org/10.1016/j.intermet.2020.106975.

Magneto-controlled static and dynamic optical properties of ferro-nematic liquid molecular crystals

A. M. Korostil

V.G.Baryakhtar Institute of Magnetism of the NAS of Ukraine,
36-b Vernadsky Ave., Kyiv, 03142, Ukraine
e-mail: imag@nas.gov.ua

Magneto-nematic liquid crystals represent a class of composite soft materials formed by dispersing magnetic nanoparticles into nematic liquid crystal matrices. Such systems combine the long-range orientational order typical for nematic phases with magnetic sensitivity introduced by the embedded magnetic particles. As a result, magneto-nematic systems exhibit enhanced responses to external magnetic fields compared with conventional nematic liquid crystals. This property makes them promising materials for magnetically controlled photonic and optoelectronic devices.

The optical properties of nematic liquid crystals are determined by the orientation of the director, which defines the anisotropic dielectric tensor of the medium. In magneto-nematic systems, the magnetic nanoparticles interact with the nematic director through surface anchoring and elastic distortions of the liquid crystal matrix. When an external magnetic field is applied, the magnetic moments of the nanoparticles tend to align with the field. Due to the coupling between the nanoparticles and the director field, this alignment induces a reorientation of the nematic director, which leads to changes in the optical anisotropy of the medium.

In the static regime, the reorientation of the director modifies the birefringence of the magneto-nematic layer and therefore changes the intensity of transmitted light in a typical polarizer–liquid crystal–analyzer configuration. The threshold conditions for magnetically induced reorientation depend on several parameters, including the elastic constants of the nematic phase, the magnetic susceptibility of the nanoparticles, the particle concentration, and the strength of the anchoring between nanoparticles and the liquid crystal molecules.

In the dynamic regime, the director response to time-dependent magnetic fields becomes important.

The relaxation and oscillatory dynamics of the director are governed by the balance between magnetic torques, elastic restoring forces, and viscous damping in the liquid crystal. Magnetic nanoparticles can significantly modify the characteristic response times due to additional magnetic torques and particle–director coupling mechanisms. As a consequence, magneto-nematic systems may exhibit enhanced sensitivity and faster response to magnetic stimuli compared with pure nematic liquid crystals.

Understanding the physical mechanisms governing both static and dynamic optical responses is important for the development of magnetically controlled liquid crystal devices. These include tunable optical elements, sensors, and magnetically driven modulators. Theoretical modeling based on continuum descriptions of the director field, coupled with magnetic interactions of nanoparticles, provides insight into the interplay between magnetic, elastic, and viscous effects responsible for the observed optical phenomena.

The analysis of magneto-controlled optical behavior in magneto-nematic liquid crystals opens new possibilities for designing multifunctional soft materials whose optical properties can be tuned by relatively weak magnetic fields. Such systems offer prospects for applications in adaptive photonics, smart optical materials, and magnetically controlled display technologies.

Equilibrium of kink-like torsional deformation of a magnetoactive elastomer in a magnetic field

A. V Kyryliuk[1], Yu. I. Dzhezherya[1,2,3], S. V. Cherepov[1], Yu. B. Skirta[1], S. O. Reshetnyak[1,2], S. M. Ryabchenko[3], V. M. Kalita[1,2,3]

[1]V. G. Baryakhtar Institute of Magnetism of the National Academy of Sciences of Ukraine, 36-b, Akademika Vernads'koho Blvd., Kyiv 03142, Ukraine
[2]National Technical University of Ukraine "Igor Sikorsky Kyiv Polytechnic Institute", 37 Beresteiskyi Ave., Kyiv, 03056, Ukraine
[3]Institute of Physics, NAS of Ukraine, Prospekt Nauky 46, Kyiv 03028, Ukraine
e-mail: ankir007@gmail.com

In this work, we investigate the effect of magnetoelastic moment of forces on the torsional deformation of a MAE beam. [1]. It was found that the moment of force generated by the magnetic field in a magnetized MAE can cause localized kink-like torsional deformation in the MAE beam. Figure 1(a) shows an image of a thin, long MAE beam with aspect ratio $a>>b>>c$. Figure 1(b) shows an image of this beam with uniform torsional deformation in the absence of a magnetic field (**H**=0).

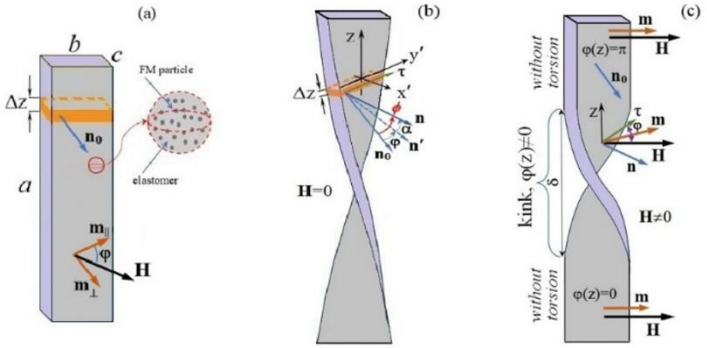

Fig.1

We place a uniformly twisted beam in a uniform magnetic field, H||b. The effect of the moment of forces created by the magnetic field leads to the localization of the torsion region, forming a kink-shaped torsion (Fig. 1(c)) of length δ, outside the torsion region there is no torsion. During the torsion of the beam, its initial normal vector after rotations around the z axis, and then around the y' axis turns into the normal vector of the deformed beam [2] (Fig. 1(b)). The rotation of the normal vector will be equal to the angle between the magnetic field strength vector H and the unit vector $\boldsymbol{\tau}$, which is directed along the selected section in Fig. 1(c).

The total torsional bending energy of the beam can be written as:

$$W = \int_{-\infty}^{+\infty} (w_e(z) + w_m(z))dz = -\frac{aS}{2}\chi_\perp H^2 + \frac{1}{2}\int_{-\infty}^{+\infty} (GJ(\frac{\partial\varphi}{\partial z})^2 - S\Delta\chi H^2\cos^2\varphi)dz\,.$$

Minimizing the energy by finding variational derivatives leads to the differential equation:

$$GJ\frac{\partial^2\varphi}{\partial z^2} - S\Delta\chi H^2\cos\varphi\sin\varphi = 0\,,$$

and its solution for the case of buckling torsion of a beam, regardless of its length:

$$\varphi(z) = 2\arctan e^{z/\lambda}\text{, де } \lambda = \frac{1}{H}\sqrt{\frac{GJ}{S\Delta\chi}}\,.$$

Thus, a kink-like torsion can be stabilized in a beam by a magnetic field if the kink length is less than the beam length, $\delta = \pi\lambda < a$.

[1] A. M. Menzel, Phys. Rep. 554, 1-45 (2015). https://doi.org/10.1016/j.physrep.2014.10.001.
[2] Landau L D and Lifshits E M, *Theory of Elasticity*, Pergamon press, New York, 1959.
.

Residual magnetization of magnetic field-induced bending deformation of a magnetically active elastomer beam

A. V. Kyryliuk[2], V. M. Kalita[1,2,3], Yu. I. Dzhezherya[2,3], S. V. Cherepov[2], Yu. B. Skirta[2], S. O. Reshetnyak[3], A. V. Bodnaruk[1], S. M. Ryabchenko[1]

[1]Institute of Physics, NAS of Ukraine, Prospekt Nauky 46, Kyiv 03028, Ukraine
[2]Institute of Magnetism of the NAS of Ukraine and MES of Ukraine, 36-b Vernadsky Blvd., Kyiv 03142, Ukraine
[3]National Technical University of Ukraine "Igor Sikorsky Kyiv Polytechnic Institute", Prospekt Peremohy 37, Kyiv 03056, Ukraine
e-mail: ankir007@gmail.com

Magnetoactive elastomers (MAE), which belong to the class of "smart" materials, are composites with a filler of magnetic micro- or nanoparticles in a matrix of a highly elastic elastomer [1].

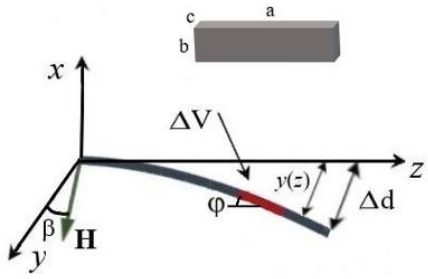

Fig.1

We studied the bending of a beam MAE [2] with one fixed end and the other end free, induced by a transverse magnetic field. In the experiment, we measured the displacement of the free end of the beam, which is indicated by Δd in Fig. 1. During bending, a small section of the beam ΔV rotates in the yz plane, the angle of rotation for the selected section of the beam is indicated by $\varphi(z)$. The angle between the magnetic field **H** and the normal to this small section of the beam is equal to the difference $\beta - \varphi(z)$.

Results: The magnitude of the bending is affected by the direction of the magnetic field sweep, the curves $\delta(H)$, where $\delta=\Delta d/L$ (L- length of the beam), for an increasing or decreasing magnetic field are shifted against each other (Fig. 2).

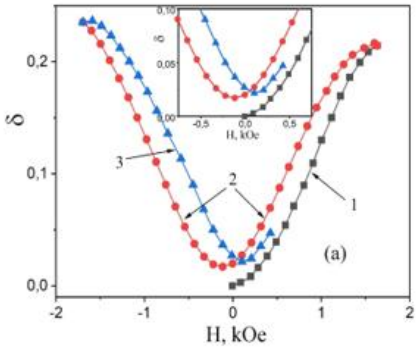

Fig.2

The sign of $\delta(H)$ does not depend on the sign of the field, when the direction of the field changes, $H \rightarrow -H$, the beam bends in the same direction, in a small field it is proportional to H^2.

After the first introduction of the output of the positive field, the beam acquires residual plastic deformation.

Hysteresis $\delta(H)$ can occur:

- due to averaging of local plastic (inelastic) deformations of the elastomer matrix in the vicinity of magnetic nanoparticles.

- due to the slow evolution of displacements of magnetic nanoparticles and matrix environments in the vicinity of their fixation due to the magnetorheological effect.

Conclusion: The change in the shape of the sample occurs mainly due to elastic deformations of the MAE matrix. When the field is removed, the shape of the MAE is almost completely restored. The magnitude of the contribution to the bending from plastic deformation is directly proportional to the square of the magnetic field strength. This fully explains why, due to the residual bending, there is no change in the sign of the bending when the field sign is inverted.

[1] A. M. Menzel, Phys. Rep. 554, 1-45 (2015). https://doi.org/10.1016/j.physrep.2014.10.001.
[2] Y. I. Dzhezherya, W. Xu, S. V. Cherepov, Y. B. Skirta, V. M. Kalita, A. V. Bodnaruk, N. A. Liedienov, A. V. Pashchenko, I. V. Fesych, B. Liu, and G. G. Levchenko, Materials & Design 197, 109281 (2021). https://doi.org/10.1016/j.matdes.2020.109281.

Ab initio study of the electronic structure of orthorhombic iron selenide

A. A. Lyogenkaya, A. S. Panfilov, I. P. Kobzar, A. V. Logosha, G. E. Grechnev, A. V. Fedorchenko

B.Verkin Institute for Low Temperature Physics and Engineering of the NAS of Ukraine, 47 Nauky Ave., Kharkiv, 61103, Ukraine
e-mail: lyogenkaya@ilt.kharkov.ua

FeSe remains one of the most actively studied iron-based superconductors owing to its structural simplicity and the rich interplay between nematicity, magnetism, and superconductivity. Upon cooling below 70–100 K, stoichiometric FeSe undergoes a tetragonal (P4/nmm) to orthorhombic (Cmma) structural transition associated with nematic electronic order. While the electronic structure of the tetragonal phase has been extensively addressed in the literature, the low-temperature orthorhombic phase has received considerably less theoretical attention. In the present work, we report full-potential linearized augmented plane wave (FP-LAPW) calculations for the orthorhombic Cmma phase of FeSe, performed using the Elk code.

We obtain the ground-state electronic structure and analyze the site-projected magnetic moments at the Fe and Se sites, decomposed into spin (S) and orbital (L) contributions, for field orientations along the principal crystallographic axes. The calculations reveal a pronounced magnetic anisotropy governed by a delicate balance between spin and orbital (Van Vleck) moments on the iron sublattice, with the Se sublattice carrying an antiferromagnetically coupled induced moment. The total moment J along the c-axis exceeds that along the a-axis by approximately a factor of three at ambient conditions, reflecting the strong anisotropy of the paramagnetic response in this phase.

Pilot calculations performed for a modest applied pressure of 0.25 GPa demonstrate that even a small compression of the Cmma lattice leads to a marked enhancement of the total moment on iron, driven primarily by a breakdown of spin-orbital compensation: the spin moment increases while the orbital contribution is partially suppressed. This behavior is qualitatively consistent with available experimental susceptibility data for the Cmma phase, where an increase of the magnetic response under pressure is observed.

This work was supported by the Department of Physics and Astronomy of the NASU under fundamental scientific programs 0122U001501.

Temperature changes of magnetic states in Co-doped YIG films probed by magnetic circular dichroism hysteresis loops

M. F. Kharchenko, Yu. M. Kharchenko, O. V. Myloslavska

B.Verkin Institute for Low Temperature Physics and Engineering of NAS of Ukraine,
47 Nauky Ave., Kharkiv, 61103, Ukraine
e-mail: olga.miloslav@gmail.com

In recent years, interest in compounds of the ferrite-garnet family has not waned. In addition to their undoubted value as model objects for fundamental research, these materials are widely used in modern photonics, spintronics, and nanoplasmonics devices. This is to a great extent true for cobalt-doped yttrium iron garnet, known for its unique photomagnetic properties and non-trivial temperature changes in magnetic anisotropy [1].

This work presents the results of studies of the magnetization curves of a 5.8 μm thick $Y_2CaFe_{3.9}Co_{0.1}GeO_{12}$ film grown by liquid-phase epitaxy on a transparent single-crystal $Gd_3Ga_5O_{12}$ substrate with a crystallographic plane (001); the temperature ranged from 200 to 27K.

For measurements of hysteresis curves, the value $(I_1-I_2)/(I_1+I_2)$, was used, where I_1 and I_2 are the intensities of circularly polarized modes with the opposite direction of rotation, at the constant wavelength, λ = 545nm, for which the maximum in the circular dichroism spectrum was earlier observed. The magnetic induction vector and the light wave vector were collinear with the [001] axis and oriented perpendicular to the sample surface.

It is known that in the temperature range from 25 to 300 K, reorientations and rearrangement of the easy magnetization axes of the YIG:Co crystal occur [1]. This temperature behavior of magnetic anisotropy is due to the fact that cobalt ions, which have strong uniaxial anisotropy, replace magneto-isotropic iron ions in the octahedral and tetrahedral sites of iron sublattices. Cobalt doping considerably changes the exchange interaction between magnetic sublattices in the YIG:Co crystal, which causes temperature changes in its magnetic states.

A decrease in temperature from 200 to 27 K leads to a radical change in the profile and parameters of the hysteresis loops in the experimental magnetization curves. The study of the characteristic features of the magnetization curves makes it possible to determine the nature of the temperature evolution of magnetic anisotropy and serves as additional confirmation of the previously obtained experimental results. The identified features allow us to have an idea of the states of domain structures and draw conclusions about their changes with temperature in the $Y_2CaFe_{3.9}Co_{0.1}GeO_{12}$ film. This information may be particularly important for selecting optimal conditions for creating certain magnetic states for practical purposes.

[1] M. Tekielak, A. Stupakiewicz, A. Maziewski and J. M. Desvignes, J. Magn. Magn. Mater. 254–255, 562 (2003). http://doi.org/10.1016/S0304-8853(02)00881-8.

Magnetic fields induced structural modification in magnetoelastic $KEr(MoO_4)_2$

V. Khrustalyov[1], K. Kutko[1], N. Nesterenko[1], D. Kamenskyi[2,3]

[1]B.Verkin Institute for Low Temperature Physics and Engineering of NAS of Ukraine, 47 Nauky Ave., Kharkiv, 61103, Ukraine
[2]Institute of Optical Sensor Systems, German Aerospace Center (DLR), Rutherfordtstr. 2, 12489 Berlin, Germany
[3]Department of Physics, Humboldt-Universität zu Berlin, Newtonstr. 15, 12489 Berlin, Germany
e-mail: nesterenko@ilt.kharkov.ua

The $KEr(MoO_4)_2$ is a "virtual" Jahn–Teller (JT) crystal (space group D_{2h}^{14}), which contains four energy-equivalent rare-earth (RE) Er^{3+} ions in the unit cell, forming two pairs located in different layers [1]. Each RE ion with C2 site symmetry is surrounded by oxygen ions belonging to the tetrahedra formed by $(MoO_4)^{2-}$ complexes. The pairs of RE ions within the layers are coupled by inversion symmetry, while the pairs of RE layers in the unit cell are transformed into each other by a two-fold axis.

In this work, we analyze the origin of the anomalous behavior of low-energy excitations obtained from the study of the Zeeman effect in $KEr(MoO_4)_2$ in external magnetic fields up to 30 T using far-infrared (FIR) spectroscopy. The measured spectra show that in the magnetic field region below $H_{cr1} \approx 5$ T ($\mathbf{H}||a$) and $H_{cr2} \approx 15$ T ($\mathbf{H}||b$), the magnetic field induces mixing of the energy states, which manifest themselves as "anticrossing-type" behavior of some excitations. In this magnetic field range, anomalies are also observed in the magnetic [2], magnetostriction [3], and magnetoresonance [4] properties of $KEr(MoO_4)_2$.

Based on a mathematical analysis of the frequency–field dependences of the energies of low-energy excitations, the magnetic-field dependences of the projection of the magnetic moment of the excited states, m_j, were obtained. Their behavior indicates a strong field dependence of the magnetic anisotropy, which may serve as an indicator of a local lowering of symmetry and point to the presence of magnetic-field-induced structural phase transitions in the studied compound. Taking into account the peculiarities of the crystal structure of $KEr(MoO_4)_2$ and the fact that an external magnetic field, via spin–orbit coupling, affects the magnetic moments orientation of the RE ions, we assume that a field-induced structural phase transition near H_{cr} may occurs. This is accompanied by rotations of the molybdenum tetrahedra surrounding the Er^{3+} ions, which play a significant role in the elastic-type ordering. A similar scenario may also be realized in other members of series of double rare-earth molybdates, and this approach allows us to discuss the nature of magnetoelasticity in these compounds.

[1] S. Chong, S. Perry, B. J. Riley and Z. J. Nelson, Acta Crystallogr., Sec. E 76, 1871 (2020). https://doi.org/10.1107/S205698902001542X.
[2] K. Kutko, B. Bernáth, V. Khrustalyov, et al., Phys. Rev. B 109, 024438 (2024). https://doi.org/10.1103/PhysRevB.109.024438.
[3] B. Bernáth, K. Kutko, S. Wiedmann, et al., Adv. Electron. Mater. 8, 2100770 (2022). https://doi.org/10.1002/aelm.202100770.
[4] V. I. Kut'ko, Low Temp. Phys. 31, 1 (2005). https://doi.org/10.1063/1.1820349.

Anomalous Hall effect in graphite intercalation compounds with cobalt

I. Ovsiienko[1], T. Len[1], L. Matzui[1], Yu. Prylutskyy[2], I. Mirzoiev[3], P. Lishchuk[1]

[1,2]Taras Shevchenko National University of Kyiv, Departments of Physic[1] and Biophysics[2], Volodymyrska Str., 64/13, 01601, Kyiv, Ukraine
[3]B.Verkin Institute for Low Temperature Physics and Engineering of NAS of Ukraine, 47 Nauky Ave.,61103, Kharkiv, Ukraine
e-mail: iaryna2002@gmail.com

The work presents the results of experimental investigations of Hall effectin graphite intercalation compounds (GICs) with cobalt.

For intercalation highly oriented pyrolytic graphite (HOPG) with a crystallite size (L) of ~ 100 nm, a distance between nearest graphite layers (d_{002}) of 0.335 nm, and a preferred orientation parameter(η) of 10^5 was chosen as the source. A two-step procedure was used for graphite intercalation, with compound C_8K serving as the precursor. According to X-ray diffraction data, intercalated compound of the second stage with cobalt (an identity period $I_s = 0.975$ nm) were obtained. The electrical resistance and Hall voltage of the GIC samples were measured using the standard four-probe method, with a constant current, over a temperature interval of (1.6–293) K, and in a magnetic field of up to 5 T.

The studies have revealed that the intercalation of graphite with cobalt causes significant changes in its transport properties. In particular, after intercalation, the sign of the temperature coefficient of resistance changes from negative (for the source HOPG) to positive (for GIC).Also, the temperature dependence of the Hall coefficient disappears for GIC, and its value decreases by almost two orders of magnitude.Such changes in transport properties are typicalfor intercalation compounds of low stages and are associated with enrichment of graphite layers with additional charge after intercalation.As a result, the concentration of free charge carriers in the intercalation compound increases significantly, while the concentration of charge carriers is almost independent of temperature.

However, the studies revealed anomalous field dependencies of the Hall coefficient $R_H(B)$ at different temperatures GIC with Co, as shown in the Figure.

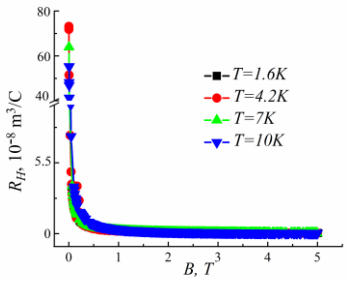

Fig. Field dependences of the Hall coefficient $R_H(B)$ for GIC with Co at different temperatures

As can be seen from the Figure, dependence $R_H(B)$ shows two distinct intervals: one where the Hall coefficient decreases sharply with increasing magnetic field magnitude, and one where the Hall coefficient is independent of the magnetic field.

As is well known, the Hall effect is caused by the action of the Lorentz force on current carriers in a magnetic field that is perpendicular to their direction of motion. The Hall coefficient is independent of the magnetic field strength. The expression for the Hall coefficient in magnetic materials includes a second term that is proportional to the material's magnetisation. This term is known as the anomalous Hall effect (AHE). As shown in [1], the anomalous Hall coefficient (R_{AH}) for magnetic granular alloys varies non-monotonically with the change in the magnetic field due to the influence of the latter on the scattering of charge carriers. Additionally, the dependence $R_{AH}(B)$ is determined by the size of the magnetic granules.Given the high concentration of charge carriers in graphite layers and the presence of magnetic inclusions at the GICs boundaries, it is reasonable to assume that asymmetric scattering, which is caused by the spin-orbit interaction between the charge carriers and the magnetic moments of the intercalate atoms, leads to the formation of AHE in GIC with Co.

[1] A. Granovsky, F. Brouers, A. Kalitsov and M. Chshiev, J. Magn. Magn. Mater. 166, 193 (1997) https://doi.org/10.1016/S0304-8853(96)00494-5.

Raman spectroscopy studies of the $HoFe_3(BO_3)_4$ single crystal

A. V. Peschanskii[1], A. Yu. Glamazda[1,2], V. P. Gnezdilov[1]

[1]B.Verkin Institute for Low Temperature Physics and Engineering of the NAS of Ukraine, 47 Nauky Ave., Kharkiv, 61103, Ukraine
[2]V.N. Karazin Kharkiv National University, 4 Svobody Sq., Kharkiv, 61022, Ukraine
e-mail: peschansky@ilt.kharkov.ua

In recent years, the physical properties of the rare-earth ferroborate multiferroic family, $ReFe_3(BO_3)_4$ (where Re = La – Lu), have been under intensive study. This interest is caused by the observation of a large magnetoelectric effect, which enables the control of electrical properties via an external magnetic field. While Raman scattering spectra for a number of crystals (Re = Sm, Gd, Nd, Tb, Er, and Y) have been investigated over a wide temperature range covering various structural and magnetic phases, such studies for the $HoFe_3(BO_3)_4$ single crystal in the low-temperature range have not yet been conducted.

In this work, we investigated the polarized Raman spectra of a $HoFe_3(BO_3)_4$ single crystal in the frequency range of 3–1500 cm^{-1} and at temperatures from 10 to 300 K. Figure 1 shows the spectra obtained at 10 K. The Raman-active modes are identified as follows: A_1 – (*ZZ)* and E – (*YX*, *ZX*, and *YZ)*.

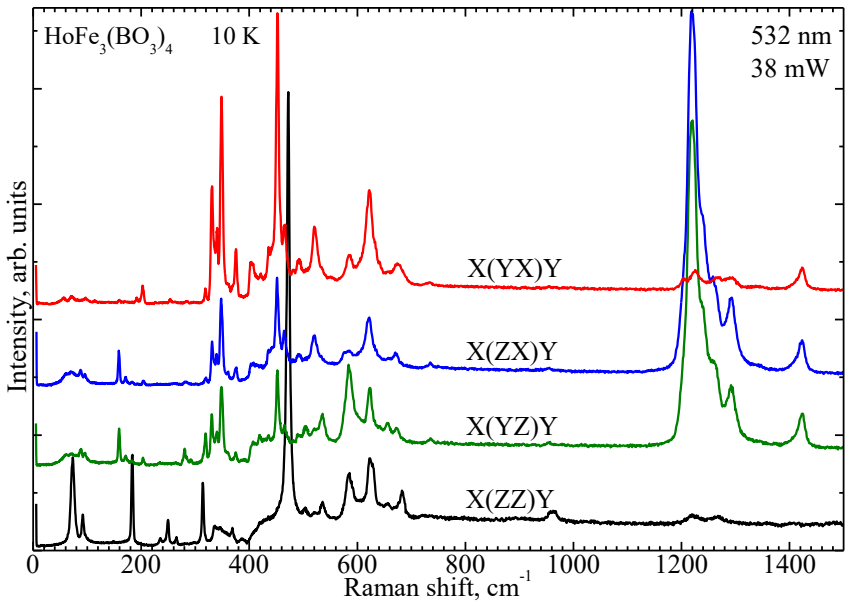

Fig. 1. Polarized Raman spectra of $HoFe_3(BO_3)_4$ crystal at 10 K. Spectral resolution 3.0 cm^{-1}.

At low temperatures, the Raman spectrum (Fig. 1) exhibits phonon modes characteristic of both high-temperature and low-temperature phases (T_C = 366 K). Below the Neel temperature (T_N = 38 K), two-magnon scattering is observed in the low-frequency region of the spectrum. Additionally, in the range of 330 – 680 cm^{-1}, the phonon spectrum and the luminescence spectrum overlap. To identify and extract these excitations, we have studied the temperature evolution of the spectra and conducted a comparative analysis with the spectra of $TbFe_3(BO_3)_4$ [1] and $SmFe_3(BO_3)_4$ [2], the latter of which does not undergo a structural phase transition.

The work was carried out with the support of the budget research project: code 1.4.10.4.14 state registration number 0122U001502.

[1] A. V. Peschanskii, A. V. Yeremenko, V. I. Fomin, L. N. Bezmaternykh, I. A. Gudim, Low Temp. Phys. 40, 171 (2014). https://doi.org/10.1063/1.4865566.
[2] A. V. Peschanskii, V. I. Fomin, I. A. Gudim, Low Temp. Phys. 42, 475 (2016). https://doi.org/10.1063/1.4954783.

Low temperature optical absorption spectra of $Nd_{0.75}Dy_{0.25}Fe_3(BO_3)_4$ ferroborate

V. G. Piryatinskaya, I. S. Kachur

B.Verkin Institute for Low Temperature Physics and Engineering of the NAS of Ukraine,
47 Nauky Ave., Kharkiv, 61103, Ukraine
e-mail: piryatinskaya@ilt.kharkov.ua

$Nd_{1-x}Dy_xFe_3(BO_3)_4$ compounds belong to the family of rare-earth trigonal ferroborates which are of interest due to a wide variety of magnetic properties and multiferroic effects. Substituted ferroborates can exhibit new magnetic reorientation transitions caused by the competition of magnetic anisotropies of different rare-earth ions. In $Nd_{0.75}Dy_{0.25}Fe_3(BO_3)_4$ antiferromagnetic ordering occurs at T_N = 32 K. The crystal exhibits two spontaneous spin-reorientation transitions at T_{cr1} = 25 K and T_{cr2} = 16 K [1]. It was established that at $T_{cr1} < T < T_N$ easy-plane magnetic structure is realized and the range $T < T_{cr2}$ corresponds to easy-axis phase [1].

In the present work we study low temperature optical absorption spectra of the $Nd_{0.75}Dy_{0.25}Fe_3(BO_3)_4$ crystal in the region of optical transition $^4I_{9/2} \rightarrow {}^2H_{11/2}$ of Nd^{3+} in σ- and π-polarizations. Both reorientation phase transitions, T_{cr1} and T_{cr2}, reveal themselves in the absorption spectra. However, no significant changes are observed in the σ-spectra, indicating that the reorientation of magnetic moments has a very weak effect on the energies of electron transitions and the exchange splitting of states. The substantial transformation of the π-polarized spectra (Fig. 1) is associated with a change in the intensities of transitions between different splitting components of neodymium Kramers doublets. The latter is caused by modification of selection rules of optical transitions with the change of magnetic structure from the easy-axis to the easy-plane type.

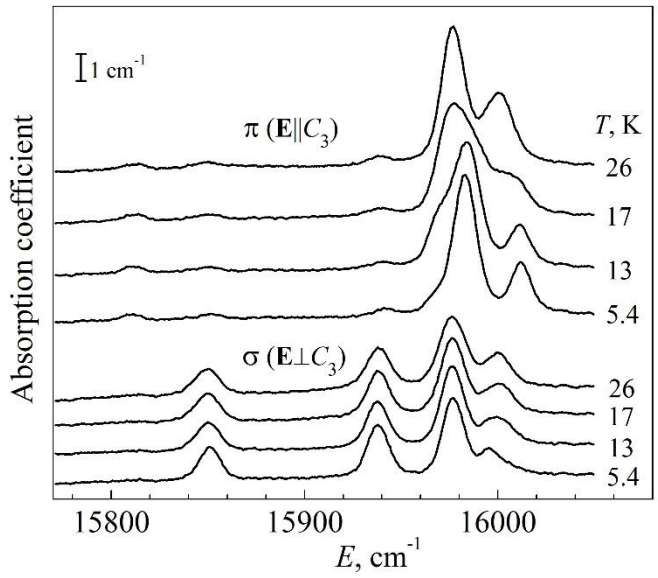

Fig. 1. Absorption spectra of $Nd_{0.75}Dy_{0.25}Fe_3(BO_3)_4$ in the region of optical transition $^4I_{9/2} \rightarrow {}^2H_{11/2}$ in σ- and π-polarizations at different temperatures.

[1] G. A. Zvyagina, K. R. Zhekov, A. A. Zvyagin, I. A. Gudim, and I. V. Bilych, Low Temp. Phys. 38, 446 (2012). https://doi.org/10.1063/1.4707947.

Low-temperature magnetometry and EPR studies of $Ca_3Y_2(BO_3)_4$:Nd (0.75 wt.%) single crystal

S. N. Poperezhai[1], D. N. Merenkov[1], V. A. Bedarev[1], A. N. Shekhovtsov[2], M. B. Kosmyna[2], A. A. Prokhorov[3], A. Sedda[4], E. Lähderanta[4]

[1]B.Verkin Institute for Low Temperature Physics and Engineering of NAS of Ukraine, 47 Nauky Ave., 61103, Kharkiv, Ukraine
[2]Institute for Single Crystals, National Academy of Sciences of Ukraine, 60 Nauky Ave., 61072, Kharkiv, Ukraine
[3]Institute of Physics of the Czech Academy of Sciences, Na Slovance 1999/2, 182 00, Prague, Czech Republic
[4]Lappeenranta-Lahti University of Technology, LUT School of Engineering Science, Yliopistonkatu 34, 53850 Lappeenranta, Finland
e-mail: dr.bedarev@gmail.com

The isostructural single crystals of the $Ca_3RE_2(BO_3)_4$ (space group Pnma, Z = 4, RE - rare-earth element) family are known as promising laser materials. Moreover, an application area of these crystals may be extended to magneto-optics, quantum memory and optical signal processing. Recently a number of pure and doped $Ca_3RE_2(BO_3)_4$ crystals have been grown and their spectroscopic characteristics and laser operation have been reported. At the same time, the low-temperature magnetic properties of RE-calcium borates remain mostly unexplored. Calcium and RE cations are statistically distributed over three cationic sites in these compounds. This may affect their magnetic properties and lead to interesting effects. In addition, spin-spin interactions have been observed in $Ca_3Nd_2(BO_3)_4$ crystals with complete replacement of non-magnetic Y by magnetic Nd at temperatures close to the temperature of liquid helium. Therefore, low-temperature studies of the magnetic and resonance properties of $Ca_3Y_2(BO_3)_4$:Nd single crystals are relevant.

A single crystal of $Ca_3Y_2(BO_3)_4$:Nd (0.75 wt.%) was grown in the [100] direction using the Czochralski method. The grown crystals was examined by X-ray diffraction. No impurity phases and gas bubble inclusions were detected. In further studies, the direction of the external field ***H*** coincided with the direction of crystal growth.

The results of low-temperature (T = 2 – 25 K) measurements of the magnetic moment of the $Ca_3Y_2(BO_3)_4$:Nd (0.75 wt.%) crystal as a function of H and T are well described by Curie's law with an effective g-factor of the main doublet $g_{eff} \approx 3.52$. The EPR spectra were measured in X-band at T = 5 – 25 K. All of them show a clearly distinguishable line with the intensity increases with decreasing temperature. The line was observed in the field $H_1 \approx 1.7$ kOe. The g-factor of this line is estimated to be $g_{epr} \approx 3.5$. The intense line is associated with transitions between the levels of the ground doublet. Furthermore, at temperatures of 11 K and below, a less intense absorption line is clearly observed in the spectrum in the field $H_2 \approx 3.4$ kOe. It is twice as high as the resonance field of the main line. The second line may be associated with two-photon absorption in the $Ca_3Y_2(BO_3)_4$:Nd crystal with a change in the magnetic quantum number $\Delta m_s = \pm 2$. These transitions are forbidden by selection rules. However, they can become observable due to various interactions in the system, such as spin-spin or spin-orbit interactions. In addition, the low symmetry of the $Ca_3Y_2(BO_3)_4$:Nd single crystal can lead to mixing of quantum states and weaken selection rules, making two-photon absorption possible and observable. The intensity of two-photon absorption is very sensitive to the direction of the magnetic field. It has been established that a small deviation (~ 1°) of the magnetic field from the orthorhombic axis of the crystal leads to a sharp drop in the intensity of the higher field line.

As a result, based on magnetic and resonance low-temperature measurements of a $Ca_3Y_2(BO_3)_4$:Nd (0.75 wt.%) single crystal, the g-factor of the ground doublet at the [100] direction was evaluated. A resonance line associated with two-photon absorption was identified in the EPR spectra.

Low-temperature thermal properties of Dy-doped $Dy_xY_{1-x}(PO_3)_3$ phosphate glasses

V. Stadnyk[1], V. Tkáč[1], M. Tokarčík[1], P. Baloh[2], R. Tarasenko[1], E. Čižmár[1], M. Orendáč[1], A. Orendáčová[1], J. Holubová[3], E. Černošková[3], Z. Černošek[3] and A. Feher[1]

[1]Institute of Physics, Faculty of Science, P. J. Šafárik University in Košice, Park Angelinum 9, 041 54 Košice, Slovakia
[2]International Institute for Carbon-Neutral Energy Research, Kyushu University (I2CNER), 744 Motooka, Nishi-ku, Fukuoka 819-0395, Japan
[3]Department of General and Inorganic Chemistry, Faculty of Chemical Technology, University of Pardubice, Studentská 573, 532 10 Pardubice, Czech Republic
e-mail: vladyslav.stadnyk@student.upjs.sk

This work focuses on the investigation of the low-temperature thermal behaviour of $Dy_xY_{1-x}(PO_3)_3$ phosphate glasses containing different concentrations of Dy^{3+} rare-earth ions. A set of samples with Dy^{3+} content x = (0, 0.0001, 0.001, 0.01, 0.1, 1) was examined using heat-capacity and thermal conductivity measurements. The heat capacity C_P was determined by the relaxation method over the temperature range 0.4-20 K in magnetic fields up to 9 T. Thermal conductivity $\kappa(T)$ was measured by a two-probe technique over a broad temperature range from 1.8 to 300 K.

The obtained heat-capacity data exhibit a pronounced boson peak in the Cp/T^3 representation for all investigated compositions, indicating the presence of universal low-energy excitations typical for disordered glassy systems. In samples containing Dy^{3+} ions, an additional contribution appears in the form of a Schottky-type anomaly, which originates from the splitting of the Dy^{3+} energy levels.

The temperature dependence of thermal conductivity $\kappa(T)$ shows typical glass-like behaviour, including a plateau in the temperature region between about 5 K and 20 K. Below approximately 5K, $\kappa(T)$ follows an almost quadratic temperature dependence, whereas above ~15 K a gradual increase in thermal conductivity is observed. The introduction of magnetic Dy^{3+} ions leads to a noticeable modification of phonon transport and changes the absolute values of thermal conductivity. These findings highlight the importance of magnetic scattering processes and phonon–spin interactions in heat transport in Dy^{3+}-doped phosphate glasses.

This work was supported by Projects APVV-22-0172 and VEGA 1/049/26.

OPTICS, PHOTONICS AND OPTICAL SPECTROSCOPY

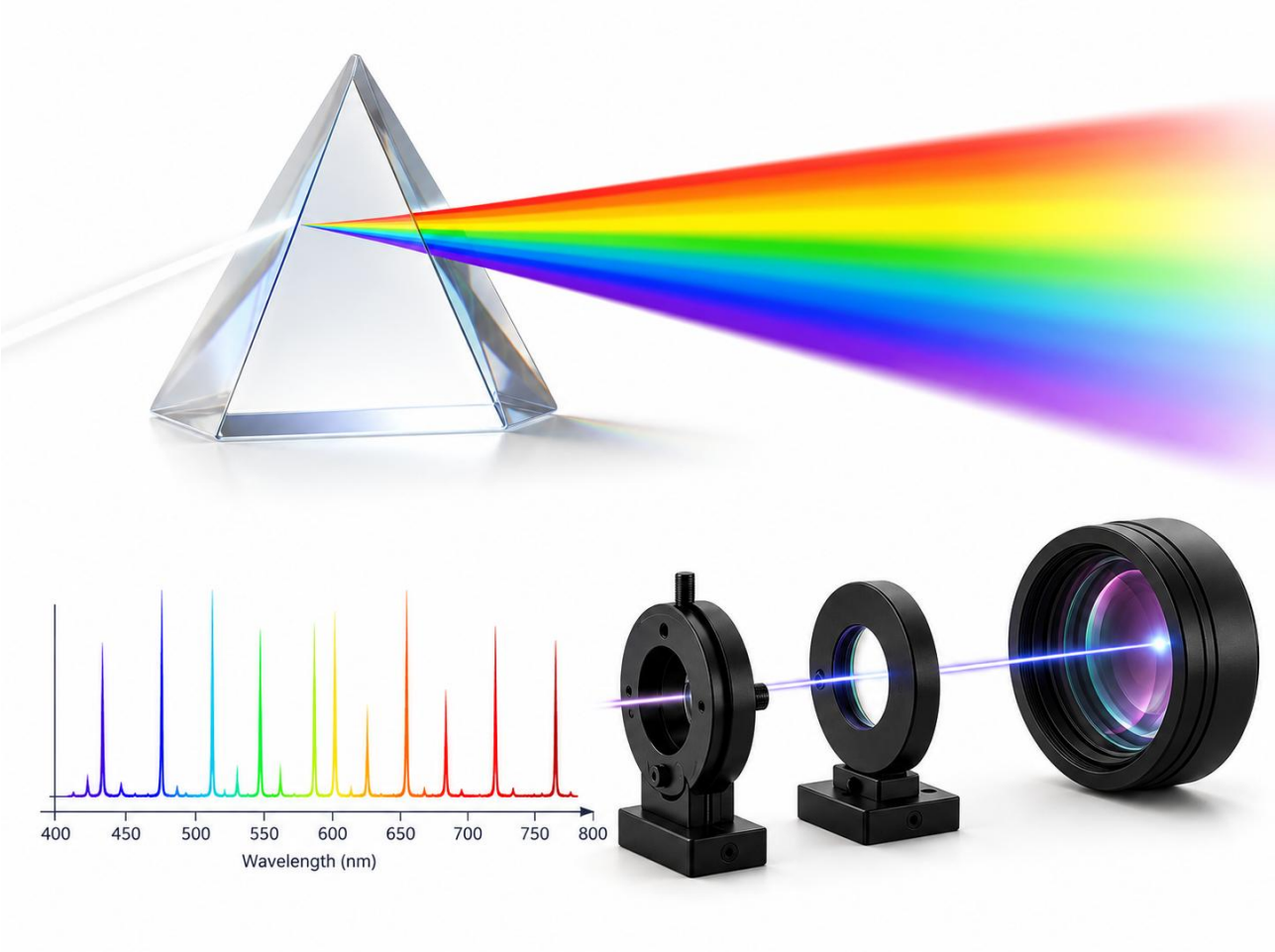

High-speed photonic VQE: overcoming optimization latency with liquid crystals

B. Bilash[1,2*], I. Ali[1,2], J. Lee[1,2], D. Parvatharajan[1], H.-T. Lim[1,2], and Y.-S. Kim[1,2†]

[1]Center for Quantum Technology, KIST, Seoul, Republic of Korea
[2]Division of Quantum Information, KIST School, UST, Seoul, Republic of Korea
e-mail: bohdan@kist.re.kr

The Variational Quantum Eigensolver (VQE) relies on a continuous feedback loop: a quantum processor evaluates the energy of a parameterized trial state, and a classical computer updates those parameters to search for a molecular ground-state energy. Photonic platforms are highly advantageous for this task; a single photon can encode multi-dimensional ququart states using both path and polarization, enabling Bell State Measurements (BSM) that significantly reduce the number of required energy measurements [1,2]. However, the classical-quantum feedback loop suffers from a severe physical bottleneck: updating the trial state traditionally requires mechanically rotating motorized waveplates, which inflates the runtime of a single VQE experiment to several hours. To resolve this latency, we introduce a motionless state-preparation architecture using voltage-controlled Liquid Crystals (LCs). By modulating LC voltages, we achieve millisecond-scale parameter switching. Integrating this ultrafast LC preparation with the measurement-reducing BSM scheme entirely eliminates mechanical delays. Validated through the energy estimation of molecular Hamiltonians, our approach slashes VQE runtimes from hours to minutes, unlocking the potential for dynamic, real-time photonic quantum simulations.

[1] Lee, Donghwa, et al., Error-mitigated photonic variational quantum eigensolver using a single-photon ququart, Optica 9, 88-95 (2022).
[2] Lee, Jinil, et al., Photonic variational quantum eigensolver using entanglement measurements, Quantum Science and Technology 9 045028 (2024).

Features of surface waves in extremely anisotropic media

A. F. Bukhanko

Donetsk Institute for Physics and Engineering named after O.O. Galkin of NAS of Ukraine,
46 Nauky ave., Kyiv, 03028, Ukraine
e-mail: metatem@ukr.net

We have been interested in extremely anisotropic metamaterials with the surface waves [1-3]. We have reinvestigated the propagation of a surface waves on interface with a discontinuity. By the boundary conditions we obtained analytical relations based on the existence of radiation modes. This phenomenon was demonstrated by numerical simulations.

We report about the existence of quasi-surface waves characterized radiative components in extremely anisotropic metamaterials. We identify the conditions for the existence of such modes, and explain their properties.

We demonstrate that the characteristics of surface waves can be changed by reflection and refraction. The generalized refraction laws for surface waves were obtained. We present simple mathematical model based on Fresnel equations to calculate the reflection and refraction characteristics of the surface waves in extremely anisotropic metamaterials.

[1] O. El Gawhary, A. J. L. Adam, and H. P. Urbach, Phys.Rev. A 89, 023834 (2014) https://doi.org/10.1103/PhysRevA.89.023834.
[2] Jie Luo, Ping Xu, Huanyang Chen, Bo Hou, Lei Gao, and Yun Lai, Applied Physics Letters 100, 221903 (2012) http://dx.doi.org/10.1063/1.4723844.
[3]. Shu Wei-Xing, Luo Hai-Lu, Li Fei and Ren Zhong-Zhou, Chinese Phys. Lett. 23, 3084 (2006) http://dx.doi.org/ 10.1088/0256-307X/23/11/055.

Influence of the distribution of energies of monomers on dynamical characteristics of molecular aggregates

I. Yu. Ropakova[1], A. A. Zvyagin[2]

[1]Institute for Scintillation Materials of the NAS of Ukraine,
60 Nauky Ave., Kharkiv, 61001, Ukraine
[2]B.Verkin Institute for Low Temperature Physics and Engineering of the NAS of Ukraine,
47 Nauky Ave., Kharkiv, 61103, Ukraine
e-mail: adelma@ukr.net

Organic molecules of dyes often aggregate in solutions or at the interfaces between solids and liquids. That self-association is mostly caused by the strong inter-molecular van der Waals-like attraction between molecular monomers. Such molecular aggregates exhibit optical properties different from the ones of molecular monomers, which form aggregates. The main difference of optical spectra of molecular aggregates is their bathochromic red shifts and narrowing of lines (comparing to the ones of monomers), caused by the inter-monomer aggregation. Such molecular aggregates are known as J-aggregates (due to E.E. Jelly). Other molecular aggregates manifest hypsochromic blue shifts, comparing to the spectrum of a monomer. They are known as H-aggregates. Aggregates of organic dyes have been the subject of many investigations by various methods.

In molecular aggregates charge overlaps of wave functions of neighboring molecules is small. Their binding energy is large. Therefore, optical properties of molecular aggregates are described by Frenkel excitons (i.e., electron-hole pairs carrying no charge). For Frenkel excitons typical space separations between electrons and holes are essentially zero. An electron and a hole of the Frenkel exciton occur at the same molecule. Most of molecular aggregates are low-dimensional systems. In our theoretical study we limit ourselves with dynamical properties of one-dimensional molecular aggregates. For that purpose we develop the linear response quantum many-body theory of Frenkel excitons within the one-dimensional model, to which the electromagnetic field of optical frequency is applied. In our study we exactly take into account the Pauli statistics of excitons.

Randomness in distributions of parameters of molecular aggregates often play the essential role in their optical properties. We assume that the energies of monomers, which form molecular aggregates, are randomly distributed according to the Lorentz (Cauchi) distribution. The calculated real and imaginary parts of the dynamical susceptibility and other dynamical characteristics of the considered system manifest the reduction of magnitudes and broadening of the resonance features of those characteristics close to the edges of exciton band (red, or blue ones for J- or H-aggregates, respectively). Those reduction and broadening depend on the strength of randomness: The stronger level of randomness, the broader and weaker features of dynamical characteristics near the edges of the exciton band of the molecular aggregate. We show that similar behavior is related to the normal (Gaussian), or Levi distributions of the energies of monomers.

We prove that such a behavior is very different from the one of the one-dimensional exciton model with randomly distributed (according to the Bernoulli law) amplitudes of hopping between neighboring molecular monomers. For the latter the spectral weight of dynamical characteristics of the molecular aggregate is distributed over the total exciton band, revealing features at both edges of the band, depending on the strength of randomness.

The research of I.Yu.R. is performed within the program "Splinter" of the NAS of Ukraine. The research of A.A.Z. is performed within the program "Ensembles of random matrices, models of quantum multi-level and multi-particle systems, nonlinear integrable equations and abstract evolution equations" of the NAS of Ukraine, the registration number 0126U001858.

Using an optimization algorithm to improve the metrological performance of a surface plasmon resonance biosensor

R. S. Terekhov[1], Z. E. Eremenko[1,2], S. M. Kulish[1,3]

[1]O. Ya. Usikov Institute for Radiophysics and Electronics of NAS of Ukraine
[2]Leibniz Institute for Solid State and Materials Research
[3]National Aerospace University "Kharkiv Aviation Institute", NAU "KhAI"
e-mail: r.s.terekhov@gmail.com

The use of biosensors based on the surface plasmon resonance (SPR) phenomenon in the fields of medicine and ecology plays a significant role in the modern world [1]. Current research on SPR sensors employing layered nanomaterial structures to enhance sensitivity is primarily focused on selecting the optimal thickness of each layer in order to achieve the desired metrological characteristics. However, this approach becomes inefficient as the number of layers or materials increases, since it requires considerable computational time and resources [2].

To address this limitation, the application of optimization algorithms is proposed. This approach is particularly promising for determining the optimal geometric parameters of thin-film SPR sensor structures, as it enables the solution of a multi-parameter problem that lacks an analytical formulation.

Numerical modeling was carried out using COMSOL Multiphysics 6.4. The optimization problem was solved using the Nelder-Mead algorithm, a gradient-free numerical method for function minimization based on iterative transformations of a simplex in parameter space. The optimal thickness of the MXene layer was found to be 4.27 nm, which is relatively large; compared to our previous work [3], this value is approximately twice as high. Silver was used as a plasmon-supporting layer, with an optimal thickness of 56 nm, which is typical for such sensor configurations. The additional graphene layer acts as a damping medium for surface plasmons due to its high electrical conductivity [4]. This results in stronger localization of surface plasmons at the interface and an increase in the quality factor of the resonant structure.

As a result of the optimization and modeling, a sensor with a sensitivity of 145°/RIU was obtained. This value is 14% higher than that reported in our previous work [3], where no optimization algorithm was applied (127.6°/RIU), and 18% higher than that of a similar structure reported by Kirki [5] (123°/RIU).

[1] M. A. Butt, Surface Plasmon Resonance-Based Biodetection Systems: Principles, Progress and Applications—A Comprehensive Review, Biosensors, vol. 15, no. 1, p. 35, Jan. 2025, doi: 10.3390/bios15010035.
[2] M. R. Villarim, D. R. Belfort, and C. P. De Souza, A Surface Plasmon Resonance (SPR)-Based Biosensor Simulation Platform for Performance Evaluation of Different Constructional Configurations, Coatings, vol. 13, no. 3, p. 546, Mar. 2023, doi: 10.3390/coatings13030546.
[3] R. Terekhov, Z. Eremenko, and S. Kulish, Increasing the sensitivity of a surface plasmon resonance sensor using Ti3C2 MXene, Low Temp. Phys., vol. 52, no. 2, pp. 218–223, Feb. 2026, doi: 10.1063/10.0042358.
[4] M. Sang, J. Shin, K. Kim, and K. J. Yu, Electronic and Thermal Properties of Graphene and Recent Advances in Graphene Based Electronics Applications, Nanomaterials, vol. 9, no. 3, p. 374, Mar. 2019, doi: 10.3390/nano9030374.
[5] B. Karki, A. Jha, A. Pal, and V. Srivastava, Sensitivity enhancement of refractive index-based surface plasmon resonance sensor for glucose detection, Opt. Quantum Electron., vol. 54, no. 9, p. 595, Sep. 2022, doi: 10.1007/s11082-022-04004-z.

An ordered composite based on dimers of metal nanoshells as a "left-handed" medium

L. O. Abramenko[1], A. V. Korotun[1,2], V. P. Kurbatsky[1]

[1]National University Zaporizhzhia Politechnic, 64 Universytetska Str., Zaporizhzhia, 69011, Ukraine
[2]G.V. Kurdyumov Institute for Metal Physics of the NAS of Ukraine, 36 Academician Vernadsky Blvd., Kyiv, 03142, Ukraine
e-mail: andko@zp.edu.ua

Currently, there is an intensive search for architectures of synthetic materials with unique optical properties, including negative refraction, the inverse Doppler effect, and superresolution. Such materials are metal-dielectric composites consisting of periodically arranged subwavelength unit cells (meta-atoms). In [1], a cubic cell with dimers of spherical metal nanoparticles located on its faces was considered as a meta-atom in an ordered composite. A drawback of the architecture proposed in this work is the extremely narrow spectral range in which the nanocomposite has a negative refractive index. Finding the shape and size of structural elements that make a nanocomposite become a "left-handed" medium is a pressing task.

This paper examines the optical properties of an ordered nanocomposite based on cubic unit cells with dimers of spherical shell particles, which represent a dielectric core covered by a metal shell. Using effective medium theory, the frequency dependences of the permittivity and magnetic permeability, as well as the absorption coefficient, of this composite are obtained. The evolution of the extremes of the real and imaginary parts of the dielectric and magnetic polarizability for a cubic unit cell with dimers of shell particles on its faces is studied. Spectral ranges are found in which nanocomposites with dimers of particles of different sizes and made of different materials exhibit the properties of a "left-handed" medium.

[1] L. O. Abramenko, V.M. Matiushyn, and A. V. Korotun, Funct. Mater., 32, 21 (2025). http://dx.doi.org/ 10.15407/fm32.01.21.

Optical phenomena in a hybrid system based on a semiconductor quantum dot and prolate spheroidal metallic nanoparticle

R. Yu. Korolkov, O. Yu. Berezhnyi

National University Zaporizhzhia Politechnic,
64 Universytetska Str., Zaporizhzhia, 69011, Ukraine
e-mail: romankor@zp.edu.ua

The study of the interaction between light and matter in the semiconductor nanostructures attracts the attention of the researchers for the use in optoelectronics. In order to optimize this interaction, it is proposed to create the quantum dots in the neighborhood of the metallic nanoparticles of different geometries and, accordingly, to obtain the hybrid "metal-semiconductor" nanostructures. An interesting effect observed in the hybrid systems, which are under the consideration, is the excitation of excitons and the presence of various modes of plasmon-exciton interaction. It should be pointed out that the optical properties of the hybrid system "spherical metallic nanoparticle – semiconductor quantum dot" are fairly well described in the scientific literature. For example, in [1], light absorption in such a hybrid system was studied and the factors, which influence the spectral position of the absorption coefficient maxima were established. At the same time, the optical properties of the considered nanosystems with metallic nanoparticles of non-spherical geometry have been poorly studied, so such problems are relevant.

We investigate the hybrid system, which consists of the prolate spheroidal metallic nanoparticle and the semiconductor quantum dot located on its axis. It should be pointed out that the optical properties of the spheroidal nanoparticle can be described within the framework of the quasi-static approximation (since the characteristic sizes of the system are significantly less than the wavelength). In this case, the semiconductor quantum dot is considered to be two-level system, and the spatial dispersion of the permittivity is taken into account for the nanoparticles. In addition, the paper investigates the influence of the electron relaxation processes in the nanoparticles on the absorption of light by the hybrid system.

The results of the calculations indicate the presence of the sharp maxima of the susceptibilities of the spheroidal metallic nanoparticles and semiconductor quantum dots, as well as the sharp maxima of the the absorption coefficient of the hybrid nanosystem. It is shown that in the system, which is under consideration, it is necessary to take into account the relaxation processes that determine the width of the resonance peaks observed in the experiment.

[1] R. Korolkov, O. Berezhnyi, and A. Korotun, Proc. 2025 IEEE 15th Intern. Conf. NAP 2025, UBMP041 (September, 07-12, 2025). http://dx.doi.org/10.1109/NAP68437.2025.11216264.

Electromagnetic waves on the surface of a composite with spheroidal nanoshells

N. I. Pavlyshche[1], A. V. Korotun[1,2], V. I. Reva[1], D. O. Chyslov[1], I. M. Titov[1]

[1]National University Zaporizhzhia Politechnic,
64 Universytetska Str., Zaporizhzhia, 69011, Ukraine
[2]G.V. Kurdyumov Institute for Metal Physics of the NAS of Ukraine,
36 Academician Vernadsky Blvd., Kyiv, 03142, Ukraine
e-mail: andko@zp.edu.ua

The study of the waves, which propagate at the interface between a composite with the inclusions of different geometry and composition and the surrounding environment is the relevant problem related to the applications in optoelectronic and nanophotonic technologies. It should be pointed out that virtually all available scientific literature is devoted to the study of the optical properties of the composites with the monometallic inclusions of the different shapes. The use of the shell nanoparticles as the inclusions is of interest due to the additional possibilities for controlling the optical properties of the particle inclusions (and thus the entire nanocomposite) by changing the materials and sizes of the core and shell.

Let us consider the composite with the spheroidal metallic nanoshells randomly embedded into the matrix dielectric. Applying the effective medium theory and assuming a low concentration of the particle inclusions, the following formula can be obtained for the frequency dependence of the effective permittivity of the nanocomposite, which is under the study

$$\varepsilon_{\text{eff}}(\omega) = \varepsilon_{\text{m}} \frac{a_4\varepsilon_{\text{s}}^4 + a_3\varepsilon_{\text{s}}^3 + a_2\varepsilon_{\text{s}}^2 + a_1\varepsilon_{\text{s}} + a_0}{b_4\varepsilon_{\text{s}}^4 + b_3\varepsilon_{\text{s}}^3 + b_2\varepsilon_{\text{s}}^2 + b_1\varepsilon_{\text{s}} + b_0}, \quad (1)$$

where ε_{m} is the permittivity of the matrix dielectric; the coefficients a_i and b_i depend on the depolarization factors, electrophysical characteristics of the matrix dielectric and the dielectric core of spheroid, the volume content of the dielectric in the particle and the particles in the composite, and the dielectric function of the spheroid shell material $\varepsilon_{\text{s}}(\omega)$ is determined by Drude formula in the dissipation-free approximation.

It should be pointed out that the obtained formula (1) differs significantly from similar formulas for the composites with the spherical shell and spheroidal monometallic particles. Thus, unlike the above cases, the numerator and denominator in (1) contain fourth-degree polynomials with respect to ε_{s} and, respectively, eighth-degree polynomials with respect to the frequency. However, each of these polynomials has three pairs of the complex conjugate roots and two real roots, which correspond to the longitudinal and transverse optical modes. In addition, the equation $\varepsilon_{\text{eff}}(\omega_{sp}) = -\varepsilon_{\text{h}}$ (where ε_{h} is the permittivity of the medium bordering the nanocomposite) also has two real roots, which correspond to the resonances at the composite/environment interface. Thus, as in the case of the composites mentioned above, we have six characteristic frequencies that divide the frequency range, which is under the study, into seven regions, three of which contain surface electromagnetic waves, two regions contain surface plasmon polaritons, and two regions are the forbidden zones – the frequency regions at which the electromagnetic waves cannot propagate along the boundaries between the composite and the surrounding environment.

Multilayer cylindrical invisible cloaks with elliptical cross-section

V. I. Reva[1], R. Yu. Korolkov[1], A. V. Korotun[1,2], R. V. Fliahin[1]

[1]National University Zaporizhzhia Politechnic,
64 Universytetska Str., Zaporizhzhia, 69011, Ukraine
[2]G.V. Kurdyumov Institute for Metal Physics of the NAS of Ukraine,
36 Academician Vernadsky Blvd., Kyiv, 03142, Ukraine
e-mail: romankor@zp.edu.ua

Over the past two decades, the intensive research has been conducted into the possibility of creating invisibility cloaks of various geometries. The basis for this research is the concept of "wave flow" proposed in [1] – the use of the spatial transformation to achieve the invisibility of material objects. There are two known approaches to achieving near-perfect invisibility. The first of these approaches is based on transformational optics and uses materials with the heterogeneous and anisotropic permittivity and permeability. These materials have high losses and narrow bandwidths in the optical frequency range, which significantly limits their use in the visible spectrum. Therefore, the second approach, which consists of minimizing scattering by the plasmonic or dielectric layers, is more relevant.

Any nanoparticle does not contribute to the scattered field if its scattering cross-section, and therefore its polarizability, is equal to zero. In order to find the polarizability, it is necessary to solve the boundary problem of electrostatics for an infinitely long multilayer cylindrical structure with the elliptical cross-section. Let us limit ourselves to considering three-layer structure, the transverse cross-section of which differs slightly from the circular one. In this case, according to the boundary shape variation method [2], the task is to solve Laplace equation for each layer and the surrounding environment in a polar coordinate system with "deformed" boundary conditions.

The numerical experiments show that the shielding of the electric field in the inner region of the cylindrical structure is possible due to the layer with quasi-zero permittivity ($\varepsilon_2 \to 0$) when the resonant plasmon is excited in the shielding layer. In addition, the masking is possible in the presence of the singularity of the permittivity ($|\varepsilon_2| \to \infty$). Both of these cases can be realized using natural materials. The approach proposed in this work also allows the optimal thicknesses of the compensating shell to be determined for these cases.

[1] J. B. Pendry, D. Schurig, D. R. Smith, Science. 312, 1780 (2006). http://dx.doi.org/10.1126/science.1125907.
[2] A. V. Korotun, Phys. Sol. St. 56, 1245 (2014). http://dx.doi.org/10.1134/S1063783414060195.

Calculation of atomic structure of doubly ionized vanadium

S. V. Gedeon, V. Yu. Lazur, V. I. Kazakov

Department of Theoretical Physics, Uzhhorod National University,
54 Voloshyna str., Uzhhorod, 88000, Ukraine
e-mail: sergej.gedeon@uzhnu.edu.ua

Determination of spectroscopic and transition properties of vanadium ions is important for understanding the processes that occur in astrophysical and industrial plasma. The spectroscopic methods of plasma diagnostics require a large amount of atomic data on the vanadium atom and its ions.

This work is a logical continuation of the research begun in our previous works [1, 2] on the study of neutral and singly ionized vanadium respectively. We employed the same combination of multi-configuration Hartree–Fock method (MCHF) [3] and the configuration interaction (CI) approach with non-orthogonal orbitals and *B*-splines as basis functions [4, 5] to calculate the wave functions of the ground and lower excited states of vanadium ion V VIII.

To cover main allowed transitions, in present research we considered the ground and lower excited states of the V VIII ion with the excitation energies up to 16 eV. In the *LS* coupling approximation these states have electronic configurations $3d^3$ (terms $^{2,4}P^2D^{2,4}F^2GH$), $3d^24s$ (terms $^2S^{2,4}P^2D^{2,4}F^2G$), and $3d^24p$ (terms $^{2,4}SPDFG^2H^o$). Similarly to our previous calculations [1, 2], for all states under consideration we use the same set of deep core orbitals 1*s*, 2*s*, and 2*p*, which was generated using the Hartree–Fock (HF) method for the ground state $3d^3\ ^4F$ of doubly ionized vanadium. Outer electron orbitals 3*spd* and 4*sp* were generated for each of principal electronic configurations of V VIII in the separate term-average HF-calculations. Finally, the sets of the correlation orbitals 4*l* and 5*l* (*l* = 0–4) were obtained in separate MCHF calculations for the lowest term for each of the selected configurations. The same set of orbitals was used for other terms with given configuration.

As a result, in scope of non-relativistic *LS* approximation, we obtained wave functions of the ground and 33 lower excited states of doubly ionized vanadium. Calculated excitation energies are in good agreement with the averaged by fine structure levels experimental values compiled by NIST [6]. For each of the three types of electronic configurations under consideration ($3d^3$, $3d^24s$, and $3d^24p$) the main correlation contributions were studied in details. All configurations with mixing coefficients less than 0.001 were excluded from the final CI-expansions. This approach allows to keep an acceptable size of the configuration expansions.

Obtained sets of the wave functions will be used in further atomic structure calculations of V VIII with the quasi-relativistic Breit–Pauli corrections in order to accumulate data on transitions between levels, taking into account fine structure splitting.

[1] S.V. Gedeon, V.Yu. Lazur, and A.A. Kochemba, Semicond. phys. quantum electron. optoelectron. 28, 221 (2025). https://doi.org/10.15407/spqeo28.02.221.
[2] S.V. Gedeon, V.Yu. Lazur, V.I. Kazakov, Low Temp. Phys. 52(2), 257 (2026). https://doi.org/10.1063/10.0042377.
[3] C.F. Fischer, G. Tachiev, G. Gaigalas, and M.R. Godefroid, Comput. Phys. Commun. 176, 559 (2007). https://doi.org/10.1016/j.cpc.2007.01.006.
[4] O. Zatsarinny and C.F. Fischer, Comput. Phys. Commun. 124, 247 (2000). https://doi.org/10.1016/S0010-4655(99)00441-5.
[5] O. Zatsarinny and C.F. Fischer, Comput. Phys. Commun. 180, 2041 (2009). https://doi.org/10.1016/j.cpc.2009.06.007.
[6] A. Kramida, Yu. Ralchenko, J. Reader, and NIST ASD Team. NIST Atomic Spectra Database (ver. 5.10) (2022). Available: https://physics.nist.gov/asd.

Directivity analysis of microlaser with silver film and DBR reflectors

S. S. Herasymov

Department of Theoretical Radiophysics, The Institute of Radio Astronomy NASU,
4 Mystetstv St., Kharkiv, 61002, Ukraine
e-mail: serhii.heras@gmail.com

In this work, we analyse the directivity of a microlaser made of a silver film superstrate, active layer, and distributed Bragg reflector (DBR) substrate, depicted in Fig 1.

The periodic layered structures are common configurations for different photonic applications [1, 2]. The noble-metal resonant films sustain the plasmonic modes, which exist in the visible and near-infrared ranges. In considered plasmon periodic microlaser configuration, the silver film characterized by silver dielectric permittivity given from experimental data in [3].

The general electromagnetic analysis implements the Lasing Eigenvalue Problem (LEP) that involves neglecting non-electromagnetic effects, and leveraging the Maxwell equations linear set without the source of the incident field. The LEP approach allows us to find the electrical field component scalar function and a corresponding pair of eigenvalues, namely, real numbers of wavelength and threshold gain index of the mode [2]. As far as DBR is considered, the transmission matrix method (TMM) was used. The microlaser directivity can be defined as the ratio of the difference of the powers radiated upwards and downwards to the sum of these powers, as follows $D = (P^+ - P^-)/(P^+ + P^-)$.

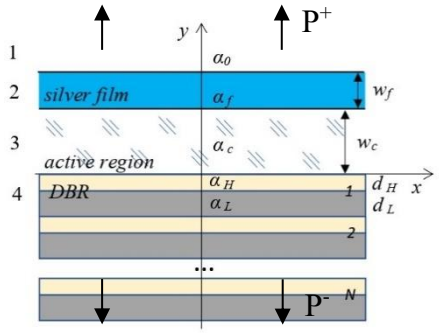

Fig. 1 Geometry cross-section of microlaser configuration

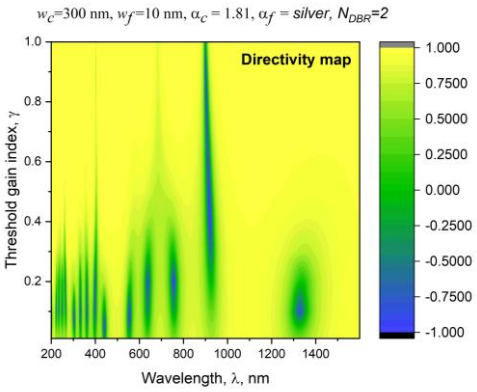

Fig. 2 Color map of microlaser directivity, D=1 corresponds to upwards power (P^+) while D=-1 corresponds to downwards power (P^-)

The Fig. 2 shows the relief map of directivity of the proposed microlaser. As one can see, the main amount of radiated power is directed upwards ($D = 1$), the blue spots indicate downwards radiation ($D = -1$) and they are close to lasing modes. We analysed the influence of silver film thickness and the number of layers of DBR on the microlaser directivity.

Overall, the directivity analysis of the multilayered microlaser configuration was shown. We observed that the thick silver film with 20-pair DBR microlaser structure yields mostly unidirectional upward radiation.

[1] V. V. Yachin, et al., Resonance enhancement of Faraday rotation in double-periodic gyromagnetic layers analyzed by the method of integral functionals, JOSA B, 35, 4, 851 (2018).
[2] S. S. Herasymov, et al., Electromagnetic analysis of threshold conditions for modes of 1-D microcavity laser with noble metal and distributed Bragg reflectors, JEWA, 39, 16, 1969–1984 (2025).
[3] P. B. Johnson and R. W. Christy, Optical constants of the noble metals, Phys. Rev. B, 6, 4370–4379, (1972).
[3] V. O. Byelobrov, A. I. Nosich, Mathematical analysis of the lasing eigenvalue problem for the optical modes in a layered dielectric microcavity with a quantum well and distributed Bragg reflectors. Opt. Quant. Electron., 39, 10-11, 927-937 (2007).

Plasmonic enhancement of photoemission in new-generation solar cells

A. V. Korotun[1,2], S. I. Shylo[1], O. O. Kapliienko[1]

[1]National University Zaporizhzhia Politechnic,
64 Universytetska Str., Zaporizhzhia, 69063, Ukraine
[2]G.V. Kurdyumov Institute for Metal Physics of the NAS of Ukraine,
36 Academician Vernadsky Blvd., Kyiv, 03142, Ukraine
e-mail: andko@zp.edu.ua

Increasing the efficiency of the solar cells is a fundamental problem in modern photovoltaics. One promising approach to solving this problem is to modify the absorbing semiconductor layer of the solar cells with the metallic nanoparticles. The main idea of this approach is that the excitation of the plasmon resonances on the surfaces of the nanoparticles results in the enhancement of the local electric fields and the generation of the hot charge carriers. In this case, the hot carriers are injected into the semiconductor absorbing layer, amplifying the photocurrent. It should be pointed out that in works [1, 2], the amplification of the current in the photocell due to the excitation of the surface plasmon resonance and the change in the photoemission cross-section when changing the size of the metallic nanoparticles embedded into the semiconductor layer were investigated. However, the influence of the optical phenomena in the semiconductor layer itself on the physical and technical characteristics of the solar cells has not been studied, and therefore these issues remain relevant.

The paper shows that the photoemission cross-section is proportional to the enhancement factor of the local electric fields, which, in turn, depends on the dielectric functions of the nanoparticle and absorbing layer materials. In order to determine these functions, the Drude and Lorentz–Tauka models are used [3]. In addition, the work takes into account the relaxation processes in the metallic nanoparticles. The results of the numerical experiments indicate the advisability of using small-radius gold nanoparticles to modify absorbing semiconductor layers in order to obtain the maximum photoemission cross-section.

[1] A. Korotun, H. Moroz, I. Titov, V. Reva, and S. Shylo, Proc. IEEE 42nd Intern. Conf. ELNANO. (May, 13-16, 2024), 197. http://dx.doi.org/10.1109/ELNANO63394.2024.10756911.
[2] A. V. Korotun, S. I. Shylo, V. I. Reva, and I. M. Titov, J. Nano Electron. Phys. 17, 01013 (2025). http://dx.doi.org/10.21272/jnep.17(1).01013.
[3] S. Adachi, H. Mori, and S. Ozaki, Phys. Rev. B. 66, 153201 (2002). http://dx.doi.org/10.1103/PhysRevB.66.153201.

THz properties of rare earth double molybdate $KLu(MoO_4)_2$

D. Kamenskyi[1,2,3], L. Prodan[3], K. Vasin[3], V. Khrustalyov[4], K. Kutko[4]

[1]Institute of Optical Sensor Systems, German Aerospace Center (DLR), Rutherfordtstr. 2, 12489 Berlin, Germany
[2]Department of Physics, Humboldt-Universität zu Berlin, Newtonstr. 15, 12489 Berlin, Germany
[3]Experimental Physics V, Center for Electronic Correlations and Magnetism, Institute of Physics, University of Augsburg, 86159 Augsburg, Germany
[4]B.Verkin Institute for Low Temperature Physics and Engineering of the NAS of Ukraine, 47 Nauky Ave., Kharkiv, 61103, Ukraine
e-mail: khrustalyov@ilt.kharkov.ua

Recently, we have demonstrated that in the dielectric compound $KY(MoO_4)_2$, low-frequency optical phonons excited by broadband THz pulse exhibit long-lived (lasting over 100 ps) narrowband re-emission of THz electromagnetic radiation [1]. Similar effect has been found in other compounds of $KRe(MoO_4)_2$ family including compounds with magnetic lanthanide ions (Re^{3+}) Here, we investigate the THz properties of another non-magnetic compound of this family, $KLu(MoO_4)_2$, with heavier lanthanide ion, Lu^{3+}. The absence of magnetic contributions together with mass-related effects influences the lattice dynamical parameters and, consequently, the frequencies of the layer phonons involved in the re-emission process.

$KLu(MoO_4)_2$ was investigated by means of THz time-domain spectroscopy (THz-TDS) in the frequency range 0.3 – 3.5 THz at the temperatures 5 – 200 K. Fig.1(a) shows the transmittance spectra of $KLu(MoO_4)_2$ single crystal at 5 K, typical of compounds belonging to this series [2]. The re-emission spectra at the phonon mode frequencies S_{1a} and S_{1c} are attributed to dipole-active shear lattice vibrations of the $[Lu(MoO_4)_2]^-$ and K^+ layers, is represented in Fig.1(b). The obtained decay time for this re-emission is about 50 ps.

Analysis of the temperature evolution of the transmittance spectra allowed us to determine the critical temperature at which the D_1 mode, attributed to rotational vibrations of the $(MoO_4)^{2-}$ tetrahedra, disappears. This may indicate the presence of a structural phase transition.

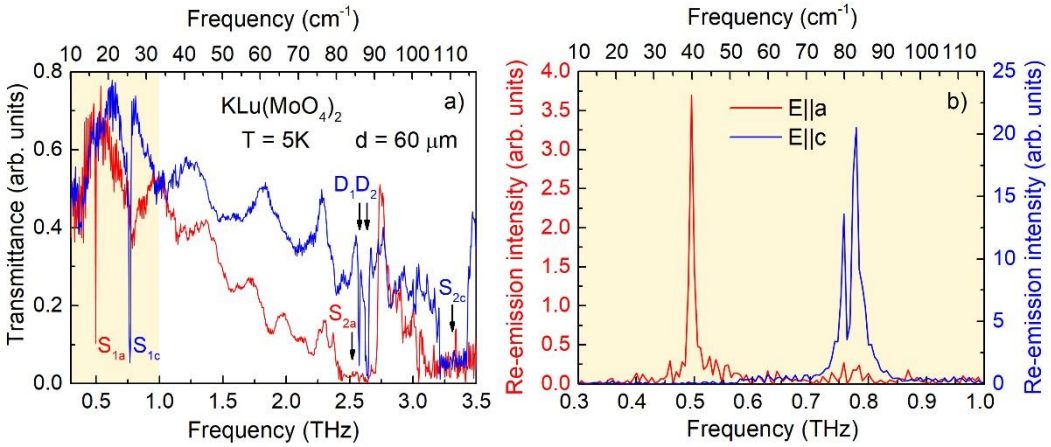

Fig.1. a) Transmittance spectra of $KLu(MoO_4)_2$ single crystal at 5K for two polarizations E||a and E||c (red and blue curves, consequently). S_1 and S_2 modes correspond to shear lattice vibrations and the doublet (D_1, D_2) – rotational vibrations of the $(MoO_4)^{2-}$ tetrahedra; b) re-emission intensity at the S_{1a} and S_{1c} phonon modes.

[1] D. Kamenskyi, K. Vasin, L. Prodan et al., Adv. Science, 12, 2, 202407028 (2025). https://doi.org/10.1002/advs.202407028.
[2] S. Poperezhai, P. Gogoi, N. Zubenko, et al., J. Phys.: Condens. Matter 29, 095402 (2017). https://doi.org/10.1088/1361-648X/aa55a8.

Enhancement of local electric fields in the gap between the metallic substrate and the scanning microscope probe

A. V. Korotun[1,2]

[1]*National University Zaporizhzhia Politechnic,*
64 Universytetska Str., Zaporizhzhia, 69011, Ukraine
[2]*G.V. Kurdyumov Institute for Metal Physics of the NAS of Ukraine,*
36 Academician Vernadsky Blvd., Kyiv, 03142, Ukraine
e-mail: andko@zp.edu.ua

The study of the optical resonance phenomena in a nanometer-scale "probe-substrate" gap is important for the applications such as surface-enhanced Raman scattering (SERS), surface fluorescence, adsorbed molecule spectroscopy, and near-field microscopy [1]. In the case when the probe and substrate materials are metals, the picture of the resonance phenomena in the small gap is quite complex. This is due to the fact that the permittivity of metal in the optical frequency range is negative, and the optical resonances (plasmons) are excited in the gap, providing the significant enhancement of the local electric field. Thus, the probe and the substrate, which support the localized resonances in the gap, behave like an open resonator. In this case, the controlling parameters that determine the spectral characteristics are geometry and dimensions of the probe, as well as the width of the gap. It should be pointed out that the scientific literature contains a very limited number of the studies of the optical phenomena in the nanometer gap between the metallic nanostructures, which are restricted by certain probe geometries, and therefore such studies are relevant.

This paper investigates resonance phenomena in the nanometer-scale gap between the axisymmetric metallic probe and the metallic substrate. The consideration is performed in the quasi-static approximation, since the characteristic dimensions (gap width and probe thickness) are significantly less than the wavelength. The results of the calculations show that in modes of the weak and moderate interaction in the system "the elongated spheroidal probe – the substrate", which is most often used in the experiments, the dipole resonance mode dominates. At the same time, the enhancement of the local electric field is more significant in the case of the convex shape of the tip than in the case of the probe in the shape of ideal cone.

[1] B.-Y. Jiang, L. M. Zhang, A. H. Castro Neto, D. N. Basov, M. M. Fogler, J. Appl. Phys. 119, 054305 (2016). http://dx.doi.org/10.1063/1.4941343.

Optical response of metallic nanotube with the variable thickness

R. Yu. Korolkov[1], V. I. Reva[1], R. O. Malysh[1], A. V. Korotun[1,2], I. M. Titov[1]

[1]National University Zaporizhzhia Politechnic,
64 Universytetska Str., Zaporizhzhia, 69063, Ukraine
[2]G.V. Kurdyumov Institute for Metal Physics of the NAS of Ukraine,
36 Academician Vernadsky Blvd., Kyiv, 03142, Ukraine
e-mail: revvi@zp.edu.ua

The cylindrical metallic nanoshells (nanotubes) attract the attention of the researchers due to their tunable sensory properties for the optical measurements. Currently, the process of exciting the surface plasmon resonances in the metallic nanotubes of the constant thickness is well studied [1]. In particular, it is established that the plasmonic hybridization of the inner and outer surfaces and changes in the shell thickness regulate the position of the surface plasmon resonance peaks. The violation of the symmetry in the metal-dielectric cylindrical nanostructures due to the displacement of the dielectric core leads to the significant complication in the behavior of the plasmonic modes. It should be pointed out that these issues remain poorly studied, and therefore their study is relevant.

Let us consider the interaction of light with the metal-dielectric non-coaxial cylindrical nanostructure located in the dielectric medium. We consider this interaction in the quasi-static approximation, since the characteristic dimensions of the system are significantly less than the wavelength of light. This approach allows us to analytically determine the frequency dependence of the transverse polarizability of the composite cylindrical nanostructure, which is under the consideration. In turn, the analysis of the obtained expression for the polarizability allows us to obtain the size dependencies of the surface plasmon resonance frequencies and the invisibility frequencies. These dependencies in the dissipation-free approximation are obtained from the conditions of zero denominator and numerator of the expression for the polarizability. However, unlike the metallic nanotube of the constant thickness, which has two frequencies of the invisibility and two frequencies of the surface plasmon resonance, the nanostructure, which is under the study, has four frequencies of the invisibility and four frequencies of the surface plasmon resonance due to the non-coaxiality of this nanostructure.

The results of the calculations show that if the splitting of the surface plasmon resonance frequencies is noticeable, then the splitting of the invisibility frequencies is insignificant. This behavior of the invisibility frequencies, which is close to the degeneracy, is due to the fact that they are practically independent of the distance between the axes of the inner cylinder and the entire metal-dielectric nanostructure.

[1] A. V. Korotun, Y. V. Karandas, Phys. Met. Metallogr. 123, 7 (2022). http://dx.doi.org/10.1134/S0031918X22010070.

Plasmonic phenomena in a chain of toroidal metal nanoparticles on a dielectric substrate

M. S. Maniuk[1], A. V. Korotun[1,2], V. P. Kurbatsky[1]

[1]National University Zaporizhzhia Politechnic,
64 Universytetska Str., Zaporizhzhia, 69063, Ukraine
[2]G.V. Kurdyumov Institute for Metal Physics of the NAS of Ukraine,
36 Academician Vernadsky Blvd., Kyiv, 03142, Ukraine
e-mail: andko@zp.edu.ua

Chains of metal nanoparticles of various geometries are currently being actively studied both experimentally and theoretically. This interest stems from their wide range of practical applications. In particular, chains of metal nanoparticles are used as discrete plasmonic waveguides for transmitting modulated signals with a high degree of spatial confinement. Researchers expect that subwavelength spatial localization of optical excitations in plasmonic discrete waveguides will minimize parasitic interactions between the structural elements of the optical circuit. Another advantage of plasmonic chains is the easy tuning of their properties by varying the particle sizes in the chain and the distance between them. The optical response of chains of oblate and prolate spheroids has already been studied [1, 2]. However, plasmonic phenomena in chains of nanoparticles of other geometries remain unexplored, making such research relevant.

This paper examines the optical response of a chain of toroidal metal nanoparticles on a dielectric substrate. The toroids in the chain have a common axis parallel to the plane of the substrate.

In the local field approximation, the frequency dependence of the transverse component of the chain polarizability tensor and the size dependence of the chain optical resonance frequency were obtained. Spectral shifts of the maxima of the transverse polarizability imaginary part were compared for the chain and an isolated toroid. The influence of the particle and substrate materials, and surrounding medium on the positions of the chain resonances was studied.

The calculation results indicate a significant decrease in the frequency of chain optical resonance with a decrease in the distance between toroidal particles.

[1] M. S. Maniuk, A. V. Korotun, V. I. Reva, I. M. Titov, Cond. Matt. Phys., 27 43701 (2024). http://dx.doi.org/10.5488/CMP.27.43701.
[2] M. S. Maniuk, A. V. Korotun, V. P. Kurbatsky, Low Temp. Phys. 51, 143 (2025). http://dx.doi.org/10.1063/10.0034659.

Characteristics of laser dye Nile red in a series of solvents

V. V. Maslov[1], I. M. Pritula[2]

[1]O.Ya.Usikov Institute for Radiophysics and Electronics of NAS of Ukraine, 12, Ac. Proscury St., Kharkiv, 61085, Ukraine
[2]Institute for Single Crystals of NAS of Ukraine, 60, Nauky Ave., Kharkiv, 61072, Ukraine
e-mail: maslov@ire.kharkov.ua

Continuing our studies of the influence of the molecular environment on the spectral and emission characteristics of solutions of laser oxazine dyes in order to expand the possibilities of creating active photonic elements for the red region of the spectrum based on them [1], we conducted a series of similar measurements of the characteristics of their close structural analogue - the effective laser dye Nile Red (NR):

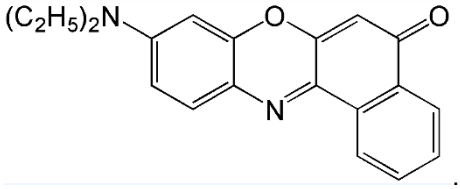

This dye, from the very beginning of its use in lasers [2], differed from other laser dyes in its energy photostability. In addition, its ability to bind to a number of biological tissues makes it a common probe for their visualization [3].

The measurements of spectral, fluorescent, and laser characteristics of Nile red in methanol (Met), acetonitrile (AcN), and dimethyl sulfoxide (DMSO) showed its significant differences from the previously studied [1] oxazine derivatives CV670 and Ox720. The presence in its structure of a carbonyl group, which has proton-acceptor properties, changed the nature of the interaction of this dye with its solvate environment. As a result, the solvents acetonitrile and DMSO showed themselves in this case as aprotic, and in the absorption spectra of this dye in all solutions only one long-wave band is observed, which is shifted to the green region by 40–50 nm relative to CV670 and by 65–75 nm relative to Ox720.

The laser characteristics of the NR dye were investigated when its solutions were excited by the radiation of a G283+ iminocoumarin laser with flashlamp pumping [4] and wavelength of 554 nm and output energy of up to 120 mJ under the same conditions and on the same setup as the oxazine derivatives [1]. The measurements of these characteristics showed that all the studied NR solutions effectively generate radiation in a non-selective resonator in the region of 630–660 nm with a bandwidth of 10 nm, and at a pump of 100 mJ their output energy significantly (by 1.5–6.5 times) exceeds the similar values obtained at the same pump for CV670 and Ox720.

[1] V. V. Maslov and I. M. Pritula, Low Temp. Phys. 52, 28 (2026). https://doi.org/10.1063/10.0042159.
[2] D. Basting, D. Ouw, F. P. Schafer, Optics Commun. 18, 260 (1976). https://doi.org/10.1016/0030-4018(76)90126-7.
[3] J. Sot, Y. R. Varela, L. R. Montes, F. M. Goñi, A. Alonso, Sci. Rep. 15, 34571 (2025). https://doi.org/10.1038/s41598-025-18016-8.
[4] V. V. Maslov, O. M. Bezkrovna, and I. M. Pritula. Appl. Phys. B. 127, 166 (2021) https://doi.org/10.1007/s00340-021-07706-6.

Features of exciton self-trapping in J-aggregates under exciton–plasmon interaction

P. V. Pisklova[1], I. I. Bespalova[1], S. L. Yefimova, O. V. Sorokin[1], S. Wolter[2], J. Schröer[2], T. Korn[2], S. Lochbrunner[2]

[1]Institute for Scintillation Materials of the NAS of Ukraine, 60 Nauky Ave., Kharkiv, 61072, Ukraine
[2]Institute of Physics, University of Rostock, 23 Albert-Einstein-Str., Rostock, 18059, Germany
e-mail: polinkapisklova@gmail.com

Supramolecular highly ordered assemblies, known as J-aggregates, exhibit a number of unique spectral properties that differ markedly from those of individual molecules. These include a narrow and intense absorption band, near-resonant fluorescence with a small Stokes shift, high oscillator strength, giant third-order nonlinear susceptibility, and efficient resonant energy migration. The distinctive optical properties of J-aggregates originate from electronic excitations delocalized along the molecular chain and from the formation of molecular (Frenkel) excitons arising due to translational symmetry and strong dipole–dipole interactions between the molecules within the aggregate. A characteristic feature of J-aggregates is a narrow red-shifted excitonic absorption band, known as the J-band, whose width is governed by the exciton coherence (or delocalization) length. J-aggregates therefore represent a class of molecular nanocrystals formed by various dyes, including cyanines, porphyrins, merocyanines, perylenes, and related chromophores.

The unique spectral properties of J-aggregates make them promising candidates for novel photonic materials, particularly in the form of thin films such as polymer matrices. In solution, J-aggregates often exhibit limited photostability; however, their stability increases significantly when incorporated into polymer films. Despite this advantage, the formation of J-aggregates in polymer matrices may also present certain drawbacks, including a reduced fluorescence quantum yield. One possible reason for this behavior is exciton self-trapping in the more rigid environment of the polymer matrix. Exciton self-trapping occurs when excitons become localized in a self-induced potential well created by significant lattice distortion under conditions of strong exciton–phonon coupling.

Recently, it was demonstrated that plasmon-enhanced fluorescence can suppress exciton self-trapping in cyanine dye J-aggregates formed in thin polymer films [1]. The present study is devoted to further investigation of this phenomenon in other types of J-aggregates, with particular attention to the influence of J-aggregate dimensionality in polymer films on exciton self-trapping under conditions of plasmon-enhanced fluorescence.

[1] A. V. Sorokin, I. I. Grankina, I. I. Bespalova, A. V. Aslanov, S. L. Yefimova, Yu. V. Malyukin, J. Phys. Chem. C 124, 10167 (2020) https://dx.doi.org/10.1021/acs.jpcc.0c00583.

Study of optical absorption of leukosapphire and ruby irradiated with electrons with an energy of 12.5 MeV

O. M. Pop, V. T. Maslyuk, I. G. Megela, I. Yu. Roman

Institute of Electron Physics of the NAS of Ukraine, Uzhhorod
e-mail: oksana_pop@i.ua

Leucosapphire and ruby are varieties of corundum (α-Al_2O_3) that share the same crystal structure but differ significantly in their optical properties due to the presence of impurity centers. Ruby is an impurity-activated Al_2O_3 crystal, in which Cr^{3} ions replace part of the Al^{3+} ions. It is these impurity ions that form localized energy levels in the band gap, causing absorption in the visible region of the spectrum, a characteristic red color, and the presence of narrow R-lines. In contrast, leucosapphire (pure Al_2O_3) contains practically no impurities; it demonstrates high transparency in a wide spectral range, and its optical properties are determined mainly by interband transitions and intrinsic defects of the crystal lattice. Thus, despite the matrix's structural identity, the presence of Cr^{3+} ions fundamentally changes the electronic structure and spectral characteristics of ruby relative to leucosapphire, making a comparative analysis in the context of optical absorption studies advisable.

In the presented work, crystals of leucosapphire (Al_2O_3) grown by the Stepanov method and ruby (Al_2O_3:Cr) grown by the Verneuil method were studied.

The irradiation of the studied samples was carried out at room temperature in a radiation field of scattered electrons with an energy of 12.5 MeV at the M-30 microtron of the Department of Photonuclear Processes of the Institute of Electron Physics of the NAS of Ukraine. Irradiation with electrons is accompanied by irradiation with bremsstrahlung gamma quanta, which inevitably arise during the interaction of accelerated electrons with structural elements.

After irradiation, the phosphorescence decay kinetics were measured. The optical absorption of the studied samples was measured with a spectrophotometer SF-46 after phosphorescence decay.

The optical absorption of ruby (Al_2O_3:Cr^{3+}) is significantly different from the absorption of leucosapphire (pure Al_2O_3), which is due to the presence of impurity ions Cr^{3+} in the crystal lattice of corundum.

In the studied ruby crystals, intense bands are observed in the visible region ~400–450 nm (3 eV) and ~550–560 nm (2.3 eV) (corresponding to intraconfigurational d–d transitions of Cr^{3+} ions: $^4A_2 \rightarrow {}^4T_1$ and $^4A_2 \rightarrow {}^4T_2$). As a result of irradiation of the studied samples, a slight decrease in the optical coefficients is observed, which corresponds to a relative change of approximately 4–5%. The small magnitude of the changes indicates the preservation of the crystal lattice and the insignificant effect of ionization on radiation exposure.

Unlike ruby crystals, undoped leucosapphire samples exhibit practically no absorption in the visible region and high optical transparency. After irradiation, a decrease in absorption is observed in the entire wavelength range of 200–1000 nm. This is explained by the low-dose effect, which results from a decrease in crystal defectivity due to radiation-stimulated diffusion of existing technological defects to the drains under irradiation.

The effect of copper impurity on photochemical transformations in cadmium iodide

M. M. Rudka

Lviv Polytechnic National University, 12 Bandery street, Lviv, 79013, Ukraine
e-mail: mykola.m.rudka@lpnu.ua

Cadmium iodide CdJ_2 is a layered material of I-Cd-I packages, in which anions (iodine) realize a close hexagonal packing, and cations (cadmium) occupy half (!) of the octahedral voids between the anions. Crystals are formed by parallel packing of such layers. Weak molecular (van der Waals) interactions operate between the layers, and within the structural package the interactions between the components are an order of magnitude stronger, are of a covalent-ionic nature, and with a significant predominance of the covalent component over the ionic one. CdI_2 crystals are wide-band materials with almost dielectric characteristics, their fundamental absorption edge at room temperatures (~290 K) lies at about 3.2 eV and shifts to 3.5 eV with a decrease in temperature to 80 K.

Structural anisotropy and features of intracrystalline bonding make layered cadmium iodides objects with unique properties: they are good phosphors in the visible region of the spectrum, scintillators, electrets, etc. All of these properties can be changed or enhanced, for example, by doping with various impurities.

A special role belongs to the impurities of noble metals - copper, silver and gold, which transform CdX_2 crystals (X = Cl, Br, I) into photochromic materials sensitive to ultraviolet radiation. However, the course of photochemical transformations in different cadmium halides differs significantly depending on the crystal matrix and the type of impurity.

We have applied a comprehensive approach to the study of photochemical processes in a highly anisotropic crystalline matrix of CdI_2 and have shown the features of photochemical reactions in it when copper is added to cadmium iodide. We have established the conditions for the occurrence of such processes, and have shown that the efficiency of stimulated defect transformations in these materials depends on the irradiation energy, its dose, and the temperature of the objects under study and is determined by the concentration of copper in them.

We have shown that the photochromic of CdI_2:Cu is due to the unique choice of the "crystal matrix – impurity" system, and one of the main reasons is that in the CdI_2 crystal lattice, copper is an amphoteric impurity and generates both acceptor (A) and donor (D) energy levels in the band gap. These impurity defects are part of donor-acceptor complexes of defects – trimers of DADi centers, which significantly affect the optical-luminescent and electrical properties of cadmium iodides [1, 2]. Such intrinsic impurity and purely impurity DADi complexes of defects are sensitive to electromagnetic radiation of a certain spectral composition.

We have established that photochemical transformations in CdI_2:Cu crystals are multistage in nature and are caused by the occurrence of a number of photochemical reactions that end with the formation of impurity coagulates - image centers. We have revealed the types of these reactions and their mechanism.

[1] M. Rudka, I. Matviishyn, B. Seredyuk, N. Tovstyuk, M. Karkulovska, I. Kravchuk, 2020 IEEE 40th International Conference on Electronics and Nanotechnology (ELNANO), 268 (2020). https://doi.org/10.1109/ELNANO50318.2020.9088922.
[2] Mykola Rudka, Low Temp. Phys. 52, 200 (2026). https://doi.org/10.1063/10.0042295.

Absorption and scattering of light in a dimer of the "solid metallic nanocylinder – metallic nanotube" type

V. I. Reva[1], A. V. Korotun[1,2], O. O. Shyrokopoias[1]

[1]National University Zaporizhzhia Politechnic,
64 Universytetska Str., Zaporizhzhia, 69011, Ukraine
[2]G.V. Kurdyumov Institute for Metal Physics of the NAS of Ukraine,
36 Academician Vernadsky Blvd., Kyiv, 03142, Ukraine
e-mail: andko@zp.edu.ua

It is well known that a significant enhancement of local electric fields and the formation of "hot spots" are possible in the gaps between metallic nanostructures. Therefore, the study of optical phenomena in dimers of nanoparticles with different shapes is of great practical interest.

We shall investigate the absorption and scattering of light in a dimer of a cylinder and a nanotube parallel to each other. The transformation plasmonics approach allows us to obtain the following relations for the absorption and scattering cross-sections of horizontally (x) and vertically (y) polarized radiation for the nanosystem under consideration.

$$C_{\text{abs}}^{(x,y)} = \frac{\omega}{c}\sqrt{\varepsilon_{\text{m}}}V\frac{\operatorname{Im}\xi_{x,y}}{\left|1+\mathrm{i}\pi\left(\frac{\omega D}{2c}\sqrt{\varepsilon_{\text{m}}}\right)^2\xi_{x,y}\right|},$$

$$C_{\text{sca}}^{(x,y)} = \frac{1}{6\pi}\left(\frac{\omega}{c}\sqrt{\varepsilon_{\text{m}}}\right)^4 V^2\left|\frac{\xi_{x,y}}{1+\mathrm{i}\pi\left(\frac{\omega D}{2c}\sqrt{\varepsilon_{\text{m}}}\right)^2\xi_{x,y}}\right|^2, \tag{1}$$

where

$$\xi_x = \pi\mathrm{e}^{\alpha}\sum_{l=1}^{\infty}\frac{\eta^{2l}+\mathrm{e}^{\alpha}-\mathrm{e}^{\alpha}\eta^{2l}\left(1+\eta^{2l}\operatorname{ch}\alpha\right)}{\eta^{4l}-\mathrm{e}^{2\alpha}\left(1+\eta^{6l}-\eta^{2l}\right)},$$

$$\xi_x = \pi\mathrm{e}^{\alpha}\sum_{l=1}^{\infty}\frac{\eta^{2l}-\mathrm{e}^{\alpha}+\mathrm{e}^{\alpha}\eta^{2l}\left(1-\eta^{2l}\operatorname{ch}\alpha\right)}{\eta^{4l}-\mathrm{e}^{2\alpha}\left(1+\eta^{6l}-\eta^{2l}\right)}, \tag{2}$$

$$\alpha = \ln\frac{\varepsilon(\omega)-\varepsilon_{\text{m}}}{\varepsilon(\omega)+\varepsilon_{\text{m}}},\ \eta = \frac{\sqrt{2+\mathrm{c}}+\sqrt{\mathrm{c}}}{\sqrt{2+\mathrm{c}}-\sqrt{\mathrm{c}}}, \tag{3}$$

ω and c are the frequency and speed of light; ε_{m} is the permittivity of the surrounding dielectric; $\varepsilon(\omega)$ is the dielectric function of the cylinder and nanotube material (determined by the Drude model); l is the multipolarity order; $\mathrm{c} = \delta/D$, δ is the distance between the cylinder and the nanotube, D is their diameter; $V = \frac{\pi}{4}\left(D^2+\left(D-d\right)^2\right)$ is the volume of the metallic part of the nanosystem, d is the diameter of the dielectric core of the nanotube.

The results of calculations using formulas (1) indicate the presence of a large number of absorption and scattering cross-section maxima arising from the strong interaction of plasmonic modes of different multipolarity.

Microwave two-photon threshold detector based on a Josephson photomultiplier

E. V. Stolyarov[1], R. A. Baskov[2,3]

[1]Quantum Optics and Quantum Information Group, Bogolyubov Institute for Theoretical Physics, National Academy of Sciences of Ukraine, vul. Metrolohichna 14-b, Kyiv 03143, Ukraine
[2]Department of Physics and Applied Physics, Yale University, P.O. Box 208120, New Haven, Connecticut 06520-8120, USA
[3]Yale Quantum Institute, 17 Hillhouse Avenue, P.O. Box 208334, New Haven, Connecticut 06520-8263, USA
e-mail: eugene.stolyarov@bitp.kyiv.ua

Fast and efficient detection of microwave photons in superconducting circuit QED systems is essential for various applications. Moreover, employing on-chip microwave photodetectors could eliminate the need for bulky cascades of amplifiers and non-reciprocal elements, thereby improving the scalability of circuit QED systems.

A Josephson photomultiplier (JPM) [1—3] is an example of such a detector, featuring an on-chip design that is fully compatible with superconducting circuit QED architecture. Essentially, the JPM is a phase qubit [4] that serves as a narrowband *absorbing* detector with a single-photon threshold, delivering a "click" only when there is at least one photon in the measured mode.

We propose the extension [5] to the JPM that transforms it into a two-photon threshold detector. Such a detector absorbs a pair of photons and delivers a "click" only when there are at least two photons in the measured mode. For achieving a two-photon threshold, we couple the JPM to a dimer of resonators composed of two lumped-element resonators interacting via an asymmetric dc SQUID. Specific tuning of the resonator frequencies and the external flux through the SQUID coupler allows us to engineer a two-photon coupling between the resonators. This coupling gives rise to the conversion of a photon pair from one resonator into a single photon in another resonator that enables a selective response to quantum states with at least two photons.

We derive the effective Hamiltonian of the system and the master equation that governs the evolution of its quantum state. By numerically solving the master equation, we evaluate the click probability, which allows us to estimate the detection fidelity. Calculations demonstrate that, for realistic circuit parameters, more than 99% fidelity of photon pair detection can be achieved in less than 50 ns.

E.V.S. acknowledges support from the National Research Foundation of Ukraine through Project No. 2023.03/0165, Quantum correlations of electromagnetic radiation.

[1] Y.-F. Chen et al., Phys. Rev. Lett. 107, 217401 (2011). https://doi.org/10.1103/PhysRevLett.107.217401.
[2] A. Opremcak et al., Science 361, 1239 (2018). https://doi.org/10.1126/science.aat4625.
[3] A. Opremcak et al., Phys. Rev. X 11, 011027 (2021). https://doi.org/10.1103/PhysRevX.11.011027.
[4] J. M. Martinis, Quantum Inf. Process. 8, 81 (2009). https://doi.org/10.1007/s11128-009-0105-1.
[5] E. V. Stolyarov and R. A. Baskov, Phys. Rev. Res. 7, 033263 (2025). https://doi.org/10.1103/6p8x-snzm.

Emission properties of low-temperature plasma based on a helium-methionine mixture

E. A. Svitlichnyi

Institute of Electron Physics, 21 Universitetska str., 88017 Uzhhorod, Ukraine
e-mail: bercheni14@gmail.com

The study of the interaction processes of methionine with components of gas discharge plasma is highly relevant given the rapid development of plasma medicine and oncology, as this sulfur-containing amino acid plays a critical role in the metabolism of tumor cells. Studying the mechanisms of fragmentation and stability of methionine's molecular bonds is essential for understanding the evolution of organic matter under extreme environmental conditions and deep space conditions.

This work is dedicated to the experimental study of the luminescence characteristics of low-temperature gas-discharge plasma in a mixture of methionine amino acid vapors ($C_5H_{11}NO_2S$) and helium.

The experiment used methionine powder produced by Sigma-Aldrich with a purity of 99.4%. The plasma luminescence source was a gas discharge chamber (GDC) made of melted quartz, 14 cm in length, with an internal diameter of 3 cm and an interelectrode gap of 2.5 cm. The methionine powder was placed inside the GDC. Metal electrodes were located at the opposite ends of the chamber. The emission from the GDC for analysis was recorded through the walls of a quartz tube. Luminescence spectra were recorded using an MS 7504i monochromator. Time-integrated discharge luminescence spectra were captured by an HS 101H CCD camera. To excite the longitudinal pulse-periodic discharge, a generator with resonant charging of an 825 pF storage capacitor and a TGI1-2000/35 thyratron as a commutator was used [1]. The generator provided a pulse repetition frequency of up to 10 kHz at charging voltages not exceeding 5 kV. As a result of self-heating, the GDC temperature reached 250°C. The pressure of the inert helium gas was 25 Torr. Temperature control was maintained using a platinum-platinum-rhodium thermocouple and a portable pyrometer.

For the first time, the luminescence of the plasma mixture and the emission spectra of methionine molecules were experimentally investigated in a low-temperature longitudinal pulse-periodic discharge plasma. It was established that under the influence of the plasma discharge, intensive fragmentation of methionine molecules occurs, involving the destruction of major functional groups and the formation of several light gas-phase products and radical compounds.

[1] Svitlichnyi, E.A., Kelman, V.A. & Zhmenyak, Y.V. About universal mechanism of the influence of metal additives on the copper vapor laser output parameters. Opt Quant Electron 50, 331 (2018).

Study of the properties of gas discharge plasma in mixtures of inert gases with tellurium vapor

E. A. Svitlichnyi[1], V. Yu. Loya[1], A. K. Shuaibov[2], A. I. Minya[2], A. A. Malinina[2], R. V. Gritsak[2], A. N. Malinin[2], M. M. Pop[2], M. M. Feldii[2]

[1]Institute of Electron Physics of NAS of Ukraine,
Universitetska str., 21, 88017 Uzhhorod, Ukraine
[2]Uzhgorod National University, Voloshin str. 54, 88000 Uzhgorod, Ukraine
e-mail: bercheni14@gmail.com

The study of the properties of gas discharge plasma in mixtures of inert gases with tellurium vapor is of particular interest due to the combination of fundamental energy transfer processes and applied possibilities in nanotechnology. The study of the kinetics of the interaction of metastable inert gas atoms with tellurium atoms allows for a deeper understanding of the mechanisms of selective excitation and ionization, which is key to the development of highly efficient gas-discharge light sources. The relevance of this topic is reinforced by needing for modern microelectronics and photonics in new semiconductor materials with a direct band gap, the production of which requires a deep understanding of the physicochemical processes occurring in non-equilibrium plasma of chalcogen mixtures [1].

For the experiment was used "Plasma" experimental setup [2]. The longitudinal pulse-periodic discharge in the gas discharge chamber was excited using a thyratron generator with a TGI1-2000/35 switch and resonant recharging of a storage capacity of 1650 nF.

In the experiment, the voltage on the high-voltage rectifier was up to 5 kV, the average discharge current was up to 0.5 A, and the pump pulse frequency was up to 5 kHz. Tellurium electrodes were used in the work.

Time-integrated emission characteristics of the discharge were recorded using a MS 7504i spectral monochromator and an HS 101H CCD camera. The information was recorded and analyzed using a personal computer.

The results of the first measurements of the spectral characteristics of the radiation of a mixture of tellurium vapor with an inert gas in a gaseous pulse-periodic discharge in the ultraviolet and visible spectrum were obtained.

[1] Zhao, X., et al. (2024). "Low-temperature growth of 2D tellurium for high-performance flexible electronics via plasma-enhanced chemical vapor deposition". Nature Communications / Advanced Functional Materials.
[2] A.A. General, E.A. Svitlychny: Abstracts of the International Conference of Students and Young Scientists in Theoretical and Experimental Physics "Eureka-2023". Lviv, Ukraine. May 16–18, 2023. P. B2 (in Ukrainian).

Transformation of photoluminescence and structure of C60 fullerite under the influence of nitrogen chemical and diffusion sorption

V. N. Zoryansky, P. V. Zinoviev, N. N. Galtsov and Yu. O. Semerenko

B. Verkin Institute for Low Temperature Physics and Engineering of NAS of Ukraine, 47 Nauky Ave., Kharkiv, 61103, Ukraine
e-mail: zoryansky@gmail.com

Polycrystals of C_{60} with an admixture of N_2 molecules were studied using X-ray diffractometry [1] and photoluminescence spectroscopy [2-4] in a wide temperature range (10-300 K). Saturation was carried out at various sorption temperatures (T_s) from 200 °C to 550 °C in a nitrogen atmosphere under a pressure of 30 atm. Consistent studies of the optical and structural characteristics of the C_{60}+N_2 complex, as well as their temperature behavior, were carried out. The kinetics of nitrogen sorption for different T_s and the efficiency of impurity diffusion were studied. The influence of the impurity on the orientational phase transition, the processes of glass state formation and the dynamics of electron excitation transfer were determined depending on the mechanism of interaction in the impurity-matrix system.

A combined analysis of experimental spectroscopy and diffractometry data showed the presence of an adsorption crossover at a sorption temperature of about 420 °C - a transition from the diffusion mechanism of filling intermolecular voids with an impurity (physisorption) to the chemical impurity-matrix interaction (chemisorption).

For solid solutions of C_{60}+N_2 (T_s<420 °C), curves of the increase in the lattice parameter from the saturation time were established and an increase in the luminescence of impurity glow centers ("deep X-traps") was shown, correlating with an increase in the concentration of octahedral voids of the C_{60} lattice filled with N_2 molecules. The different dynamics of these processes indicate a significant gradient in impurity concentration over the penetration depth. In the case of extremely saturated solid solutions of C_{60}+N_2, as shown by the temperature dependences of the luminescence intensity and the lattice parameter, the temperature of formation of the glass state (T_g) decreases, but not as significantly as the temperature of the orientational phase transition (T_c). At the same time, in the case of chemical sorption of nitrogen (T_s>420 °C) in C_{60}, the orientational phase transition is completely suppressed, and the temperature boundaries of the glass transition processes are greatly blurred with a simultaneous significant increase in the volume of the cubic cell and thermal expansion of the crystals. Also, for this saturation mechanism, reformatting and a shift towards low energies with a significant inhomogeneous broadening of the luminescence spectrum were found, the primary analysis of which showed the presence of biazafullerite $(C_{59}N)_2$ in the resulting new multicomponent complex of nitrogen-containing substances. Significant changes in the behavior of the temperature dependence of the integrated radiation intensity indicate the presence of additional mechanisms of electron excitation transport in crystals with a new chemical composition. The quenching of photoluminescence at low temperatures observed here may be associated with the emergence of many additional Frenkel exciton capture centers with high efficiency of their nonradiative deactivation.

[1] I. V. Legchenkova, K. A. Yagotintsev, N. N. Galtsov, V. V. Meleshko, Yu. E. Stetsenko, A. I. Prokhvatilov, Low Temp. Phys. 40 (8), 685 (2014). https://doi.org/10.1063/1.4894316.
[2] P. V. Zinoviev, V. N. Zoryansky, V. V. Meleshko, Yu. E. Stetsenko, Low Temp. Phys. 41 (3), 236 (2015). https://doi.org/10.1063/1.4915916.
[3] P. V. Zinoviev, V. N. Zoryansky, Low Temp. Phys. 47 (2), 173 (2021). https://doi.org/10.1063/10.0003180.
[4] P. V. Zinoviev, V. N. Zoryansky, Low Temp. Phys. 48 (3), 268 (2022). https://doi.org/10.1063/10.0009547.

QUANTUM LIQUIDS AND QUANTUM CRYSTALS, CRYOCRYSTALS

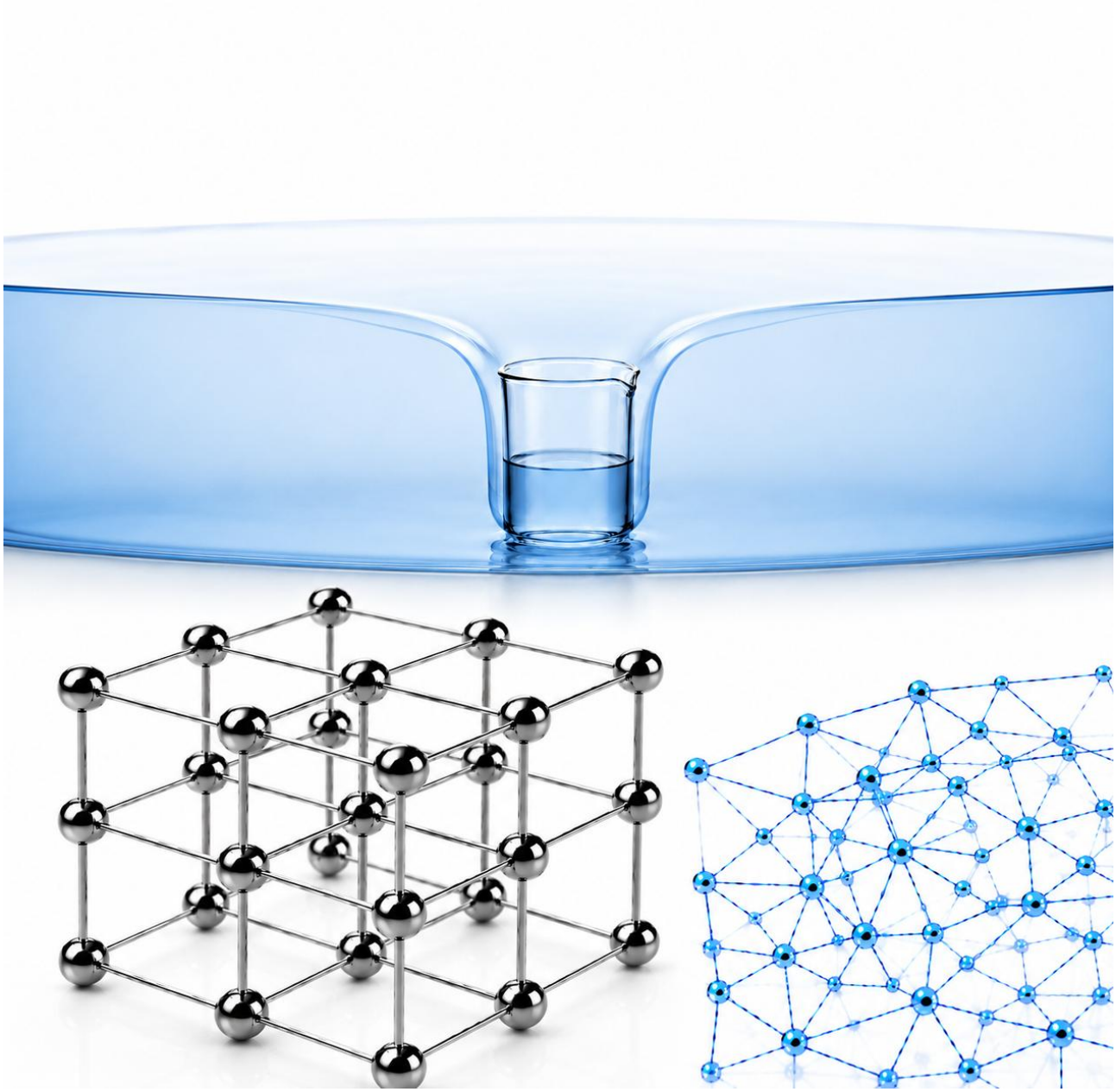

Photon-driven relaxation in cryogenic solids and the role of charged particles

E. V. Savchenko, I. V. Khyzhniy, M. A. Bludov, S. A. Uyutnov

B.Verkin Institute for Low Temperature Physics and Engineering of the NAS of Ukraine, 47 Nauky Ave., Kharkiv, 61103, Ukraine
e-mail: savchenko@ilt.kharkov.ua

Despite the long story of research on cryogenic solids, specifically nitrogen, the fascinating problem of charged species dynamics and their role in a variety of radiation-induced phenomena has only become a focus of study in the last few decades ([1] and references therein). The complex relaxation pattern includes processes in the atomic, electronic, and charge subsystems and their interconnection, which is the subject of our present study. We used a number of emission techniques in combination with matrix isolation to get information on different channels of relaxation in electron beam pre-irradiated films of cryogenic Ar matrix doped with N_2 and O_2. The combination of current and optical activation spectroscopy methods – thermally and optically stimulated exoelectron emission (TSEE, OSEE) as well as thermally and optically stimulated luminescence (TSL, OSL) over a wide spectral range was applied.

It was found that the photons of long visible range afterglow of the N atom in the ^2D state with τ=20±4 s drive not only the afteremission of electrons, but also the VUV "afterglow" of the matrix recombination radiation, which occurs in the reaction: $Ar_2^+ + e^- \rightarrow Ar_2^*$. This VUV emission was also observed upon heating of the pre-irradiated sample up to 42 K, yielding a multi-peak structure. It was ascertained that the lowest-temperature peak near 12 K is connected with the release of electrons from shallow traps in the subsurface layer. In order to isolate more high-temperature peaks and estimate activation energies needed for electron detrapping, we resorted to the "cleaning curve" technique – irradiating the sample at a higher temperature or pre-annealing the irradiated sample. Such a procedure revealed the TSL peaks at 18 and 23 K in O_2-doped Ar in good agreement with our previous results [2]. Comparison of the found activation energies E_{ac} with theoretical results [3] allows the identification of these peaks as related to the temperature-induced migration of O atoms via interstitial sites and vacancy-assisted migration via substitution ones. Possible migration routes of N atoms are discussed, but their final assignment is a challenging task. Correlation studies of the spectrally resolved TSL and TSEE provided strong evidence of the relaxation cascades stimulation via radiative atom-atom recombination reactions. The electronic transitions $A^3\Sigma_u^+ \rightarrow X^1\Sigma_g^+$ and $C^3\Delta_u \rightarrow X^3\Sigma_g^-$ represent the "internal source" of photons in the case of N_2- and O_2-doped Ar, respectively. The experiments with laser-induced electron detachment from O^- centers demonstrated an enhancement of the relaxation emissions of electrons and VUV photons via the reaction $O+O \rightarrow O_2^* \rightarrow O_2$. Our new data support the long-range photon-induced mechanism of relaxation triggering in pre-irradiated rare-gas matrices and contribute a fresh aspect interconnecting atomic and electronic subsystems with charge carriers. The suggested radiative mechanism of electron detrapping provides a long-range energy transfer through the solid transparent to visible light. The observed "conversion" of low-energy chemiluminescence photons into high-energy photons of recombination luminescence clearly demonstrates the prominent role of chemiluminescent reactions and charge particles in the branching of relaxation paths and their effect on the stability of charged centers.

[1] E. Savchenko, I. Khyzhniy, V. Bondybey, Low Temp. Phys. 45, 975 (2019). https://doi.org/10.1063/1.5121267.
[2] E. V. Savchenko, I. V. Khyzhniy, S. A. Uyutnov, G. B. Gumenchuk, A. N. Ponomaryov, M. K. Beyer, V. E. Bondybey, J. Phys. Chem. A 115**,** 7258 (2011). https://doi.org/10.1021/jp2004419.
[3] I. V. Leibin, D. S. Bezrukov, and A. A. Buchachenko, Phys. Chem. Chem. Phys. 26**,** 958 (2024). https://doi.org/10.1039/D3CP04178F.

Molecular-shape control of Boson-peak-like heat-capacity anomalies in polycyclic aromatic hydrocarbon crystals

V. Sokolenko[1], D. Szewczyk[1], A. I. Krivchikov[1,2], A. Jeżowski[1]

[1]Institute for Low Temperatures and Structure Research, Polish Academy of Sciences, Okólna 2, 50-422 Wroclaw, Poland
[2]B. Verkin Institute for Low Temperature Physics and Engineering of the NAS of Ukraine, 47 Nauky Ave., Kharkiv, 61103, Ukraine
e-mail: v.sokolenko@intibs.pl

Boson-peak-like anomalies are typically identified as an excess contribution to the low-temperature heat capacity relative to the Debye baseline, appearing as a maximum in the reduced representation Cp/T3 in the ~1-10 K range. While traditionally associated with structural disorder in glasses [1], similar anomalies have also been reported in fully ordered molecular crystals [2], raising the question of whether such features are universal or instead governed by deterministic structural factors. Here, we analyse the dependence of Boson-peak-like behaviour on molecular shape using specific-heat measurements of polycyclic aromatic hydrocarbon (PAH) crystals.

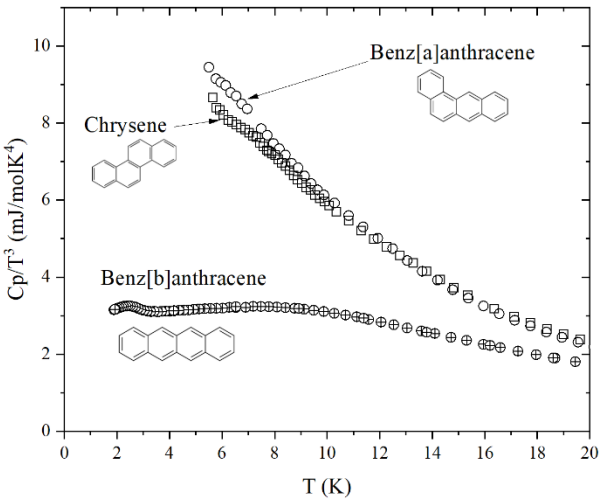

Fig. 1. Low-temperature heat capacity anomalies in two PAH crystals.

PAH crystals are well-suited model systems because they are structurally ordered yet often strongly anisotropic, owing to rigid π-conjugated backbones, layered packing, and weak intermolecular cohesion dominated by π–π interactions. This combination enables systematic variation of molecular geometry and packing without introducing topological disorder. We therefore test the hypothesis that Boson-peak-like contributions are not universal even within a chemically coherent PAH family, but depend on molecular symmetry, aspect ratio, and the resulting packing geometry.

Figure 1 compares the reduced heat capacity Cp/T3 of structurally related PAH crystals. Literature data for chrysene and benz[a]anthracene [3] exhibit a pronounced Boson-peak-like maximum in the ~5-8 K range, indicating enhanced low-frequency vibrational contributions relative to the Debye baseline. In contrast, our measurements for benz[b]anthracene show a markedly lower and smooth dependence over the same temperature interval, without a distinct maximum. This comparison indicates that the presence and strength of Boson-peak-like anomalies can vary strongly even among closely related PAH crystals, consistent with structure- (molecular-shape and packing-) controlled rather than universal behaviour.

[1] R. C. Zeller and R. O. Pohl, Thermal Conductivity and Specific Heat of Noncrystalline Solids, Phys. Rev. B 4, 2029 (1971). http://dx.doi.org/10.1103/PhysRevB.4.2029
[2] D. Szewczyk et al., Specific heat at low temperatures in quasiplanar molecular crystals: Origin of glassy anomalies in minimally disordered crystals, Phys. Rev. B 110, 174204 (2024). http://dx.doi.org/10.1103/PhysRevB.110.174204
[3] M. I. Lelet, V. N. Larina, E. O. Silyakova, and E. V. Suleimanov, Thermodynamic Properties from Adiabatic and Combustion Calorimetry of Two Polycyclic Aromatic Hydrocarbons, Benz[a]anthracene and Chrysene, J. Chem. Eng. Data 66, 3667 (2021). http://dx.doi.org/10.1021/acs.jced.1c00152

Low-temperature heat capacity scaling patterns in cryocrystals

M. Barabashko[1], A. Jeżowski[2], A. Krivchikov[1,2]

[1]B.Verkin Institute for Low Temperature Physics and Engineering of the NAS of Ukraine, 47 Nauky Ave., Kharkiv, 61103, Ukraine
[2]Institute for Low Temperatures and Structure Research, Polish Academy of Sciences, P.O. Box 1410, 50-950 Wroclaw, Poland
e-mail: barabaschko@ilt.kharkiv.ua

The low-temperature heat capacity of solids reflects the quantum nature of atomic vibrations and the lattice dynamics. Cryocrystals provide particularly suitable systems for such studies because of their structural simplicity and the well-defined character of their intermolecular interactions. A universal empirical scaled relation, denoted Δ^*, was previously shown to describe the non-Debye excess in the isochoric heat capacity of Ne cryocrystals with different molar volumes [1]. In this work, we extend the analysis of the universal scaled relation Δ^* to a broader class of atomic and quantum cryocrystals, including ^{4}He, ^{3}He, H_2. We examine the low-temperature isochoric heat capacity across a wide set of cryocrystals and demonstrate that the characteristic hump in the Debye-reduced function $C_v(T)/T^3$, originating from the first van Hove singularity in the phonon spectrum—can be captured within a single universal description. Specifically, we show that this feature is reproduced by a dimensionless function Δ^* that depends only on the magnitude of the excess and on the characteristic temperature T_{max}, without invoking any system-specific assumptions beyond the standard behavior of the phonon density of states near a van Hove maximum. Across atomic (Ar, Ne, Kr, Xe), molecular (N_2, CO, CO_2, N_2O), and quantum (^{4}He, ^{3}He, H_2) crystals, we find that Δ^* scales with molar volume in a manner consistent with Brillouin-zone scaling of the corresponding phonon frequencies [2].

Taken together, these results demonstrate that classical and quantum cryocrystals can be consistently described within a unified vibrational framework in which the first van Hove singularity plays a central role in governing the low-temperature heat capacity. The universal scaling established here provides a practical basis for approximating and predicting the heat capacity of crystalline solids over finite ranges of density or pressure, even in the absence of detailed phonon spectra. Its applicability to both classical and quantum cryocrystals makes it especially valuable for high-pressure studies and for lighter quantum systems, where zero-point motion and anharmonicity exert strong influence on lattice dynamics. By defining a robust van Hove–based reference for crystalline solids, this approach also offers a reliable baseline for distinguishing conventional phonon behavior from genuinely unresolved low-frequency anomalies in more complex or disordered materials.

Acknowledgements

This work was partly supported by the National Research Foundation of Ukraine (Grant 2023.03/0012) and National Science Centre, Poland (Grant 2022/45/B/ST3/02326).

[1] M. S. Barabashko and A. I. Krivchikov, About the hump in the low-temperature isochoric heat capacity of Ne cryocrystals, Low Temp. Phys. 51, 157–161, (2025). https://doi.org/10.1063/10.0034896.
[2] M. Barabashko, A. Jeżowski and A. Krivchikov, Scaling of Low-Temperature Heat Capacity in Cryocrystals, arXiv preprint arXiv:2511.14409, (2025).

Rotation of chains of vortices and dipoles in circular cylinders

T. I. Zueva

B.Verkin Institute for Low Temperature Physics and Engineering of the NAS of Ukraine,
47 Nauky Ave., Kharkiv, 61103, Ukraine
e-mail: zueva@ilt.kharkov.ua

The flow of a liquid with two types of singularities is considered: vortices and dipoles. These problems became relevant again when, in 1994, the model of Bose-Einstein condensates in magnetic trap was successfully implemented.

We now consider the simplest problem: 2D-flow of ideal liquid with vortices and dipoles in the circular cylinder of radius *R*. The motion of dipoles has been studied much less than the motion of individual vortices, and many works describing the motion of dipoles in Bose-Einstein condensates consider them just as pairs of free individual vortices of opposite signs [1,2]. Here we consider a dipole as two vortices with intensities ±γ, fixed at a small distance *2a* from each other, and study their motion.

The flow complex potentials around the vortex and dipole are well-known. We study the chains of these singularities. It is shown that for a chain *N* identical vortices or dipoles uniformly distributed in a circle of radius r_1, the complex potential is a periodic function with an angular period $2\pi/N$. The complex conjugate velocity of any vortex $z_1=r_1 \exp(i\theta_1)$ in the chain is:

$$\overline{V_v} = -\frac{i\gamma(N-1)}{2z_1} + \frac{i\gamma N z_1^{N-1}}{z_1^N - z_2^N}$$

and for any dipole we obtain:

$$\overline{V_d} = \frac{ia_1\gamma e^{i\alpha_1}(N^2-1)}{3z_1^2} - \frac{2ia_2\gamma e^{i\alpha_2}N^2(z_1z_2)^{N-1}}{(z_1^N - z_2^N)^2}.$$

Here z_2 is a point that is symmetrical to z_1 with respect to the boundary, α_1 is the slope of the dipole axis relative to the horizontal axis, $\alpha_2=-\alpha_1+2\theta_1$, $a_2=a_1R^2/r_1^2$. It is shown that a ring of vortices always rotates as a rigid structure, but dipoles rotate as a fixed structure if and only if the axes of all dipoles are directed along the radius vector.

The equation of motion of any vortex or dipole from the ring can be written as $\chi_1' = \mathbf{\Omega}_N \times \chi_1$, where we have defined $\chi_1=(x_1,y_1,0)$, $\mathbf{\Omega}_N = (0,0,\Omega_N)$, $r_1^2 = x_1^2 + y_1^2$. For *N* uniformly distributed vortices angular velocity is:

$$\Omega_N^{(v)} = \frac{\gamma}{r_1^2}\left(\frac{N-1}{2} + \frac{Nr_1^N}{(R^2/r_1)^N - r_1^N}\right)$$

and for *N* dipoles we obtain:

$$\Omega_N^{(d)} = \frac{\gamma a_1}{r_1^3}\left(\frac{N^2-1}{3} - \frac{2N^2R^{2N}}{((R^2/r_1)^N - r_1^N)^2}\right).$$

If we add the rotation of the cylinder as whole with an angular velocity Ω_0, we can get the chain to rotate with any angular velocity.

[1] B. Gertjerenken, P. G. Kevrekidis, R. Carretero-Gonzalez, B. P. Anderson, Phys. Rev. A 93, 023604 (2013). http://dx.doi.org/10.1103/PhysRevA.93.023604.
[2] S. Middelkamp, P. J. Torres, P. G. Kevrekidis, D. J. Frantzeskakis et al, Phys. Rev. A 84, 011605(R) (2011). http://dx.doi.org/10.1103/PhysRevA.84.011605.

Condensed-state rearrangements in N_2O-CO_2 alloys according to THEED data

O. P. Konotop, A. A. Solodovnik

B.Verkin Institute for Low Temperature Physics and Engineering of NAS of Ukraine,
47 Nauky Ave., Kharkiv, 61103, Ukraine
e-mail: solodovnik@ilt.kharkov.ua

The structural properties and phase behavior of binary molecular solids formed by nitrous oxide (N_2O) and carbon dioxide (CO_2) are of significant interest due to their nearly identical molecular geometries and electronic configurations. Despite their similarities, the subtle differences in their dipole moments and intermolecular potentials lead to complex solubility limits and decomposition mechanisms at cryogenic temperatures.

In this study, the structural characteristics of N_2O–CO_2 alloys were investigated across the entire range of mutual concentrations. Samples were synthesized via vapor deposition onto substrates at condensation temperatures of 5 K and 65 K. Structural analysis was performed using transmission high-energy electron diffraction (THEED). To delineate solubility regions, we monitored the concentration dependence of the lattice parameters and analyzed the intensity distribution of the diffraction patterns.

It was found that, under both temperature conditions, alloys dominated by either N_2O or CO_2 crystallized in a face-centered cubic (fcc) lattice characterized by the *Pa3* space group, which is consistent with the structures of the pure components. The ranges in which regular solutions exist and intervals of alloy phase separation have been identified. At 5 K, the N_2O matrix can accommodate up to 20 mol.% CO_2, while the solubility of N_2O in solid CO_2 reaches approximately 35 mol.%. As the temperature increased to 65 K, these limits contracted significantly to 11 mol.% for CO_2 in N_2O and 30 mol.% for N_2O in the CO_2 lattice. Detailed investigations of low-fraction components allowed for the calculation of relative excess volumes. These values quantify the local lattice distortion induced by CO_2 impurities in the N_2O matrix and vice versa. Analysis of the diffraction profiles suggests that the phase separation in N_2O–CO_2 cryosolutions does not follow classical nucleation and growth but instead corresponds to a spinodal decomposition mechanism.

The findings indicate that while N_2O and CO_2 are nearly isostructural, their solid solutions exhibit restricted solubility that is dependent on temperature. The identification of spinodal decomposition as the primary separation mechanism provides new insights into the thermodynamic stability and kinetic evolution of molecular cryo-alloys.

Persistent current oscillation in double-ring quantum gas

A. A. Chaika[1], A. O. Oliinyk[1], I. V. Yatsuta[2], Y. O. Nikolaieva[1], M. Edwards[3], N. P. Proukakis[4], T. Bland[5], A. I. Yakimenko[1,6]

[1]Taras Shevchenko National University of Kyiv, 64/13, Volodymyrska Street, Ukraine
[2]Weizmann Institute of Science, Rehovot 7610001, Israel
[3]Georgia Southern University, Statesboro, Georgia 30460-8031, USA
[4]Newcastle University, Newcastle upon Tyne, NE1 7RU, United Kingdom
[5]LTH, Lund University, S-22100 Lund, Sweden
[6]Universit´a di Padova, Via Marzolo 8, 35131 Padova, Italy
e-mail: andriy31415@gmail.com

Atomtronic quantum sensors [1] based on trapped superfluids offer a promising platform for high precision inertial measurements where the dynamics of quantized vortices can serve as sensitive probes of external forces. In our series of theoretical works [2-4], we studied how quantized vorticity is transported between two density-coupled Bose–Einstein condensate rings of equal radius, with a tunable weak link, that can separate and reconnect rings. Under reconnect configuration we observe periodic transfer of the vorticity across two rings. Our extensive quasi-2D and 3D simulations revealed such oscillations to be long-lived, even at finite temperature [2]. At low temperatures and with minimal damping, these oscillations dissipate until the vortex, the carrier of the persistent current, sits in the center of the system. For the large enough damping, there are no oscillations, the vortex stays whenever it was initially.

Further study [4] revealed that these oscillations originate from low-energy collective excitations with phonon-like character. Therefore, persistent current oscillation can be interpreted as an angular momentum transfer mediated by sound waves propagating through the system. The oscillation frequency and damping rate are quantitatively predicted by a simplified hydrodynamic model, in agreement with Bogoliubov–de Gennes analysis and Gross–Pitaevskii simulations. The absence of oscillations with critical damping is identified with overdamped oscillations, explaining vortex localization. Also, we demonstrated that periodic modulation of the weak link barrier at resonant frequencies enables controlled vortex transfer even for lower barrier amplitudes, where a finite density persists in the central region of the double-ring system, through selective excitation of collective modes.

Despite a purely theoretical framework, our studies within observational reach are based on current experimental capabilities and detection schemes and provide explanations of essential physics of the given setup, which pave the way for potential quantum devices and sensors [3].

[1] L. Amico, G. Birkl, M. Boshier, L.-C. Kwek, C. Miniatura, A. Minguzzi, C. Ryu, B. Seaman, S. Stringari, G. Tino, et al., Roadmap on atomtronics: State of the art and perspective, AVS Quantum Science 3, 039201 (2021).
[2] T. Bland, I. V. Yatsuta, M. Edwards, Y. O. Nikolaieva, A. O. Oliinyk, A. I. Yakimenko, and N. P. Proukakis, Persistent current oscillations in a double-ring quantum gas, Physical Review Research 4, 043171 (2022).
[3] A. Chaika, A. Oliinyk, I. Yatsuta, N. Proukakis, M. Edwards, A. Yakimenko, and T. Bland, Acceleration induced transport of quantum vortices in joined atomtronic circuits, SciPost Phys. 19, 005 (2025).
[4] A. Chaika, A. Oliinyk, I. Yatsuta, N. Proukakis, M. Edwards, A. Yakimenko, and T. Bland, Controlled acoustic-driven vortex transport in coupled superfluid rings, arXiv:2510.26591.

Optimization of phonon transmission through the interface between superfluid ^{4}He and bilayer solid structures

J. Amrit[1], V. Luzik[2], K. Nemchenko[2], Ye. Niemchenko[2], T. Vikhtynska[2]

[1]LISN, Université Paris-Saclay, CNRS, 91405, Orsay, France
[2]V.N.Karazin Kharkiv National University, 61022, Kharkiv, Ukraine
e-mail: nemchenko@karazin.ua

This work is devoted to the study of phonon transfer mechanisms from superfluid 4He across a bi-layered solid, made up of a film layer, of a few tens of nanometers in thickness, deposited on a solid [1]. The main problem considered is the thermal boundary resistance [2] (Kapitza resistance), which arises due to acoustic mismatch and significantly limits the efficiency of heat exchange at low temperatures.

The study considered a method for minimizing thermal boundary resistance by applying a film layer at the interface between superfluid helium and a solid body as an anti-reflective coating. The calculations were performed within the framework of an acoustic mismatch model [3], taking into account phase coherence caused by interference effects arising as a result of multiple phonon reflections inside the film.

As a result, it was shown that maximum phonon transmission is achieved when the thickness of the intermediate layer becomes comparable to the wavelength of phonons in the film, due to constructive interference that minimizes total reflection. The results obtained emphasize the importance of nanoscale engineering for controlling phonon transport. The method considered allows improving the parameters of cryogenic systems and can be used to develop new thermoregulation strategies in low-temperature physics.

[1] J. Amrit, V. Luzik, K. Niemchenko, Ye. Niemchenko, A. Tonkonozhenko, and T. Vikhtynska, Low Temp. Phys. 52, 4 (2026).
[2] P. L. Kapitza, Phys. Rev. 60, 354 (1941).
[3] I. M. Khalatnikov, Introduction to the Theory of Superfluidity (Addison-Wesley, Redwood 1989).

Comprehensive analysis of low-temperature thermal conductivity of various epoxy resins and epoxy resin-based composites

Yu. V. Horbatenko[1], A. I. Krivchikov[1], O. A. Korolyuk[1], V. V. Sagan[1], O. O. Romantsova[1,2]

[1]B.Verkin Institute for Low Temperature Physics and Engineering of the NAS of Ukraine, 47 Nauky Ave., Kharkiv, 61103, Ukraine
[2]Institute for Low Temperatures and Structure Research, Polish Academy of Sciences, P.O. Box 1410, 50-950 Wroclaw, Poland
e-mail: horbatenko@ilt.kharkov.ua

We have processed a significant amount of literature data on low-temperature thermal conductivity data of various epoxy resins in the temperature range from 1 K to 100 K: they demonstrate the so-called glassy behavior of thermal conductivity, which can be represented as the sum:

$$\kappa(T) = \kappa_{pl}(T) + \kappa_0 \cdot exp(-E/T) \quad (1)$$

where the first term is the thermal conductivity plateau, $\kappa_{pl.}$, which occurs in disordered solids in the range 2-10 K; and the second term describes a smooth gradual increase in thermal conductivity - and it is similar to the Arrhenius expression, which, in turn, has two fitting parameters – pre-exponential factor and some characteristic energy[1].

It should be noted that the representation of $\kappa(T)$ data as a sum of two terms is consistent with the "Unified theory of thermal transport in crystals and glasses" proposed by Simoncelli- Marzari-Mauri [2], and manifested that heat transfer in a solid is realized in two ways: particle-like (first term) and wave-like tunneling (second term) – $\kappa(T) = \kappa_p(T) + \kappa_c(T)$.

At low temperatures, the particle-like contribution κ_p in amorphous polymers is described using a Matthiessen-type relation [3]:

$$1/\kappa_p = 1/\kappa_{TLS} + 1/\kappa_{pl} \quad (2)$$

where κ_{TLS} represents resonant scattering by two-level system (TLS), following a power law: $\kappa_{TLS} = \beta T^n$ with $n \approx 2$: so thermal conductivity data for the low-temperature range of epoxy resins (to the left of the plateau) demonstrate a dependence of $\kappa(T)$ close to T^2 [3]. So, in general, the temperature dependences of thermal conductivity can be described as:

$$\kappa(T) = \kappa_p(T) + \kappa_c(T) = \frac{\beta T^n \cdot \kappa_{pl.}}{\beta T^n + \kappa_{pl.}} + \kappa_0 \cdot \exp(-E/T) \quad (3)$$

where β is the intensity of low-temperature scattering processes; n is the power-law exponent. Expression (4) describes all thermal conductivity data well, and all fitting parameters were calculated. Finally, we compared data for various epoxy resins with thermal conductivity data for epoxy resin-based composites.

Acknowledgements

This work was supported by the Research Project for Young Scientists of the National Academy of Sciences of Ukraine No. 0125U002900: 12/04-2026.

[1] Y. V. Horbatenko, V. V. Sagan, O. A. Korolyuk, O. O. Romantsova, and A. I. Krivchikov, Low Temp. Phys. 50(5), 379 (2024). https://doi.org/10.1063/10.0025621.
[2] M. Simoncelli, N. Marzari, and F. Mauri, Nature Physics, 15, 809 (2019). https://doi.org/10.1038/s41567-019-0520-x.
[3] Y. V. Horbatenko, O. A. Korolyuk, A. I. Krivchikov, and M. S. Barabashko, Low Temp. Phys. 52(4), 418 (2026).

Thermal conductivity analysis of graphene-containing epoxy composites

Yu. V. Horbatenko, V. V. Sagan, A. I. Krivchikov

B.Verkin Institute for Low Temperature Physics and Engineering of the NAS of Ukraine,
47 Nauky Ave., Kharkiv, 61103, Ukraine
e-mail: horbatenko@ilt.kharkov.ua

We have analyzed experimental data on the temperature dependences of the thermal conductivity of graphene-containing epoxy composites with different percentages of graphene in the temperature range of 4.5-300 K. The obtained results were compared with the data for pure epoxy resin, and it was shown that the addition of graphene to epoxy resin at first glance leads to minor changes in thermal conductivity curves at medium temperatures, while in the low- and high-temperature range these thermal conductivity curves exhibit some features, most likely related to some molecular interactions in the composite.

As previously established [1, 2], the temperature dependence of thermal conductivity for complex molecular substances is well described by a simple approximation:

$$\kappa(T) = \kappa_p(T) + \kappa_C(T) \quad (1)$$

where the first term corresponds to the particle-like contribution of the heat-carriers to the thermal conductivity, and the second term refers to the wave-like tunneling of these carriers. We have considered the description of thermal transport within the framework of advanced concepts of multi-channel heat transfer proposed in [3].

Finally, we found that the temperature dependences of thermal conductivity of graphene-containing epoxy composites with different percentages of graphene and pure epoxy resin are described by three terms – a particle-like term and two exponential terms:

$$\kappa(T) = \kappa_p(T) + \kappa_{01}\cdot exp(-E_1/T) + \kappa_{02}\cdot exp(-E_2/T) \quad (2)$$

Most likely, this is a consequence of the layered structure of carbon materials and intramolecular interactions between the components of the composite.

Acknowledgements

This work is supported by the National Research Foundation of Ukraine (Grant 2023.03/0012).

[1] A. I Krivchikov, Y. V. Horbatenko, O. A. Korolyuk, O. O. Romantsova, O. O. Kryvchikov, D. Szewczyk, and A. Jezowski, Materialia, 32, 101944 (2023). https://doi.org/10.1016/j.mtla.2023.101944.
[2] Y. V. Horbatenko, V. V. Sagan, O. A. Korolyuk, O. O. Romantsova, and A. I. Krivchikov, Low Temp. Phys. 50(5), 379 (2024). https://doi.org/10.1063/10.0025621.
[3] O. A. Korolyuk, V. V. Sagan, A. I. Krivchikov, V. A. Konstantinov, Yu. V. Horbatenko, Low Temp. Phys. 51(9), 1048 (2025). https://doi.org/10.1063/10.0038988.

Comparative analysis of thermal conductivity of polymers under varying temperature and pressure

V. V. Sagan, V. A. Konstantinov

B. Verkin Institute for Low Temperature Physics and Engineering of NAS of Ukraine,
47 Nauky Ave., Kharkiv 61103, Ukraine
e-mail: sagan@ilt.kharkov.ua

In recent years, there has been significant interest in studying heat transfer mechanisms in solids, including polymeric materials, whose properties depend strongly on the degree of structural order. Despite numerous experimental studies, the influence of thermal expansion and volumetric changes on thermal conductivity often remains unexamined, while theoretical estimates are typically made at constant volume.

The aim of this study is to comparatively analyze the temperature and pressure dependences of polymer thermal conductivity under isochoric and isobaric conditions. The study is limited to the low-pressure region (up to ~1 GPa) in the absence of pressure-induced phase transitions, as well as to temperatures at and above the Debye temperature.

It is shown that the temperature dependence of polymer thermal conductivity is determined by morphology and phase state. The effect of pressure on polymer thermal conductivity is analyzed based on a synthesis of experimental literature data and theoretical heat-transfer models [1-3]. It is found that the increase in thermal conductivity with pressure correlates with the compressibility of the material, consistent with the theory of elementary thermal resistance. The Bridgman coefficient, which characterizes the volumetric sensitivity of heat transfer, is examined; it is shown that for most polymers, its value lies in the range of ~2–3.5 and depends only weakly on temperature.

Isochoric and isobaric thermal conductivities are compared for polystyrene (PS) and polycarbonate (PC) [4]. It is shown that even with relatively small Bridgman coefficients, the differences between them can be significant due to the high thermal expansion coefficients of these polymers.

Thus, it is established that volumetric effects play an important role in determining the thermal conductivity of polymeric materials. Accounting for pressure, density, and thermal expansion is necessary for an accurate description of heat transfer and for predicting the thermophysical properties of polymers over a wide temperature range.

[1] M. C. Wingert, J. Zheng, S. Kwon, and R. Chen, Semiconduct. Sci. Technol. 31, 11300 (2016). https://doi.org/10.1088/0268-1242/31/11/113003.
[2] M. Simoncelli, N. Marzari, and F. Mauri, npj Comput. Mater. 9, 106 (2023). https://doi.org/10.1038/s41524-023-01033-4.
[3] R. Hanus, R. Gurunathan, L. Lindsay, M. T. Agne, J. Shi, S. Graham, and G. J. Snyder, Appl. Phys. Rev. 8, 031311 (2021). https://doi.org/10.1063/5.0055593.
[4] T. Kikuchi, T. Takahashi, and K. Koyama, J. Macromolec. Sci. B. 42, 1097 (2003). https://doi.org/10.1081/MB-120023560.

Peculiarities of phase diagram for dense superfluid neutron matter with spin-triplet anisotropic pairing in superstrong magnetic fields

A. N. Tarasov

A. I. Akhiezer Institute for Theoretical Physics, NSC "Kharkov Institute of Physics and Technology" of NAS of Ukraine, 1 Akademicheskaya Str., Kharkiv, 61108, Ukraine
e-mail: antarasov@kipt.kharkov.ua

Within the framework of the generalized nonrelativistic Fermi-liquid approach [1-4], analytical expressions for the phase transition temperatures of neutron matter of supranuclear densities from normal to superfluid states with anisotropic spin-triplet *p*-wave pairing in steady and uniform extremely strong magnetic fields (from the range $10^{17}\div10^{18}$ G) have been obtained [5]. These phase transition temperatures depend nonlinearly on both the neutron matter density and the magnetic field. The expressions for them contain both terms with symmetric and linear field-dependent splitting (as was previously derived in [6,7] for "moderately strong" fields $H \leq 10^{17}$ G), and new additional terms that depend nonlinearly on the superstrong magnetic field (from the interval 10^{17} G $\leq H \leq 10^{18}$ G), which leads to asymmetry and nonlinearity of the splitting of phase transition temperatures relative to the phase transition temperature at zero field. Phase transitions to superfluid states of this type can occur at nuclear and supranuclear densities in the liquid outer core of magnetars (strongly magnetized neutron stars).

[1] A. I. Akhiezer, V. V. Krasil'nikov, S. V. Peletminskii, and A. A. Yatsenko, Phys. Usp. 36, 35 (1993). https://doi.org/10.1070/pu1993v036n02abeh002127.
[2] A. I. Akhiezer, V. V. Krasil'nikov, S. V. Peletminskii, and A. A. Yatsenko, Phys. Rep. 245, 1 (1994). https://doi.org/10.1016/0370-1573(94)90060-4.
[3] A. N. Tarasov, Low Temp. Phys. 24, 324 (1998). https://doi.org/10.1063/1.593593.
[4] A. N. Tarasov, Low Temp. Phys. 26, 785 (2000). https://doi.org/10.1063/1.1330536.
[5] A. N. Tarasov, Low Temp. Phys. 51, 1301 (2025). https://doi.org/10.1063/10.0039547.
[6] A. N. Tarasov, J. Phys.: Conf. Ser. 400, 032101 (2012) [LT26]. https://doi.org/10.1088/1742-6596/400/3/032101.
[7] A. N. Tarasov, EPL (Europhysics Letters) 105, 52001 (2014). https://doi.org/10.1209/0295-5075/105/52001.

The conductivity dip-effect of quasi-one-dimensional electrons over superfluid helium

V. A. Nikolaenko, A. V. Smorodin, S. S. Sokolov

B.Verkin Institute for Low Temperature Physics and Engineering of the NAS of Ukraine,
47 Nauky Ave., Kharkiv, 61103, Ukraine
E-mail: nikolaenko@ilt.kharkov.ua

The conductivity of quasi-one-dimensional surface electrons (Q1D-SEs) over superfluid helium in grooves between rows of dielectric threads is investigated. The measurements performed at frequency 20 kHz by a technique that uses a capacitive coupling of the two plane electrodes 1x0.5 cm in size under a profiled substrate with the subsystem of the surface electrons. Experiments were carried out with the use of nylon threads 100 μm in diameter at temperatures 0.5–1.5 K by scanning the pressing electric field, $E_\perp$, in both directions between 1.1–1.6 kV/cm in magnitude (Fig 1). The difference of levels between substrate and helium, *h,* sets the curvature radius, *R,* of the liquid surface in grooves $R = \alpha / (\rho \cdot g \cdot h)$ (here α and ρ are the surface tension and the density of superfluid helium; g is the gravity constant). The value of R in the present experiments is 35 μm in magnitude. The dip-effect maximum takes place at the pressing field value $E_\perp \sim 1.3$ kV/cm (as shown in the figure). It must be noted: the value of the field minimum essentially depends on the curvature radius. The effect doesn't depend on temperature or parameters of the measurement signal. The field dip-effect disappears at a very large radius curvature in the substrate profiled channels, as well as at a very rough substrate surface.

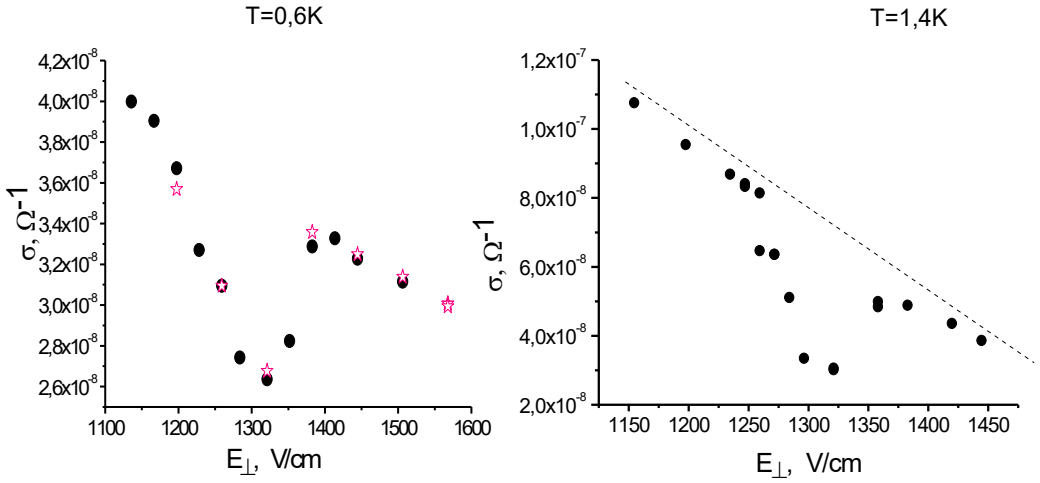

Fig 1. The dependence of the conductivity surface electrons, σ, in profiled channels on the pressing field, $E_\perp$. The left dependence is obtained at T=0.6 K (riplon scattering region), and the right dependence is performed at T=1.4K (gas scattering region).

It must be noted that the position dip minimum practically does not depend on the field, $E_\perp$. The qualitative explanation can be next. The SEs stripe on a non-smooth substrate and relatively large $E_\perp$ is divided into segments, and so an electron percolation through quantum size distance takes place (which is accompanied by noise in experimental measurements). The dip-effects of conductivity have been observed early for 2*D* electrons on a helium film with a rough substrate [1].

[1] P. Leiderer, S. Nazin, and V. Shikin, Low Temp. Phys. 34, 489 (2008).

NANOPHYSICS AND NANOTECHNOLOGIES

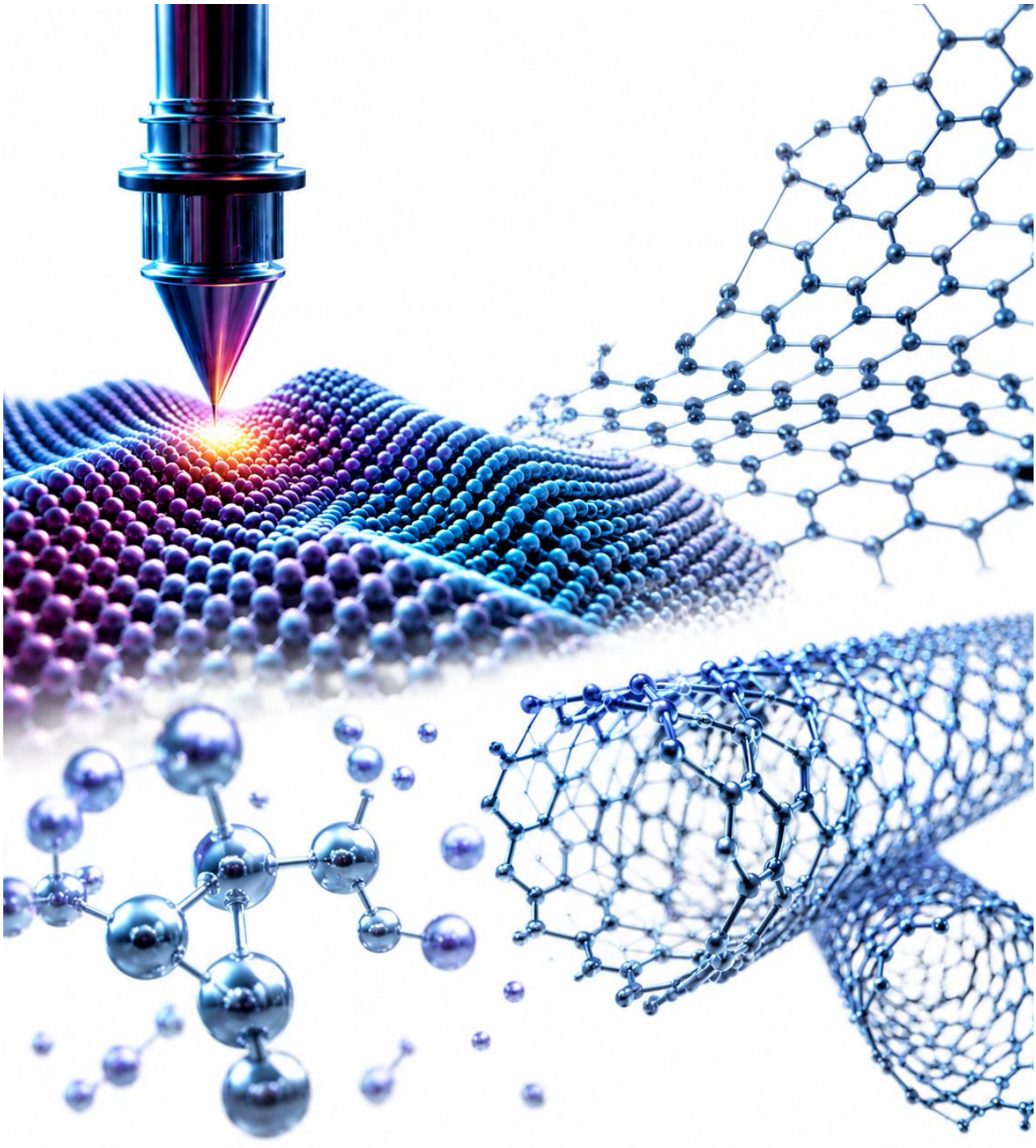

The effect of $BaTiO_3$ nanoparticles on the dielectric properties of the 5CB nematic liquid crystal

J. M. Gudenko[1], V. V. Vainberg[1], O. S. Pylypchuk[1], S. E. Ivanchenko[2], V. N. Poroshin[1], D. O. Stetsenko[1], I. A. Gvozdovskyy[1], A. N. Morozovska[1]

[1]Institute of Physics of the National Academy of Sciences of Ukraine, 46 Nauky Avenue, Kyiv, 03028, Ukraine
[2]Frantsevich Institute for Problems in Materials Science, National Academy of Sciences of Ukraine, 3 Omeliana Pritsaka Str, Kyiv, 03142, Ukraine
email: gudenko.juliya@gmail.com

The influence of ferroelectric nanoparticles on the dielectric properties of liquid crystal (LC) suspensions has been studied. To prepare the liquid crystal suspensions, nematic 4-pentyl-4'-cyanobiphenyl (5CB) and $BaTiO_3$ nanopowder with an average particle diameter of 24 nm were used (Fig. 1). The thicknesses of the samples studied were 21 ± 0.5 μm. The samples contain 0, 0.5, 1.0, 2.0,3.0 and 5.0 wt.% of $BaTiO_3$ nanoparticles [1, 2].

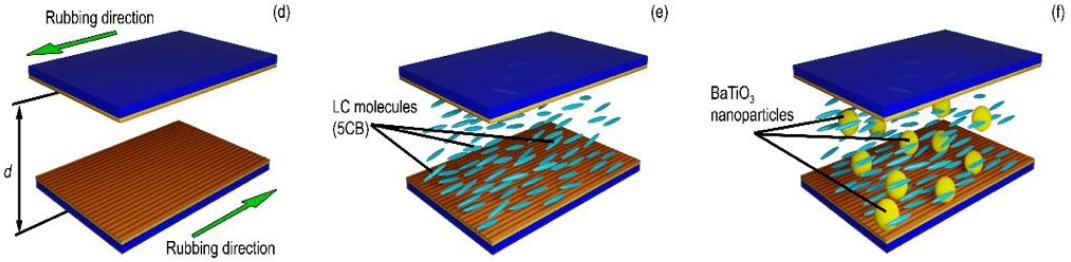

Fig. 1. Schematic diagram of the studies cells: pure LC (left) and an LC suspension with $BaTiO_3$ nanoparticles (right).

The obtained experimental results demonstrated a significant effect of the ultra-low concentrations of $BaTiO_3$ nanoparticles (1 wt% or less) on the electrophysical properties and effective capacitance of the 5CB LC [1]. This effect is explained by the leading role of screening charges, since the surface of a ferroelectric nanoparticle is screened by an ionic-electronic charge, which partially compensates for its spontaneous polarization in the single-domain and/or multi-domain states. A study was performed on the combined (competing and/or complementary) effect of the presence of dispersed nanoparticles and uncontrolled ionic impurities on the anisotropy of the dielectric constant and the phase transition of nematic-isotropic phases. The temperature dependencies of the dielectric permittivity and electric resistance of the samples were measured in the temperature range from 0 to 50 °C, for two perpendicular orientations of the LC director.

Acknowledgments. The work of D.O.S., O.S.P. and A.N.M. are funded by the National Research Foundation of Ukraine (project "Manyfold-degenerated metastable states of spontaneous polarization in nanoferroics: theory, experiment and perspectives for digital nanoelectronics", grant application 2023.03/0132). The work of V.V.V. and V.N.P. are funded by the Target Program of the National Academy of Sciences of Ukraine, Project No. 5.8/26-П "Energy-saving and environmentally friendly nanoscale ferroics for the development of sensorics, nanoelectronics and spintronics".

[1] Ju. M. Gudenko, O. S. Pylypchuk, V.V. Vainberg, et al. Ferroelectric nanoparticles in liquid crystals: Role of ionic transport at small nanoparticle concentrations, SPQEO, 28 (1), P. 010-018 (2025); https://doi.org/10.15407/spqeo28.01.010.
[2] Ju. M. Gudenko, O. S. Pylypchuk, V.V. Vainberg, et al. Dynamics of charge states at the surface of ferroelectric nanoparticle in a liquid crystal, SPQEO, 28 (3), P. 258-266 (2025); https://doi.org/10.15407/spqeo28.03.258.

Universal method of selective detection of a wide range of pollutants in liquids using conductance quantization

A. Herus[1], O. Pospelov[2], A. Savytskyi[1], V. Vakula[1], M. Sakhnenko[2], N. Kalashnyk[3], E. Faulques[3], G. Kamarchuk[1]

[1]B.Verkin Institute for Low Temperature Physics and Engineering of the NAS of Ukraine, 47 Nauky Ave., Kharkiv, 61103, Ukraine
[2]National Technical University "Kharkiv Polytechnic Institute", 2 Kyrpychov Str., Kharkiv, 61002, Ukraine
[3]Univ. Lille, CNRS, Centrale Lille, Yncréa ISEN, Univ. Polytechnique Hauts -de -France, UMR 8520 -IEMN, F -59000, Lille, France
e-mail: agerus579@gmail.com

The development of modern sensor technologies requires new approaches for rapid and highly sensitive analysis of complex chemical systems. In particular, the detection of pollutants in liquid media, including heavy metals and organic compounds, is essential for environmental monitoring and water quality control. Conventional analytical techniques such as optical spectroscopy and chromatography provide high sensitivity but require complex instrumentation and expensive laboratory infrastructure. Advances in nanoscale physics have enabled the development of affordable, low-cost techniques capable of probing electronic transport at the atomic scale for sensor applications. A prominent example of such techniques are quantum point-contact sensors, which utilize conductance quantization in Yanson point contacts [1].

In this work, quantum point-contact sensors based on dendritic Yanson point contacts were employed. The contacts were formed in a "needle–anvil" configuration via electrochemical growth of metallic dendrites in an electrolyte solution. Experiments were performed in a constant current regime, where the cyclic switchover effect leads to periodic formation and dissolution of the conductive channel of the point contact. The structural evolution of the contact is governed by the quantum shell effect, which determines the stability of metastable atomic configurations in the conduction channel. During the experiments, the temporal dependence of electrical resistance $R(t)$ was recorded and conductance histograms were constructed.

The results show that the distribution of quantized conductance states strongly depends on the composition of the surrounding liquid medium and can serve as an energetic fingerprint of the analyzed substance [2]. Quantum point-contact sensors were shown to detect copper, zinc, and lead ions over a wide concentration range, including trace levels down to several parts per billion (ppb). Variations in the position and shape of conductance histogram maxima allow reliable identification of specific ions in solution. Additionally, the detection of organic compounds was demonstrated using acetic acid as a model system.

The nature of the discovered phenomenon can be described as follows. The cyclic formation and dissolution of dendritic Yanson point contacts lead to discrete conductance steps in the $R(t)$ dependence corresponding to metastable atomic configurations determined by the quantum shell effect. The presence of a gapless electrode system ensures localization of electrochemical processes within the conductive contact channel. As a result, even small changes in the chemical composition of the liquid medium significantly modify the conductance histogram structure.

These results indicate that quantum point-contact sensors represent a new approach to chemical detection based on quantum transport phenomena and conductance quantization.

[1] G.V. Kamarchuk, A.P. Pospelov, A.V. Savytskyi, A.O. Herus, Yu.S. Doronin, V.L. Vakula, E. Faulques, SN Appl. Sci. 1, 244 (2019). https://doi.org/10.1007/s42452-019-0241-x.
[2] O. Pospelov, A. Herus, A. Savytskyi, V. Vakula, M. Sakhnenko, N. Kalashnyk, E. Faulques, G. Kamarchuk, Microchem. J., 117555 (2026). https://doi.org/10.1016/j.microc.2026.117555.

Correlations between the dielectric properties and phase diagrams of $Bi_{1-x}Sm_xFeO_3$ nanopowders

V. O. Kolupaiev[1], O. S. Pylypchuk[1], V. V. Vainberg[1], V. N. Poroshin[1], I. V. Fesych[2], L. D. Demchenko[3,4], E. A. Eliseev[5], A. N. Morozovska[1]

[1]Institute of Physics, National Academy of Sciences of Ukraine, 46 Nauky Ave., Kyiv, 03028, Ukraine
[2]Taras Shevchenko National University of Kyiv, Volodymyrska Str., Kyiv, 01030, Ukraine
[3]Stockholm University, Department of Chemistry, 8 Frescativägen, Stockholm, SE-114 18, Sweden
[4]University of Ukraine "Igor Sikorsky Kyiv Polytechnic Institute", 37 Beresteisky Ave., Kyiv, 03056, Ukraine
[5]Frantsevich Institute for Problems in Materials Science of the National Academy of Sciences of Ukraine, 3 Omeliana Pritsaka Str., Kyiv, 03142, Ukraine
e-mail: kolupaiev.v.o@gmail.com

Nanoscale multiferroics with different sizes and shape parameters are basic model objects for studying polar, antipolar, and magnetic orientation as well as magnetoelectric interaction. Bismuth-Samarium ferrite ($Bi_{1-x}Sm_xFeO_3$) is a model orthoferrite, whose polar and magnetic properties have been studied enough for the bulk and thin film samples. Although, the properties of $Bi_{1-x}Sm_xFeO_3$ nanoparticles have been studied much less theoretically and experimentally, despite they have properties, which can be used in a wide range of applications, for example, in energy storage [1] and magnetic hyperthermia [2].

A series of experimental measurements and analysis of the temperature dependence of the $Bi_{1-x}Sm_xFeO_3$ nanopowders dielectric permittivity were conducted. The effective dielectric permittivity of Sm-doped $BiFeO_3$ has an interesting tendency within two characteristic temperature ranges, namely a slow increase from 20°C to 250 – 300°C followed by a sharp increase in the range 300°C - 400°C that may lead to the maximum formation at higher temperatures. Theoretical estimations and computer modelling results [3] explain the main trends of experimentally observed temperature dependences of the effective dielectric permittivity, which allows us to understand the correlations between the temperature behavior of dielectric properties, domain structure morphology and phase state of $Bi_{1-x}Sm_xFeO_3$ nanoparticles. The chemically controlled dielectric permittivity is a key for controlling the electrophysical properties, such as magnetoelectric effect and electric conduction. Therefore, the results of the work can help to create ferroics with custom and/or controllable polar and dielectric properties, as well as to find advanced applications in nanoelectronics and energy storage.

Acknowledgments. The work of O.S.P. and A.N.M. are funded by the National Research Foundation of Ukraine (project "Manyfold-degenerated metastable states of spontaneous polarization in nanoferroics: theory, experiment and perspectives for digital nanoelectronics", grant application 2023.03/0132). The work of E.A.E. is funded by the National Research Foundation of Ukraine (project 2023.03/0127 "Silicon-compatible ferroelectric nanocomposites for electronics and sensors"). The work of V.V.V. and V.N.P. are funded by the Target Program of the National Academy of Sciences of Ukraine, Project No. 5.8/26-П "Energy-saving and environmentally friendly nanoscale ferroics for the development of sensorics, nanoelectronics and spintronics"

[1] Amira Bougoffa, E. M. Benali, A. Benali, M. Bejar, E. Dhahri, M. P. Graça, M. A. Valente, G. Otero-Irurueta, B. F. Costa, RSC Advances, 12 (11), 6907–6917, (2022). https://doi.org/10.1039/D1RA08975G
[2] K. Papadopoulos, E. Myrovali, D. Karfaridis, M. Farle, U. Wiedwald, M. Angelakeris, Journal of Alloys and Compounds, 969, 172337, (2023). https://doi.org/10.1016/j.jallcom.2023.172337.
[3] O.S. Pylypchuk, V.O. Kolupaiev, I.V. Fesych, V.N. Poroshin, and A.N. Morozovska, Ukrainian Journal of Physics, 70 (10), 717, (2025). https://doi.org/10.15407/ujpe70.10.717.

Optimization of thermal transport properties in silicon structures with inhomogeneous porosity: experiment and machine learning

P. O. Lishchuk, L.I. Chepela, V. B. Shevchenko, M. O. Borovoy, V. V. Kuryliuk, O. Ya. Olikh

Taras Shevchenko National University of Kyiv, 64/13, Volodymyrska Str., Kyiv, 03028, Ukraine
e-mail: pavel.lishchuk@knu.ua

Understanding heat transport in porous and multilayer silicon structures is of great importance for modern micro- and nanoelectronics, thermoelectric systems, and thermal insulation technologies, where accurate control of thermal conductivity is essential for device reliability. To address these challenges, this study employs a comprehensive approach combining experimental measurements, molecular dynamics (MD) simulations, and machine learning.

Firstly, the thermal and transport properties were investigated using the photoacoustic (PA) method. This non-destructive technique is based on the generation of acoustic waves resulting from periodic heating of a sample by modulated light. The thermophysical parameters, specifically thermal diffusivity and thermal conductivity, were determined from the frequency-dependent amplitude and phase of the PA signal.

In parallel, MD simulations were performed using the Green–Kubo method, which involves integrating the heat current autocorrelation function. Furthermore, a Physics-Informed Neural Network (PINN) was employed to solve the 2D Fourier heat conduction equation for porous models generated using the Quartet Structure Generation Set (QSGS) algorithm. The figure presents the results obtained for a homogeneous structure at room temperature. A strong correlation is observed between the thermal conductivity values obtained using the different approaches. The slightly lower thermal conductivity predicted by MD simulations can be attributed to finite-size effects that limit the contribution of long-wavelength phonons, as well as to the finite simulation time. As porosity increases, phonon scattering at pores becomes the dominant heat-transport mechanism, reducing the discrepancy between the methods.

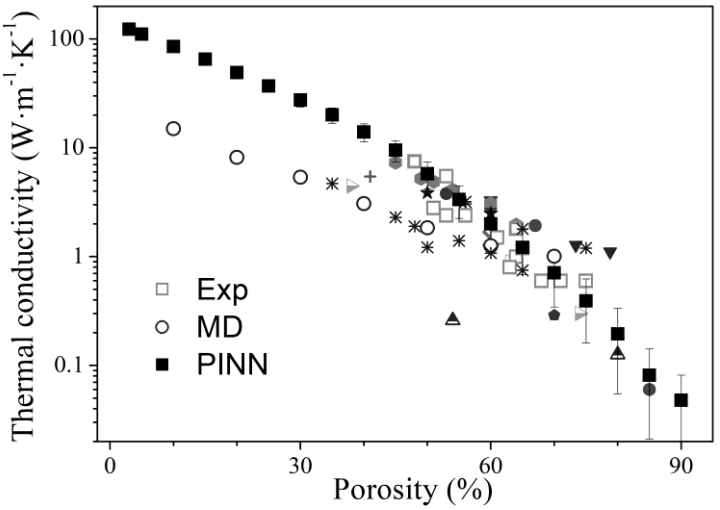

Fig. 1. Thermal conductivity of porous silicon as a function of porosity obtained using various methods. Experimental data reported in the literature are also included for comparison.

Finally, the study evaluated multilayer silicon structures with varying porosity. Both experimental and PINN-based data deviate from the effective medium approximation, with discrepancies increasing alongside the porosity contrast between layers. The interfacial thermal resistance was quantitatively estimated, providing essential data for the design of advanced thermal insulation components.

The work was supported by National Research Foundation of Ukraine (project No. 2023.03/0252).

Controlling the pro-oxidant properties of cerium oxide nanocrystals by Fe^{3+} doping and morphology modification

M. I. Lupan, G. V. Grygorova, V. V. Seminko, P. O. Maksimchuk, S. L. Yefimova

Institute for Scintillation Materials of NAS of Ukraine, 60 Nauky Ave., Kharkiv, 61072, Ukraine
e-mail: nikita.lupan4@gmail.com

Since the discovery of their antioxidant properties in the early 2000s, cerium oxide nanocrystals have been extensively investigated by global research groups as therapeutic agents with predominantly beneficial effects, such as radioprotection and ROS-scavenging. While this line of research remains highly relevant, recent years have seen a shift toward more active investigation of the pro-oxidant properties of various particles. Key applications of such pro-oxidant particles include their use in antitumor therapy, antimicrobial formulations, and water purification systems.

Numerous studies have demonstrated that cerium oxide exhibits pro-oxidant properties at low pH levels. This characteristic makes it a compelling therapeutic agent, as it protects cells at neutral pH while inducing oxidative stress and subsequent cell death under the acidic conditions typical of the cancer microenvironment. However, the transition from antioxidant to pro-oxidant behavior in cerium oxide occurs relatively slowly, which limits its direct clinical application. Consequently, there is a significant interest in developing methods to modulate and control the pro-oxidant properties of these nanocrystals.

In this study, we investigated two distinct strategies to enhance the pro-oxidant activity of cerium oxide nanocrystals: doping with iron ions and surface morphology modification. An increase in pro-oxidant activity was observed in both cases. The incorporation of Fe^{3+} ions into the CeO_{2-x} lattice promotes the formation of additional oxygen vacancies due to charge compensation, which subsequently increases the concentration of Ce^{3+} ions and enhances the overall catalytic activity. Furthermore, surface-bound Fe^{3+} ions may directly participate in redox reactions. Our findings demonstrate that iron doping significantly boosts the pro-oxidant properties of nanoceria; however, this relationship is non-linear. Specifically, the peroxidase-like activity reaches a pronounced maximum at 5% iron doping, significantly outperforming the activities observed at 3% and 10% doping levels.

Study of nanoparticles with different morphologies further revealed that the activity of cerium oxide nanocrystals can vary by up to an order of magnitude depending on the specific crystallographic facets exposed. Specifically, rhombohedral nanocrystals predominantly enclosed by (111) planes exhibit peroxidase-like activity approximately 7–8 times higher than that of nanocubes of similar dimensions characterized by (100) facets. Consequently, the distinct surface planes—and their corresponding energies of defect formation, primarily oxygen vacancies—exert a profound influence on the pro-oxidant activity of cerium oxide.

In summary, iron doping and morphology engineering provide effective routes for controlling the pro-oxidant activity of cerium oxide nanocrystals. These results highlight the importance of defect structure and surface facets in determining the catalytic behavior of nanoceria.

Acknowledgments: This research was supported by National Research Foundation of Ukraine, Grant № 2025.07/0093.

Defect evolution in irradiated multilayer graphene

S. I. Menshykova[1*], S. I. Khaldeev[1], A. Ruhtinas[2], S. Moulick[1], J. T. Mäkinen[1], P. Hakonen[1]

[1]Department of Applied Physics, Aalto University, P. O. Box 15100, FI-00076 Aalto, Finland
[2]Nanoscience Center, Department of Physics, University of Jyväskylä,
P. O. Box 35, FI-40014 Jyväskylä, Finland
e-mail: svitlana.menshykova@aalto.fi

Control and characterization of defects in graphitic systems are crucial for tailoring their electronic and structural properties. Defect engineering is a promising strategy to create a periodic defect-induced potential to modify the electronic band structure, which may potentially lead to the opening of a superconducting gap. It is known that Raman spectroscopy is a standard method for structural and defect analysis [1]. Detailed analysis of the intensity ratio of defect-induced features allows for distinguishing between different types of disorder (vacancies, grain boundaries, sp3-type defects). While our long-term goal focuses on creating periodic defect-induced potentials, it is essential to investigate the controlled generation of defects and their subsequent healing through a thermal annealing.

Natural graphite flakes with a thickness of 30 nm were prepared by the method of mechanical exfoliation onto pre-cleaned Si substrates with a SiO_2 layer (290 nm) on top. The morphology and thickness of the flakes were investigated using atomic force microscopy (AFM). Raman spectroscopy was used to characterize the structure of the flakes before and after the irradiation and annealing processes. Helium ion irradiation using a Focused Ion Beam (FIB) system was used to create controlled lattice disorder according to a given pattern. To recover the damaged crystalline lattice and to stabilize the induced defects a thermal annealing process at 200°C for 9 hours in vacuum was performed. The collected Raman spectra at each stage of the process (pristine, irradiated and annealed) were analyzed.

Irradiation with Helium ions led to a significant increase in the D peak (so-called defect peak) intensity, accompanied by the emergence of a distinct D' shoulder. The appearance of both peaks indicates the transition from high-quality pristine graphite to a disordered structure [2]. The calculated ratio between defect peaks after irradiation indicates the creation of different types of defects depending on the pattern.

Low-temperature annealing at 200°C led to a substantial reduction in the D peak intensity, while the D' peak nearly vanished across the sample. The analysis of the ID/ID’ ratio after annealing indicates a change in the dominant defect type from vacancies to boundary-like defects [2]. This effect was interpreted as selective annihilation of Frenkel defects (point-like vacancies and interstitial atoms), which have higher mobility at the annealing temperature, leaving behind more stable extended defects such as grain boundaries or reconstructed lattice edges. This study highlights the effectiveness of the ID/ID’ ratio as a sensitive probe for monitoring the "healing" kinetics of graphitic materials.

This work was supported by the Research Council of Finland through the mobility grant for Ukrainian researchers (Decision No. 359743) and within the framework of the SuperC project. The experimental work benefited from the Aalto University OtaNano/LTL facilities.

[1] M. Lucchese, F. Stavale, E. Martins Ferreira, C. Vilani, M. Moutinho, Rodrigo B. Capaz, C. Achete, A. Jorio, Carbon 48 (5), 1592 (2010). https://doi.org/10.1016/j.carbon.2009.12.057.
[2] A. Eckmann, A. Felten, A. Mishchenko, L. Britnell, R. Krupke, K. S. Novoselov, C. Casiraghi, Nano Lett. 12, 8, 3925 (2012). https://doi.org/10.1021/nl300901a.

[*]*Permanent address: National Technical University "Kharkiv Polytechnic Institute", 2 Kyrpychova Str., Kharkiv, 61002, Ukraine*

Nanoceria-based complexes for improved sensing of redox-active molecules in biological media

V. V. Seminko, Ye. I. Neuhodov, P. O. Maksimchuk, G. V. Grygorova, S. L. Yefimova

Institute for Scintillation Materials, National Academy of Sciences of Ukraine,
60 Nauky Ave., Kharkiv, 61072, Ukraine
e-mail: seminko@ukr.net

Today, direct and indirect methods for detecting redox-active biomolecules (in particular, reactive oxygen species) are represented by fluorimetry, chemiluminescence and spectrophotometry. In recent years, a large number of new sensors have been developed (in particular, based on Prussian blue (PB), heme proteins, carbon nanotubes and various metal nanoparticles), which has increased the sensitivity and efficiency of methods for detecting hydrogen peroxide. The redox sensitive luminescence of Ce^{3+} ions in cerium oxide nanocrystals opens the possibility of detecting redox-active biomolecules in aqueous solutions using optical spectroscopy methods, which in many applications (primarily biological) is much more convenient than the use of amperometric methods or enzymes. Our previous studies have revealed that Ce^{3+} ions in ceria NPs possess characteristic 5d-4f luminescence, which intensity changes during interaction with reactive oxygen species (ROS) or other redox active molecules. Linear dependence of Ce^{3+} luminescence intensity on the concentration of HP in water solutions allowed us proposing these NPs as multifunctional agents with both ROS scavenging and ROS sensing properties [1]. At the same time, the dynamic range of concentrations detectable by the change of Ce^{3+} luminescence is limited to millimolar values due to relatively low intensity of 5d-4f Ce^{3+} transitions in this crystal host. This fact limits sufficiently the possible applications of these NPs as HP sensors in biomedical field as HP concentrations in living cells rarely exceed tens of micromoles per liter.

In order to remove the restriction determined by low HP sensitivity of Ce^{3+} luminescence and improve both sensing and physicochemical properties of nanoceria we have obtained nanoceria-FBS (fetal bovine serum) complexes. Besides improving aggregation stability in biological environments (DMEM, C199, and Hanks), fetal bovine serum had a sufficient effect on the luminescence intensity of 5d-4f transitions of Ce^{3+} ions in nanoceria due to enhanced $Ce^{4+} \rightarrow Ce^{3+}$ reduction in the presence of FBS acting as a reducing agent. We have revealed that the presence of protein corona formed by FBS proteins do not deteriorate the ROS sensing properties of nanoceria, moreover, the increase in the luminescence intensity of Ce^{3+} ions allows widening sufficiently the dynamic range of HP concentrations detectable by the change in Ce^{3+} luminescence intensity (from mM to tens of μM) [2]. The luminescence sensors based on the FBS-stabilized cerium oxide nanoparticles are reversible due to $Ce^{3+} \leftrightarrow Ce^{4+}$ regeneration ability in nanoceria and able for multi-use in biological media. Generally, FBS-induced improvement in biocompatibility, aggregation stability and sensitivity of CeO_{2-x} luminescent sensors opens the direct way for their biological applications.

This work was supported by Verkhovna Rada of Ukraine Scholarship for Young Scientists (Doctors of Sciences) for 2025, recipient – Dr. Vladyslav Seminko.

[1] Y. Malyukin, V. Seminko, P. Maksimchuk, E. Okrushko, O. Sedyh, Y. Zorenko, Optical Materials. 85, 303-307 (2018). https://doi.org/10.1016/j.optmat.2018.08.063.
[2] Y. Neuhodov, V. Seminko, P. Maksimchuk, G. Grygorova, K. Hubenko, N. Kavok, G. Dudetskaya, Yu. Kot, S. Yefimova, Journal of Molecular Liquids. 433, 127798 (2025). https://doi.org/10.1016/j.molliq.2025.127798.

Dimensional effect on relaxation processes of polypropylene glycol 1000 confined in silica-gel nanopores

A. O. Sobchuk[1], D. A. Andrusenko[1], V. B. Shevchenko[1], S. A. Alekseev[1], K. S. Yablochkova[1], R. V. Dinzhos[2,3]

[1]Taras Shevchenko National University of Kyiv, Faculty of Physics,
4 Akademika Hlushkova Ave., Kyiv, 03187, Ukraine
[2]Petro Mohyla Black Sea National University, 68 Desantnykiv Str., Mykolaiv, 54003, Ukraine
[3]Institute of Polymers, Bulgarian Academy of Sciences,
Acad. Georgi Bonchev Str., Block 103A, Sofia, 1113, Bulgaria
e-mail: sobchukandriii@gmail.com

Polypropylene glycol (PPG) and related polyethers are widely used in functional material. When confined in silica-based nanopores, PPG forms nanocomposite systems whose molecular dynamics are governed by the interplay between finite-size confinement and interfacial interactions with the pore walls. Previous studies of confined PPG have shown slower translational diffusion compared with the bulk state, the formation of interfacial regions with different mobility, and pore-size-dependent changes in the segmental and normal-mode relaxation processes. These features make nanoconfined PPG a convenient model system for studying dimensional effects in relaxation phenomena.

The present research aims to determine the influence of dimensional effects on the relaxation processes of polypropylene glycol 1000 confined in silica-gel nanopores. The object of this study is PPG 1000/silica-gel nanocomposites, in which restricted geometry and polymer–surface interactions jointly affect molecular mobility. Our research methods include IR spectroscopy, differential scanning calorimetry, dielectric spectroscopy, and X-ray diffraction. We show that the thermal and dielectric relaxation behavior of confined PPG 1000 differs from that of the bulk polymer and depends on the pore size of the host matrix. The mechanisms of thermal mobility and relaxation in these nanocomposites are discussed in terms of the contribution of interfacial polymer layers and confinement-induced changes in molecular packing.

Analytical approaches to describe phonon heat transfer in two-dimensional nanoconductors

J. Amrit[1], I. Kudriavtsev[2], K. Nemchenko[2], Y. Niemchenko[2], M. Spotar[2], T. Vikhtynska[2]

[1]LISN, Université Paris-Saclay, CNRS, 15 Rue Georges Clemenceau, Orsay, 91405, France
[2]V. N. Karazin Kharkiv National University, 4 Svobody Sq, Kharkiv, 61022, Ukraine
e-mail: xa12283354@student.karazin.ua

In this report we analyze the mechanism of phonon heat transport in nanoribbons with diffuse scattering on boundaries. The temperature profile of heat flow in a two-dimensional nanoconductor is given by the integral equation [1, 2]:

$$t(x) = \frac{1}{2}\left[1 - \frac{x}{\sqrt{w^2+x^2}}\right] + \frac{1}{2w}\int_0^1 dx_1 \frac{1}{[1+(x-x_1)^2]^{\frac{3}{2}}} t(x_1), \quad (1)$$

in which $w = W/L$ is the ratio of the width W to the length L of the conductor, $t(z)$ is the normalized temperature and z is the normalized coordinate along the conductor. Numerical solutions of similar equations that describe radiative heat transfer by phonons in the ballistic regime with diffusive [3] and reflective [4] scattering mechanisms show a near-linear distribution of temperature profile in samples. A linear first-order approximation is proposed to describe temperature dependence on the coordinate along the sample [5]:

$$t^{(1)}(x) = \frac{[1+\Delta T(w)(1-2x)]}{2}, \quad (2)$$

where $\Delta T(w) = \left\{1 + 4w\left[1 + (1 + \frac{w}{\sqrt{1+w^2}})\right]^{-1}\right\}^{-1}$ derivative of the temperature profile is defined using boundary conditions. Using linear solution (2) as a first-order approximation, allowing analytically obtaining higher-order iterations applying the iterative method:

$$t^{(N+1)}(x) = \frac{1}{2}\left[1 - \frac{x}{\sqrt{w^2+x^2}}\right] + \frac{1}{2w}\int_0^1 dx_1 \frac{1}{[1+(x-x_1)^2]^{\frac{3}{2}}} t^{(N)}(x_1). \quad (3)$$

Examination of linear solution deviations from numerical suggests adding a cubic term that is equal to zero in the middle and at the boundaries of the sample and, subsequently, correcting the derivative of the temperature profile in the middle of the sample:

$$t_{cubic}(x) = \frac{[1+\Delta T_q(w)(1-2x)+Qx(1-x)(1-2x)]}{2}, \quad (4)$$

as an alternative method to achieve a more precise model of temperature distribution. Parameters $\Delta T(w)$ and Q calculated applying corresponding boundary conditions.

The methods demonstrated in this work provide results that compare well with results of numerical calculations [3, 5] outside very long conductors with a width to length ratio $\frac{W}{L} < 0.05$. The problem of very long conductors emerged in nearly all methods [3] for solving equation (1) due to the extremely small value of the heat flux in such structures that makes it highly sensitive to calculation errors and features of particular methods. To take into account the case of a very long conductor, we showed a fitting-coefficient method for linear approximation (2):

$$\Delta T_f(w) = \Delta T(w)\left[1 - \frac{0.02}{1+w}\right], \quad (5)$$

that demonstrates a fairly accurate description for the entire range of ratios of the width to length of the nanoribbons.

[1] J. Amrit, K. Nemchenko, T. Vikhtinskaya, Journal of Applied Physics, 129, 085105 (2021). https://doi.org/10.1063/5.0036935.
[2] D. Clausing, Ann. D. Physik, 404, 961 (1932). https://doi.org/10.1002/andp.19324040804
[3] T. Klitsner, J. E. VanCleve, H. E. Fischer, R. O. Pohl, Phys. Rev. B, 38, 7576 (1988). https://doi.org/10.1103/PhysRevB.38.7576.
[4] M. Perlmutter, R. Siegel, J. Heat Transfer, 85, 55-62 (1963). https://doi.org/10.1115/1.3686010.
[5] J. Amrit, T. Medintseva, Ye. Nemchenko, K. Nemchenko, M. Spotar, S. Rogova, T. Vikhtinskaya, Low Temp. Phys. 49, 961 (2023). https://doi.org/10.1063/10.0020163.

Long-range tunneling of magnons between nanomagnets connected by a ferromagnetic chain

S. M. Tunyk, E. G. Petrov

Bogolyubov Institute for Theoretical Physics, National Academy of Sciences of Ukraine,
14-B Metrolohichna Str., Kyiv, 03143, Ukraine
e-mail: toonik@ukr.net

In the field of quantum technologies, the precise control of physical processes at the atomic-molecular level is essential. Cavity magnonics has emerged as a key area of study, focusing on hybrid microwave structures (magnon cavities) where electromagnetic field energy is transduced into magnetostatic spin excitations, known as Kittel magnons, of an embedded nanomagnet. While traditional spintronics relies on charged particles, the resulting Joule heat limits long-distance information transmission. Magnons, as uncharged carriers, offer a promising alternative for quantum communication without thermal losses.

This work proposes a physical mechanism for the coherent long-range transfer of spin excitations between nanomagnets connected by a bridge consisting of a ferromagnetic chain (the AFB system). We demonstrate that Kittel magnons can facilitate communication between magnon cavities through coherent one-step tunneling. Using a semiphenomenological approach, analytical expressions for the magnon transport rate were obtained, identifying parameters that control both off-resonant and resonant tunneling regimes.

In the off-resonant regime, the transfer rate decreases exponentially as the number of units in the bridge chain increases. Conversely, in the resonant regime, where the Kittel magnon energy falls within the chain's magnon band, the transport efficiency increases by several orders of magnitude. We define the physical conditions under which peak transport rates occur, whether at fixed tunneling energies or varying chain lengths. Furthermore, it is shown that strong photon-magnon coupling within the cavity leads to additional peaks in the tunneling flow, reflecting the resonant conversion of photons to magnons. These results suggest that switching magnon tunneling modes via external magnetic fields can serve as an effective tool for controlling information transfer in ferromagnetic nanostructures.

[1] E. G. Petrov, S. M. Tunyk, V. V. Gorbach, Phys. Rev. Appl. 25, 024072 (2026). https://doi.org/ 10.1103/v979-v754.

Influence of post annealing temperature and aging effect on electrical properties of chromium nanofilms

S. Udachan[1], S. B. Kolavekar[1], N. H. Ayachit[1], L. A. Udachan[2], S. S. Kolkundi[3], S. Ramya[4], S. Veeresh[4]

[1]Department of Physics, School of Advanced Sciences, KLE Technological University, Hubballi-580031, India
[2]S. S. Tegnoor Degree College, Kalaburagi-585105, India
[3]Government First Grade College, Shahapur-585223, Yadgir, India
[4]Shree Sangam Vidya Mandir, Kalburagi-585104, India
e-mail: shivaudachan8@gmail.com

It is possible that diffusion processes can be triggered by annealing. It is true that in most cases annealing releases stress in the crystal structure, but there are cases where the opposite happens. wherein some cases, the electronic resistance is increased with the post-annealing process [1-2]. Aging [3] involves just annealing the films at room temperature and determining the resistance of the films over time. The resistance (R) of films is shown to expand significantly in extremely thin films for a period of up to 15 hours for Cr and to remain rather constant thereafter.

[1] Sunil Jagannath Patil, International Journal of Scientific Development and Research (IJSDR) 302, 8, 8 (2023). https://ijsdr.org/papers/IJSDR2308041.pdf.
[2] Andreas Kaidatzis, Vassilios Psycharis, Konstantina Mergia, Dimitrios Niarchos, Thin Solid Films. 619, 61-67, (2016), https://doi.org/10.1016/j.tsf.2016.10.027
[3] Halyna Klym, Ivan Hadzaman, Yuriy Kostiv & Dmytro Chalyy, Molecular Crystals and Liquid Crystals. 767, 1, 42-50, (2023). https://doi.org/10.1080/15421406.2023.2224987.

Impact of nanocomposite polymer film formulation on the corrosion resistance of cold-rolled steel surfaces

M. V. Borysenko, B. M. Gorelov, L. I. Borysenko, V. L. Roshchenko

Chuiko Institute of Surface Chemistry of NAS of Ukraine,
17 Oleha Mudraka Str., Kyiv, 03164, Ukraine
e-mail: borysenko@nas.gov.ua

The search for sustainable anticorrosive coatings for metal surfaces capable of operating across a wide temperature range and in aggressive environments based on epoxy polymer materials remains a critical scientific challenge today. This study focuses on investigating coating stability by determining the impact of salt spray on the surface corrosion of cold-rolled steel coated with an epoxy-polymer nanocomposite film. The composite is based on ED-20 epoxy resin cured with PEPA (polyethylenepolyamine) and PO-300 (polyamide resin). Highly dispersed oxides of silicon, aluminum, and titanium, as well as asbestos, basalt, tuff, and talc, were utilized as nanofillers, along with heat-resistant organic additives to enhance the mechanical strength of the composites.

A salt spray atmosphere with a constant temperature of 35±1.7 °C was generated in an Auto Technology climatic chamber. The concentration of the sprayed NaCl solution was 5%, with the pH maintained within the range of 6.5–7.2. Standard 0.5 mm wide scribes were applied to the center of the 100×100×0.77 mm steel plates, reaching the metal substrate through the 30–50 μm thick polymer films. The panels (Fig. 1.), previously heat-treated at 25 °C and 100 °C, were exposed to the aggressive environment with inspections conducted after 48, 100, 200, 300, 500, 800, and 1000 hours, in accordance with DSTU ISO 9227:2015. Adhesion was evaluated using the cross-cut method (ISO 2409) both before and after the corrosion tests, as well as after exposure to liquid nitrogen (-196 °C).

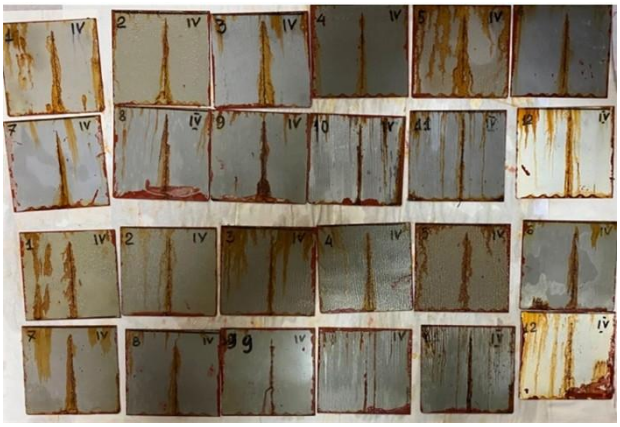

Fig. 1. Visual inspection of the test panels after 200 hours of exposure. Samples cured at 25 °C (Rows 1–2) versus post-cured at 100 °C (Rows 3–4).

The corrosion resistance of the coating on cold-rolled steel depends on several factors, ranked in the following order of importance:

1. Optimal composition (synergy): The best results (1000 hours) are achieved through the synergy of the epoxy resin with active fillers (TiO_2, SiC, basalt) and complex curing agents (PEPA or PO-300).

2. Thermal conditions: For most epoxy systems, post-curing (heating up to 100 °C) is desirable to ensure the completion of polymerization processes.

3. Barrier effect: Fillers with plate-like (lamellar) or needle-like (acicular) structures provide superior protection against salt spray penetration compared to a thick layer of pure polymer.

Atomic ordering in M2X-type MXenes: statistical thermodynamics and kinetics

A. V. Chystota, T. M. Radchenko, V. A. Tatarenko

G. V. Kurdyumov Institute for Metal Physics of the N.A.S. of Ukraine,
36 Academician Vernadsky Blvd., Kyiv, 03142, Ukraine
e-mails: chystota@imp.kiev.ua, tarad@imp.kiev.ua, tatar@imp.kiev.ua

As is known, the re-distribution of atoms of components in MXenes can lead to the formation of the in-plane (intra-planar) or out-of-plane (inter-planar) atomic-ordering structures. Apparently, the properties of crystalline systems are determined not only by the large composition of components, but also by the distribution of atoms over the crystal-lattice sites. Interactions between atoms of different types lead to deviation from their random spatial distribution and the appearance of the short-range (correlation) or long-range order (LRO). Changes in the degree of perfection (LRO parameter) of the crystalline system, related to the ordering of atoms, strongly affect the properties of materials: structural, mechanical, thermal, electrical, magnetic, and optical ones [1, 2]. The possibility of control of the arrangement of metal (M) and/or non-metal (X) atoms to form ordered (super)structures gives control over the MXenes' properties that is unique to the field of quasi-two-dimensional (quasi-2D) materials [3].

The statistical-thermodynamics and kinetics models of long-range atomic order in the interstitial solid solution M–X based on a quasi-2D M2X-type MXene lattice are proposed. Ordered distributions of interstitial atoms (X) over the interstices of the hexagonal host-metal (M) lattice at the different compositions and temperatures are described theoretically. (If interstitial positions in the host-metal lattice are vacant, then, we denote them as ∅. In this case, the distribution of the interstitial components (X and ∅) over the interstices of the hexagonal lattice can be described by a single-particle function that defines the probability of finding an interstitial atom in a given interstitial position of the solvent crystal lattice.)

The ranges of values of interatomic-interaction parameters, which correspond to the generation of the ordering of a subsystem of interstitial atoms characterized by a certain superstructure type (M2X, M4X, M6X or M8X), are obtained. All predicted interstitial superstructures could be stable at certain (appropriate) energy-parameter values, even if taking into account the latter only for the first three interstitial coordination shells. However, their account taken only for the first shell renders the impossibility of predicting some superstructures. The contribution of interactions between atoms at different distances, depending on the sign of their 'mixing' (ordering) energy, contributes to or impedes the atomic ordering that determines the structure symmetry.

[1] 2D Metal Carbides and Nitrides (MXenes): Structure, Properties and Applications, Editors: Babak Anasori and Yury Gogotsi (Springer, Nature, Switzerland 2019). https://doi.org/10.1007/978-3-030-19026-2
[2] Shrabani De, Sourav Acharya, Sumanta Sahoo, and Ganesh Chandra Nayak, Current trends in MXene research: properties and applications, Materials Chemistry Frontiers 5, 7134–7169 (2021).https://doi.org/10.1039/D1QM00556A
[3] Weichen Hong, Brian C. Wyatt, Srinivasa Kartik Nemani, and Babak Anasori, Double transition-metal MXenes: Atomistic design of two-dimensional carbides and nitrides, MRS Bulletin 45, 850–861 (2020). https://doi.org/10.1557/mrs.2020.251

Surface adsorption of eosin Y on carbonate-intercalated Mg_2Al layered double hydroxide

E. Dukhopelnikov[1], K. Bereznyak[1], A. Laguta[2], N. Hladkovska[1], Iu. Blyzniuk[1], A. N. Salak[3]

[1]O.Ya. Usikov Institute for Radiophysics and Electronics NAS of Ukraine, 12 Akad. Proskury Str., Kharkiv 61085, Ukraine
[2]V.N. Karazin Kharkiv National University, 4 Svobody Sq., Kharkiv, 61022, Ukraine
[3]DEMaC-CICECO-Aveiro Institute of Materials, University of Aveiro, Aveiro 3810-193, Portugal
e-mail: dukhopelnikov@gmail.com

Layered double hydroxides (LDH) are of great interest due to their sorption properties caused by huge specific surface area of 2-D frames formed by positively charged mixed M^{2+}/M^{3+} metal hydroxide layers with anions in the interlayer. Anionic dyes can interact with LDH nanoparticles through two mechanisms (surface adsorption and intercalation) [1], which complicates the interpretation of binding processes. We used $Mg_2Al–CO_3$ LDH to focus on surface adsorption because intercalated $CO_3$2- anions bind strongly to hydroxide layers, reducing the interlayer spacing and making impossible intercalation of bulky organic anions [2]. Accordingly, the dianionic dye Eosin Y (EY) interacts with $Mg_2Al–CO_3$ in aqueous suspensions through surface adsorption within the time frame of the experiment, allowing exclusive investigation of surface binding mechanism.

According to Dynamic Light Scattering (DLS) study, the LDH nanoparticles have low colloidal stability, i.e. time stability is limited. The increase in size and polydispersity index was slight on day 3 and significant on day 7. Laser Doppler Electrophoresis (LDE) measurements revealed a pronounced drop in ζ-potential of nanoparticles with increased hydrodynamic size at short-range EY concentrations, indicating strong affinity of EY to the positively charged LDH surface. This range falls at a small electrolyte concentration that provides clear evidence of specific binding of dianion to the particle surface. Aggregated particles with dye precipitate.

UV–Vis titration spectra showed an overall increase in optical density due to light scattering and intrinsic LDH absorption, without any significant shift of the EY absorption maximum. Spectral decomposition by the MCR-ALS algorithm indicates only two absorbing species in the system, namely free dye and LDH particles. Thus, surface binding of EY to LDH, assumed by DLS&LDE analysis, is not accompanied by noticeable spectral changes. Therefore, the concentration of the adsorbed dye cannot be directly determined from titration experiments. To quantify binding efficiency, absorption spectra of the supernatants of the centrifuged mixtures with different LDH concentrations were studied and showed no nanoparticle contribution. It indicates LDH sedimentation together with the bound dye and allows the determination of the free EY concentration. Fitting the dependence of the dye binding degree on LDH concentration using the Verhulst logistic equation revealed a low value of encapsulation efficiency, with $EE_{max} \approx 40\%$.

In summary, surface adsorption of Eosin Y on $Mg_2Al–CO_3$ LDH changes particle surface charge but does not affect the dye absorption spectrum. Centrifugation-based separation of free and adsorbed fractions enables quantitative evaluation of adsorption parameters when spectral differences are absent.

[1] R.K. Kankala, Adv. Drug Deliv. Rev. 186, 114270 (2022). https://doi.org/10.1016/j.addr.2022.114270.
[2] A. Ali Khan, M. Tahir, N. Khan, J. Energy Chem. 84, 242 (2023). https://doi.org/10.1016/j.jechem.2023.04.049.

Structure and morphology of thermally reduced graphene oxide under high temperatures

D. E. Hurova[1], S. V. Cherednychenko[1], A. G. Bulova[1], A. Yu. Glamazda[1], T. J. Bednarchuk[2], A. I. Krivchikov[1], N. N. Galtsov[1]

[1]B. Verkin Institute for Low Temperature Physics and Engineering of the NAS of Ukraine, 47 Nauky Ave., Kharkiv, 61103, Ukraine
[2]Institute for Low Temperatures and Structure Research, Polish Academy of Sciences, P.O. Box 1410, 50-950 Wroclaw, Poland
e-mail: hurova@ilt.kharkov.ua

This work presents a detailed study of the structural and morphological evolution of thermally reduced graphene oxide (trGO) [1, 2] subjected to high-temperature treatment at 500 °C and 700 °C. The resulting materials were characterized by X-ray diffraction and Raman spectroscopy.

The analysis indicates that high-temperature treatment leads to a substantial reorganization of the carbon planes. In the X-ray diffraction patterns, additional peaks appear at ~36°. For the sample reduced at 700 °C, an additional broad maximum is observed at 2θ=17.51°, which may indicate corrugation of the carbon surfaces and the formation of an additional identity period of d = 5.06 Å.

Raman spectra show that thermal reduction induces significant local mechanical strain due to structural rearrangement and crumpling of the graphene sheets. The increase in reduction temperature leads to an apparent decrease in the ratio of carbon atoms to oxygen atoms (C/O), derived from the analysis of Raman peak positions. This observed effect reflects a transition toward a more disordered, 'rippled' state characterized by alternating nanodomains of mechanical relaxation and compression. These local variations in the strain field manifest as bidirectional shifts in the Raman bands: tensile stress leads to a red-shift of phonon modes, while compressive stress results in a blue-shift. This phenomenon arises from the dissipation of elastic energy in regions with a high density of structural defects, where the lattice undergoes out-of-plane deformation to minimize internal stress.

The revealed structural transformation provides new insight into the organization of trGO at high-temperature treatment and directly impacts its functional properties. In particular, the presence of an additional periodicity makes trGO a highly promising material for application as a nanoscale spacer or functional interlayer in multilayer systems [3].

This work was partly supported by NASU (RSW of young scientist №12/04-2025) and the National Research Foundation of Ukraine (Project № 2023.03/0012).

[1] A. V. Dolbin, N. A. Vinnikov, V. B. Esel'son et. al., Applied Surface Science 361, 213–220 (2016). http://dx.doi.org/10.1016/j.apsusc.2015.11.167.
[2] A. V. Dolbin et. al., Low Temp. Phys. 46, 293 (2020); https://doi.org/10.1063/10.0000701.
[3] L. Mei et al., Optics Express, 31(18), 29768 (2023) https://doi.org/10.1364/OE.497888.

Features of voltage-driven magnetic anisotropy in tunnel junctions

A. M. Korostil

V. G. Baryakhtar Institute of Magnetism of the NAS of Ukraine,
36-b Vernadsky Ave., Kyiv, 03142, Ukraine
e-mail: imag@nas.gov.ua

Magnetic anisotropy plays a fundamental role in determining the stability and switching behavior of magnetic states in nanoscale magnetic junctions. In systems composed of ferromagnetic and antiferromagnetic layers based on transition metals and rare-earth elements, the anisotropy energy governs the orientation of magnetization and strongly influences magnetization dynamics. Understanding the mechanisms controlling magnetic anisotropy in such materials is essential for the development of modern spintronic devices, magnetic sensors, and memory elements.

The present study is devoted to the investigation of magnetic anisotropy and magnetically induced orientational transitions in magnetic junctions composed of ferromagnetic and antiferromagnetic materials formed from transition-metal and rare-earth compounds. Special attention is paid to the role of elastic waves and external electric fields in modifying the magnetic anisotropy and inducing magnetic phase transitions.

In transition-metal and rare-earth magnetic systems, the magnetic anisotropy arises from several mechanisms, including spin–orbit coupling, crystal-field interactions, and exchange interactions. In rare-earth elements, the strong spin–orbit coupling and the interaction between localized 4f electrons and the crystal field produce particularly large anisotropy energies. As a result, rare-earth–transition-metal heterostructures exhibit rich magnetic behavior and pronounced anisotropic properties.

The proposed model developed in this work takes into account the coupling between magnetic degrees of freedom and elastic lattice deformations. Propagating elastic waves generate time-dependent strain fields in the magnetic layers. These strains modify the magnetoelastic energy of the system and can therefore influence the effective magnetic anisotropy. As a consequence, elastic waves may act as a mechanism for controlling magnetic states and triggering magnetic transitions in the junction.

Within the framework of the given model, the free energy of the system includes contributions from exchange interaction, magnetic anisotropy, Zeeman interaction with external magnetic fields, magnetoelastic coupling, and the interaction with external electric fields in anisotropic media. The electric field can influence the magnetic anisotropy indirectly through magnetoelectric and strain-mediated coupling mechanisms, particularly in heterostructures containing anisotropic layers.

It is shown that the combined action of elastic waves and electric fields can significantly modify the effective magnetic anisotropy energy. Under certain conditions, the anisotropy barrier separating different magnetic configurations may decrease, leading to induced magnetic phase transitions. In particular, elastic waves can dynamically modulate the anisotropy constant, while the electric field can shift the equilibrium orientation of magnetization in anisotropic structures.

The obtained results show that the cooperative influence of magnetoelastic and electric-field effects provides an efficient mechanism for controlling magnetic states in transition-metal and rare-earth magnetic junctions. Such control mechanisms are of great interest for the design of low-energy spintronic devices and electrically controlled magnetic memory elements.

In conclusion, the developed approach provides a consistent framework for describing magnetic anisotropy and field-induced magnetic transitions in complex magnetic heterostructures. The results indicate that elastic waves and electric fields can be used as effective external parameters for tuning magnetic anisotropy and inducing magnetic transitions in transition-metal and rare-earth magnetic systems. These findings may be useful for future studies of magnetoelastic phenomena and for the development of advanced functional magnetic materials.

Influence of nanoscale effects on the surface of sensors with Au–Ni nanoparticles.

I. Kruglenko, Ju. Burlachenko, S. Kravchenko, Ju. Kyyak, B. Snopok

V. Lashkaryov Institute of Semiconductor Physics NAS of Ukraine,
41 Nauky Ave., Kyiv, 03028, Ukraine
e-mail: kruglen@isp.kiev.ua

Quartz crystal microbalance (QCM) sensors operating at a frequency of 10 MHz [1] were modified with nanostructured Au and Ni adsorption layers to study the response to water vapor and polar organic vapors. The deposition of nanostructured Au and Ni layers resulted in the formation of coatings with a developed and increased effective adsorption area, as confirmed by AFM analysis (Fig. 1).

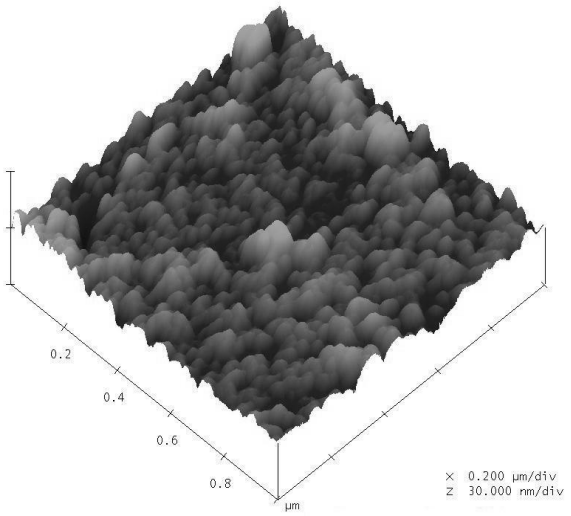

Fig.1. The AFM of nanoparticles Au-Ni on the glass surface in water vapor.

This morphology promotes enhanced analyte absorption. The Au–Ni nanoparticle mixture system is more adaptable for detecting polar gases and water vapor compared to single-component coatings. QCM sensors with an adsorption nanosurface based on a mixture of Au and Ni nanoparticles demonstrate a synergistic effect that combines the high sensitivity of Ni and the stability of Au. The heterogeneous chemical nature of the surface, together with the developed nanostructure, forms a multi-level system of adsorption centers, which provides increased efficiency in the detection of water vapor and polar gases. KCM gas sensors modified with nanostructured Au and Ni adsorption layers demonstrate different sensing characteristics, which are determined by their own surface chemistry and nanoscale morphology [2]. The chemical nature of the surface, together with the developed nanostructure, forms a multi-level system of adsorption centers, which provides increased efficiency in the detection of water vapor and polar gases. Metal oxide-based gas-sensitive materials have attracted considerable attention for the detection of air pollution, as well as accidental leaks of life-threatening toxic substances.

[1] Kruglenko I., Snopok B., Nonexponential relaxations in sensor arrays: forecasting strategy for electronic nose performance, Sensors and Actuators B: chemical 106, I.1, P.101, 2005. https://doi.org/10.1016/j.snb.2004.05.064.
[2] Qingting Li, Wen Zeng, and Yanqiong Li, NiO-Based Gas Sensors for Ethanol Detection: Recent Progress, Journal of Sensors Volume 2022, Article ID 1855493, https://doi.org/10.1155/2022/1855493.

Terahertz metasurface sensor based on multi-walled carbon nanotube aggregates for protein detection

K. S. Kuznetsova, Z. E. Eremenko

O.Ya. Usikov Institute for Radiophysics and Electronics of the NAS of Ukraine,
12 Academ. Proskury Str., Kharkiv, 61085, Ukraine
e-mails: kuznetsova.ire@gmail.com, zoya.eremenko@gmail.com

Metasurfaces operating in the terahertz range provide a promising platform for label-free biosensing owing to their ability to support localized plasmonic resonances with strong near-field and high sensitivity to changes in the surrounding dielectric environment. The terahertz region is also particularly relevant for biological sensing because water, which is the main component of most biomolecular systems, exhibits strong absorption in this frequency range. Moreover, biological molecules such as proteins, DNA, and lipids exhibit characteristic absorption features in the terahertz spectral range [1]. In this work, a terahertz metasurface based on a nanocomposite unit cell containing a carbon fillers – multiwalled multi-walled carbon nanotubes (MWCNT) embedded in a dielectric layer is numerically investigated. The modeled metasurface structure consists of a periodic array of unit cells P = 1 μm including with a MWCNT (diameter D=45 nm and a length L=0.95 μm) per unit cell inside a dielectric substrate of thickness d = 0.15 μm, while a thin analyte layer representing an aqueous human serum albumin (HSA) solution is placed above the polymer-based nanocomposites. The geometrical parameters of the unit cell are chosen to ensure resonant behavior in the frequency range near 46–49 THz. These frequencies are selected based on reported experimental data [1], where HSA exhibits characteristic dispersive and absorptive dielectric features associated with collective vibrational modes and hydration shell dynamics. Optimization of the carbon filler content in the composite was performed to achieve maximum sensitivity for HSA concentration detection. To enhance the sensor performance, aggregates of MWCNTs were considered instead of individually distributed nanotubes. Higher MWCNT concentrations enhance material polarization through interfacial charge trapping, creating electromagnetic hot spots between aggregates that drive stronger absorption than isolated nanotubes. MWCNTs are selected as resonant elements due to their unique electromagnetic properties in the THz range, including strong field localization, tunable conductivity, and enhanced interaction of the electromagnetic field with biological layers. The resonance frequency of the metasurface nanostructure was tuned to near 46–50 THz to enable sensitive detection of changes in the concentration of HSA, since pronounced protein-related vibrational features, including the amide-I and -II bands were reported in this terahertz range [1]. By analyzing resonance frequency shifts in these frequency regions, the potential of MWCNT-based THz metasurfaces for label-free detection of biomolecular markers is assessed. The first dipole resonance was selected and tuned to occur near 46 THz, where the MWCNT exhibits enhanced electromagnetic field localization at its ends. This effect is particularly favorable for biosensing applications, as it ensures strong interaction with the surrounding analyte and results in high sensitivity of MWCNT-based metasurfaces to variations in the refractive index (RI). In the region near 46 THz, the real part of the permittivity varies from 1.586 to 1.705, while the imaginary part increases from 0.1 to 0.204 with increasing protein concentration 0–150 mg/ml. This behavior indicates an enhancement of collective vibrational modes and hydration-shell dynamics of HSA. Refractive Index Unit (RIU) represents a unit change in the RI of the analyte medium. The resonance frequency shifts from 46.78 THz for water to 46.54 THz for HSA concentration of 150 mg/mL. Considering the refractive index variation from 1.259 to 1.306, the sensitivity of the metasurface is approximately 5.1 THz/RIU.

[1] K. Shiraga, Y. Ogawa, N. Kondo, Hydrogen Bond Network of Water around Protein Investigated with Terahertz and Infrared Spectroscopy, Biophys J., 111(12), 2629-2641 (2016). https://doi.org/ 10.1016/j.bpj.2016.11.011.

Controlled pro-oxidant action of (Gd,Y)VO_4:Eu^{3+} nanocrystals through delayed ROS generation

O. Ivanov[1], P. Maksimchuk[1], V. Seminko[1], M. Lupan[1], G. Grygorova[1], O. Samoilov[1], A. Onishchenko[2], V. Klochkov[1], S. Yefimova[1]

[1]Yu. V. Malyukin Department of Nanostructured Materials, Institute for Scintillation Materials NAS of Ukraine, 60 Nauky Ave., Kharkiv, 61072, Ukraine
[2]Department of Physics, Kharkiv National University of Radio Electronics, 14 Nauky Ave., Kharkiv, 61166, Ukraine
e-mail: pavel.maksimchuk@gmail.com

A significant challenge in traditional photodynamic therapy (PDT) is its dependence on oxygen to generate singlet oxygen ($^1O_2$) [1]. Because solid tumors often exhibit hypoxia, the efficacy of classical PDT is frequently compromised [2]. In contrast, the generation of hydroxyl radicals (•OH) presents a superior alternative for cancer treatment, as these radicals can be produced directly from water molecules rather than dissolved oxygen. This study focuses on (Gd,Y)VO_4:Eu^{3+} orthovanadate nanocrystals (NCs) that exhibit controlled pro-oxidant action by generating •OH in a delayed manner, after UV pre-irradiation in the absence of continuous external stimuli.

The (Gd,Y)VO_4:Eu^{3+} NCs (~2.1 nm) possess a high density of oxygen vacancies (V_O) and structural defects [3]. Under UV pre-irradiation, photo-induced holes are created. Instead of immediate recombination, these holes are captured by localized metastable levels formed by the scattering potentials of the oxygen vacancies. These trapped holes eventually migrate to the surface of the NCs and react with water molecules to produce hydroxyl radicals long after the light source has been removed.

The delayed generation of •OH radicals after UV pre-irradiation in the dark was confirmed using several analytical techniques:

1) Luminescence spectroscopy: using coumarin as a fluorescent probe, which reacts with •OH to form highly fluorescent 7-hydroxycoumarin.

2) EPR spectroscopy: using DMPO as a spin trap, which reacts with •OH to form DMPO-OH adducts.

3) Overall pro-oxidant activity: the oxidative capacity was further evidenced by the degradation of DiD-C3S dye in solutions containing UV pre-irradiated NCs.

The ability to trigger and then sustain the release of •OH radicals provides a unique mechanism for controlled pro-oxidant action. By bypassing the need for high oxygen concentrations and continuous irradiation, (Gd,Y)VO_4:Eu^{3+} NCs offer a promising strategy for the treatment of hypoxic malignant cells, potentially overcoming the limitations of oxygen-dependent therapeutic modalities.

Acknowledgments: This research was supported by National Research Foundation of Ukraine, Grant № 2025.07/0093

[1] M. Valko, D. Leibfritz, J. Moncol, M. T. Cronin, M. Mazur, J. Telser, «Free radicals and antioxidants in normal physiological functions and human disease», Int. J. Biochem. Cell Biol., 39, 44 (2007). https://doi.org/10.1016/j.biocel.2006.07.001.
[2] L. Tong, C. C. Chuang, S. Wu, L. Zuo, «Reactive Oxygen Species in Redox Cancer Therapy», Cancer Letters, 367, 18 (2015). https://doi.org/10.1016/j.canlet.2015.07.008.
[3] P. O. Maksimchuk, K. O. Hubenko, V. V. Seminko, V. L. Karbivskii, A. S. Tkachenko, A. I. Onishchenko, V. Yu. Prokopyuk, S. L. Yefimova, «High antioxidant activity of gadolinium–yttrium orthovanadate nanoparticles in cell-free and biological milieu», Nanotechnology, 33, 055701 (2022). https://doi.org/10.1088/1361-6528/ac31e5.

Enhancement of electric fields in the gap between two metal nanoparticles. Dipole approximation

A. V. Korotun[1,2], V. P. Kurbatsky[1], H. V. Moroz[1]

[1]Zaporizhzhia Polytechnic National University,
64 Universytetska Str., Zaporizhzhia, 69063, Ukraine
[2]G. V. Kurdyumov Institute for Metal Physics of the NAS of Ukraine,
36 Academician Vernadsky Blvd., Kyiv, 03142, Ukraine
e-mail: garrymrz@zp.edu.ua

One of the most important applications of plasmonic nanoparticles is their use as optical antennas. This application is possible due to the enhancement of electric fields in the vicinity of nanoparticles when plasmon resonances are excited on their surfaces. The problem of field enhancement near isolated nanoparticles is well studied. However, the scientific literature contains virtually no studies investigating field enhancement in the gap between two nanoparticles. Since such dimeric optical nanoantennas can be used to observe fluorescence or Raman scattering, studying the enhancement of electric fields in the gap between metal nanoparticles of various shapes is relevant.

A rigorous approach to studying the optical response of dimers is the T-method, which takes into account the contributions of all multipole modes [1]. However, this method has a significant drawback: it is cumbersome and, consequently, requires a large amount of calculations. It is well known that the main contribution to the optical response of both isolated nanoparticles and their dimers comes from the dipole resonant mode. Therefore, in this study, the diagonal components of the field enhancement tensor in the gap between nanoparticles are calculated using the dipole polarizability tensor.

Calculations were performed for dimers of spherical and prolate spheroidal nanoparticles. The results indicate the presence of significant longitudinal enhancement (especially near the optical resonance) and the absence of transverse enhancement. A comparison of the results with corresponding results obtained taking into account higher multipoles revealed their similarity. This fact confirms the adequacy of the dipole approximation used.

[1] V. Klimov, Nanoplasmonics (Pan Stanford Publishing, 2014). https://doi.org/10.1201/b15442.

Simultaneous turn-off and ratiometric detection of HP using redox-active $CeO_{2-x}:Eu^{3+}$ colloidal nanosensors

Y. Neuhodov[1], P. Maksimchuk[1], A. Onishchenko[2], N. Kavok[1], G. Dudetskaya[1], Y. Kot[3], S. Yefimova[1], V. Seminko[1]

[1]Yu. V. Malyukin Department of Nanostructured Materials, Institute for Scintillation Materials of NAS of Ukraine, 60 Nauky Ave., Kharkiv, 61072, Ukraine
[2]Department of Physics, Kharkiv National University of Radio Electronics, 14 Nauky Ave., Kharkiv, 61166, Ukraine
[3]School of Biology, V. N. Karazin Kharkiv National University, 14 Svobody sq., Kharkiv, 61022, Ukraine
e-mail: e.i.neugodov@gmail.com

Hydrogen peroxide (HP) is a central signaling molecule in physiological systems and a critical byproduct of enzymatic activities involving catalase and superoxide dismutase [1]. Despite the high sensitivity of traditional organic fluorescent probes, their practical application is often restricted by poor chemical stability, susceptibility to photobleaching, and a fundamental lack of reversibility [2]. To address these challenges, this study introduces ultra-small (3 nm and 6 nm) Eu^{3+}-doped colloidal ceria nanoparticles ($CeO_{2-x}:Eu^{3+}$) as a robust and stable inorganic alternative. These nanoparticles, synthesized via a controlled hydrolysis process, maintain a face-centered cubic structure and offer a unique multi-channel sensing platform that combines turn-off and ratiometric detection modes [3].

The operational logic of the $CeO_{2-x}:Eu^{3+}$ sensor is based on the complex interplay between surface redox reactions and luminescence properties. The turn-off channel utilizes the reversible quenching of Ce^{3+} (430 nm) and Eu^{3+} (591 nm) luminescence bands. Detailed statistical analysis demonstrates that this quenching does not follow the standard Stern-Volmer model but is instead governed by surface-adsorption mechanisms. Specifically, the Ce^{3+} band quenching aligns with the Temkin adsorption model, reflecting the energetic inhomogeneity of the nanoparticle surface, while the Eu^{3+} band follows a Langmuir-like behavior. Mechanistically, HP molecules adsorbed on the surface oxidize Ce^{3+} to Ce^{4+}, while the hydroxyl radicals produced during HP decomposition act as the primary quenchers for Eu^{3+} ions.

Furthermore, the system provides a self-calibrating ratiometric signal based on the intensity ratio of Eu^{3+} transitions ($^5D_0 \rightarrow {}^7F_1$ and $^5D_0 \rightarrow {}^7F_2$). As HP-induced oxidation reduces the concentration of oxygen vacancies in the lattice, the local symmetry surrounding the Eu^{3+} ions increases, leading to a measurable shift in the 591/606 nm ratio. This ratiometric sensitivity is particularly pronounced in 3 nm nanoparticles due to their higher initial defect density.

Thus, $CeO_{2-x}:Eu^{3+}$ nanoparticles represent an effective inorganic platform for multi-channel hydrogen peroxide detection, providing high reliability through the combination of ratiometric and turn-off sensing modes.

Acknowledgments: This research was supported by National Research Foundation of Ukraine, Grant № 2023.03/0050.

[1] B. Halliwell, J.M. Gutteridge, Free radicals in biology and medicine, fifth ed., Oxford University Press, Oxford, 2015. https://doi.org/10.1093/acprof:oso/9780198717478.001.0001.
[2] M. Schäferling, D.B.M. Grögel, S. Schreml, Luminescent probes for detection and imaging of hydrogen peroxide, Microchim. Acta., 2011, 174, 1-18. https://doi.org/10.1007/s00604-011-0606-3.
[3] Ye. Neuhodov, P. Maksimchuk, K. Hubenko, N. Kavok, G. Dudetska, Yu. Kot, O. Sedyh, V. Klochkov, V. Seminko, Ultra-small CeO2-x:Eu3+ colloidal nanoparticles for simultaneous turn-off and ratiometric hydrogen peroxide sensing, J. Mol. Liq., 2025, 441, 129027. https://doi.org/10.1016/j.molliq.2025.129027.

Atomic-scale contact mechanics of Al and Cu nanoislands

M. V. Prodanov, O. V. Khomenko

Sumy State University, 116 Kharkivska Str., Sumy, 40007, Ukraine
e-mail: prodkolya@gmail.com

Aluminum and copper nanoparticles (NPs) have attracted attention due to their size-dependent structural, thermodynamic, and chemical properties [1, 2]. However, no thorough research on the scaling of their contact mechanics (CM) quantities, such as the mean distance between the contacting surfaces (also called interfacial separation u), the relative contact area A_r, and the height power spectrum density (PSD), has been reported in the literature.

In this work, we perform large-scale classical molecular dynamics simulations to study the size scaling of CM properties of Al and Cu NPs adsorbed on a suspended graphene sheet. The calculations suggest that size effects exist in the scaling of the CM quantities. Properties of the NPs smaller than around 3 – 6 nm scale differently compared to the larger ones. In particular, the u and A_r values of the smaller NPs strongly fluctuate and differ from the thermodynamic values of the larger NPs. PSDs are smeared for the smaller NPs, whereas the larger nanoislands' PSDs have anisotropic frequency structure. It can be attributed to the ordering of the interface atomic layer of the NPs into the lowest-energy (111) atomic plane, with a hexagonal atomic arrangement. 2D height PSDs exhibit sixfold symmetry with a central region, bounded by the frequencies whose wavelengths approximately equal to the nearest neighbor distances of the metal atoms. Another noticeable result is that the isotropic height PSD of the larger NP samples has relatively narrow regions that scale as power laws (cf. Fig. 1), some of which exhibit self-affine surface roughness with Hurst exponents 0.1 – 0.56. This means that even though the graphene substrate surface is smooth, the NPs formed on it can still exhibit random atomic-scale roughness.

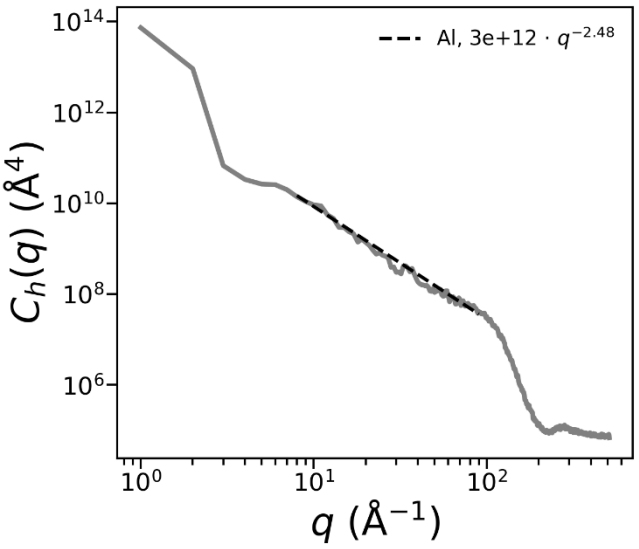

Fig. 1. Thermal conductivity of porous silicon as a function of porosity obtained using various methods. Experimental data reported in the literature are also included for comparison.

The surface height distribution has a narrow peak that can be fit to a Gaussian, as well as the Gaussian tail. The surface height spread can exceed 1 nm for the largest NPs. In contrast, the interfacial separation distribution is close to a single Gaussian, as observed for macroscopic randomly rough surfaces at zero squeezing pressure [3]. This suggests that the graphene substrate deforms elastically, resulting in a normally distributed mean gap, in contrast to the surface topography, which mainly depends on the preparation process.

[1] K. Chung, J. Bang, A. Thacharon, H. Y. Song, S. H. Kang, W.-S. Jang, N. Dhull, D. Thapa, C. M. Ajmal, B. Song, S.-G. Lee, Z. Wang, A. Jetybayeva, S. Hong, K. H. Lee, E. J. Cho, S. Baik, S. H. Oh, Y.-M. Kim, Y. H. Lee, S.-G. Kim and S. W. Kim, Nature Nanotechnology, 17, 285 (2022). https://doi.org/10.1038/s41565-021-01070-4.
[2] A. Yalamanchali, K. L. Pyfer and M. F. Jarrold, The Journal of Physical Chemistry C, 121, 10242 (2017). https://doi.org/10.1021/acs.jpcc.7b02768.
[3] A. Almqvist, C. Campaña, N. Prodanov and B. Persson, Journal of the Mechanics and Physics of Solids, 59, 2355 (2011). https://doi.org/10.1016/j.jmps.2011.08.004.

Peculiarities of behavior of composite charged particles in the electric field

V. V. Yanovsky, M. A. Ratner

Institute for Single Crystals, NAS Ukraine, 60 Nauky Ave., Kharkiv, 61072, Ukraine
e-mail: marinaratner2017@gmail.com

The motion of one-dimensional and two-dimensional charged composite particles in a constant electric field is considered. Using the billiard formalism, precise laws of motion for a one-dimensional particle with a small number of internal degrees of freedom are established, and the laws of motion for a two-dimensional particle are numerically integrated. A generalized Schwarz method for trajectory straightening in the presence of a field is proposed. Within the framework of the billiard formalism, motion regimes for such particles in a constant field are obtained. The existence of periodic motion regimes for such particles was demonstrated. With an increase in the number of internal degrees of freedom, as well as upon transitioning to the two-dimensional case, the main change in the shell's behavior consists in the emergence of chaotic regimes of acceleration. More complex periodic acceleration components with a wide variety of values by which the shell's velocity changes during a single period also become possible. It has been shown that the kinetic energy of a composite particle exceeds that of a monolithic particle with the same mass. The presence of periodic components is interesting for the creation of emitting nanodevices, especially in the case of zero net charge, when the emitting device can be stationary and emit radiation under the influence of a constant electric field.

This work was supported by the National Research Foundation of Ukraine, grant number 2025.07/0030.

[1] V.V. Yanovsky, A.V. Tur, Yu.N. Maslovsky, JETP, 133:1, 220 (2008).
[2] B.W. Smith, M. Monthioux, D. E. Luzzi, Nature, 396:6709, 323 (1998). https://doi.org/10.1038/24521.
[3] M. Monthioux, Carbon, 40:10, 1809 (2002). https://doi.org/10.1016/S0008-6223(02)00102-1.
[4] K. Suenaga, T. Okazaki, K. Hirahara, S. Bandow, H. Kato, A. Taninaka, H. Shinohara, S. Iijima, Appl. Phys. A, 76:4, 445 (2003). https://doi.org/10.1021/la9017932.

Morphology and interfacial forces of Pb nanoparticles

A. A. Samilyk, O. V. Khomenko, M. V. Prodanov

Sumy State University, 116 Kharkivska Str., Sumy, 40007, Ukraine
e-mail: samilykanton@gmail.com

Understanding the morphology of Pb nanoparticles (NPs) and their interactions with carbon surfaces, particularly with graphene, is important from a practical perspective. Examples of relevant industrial applications include next-generation sensors for real-time detection of toxic heavy metals [1], membrane separation technologies [2], and hybrid lead–carbon battery systems [3]. However, there is a lack of research on the size scaling of morphological and interfacial properties of Pb NPs on carbon surfaces.

In this study, large-scale molecular dynamics (MD) simulations are employed to investigate the scaling behavior of morphological properties of Pb NPs physisorbed on a graphene substrate. We analyzed quantities such as the total surface area S, the total volume V, and the surface area-to-volume ratio of Pb nanoislands. The mentioned quantities were calculated using the corresponding surface-mesh approximations obtained via the Poisson surface reconstruction algorithm, where each atom normal was estimated using the point cloud library wrapper in CloudCompare [4]. Additionally, distributions of interfacial forces and potential energies were calculated.

One important peculiarity of the current model is that the nanoislands are not prepared manually but rather obtained via a process that mimics thermal dewetting of thin metal films. This makes the model more realistic, avoiding some assumptions regarding the roughness of the contact interface. Thermal dewetting incorporates depositing a thin metal film on a substrate, then heating it until it melts, forming separate nanodroplets that transform into solid NPs upon cooling. The model also accounts for the fact that Pb atoms weakly interact with perfect graphene, as evidenced by both experimental and theoretical results [5], which was taken into account for the Lennard-Jones potential describing carbon-metal interactions. The temperature was controlled using the Berendsen thermostat, and the equilibration temperature of around 300 K was maintained.

Our calculations suggest that simulating the thermal dewetting process in MD can yield NPs with different shapes and surface topographies. In particular, the shape of Pb NPs on the substrate plane can vary from square to round, depending on when cooling begins. All the NPs exhibit a polycrystalline structure, as confirmed by their radial distribution functions. Size scaling of S and V of the larger NPs obeys the expected quadratic and cubic laws. Distributions of the interfacial forces and potential energies show size-dependent behavior. Additionally, the 2D power spectrum densities of the interfacial quantities exhibit anisotropic symmetry, reflecting the interface's structure.

[1] I. Shtepliuk, N.M. Caffrey, T. Iakimov, T. et al. Sci Rep 7, 3934 (2017).https://doi.org/10.1038/s41598-017-04339-8.
[2] D. G. Chandran, L. Muruganandam, R. Biswas, Chemical Engineering Journal Advances 24,100891 (2025). https://doi.org/10.1016/j.ceja.2025.100891
[3] S. Thangarasu, G. Palanisamy, S.-H. Roh, H. Jung, ACS Sustainable Chem. Eng., 8, 8868 (2020). https://doi.org/10.1021/acssuschemeng.0c03461.
[4] GPL software (2025) CloudCompare (version 2.14), http://www.cloudcompare.org
[5] D. Ma, Zh. Yang, New J. Phys. 13, 123018 (2011). https://doi.org/10.1088/1367-2630/13/12/123018.

Catalytic mechanism of hydrogen peroxide decomposition by redox-active manganese oxide nanocrystals

O. Samoilov[1], P. Maksimchuk[1], V. Seminko[1], M. Lupan[1], G. Grygorova[1], A. Onishchenko[2], V. Klochkov[1], S. Yefimova[1]

[1]Institute for Scintillation Materials National Academy of Sciences of Ukraine,
60 Nauky Ave., Kharkiv, 61072, Ukraine
[2]Kharkiv National University of Radio Electronics,
14 Nauky Ave., Kharkiv, 61166, Ukraine
e-mail: samoilovisma@gmail.com

Reactive oxygen species (ROS) play an essential role in cellular functioning, regulating signaling pathways, metabolism, proliferation, and apoptosis. While physiological ROS levels are maintained by antioxidant defense systems, their overproduction induces oxidative stress and biomolecular damage associated with various diseases. At the same time, controlled ROS elevation can be utilized for selective elimination of pathological cells, particularly cancer cells, which are highly sensitive to oxidative stress.

ROS levels can be regulated using low-molecular antioxidants, enzyme mimetics, and radical scavengers; however, conventional agents often exhibit limited stability, rapid clearance, and low selectivity. Inorganic nanocrystals have recently emerged as promising ROS regulators due to their high surface area, tunable composition and morphology, and enzyme-like catalytic activity, enabling them to act as either ROS scavengers or generators while maintaining high chemical stability and prolonged activity.

In this study, manganese oxide nanocrystals were proposed as ROS-modulating agents. Their size distribution and crystalline structure were characterized by transmission electron microscopy (TEM) and X-ray diffraction (XRD). X-ray photoelectron spectroscopy (XPS) revealed the presence of manganese ions in lower oxidation states on the nanocrystal surface, indicating catalytically active centers. Using a selective fluorescent probe for hydrogen peroxide (DPPP), the nanocrystals were shown to efficiently decompose H_2O_2. The process proceeds via a Fenton-like reaction with generation of highly reactive hydroxyl radicals (•OH), confirmed by fluorescence measurements and electron paramagnetic resonance (EPR) spectroscopy.

These results demonstrate that manganese oxide nanocrystals efficiently modulate ROS levels through catalytic hydrogen peroxide decomposition accompanied by formation of highly cytotoxic •OH radicals, highlighting their potential as promising nanoplatforms for controlled ROS regulation and ROS-based therapeutic applications.

Acknowledgments: This research was supported by National Research Foundation of Ukraine, Grant № 2025.07/0093.

Thermal phenomena in the neighborhood of spheroidal metallic nanoparticles under the excitation of plasmon resonances on their surface

R. Yu. Korolkov[1], V. I. Reva[1], M. A. Shvydkyi[1], E. V. Stegantsev[2]

[1]National University Zaporizhzhia Politechnic,
64 Universytetska Str., Zaporizhzhia, 69011, Ukraine
[2]Zaporizhzhia Institute of Economics and Information Technologies,
16-B Kyiashka Str., Zaporizhzhia, 69041, Ukraine
e-mail: romankor@zp.edu.ua

As is well known, the excitation of the surface plasmon resonances in the metallic nanoparticles of various shapes is accompanied by the heating of their neighborhoods. This is due to the conversion of the absorbed light energy into heat energy. It should be pointed out that the thermoplasmonic effects are widely used in nanomedicine, in particular for the thermal destruction of the malignant neoplasms. In [1], the thermoplasmonic phenomena in the metallic nanoparticles of the spherical, cylindrical, and disc shapes were investigated, and the recommendations were presented for the practical use of the overheating in the particles of such shapes. However, the issues related to the heating of the neighborhoods of the spheroidal nanoparticles under the excitation of the surface plasmon resonances remain unexplored and therefore relevant.

The study investigates the influence of geometry of the metallic nanoparticles and their composition on the heating of their neighborhoods. The calculations show a slight (on the order of fractions of a degree or several degrees) overheating near the oblate spheroidal nanoparticles and prolate spheroids with low eccentricity (when their shape is close to spherical one). At the same time, near highly prolate spheroids (needles), the overheating is significant. Thus, in practical applications where slight overheating is required, it is advisable to use oblate spheroidal particles and slightly prolate spheroids, and where the significant overheating is required, it is advisable to use highly prolate spheroids. It is demonstrated that the material of nanospheroids significantly affects maximum overheating and is determined by the frequency of bulk plasmons. It is established that at frequencies falling within the biological transparency windows, the overheating is sufficient for the photothermal therapy of the malignant tumors.

[1] V. I. Reva, M. A. Shvydkyi, R. Yu. Korolkov, A. V. Korotun, E. V. Stegantsev and O. S. Hnatenko, J. Nano- Electron. Phys. 17, 02006 (2025). http://dx.doi.org/10.21272/jnep.17(2).02006.

Enhancement of light emission by capped III-V QDs under gamma-irradiation

G. Yu. Rudko[1,2], O. M. Strilchuk[1,2], E. G. Gule[1], Yu. I. Mazur[3]

[1]V. Lashkaryov Institute of Semiconductor Physics, National Academy of Sciences of Ukraine, 45 Nauky Ave., Kyiv, 03028, Ukraine
[2]National University of Kyiv-Mohyla Academy, 2 Skovorody Str., Kyiv, 04070, Ukraine
[3]Institute of Nano Science and Engineering, University of Arkansas, Fayetteville, AR 72701, USA
e-mail: ostrilchuk@gmail.com

The evolution of modern optoelectronics is increasingly defined by the development of nanoscale devices that extend the operational horizons of conventional semiconductors; especially the domain of nano-light-emitters has become the focus of research for display applications [1]. Among these, III-V quantum dots (QDs) have emerged as a foundational platform for high-speed lasers, LEDs, and advanced sensors, including NH_3 detectors and shortwave infrared (SWIR) imaging systems.

III-V QDs are predominantly produced using the techniques like molecular-beam epitaxy (MBE) which allows for precise control over QD size and composition during the growth phase. However, the ability for post-growth modification of the properties of QDs remains a challenge. The strategies for post-growth tuning are often complex or chemically invasive. Recently, we have advanced a previously unforeseen method for tuning the light emission of surface QD arrays by exposure to γ-irradiation [2].

While radiation is traditionally associated with the deterioration of semiconductor properties due to atoms displacements, the interaction of high-energy electromagnetic waves with surface nanostructures revealed a different physical mechanism. By utilizing ionization and Compton-electron-enhanced surface diffusion, we demonstrated that γ-treatment can be used not as a destructive force for surface QDs, but as a precision tool for structural "healing" and optical efficiency improvement.

This study explores the application of the above unconventional approach in order to achieve sensibilization of low-temperature light emission from the capped $In_{0.4}Ga_{0.6}As$ QDs. We showed that upon exposure to increasing doses of 1.2 MeV γ-quanta PL intensity of III-V capped QDs exhibits a non-monotonic dependence on the radiation dose: at first, a persistent increase in low temperature PL intensity occurs, reaching a maximum before a sharp decline at the threshold of 1×10^8 rad. This enhancement is highly unusual in the context of radiation physics, as ionizing radiation is typically associated with the creation of non-radiative recombination centers (Frenkel pairs and lattice displacements). A maximum PL enhancement factor for capped QDs was ~1.6, which was observed at 970 nm. On the other hand, the spectral position of PL peak of capped QDs remained unchanged under irradiation which indicates that the core electronic confinement and the average composition of the InGaAs capped QDs are preserved. Thus, one can state that, unlike the surface QDs, light emission improvement in capped QDs occurs independently on the changes of QDs morphology. We attribute this to the ionization-assisted annihilation of growth-related defects with newly formed radiation defects. These results challenge the traditional view of radiation-matter interactions and suggest a non-invasive pathway for the "athermal" optimization of buried nanostructures.

[1] Z. Liu, C.-H. Lin, B.-R. Hyun, C.-W. Sher, Z. Lv, B. Luo, F. Jiang, T. Wu, C.-H. Ho, H.-C. Kuo, J. H. He, Light: Sci. Appl. 9, 1 (2020). https://doi.org/10.1038/s41377-020-0268-1.
[2] O. M. Strilchuk, G. Yu. Rudko, E. G. Gule, O. S. Lytvyn, V. P. Maslov, B. Liang, Yu.I. Mazur, IEEE Transactions on Nuclear Science 72(9), 3064 (2025) https://doi.org/10.1109/TNS.2025.3594156.

Benzene on graphene surface: domain and domain boundaries

Y. M. Trotskyi[1], E. S. Syrkin[1], V. O. Lykah[2]

[1]B.Verkin Institute for Low Temperature Physics and Engineering of the NAS of Ukraine, 47 Nauky Ave., Kharkiv, 61103, Ukraine
[2]National Technical University "Kharkiv Polytechnic Institute", 2 Kyrpychova Str., Kharkiv, 61002, Ukraine
e-mail: trotskyi@ilt.kharkov.ua

A hexagonal close packed (hcp) organic-inorganic molecular systems demonstrate complex geometric and physical properties even for benzene, the simplest type of cyclic hydrocarbons. We consider a set of topological defects in placement of benzene molecules adsorbed on graphene [1]. These defects are visually similar to ferroelectric domains in terms of molecular orientation relative to graphene atoms. We describe the case of 180-degrees domain boundary. This model shows the hybrid molecular system with the minimal possible distance between benzene molecules, below which they repel each other, preventing nucleation. The quantity of existing structural domains, possible mutual orientations on vertical (Fig.1, *a*) and horizontal (Fig.1, *b*) boundaries and the interaction of benzene molecules on the boundaries have been calculated.

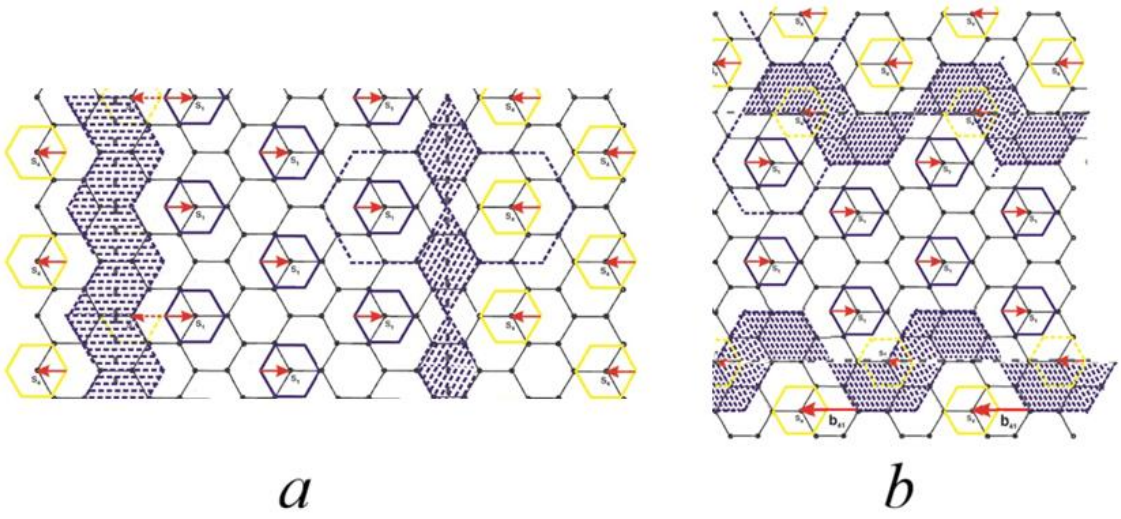

a *b*

Fig. 1. *a* – vertical 180° left and right boundaries; *b* – horizontal boundaries. Filled areas show regions with no atoms adsorbed.

The linear energy density of molecular interaction on vertical left w_{VL}, vertical right w_{VR} and horizontal w_H are calculated by using corresponding formulas:

$$w_{VL} = \frac{2w_{vdw}}{a\sqrt{3}};\ w_{VR} = \frac{4w_{vdw} - w_{180}}{2a\sqrt{3}};\ w_H = \frac{8w_{vdw} - w_{180}}{6a}.$$

It follows that the potential interaction of molecules is greater on the horizontal boundary and, consequently, has a less stable configuration than on vertical boundaries.

[1] V. A. Lykah and E. S. Syrkin, Low Temp. Phys. 48(4), 353 (2022). https://doi.org/10.1063/10.0009743.

Kinetics of electrophysical properties of diluted aqueous colloidal solutions of fullerene $C_{60}@\{H_2O\}_n$

M. A. Vinnikov, M. T. Pohribnyi, O. V. Dolbyn, R. M. Basnukaeva, L. M. Buravtseva, S. V. Cherednychenko

B.Verkin Institute for Low Temperature Physics and Engineering of the NAS of Ukraine, 47 Nauky Ave., Kharkiv, 61103, Ukraine
e-mail: vinnikov@ilt.kharkov.ua

The kinetics of the dielectric loss tangent δ and permittivity ε of diluted aqueous colloidal solutions of fullerene $C_{60}@\{H_2O\}_n$ obtained using the cryogenic vacuum-sublimation technique were studied [1]. A colloidal solution of hydrated fullerene $C_{60}@\{H_2O\}_n$ with a base concentration of 3 mg C_{60} per 1 L was obtained by melting the solid phase of $C_{60}@\{H_2O\}_n$ obtained by condensing fullerene C_{60} vapor and water on a substrate cooled with liquid nitrogen. Dilute solutions of $C_{60}@\{H_2O\}_n$ were obtained by adding a $C_{60}@\{H_2O\}_n$ solution with a base concentration to pure distilled water and subsequent stirring with a magnetic stirrer for 1 minute. In this way, solutions with relative concentrations to the base of 1:10, 1:100, and 1:1000 were obtained. Changes in the dielectric loss tangent δ and permittivity ε over time were studied for each solution in the frequency range of 100-10^4 Hz.

Measurements showed that the dielectric loss tangent δ of the colloidal $C_{60}@\{H_2O\}_n$ solution is significantly higher than that of plain water, with a maximum shifted to higher frequencies. This phenomenon is presumably due to the formation of metastable spherical layers of water molecules around the fullerene molecules due to donor-acceptor bonds between the water molecules and the C_{60} surface [2].

The permittivity of the $C_{60}@\{H_2O\}_n$ solution was also higher than that of pure water, which is likely explained by the polarization of water molecules by the fullerene molecules.

An increase in the dielectric loss tangent and permittivity was observed over time, which can be explained by the growth of hydration shell layers around the C_{60} molecules. The obtained effect depends on the concentration of C_{60} molecules in the solution and can be used for subsequent biophysical studies.

This work was partly supported by the National Academy of Sciences of Ukraine [Project reg. no 0122U001504, Contract no 2H/48-26] and the National Research Foundation of Ukraine [Grant 2023.03/0012]

[1] N.A. Vinnikov, S.V. Cherednichenko, A.V. Dolbin, et al., Low Temp. Phys. 48, 336 (2022). http://dx.doi.org/10.1007/b985410.
[2] J. Herna´ndez-Rojas, J. Breto´n, and J. M. Gomez Llorente, J. Phys. Chem. B 2006, 110, 13357-13362. http://dx.doi.org/10.1073/1.5030456.

Study of early stages of clustering in a supersonic nitrogen jet

Yu. S. Doronin, A. A. Tkachenko, V. L. Vakula, G. V. Kamarchuk

B. Verkin Institute for Low Temperature Physics and Engineering of the NAS of Ukraine,
47 Nauky Ave., Kharkiv, 61103, Ukraine
e-mail: doronin@ilt.kharkov.ua

Research into electron-excited supersonic nitrogen jets is important for many areas of science and technology, in particular: fundamental plasma physics, astrophysics, Earth's atmosphere physics, plasma chemistry, and surface modification [1].

The report presents a study of the VUV radiation from a supersonic nitrogen jet excited by an electron beam with 1000 eV of energy and 20 mA of current. The spectra were recorded with a vacuum monochromator over the wavelength range 1400-1800 Å, at a nitrogen pressure at the nozzle inlet, P_0= 0.2 MPa, and temperatures T_0 = 270, 200, and 130 K.

The recorded spectra contain intense resonance lines of atomic nitrogen ***NI*** λ=1492 Å and λ=1742 Å, which are emitted mainly as a result of dissociative excitation of nitrogen molecules by electrons. Between them are the most intense molecular nitrogen bands of the Lyman-Birge-Hopfield (LBH) system ($a^1\Pi_g - X^1\Sigma^+_u$): 1501 Å (0-1), 1555 Å (0-2), 1611 Å (0-3), 1672 Å (0-4), 1736 Å (0-5), which can be emitted by both gaseous nitrogen and nitrogen clusters.

Analysis of the results showed that the ratios of the intensities ***I*** of the Lyman-Birge-Hopfield system nitrogen molecular bands to the intensity of the ***NI*** λ=1492 Å atomic line, ***Im/Ia***, can serve as an indicator of the clustering process in a supersonic nitrogen jet. At T_0 = 200 K, we obtained the maximum value of ***Im/Ia***, which is explained by the suppression of the dissociative channel of excited nitrogen atom formation as a result of the initial stage of clustering. We attribute the observed decrease in the ***Im/Ia*** ratio with a decrease in T_0 to 130 K to the further growth of clusters due to coalescence. This increases the number of free nitrogen molecules in the jet during the decay of unstable condensation nuclei and, accordingly, the number of excited nitrogen atoms.

It should be noted that we did not observe the spectral shift and broadening of the analysed molecular bands of the Lyman-Birge-Hopfield system characteristic of solid nitrogen [2]. This indicates that the cluster contribution to the radiation of the observed molecular bands is mainly due to excited molecules on the cluster surface.

[1] M. Patel, J. Thomas, and H. Chandra Joshi, Vacuum, 192, 110440 (2021). https://doi.org/10.1016/j.vacuum.2021.110440.
[2] E. V. Savchenko, I. V. Khyzhniy, S. A. Uyutnov, A. P. Barabashov, G. B. Gumenchuk, M. K. Beyer, A. N. Ponomaryov, and V. E. Bondybey, J. Phys. Chem. A, 119, 2475 (2014). https://doi.org/10.1021/jp5087575.

BIOPHYSICS AND PHYSICS OF MACROMOLECULES

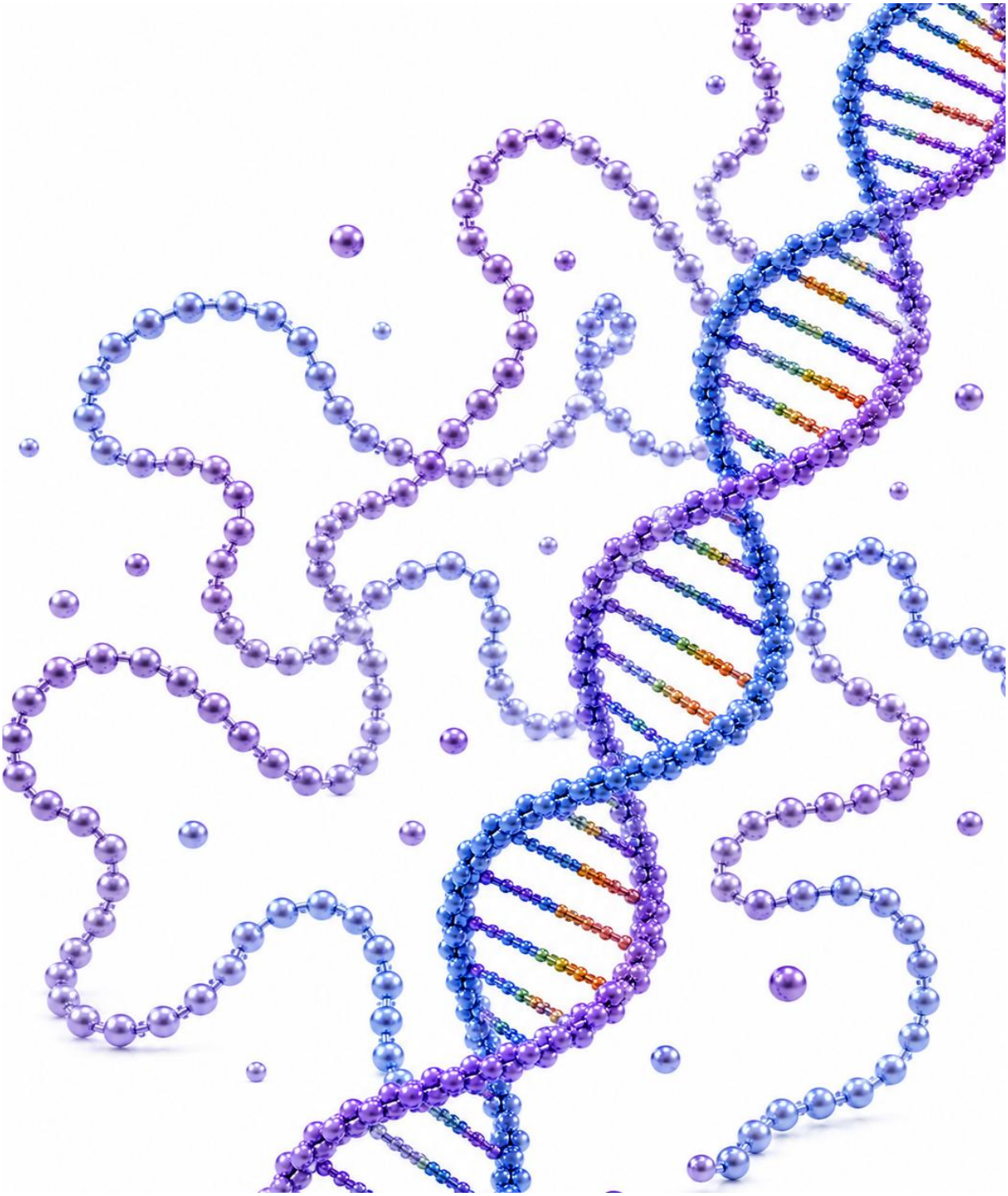

Enzyme adsorption on single-walled carbon nanotubes: Raman spectroscopy analysis

A. Glamazda and V. Karachevtsev

B.Verkin Institute for Low Temperature Physics and Engineering of the NAS of Ukraine, 47 Nauky Ave., Kharkiv, 61103, Ukraine
e-mail: alex.glamazda@gmail.com

Single-walled carbon nanotubes (SWNTs) have attracted considerable attention from researchers as functional nanomaterials for biosensing and bioelectronic applications due to their unique electronic structure, high surface area, and sensitivity to changes in the local chemical environment. The adsorption of biomolecules on the nanotube surface can significantly modify their electronic and vibrational properties through mechanisms such as charge transfer, dielectric screening, and mechanical strain. Therefore, understanding the interactions between SWNTs and biological macromolecules is essential for the development of nanotube-based biosensors and nanobiohybrid systems. Among various biomolecules, enzymes are of particular interest because their immobilization on nanostructured materials enables the creation of highly sensitive and selective biosensing platforms. The development of enzyme-based sensors strongly depends on the interactions between the enzyme and the nanomaterial surface. SWNTs are extremely sensitive to changes in their environment, which are manifested by shifts in the position, shape, and intensity of their characteristic Raman bands.

In this work, the adsorption of the enzyme, lactate oxidase (LOX), on the surface of single-walled carbon nanotubes (SWNTs) was studied using Raman spectroscopy. The Raman spectra were recorded in the regions corresponding to the radial breathing mode (RBM) (200-350 cm^{-1}) and tangential (G) modes (1500-1650 cm^{-1}). Individual nanotubes were prepared by ultrasonication of SWNTs dispersed in an aqueous solution of Poly(rC), followed by ultracentrifugation. The resulting suspension of Poly(rC)-wrapped nanotubes was sprayed onto quartz substrates, forming a network of nanotubes. Previous analysis of atomic force microscopy images of such samples showed that the biopolymer forms discrete bulges along the nanotube, leaving certain areas of the nanotube surface free of the biopolymer [1]. Subsequently, the enzyme was sprayed onto this nanotube network from an aqueous solution. The pristine Poly(rC)-SWNT sample and the LOX-treated sample were analyzed by Raman spectroscopy, focusing on spectral changes induced by enzyme deposition, including variations in peak positions, bandwidths, and intensities. The observed spectral transformations were attributed to enzyme adsorption on regions of the nanotube surface not covered by the biopolymer. The possible contributions of charge transfer between the nanotube and the adsorbed enzyme, dielectric screening effects associated with the local environment changes, and mechanical stress exerted on the nanotube by adsorbed enzymes were considered in interpreting the Raman spectral changes.

This work was supported by the National Academy of Sciences of Ukraine (Grant 0126U001857).

[1] N. V. Kurnosov, V. S. Leontiev, A. S. Linnik, O. S. Lytvyn, V. A. Karachevtsev, Chem. Phys. 438, 23 (2014). https://doi.org/10.1016/j.chemphys.2014.04.006.

Quantitative assessment of tryptophan content in the blood plasma of oropharyngeal cancer patients after COVID-19

I. Gnatyuk[1], D. Doni[2], S. Verevka[2], A. Tarasenko[3], O. Gnatyuk[1], T. Isokov[1], G. Dovbeshko[1]

[1]Institute of Physics NAS of Ukraine, 46 Nauky Ave., Kyiv, 03028, Ukraine
[2]State Institution "O. S. Kolomiychenko Institute of Otolaryngology NAMS of Ukraine", 3 Zoolohichna St., Kyiv, 03057, Ukraine
[3]A.V. Palladin Institute of Biochemistry NAS of Ukraine, 9 Leontovycha St., Kyiv, 02000, Ukraine
e-mail: isokovtd@gmail.com

Quantitative determination of metabolites in blood plasma is an important tool for assessing metabolic disturbances associated with various pathological conditions [1]. In particular, the analysis of definite free amino acids provides valuable information for the diagnosis and monitoring of oncological diseases [2]. However, comprehensive amino acid profiling usually requires complex analytical instrumentation and expensive reagents, which limits its application in routine clinical practice. Due to its pronounced intrinsic fluorescence, tryptophan can be quantitatively determined using relatively simple fluorimetric methods, making it a convenient marker for spectroscopic analysis of biological fluids.

The work examined blood plasma samples from 17 patients with oropharyngeal cancer who had previously suffered from COVID-19. Plasma samples were obtained by centrifugation at 4000 rpm for 20 min. A mixture of plasma samples from three healthy individuals was used as a control.

Precipitation of high-molecular proteins and peptides was performed by adding an equal volume of 10% perchloric acid followed by centrifugation. The resulting supernatant was diluted in phosphate buffer with a final pH of 7.5. Fluorescence spectra were recorded using an Edinburgh Instruments FS5 spectrofluorometer in the wavelength range of 280–550 nm. The spectra exhibited a characteristic emission maximum near 360 nm under excitation at 280 nm. Quantitative determination of tryptophan concentration in blood plasma was performed using a calibration curve constructed from fluorescence intensities of tryptophan solutions with known concentrations in a system similar in composition to that used for sample preparation.

The experimental results demonstrate a noticeable difference in the content of free tryptophan in the blood plasma of cancer patients compared with the control sample. However, the obtained values show no pronounced correlation and may be either higher or lower than the control level. This variability may result from the combined influence of two pathological processes. On the one hand, enhanced tissue catabolism associated with oncological disease alters the composition of circulating amino acids. On the other hand, previous studies indicate that both COVID-19 and oncological pathology may lead to decreased tryptophan levels in the bloodstream [3, 4].

The obtained results indicate the feasibility of long-term monitoring of free tryptophan levels in the blood plasma of cancer patients who have experienced COVID-19 or other viral infections.

[1] C. A. Kraft, et al. Quantitative Analysis of Protein-Lipid Interactions Using Tryptophan Fluorescence. Sci. Signal. 2, pl4-pl4 (2009). https://doi.org/10.1126/scisignal.299pl4.
[2] M. Liu, X. Wang, L. Wang, et al. Targeting the IDO1 pathway in cancer: from bench to bedside. J Hematol Oncol. 11(1), 100 (2018). https://doi.org/10.1186/s13045-018-0644-y.
[3] L.A. Cysique, D. Jakabek, S.G. Bracken, et al. The kynurenine pathway relates to post-acute COVID-19 objective cognitive impairment and PASC. Ann Clin Transl Neurol, 10: 1338-1352 (2023). https://doi.org/10.1002/acn3.51825.
[4] A.J. Muller, M.G. Manfredi, Y. Zakharia, et al. Inhibiting IDO pathways to treat cancer: lessons from the ECHO-301 trial and beyond. Semin Immunopathol 41, 41–48 (2019). https://doi.org/10.1007/s00281-018-0702-0.

Machine learning–based conformational sampling does not improve rigid protein–protein docking performance

I. Koleiev[1,2], T. Voitsitskyi[1,2], I. Savchenko[1,2], S. Starosyla[2], S. Yesylevskyy[1,2]

[1]Institute of Physics, NAS of Ukraine, 46 Nauky Ave., Kyiv, 03038, Ukraine
[2]Receptor.AI Inc., 20-22 Wenlock Road, London N1 7GU, United Kingdom
e-mail: koleev.igor@gmail.com

Protein–protein interactions play a central role in cellular processes and drug discovery. Accurate computational docking of protein complexes remains challenging, particularly when significant conformational changes occur upon binding. Recent advances in machine learning (ML), especially AlphaFold2-based approaches [1], have enabled large-scale conformational sampling of protein structures. In this work, we systematically evaluate whether ML-generated conformational ensembles can improve rigid protein–protein docking performance compared to experimentally determined Apo structures.

We performed a comprehensive benchmark study using a subset (N = 30) of the PINDER-AF2 dataset [2]. For each target, experimentally resolved Apo structures and ML-sampled conformations were subjected to rigid docking with HDOCK [3]. Generated docking complexes were evaluated using the DockQ metric with CAPRI quality classification [4]. We compared Top-1, Top-5, Top-40 ranked models with different scoring strategies, including physics-based, knowledge-based, and ML-based scoring functions.

Our results demonstrate that ML-based conformational sampling does not consistently improve docking outcomes over Apo baselines. These findings highlight two primary bottlenecks: (i) limited ability of current ML sampling methods to generate Holo-like conformations suitable for docking, and (ii) insufficient robustness of scoring functions to recognize near-native solutions within diverse conformational ensembles. This study underscores the need for next-generation scoring functions trained on modern predicted structure distributions and capable of handling increased conformational variability.

[1] Evans, R., O'Neill, M., Pritzel, A., Antropova, N., Senior, A., Green, T., Žídek, A., Bates, R., Blackwell, S., Yim, J., Ronneberger, O., Bodenstein, S., Zielinski, M., Bridgland, A., Potapenko, A., Cowie, A., Tunyasuvunakool, K., Jain, R., Clancy, E., Hassabis, D. Protein complex prediction with AlphaFold-Multimer. bioRxiv (Cold Spring Harbor Laboratory). (2021). https://doi.org/10.1101/2021.10.04.463034.
[2] Durairaj, J., Adeshina, Y., Cao, Z., Zhang, X., Oleinikovas, V., Duignan, T., McClure, Z., Robin, X., Studer, G., Kovtun, D., Rossi, E., Zhou, G., Veccham, S., Isert, C., Peng, Y., Sundareson, P., Akdel, M., Corso, G., Stärk, H., Naef, L. PLINDER: The protein-ligand interactions dataset and evaluation resource. bioRxiv. (2024). https://doi.org/10.1101/2024.07.17.603955.
[3] Yan, Y., Tao, H., He, J., & Huang, S. The HDOCK server for integrated protein–protein docking. Nature Protocols, 15(5), 1829–1852. (2020). https://doi.org/10.1038/s41596-020-0312-x.
[4] Basu, S., Wallner, B. DockQ: A quality measure for Protein-Protein docking models. PLoS ONE, 11(8), e0161879. (2016). https://doi.org/10.1371/journal.pone.0161879.

Composite film of N-doped reduced graphene oxide with MoS_2: spectroscopy characterization and analysis of low-temperature electron transport

N. V. Kurnosov, A. Yu. Glamazda, A. M. Plokhotnichenko, V. A. Karachevtsev

B.Verkin Institute for Low Temperature Physics and Engineering of the NAS of Ukraine,
47 Nauky Ave., Kharkiv, 61103, Ukraine
e-mail: nick.kurnosov@gmail.com

Currently the graphene-related materials such as graphene oxide and few-layered molybdenum disulfide (MoS_2) are among the nanostructures which draw persistent research interest from both fundamental and applied standpoints. Reduced graphene oxide (rGO) is the nanomaterial that can be synthesized directly from graphite using cost-effective modified Hummers method. Physical properties of rGO are essentially governed by the amount of bound oxygen groups which determine the C/O ratio and relative content of sp^2 and sp^3 hybridized atoms. Few-layered MoS_2 which properties are mostly determined by number of stacked S-Mo-S layers can be obtained by exfoliation of bulk MoS_2 crystals. Both rGO and MoS_2 nanostructures can be considered as 2D semiconductors with tunable, structure-dependant electronic properties. The potential applications of these nanomaterials and composites (nanoelectronics, electrochemical sensors etc.) may require detailed information on charge transport mechanisms.

In our previous study we have shown that rGO mostly provides the conductivity in rGO-MoS_2 composite [1] while presence of MoS_2 nanoflakes can affect ordering and local dielectric environment of rGO and thus electron transport parameters. rGO is intrinsically a p-type semiconductor due to bound oxygen groups, however, the n-type doping can also be applied to rGO nanostructures. Inclusion of nitrogen which can occupy several different positions in rGO sheets (pyridinic, pyrrolic, graphitic) was shown to alter the rGO electronic properties. The aim of our current work is to elucidate the impact of N doping of rGO on low-temperature electron transport mechanisms in N-rGO-MoS_2 composite.

The composite material studied in this work was formed by nanoflakes of MoS_2 and N-rGO. The N and O content in raw N-rGO material was estimated as ~4% and ~16%, respectively [2]. The composite film was obtained by vacuum filtration from the suspension of N-rGO-MoS_2 hybrids. Preparation of the suspension was based on ultrasound treatment (60 min, 22 kHz) with following centrifugation (3000g, 15 min) of N-rGO and MoS_2 with 1:2 weight ratio.

The SEM, UV-Vis and Raman spectroscopy characterizations of N-rGO-MoS_2 composite were performed. The defect-induced (D) and tangential (G) Raman bands of N-rGO were located in the 1200–1700 cm^{-1} range. The presence of few-layered MoS_2 was confirmed by analysis of characteristic E^1_{2g} and A_{1g} bands observed in Raman spectrum (532 nm excitation wavelength). Weak multi-phonon MoS_2 bands which are usually observed at resonance conditions were also revealed.

The temperature dependence of resistance R(T) of the N-rGO-MoS_2 composite was measured in the 5–286 K range. We analyzed the R(T) dependence using Efros-Shklovskii and Mott variable-range hopping transport models [3] in different temperature ranges and also performed comparison of electronic transport properties of N-rGO-MoS_2 composite with N-rGO film.

This work was supported by the National Academy of Sciences of Ukraine (Grant 0126U001857).

[1] N. V. Kurnosov, A. M. Plokhotnichenko, and V. A. Karachevtsev, Appl. Phys. A 131, 190 (2025). https://doi.org/10.1007/s00339-025-08302-7.
[2] A. A. Abakumov, I. B. Bychko, A. S. Nikolenko, and P. E. Strizhak, Theor. Exp. Chem. 54, 218 (2018). https://doi.org/10.1007/s11237-018-9566-6.
[3] B. I. Shklovskii and A. L. Efros, Electronic Properties of Doped Semiconductors (Springer-Verlag, Berlin 1984). https://doi.org/10.1007/978-3-662-02403-4.

Correlative nanoscale imaging of adherent Lewis lung carcinoma cells

G. Monastyrskyi[1], O. Gnatyuk[1], M. Olenchuk[1], D. Kolesnik[2], A. Boisen[3], Z. Zhang[3], S. Karakhim[4], G. Solyanik[2], G. Dovbeshko[1]

[1]Institute of Physics of the NAS of Ukraine, Kyiv, Ukraine
[2]R.E. Kavetsky Institute of Experimental Pathology, Oncology and Radiobiology of the NAS of Ukraine, Kyiv, Ukraine
[3]Technical University of Denmark, Lyngby, Denmark
[4]O.V. Palladin Institute of Biochemistry of the NAS of Ukraine, Kyiv, Ukraine
e-mail: g.monastyrskyi@gmail.com

Adhesive structural organization of carcinoma cells determines the spatial distribution of adhesion complexes, cytoskeletal tension, and membrane topography, which collectively regulate force transmission, signaling activity, and migration potential of Lewis lung carcinoma (LLC) cancer cells, thereby directly influencing their proliferative capacity, invasive behavior, and progression toward metastatic phenotypes. In this study, substrate-attached cells were examined using an imaging centered on high-resolution scanning electron microscopy (SEM), supported by optical microscopy, vibrational spectroscopy, and Coherent Anti-Stokes Raman Scattering (CARS).

Following controlled dehydration and CO_2 critical point drying, SEM in secondary electron mode enabled detailed visualization of membrane surface architecture and adhesion-associated structures. The adherent phenotype was characterized by pronounced lamellar extensions, elongated filopodia, and structured peripheral zones corresponding to focal anchoring regions. At higher magnification, the plasma membrane displayed heterogeneous nanoscale relief, including protrusive domains and vesicular elements indicative of dynamic membrane turnover.

Optical and confocal imaging confirmed cytoskeletal alignment along substrate interaction axes. CARS imaging targeting CH_2 vibrational modes revealed non-uniform lipid distribution, particularly enriched in cell peripheries and protrusive regions. Spectroscopic analysis suggested localized lipid–protein rearrangements associated with mechanical coupling to the substrate.

The integration of ultrastructural and chemically selective imaging demonstrates that adhesion induces coordinated remodeling of membrane topology and intracellular organization.

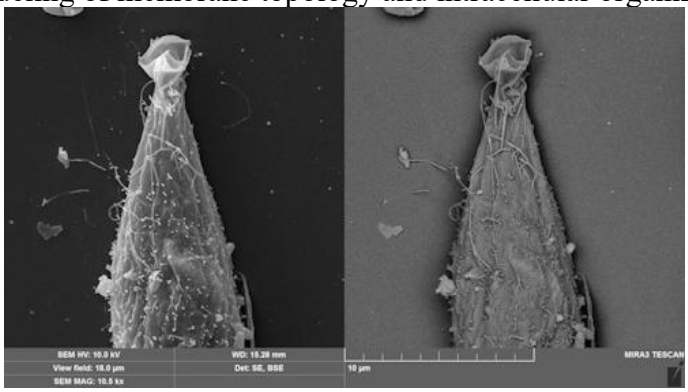

Fig.1. Adherent LLC cell in SE and BSE modes (HV 10 kV, mag. 10.5 k×, scale bar 10 µm).

These findings are consistent with recent studies demonstrating that adhesion-mediated cytoskeletal remodeling and membrane nanostructuring are key determinants of tumor cell mechanoadaptation and metastatic potential, and they support the use of SEM-based correlative microscopy as a quantitative approach for resolving ultrastructural features of carcinoma cells.

Acknowledgement. This work was supported by the project: NRFU № 2021.01/0229 “Biophysical characteristics of circulating metastatic cells as potential targets of antimetastatic therapy” (2022-2025) and 0123U100990, «Physical effects and molecular mechanisms of interaction of biological molecules and biological systems of different levels of structural organization with small molecules, nanoscale and supramolecular complexes».

Protein-ligand molecular docking with unbound protein conformations using machine learning

T. Voitsitskyi[1,2], I. Koleiev[1,2], I. Savchenko[1,2], S. Starosyla[2], S. Yesylevskyy[1,2]

[1]Institute of Physics, NAS of Ukraine, 46 Nauky Ave., Kyiv, 03038, Ukraine
[2]Receptor.AI Inc., 20-22 Wenlock Road, London N1 7GU, United Kingdom
e-mail: taras270698@gmail.com

Traditional protein-ligand docking methods have been a cornerstone of computational drug discovery for decades, yet their predictive performance has seen little improvement recently. Docking approaches based on Machine Learning (ML) have emerged as a promising alternative, though their practical adoption remains limited by several unresolved challenges – including the trade-off between computational efficiency and predictive accuracy, the lack of standardized evaluation frameworks, and questions surrounding the physical realism of the generated binding poses. This study assesses the performance of ArtiDock, an ML-driven docking method trained on experimentally determined protein-ligand complex structures. The assessment focuses on predicting ligand binding pose under realistic docking conditions when the optimal (holo) protein structure is unknown and unbound protein conformations (apo) are used as input.

To minimize evaluation bias, the model was trained on the PLINDER [1] dataset, a large and structurally diverse collection derived from the Protein Data Bank with a predefined training subset. Final performance was evaluated on the test set with apo protein structures (PLINDER MLSB) and compared against prominent open-source and commercial classical docking tools, including AutoDock [2], Vina [3], and Glide [4].

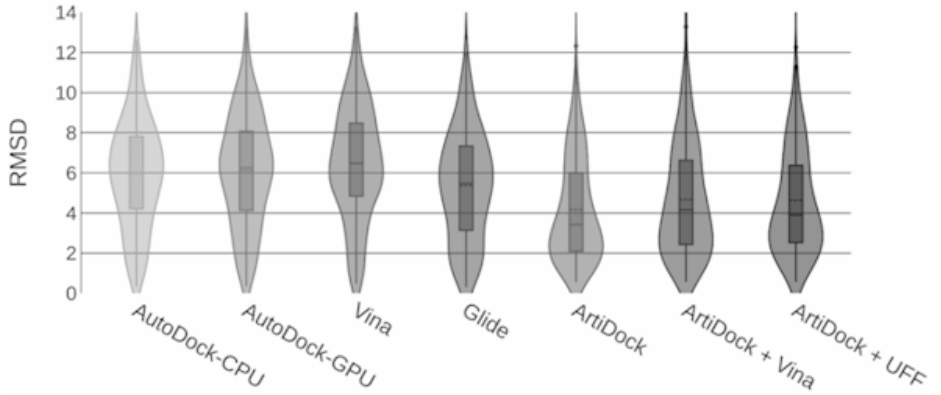

Fig. 1. Violin plot of docking top-ranked pose RMSD (Å, smaller is better) distributions on the PLINDER MLSB test dataset (N=344).

Our results indicate that ArtiDock achieves a median RMSD improvement of 2.1 Å over the top-performing classical docking method when comparing predicted ligand poses to experimentally determined structures (Fig. 1).

[1] J. Durairaj, Y. Adeshina, Z. Cao, X. Zhang, V. Oleinikovas, T. Duignan, Z. McClure, X. Robin, G. Studer, D. Kovtun, E. Rossi, G. Zhou, S. Veccham, C. Isert, Y. Peng, P. Sundareson, M. Akdel, G. Corso, H. Stärk, G. Tauriello, Z. Carpenter, M. Bronstein, E. Kucukbenli, T. Schwede, and L. Naef, bioRxiv (2024). https://doi.org/10.1101/2024.07.17.603955.
[2] D. S. Goodsell, M. F. Sanner, A. J. Olson, and S. Forli, Protein Sci. 30, 31 (2021). https://doi.org/10.1002/pro.3934.
[3] J. Eberhardt, D. Santos-Martins, A. F. Tillack, and S. Forli, J. Chem. Inf. Model. 61, 3891 (2021). https://doi.org/10.1021/acs.jcim.1c00203.
[4] R. A. Friesner, J. L. Banks, R. B. Murphy, T. A. Halgren, J. J. Klicic, D. T. Mainz, M. P. Repasky, E. H. Knoll, M. Shelley, J. K. Perry, D. E. Shaw, P. Francis, and P. S. Shenkin, J. Med. Chem. 47, 1739 (2004). https://doi.org/10.1021/jm0306430.

Ions binding to model lipid membranes: obtaining the adsorption value from indirect measurements

R. Ye. Brodskii[1], O. V. Vashchenko[2]

[1]Institute for Single Crystals of the NAS of Ukraine, 60 Nauky Ave., 61072 Kharkiv, Ukraine
[2]Institute for Scintillation Materials of the NAS of Ukraine, 60 Nauky Ave., 61072 Kharkiv, Ukraine
e-mail: r.brodskii@gmail.com

Ions binding to lipid membranes is commonly considered from an adsorption viewpoint. Meanwhile, all canonical adsorption models [1] contain equilibrium adsorbate concentration, c, which may not always be determined properly in a lipid medium. So, it would be helpful to obtain the adsorption value, s, from indirect measurements, *e.g.*, from phase transition temperatures of model lipid membranes. As it was shown earlier [2], the shift of the phase transition temperature, ΔT, is proportional to s, which obeys the Freundlich isotherm $s = kc^{\beta}$ (k, β are constants). So,

$$\Delta T = \gamma s = \gamma k c^{\beta} . \qquad (1)$$

As one can see from (1), determination of s from ΔT is based on obtaining the value of the proportional constant, γ. The problem is that γ cannot be obtained on the basis of $\Delta T(c)$ (1), since this dependence contains γ only in a combination with another constant, k.

We have recently shown [3], that there is a form of isotherm, where these constants become separated. Such a form can be found by means of explicit accounting of both adsorbate uptake and solvent uptake by the adsorbent. As a result, we obtained in the case of Freundlich adsorption:

$$\Delta T = \gamma k c_0^{\beta} \left(\frac{\kappa_a - \alpha / c_0 \cdot (\Delta T / \gamma)}{\kappa_a - \eta} \right)^{\beta} , \qquad (2)$$

where c_0 is the initial adsorbate concentration in solution, the constant α includes such parameters as the molar mass of the adsorbent and the solvent density, $\kappa_a = C_a / (1 - C_a)$ is the solvent : adsorbent mass ratio, C_a is the mass fraction of solvent; η is the value of κ_a corresponding to full membrane hydration. Note that analytical dependence (2) fitted well the experimental data on $\Delta T(C_a)$ obtained for the dipalmitoylphosphatidylcholine (DPPC) membrane hydrated with KCl aqueous solution ($c_0 = 0.45$ M), which confirms the applicability of the model to our system. Using (2), one can determine k and γ separately by means of setting up a system of two equations for two pairs $(c_0, \Delta T)$ or $(C_a, \Delta T)$. Knowing γ, one can find the value of s on the basis of ΔT from (1). Applicating this method to our experimental data, we determined the lipid : ion ratio at DPPC membrane surface as *ca*. 10 : 1 at $C_a \approx 0.9$.

Finally, it should be emphasized that, albeit the method was initially developed for the determination of lipid : ion ratio on a membrane surface, it only utilizes such common physical parameters as the amount of adsorbent and adsorbate, solvent volume, density, *etc.*, and therefore it seems quite applicable to various adsorption processes on liquid-solid, gas-solid, and gas-liquid interfaces.

[1] K.Y. Foo and B.H. Hameed, Chem. Eng. J. 156(1), 2 (2010). https://doi.org/10.1016/j.cej.2009.09.013.
[2] O.V. Vashchenko, N.A. Kasian, R.Ye. Brodskii, L.V. Budianska, D.S. Sofronov, L.N. Lisetski, Func. Materials, 25(3), 422 (2018). https://doi.org/10.15407/fm25.03.
[3] R.Ye. Brodskii and O.V. Vashchenko, J. Mol. Liq., 449, 129423 (2026). https://doi.org/10.1016/j.molliq.2026.129423.

Virtual screening and molecular dynamics simulation of phytochemicals as potential inhibitors of extended-spectrum beta-lactamases

N. V. Khmil[1,2], M. O. Kryvobok[2], A. V. Shestopalova[1]

[1]O. Ya. Usikov Institute for Radiophysics and Electronics National Academy of Sciences of Ukraine, 12 Acad. Proskura str., Kharkiv, 61085, Ukraine
[2]Kharkiv National University of Radio Electronics, Nauky ave., 14, Kharkiv, Ukraine, 61166
e-mail: khmilnatali@gmail.com

The global spread of extended-spectrum в-lactamases (ESBLs) in *Klebsiella pneumoniae*, particularly the SHV-1 and SHV-2 variants, represents a critical challenge in the management of hospital-acquired infections [1]. Point mutations in the ESBL enzymes expand the active site, thereby conferring resistance to third-generation cephalosporins and reducing the efficacy of classical в-lactamase inhibitors. This study investigates the potential of phytochemical core structures as alternative non-в-lactam inhibitors to counteract these resistance mechanisms.

Comparative molecular docking was performed using AutoDock Vina (v1.2.5) and the CB-Dock2 web server [2]. A total of 18 phytochemicals, including flavonoids and polyphenols, as well as clavulanic acid, were retrieved from the PubChem database (https://pubchem.ncbi.nlm.nih.gov). Docking simulations were carried out against both the wild-type sulfhydryl variable в-lactamase SHV-1 (PDB ID: 1SHV) and its mutant variant, SHV-2, carrying the Gly238Ser substitution (PDB ID: 1N9B), obtained from the RCSB Protein Data Bank (https://www.rcsb.org). Molecular dynamics simulations of 100 ns were performed using GROMACS (v2024.4) with the CHARMM27 force field and the TIP3P water model to evaluate the conformational stability of the most energetically favorable docked complexes.

Among the investigated compounds, Epigallocatechin gallate (EGCG) demonstrated the strongest binding affinities toward both protein variants across both docking platforms. Using AutoDock Vina, EGCG exhibited binding energies of –8.0 kcal/mol for the wild-type enzyme (1SHV) and –10.0 kcal/mol for the mutant (1N9B). CB-Dock2 produced comparable results, with docking scores of –7.7 kcal/mol (1SHV) and –8.8 kcal/mol (1N9B). Both docking methods consistently showed stronger binding to the Gly238Ser mutant compared to the wild-type structure. EGCG possesses multiple phenolic hydroxyl groups distributed across three aromatic rings. This structure enables the formation of numerous hydrogen bonds with catalytic and surrounding residues, including Ser70, Ser130, Glu166, and Thr235. In addition, electrostatic interactions with polar residues and π-π stacking with a polar, uncharged amino acid possessing pronounced hydrophobic properties (Tyr105) contribute to stabilization within the binding pocket. These combined interactions likely facilitate improved accommodation of EGCG within the expanded active site of the Gly238Ser mutant. Clavulanic acid was selected as a reference inhibitor of class A в-lactamases to benchmark the docking performance of the studied phytochemicals. The *in silico* docking study demonstrated that clavulanic acid exhibited weaker predicted binding affinities in both docking approaches. AutoDock Vina produced binding energies of –6.1 kcal/mol for 1SHV and –7.2 kcal/mol for 1N9B, while CB-Dock2 yielded –6.6 kcal/mol and –6.3 kcal/mol, respectively. These less negative docking scores indicate lower predicted non-covalent affinity compared to the investigated flavonoids. Molecular dynamics simulations revealed that EGCG exhibits stable binding and structural stability in complexes with both SHV-1 and SHV-2 в-lactamases over a 100 ns trajectory. Our findings emphasize that integrating computational binding affinity data with dynamic stability analysis and structural insights is essential for predicting effective inhibitors of sulfhydryl variable в-lactamases that contribute to antibiotic resistance.

[1] A. Liakopoulos, D. Mevius, and D. Ceccarelli, Frontiers in microbiology. 7, 1374 (2016). https://doi.org/10.3389/fmicb.2016.01374.
[2] O. Trott, and A. J. Olson, Journal of computation chemistry. 31, 2 (2010). http://doi.org/10.1002/jcc.21334.

Biomechanical adaptation of Lewis lung carcinoma (LLC) cells to circulation conditions and metabolic stress

M. V. Olenchuk[1], O. P. Gnatyuk[1], S. V. Romanenko[2], D. L. Kolesnik[3], G. I. Solyanik[3], G. I. Dovbeshko[1]

[1]Institute of Physics of the NAS of Ukraine, 46 Nauky Ave., 03028, Kyiv, Ukraine
[2]O.O. Bogomolets Institute of Physiology of the NAS of Ukraine, 4 Akademik Bogomolets str., 01601, Kyiv, Ukraine
[3]R.E. Kavetsky Institute of Experimental Pathology, Oncology and Radiobiology of the NAS of Ukraine, 45 Vasyl'kivs'ka St., 03022, Kyiv, Ukraine
e-mail: m.olenchuk@yahoo.com

The mechanical properties of the cell membrane and the underlying cytoskeleton are key determinants of the metastatic potential of tumor cells. Passive mechanical characteristics—elasticity, viscosity, and strength—define a cell's ability to undergo deformation under external forces without active cellular participation, which is critical for the passage of circulating tumor cells (CTCs) through narrow capillaries.

Lewis lung carcinoma (LLC) cells were used as the experimental model. The study investigated the impact of two factors: adhesive growth conditions and glucose deficiency. To simulate the state of CTCs, deadhesive growth was modeled using poly(2-hydroxyethyl methacrylate) (polyHEMA)-coated dishes, compared with standard adhesive growth. The impact of energy deficit was studied by incubating cells in a glucose-free medium for 24 hours. Mechanical properties were quantified using the micropipette aspiration technique, which allows for the non-invasive measurement of integral macroscopic elastic characteristics based on the pressure-induced cell entry into a capillary.

The study demonstrated that cultivation conditions significantly modulate the biomechanical profile of LLC cells. It was established that the transition to a deadhesive state (CTC model) leads to a shift in the Young's modulus, indicating an adaptive reorganization of the actin cortex. Glucose deficiency acts as an additional stress factor that reduces the cell's resistance to deformation. Quantitative assessment of aspiration parameters showed that the combination of metabolic stress and loss of adhesion significantly increases cell deformability, potentially facilitating survival during passive transport through the vasculature.

The micropipette aspiration method is an effective tool for assessing the functional state of tumor cells under changing microenvironmental conditions. It was established that glucose deficiency and the lack of adhesive contact significantly affect the passive mechanical properties of LLC cells, leading to decreased stiffness. Understanding the mechanisms that transform external stimuli into biomechanical responses is essential for uncovering the molecular aspects of cancer progression, developing strategies to control metastasis and antimetastatic therapy.

Acknowledgement

Authors acknowledge the projects №2021.01/0229 “Biophysical characteristics of circulating metastatic cells as potential targets of antimetastatic therapy” and №1.4. B/218 “Physical effects and molecular mechanisms of interaction of biological molecules and biological systems of different levels of structural organization with small molecules, nanoscale and supramolecular complexes”.

Reconstruction of the real distribution of the relative yields of the clusters of polyisotopic elements sputtered from MoS_2 under laser desorption/ionization

V. V. Orlov[1], O. A. Boryak[1], V. S. Shelkovsky[1], M. V. Kosevich[1], P. O. Kuzema[2]

[1]B.Verkin Institute for Low Temperature Physics and Engineering of the NAS of Ukraine, 47 Nauky Ave., Kharkiv, 61103, Ukraine
[2]Chuiko Institute of Surface Chemistry of the National Academy of Sciences of Ukraine, 17 Oleg Mudrak Str., Kyiv 03164, Ukraine
e-mail: orlov@ilt.kharkov.ua

In cluster science, mass spectrometry is an efficient tool that permits the simultaneous generation and study of small atomic and molecular clusters. The clusters can either assemble in the gas phase or be sputtered from condensed matter. As a rule, the relative yield of a cluster M_n to the total population monotonically decreases with increasing n for a monocomponent object. However, the situation may be different for multicomponent objects, when the cluster assembling is governed by intermolecular interactions of varying strengths between different components. This is the case of clusters sputtering from oxidized transition metal dichalcogenides, MoS_2 in particular. The pattern of $Mo_xS_yO_z$ clusters sputtered under laser desorption/ionization (LDI) mass spectrometric conditions from MoS_2 consists of several groups of clusters formed due to assembling of chalcogens (S, O) around molybdenum atoms (x = 1÷4) (Fig. 1a). The estimation of the yield of each cluster is hampered, however, by the polyisotpic nature of Mo element, which is represented in nature by 7 stable isotopes (92, 94, 95, 96, 97, 98, 100 u). Due to this, 100% of the cluster content is distributed over the related isotopic distribution, that is, the set of peaks in the mass spectrum: 15 peaks for Mo_2, 23 for Mo_3, 31 for Mo_4, 39 for Mo_5, etc. As a consequence, the intensity of the maximal peak in the set decreases with x increase from 23% of the total 100% for clusters containing one Mo atom to 8% for clusters with four Mo atoms.

The aim of this work was to "reconstruct" the real contributions of $Mo_xS_yO_z$ clusters sputtered under LDI from MoS_2 by recalculating the value of 100% abundance of isotopic distributions for each cluster in the spectrum. The results of the reconstruction are presented as a histogram where the calculated abundances are plotted versus average mass values of the clusters (Fig. 1b). It can be seen that the total pattern of the two clusters' distributions is similar, while maximum intensities in the experimental envelopes of peaks for larger clusters are lower than the calculated ones.

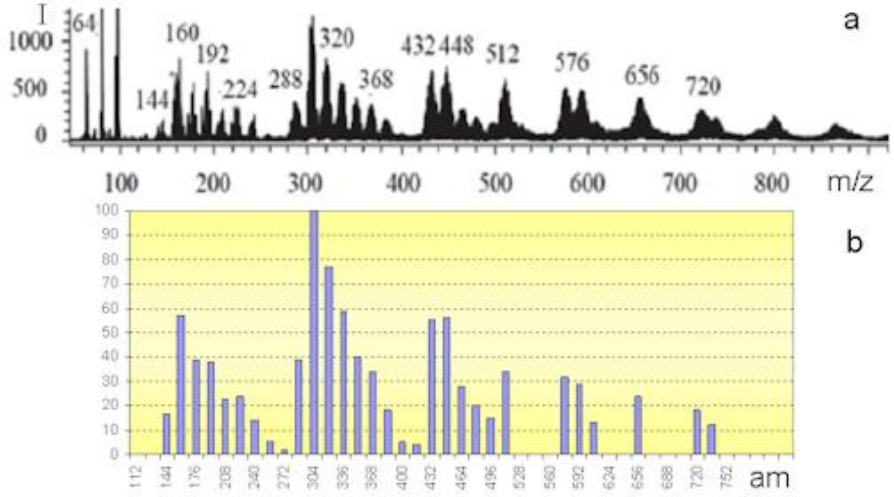

Fig. 1. Experimental LDI mass spectrum of MoS_2 (a) and calculated relative yields of $Mo_xS_yO_z$ clusters (b); am – average mass of polyisotopic clusters.

This work was supported by the grant 0126U001857 of the NAS of Ukraine.

Infrared and Raman spectra of the MoS_2-adenine and MoS_2-guanine complexes: a DFT/M06-2X study

T. Piddubnyi[1], S. Stepanian[1], L. Adamowicz[2]

[1]B.Verkin Institute for Low Temperature Physics and Engineering of the NAS of Ukraine, 47 Nauky Ave., Kharkiv, 61103, Ukraine
[2]Department of Chemistry and Biochemistry, University of Arizona, 85721 Tucson AZ, USA
e-mail: piddubnyi@ilt.kharkov.ua

The main aim of this work is to determine the effect of interaction with molybdenum disulfide on the vibrational spectra of purine nucleobases: adenine and guanine, and to identify spectral markers of this interaction for each base. We employed the quantum-mechanical DFT/M06-2X method to calculate the structure, infrared, and Raman spectra of the nucleobases with the MoS_2 monolayer. The calculations were performed for the complexes with the pristine MoS_2 fragment as well as with the MoS_2 fragment having point surface defects.

Two types of complexes were calculated for the pristine MoS_2. These are stacking complexes in which adenine and guanine interact with the MoS_2 surface formed by sulfur atoms, and covalently bonded complexes in which coordination bonds are formed between under-coordinated edge molybdenum atoms and base atoms with lone electron pairs.

Analysis of the calculated vibrational spectra of the MoS_2-adenine and MoS_2-guanine complexes revealed that the formation of the stacked complexes is accompanied by a decrease in the intensities of vibrations both in infrared and Raman spectra. In most cases, the shifts of the bands demonstrate weak sensitivity to the structure of the complexes. At the same time, the formation of covalently bonded complexes leads to a significant increase in the intensities of vibrations, especially in Raman spectra. In infrared and Raman spectra of the complexes, the most significant changes are observed for vibrations of different types. The spectra of covalently bonded complexes demonstrate high sensitivity to the structure of the complexes, which made it possible to identify characteristic spectral markers of the formation of complexes for all purine bases. There is the dependence between the energies of interaction in the complexes and the values of the shifts of the spectral stripes during their formation.

Acknowledgements

The authors acknowledge financial support from National Academy of Sciences of Ukraine (Grant № 0126U001857). An allocation of computer time from the Computational Center at Institute for Low Temperature Physics and Engineering and from UA Research High Performance Computing (HPC) and High Throughput Computing (HTC) at the University of Arizona is gratefully acknowledged.

Modification of transition metal dichalcogenides by organic compounds, reflected in the composition of laser-desorbed clusters

V. G. Zobnina[1], V. S. Shelkovsky[1], M. V. Kosevich[1], O. A. Boryak[1], P. O. Kuzema[2], V. A. Karachevtsev[1]

[1]B.Verkin Institute for Low Temperature Physics and Engineering of the NAS of Ukraine, 47 Nauky Ave., Kharkiv, 61103, Ukraine
[2]Chuiko Institute of Surface Chemistry of the National Academy of Sciences of Ukraine, 17 Oleg Mudrak Str., Kyiv 03164, Ukraine
e-mail: valezobnina@gmail.com

Transition metal dichalcogenide (TMD) layered 2D nanomaterials are combined with organic compounds to obtain materials possessing new properties. The properties of the composite as a whole are usually considered. In the current study, we have observed changes in the chemical composition of the TMD MoS_2 and WS_2 nanosheets due to their interactions with organic compounds methylene blue (MB), PEG, and thioglycerol (TG), which was reflected in the changes of composition of clusters desorbed from the TMD-organics nanohybrides under the conditions of laser desorption/ionization (LDI) mass spectrometry.

It is believed that small clusters of atoms are cleaved from the edges of the TMD nanosheets by the laser heating. The modification of the TMD occurs mainly at edges as well. Sets of negatively charged clusters $TM_xCh_y^-$ (where Ch is a chalcogene) are expected to be sputtered from the TMD under LDI. It was shown that the oxidation of TMD occurs during their ultrasound exfoliation in aqueous media, as reflected in the formation of oxygen-containing $TM_xS_yO_z^-$ clusters [1]. More detailed inspection of the isotopic distributions of the clusters permitted us to reveal attachment of hydrogen atoms to some small clusters: $TM_1SO_2H^-$, $TM_1S_2OH^-$, $TM_1S_3O_zH^-$ (z = 0-3). Interestingly, these clusters disappear in the mass spectra of the (TMD + PEG) nanocomposites.

In the LDI mass spectra of a nanocomposite of MoS_2 with MB (which is an organic salt consisting of organic cations and Cl^- counterion), chlorine-containing cluster $MoSOCl^-$ was registered. This means that some share of the chlorine counterions become covalently attached to the TMD, more probably, at the edges of the nanosheets.

While molybdenum and tungsten-containing ions are recorded in the mass spectra of pristine TMD in the negative ion mode only, positively charged ions appear in the spectra of the (TMD + TG) nanocomposites. Mo^+ (or W^+) ions and $MoS_xO_y^+$ (x=1,2, y=0,1) or $WS_xO_y^+$ (x=1,2, y=0,1) clusters are desorbed. It may be assumed that interaction with thiol TG causes noticeable distortion of the nanosheets' edges, which makes possible the release of the naked TM^+ ions and small clusters.

Information on the modification of TMD nanomaterials on their interaction with organic molecules is of practical importance for the elaboration of biomedical applications of TMD-based nanocomposites.

This work was supported by the N 0126U001857 grant of the NAS of Ukraine.

[1] O. A. Boryak, M. V. Kosevich, V. A. Psahynska, P. O. Kuzema, and V. A. Karachevtsev, Chem., Phys. Technol. Surf. 16(2) 178 (2025). https://doi.org/10.15407/hftp16.02.178

The effect of temperature and thionine concentration on DNA stability

E. L. Usenko, A. Yu. Glamazda, V. A. Valeev, V. A. Karachevtsev

B. Verkin Institute for Low Temperature Physics and Engineering of NAS of Ukraine,
47 Nauky Ave., Kharkiv, 61103, Ukraine
e-mail: usenko@ilt.kharkov.ua

Interest in studying the interaction of small molecules with DNA is caused by the need to develop new, highly effective, and low-toxic drugs for cancer treatment [1]. The strong and highly specific binding of thionine with DNA makes it a promising candidate for use in medicine and pharmacology [2].

In this study, DNA-thionine complexes in aqueous solutions were investigated using UV-Vis absorption spectroscopy. The thermal stability of native DNA was studied in a broad range of thionine concentrations.

The mechanisms of thionine binding to DNA, depending on the concentration of thionine, have been established. At low thionine concentrations ($[c_{th}] \leq 1.5$ mg/L), thionine molecules intercalate between the base pairs of the DNA double helix. At a thionine concentration of 1.5 – 10 mg/L, the groove binding and external electrostatic interaction of positively charged thionine with negatively charged biopolymer phosphate groups of the DNA backbones is preferable. In all cases, the interaction of thionine with DNA leads to an increase in the thermal stability of the polynucleotide.

These findings provide valuable insight into the concentration-dependent molecular mechanisms of DNA-small molecule interactions, supporting the rational design of anticancer and antimicrobial agents, as well as exploiting molecular probes for nucleic acid detection, imaging, and other biomedical applications.

[1] R. Martínez and L. Chacón-García, Curr. Med. Chem. 12, 127 (2005).
https://doi.org/10.2174/0929867053363414.
[2] P. Paul and G.S. Kumar, J. Hazard Mater. 184, 620 (2010).
https://doi.org/10.1016/j.jhazmat.2010.08.081.

"Poor man's" depth profiling: microscopy and laser desorption/ionization mass spectrometry of a thin film of (MoS_2 + PEG + thioglycerol) system

V. G. Zobnina[1], P. O. Kuzema[2], O. A. Boryak[1], V. S. Shelkovsky[1], M. V. Kosevich[1], V. A. Karachevtsev[1]

[1]B.Verkin Institute for Low Temperature Physics and Engineering of the NAS of Ukraine, 47 Nauky Ave., Kharkiv, 61103, Ukraine
[2]Chuiko Institute of Surface Chemistry of the National Academy of Sciences of Ukraine, 17 Oleg Mudrak Str., Kyiv 03164, Ukraine
e-mail: valezobnina@gmail.com

A jocular term, "poor man's" experimental methods, was coined to refer to a relatively simple technique that permits obtaining some experimental results similar to those expected from more intricate ones. In this report, we present data on distinguishing the upper and bottom layers, i.e., a simplified "depth profiling" of a thin film of a (MoS_2 + PEG + thioglycerol) sample probed by optical microscopy and laser desorption/ionization (LDI) mass spectrometry.

The triple mixture of MoS_2 inorganic nanomaterial, the organic polymer PEG-600, and thioglycerol (TG, as an exfoliation-assisting agent) intended for nanocomposite preparation was treated by ultrasound in an aqueous medium. PEG-600 and TG are components with low vapour pressure that can remain in the liquid state under vacuum.

During the inspection of the dehydrated film (about 0.1 mm thick) of the composite by optical microscopy, it appears that the image changes qualitatively with the change of focusing of the optical lens: upper layer of the film was enriched by chains of particles, virtually, bound due to PEGylation effect of PEG (insert in Fig. 1a). Focusing on the lover layer of the transparent film reveals small separate particles (Fig. 1b). Such a film was probed by the LDI mass spectrometry operating in two modes. At relatively low laser pulse power, ensuring desorption mode from the surface layer, the bell-shaped distribution of oligomers characteristic of PEGs dominated the spectrum (Fig. 1a), while the signals characteristic of MoS_2 were relatively low. Such a spectral pattern agrees with the surface localization of MoS_2 particles covered with (and shielded by) PEG. A substantial increase in laser power provides the ablation mode with atomization of deeper layers of the sample film. In this mode, the total ion current increases, but the re-distribution of the yields of the sample components is observed (Fig. 1b): PEG-related spectrum is substantially suppressed in favour of noticeable growth of MoS_2-related ions.

The present observation is of practical value for analytical applications of LDI mass spectrometry. Usually, the heterogeneous sample composition is accounted for only the surface distribution of so-called "sweet spots" (with a higher content of the studied compound). A possible heterogeneous layered structure of a multicomponent sample is rarely accounted for in standard analyses.

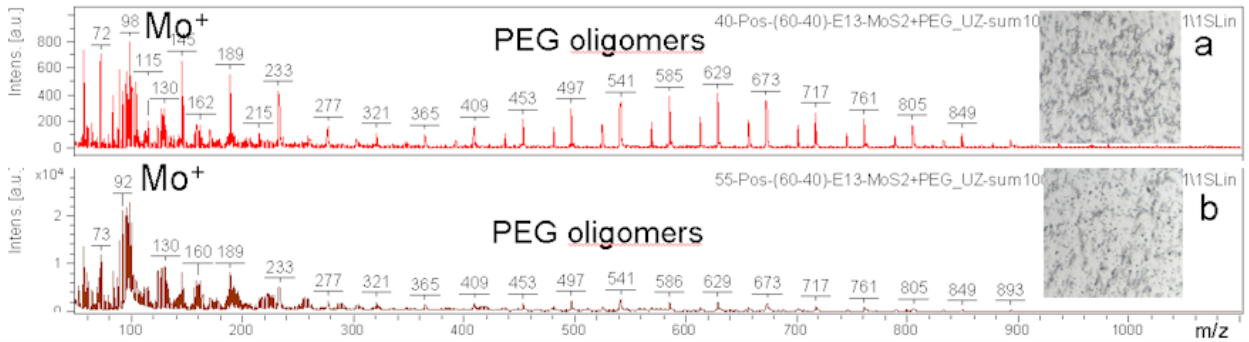

Fig. 1. LDI mass spectra and microphotographs of (MoS_2 + PEG + thioglycerol) system.

This work was supported by the grant N 0126U001857 of the NAS of Ukraine.

Nanocomposites of two-dimensional transition metal dichalcogenides with anticancer drug 5-fluorouracil: biophysical examination of drug delivery applicability

V. A. Pashynska[1], S. G. Stepanian[1], M. V. Kosevich[1], O. A. Boryak[1], P. O. Kuzema[2]

[1]B.Verkin Institute for Low Temperature Physics and Engineering of the NAS of Ukraine, 47 Nauky Ave., Kharkiv, 61103, Ukraine
[2]Chuiko Institute of Surface Chemistry of the National Academy of Sciences of Ukraine, 17 Oleg Mudrak Str., Kyiv, 03164, Ukraine
e-mail: vlada.pashynska@gmail.com

Two-dimensional (2D) transition metal dichalcogenides (TMDs), notably MoS_2 and WS_2, are considered and deeply studied as efficient, biocompatible nanocarriers for drug delivery and cancer therapy due to their high surface area, excellent photothermal conversion, and other prominent physicochemical properties. These TMD nanomaterials can be excellently loaded with low water-soluble hydrophobic drugs via noncovalent interactions, providing sustained, pH-sensitive, and light-activated drug release [1]. At the same time, TMDs are characterized by high catalytic activity, in particular edge-site activity and defects stimulated catalysis, that can affect the drug delivery. Therefore, the study on the peculiarities of biophysical interactions between nanoparticles and drug molecules can become the basis for the understanding and development of the controllability of drug compound loading and release processes, as well as may provide the opportunity to assess the applicability of TMDs for the delivery of specific drugs. Our recent study focused on the combined – experimental and theoretical – characterization of interactions between the components of a nanocomposite of MoS_2 with anticancer thioderivatives of purine nucleobases 6-thiopurine (TP) and 2-thioadenine (TA) [2]. The biologically significant noncovalent and covalent interactions of TP and TA with MoS_2 nanosheets were revealed.

In the current study, we used the same approach combining laser desorption/ionization (LDI) mass spectrometry and ab initio DFT/M06-2X calculations to characterize the nanocomposites of TMD (MoS_2 or WS_2) with the widely used anticancer drug 5-fluorouracil (FU). The LDI data showed the presence of appropriate peaks of intact molecular ions of FU in the positive- and negative-ion mass spectra for both (MoS_2 + FU) and (WS_2 + FU) nanocomposites. This result testifies to the effective drug loading onto the TMD nanoparticles during composite production by ultrasonic treatment and to effective drug release under LDI. Note that LDI conditions can be considered as modeling other light-activated drug release conditions and photothermal cancer treatment with TMD nanomaterials. The comparison of spectral data for MoS_2 or WS_2 containing composites with FU was performed, as well as the difference in intercomponent interactions in FU and TP or TA-based composites was revealed.

DFT/M06-2X modelling of nanocomplexes of MoS_2 nanosheets with FU molecule allowed us to obtain the structural and energetic parameters of biophysical interactions of the drug with the nanoparticles. It was revealed that FU can form stable staking complexes with the MoS_2 nanosheet surface as well as covalent complexes with the nanosheets` edges. The effect of the revealed peculiarities of interactions of TMD nanoparticles with FU on the nanoparticles' applicability for this drug delivery purposes is discussed.

This work is supported by the National Academy of Sciences of Ukraine (grant No 0126U001857).

[1] R. Zhang, Z. Yan, M. Gao, B. Zheng, B. Yue, and M. Qiu, J. Mater. Chem. B, 12, 12437 (2024) https://doi.org/10.1039/D4TB01787K.
[2] V. A. Pashynska, M. V. Kosevich, S. G. Stepanian, O. A. Boryak, P. O. Kuzema, L. Adamowicz, and V. A. Karachevtsev, Low Temp. Phys, 52, N 5 (2026) *in press.*

MATERIALS SCIENCE

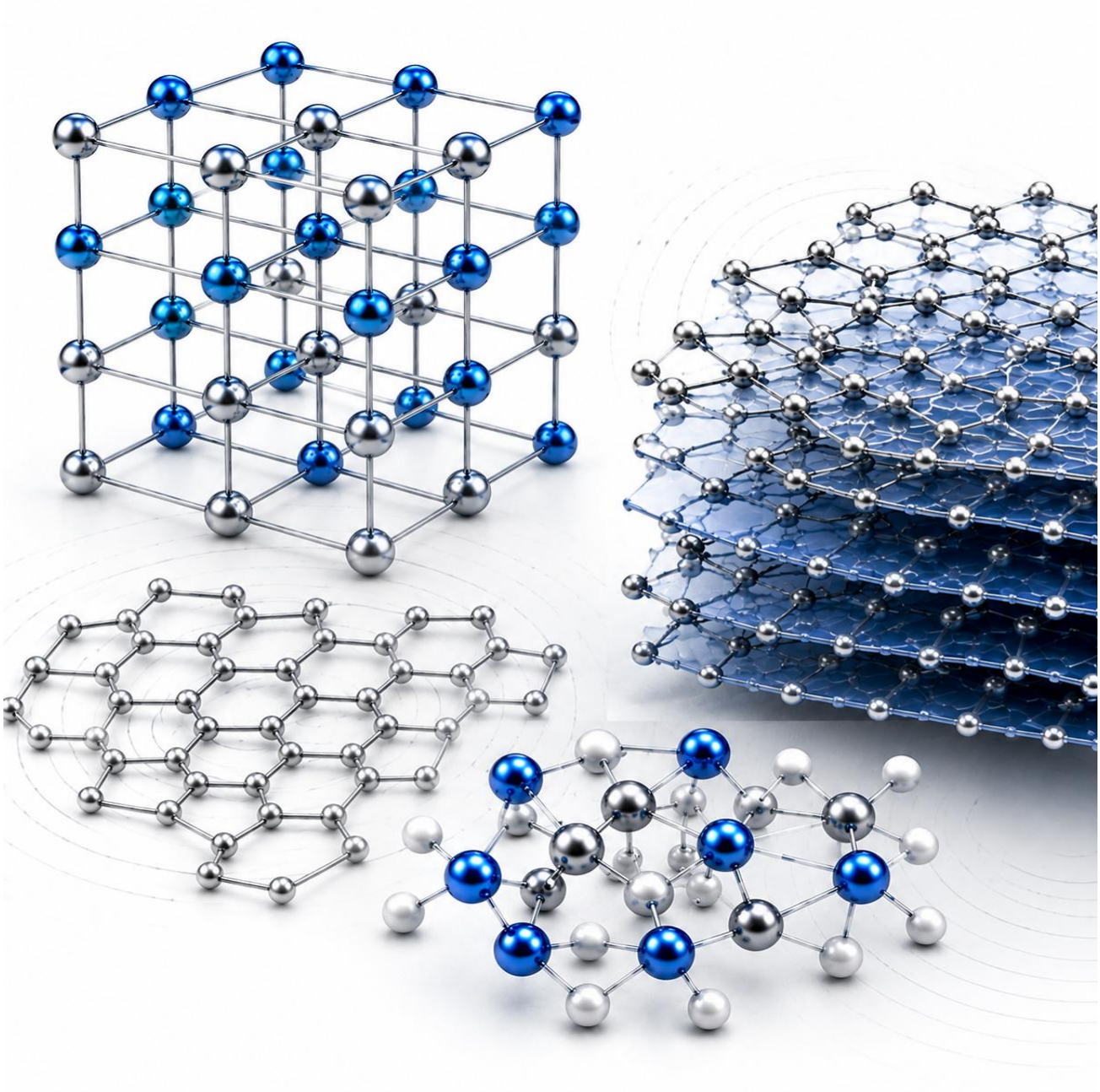

Crystallization of amorphous films of ytterbium oxide sulfide at thermal and electron beam influence

A. G. Bagmut

National Technical University "Kharkiv Polytechnic Institute",
2, Kyrpychova str., 61002, Kharkiv, Ukraine
e-mail: agbagmut@gmail.com

Amorphous films of ytterbium oxide sulfide (Yb_2O_2S) are formed on substrates at room temperature in the process of electron-beam evaporation of YbS in vacuum and subsequent oxidation at separation of the film from the substrate in distilled water. Thermal and electron beam influence causes their crystallization with the formation of Yb_2O_2S micro crystals with hexagonal crystal lattice (Fig. 1).

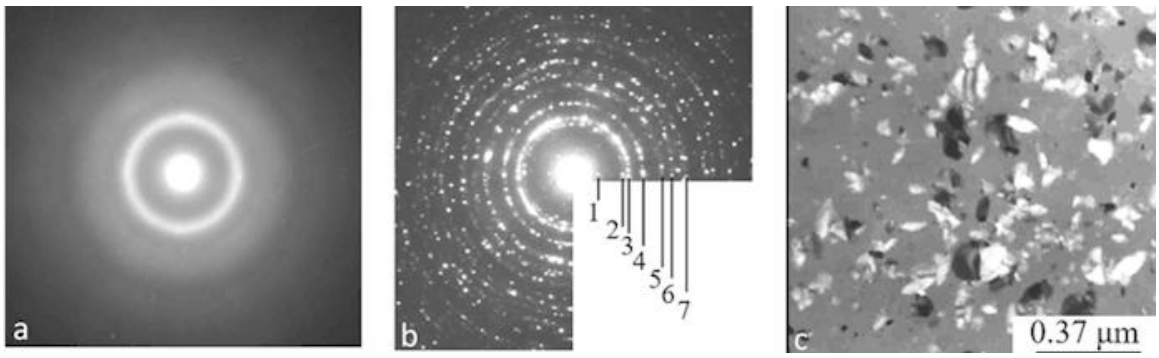

Fig. 1. Electron-beam crystallization of the amorphous Yb_2O_2S film: SAED pattern of the initial state (a) and after partial crystallization (b); TEM image of the film after partial crystallization (c)

In situ electron microscopy studies with the video recording method demonstrated, that phase transformation occurs in the island polymorphous crystallization mode with the relative length $\delta_0 \approx 1030$ [1]. In this case, the dependence of the fraction of the crystalline phase x on time t has an exponential character, described by the Johnson-Mail-Avrami-Kolmogorov formula.

The formation of a film occurs at the constant crystal growth rate and at the constant intensity of nucleation of crystallization centers α, that corresponds to the α-version of the Kolmogorov's model (Fig. 2).

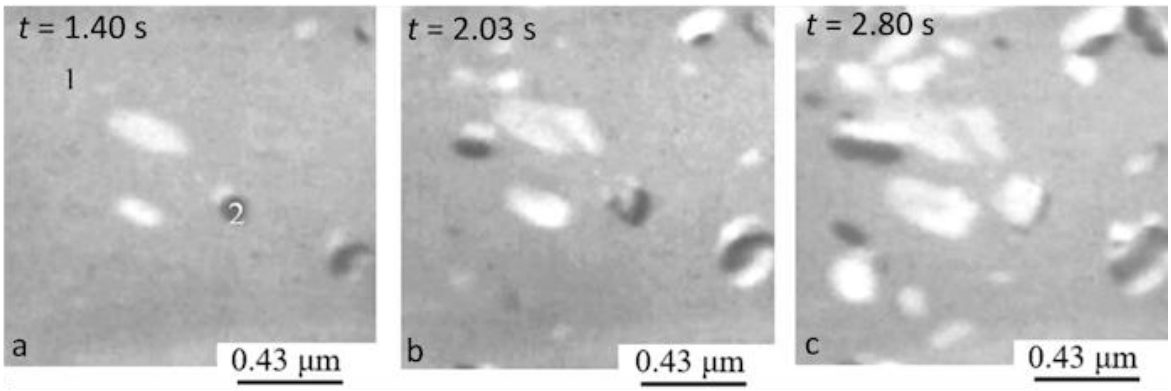

Fig. 2. Video footage of crystallization of amorphous Yb_2O_2S film

[1] A. Bagmut, Problems of Atomic Science and Technology. 137, 64 (2022). https://doi.org/10.46813/2022-137-064.

UVC up-conversion and vis-luminescence of $CaF_2:Pr^{3+}$ crystallites

O. Bezkrovna[1,2], R. Lisiecki[1], P.J. Dereń[1]

[1]Institute of Low Temperature and Structure Research, Polish Academy of Sciences, Okólna 2, Wrocław, 50-422, Poland
[2]Institute for Single Crystals, NAS of Ukraine, Nauky Ave. 60, Kharkiv, 61001, Ukraine
e-mail: o.bezkrovna@intibs.pl

Increasing attention is being paid to the development of self-disinfecting surfaces that could replace mercury lamps. The materials suitable for this purpose can be created using phosphors doped with active ions capable of converting visible light into ultraviolet (UV) radiation through up-conversion (UPC) processes. In UPC processes, two or more low-energy photons combine to produce a single high-energy photon [1]. The resulting UV radiation, particularly in the UVC region (200–280 nm), can damage DNA and RNA in microorganisms and viruses, inhibiting their reproduction [2]. Various host matrices have been investigated for UPC phosphors. The use of CaF_2 is especially promising due to the low phonon energy of its crystalline phases (466 cm^{-1} [3]) which makes them ideal host matrices for the UPC emission.

Lanthanide ions are suitable dopants due to their rich energy level structures and long-lived excited states caused by shielding of the *4f*-electrons by the *5s*- and *5p*-shells [1]. Among them, Pr^{3+} ions can emit UV radiation under visible excitation.

In our work, $CaF_2:Pr^{3+}$ crystallites were synthesized by the precipitation method and annealed at high temperature. The structural and optical (luminescence and excitation spectra, luminescence lifetime, up-conversion emission at excitation by the 444-nm laser) properties of the samples were investigated accompanied by transmission electron microscopy (TEM).

The samples exhibited visible photoluminescence bands at 496 nm and 655 nm corresponding to the $^3P_0 \rightarrow {}^3H_4$ and $^3P_0 \rightarrow {}^3F_2$ transitions. Their positions remained stable with increasing temperature, although the intensities decreased significantly above 400 K [4].

The UPC emission from a visible excitation produced the UVC emission in the 230–320 nm range with a maximum at 265 nm. The quadratic dependence of emission intensity on excitation power indicates a two-photon UPC process. The optimal Pr^{3+} concentration was 0.2–0.3%, and the CaF_2:0.3%Pr^{3+} sample showed about three times higher integrated UPC intensity than that of Y_2SiO_5:1%Pr^{3+}. Lifetime measurements showed concentration quenching due to the cross-relaxation as the Pr^{3+} content increased.

These results indicate that $CaF_2:Pr^{3+}$ is a promising material for self-disinfecting surfaces that convert visible light into UV radiation via UPC processes.

[1] S. L. Cates, E. L. Cates, M. Cho, J.-H. Kim. Environ. Sci. Technol. 48, 2290, (2014). https://dx.doi.org/10.1021/es405229p
[2] M. Raeiszadeh, B. Adeli, ACS Photonics. 7, 2941, (2020). https://dx.doi.org/10.1021/acsphotonics.0c01245
[3] N. Pawlik, B. Szpikowska-Sroka, T. Goryczka, W. A. Pisarski, Phys. Status Solidi B. 257, 1900478 (2020). https://doi.org/10.1002/pssb.201900478
[4] O. Bezkrovna, R. Lisiecki, O. S. Bezkrovnyi, P.J. Dereń, J. Alloys Compd. 1047, 185075 (2025). https://doi.org/10.1016/j.jallcom.2025.185075.

Acknowledgements
This research was funded by the National Science Center, grant number 2021/41/B/ST5/03792, which is gratefully acknowledged, and by the Program supporting scientists from Ukraine (PAS and NASU).

Quantum tunneling and above-barrier reflection of high-energy positively charged particles in oriented crystals

M. V. Bondarenco[1,2]

[1]*NSC Kharkov Institute of Physics & Technology, 1 Academic St., Kharkiv, 61108, Ukraine*
[2]*V.N. Karazin Kharkov National University, 4 Svobody Sq., Kharkiv, 61077, Ukraine*
e-mail: bon@kipt.kharkov.ua

Channeling of fast charged particles in oriented crystals is usually amenable to classical treatment. Quantum effects, though, are known to exist for electrons with energies up to 100 MeV, manifesting themselves as a zone structure in the transverse energy spectrum. For positrons, the top of the potential barrier is narrower, so tunneling and above-barrier reflection is expected to occur at higher energies. In [1], such effects were studied for an idealized case of a sharp wedge potential, corresponding to a static atomic plane. The estimates indicated the significance of quantum effects for positrons or protons at 1 GeV energies. Thermal smearing of the continuous potential, however, makes the potential barrier intermediate between sharp wedge and smooth turnover, requiring a numerical study. In the present work, quantum transmission through such a barrier is calculated based on the generic representation [1] for probability of transmission through a symmetric potential $V(-x) = V(x)$

$$T(E_\perp) = \frac{1}{1 + J^{-2}\left[\frac{\partial}{\partial x}|\psi|^2\Big|_{x=+0}\right]^2},$$

where

$$J = \frac{1}{i}\left(\psi^* \frac{\partial}{\partial x}\psi - \psi \frac{\partial}{\partial x}\psi^*\right)$$

is real and proportional to the probability current, which for a real potential $V(x)$ is real and locally conserved: $\partial J/\partial x = 0$.

The continuous potential is approximated by a thermally smeared linear wedge, involving a single spatial scale parameter [2]. Granted that away from the smearing region the potential is regarded as linear, the transmitted wave function assumes an Airy form. Adopting it as an initial value, we solve the Schrodinger equation for a definite energy as an initial-value problem. The results for the transmission probability depending on the transverse energy and the smearing parameter indicate that for room temperature, quantum effects for 1 GeV positrons or protons can be noticeable, although the course of the transverse energy dependence of the transmission probability differs significantly from that for a static plane.

[1] M. V. Bondarenco, Semiclassical transmission through a curved wedge potential barrier. J. Phys. A: Math. Theor. 58, 415305 (2025) https://doi.org/10.1088/1751-8121/ae0202.
[2] M. V. Bondarenco and N. S. Moskvitin, Truncated Coulomb potential for planar channeling. Phys. Rev. B 110, 205205 (2024) https://doi.org/10.1103/PhysRevB.110.205205.

DFT investigation of native and carbon defects in oxides grown under a CO atmosphere: a case study of YAG

K. V. Hermash[1], D. V. Fil[1,2]

[1]Institute for Single Crystals of the NAS of Ukraine, 60 Nauky Ave., Kharkiv, 61072, Ukraine
[2]V. N. Karazin Kharkiv National University, 4 Svobody Sq., Kharkiv, 61022, Ukraine
e-mail: kostiantyn.hermash@gmail.com

Carbon is a common unintentional impurity in yttrium aluminium garnet (YAG), readily introduced during crystal growth from graphite heating elements or CO-containing atmospheres. It strongly affects the luminescence, scintillation, and charge-compensation behavior of YAG. Previous *ab initio* studies [1, 2] have provided qualitative insight but were limited to zero temperature, leading to thermodynamic inconsistencies and preventing quantitative predictions of defect concentrations.

Here, we present a thermodynamically consistent analysis of carbon incorporation and defect equilibria in YAG using density functional theory (DFT) implemented in the SIESTA code [3], combined with thermochemical data. Building on our previously developed methodology for Ti-doped Al_2O_3 [4, 5], we determine the dominant carbon-related defect species in YAG. The formation energies of carbon-related defects are evaluated at the melting temperature of YAG, and their equilibrium concentrations are determined as functions of the partial pressures of CO, CO_2, and O_2 in the growth atmosphere.

We find that under reducing conditions, carbon preferentially forms negatively charged C_O defects, whereas positively charged C_{Al} defects dominate under oxidizing conditions. Only a small fraction of carbon-related defects (approximately 1%) participates in the formation of defect complexes. Carbon solubility in YAG is predicted to exhibit a pronounced minimum under moderately reducing conditions and to reach a maximum under either strongly reducing or oxidizing atmospheres. Carbon-related defects in YAG grown under strongly reducing conditions significantly enhance the concentration of charged oxygen vacancies, increasing their concentration by several orders of magnitude.

The results presented in this talk are largely based on our recently published paper [6].

[1] J. Zhu, O. Sidletskiy, Y. Boyaryntseva, and B. Grynyov, Structure and role of carbon-related defects in yttrium aluminum garnet, Opt. Mater. 111, 110561 (2021). http://dx.doi.org/10.1016/j.optmat.2020.110561.
[2] L. Jia, J. Zhu, Y. Boyaryntseva, I. Gerasymov, B. Grynyov, and O. Sidletskiy, Effect of carbon doping on F-type defects in YAG and YAG:Ce crystals, Phys. Status Solidi B 258, 2100325 (2021). http://dx.doi.org/10.1002/pssb.202100325.
[3] J. M. Soler, E. Artacho, J. D. Gale, A. García, J. Junquera, P. Ordejón, and D. Sánchez-Portal, The SIESTA method for ab initio order-N materials simulation, J. Phys.: Condens. Matter 14, 2745 (2002). http://dx.doi.org/10.1088/0953-8984/14/11/302.
[4] L. Yu. Kravchenko and D. V. Fil, Defect complexes in Ti-doped sapphire: A first principles study, J. Appl. Phys. 123, 023104 (2018). http://dx.doi.org/10.1063/1.5002532.
[5] L. Yu. Kravchenko and D. V. Fil, Control of charge state of dopants in insulating crystals: Case study of Ti-doped sapphire, Phys. Rev. Research 2, 023135 (2020). http://dx.doi.org/10.1103/PhysRevResearch.2.023135.
[6] K. V. Hermash and D. V. Fil, DFT study of carbon-related defects in yttrium aluminum garnet in a CO-containing atmosphere, J. Appl. Phys. 139, 125104 (2026). https://doi.org/10.1063/5.0310889.

Crystal growth and properties of co-doped (Cr, Co, Fe):ZnSe

O. K. Kapustnyk, S. V. Naydenov, O. K. Kosteniukova, D. S. Sofronov, and I. M. Pritula

Institute for Single Crystals of NAS of Ukraine, 60 Nauky Ave., Kharkiv, 61072, Ukraine
e-mail: mrlex.nauka@gmail.com, sergei.naydenov@gmail.com

ZnSe-based crystals are among the most in-demand II–VI semiconductor materials. Undoped ZnSe crystals have long been used as optical elements for infrared optics. Tellurium-activated ZnSe:Te scintillation crystals are highly efficient for detecting X-rays or low-energy gamma rays. Chromium-doped Cr^2:ZnSe crystals dominate in the market of infrared laser materials for 2-3 μm emission range [1]. Due to the scientific, industrial, and military applications, extending the laser emission range of ZnSe-based materials to 4-5 μm is an important task. Divalent iron ions in Fe^2:ZnSe crystals emit in this spectral region. However, these crystals require pumping in the range above 3 μm. At the same time, laser media that can be pumped in the 1.5-2 μm range – where numerous compact diode and fiber laser sources are available – are in high demand. The development of advanced laser materials may therefore require the incorporation of multiple active ions, enabling energy transfer between them within a single crystal. Promising candidates for such materials include double- (Cr, Fe):ZnSe and triple-doped (Cr, Co, Fe):ZnSe single crystals.

Experimental results of crystal growth of ZnSe crystals (Ø50x90 mm), doped with chromium, cobalt and iron ions for laser applications in the range 2-5 μm, grown by the vertical Bridgman method under high argon pressure are reported. Triple-doped crystals were grown for the first time in the Institute for Single Crystals [2]. A study involving crystallography and microscopy methods, FTIR-transmission spectroscopy, microhardness testing and other techniques was carried out for the grown crystals. The growth features, morphology, optical and mechanical properties of the crystals were investigated. The feasibility of producing homogeneous crystals with a controlled distribution of multiple activators throughout the crystal volume was demonstrated. A comparative study of the optical and mechanical properties of these crystals revealed that co-doping may some reduce optical transparency in the range 4-5 μm and microhardness (Figure). This effect may be associated with an increased density of growth as well as with structural defects induced by co-doping and indicates the need for further optimization of melt-based growth techniques to obtain higher-quality crystals.

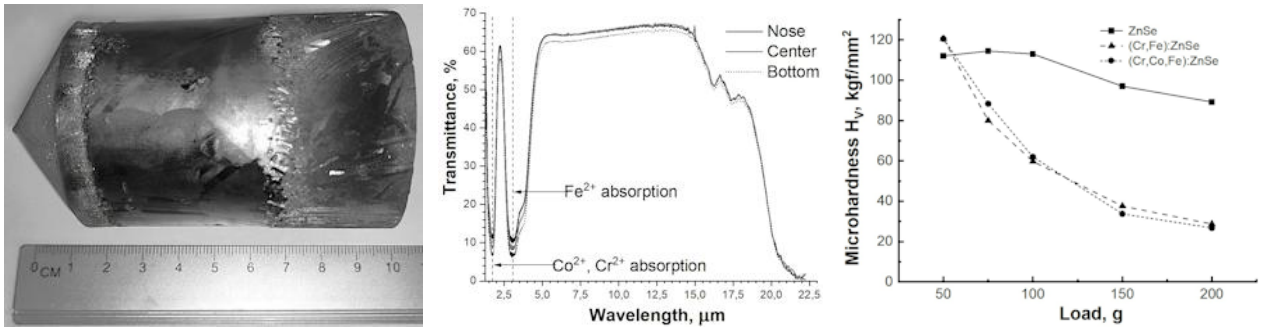

Figure. As-grown crystal (Cr_{150}, Co_{75}, Fe_{125}):ZnSe (a); IR-spectra and absorption maxima (b) for samples from different parts of the ingot; the Vickers microhardness (c).

Acknowledgements. This work was supported by the National Research Foundation of Ukraine (NRFU), grant number 2025.06/0006.

[1] S. B. Mirov, I. S. Moskalev, S. Vasilyev et al., Frontiers of Mid-IR Lasers Based on Transition Metal Doped Chalcogenides, IEEE J. of Selected Topics in Quantum Electronics 24, 1-29 (2018). https://doi.org/10.1109/JSTQE.2018.2808284.
[2] S. Naydenov, O. Kapustnyk, I. Pritula, D. Sofronov, Acta Crystallographica B, B52 (2026). https://doi.org/10.1107/S2052520626000673.

Low-temperature ultrasonic studies of $CoCrFeMnNiV_{0.85}$ high-entropy alloy in different structural states

V. S. Klochko, A. V. Korniiets, V. I. Sokolenko, I. V. Kolodiy, O. O. Kondratov, I. F. Kislyak, Yu. S. Lypovska, T. M. Tykhonovska

National Science Center "Kharkiv Institute of Physics and Technology" of the NAS of Ukraine, 1 Academichna St., UA-61108 Kharkiv, Ukraine
e-mail: korniets@kipt.kharkov.ua

We present the results of structural and ultrasound studies of the $CoCrFeMnNiV_{0.85}$ high-entropy alloy in the as-cast (state I) structural state and after annealing at 1050°C temperature (state II). The equiatomic single-phase fcc CoCrFeMnNi alloy (Cantor alloy) was also investigated for comparison.

Both the CoCrFeMnNi and $CoCrFeMnNiV_{0.85}$ alloys were obtained by re-melting the components (purity ~99.9%) on a copper water-cooled hearth in an arc furnace in a purified argon environment, using a tungsten electrode. XRD analysis revealed that the $CoCrFeMnNiV_{0.85}$ alloy exhibited a heterogeneous structure, consisting of an fcc matrix and a tetragonal (σ) phase, with the latter accounting for approximately 73 wt.% and 83 wt.% in structural states I and II, respectively. The texture with the predominant crystallographic orientation [200] of the fcc grains along the crystallization axis of the ingot were revealed in both structural states of the CoCrFeMnNi and in the state II of the $CoCrFeMnNiV_{0.85}$ alloy. The predominant crystallographic orientation [220] of the fcc grains along the crystallization axis of the ingot was revealed in the state I of the $CoCrFeMnNiV_{0.85}$ alloy.

ltrasonic studies in the range of 77-300 K were performed using a pulsed phase-sensitive method. Excitation and detection of ultrasonic oscillations were carried out using the broadband (±2 MHz) lithium niobate piezotransducers with a natural resonant frequency of 50 MHz.

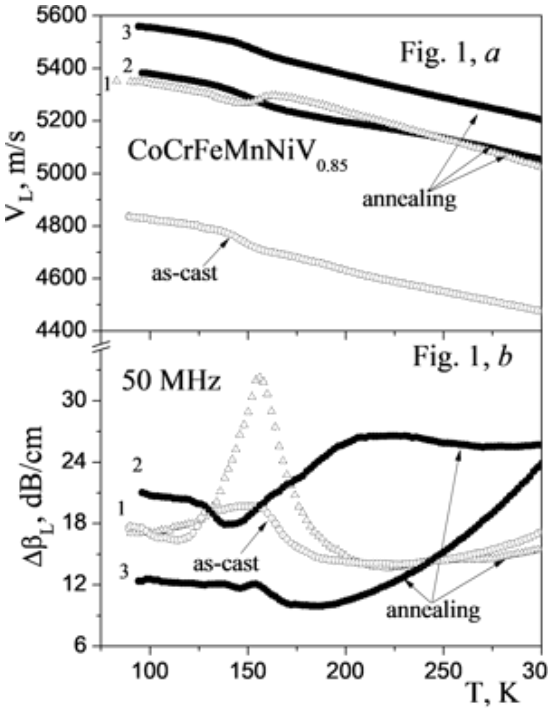

Fig. 1, *a* shows the temperature dependences of the velocity of longitudinal ultrasound of the $CoCrFeMnNiV_{0.85}$ alloy in the as-cast and in the annealed states (1, 2 and 3 – numbers of cooling-heating cycles). The revealed difference (~11%) in the magnitude of the sound velocity of the alloy for different structural states is due to both the increase in the σ-phase content and change in the texture. Fig. 1, *b* shows the temperature spectrum of acoustic absorption. Anomalies in $\Delta\beta_L(T)$ near 150 K were found for both structural states of the alloy. The determined value of the activation energy of the detected process corresponds to the dislocation relaxation resonance of the Bordony type, which occurs in fcc metals. During subsequent measurements, both the $V_L(T)$ and $\Delta\beta_L(T)$ anomalies near 150 K changed noticeably due to microstructural changes caused by thermal micro-stresses that arise in the alloy as a result of a noticeable difference in the thermal expansion of the phases. This behaviour of acoustic characteristics occurred only in the annealed sample (state II). The results of studies of the $CoCrFeMnNiV_{0.85}$ alloy were compared with data for the Cantor alloy in structural states I and II.

The research presented in this work was financially supported by the Simons Foundation International Program: PD-Ukraine: President Directed Ukraine Support Grants, Record ID: SFI-PD-Ukraine-00014584.

Effect of iodine pentoxide evaporation on the synthesis and superconducting properties of Tl-1223

I. R. Metskhvarishvili[1,2], M. Menelaou[3], D. L. Surmanidze[1,4], T. E. Lobzhanidze[4], A. D. Tchankvetadze[1,4], B. G. Bendeliani[1], G. N. Dgebuadze[1], V. M. Gabunia[1,5], M. R. Metskhvarishvili[6]

[1]Laboratory of Cryogenic Technique and Technologies, Ilia Vekua Sukhumi Institute of Physics and Technology, Mindeli St. 7, 0186, Tbilisi, Georgia
[2]Department of Microprocessor and Measurement Systems, Faculty of Informatics and Control Systems, Georgian Technical University, Kostava St. 77, 0175 Tbilisi, Georgia
[3]Department of Mechanical Engineering and Materials Science and Engineering, Cyprus University of Technology, Limassol 3036, Cyprus
[4]Department of Chemistry, Faculty of Exact and Natural Sciences, Ivane Javakhishvili Tbilisi State University, Chavchavadze Ave. 3, 0179 Tbilisi, Georgia
[5]Petre Melikishvili Institute of Physical and Organic Chemistry of the Ivane Javakhishvili Tbilisi State University, Jikia str 5, 0186, Tbilisi, Georgia
[6]"Talga" Institute of Georgian Technical University, Zurab Anjaparidze 5, 0186 Tbilisi, Georgia
e-mail: i.metskhvarishvili@gtu.ge

The influence of iodine pentoxide (I_2O_5) pressure on $TlBa_2Ca_2Cu_3O_{8+\delta}$ superconducting samples in a sealed quartz tube was studied. The samples were synthesized using a two-step preparation method. In the first stage, Tl-free precursor materials were obtained through an in situ polymerization process. During the second stage, Tl_2O_3 was introduced and the final synthesis was performed under two different conditions: 1) under vacuum and, 2) in the presence of iodine pentoxide with concentrations of 3.0, 6.0, and 9.0 wt.%.

The obtained results indicate that pressure generated by iodine pentoxide inside the sealed quartz tube favors the formation of the pure Tl-1223 superconducting phase. The sample without iodine pentoxide (0.0 wt.%) exhibited a diamagnetic onset critical temperature T_c of 114 K. With the addition of 3.0 wt.% I_2O_5, T_c increased to 115.8 K, while the sample containing 6.0 wt.% showed the highest T_c value of 119 K. Complete diamagnetism occurred at approximately T_c = 81 K, 87 K, and 95 K for the samples containing 0.0, 3.0, and 6.0wt.% I_2O_5, respectively. However, the further increase in iodine pentoxide to 9.0 wt% resulted in a decrease in the critical temperature to about T_c = 110 K, and full diamagnetism was not observed at liquid nitrogen temperature.

X-ray diffraction analysis showed that the sample containing 6.0wt.% I_2O_5 was nearly a single phase Tl-1223 compound with a tetragonal crystal structure and exhibited the highest critical current density, J_c = 176 A/cm^2. The results suggest that the incorporation of iodine pentoxide significantly enhances the superconducting properties of the materials.

Acknowledgments
This work was supported by the Shota Rustaveli National Science Foundation of Georgia (SRNSFG) [FR-24-11856, Thin-film technology for the creation of Tl-based HTS for practical application].

Intrinsic and radiation defects in ZrO_2 powders

V. V. Nosenko, I. P. Vorona, T. L. Petrenko, L. Yu. Khomenkova

V. Lashkaryov Institute of Semiconductor Physics, National Academy of Sciences of Ukraine,
45 Pr. Nauky, Kyiv, 03028, Ukraine
e-mail: vvnosenko@ukr.net

The study of radiation-induced defects in zirconium dioxide ZrO_2 remains a highly relevant task due to the material's widespread application in extreme environments. ZrO_2 is a key component in nuclear fuel cladding, thermal barrier coatings, and solid oxide fuel cells (SOFCs), where its structural stability under high-energy irradiation is critical for safety and efficiency. Despite decades of research, the precise nature of paramagnetic centers (PCs) and the dynamics of their formation in different polymorphs have remained subjects of debate. Our research addresses these gaps by bridging Experiment and Theory**.**

We provide a comparative study of initial ZrO_2 powders annealed at different temperatures as well as electron irradiated ones. The experiment was performed by means of EPR and Raman techniques. Raman spectroscopy revealed simultaneous presence of monoclinic and tetragonal phases in ZrO_2 powders. The *m*-ZrO_2 phase is the dominant one, while the contribution of *t*-ZrO_2 decreases as annealing temperature increases. EPR spectra of non-irradiated ZrO_2 powders are determined by two signals with parameters: 1) $g_\perp = 1.9755$ and $g_\parallel = 1.9635$ and, 2) $g_\perp = 1.9755$ and $g_\parallel = 1.9590$. They were attributed to bulk Zr^{3+} ions in monoclinic and in tetragonal ZrO_2, correspondingly. The growth of the annealing temperature leads to a relative increase of Zr^{3+} in the *m*-ZrO_2 in accordance with change in powder phase composition. However, concentration of Zr^{3+} PCs in *t*-ZrO_2 remains higher than that in *m*-ZrO_2. This leads to the observation of Zr^{3+} (*t*-ZrO_2) in EPR spectra of a powder annealed at 1000ºC, while Raman peaks related to the tetragonal phase decrease significantly.

Electron irradiation of ZrO_2 powders causes a decrease in the amount of Zr^{3+} centers and leads to the formation of new defects. These are two singly-ionized oxygen vacancies V_O^+ in *m*-ZrO_2 ($g_\perp = 2.0029$, $g_\parallel = 2.0006$) and V_O^+ in *t*-ZrO_2 ($g_\perp = 2.004$, $g_\parallel = 2.002$), as well as a hole trapped at the oxygen atom: O^- ion in *m*-ZrO_2 ($g_x = 2.0125$, $g_y = 2.0113$, $g_z = 2.0046$). Additionally, O^- ions in *t*-ZrO_2 ($g_\perp = 2.0024$ and $g_\parallel = 2.0110$) are observed in e-irradiated Y-doped ZrO_2.

To elucidate the nature of defects induced by irradiation of ZrO_2 crystal, we performed density functional theory (DFT) calculations [1]. We employ PBE+U functional [2] together with relativistic small core pseudopotentials [3]. Our DFT+U calculations elucidate the polaron-mediated mechanisms behind transformations observed by EPR results. Notably, we identify the role of electron-hole polaron pairs and their interaction with Frenkel pairs, which explains the formation of paramagnetic centers observed in our experiments.

[1] T. D. Kuehne, M. Iannuzzi, M. Del Ben, V. V. Rybkin, P. Seewald, F. Stein, T. Laino, R. Z. Khaliullin, O. Schuett, F. Schiffmann, D. Golze, J. Wilhelm, S. Chulkov, , M. H. Bani-Hashemian, V. Weber, U. Borstnik, M. Taillefumier, A. S. Jakobovits, A. Lazzaro, H. Pabst, T. Mueller, R. Schade, M. Guidon, S. Andermatt, N. Holmberg, G. K. Schenter, A. Hehn, A. Bussy, F. Belleflamme, G. Tabacchi, A. Gloess, M. Lass, I. Bethune, C. J. Mundy, C. Plessl, M. Watkins, J. Vande Vondele, M. Krack, and J. Hutter, J. Chem. Phys. 152, 194103 (2020). https://doi.org/10.1063/5.0007045.
[2] J. P. Perdew, K. Burke, and M. Ernzerhof, Phys. Rev. Lett. 77, 3865 (1996). https://doi.org/10.1103/PhysRevLett.77.3865.
[3] M. Krack, Theor. Chem. Acc. 114, 145 (2005). https://doi.org/10.1007/s00214-005-0655-y.

DFT study of point defects in Y_2O_3 doped with fluorine

D. O. Puhachev[1] and D. V. Fil[1,2]

[1]Institute for Single Crystals of NAS of Ukraine, 60 Nauky Avenue, Kharkiv, 61072, Ukraine
[2]V. N. Karazin Kharkiv National University, 4 Svobody Square, Kharkiv, 61022, Ukraine
e-mail: pugachev.deni@gmail.com

Transparent sesquioxides have been widely studied as potential laser host materials because they combine good optical properties with excellent thermal stability. Among them, transparent Y_2O_3 ceramics are considered the most promising. The technology for synthesizing Y_2O_3-based ceramics involves the use of sintering additives. The most commonly used additive, ZrO_2, has demonstrated good experimental results [1] and has been the subject of recent theoretical study [2]. At the same time, additives containing fluorine have become increasingly promising. In several experimental studies (e.g., [3]), it has been shown that doping with fluorine could be an interesting way to improve the optical properties of sesquioxide laser ceramics.

In this talk, we present a density functional theory (DFT) study of the energetics of point defects in Y_2O_3:F. The calculations were performed with the SIESTA program [4]. Pseudopotentials were taken from the PseudoDojo database [5]. To construct the phase diagram of the Y–O–F system, the formation energies of pure compounds containing these elements were calculated. Next, a simple or complex defect was introduced into the unit cell of the Y_2O_3 crystal. Structural optimization was performed with respect to atomic positions and lattice vectors. The formation energies of point defects, binding energies of defect complexes, and structural characteristics of the resulting systems were obtained.

It was found that F ions substitute for oxygen atoms and form positively charged $F_O^{\bullet}$ defects, which are compensated by negatively charged interstitial defects O_i''. A significant fraction of such defects bind into pairs. The formation energies of these defects are relatively small, and therefore, the solubility of fluorine is expected to be rather high. The obtained results indicate that the incorporation of fluorine may significantly influence the defect chemistry of Y_2O_3 and reduce the solubility of other impurities whose defects carry a positive charge.

[1] D. Chernomorets, P. Galizia, G. Zanetti, S. Varas, A. Chiasera, A. Piancastelli, R. Yavetskiy, J. Hostasa, IR-transparent Y_2O_3 ceramics: Effect of zirconia concentration on optical and mechanical properties, Open Ceramics 20, 100666 (2024). https://doi.org/10.1016/j.oceram.2024.100666
[2] D. Pugachev, D. Fil, DFT Study of Point Defects in Y_2O_3 Doped with Zirconium, Materials Science Forum 1178, 79–84 (2026). https://doi.org/10.4028/p-V37AXc
[3] F. Delaunay et al, Effect of fluorine addition on the microstructure and emission properties of Ho: Y_2O_3 transparent ceramics, Optical Materials 168, 117523 (2025). https://doi.org/10.1016/j.optmat.2025.117523
[4] J. M. Soler, E. Artacho, J. D. Gale, A. Garcia, J. Junquera, P. Ordejon, and D. Sanchez-Portal, The SIESTA method for ab initio order-N materials simulation, J. Phys.: Condens. Matter 14, 2745 (2002). http://dx.doi.org/doi.org/10.1088/0953-8984/14/11/302
[5] M. J. van Setten, M. Giantomassi, E. Bousquet, M. J. Verstraete, D. R. Hamann, X. Gonze, and G.-M. Rignanese, The PseudoDojo: Training and grading a 85 element optimized norm-conserving pseudopotential table, Comput. Phys. Commun. 226, 39-54 (2018). http://dx.doi.org/doi.org/10.1016/j.cpc.2018.01.012.

Thermal behaviour and evaluation of individual kinetic analysis approaches in the Al_2O_3-Yb_2O_3-Er_2O_3 glass systems

L. Šedivá[1,2], K. Faturíková[3], B. Pecušová[3], P. Švančárek[2], J. Valúchová[2], A. Prnová[2], D. Galusek[2,3]

[1]Faculty of Chemical and Food Technology STU, Radlinského 9, 812 37 Bratislava. Slovakia
[2]Joint Glass Centre of the IIC SAS, TnUAD, and FCHPT STU, Študentská 2, 911 50 Trenčín. Slovakia.
[3]Centre for Functional and Surface Functionalized Glass, Alexander Dubček University of Trenčín, Študentská 2, 911 50 Trenčín. Slovakia
e-mail: lucia.sediva@tnuni.sk

Glasses constitute a versatile class of materials capable of incorporating relatively high concentrations of dopant species within their topologically disordered network structures. The amorphous and crystalline phases in the Al_2O_3–RE_2O_3 system exhibit functional and technological properties that surpass those of commercial materials currently employed for optical and mechanical applications – such as phosphors, solid-state lasers, scintillators, and damage-tolerant glasses. However, their wider technological deployment is limited by the complexity of their synthesis, which typically requires capital- and energy-intensive equipment, as well as by the high cost of raw materials and restricted production throughput.

A detailed investigation of the processes taking place during synthesis, together with their kinetics, is essential for identifying suitable compositions and processing conditions for the fabrication of glass, glass-ceramic, or ceramic materials with tailored microstructures. The present work focuses on the thermal behaviour of glasses with the nominal composition 62.5 mol.% Al_2O_3 – (37.5 – x) mol.% Yb_2O_3 – x mol.% Er_2O_3, where x = 0.25, 0.5, 0.75, 1, 3, and 5. The samples were prepared via a cost-effective route combining Pechini-type sol–gel synthesis from nitrates with flame processing. The resulting glass microspheres were initially characterized using scanning electron microscopy (SEM) and X-ray diffraction (XRD), and subsequently subjected to a detailed study of their thermal behavior using non-isothermal thermal analysis (differential scanning calorimetry, DSC; thermogravimetry, TG), isothermal crystallization experiments, and high-temperature X-ray diffraction (HT-XRD). The investigations demonstrated that the dominant transformation process was the crystallization of a garnet-type phase. The first thermally activated event was the glass transition, observed at approximately 860 °C, followed by a crystallization peak detected by DSC at around 915 °C. In contrast, HT-XRD revealed the onset of crystalline phase formation already a few degrees above the glass transition temperature T_g, at roughly 880 °C, followed by an almost linear increase in the content of crystalline fraction up to about 920 °C. Kinetic analysis of the crystallization process showed that commonly applied kinetic methodologies – both model-free (isoconversional approaches such as the Kissinger, Ozawa–Flynn–Wall, and Friedman methods) and model-based (nucleation–growth models) – provided useful, albeit not fully quantitatively accurate, insights into crystallization behavior, including estimates of kinetic parameters (activation energy, pre-exponential factor) and qualitative information on the mechanism.

For a more rigorous kinetic description, it is necessary to treat nucleation and growth as distinct, sequential processes. In this context, the induction-period method emerges as a particularly suitable tool, yielding kinetic parameters that can be directly employed in the design and optimisation of glass, glass-ceramic, and ceramic materials, especially for defining optimal processing temperatures and holding times.

Acknowledgement
Funded by the EU NextGenerationEU through the Recovery and Resilience Plan for Slovakia under the project No. 09I05-03-V02-00065.

Implementation of a methodology for crystal structure prediction using genetic algorithms integrated into the Python ASE library

B. Y. Semeniuk, O. D. Feia

Kyiv Academic University, 36 Academician Vernadsky Blvd., Kyiv, 03142, Ukraine
e-mail: semenuk.b.20@gmail.com

Crystal structure prediction is a fundamental task in modern materials science, as it enables the identification of stable and metastable phases of materials and the prediction of their physicochemical properties. In this work, we present a computational methodology for crystal structure prediction, implemented using genetic algorithms within the Atomic Simulation Environment (ASE) framework [1] and the neural network interatomic potential MACE [2]. The combination of ASE's flexibility with the DFT-level accuracy of MACE allows an efficient exploration of the energy landscape of crystalline systems while significantly reducing computational costs.

The framework integrates MACE as a high-performance relaxer during the evolutionary search. Its architecture, based on the Atomic Cluster Expansion formalism and message passing mechanisms, accurately reproduces energies, forces, and stresses from Density Functional Theory (DFT) calculations [3]. The integration of this potential substantially accelerates structure optimization and expands the capability for scalable exploration of new crystalline phases across the configuration space.

[1] A. H. Larsen, J. J. Mortensen, J. Blomqvist, et al., J. Phys.: Condens. Matter 29, 273002 (2017). https://doi.org/10.1088/1361-648x/aa680e.
[2] Y. Lysogorskiy, C. van der Oord, A. Bochkarev, et al. npj Comput Mater 7, 97 (2021). https://doi.org/10.1038/s41524-021-00559-9.
[3] R. Drautz, Phys. Rev. B 99, 014104 (2019). https://doi.org/10.1103/PhysRevB.99.014104.

Formation and characterization of TBCCO superconductor coated lanthanum aluminate films via organometalic routes

A. D. Tchankvetadze[1,2], T. E. Lobzhanidze[2], M. Menelaou[3], I. R. Metskhvarishvili[1,4], D. L. Surmanidze[2], V. M. Gabunia[1,5], G. N. Dgebuadze[1], B. G. Bendeliani[1]

[1]Laboratory of Cryogenic Technique and Technologies,
Ilia Vekua Sukhumi Institute of Physics and Technology, Mindeli St. 7, 0186, Tbilisi, Georgia
[2]Department of Chemistry, Faculty of Exact and Natural Sciences,
Ivane Javakhishvili Tbilisi State University, Chavchavadze Ave. 3, 0179 Tbilisi, Georgia
[3]Department of Mechanical Engineering and Materials Science and Engineering,
Cyprus University of Technology Limassol 3036, Cyprus
[4]Department of Microprocessor and Measurement Systems, Faculty of Informatics and Control Systems, Georgian Technical University, Kostava St. 77, 0175 Tbilisi, Georgia
[5]Petre Melikishvili Institute of Physical and Organic Chemistry of the Ivane Javakhishvili Tbilisi State University, Jikia str 5, 0186, Tbilisi, Georgia
e-mail: amiran.tchankvetadze027@ens.tsu.ge

The fabrication of Tl-based high temperature superconducting coated films was carried out through a four-step synthesis process.

In the first stage, organometallic 2-ethylhexanoate salts of barium, calcium and copper were synthesized through a chemical process.

In the second stage, the obtained organometallic solutions were homogenized and stabilized at the room temperature in order to prevent salt crystallization before deposition on lanthanum aluminate substrate. The homogeneous metal-organic solution was characterized by FTIR spectroscopy. The results showed that the acidic hydrogen proton was no longer observed in the solution.

In the third stage, homogenous solution was deposited onto a single-side polished $LaAlO_3$ substrate and subsequently dried under thermal treatment conditions. The phase analysis of the deposited film was carried out using XRD analysis. The precursor consists of only two phases $BaCuO_2$ and Ca_2CuO_3 phases.

In the final, fourth stage, the precursor-coated film underwent thalliation in a closed quartz tube under oxygen pressure.

The elemental composition of the samples obtained by thalliation was characterized using XRD and SEM. The superconducting properties were investigated using linear and nonlinear magnetic susceptibility. The results showed a high critical temperature and a suitable value of critical current density.

Acknowledgements
This work was supported by the Shota Rustaveli National Science Foundation of Georgia (SRNSFG) [MR-25-330].

Effect of pressure on electrical resistivity of tin films

S. L. Udachan[1], S. B. Kolavekar[1], N. H. Ayachit[1], L. A. Udachan[2], S. S. Kolkundi[3], S. Ramya[4], S. Veeresh[4]

[1]Department of Physics, School of Advanced Sciences, KLE Technological University, Hubballi, 580031, India
[2]S. S. Tegnoor Degree College, Kalaburagi, 585105, India
[3]Government First Grade College, Shahapur, Yadgir, 585223, India
[4]Shree Sangam Vidya Mandir, Kalaburagi, 585104, India
e-mail: shivaudachan8@gmail.com

Deposition pressure is a critical parameter in thin-film growth, particularly in techniques like thermal evaporation in vacuum, where it plays a decisive role in governing the kinetic energy, mean free path, and directionality of evaporated atoms. By directly influencing collision frequency, pressure dictates the purity, microstructure, and defect concentration of the deposited film. It is observed from our experimental results that the resistivity in the thick-film (bulk) limit increases with increasing pressure [1], because of the incorporation of defects during the film growth. Based on the size effect, Fuchs obtained an expression for electrical resistivity, ρ, also known as Fuchs-Sondheimer (F-S) equation:

$$\rho = \rho_0 \left(1 + \frac{3}{8} \cdot \frac{1-p}{\lambda} \right).$$

Here, ρ_0 is the resistivity of infinitely thick film, l is the electron mean free path, p is the scaling parameter, $\lambda = t/l > 0.1$ is a ratio of the film thickness, t, to the electron mean free path, l, therefore λ is a dimensionless quantity. The F-S model is valid for the thick film region only, $t > t_c$, where t is a thickness, while t_c is the critical thickness. The first term of equation represents the background/bulk resistivity, and the second term indicates resistivity due to size effect.

Tin thin films were deposited using 99.99% pure tin that was acquired from Vin Karola Instruments, USA. In this investigation, thin films of tin were grown using "Hind High Vacuum Coating Unit (Model 12A4D). Using an integrated Quartz Crystal Digital Thickness Monitor (Model DTM-101), film thickness [2] has been controlled or measured. At normal temperature (23°C), 99.99% pure tin has been dispersed from a molybdenum boat at a rate of 0.5nm/s under a vacuum of $2x10^{-6}$ and $2x10^{-5}$ Torr onto cleaned glass substrate surfaces. About 0.20 meters separated the substrates from the evaporation source. The sample resistance was measured by the standard four probe technique, in-situ. Ultimately, this leads to a large resistivity for tin films grown at higher pressures and results in lower mean free path of electrons. It is also seen from observations that scaling parameter value, p, decreases with increasing pressure, which indicates a diffuse scattering of conduction electrons in thin tin films. By controlling the deposition parameters, one could get desired film for specific applications.

[1] S. Wu, H. Chen, X. Du, & Z. Liu, Effect of deposition power and pressure on rate deposition and resistivity of titanium thin films grown by DC magnetron sputtering. Spectroscopy Letters 49, 514–519 (2016). https://doi.org/10.1080/00387010.2016.1212244.
[2] L. U. Shiva, N. H. Ayachit, L. A. Udachan, S. M. Sunagar, Thickness dependence of microstructure in thin chromium films, nternational Journal of Research in Engineering and Technology 6, 75-80 (2017). https://ijret.org/volumes/2017v06/i13/IJRET20170613016.pdf.

Methodological aspects of temperature-programmable desorption in studies of CO_2, CO, and CH_4 storage at cryogenic temperatures

N. N. Chigambayeva, A. Y. Nurmukan

Al-Farabi Kazakh National University, al-Farabi ave., 71, Almaty, 050040, Kazakhstan
e-mail: nurgul050490@gmail.com

The increasing concentration of greenhouse gases CO_2, CO, and CH_4 in the atmosphere requires the development of effective methods for their capture and storage. One of the promising directions is the application of cryogenic technologies, which are based on the condensation of gases at low temperatures and the formation of cryocondensates or thin films [1, 2].

To study the processes of gas retention and release in such systems, the Temperature-Programmed Desorption (TPD) method is widely used. The essence of the method lies in the gradual heating of the sample according to a predefined temperature program while simultaneously recording the flux of desorbing molecules. The analysis of desorption temperature maxima makes it possible to determine the interaction energy of molecules with the surface and the mechanisms of gas retention in the cryogenic matrix [1].

Experiments on the study of CO_2, CO, and CH_4 cryocondensates are usually carried out in cryovacuum systems at temperatures of 10–300 K and pressures on the order of 1×10^{-10} Torr. Under such conditions, amorphous or crystalline ice structures are formed, which can retain gas molecules and influence the processes of their subsequent desorption. Mass spectrometry and infrared spectroscopy are used to detect the released molecules, which makes it possible to study both the desorption kinetics and the structural changes of the cryocondensate [3].

An important methodological aspect of applying the TPD method is ensuring the accuracy and reproducibility of the experiment. This requires strict control of the heating rate, substrate temperature, pressure in the vacuum system, and the composition of the gas mixture. In this context, the principles of standardization and certification of experimental methods play a significant role. The international standard ISO/IEC 17025 establishes requirements for the competence of testing and calibration laboratories, including the calibration of measuring equipment and ensuring the traceability of measurement results [4]. Standardization of experimental conditions and certification of measuring equipment make it possible to minimize measurement errors and ensure the comparability of results obtained in different studies.

Thus, the Temperature-Programmed Desorption method is an effective tool for studying the processes of storage and release of CO_2, CO, and CH_4 in cryogenic systems. The application of standardized experimental methodologies increases the reliability of the obtained data and contributes to the development of technologies for the capture and storage of greenhouse gases.

[1] P. A. Redhead, Vacuum 12, 203-211 (1962). https://doi.org/10.1016/0042-207X(62)90978-8.
[2] K. Isokoski, J.-B. Bossa, T. Triemstra, H. Linnartz, Phys. Chem. Chem. Phys. 16, 3456-3465 (2014). https://doi.org/10.1039/c3cp54481h.
[3] O. Golikov, D. Yerezhep, A. Akylbayeva, D. Yu. Sokolov, E. Korshikov, A. Nurmukan, A. Aldiyarov, Sci. Rep. 13, 21155 (2023). https://doi.org/10.1038/s41598-023-48541-3
[4] ISO/IEC 17025:2017, General requirements for the competence of testing and calibration laboratories. https://www.iso.org/standard/66912.html.

Structure evolution of the 75-μm thick Kapton H-type polyimide film under a long-term environmental exposure: an X-ray study

V. Geidarov, I. Braude, V. Lototskaya

B. Verkin Institute for Low Temperature Physics and Engineering of NAS of Ukraine,
47 Nauky Ave., Kharkiv, 61103, Ukraine
e-mail: geydarov@ilt.kharkov.ua

Kapton H-type polyimide films are the most radiation-resistant polymeric materials. They are used on the outer surfaces of spacecraft, the service life of which currently reaches 15 years in near-Earth orbits. During this time, the degradation of their physical and mechanical characteristics begins to occur [1], the nature of which is apparently associated with changes in the structure of films.

Therefore, the aim of the present work is to investigate the nature of structural changes in the initial and deformed 75-μm thick Kapton H-type films aged under normal conditions for several years, and to compare it with the structure of "fresh" films.

In the diffraction pattern of the initially "fresh" films, a broad diffuse halo is observed in the region of $2\theta = 5–25°$, containing a diffuse maximum with the peak apex in the region of $2\theta = 5.35°$ with an amplitude of 20844 cps and the second one in the region of $2\theta = 13.42°$ with an amplitude of 15330 cps [2]. Maxima at higher angles are absent. This indicates a predominantly amorphous film structure, possibly partially oriented during the film drawing process. After aging for several years, diffraction patterns of the initially undeformed films exhibit a decrease in the amplitude, peak intensity, and integrated area of the diffraction pattern, as well as a slight broadening of the peaks. This indicates further amorphization of the structure, disorientation of polymer molecules, and an increase in the free volume [3].

In the aged sample deformed to failure by uniaxial tension at room temperature, the preservation of the amplitude of diffuse maxima, the further broadening of the main diffuse maximum as well as the increase in the integrated area of the diffraction pattern are observed.

[1] V. A. Lototskaya, Particularity of relaxation of mechanical properties of the Kapton h type polyimide films at different strain rates after long-term exposure to environmental conditions, Low Temp. Phys. 52, 342–349 (2026). https://doi.org/10.1063/10.0042905.
[2] V. G. Geidarov, I. S. Braude, N. N. Gal'tsov, Yu. M. Pohribnaya, V. A. Lototskaya, and N. A. Aksenova / Structural Studies of Polyimide Films. Size Effect / Nano Studies 19, 11-14 (2019).
[3] B. Wernisch, M. Al Otmi, E. Beauvaisa and J. Sampath, Evolution of free volume elements in amorphous polymers undergoing uniaxial deformation: a molecular dynamics simulations study, Molecular Systems Design & Engineering 9, 214–225 (2024). https://doi.org/10.1039/D3ME00148B.

Effect of a long-term environmental exposure on the structure of the 125-μm thick Kapton H-type polyimide film: an X-ray study

V. Geidarov, I. Braude, V. Lototskaya

B. Verkin Institute for Low Temperature Physics and Engineering of NAS of Ukraine,
47 Nauky Ave., Kharkiv, 61103, Ukraine
e-mail: geydarov@ilt.kharkov.ua

Kapton H-type polyimide films are widely used in aerospace engineering, electronics, and other fields due to their high radiation resistance, thermal stability, chemical resistance, and good mechanical properties. The service life of films, established by manufacturers, is 20-25 years. It has been found that the film aging for about half of the aforementioned period leads to a change in mechanical properties under normal conditions [1].

Therefore, the aim of this work is to study the structure of the 125-μm thick Kapton H-type polyimide film after a similar long-term aging under normal conditions and a subsequent deformation by the uniaxial tension at room temperature in order to further compare these data with those obtained on "fresh" films.

The diffraction patterns of all (fresh and aged) investigated samples are characterized by the presence of a broad diffuse halo up to $2\theta \cong 25°$, having two maxima ($2\theta_1 = 6^o$, $2\theta_2 = 15^o$) with an approximately equal amplitude. In the "fresh" films, weak peaks at higher angles were also found in [2], which were especially well manifested after deformation. This is typical for the partially crystalline structure of a "fresh" film. After a long-term aging of the initial film, a broadening of the diffuse halo and a change in the amplitude, shape, and position of the second maximum occur in the diffraction pattern. At high angles, peaks are practically absent. These changes indicate a decrease in the degree of the structural ordering and an increase in the free volume. Such effects can be associated with the relaxation of internal stresses, an increase in the disorientation angle of polymer macromolecules relative to the drawing direction, a change in the position of hinge atoms of the monomer and, accordingly, an increase in the degree of coiling of the molecule. This is in a good agreement with the known data on the aging of polymers [3].

In the aged sample deformed to failure, weak reverse processes occur. The integrated intensity of peaks and the total integrated area of the diffraction pattern decrease slightly. A further broadening of peaks occurs.

It is shown that the partially crystalline structure in the 125-μm thick Kapton H-type polyimide film after a long-term aging is observed neither in the initial nor in the deformed state. The aging leads to a decrease in the degree of ordering (to an amorphous state) with a subsequent loosening of the structure. The deformation leads to a further increase in the free volume.

[1] V. A. Lototskaya, Particularity of relaxation of mechanical properties of the Kapton h type polyimide films at different strain rates after long-term exposure to environmental conditions, Low Temp. Phys. 52, 342–349 (2026). https://doi.org/10.1063/10.0042905.
[2] V. G. Geidarov, I. S. Braude, N. N. Gal'tsov, Yu. M. Pohribnaya, V. A. Lototskaya, and N. A. Aksenova / Structural Studies of Polyimide Films. Size Effect / Nano Studies 19, 11-14 (2019).
[3] M.-L. Cheng, Y.-M. Sun / Relationship between free volume properties and structure of poly(3-hydroxybutyrate-co-3-hydroxyvalerate) membranes via various crystallization conditions, Polymer 50, 5298-5307, (2009). https://doi.org/10.1016/j.polymer.2009.09.035.

Visualization of a photosensitive area of infrared photodiodes using two-dimension scanning method

O. G. Golenkov, A. V. Shevchik-Shekera, V. V. Zabudsky, I. O. Lysiuk, Z. F. Tsybrii, A. S. Stanislavskyi, M. V. Vuichyk, S. V. Korinets

V. E. Lashkaryov Institute of Semiconductor Physics, NAS of Ukraine,
41, Nauky Ave., Kyiv 03028, Ukraine
e-mail: golenkov@isp.kiev.ua

Accurate characterization of the spatial uniformity of photosensitivity is an important step in the development and optimization of infrared photodetectors. Non-uniformity of the photoresponse can significantly influence the performance of detectors in imaging systems, spectroscopy, and precision optical measurements. Therefore, investigation of the spatial distribution of sensitivity provides valuable information about material quality, device fabrication processes, and the presence of local defects affecting detector performance.

The non-uniformity of photosensitivity (Fig. 1) was investigated using an *InSb* infrared photodiode developed and fabricated at the V. Lashkaryov Institute of Semiconductor Physics of the NAS of Ukraine [1]. The photodiode has performance characteristics comparable with commercially available ones. Its topology dimensions are 230×40 μm^2.

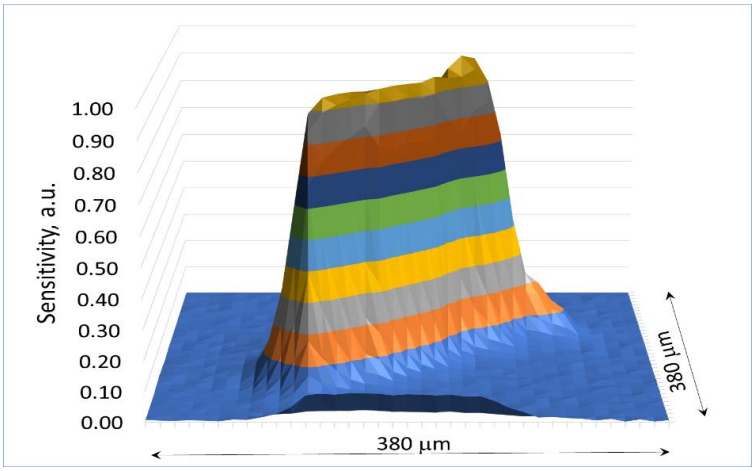

Fig. 1. 3D mapping of the *InSb* photodiode photosensitivity at liquid nitrogen temperature.

There is an increased (up to 5%) photosensitivity near the contact area (Fig. 1). This can be explained by a combination of reasons: both the increased width of the photodiode on the contact side and not sufficiently small size of the optical probe.

The surface distribution of photosensitivity was investigated with the assistance of an optical probe [2] at 4.3 μm radiation source wavelength. A spot diameter of a focused radiation was < 30 μm.

Visualization of photosensitivity allows determining the effective sensitive area of the detector, sensitivity uniformity, and crosstalk coefficient between neighboring detectors.

Results reported in the abstract were supported by the National Research Foundation of Ukraine, project No. 2025.06/0089.

[1] S. V. Sapon, M. S. Boltovets, O. A. Kulbachynskyi, V. V. Zabudsky, O. G. Golenkov, V. V. Korotyeyev, A. A. Efremov, Semiconductor physics, quantum electronics and optoelectronics 27, 356-365 (2024). https://doi.org/10.15407/spqeo27.03.
[2] O. G. Golenkov, A. V. Shevchik-Shekera, V. V. Zabudsky, I. O. Lysiuk, Z. F. Tsybrii, A. S. Stanislavskyi, S. V. Korinets, A. Yu. Shekera, Sensor Electronics and Microsystem Technologies 22, 30-39 (2025). https://semst.onu.edu.ua/article/view/343569/336882.

Dielectric properties of aged and modified by doping glassy selenium

A. A. Horvat, A. A. Molnar, V. V. Minkovych

Faculty of Physics, Uzhhorod National University,
A. Voloshin str., 54, 88000 Uzhhorod, Ukraine
e-mail: ahorvat@ukr.net

Semiconductor chalcogenide alloys, which are primarily consist of selenium (Se), have a variety of commercial and technological applications, including infrared optical and electronic devices, sensors, optical fibers and phase-change materials [1, 2]. However, the amorphous selenium is characterised by low thermal stability, which limits its applications. This report presents an analysis of the behaviour of pure selenium glasses that have been aged under normal laboratory conditions for several decades, as well as glasses doped with small concentrations of impurities such as As, Sb, In, Ga Ge, etc., which alter the crystallisation ability.

The bulky glass samples were prepared using the well-known melt-quenching technique. The ampoules containing the molten alloys were cooled in ice water. The samples were then ground into a fine powder for further analysis. Various methods were employed to study the glass transition, crystallisation kinetics, glass-forming ability and thermal stability of the alloys under non-isothermal conditions, including X-ray diffraction, differential scanning calorimetry, electrophysical and dielectric investigations.

Figure 1, for example, shows the temperature dependences of the complex dielectric constant $\varepsilon^*=\varepsilon'+i\varepsilon''$ components of selenium-based glasses at a frequency of 1 kHz. To present the results more clearly, the temperature dependences of ε' and ε'' are shown on a logarithmic scale.

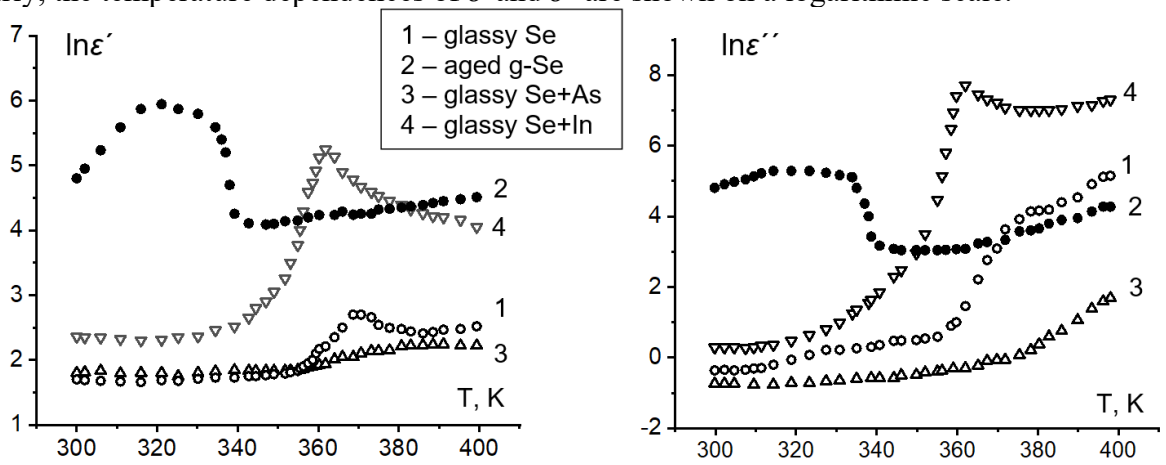

Fig. 1. Temperature dependencies of complex dielectric constants $\varepsilon^*=\varepsilon'+i\varepsilon''$ components in selenium-based glasses.

A significant difference in the behaviour of the dielectric constants was observed in the crystallisation region for aged glasses (curve 2), namely that the anomalies associated with crystallisation have a much sharper form and are observed at much lower temperatures (by about 35 K) in comparison with as-obtained samples (curve 1). Curves 3 and 4 show the behaviour of selenium glass doped with arsenic and indium, respectively. As can be seen, a small addition (up to 5 mol%) of indium leads to a lower crystallization temperature and a more pronounced anomaly of dielectric parameters, while arsenic impurities stabilise the glassy state.

[1] H. Kumar, A. Lal Saroj. Recent Advances in Chalcogenide Glasses and their Applications. In Book «Materials Science: A Field of Diverse Industrial Applications». 2023, p. 26-45. doi:10.2174/9789815051247123010004.
[2] J. D. Musgraves. Chalcogenide glasses: Engineering in the infrared spectrum, American Ceramic Society Bulletin 103, 22 – 28 (2024).

Chemical composition and alkali doping effects on structural and optoelectronic properties of $Cu(In_{1-x}Ga_x)(Se_{1-y}S_y)_2$ thin films for photovoltaic applications

M. Ibragimova[1], J. Abdullayev[2]

[1]Urgench State University, 14 Hamid Olimjon St., Urgench, 220100, Uzbekistan
[2]National Research University TIIAME, Department of Physics and Chemistry, 39 Kori Niyoziy St., Tashkent, 100000, Uzbekistan
e-mail: madinabonubahodir2024@gmail.com

$Cu(In_{1-x}Ga_x)(Se_{1-y}S_y)_2$ (CIGSSe) thin films are widely used as absorber layers in high-efficiency thin-film solar cells [1] due to their tunable band gap (1.0 –1.7 eV) and high absorption coefficient ($>10^5$ cm^{-1}). In this study, we investigate the combined influence of chemical composition, Ga/(In+Ga) ratio (x = 0 – 0.6), Se/S ratio (y = 0 – 0.3), and alkali metal (Na, K) doping on the structural, morphological, and optoelectronic properties of CIGSSe thin films.

Compositional control was achieved within ±2 at.% using energy-dispersive X-ray spectroscopy (EDX) and X-ray photoelectron spectroscopy (XPS). X-ray diffraction revealed single-phase chalcopyrite structure with a preferential (112) orientation. Lattice parameters decreased from 5.78 Å to 5.70 Å with higher Ga content, while the optical band gap increased from 1.12 eV (x = 0.2, y = 0) to 1.40 eV (x = 0.4, y = 0.2). Alkali doping enhanced grain growth, reduced secondary phases, and improved carrier concentration (10^{15} –10^{16} cm^{-3}) and resistivity (0.5–2.0 Ω·cm).

The results demonstrate that a precise control of chemical composition and alkali doping significantly influences phase purity, band gap tuning, and electronic quality of CIGSSe thin films. Optimal parameters (x ≈ 0.3, y ≈ 0.1, Cu/(In+Ga) ≈ 0.9, Na/K incorporation) provide enhanced structural homogeneity and optoelectronic performance, guiding the development of next-generation high-efficiency thin-film solar cells.

[1] V. Alberts, Thin Solid Films 517, 2115-2120 (2009). https://doi.org/10.1016/j.tsf.2008.10.127.

Modification of electrophysical and mechanical characteristics of $Fe_{40}Mn_{40}Co_{10}Cr_{10}$ alloy under ultrasound influence

E. V. Karaseva, V. I. Sokolenko, A. V. Mats, E. S. Savchuk, M. A. Tikhonovsky, V. A. Frolov, V. S. Okovit

National Science Center "Kharkiv Institute of Physics and Technology", 1, Akademicheskaya St., 61108 Kharkiv, Ukraine
e-mail: vsokol@kipt.kharkov.ua

The nonequiatomic high-entropy alloy $Fe_{40}Mn_{40}Co_{10}Cr_{10}$ belongs to the TWIP class of steels, which exhibit high tensile strength and excellent plasticity. One of the main drawbacks of these steels, limiting its use in industry, is its low yield strength. Therefore, much research into TWIP steels is aimed at increasing their yield strength.

Ultrasonic treatment can be one way to increase yield strength. Ultrasonic waves, passing through a material, interact with various types of defects and cause structural changes that depend on the ultrasound parameters, primarily its power. By varying these parameters, a structure with the desired properties can be achieved in the material.

The high-entropy alloy $Fe_{40}Mn_{40}Co_{10}Cr_{10}$ was studied in the temperature range of 77–700 K in order to establish the effect of ultrasonic treatment on mechanical and electrophysical properties.

For the as-is alloy, temperature dependence measurements of the specific electrical resistance $\rho(T)$ and absolute thermoelectric power $S(T)$ in the range of 77–300 K revealed that the former is described by a quasi-linear $\rho(T)$ dependence, while the $S(T)$ dependence exhibits a complex temperature behavior characterized by the presence of two intervals with different temperature dependences. In addition to the thermoelectric anomaly, these coefficients each exhibit two correlating anomalies below ~ 200 K. The observed anomalies in the alloy's electrophysical characteristics may be the result of conversion transformations of electron and hole quasiparticle states in the free charge carrier system, which is of theoretical interest.

The creep of the high-entropy alloy $Fe_{40}Mn_{40}Co_{10}Cr_{10}$ was studied in the temperature range of 77–700 K. It was shown that the alloy has high strength and plasticity characteristics. At the same time, the yield strength is quite low: 350 MPa at 77 K, 170 MPa at 300 K and 110 MPa at 700 K. It is known that plastic deformation in the alloy occurs through twinning, as these steels have low stacking fault energy. The high strength is due to the strong strain hardening of this material. The rate of strain hardening is explained by a decrease in the mean free path of dislocations during the nucleation and growth of mechanical twins, and twinning leads to increased plasticity.

Ultrasonic treatment using a hardening mode [1] significantly impacted the alloy's properties. Specifically, yield strength increased by ~30% while maintaining tensile strength and plasticity.

It is known that high-frequency alternating currents generate a large number of vacancies and initiate dislocation multiplication, leading to an increase in yield strength. However, the primary deformation mechanism – twinning – is unchanged, ensuring the alloy maintains its high strength and plasticity. The causes of the observed anomalies in thermal and electrical properties are also discussed.

The research presented in this article was financially supported by the Simons Foundation International Program: PD-Ukraine: President Directed – Ukraine Support Grants, Record ID: SFI-PD-Ukraine-00014584.

[1] A. V. Matz, V. M. Netesov, V. I. Sokolenko, Ultrasonic influence on nanostructure in Zr-2,5%Nb alloy, Problems of atomic science and technology 74, 108-110 (2011).

Comprehensive study of electronic, optical, and mechanical properties of the $CuInP_2S_6/MoS_2$ van der Waals heterostructures in the DFT approach

O. I. Korolov, I. Ya. Babuka, K. E. Glukhov, L. Yu. Kharkhalis, T. Ya. Babuka

Institute for Physics and Chemistry of Solid State,
Uzhhorod National University, 54 Voloshin St., Uzhhorod, 88000, Ukraine
e-mail: oleh.korolov@uzhnu.edu.ua

Today, there is a growing interest in compounds of the $M1M2P_2X_6$ family as a new class of materials with unusual physical properties and the possibility of their wide use for the creation of nanoscale monolayers and 2D van der Waals heterostructures, for example, $CuInP_2S_6/In_{4/3}P_2S_6$, $CuInP_2S_6$/InSe, $CuInP_2S_6$/Ge, and $CuInP_2S_6/MoS_2$. [1-4]. As shown in [2], in the considered systems, nanometric domains (~4nm) with controlled orientation of the spontaneous polarization vector and controlled magnetism can be achieved. It opens the way to new technologies for creating memory cells and ferroelectric non-volatile switches, as well as for high-speed data recording and storage. Nowadays, the $CuInP_2S_6/MoS_2$ van der Waals heterostructure also demonstrates the potential to create multifunctional optoelectronic transistors that convert light into electricity. Despite the promising functionalities of heterostructures based on the ferrielectric $CuInP_2S_6$ and their suitability for various devices in modern nanoelectronics, the fundamental characteristics of these nanostructures have not been systematically studied. Therefore, the main aim of the present report is to calculate the electronic energy spectra and optical properties. To identify the most stable stacking of the van der Waals lattice of the heterostructures, it is necessary to investigate their mechanical stability, too. Such a study is significant for the construction of novel heterostructures to optimize their electronic properties and enhance mechanical stability.

As an example, we shall consider the $CuInP_2S_6/MoS_2$ heterostructure. It is known that $CuInP_2S_6$ has a complex crystalline structure. It is a layered crystal described by monoclinic symmetry (C2/c). Lattice parameters equal to a = 6,0566 (4) Å, b = 10.5645 Å, c = 13.6230 (9) Å with β = 107.101(3)º. The MoS_2 crystals also have a quasi-two-dimensional structure with the hexagonal symmetry (P63/mmc) and lattice parameters: a = b = 3.1602 Å, c = 12.243 Å.

We proposed two flexible models of the $CuInP_2S_6/MoS_2$ heterostructure, consisting of 1x1 and 2x2 monolayers, respectively.

Using the DFT method, we calculated the band structures, the spatial distribution of the electron density, Mulliken charges, as well as total and partial densities for both bulk crystals in two models of the $CuInP_2S_6/MoS_2$ heterostructure. This study also compared the dielectric properties, refractive indices, and absorption characteristics of the bulk materials, $CuInP_2S_6$ and MoS_2, and two types of $CuInP_2S_6/MoS_2$.

The investigation of mechanical properties, based on the calculation of elastic moduli, Young's, and Poisson's ratios, has been carried out. According to Born's criteria, the considered $CuInP_2S_6/MoS_2$ models are mechanically stable.

[1] R. Rao, R. Selhorst, B. S. Conner, M. A. Susner, Phys. Rev. Materials 6, 045001 (2022) https:// doi.org/10.1103/PhysRevMaterials.6.045001.
[2] Z. Zhu, X. Chen, W. Li, J. Qi, J. Mater. Chem. C, 8, 17342-17348 (2020) https:// https://doi.org/10.1039/D0TC04272B.
[3] Z. Zhu, X. Chen, W. Li, J. Qi, Appl. Phys. Lett. 114, 223102 (2019), https://doi.org/10.1063/1.5100240.
[4] M. Si, P.-Y. Liao, G. Qiu, Y. Duan, P. D.Ye, ACS Nano 2018, 12, 6700−6705, https://doi.org/10.1021/acsnano.8b01810.

Amorphous-to-crystalline transition in $Ge_2Sb_{2-x}Bi_xSe_5$ phase change materials

V. M. Kryshenik[1], S. M. Hasynets[1], M. J. Filep[2], Y. S. Hasynets[3], O. O. Gomonnai[3], V. Yu. Loya[1], A. V. Gomonnai[1]

[1]Institute of Electron Physics of NAS of Ukraine, 21 Universytetska Str., Uzhhorod, 88017, Ukraine
[2]Ferenc Rákóczi II Transcarpathian Hungarian Institute, Kossuth Sq. 6, Berehovo 90200, Ukraine
[3]Uzhhorod National University, Pidhirna Str. 46, Uzhhorod, 88000, Ukraine
e-mail: kryshenik@gmail.com

Chalcogenide phase change materials are characterized by significant changes in optical parameters during reversible phase transitions between crystalline and amorphous states, which are caused by the action of ultrashort laser pulses. Among these materials, a group of Sb- and Se-based semiconductor chalcogenides are distinguished as optical phase change materials. It is worth noting that Ge–Sb(Bi)–Se alloys can be expected to exhibit significant differences in refractive index and reflectivity during phase transformations, combined with low optical losses over a wide spectral range (1–18 μm). The high glass-forming ability of the aforementioned phase change materials contributes to the stability of their characteristics when used as optical switches and modulators.

Bulk samples of $Ge_2Sb_{2-x}Bi_xSe_5$ alloys ($0 \le x \le 0.4$) were synthesized from stoichiometric elemental components in a vacuumed quartz ampoule, which was heated at a rate of 30 K/h to a temperature of 973 K, and after an hour of isothermal treatment, the ampoule with the mixture was heated again at the rate of 20 K/h until a temperature of 1243 K was reached with further eight-hour isothermal treatment. Then the ampoule with the melt was cooled at a rate of 25 K/h down to a temperature of 943 K or (in another variant) to a temperature of 853 K, then the melt was quenched by immersing the ampoule in cold water. We designated these two modes of synthesis of $Ge_2Sb_{2-x}Bi_xSe_5$ alloys as rapid quenching (RQ) mode and slow quenching (SQ) mode, since the final stage of isothermal holding (before quenching the alloy) occurred at temperatures that differed by 80–90 K.

In both synthesis modes and for the synthesized alloys of different compositions, which were investigated by X-ray diffraction (XRD) using the AXRD Benchtop diffractometer with Cu Kα radiation, the initial structure was amorphous, i.e. without any signs of the presence of crystalline inclusions in the alloy.

Kinetic analysis of non-isothermal crystallization in $Ge_2Sb_{2-x}Bi_xSe_5$ alloys ($0 \le x \le 0.4$) was carried out using differential thermal analysis data with a certain set of heating rate values: $\beta = 3$, 6, 9, 12 and 15 K/min. We recorded the onset temperatures of the phase transformation T_{ons} and the exothermic crystallization peak T_p. The thermally stimulated crystallization occurs by a single-stage mechanism for all studied samples.

As X-ray diffraction measurements showed, the formation process of crystalline inclusions in the amorphous matrix of alloys with $x \ge 0.10$ was influenced by the heating rate β, i.e. the result of crystallization was temperature-dependent. For samples after the non-isothermal heating procedure with high β, the formed crystalline phases were identified by comparison with known data.

For $Ge_2Sb_{2-x}Bi_xSe_5$ alloys, the activation energy E_a for crystallization increased with increasing x. However, for samples synthesized in the SQ mode, the E_a values were significantly higher than those for samples prepared in the RQ mode. We explain this by the peculiarity of the structure of glasses synthesized in the RQ mode, which is arranged in such a way that the contribution to the activation energy for crystallization from the primary nucleation process was significantly smaller than that for glasses prepared in the SQ mode.

Possible thermal mechanisms responsible for observed phase transformations in the studied alloys are discussed.

Investigating growth mechanisms in ultrathin amorphous Mo_xSi_{1-x} films with atomic force microscopy

O. O. Leha[1], V. Yu. Lyakhno[1,2], O. V. Zraichenko[1], S. I. Kryvonohov[3], O. G. Turutanov[4], M. Yu. Mikhailov[1]

[1]B.Verkin Institute for Low Temperature Physics and Engineering of NAS of Ukraine, 47 Nauky Ave., Kharkiv, 61103, Ukraine
[2]G.V. Kurdyumov Institute for Metal Physics, N.A.S. of Ukraine, 36 Academician Vernadsky Boulevard, 03142 Kyiv, Ukraine
[3]Institute for Single Crystals, STC "Institute for Single Crystals", National Academy of Sciences of Ukraine, 60 Nauky Ave., Kharkiv, 61001, Ukraine
[4]Department of Experimental Physics, Comenius University, 842 48 Bratislava, Slovakia
e-mail: leha@ilt.kharkov.ua

Amorphous superconducting MoSi thin films are promising materials for applications in superconducting nanoelectronics, including single-photon detectors, quantum circuits, and cryogenic amplifiers [1]. Their electrical and superconducting properties are strongly governed by growth conditions, structural homogeneity, and level of disorder [2].

In this work, we present the results of a systematic investigation of the growth of MoSi thin films deposited by DC magnetron sputtering from two separate sources in an argon atmosphere. The influence of discharge power, stoichiometry, and substrate material on film roughness, thickness as well as surface parameters was analyzed using atomic force microscopy.

Structural features arising during film growth, including nanoscale inhomogeneities, local crystallization, and disorder-related defects, can significantly affect the superconducting properties of $Mo_{1-x}Si_x$ thin films. In particular, the emergence of polycrystalline phases and increased structural disorder may lead to a suppression of the critical temperature and enhanced inhomogeneity of the superconducting state. In amorphous MoSi systems, disorder-induced localization effects additionally influence charge transport and contribute to variations in normal sheet resistance and superconducting transition width [3]. The obtained results provide a basis for optimizing the fabrication of MoSi thin films with tailored properties for next-generation superconducting devices.

This work is supported by the National Research Foundation of Ukraine, project No.22.07/0044 and by the IEEE program “Magnetism for Ukraine 2025-2026”, project number 9918”.

[1] Yu. P. Korneeva, M. Yu. Mikhailov, Yu. P. Pershin, N. N. Manova, A. V. Divochiy, Yu. B. Vakhtomin, A. A. Korneev, K. V. Smirnov, A. G. Sivakov, A. Yu. Devizenko, G. N. Goltsman, Superconducting single-photon detector made of MoSi film, Superconductor Science and Technology 27, 095012 (2014). https://doi.org/10.1088/0953-2048/27/9/095012.
[2] S. Grotowski, L. Zugliani, B. Jonas, R. Flaschmann, C. Schmid, S. Strohauer, F. Wietschorke, N. Bruckmoser, M. Müller, M. Althammer, R. Gross, K. Müller & J. Finley, Optimizing the growth conditions of superconducting MoSi thin films for single photon detection, Scientific Reports 15, 2438 (2025). https://doi.org/10.1038/s41598-025-86303-5.
[3] Z. Liu, B. Luo, J. Hu, C. Xing, Transport mechanism in amorphous molybdenum silicide thin films, Journal of Physics and Chemistry of Solids 149, 109818 (2021). https://doi.org/10.1016/j.jpcs.2020.109818.

Microstructure and low-temperature mechanical properties of carbon-alloyed CoCrFeNi high-entropy alloys: effect of heat treatment temperature

A. V. Levenets, V. S. Okovit, M. A. Tikhonovsky, O. S. Solopikhina, Yu. S. Lypovska

National Science Center "Kharkiv Institute of Physics and Technology" of NAS of Ukraine,
Akademichna str. 1, Kharkiv, 61108, Ukraine
e-mail: avlevenets@gmail.com

The equiatomic CoCrFeNi high-entropy alloy (HEA) is a promising candidate for cryogenic applications due to its exceptional ductility and impact toughness, although its yield strength and ultimate tensile strength remain relatively low [1]. In this work, we study how carbon alloying and subsequent heat treatments control the microstructure and tensile properties of $Co_{25-x}Cr_{25}Fe_{25}Ni_{25}C_x$ (x = 0, 1, 3 at.% C) at 300 K and 77 K. The alloys were produced by argon-arc melting [2], homogenized at 1100 °C for 5 h, rolled into ~0.5 mm strips with intermediate annealing at 1050 °C/1 h after 50% thickness reduction, and then annealed for 1 h in argon at 650–1100 °C. Dog-bone specimens were tested in tension at a strain rate of 10^{-3} s^{-1}, while grain and carbide sizes were characterized by transmission electron microscopy.

While the carbon-free CoCrFeNi forms a single-phase FCC solid solution, carbon-doped compositions develop a two-phase microstructure consisting of an FCC matrix and M23C6-type carbides. Carbon additions suppress grain growth during annealing: for example, after 750 °C/1 h, the average grain size decreases from ~2.75 μm (x = 0) to ~1.84–1.97 μm (x = 1–3), and after 850 °C/1 h from ~4.9 μm (x = 0) to ~1.97 μm (x = 3). Carbide precipitation and coarsening become more pronounced with increasing annealing temperature, particularly for x = 3 (average carbide size increases from ~0.125 μm at 650 °C/1 h to ~1.03 μm at 850 °C/1 h).

Mechanical testing reveals that carbon alloying essentially increases the proportional limit (Figure) and another strength characteristics at both temperatures, with the most pronounced strengthening at 77 K; the elongation decreases but remains at a practically acceptable level. The influence of annealing temperature is non-monotonic, reflecting competition between recovery/recrystallization and precipitation evolution. The observed trends are discussed in terms of grain-boundary and precipitation strengthening mechanisms relevant to optimize HEAs for cryogenic service.

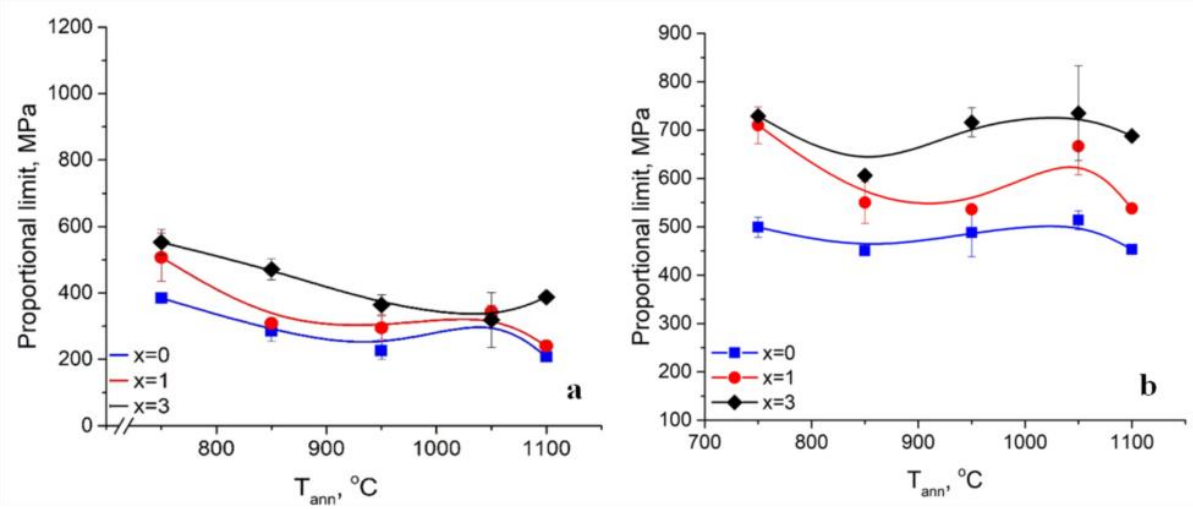

[1]. S. Wang, Z. Chen, R. Chen, et al., Journal of Alloys and Compounds 1006, 176268 (2024). https://doi.org/10.1016/j.jallcom.2024.176268
[2] A. V. Levenets, H. V. Rusakova, L. S. Fomenko et al., Low Temperature Physics 48, 560–569 (2022). http://dx.doi.org/10.1063/10.0011605.

Features of noncritical low-temperature and critical high-temperature anomalies of heat capacity in van der Waals $Cu(Ag)InP_2S(Se)_6$ crystals

V. Liubachko[1], D. Szewczyk[2], V. Sokolenko[2], P. Gluchowski[2,3], K. Glukhov[1], A. Pogodin[1], V. Yevych[1], Yu. Vysochanskii[1]

[1]Uzhhorod National University, Narodna Sq. 3, Uzhhorod, 88000, Ukraine
[2]Institute of Low Temperature and Structure Research, Polish Academy of Sciences, Okolna 2, 50-422 Wroclaw, Poland
[3]Graphene Energy LTD, Curie-Skłodowskiej 55, 50-369 Wroclaw, Poland
e-mail: vitalii.liubachko@uzhnu.edu.ua

It has recently been established that the phenomenon of ferrielectricity in $CuInP_2S_6$ can be considered within the mixed Ising model with spins s = 1/2 and S = 1 [1]. These spins (or rather pseudospins) are associated with the ordering dynamics of Cu^+ cations in the double-well local potential and with the ordering/displacive dynamics of In^{3+} cations in the three-well local potential. Therefore, the occurrence of strong lattice anharmonicity is attributable to the presence of the indium sublattice, which manifests itself below 150 K. Conversely, at higher temperatures, the anharmonicity due to the copper sublattice activates the ionic conductivity and leads to the first order ferrielectric-paraelectric phase transition at $T_C \approx 315$ K, as well as to the existence of fluctuated polar clusters above T_C. The present study focuses on the temperature evolution of the heat capacity of $Cu(Ag)InP_2S(Se)_6$ crystals. The temperature range encompassed from 2 K to 370 K, thereby covering both the low-temperature region where quantum fluctuations play a pivotal role and the high-temperature region, where classical thermal fluctuations are predominant.

For $CuInP_2S_6$, $CuInP_2Se_6$, $AgInP_2S_6$ and $AgInP_2Se_6$ crystals, a so-called "boson peak" was observed, which was analyzed using density of phonon states obtained from DFT calculations. The emergence of this peak is attributed to the specific nature of shear modes, which underlies the low-temperature heat capacity anomaly.

$CuInP_2S(Se)_6$ compounds also show an anomalous increase in C_p/T^3 dependence upon cooling below the "boson peak". Such phenomenon is not observed in $AgInP_2S(Se)_6$ crystals. This anomaly may be classified as the appearance of a Schottky-like peak [2]. The existence of such an anomaly in $CuInP_2S(Se)_6$ is consistent with the mixed Ising model [3] and can be explained by fluctuations of S = 1 pseudospins that are related to the In^{3+} cations anharmonic dynamics in the three-well local potential. In particular, when silver replaces copper, in the centrosymmetric structure, the Ag^+ cations become firmly fixed at the center of the structural layer, thereby directly constraining the role of indium fluctuations at low temperatures. This assumption is corroborated by the temperature dependence of heat capacity calculated within the framework of the quantum anharmonic oscillators model. The analysis indicated that the most significant increase in entropy within the ultralow-temperature region is linked to the anharmonic dynamics of indium. The model under consideration also predicts that the correlated relaxations related to Cu^+ cations s = 1/2 pseudospins can induce the ferroelectric clusters that occur above the transition from the ferrielectric to paraelectric state.

This work was supported by the Ministry of Education and Science of Ukraine (Grants: 0124U004302 – PH/41-2024; 0125U001555; 0126U001941) and HORIZONMSCA-2022-SE-01 (Grant 101131229 – Piezo2D).

[1] R. Yevych, V. Liubachko, V. Hryts, M. Medulych, A. Kohutych, Yu. Vysochanskii, Condens. Matter Phys. 27, 14701 (2024). https://doi.org/10.5488/cmp.27.14701.
[2] V. F. Sears, Proc. Phys. Soc. 84, 951 (1964). https://doi.org/10.1088/0370-1328/84/6/314.
[3] W. Selke, J. Oitmaa, J. Phys.: Condens. Matter 22, 076004 (2010). https://doi.org/10.1088/0953-8984/22/7/076004.

Experimental study of the palladium behavior during hydrogen saturation in the α-region of the Pd–H system

O. M. Liubymenko

State higher education institution "Donetsk National Technical University",
Sambirska st., 76, Drohobych, Lviv region, 82100, Ukraine
e-mail: e.n.lyubimenko@gmail.com

To ensure the energy independence of the state, the use of hydrogen technologies requires an in-depth study of the processes of hydrogen interaction with structural and functional materials. Thus, palladium is characterized by a high ability to absorb hydrogen and is a model material for studying phenomena associated with the penetration of hydrogen into metals. In the α-region of the Pd–H system, hydrogen dissolves in the palladium crystal lattice with the formation of a solid solution of the introduction. Even at relatively low hydrogen concentrations, such changes can significantly affect the mechanical behavior of the material. In this regard, an experimental study of the behavior of palladium during hydrogen saturation in the α-region of the Pd–H system is important for a deeper understanding of the mechanisms of hydrogen-induced deformation and for further substantiation of approaches to the creation of materials and elements resistant to the action of hydrogen.

The aim of this work is to experimentally study the behavior of a palladium cantilever during its gradual additional saturation with hydrogen in the α-region of the Pd–H system and to establish the regularities of shape change depending on the conditions of hydrogen exposure.

Within the framework of the experimental part, the hydrogen influence on the shape change of the cantilever was studied at 200°C, 240°C, 280°C, and 320 °C. A pure palladium cantilever was installed in a working chamber, where hydrogen was supplied to a given pressure, which corresponds to the concentration of $n_1 \cong \Delta n$. At this stage, the cathetometer readings were recorded, which characterized the bending of the cantilever. Next, the cantilever was kept in a hydrogen environment until it returned to its original state. Further, the hydrogen pressure was again increased by the value of ΔP_{H_2} to a concentration of $n_2 \cong n_1+\Delta n$, the bending of the sample was again recorded and it was kept in a hydrogen environment until the relaxation processes were completed. At the third stage, the pressure was increased again to a concentration of $n_3 \cong n_2+2\Delta n$, after which the cathetometer readings were recorded again and the cantilever was kept in a hydrogen environment. As a result, alloys with different hydrogen contents were obtained: α-PdH_n, α-PdH_{2n} and α-PdH_{4n}. The saturation process was recorded on video, which made it possible to obtain time dependences of the change in the shape of the cantilever.

For the first time, it was experimentally established that the dependence of the maximum palladium bending on the hydrogen concentration in the α-region of the Pd–H system has a nonlinear U-shaped character with a minimum in the range of approximately 0.01–0.02 H/Pd. The presence of such a minimum probably corresponds to the transition from an ideal to a pseudo-ideal solid solution, when the interatomic distance in the palladium crystal lattice changes. At low concentrations, the ordered filling of octahedral interstitials contributes to the partial stabilization of the lattice with the deformation response decreased. On the other hand, with higher hydrogen concentration and transition to a non-ideal state, we observe the intensification of lattice dilation, concentration stresses, as well as a decrease in the effective elastic stiffness of the lattice, which makes bending more pronounced. This confirms the complex nature of the shape change of palladium even within the α-region of the Pd–H system.

[1] E. P. Feldman, O. M. Lyubimenko, Journal Acta Mechanica 234, 1619–1626 (2023). https://link.springer.com/article/10.1007/s00707-022-03471-5.

Influence of sectoral structure on Schottky diode and ohmic contact parameters in HPHT diamond

A. Nikolenko[1], V. Strelchuk[1], I. Danylenko[1], D. Maziar[1], Ya. Kudryk[1], T. Kovalenko[2], A. Burchenia[2], V. Lysakovskyi[2], S. Ivakhnenko[2], M. Dub[3], P. Sai[3], W. Knap[3]

[1]V. E. Lashkaryov Institute of Semiconductor Physics NASU, pr. Nauky 41, 03028 Kyiv, Ukraine
[2]V. Bakul Institute for Superhard Materials NASU, Avtozavodska str. 2, 04074 Kyiv, Ukraine
[3]Center for Terahertz Research and Applications (CENTERA), Institute of High Pressure Physics PAS, ul. Sokołowska 29-37, Warsaw 01-142, Poland
e-mail: fmbfiz13.mazyar@kpnu.edu.ua

Diamond is a wide-band-gap semiconductor promising for high-power and high-temperature electronics due to its large band gap, high breakdown field, exceptional thermal conductivity, and radiation hardness. Boron provides stable p-type doping in diamond. During high-pressure high-temperature (HPHT) bulk growth with intentional boron incorporation, simultaneous growth of several crystallographic facets leads to formation of a sectoral structure. Each sector exhibits specific impurity incorporation kinetics and defect formation mechanisms, resulting in lateral modulation of dopant concentration and defect density within a single-crystalline wafer.

In this work, transport properties of planar Schottky diodes and ohmic contacts fabricated on (100)-oriented HPHT diamond plates with sectoral structure were systematically investigated. Spatial mapping of uncompensated boron concentration was performed using μ-FTIR spectroscopy and revealed distinct concentration ranges associated with {111}, {113}, and {001} growth sectors. More than 200 planar structures were fabricated on 500 μm thick substrates using Ti/Pt/Au ohmic contacts (rapid thermal annealing at 600 °C) and Ni/Pt/Au Schottky contacts (250 °C).

Current-voltage characteristics demonstrate two typical behaviors: (i) high-quality rectifying diodes and (ii) structures exhibiting increased reverse leakage and excess current at low forward bias. The latter are attributed to shunting ("killer") defects, most likely impurity-decorated dislocations intersecting the space-charge region. Statistical analysis of diodes with identical barrier area (r = 25 μm) shows that the probability of obtaining defect-free devices depends on growth sector location. However, the correlation between killer-defect density and local dopant concentration is non-trivial. In particular, the {111} sector, despite having a higher average boron concentration (~5.5×10^{18} cm^{-3}), does not exhibit the highest fraction of shunted structures, indicating that both sector-related growth conditions and edge effects contribute to defect statistics.

At higher doping (≥9×10^{18} cm^{-3}), the bulk concentration increasingly governs the reverse current, and the Schottky contact tends toward quasi-ohmic behavior due to enhanced tunneling.

A pronounced sector dependence was observed for the specific contact resistivity of Ti/Pt/Au ohmic contacts. While classical models predict approximately one order of magnitude reduction in contact resistivity per order increase in dopant concentration [1], the experimental dependence is stronger. Moreover, for identical boron concentration, contacts located in {001} and {113} growth sectors exhibit systematically lower specific contact resistivity than those in {111} sectors. Since shunting defects contribute negligibly to total current in large-area ohmic contacts, this effect is attributed to growth-sector-dependent near-surface defect structure and interfacial reactions during rapid thermal annealing (RTA).

The results demonstrate that the sectoral structure of HPHT diamond affects both leakage statistics of Schottky diodes and resistive properties of ohmic contacts. While bulk dopant concentration determines the general transport regime, growth sector dependent features play a measurable role in device yield and contact performance.

This study was supported by the NRFU project #2025.07/0197.

[1] R. K. Kupka, W. A. Anderson, Minimal ohmic contact resistance limits to n-type semiconductors, J. Appl. Phys. 69, 3623–3632 (1991). https://doi.org/10.1063/1.348509.

Fluorophore-containing sensor films for the determination of trace impurities of ammonia and acetone in air medium

V. P. Mitsai[1], Ya. P. Lazorenko[2]

[1]V.G. Baryakhtar Institute of Magnetism of the NAS of Ukraine,
36-b Akad. Vernadskogo blvd., Kyiv, 03142, Ukraine
[2]G.V. Kurdyumov Institute for Metal Physics of the NAS of Ukraine,
36 Akad. Vernadskogo blvd., Kyiv, 03142, Ukraine
e-mail: vitapok@i.ua

Recently, in the search for new opportunities in medical diagnostics, the problem of analyzing human exhaled air has gained particular interest. Gaseous ammonia and acetone in the air attract the attention of researchers. It is known that it is a marker of such diseases as renal failure, liver failure in hepatitis, cirrhosis of the liver, lung cancer, and diabetes. Humans excrete them in trace concentrations in exhaled air (at concentrations of about 0.5-10 ppm). Therefore, tools are needed that can detect gaseous ammonia and acetone at such low concentrations.

We synthesized and investigated sensor film samples with several sorbent matrices (Aerosil, butasil, silica gel, PDMS (polydimethylsiloxane)) and dopants (dyes coumarin 1 and coumarin 7, and CdTe nanocrystals). The optical properties of the created film samples and their fluorescent response to the microconcentrations of gaseous ammonia or acetone molecules were investigated using a Flx-800T fluorometer. Also, the influence of the component composition (namely, the sorbent layer of the film) on the fluorescent sensitivity of the created material to ammonia molecules in ultra-low concentrations was investigated.

The magnitude of the fluorescent response to trace concentrations of ammonia with a concentration of 10 ppm was determined for samples with coumarin 7 and CdTe quantum dots. Under interaction with ammonia vapors, a decrease in the intensity of the fluorescence signal is observed: for the film with PDMS sorbent by 12.1%, for the film with butasyl sorbent by 3.3%, for the film with Aerosil sorbent by 2.1%, and for the film with silica gel sorbent by 4.4%, compared to the initial intensity of the sample. Comparing the obtained values of the fluorescent response to the same concentration of ammonia (10 ppm) for each film with different sorbents and with the same composition of the remaining components, it was determined that the largest response value to the specified concentration was the film sample with a layer of PDMS sorbent (polydimethylsiloxane), which is 12.1%. Therefore, this sample was determined to be the most effective in detecting ammonia molecules in the air and its further application in a prototype of a fluorescent NH_3 analyzer.

Investigation of the fluorescent response of silica gel samples with coumarin 1 revealed a change of 0.25% in fluorescence intensity at an acetone concentration of 10 ppm. The magnitude of the response was proportional to the concentration of acetone in the air.

For the studied samples, multiple recovery of the fluorescent sensory response after desorption of analyte molecules was observed, which is important for sensor detection devices.

Thus, the studied samples demonstrated high sensitivity to ammonia or acetone molecules (depending on the fluorescent dye) in air, with repeated restoration of the sensory response in clean air. Films with a polydimethylsiloxane matrix demonstrated particularly high sensitivity to ammonia, compared to other matrices. These films hold promise for the development of low-cost, compact devices for the sensory detection of ammonia or acetone in human exhaled air for non-invasive disease diagnosis.

The effect of iron doping on the electrophysical properties of $Cd_2P_2S_6$ crystals

H. Bán[1], D. Gál[2], A. Horvat[1], A. Molnar[1]

[1]Uzhhorod National University, Voloshina Str. 54, Uzhhorod, 88000, Ukraine
[2]HUN-REN WIGNER Research Center for Physics, Po.Box. 49, 1525 Budapest, Hungary
e-mail: alexander.molnar@uzhnu.edu.ua

One of the ways to continue progress in increasing the switching speed and reducing the size of electronic components is to migrate to spintronics, which uses not only the charge but also the spin of electrons to store, process, and transmit information. Van der Waals antiferromagnetic materials are considered very promising for creating such devices, as they can be exfoliated to a two-dimensional (2D) limit – structural monolayers – while retaining their antiferromagnetic (AF) properties.

Cadmium trichalcogenophosphate ($Cd_2P_2S_6$) doped with iron serves a good example of a layered crystal with peculiarities mentioned above. Its properties change significantly when every second cadmium (Cd) atom is replaced with iron (Fe), forming the $CdFeP_2S_6$ compound. Despite being synthesized in 1988, the material has been studied only in three works, and almost nothing is known about its electrophysical properties. In view of these facts, our research focused on studying the temperature dependence of the conductivity and dielectric permittivity of $CdFeP_2S_6$ crystals.

We studied the temperature-dependent dielectric spectra of $CdFeP_2S_6$ single crystals in the range of 80–400 K. Our measurements revealed that the material exhibits a change in the temperature-frequency behavior of its dielectric properties. The maximum anomaly of the imaginary part (ε″) and the corresponding break in the real component (ε′) of the complex dielectric permittivity ($\varepsilon^* = \varepsilon' - i\varepsilon''$) occur at 250 K and a measurement field frequency of 10 kHz. The observed dielectric spectra can be described by the Cole–Cole formula, with a relaxation time distribution parameter α of 0.4–0.6, which is very high and decreases upon cooling. This indicates a large relaxation time distribution, strong spatial and energy inhomogeneity, and a cooperative rather than Debye relaxation mechanism. The temperature-dependent relaxation time is described by the Arrhenius law. Using this, the activation energy of the process was determined to be $E_a \approx 0.347$ eV.

In order to verify the most probable charge transfer mechanisms in these crystals, we measured the temperature dependence of the electrical conductivity of $CdFeP_2S_6$ crystals at a constant current. Two regions with different activation energies were observed in this dependence.

In the high-temperature region ($1000/T \approx 2.5–3.2$), we obtained an activation energy of $E_{a1} \approx 0.3–0.35$ eV, while for the low-temperature one ($1000/T \approx 4.2–5.8$), it was $E_{a2} \approx 0.12–0.15$ eV. The results enable us to determine the conduction mechanisms in $CdFeP_2S_6$ crystals more accurately. $E_{a1} \sim 0.33$ eV is most likely responsible for the polaron conduction caused by thermally activated charge carrier jumps, which is consistent with the mechanism associated with Fe^{2+}/Fe^{3+} centers. Meanwhile, $E_{a2} \sim 0.13$ eV should be associated with the hopping conduction, charge transfer between localized states and correlated defect transport. The nonlinearity between two of them is indicative of a transition between the two mechanisms.

[1] S. Lee, P. Colombet, G. Ouvrard and R. Brec, Inorg. Chem. 27, 1291 (1988). http://dx.doi.org/10.1021/ic00280a041.
[2] A. Bhomwick, B. Bal, S. Ganguly, M. Bhattacharya and M.L. Kundu, J. Phys. Chem. Solidv 53(10) 1279 (1992). http://dx.doi.org/10.1016/0022-3697(92)90246-A.
[3] A. Le´austic, E. Rivie`re, R. Cle´ment, E. Manova and I. Mitov, J. Phys. Chem. B 103, 4833 (1999). http://dx.doi.org/10.1021/jp9904623.

Bridging accuracy and simplicity: ML-based models for carrier mobility estimation in silicon

O. Ya. Olikh

Taras Shevchenko National University of Kyiv, 64/13, Volodymyrska Str., Kyiv, 03028, Ukraine
e-mail: olegolikh@knu.ua

Charge carrier mobility is a fundamental parameter governing semiconductor conductivity and device switching speed, linking microscopic scattering mechanisms to macroscopic transport behavior. Although rigorous theoretical formulations, such as Klaassen's model, provide high predictive accuracy, they are computationally demanding due to extensive parameterization. Consequently, simplified approaches, including the Arora model [1], are widely used despite their reduced accuracy. This work aims to develop machine learning models that retain the predictive fidelity of Klaassen's formulation while achieving computational efficiency comparable to that of the Arora approximation.

Compact analytical expressions describing the mobility of both majority and minority carriers in monocrystalline silicon over a broad range of temperatures (T = 200-500 K) and doping (N_D = 10^{13}-10^{19} cm^{-3}) were derived using a symbolic regression (SR) algorithm [2]. The general form of the resulting equations is given by:

$$\mu = \mu_0 + \frac{\mu_1}{T_n^{2,25} + a \cdot b / (a+b)} \quad (1)$$

where μ_0, μ_1, a, and b are functions of T_n=T/100 and N_{Dn}=N_D/10^{17}, with their explicit forms being carrier-type dependent. For the case of electrons, these functions are summarized in Table. The expressions are more parsimonious, require 50% fewer parameters than the Klaassen model, and eliminate preliminary impurity ionization calculations while maintaining a relative error below 0.1% (see Fig)

Table. Explicit expressions for the functions in Eq. (1) used to estimate electron mobility

	majority electron	minority electron
μ_0	0	$26.3\left(\frac{N_{Dn}}{N_{Dn}+192}\right)^{0.62}$
μ_1	$N_{Dn}+1413.2$	1412.3
a	$\left(\frac{N_{Dn}}{0.873T_n+0.0727}\right)^{0.7212}$	$1.92\left(\frac{N_{Dn}}{T_n+0,071}\right)^{0.717}$
b	$0.215N_{Dn}^{0.58}+10.5T_n-1.342$	$5.7\cdot N_{Dn}^{0.103}\cdot T_n$

In addition, set of regression models was developed and tuned for mobility prediction. These models outperform the Arora approximation in predictive accuracy, but they remain less accurate than the SR derived analytical expressions. Among the ML approaches considered, SVR and DNN demonstrated the most favorable performance.

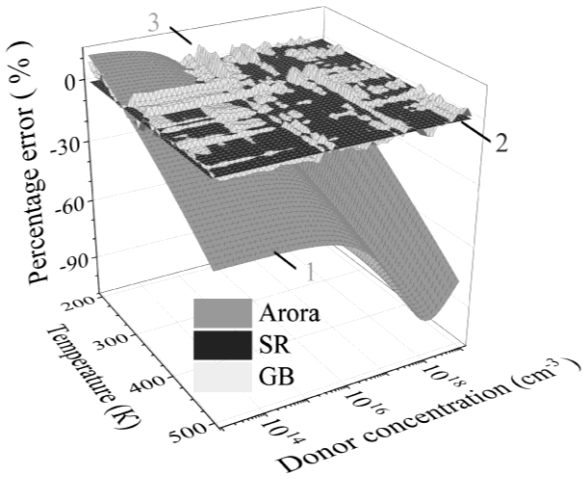

Fig. Temperature- and doping-concentration-dependent prediction errors with respect to Klaassen's hole mobility model in n-Si, evaluated using Arora's model (surface 1), an analytical expression derived via symbolic regression (2), and a Gradient Boosting regression model (3).

[1] N. Arora, J. Hauser, D. Roulston, IEEE Trans. Electron Devices 29, 292 (1982). http://dx.doi.org/ 10.1109/T-ED.1982.20698
[2] D. Angelis, F. Sofos, and T. Karakasidis. Arch. Comput. Methods Eng. 30, 3845 (2023). http://dx.doi.org/10.1007/s11831-023-09922-z.

Elastic and inelastic properties of single crystal Ni-35.6wt%W in the temperature range of 51–300 K

P. P. Pal-Val[1], O. M. Vatazhuk[1], M. A. Tikhonovsky[2], I. V. Kolodiy[2]

[1]B.Verkin Institute for Low Temperature Physics and Engineering of NAS of Ukraine, 47 Nauky Ave., Kharkiv, 61101, Ukraine
[2]National Science Center "Kharkiv Institute of Physics and Technology" of NAS of Ukraine, 1 Akademicheskaya Str., Kharkiv, 61108, Ukraine
e-mail: pppalval@gmail.com

As promising materials in the design of modern aircraft engines and gas turbine power plants, nickel-based single-crystal alloys are currently widely used, which are capable of operating under extreme conditions of high temperatures, high mechanical loads, and have high corrosion resistance and durability. The use of directionally solidified (DS) columnar grains, and later single crystal (SC) alloys, resulted in a significant increase in creep and crack resistance due to the elimination of weak grain boundaries oriented transverse to the load direction. An important factor is also the possibility of choosing the crystallographic direction of growth of <001> nickel alloy single crystals with the lowest modulus of elasticity along the turbine blades, which significantly increases the resistance to thermomechanical fatigue in regions with limited thermal expansion. In general, the absence of transverse grain boundaries, combined with a lower elastic modulus, leads to an increase in the durability of structural elements from 3 to 5 times [1].

Besides of orientation, the mechanical properties of single crystals can be affected by the dendritic structure of the alloys. Depending on the manufacturing and processing techniques chosen, products identical from a crystallographic point of view can have a different dendritic structure. In particular, the first-order dendrite axes can be located both parallel and perpendicular to the sample axis. The properties of alloys in these directions can also be different.

The study of the elastic and inelastic properties of materials can provide important and useful information about the effect of sample structure on the dynamic moduli of elasticity and sound absorption in crystals [2]. In this work, in the temperature range of 51–300 K, we have studied the elastic and inelastic characteristics of samples of the single-crystal Ni-35.6 wt.% W alloy both in amplitude independent and amplitude dependent ranges. Investigation of the acoustic properties of the alloy was carried out at frequencies of about 73 kHz using the two-component composite vibrator techniques [3]. Longitudinal standing waves were excited in the samples by the piezoelectric quartz transducers. Temperature and amplitude dependences of the logarithmic decrement and the dynamic Young's modulus were investigated. Samples in the form of rectangular rods with dimensions of 3x3x30 mm^3 were cut from the single crystal in such a way that their longitudinal axis coincided with the crystallographic direction <001>.

It is shown that the functional form of the obtained temperature dependences of the dynamic Young's modulus are corresponded to the classical concepts of the effect of thermal excitation of electrons and phonons on the elastic properties of a crystal. Dynamic effects associated with thermally activated dynamic relaxations of defect structure elements (so called internal friction peaks) were not detected in the whole temperature range studied.

The experimental results obtained in the work are discussed in the framework of the current theoretical treatments.

[1] D. V. V. Satyanarayana, N. Eswara Prasad. In: Aerospace Materials and Material Technologies, Ch. 9. Indian Institute of Metals Series, 2017, pp. 199-228.
[2] X. Tuo, Y. Liu, X. Wei, C. Xiao, X. Chen, W. Shi, L. Chen, L. Qian, Wear 571, 205862 (2025).
[3] V. D. Natsik, P. P. Pal-Val, S. N. Smirnov, Acoust. Phys. 44, 553-560 (1998).

Computational analysis of composite thermoelectric materials for energy conversion applications

R. G. Cherkez, O. M. Porubanyi

Yuriy Fedkovych Chernivtsi National University,101 Storozhynetska St., Chernivtsi, 58000, Ukraine
e-mail: r.cherkez@chnu.edu.ua

One of the promising approaches for improving the performance of thermoelectric materials is the development of composite structures that combine a thermoelectric matrix with secondary phases possessing different transport properties. The presence of such inclusions can significantly affect charge carrier transport and therefore modify the effective electrical and thermoelectric characteristics of the material [1-3]. In this work, a numerical investigation of the effective electrical conductivity of a thermoelectric composite was performed using the Representative Volume Element (RVE) approach. The simulations were carried out in the multiphysics modeling environment COMSOL Multiphysics, which enables coupled analysis of electrical and thermal transport processes in heterogeneous materials [4].

The numerical results reveal that the presence of insulating inclusions modifies the local electric field distribution within the composite. Electric current tends to circumvent low-conductivity regions, which leads to the formation of complex conduction pathways inside the matrix. As a consequence, the effective electrical conductivity of the composite decreases compared with the homogeneous thermoelectric material. The developed numerical model demonstrates that microstructural parameters such as inclusion size, volume fraction, and spatial distribution play a significant role in determining the effective transport properties of thermoelectric composites.

The presented modeling approach provides a useful tool for predicting the behavior of heterogeneous thermoelectric materials and may be applied for optimization of composite structures aimed at improving thermoelectric performance.

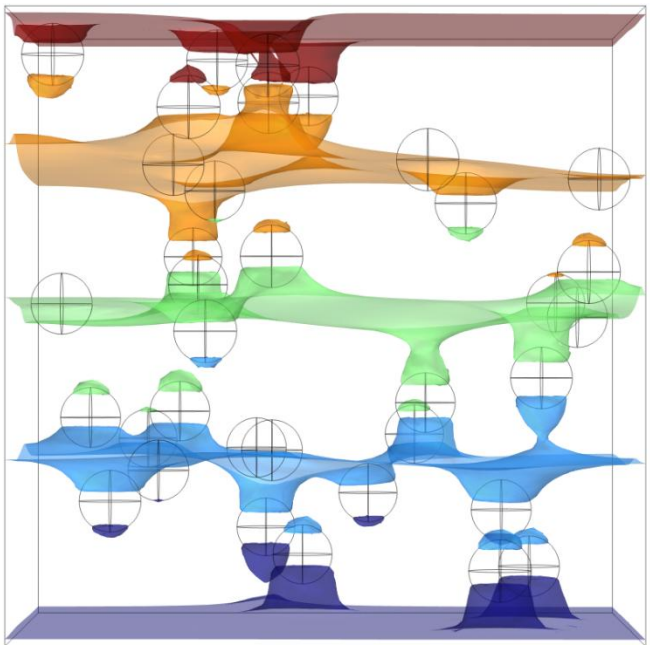

Fig. 1. Electric potential distribution inside the representative volume element of the thermoelectric composite obtained from numerical simulation.

[1] Z. L. Wang, T. Funada, T. Onda, Z.-C. Chen, Materials Today Physics 31, 100971 (2023). https://doi.org/10.1016/j.mtphys.2023.100971.
[2] M. A. Okirigiti, C. M. Kim, H. Choi, N. R. Alluri, K.-I. Park, Journal of Powder Materials 32, 1-15 (2025). https://doi.org/10.4150/jpm.2024.00395.
[3] L. Ferretti, P. Russo, J. Passaro, F. Nanni, S. D`Ascoli, F. Fabbrocino, M. Bragaglia, Materials 18, 3453 (2025). https://doi.org/10.3390/ma18153453.
[4] J. Pei, B. Cai, H.-L. Zhuang, J.-F. Li, Natl. Sci. Rev. 7, 1856–1858 (2020). https://doi.org/10.1093/nsr/nwaa259.

Multifunctional high-entropy alloy coatings for bioactive and corrosive environments: current research and future perspectives

B. Postolnyi[1,2,3], D. Mitrica[2], A. Sobetkii[2], L.-F. Mosinoiu[2], A. B. Talipova[4], L.-M. Cursaru[2], R. Basnukaeva[5], A. Pogrebnjak[2,3,6]

[1]Institute of Physics for Advanced Materials, Nanotechnology and Photonics, Faculty of Sciences of the University of Porto, 4169-007 Porto, Portugal
[2]National R&D Institute for Non−Ferrous and Rare Metals, 077145 Pantelimon, Romania
[3]Sumy State University, 116 Kharkivska st., 40007 Sumy, Ukraine
[4]Department of Biotechnology, Al-Farabi Kazakh National University, Almaty 050040, Kazakhstan
[5]B.Verkin Institute for Low Temperature Physics and Engineering of the NAS of Ukraine, 47 Nauky Ave., Kharkiv, 61103, Ukraine
[6]Institute of Materials, Faculty of Materials Science and Technology in Trnava, Slovak University of Technology in Bratislava, 917 24, Trnava, Slovakia
e-mail: b.postolnyi@gmail.com

High-entropy alloys (HEAs) provide a versatile platform for designing multifunctional materials for harsh and complex environments. Functionalization through compositional complexity enables simultaneous tuning of mechanical performance, corrosion resistance, and intrinsic antimicrobial activity, offering a materials-based strategy to control degradation processes arising from coupled chemical and biological interactions in bioactive and corrosive environments, including microbiologically influenced corrosion (MIC) [1].

Recent developments show that HEA coatings, particularly in systems such as Cu_x–Cr–Fe–Mn–Ni, can achieve a synergistic combination of mechanical robustness, corrosion resistance, and bioactive functionality [2,3]. Expanding this design space through the incorporation of refractory and high-melting-point elements (e.g., W, Nb, Ta, Mo, Re, Ti) further enhances hardness, thermal stability, and functional response, while enabling additional control over surface reactivity and antimicrobial behavior. These results highlight the central role of compositional and microstructural design in governing multifunctional performance and support the use of HEA coatings as an intrinsic, materials-based approach for advanced surface protection.

Future progress relies on accelerating exploration of vast compositional spaces and addressing multi-objective optimization challenges. Artificial intelligence (AI) and materials acceleration platforms (MAPs) provide a pathway to integrate data-driven modelling with experimental validation, enabling more efficient discovery and optimization of HEAs. Advancing such frameworks will be essential for developing next-generation coatings for demanding bioactive and corrosive environments across marine, energy, and industrial applications.

[1] B. Postolnyi, V. Buranych, L.-M. Cursaru, R.-R. Piticescu, A. Pogrebnjak, Antimicrobial high-entropy alloys as a new player against microbiologically influenced corrosion: Recent advances and comparison with steels and other conventional alloys, Appl. Phys. Rev. 12, 021325 (2025). https://doi.org/10.1063/5.0228866.
[2] A. Sobetkii, L.-F. Mosinoiu, S. Caramarin, D. Mitrica, L.-M. Cursaru, A.-C. Matei, I.-A. Tudor, B.-A. Serban, M. Ghita, N. Vitan, J. Witt, O. Ozcan, B. Postolnyi, A. Pogrebnjak, Deposition and Characterization of Cu-Enhanced High-Entropy Alloy Coatings via DC Magnetron Sputtering, Appl. Sci. 15, 1917 (2025). https://doi.org/10.3390/app15041917.
[3] L.F. Mosinoiu, A. Sobetkii, B.A. Serban, L.M. Cursaru, A.C. Matei, M. Ghita, N. Vitan, S. Caramarin, D. Mitrica, A. Pogrebnjak, B. Postolnyi, Chemical and structural characteristics of copper added high entropy alloys for corrosive applications, J. Mater. Res. Technol. 35, 6261–6268 (2025). https://doi.org/10.1016/j.jmrt.2025.02.241.

Dynamics of thermally activated processes in Cu-Mo vacuum condensates

V. Riaboshtan[1], A. Zubkov[1], M. Zhadko[2], N. Pogrebnoy[1]

[1]National Technical University "Kharkiv Polytechnic Institute",
2, Kyrpychova str., 61002 Kharkiv, Ukraine
[2]Department of Physics and NTIS – European Centre of Excellence, University of West Bohemia,
Univerzitní 8, 306 14, Plzeň, Czech Republic
e-mail: obibobbivalkinobi@gmail.com

The study of Cu-Mo composite materials can generally be divided into two major areas: the fabrication of Cu-Mo mixture films and coatings by various methods, and the production of layered structures [1]. There are also studies focused on the synthesis of bulk condensates and the enhancement of their corrosion and erosion resistance [2, 3]. These findings suggest that molybdenum tends to interact with the grain boundaries of dispersed copper. Therefore, the aim of this work is to investigate the dynamics of processes occurring during the annealing of Cu-Mo composites.

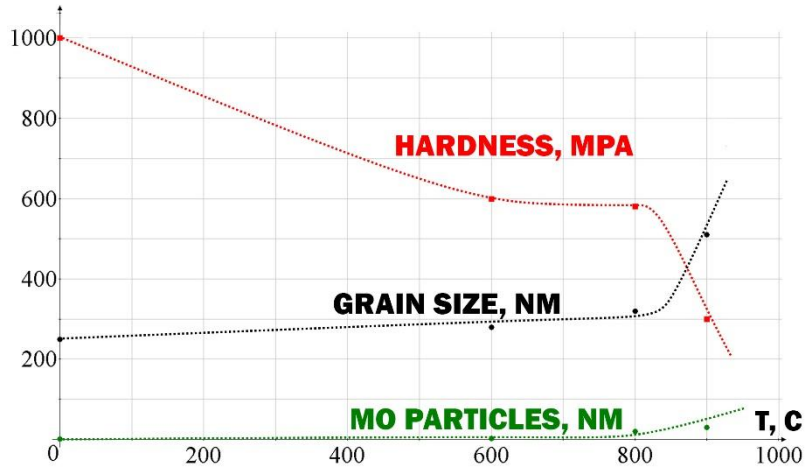

Figure 1. Composite plot showing the evolution of selected structural parameters (grain size and size of Mo particles, [nm]) and hardness (MPA) as a function of annealing temperature.

The results of the study have shown that the thermal stability of Cu-0.3%Mo condensates depends on the distribution pattern of molybdenum along the grain surfaces of the copper matrix and on the nature of the bonding that molybdenum forms with the base metal. A composite plot was also constructed to illustrate the dynamics of selected structural parameters as a function of annealing temperature (Fig. 1). Based on this plot, it can be inferred that rapid grain growth in the copper matrix and its softening commence when the average particle size of molybdenum exceeds 20 nm. This occurs at the point when lateral diffusion of molybdenum atoms along the grain boundaries leads to depletion of these boundaries in molybdenum.

[1] V. Molahalli, A. Sharma, K. Bijapur, G. Soman, A. Shetty, B. Sirichandana, B.G. M. Patel, N. Chattham, G. Hegde, Properties, synthesis, and characterization of CU-Based nanomaterials. In ACS symposium series, 1–33 (2024). https://doi.org/10.1021/bk-2024-1466.ch001.
[2] N. I. Grechanyuk, and V. G. Grechanyuk, Mechanical Properties Of Dispersed And Laminar Composite Materials On Copper And Molybdenum Base, Electrometallurgy Today 2, 43-49 (2019). https://doi.org/10.15407/SEM2019.02.07.
[3] S. Islak, U. Çalıgülü, H. R. H. Hraam, C. Özorak, V. Koç, Electrical conductivity, microstructure and wear properties of Cu-Mo coatings, Res. Eng. Struct. Mat. 5, 137-146 (2019). http://dx.doi.org/10.17515/resm2018.58is0716.

Phonon engineering in graphene oxide: effects of pressure and thermal reduction

O. Romantsova[1,2], D. Szewczyk[1], Yu. Horbatenko[2], M. Vinnikov[2], S. Cherednichenko[2], O. Kryvchikov[1,2]

[1]Institute of Low Temperatures and Structure Research, Polish Academy of Sciences, 2 Okólna str., Wrocław, 50-422, Poland
[2]B.Verkin Institute for Low Temperature Physics and Engineering of NAS of Ukraine, 47 Nauky Ave., Kharkiv, 61103, Ukraine
e-mail: romantsova@ilt.kharkov.ua

Graphene oxide (GO) and its thermally reduced derivatives (trGO) exhibit a wide range of vibrational behaviors arising from structural disorder, oxygen functional groups, and variable interlayer coupling [1, 2]. Understanding of how processing parameters influence their low-energy phonon spectra is essential for designing carbon-based materials with tailored thermal properties. In this work, we systematically investigate the effects of both mechanical compaction and thermal annealing on the low-temperature heat capacity of GO.

GO synthesized via modified Hummers method was thermally reduced at 300°C, 500°C, and 700°C, leading to controlled removal of oxygen groups and progressive graphitization. Samples compacted under pressures from 0.75 to 1.25 GPa provided insight into the mechanical tuning of interlayer interactions. Low-temperature calorimetry (1.8–100 K), complemented by X-ray diffraction and TEM, reveals that the total heat capacity can be decomposed into four components: a Schottky-type anomaly, a linear T-term, a Debye cubic T^3 contribution, and a negative T^5 term associated with flexural ZA phonons.

It is observed that thermal annealing strongly suppresses both Debye and flexural phonon contributions, indicating reduced disorder and enhanced stacking order with increasing graphitization. In contrast, the linear term remains nearly invariant, suggesting an intrinsic origin related to persistent low-energy excitations in quasi-2D GO layers. The Schottky anomaly displays a pronounced dependence on compaction pressure, highlighting its sensitivity to interlayer contacts, residual oxygen groups, and defect-related two-level systems.

A universal power-law correlation between Debye and ZA phonon coefficients places graphene oxide within the same vibrational framework as carbon nanotubes and graphite, demonstrating that low-temperature calorimetry serves as a precise probe of dimensionality, disorder, and interlayer coupling. These results provide a predictive foundation for engineering phonon spectra in graphene-based materials, with implications for cryogenic applications, composite design, and nanoscale thermal management.

O. Romantsova gratefully acknowledges the financial support from the project financing NCN MINATURA 9 2025/09/X/ST3/00153.

[1] A. A. Balandin, Thermal properties of graphene and nanostructured carbon materials, Nat. Mater. 10, 569–581 (2011). http://dx.doi.org/10.1038/nmat3064.
[2] G. Yang, L. Li, W. B. Lee, and M. C. Ng, Structure of graphene and its disorders: a review, Sci. Technol. Adv. Mater. 19, 613–648 (2018). https://doi.org/10.1080/14686996.2018.1494493.

Features of the temperature dependence of microhardness in high-entropy alloys $CoCrFeNiMnV_x$ (x = 0–2)

H. V. Rusakova[1], L. S. Fomenko[1], S. V. Lubenets[1], O. D. Tabachnikova[1], M. A. Tikhonovsky[2], I. F. Kislyak[2]

[1]B.Verkin Institute for Low Temperature Physics and Engineering of NAS of Ukraine, 47 Nauky Ave., Kharkiv, 61103, Ukraine
[2]National Science Center "Kharkiv Institute of Physics and Technology" of NAS of Ukraine, 1 Akademichna Str., Kharkiv, 61108, Ukraine
e-mail: rusakova@ilt.kharkov.ua

The main purpose of this study was to investigate the micromechanical properties of Cantor alloy, doped with vanadium, in the temperature range of 77–293 K. Depending on the phase composition of the alloys, which changes with vanadium content, the studied alloys can be divided into three main groups. (1) Alloys of the first group (x = 0–0.4) consist mainly of a single ductile FCC phase completely without or with a minimal amount of the tetragonal σ phase. (2) Alloys of the second group (x = 1.25–2) consist mainly of a single brittle tetragonal σ phase with a low content of FCC phase. (3) Alloys of the third group (x = 0.5–1) are two-phase alloys with comparable amounts of both (FCC and tetragonal) phases [1]. On the figure, one can see that with a temperature decrease from room temperature to 77 K, the microhardness of alloys from the first group monotonically increases by about 45% that indicates the thermally-activated character of plastic deformation of the material under the indenter. It turns out that its microhardness and yield strength values are about the corresponding values of the Cantor alloy CoCrFeNiMn [2, 3].

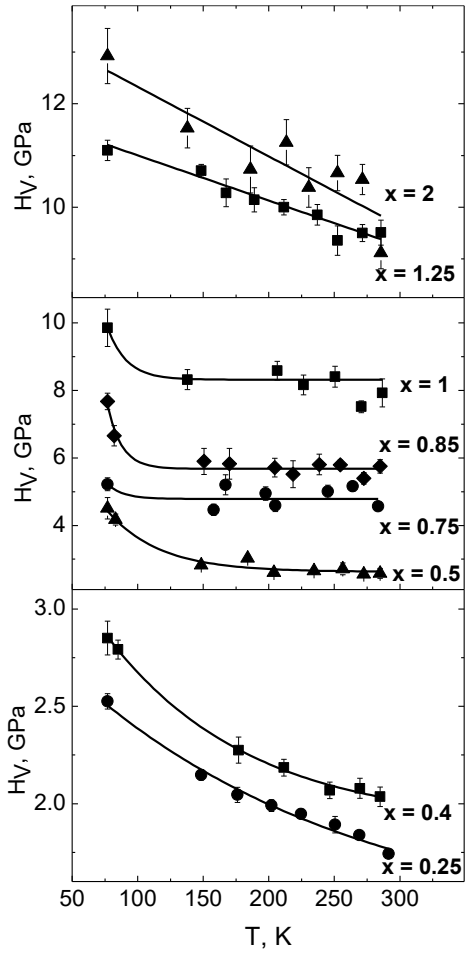

The microhardness value of alloys from the second group increases monotonically by about of 17–42% with a temperature decrease from room temperature to 77 K. A completely different microhardness behavior was observed in the case of the two-phase alloys from the third group. Specifically, in a fairly wide temperature range (150–293 K), the average microhardness remains practically unchanged. Possible reasons for this unusual microhardness behavior of two-phase alloys are discussed.

Furthermore, the effect of vanadium content on the microhardness was analyzed. At all temperatures studied, the microhardness weakly depends on the vanadium content at small and large values of x. At the same time, a sharp increase in microhardness was revealed, starting from x ~ 0.5, which is associated with the formation of a large amount of the hard intermetallic σ phase.

[1] N. D. Stepanov, D. G. Shaysultanov, G. A. Salishchev et al., J. Alloys and Compounds 628, 170-185 (2015). http://dx.doi.org/10.1016/j.jallcom.2014.12.157.
[2] H. V. Rusakova, L. S. Fomenko, S. N. Smirnov et al., Mater. Sci. Eng. A 828, 142116 (2021). http://dx.doi.org/10.1016/j.msea.2021.142116.
[3] E. D. Tabachnikova, A. V. Podolskiy, M. O. Laktionova et al., J. Alloys and Compounds 698, 501-509 (2017). http://dx.doi.org/10.1016/j.jallcom.2016.12.154.

The study of the effect of graphene oxide additive on the thermal conductivity of epoxy composites

V. V. Sagan, Yu. V. Horbatenko, A. I. Krivchikov

B. Verkin Institute for Low Temperature Physics and Engineering of the NAS of Ukraine,
47 Nauky Ave., Kharkiv, 61103, Ukraine
e-mail: sagan@ilt.kharkov.ua

Polymeric composite materials are important components in modern technologies due to their combination of low density, chemical resistance, and good mechanical properties. However, one of the main limitations of their application is low thermal conductivity, which typically ranges from 0.1 to 0.5 W/(m·K). This restricts the effective use of polymers in heat dissipation systems and electronic devices.

One of the most common approaches to improving the thermal conductivity of polymers is the incorporation of thermally conductive fillers. These include ceramic materials (Al_2O_3, AlN, BN, SiO_2) [1], metals (Cu, Ag) [2], and carbon-based nanomaterials (graphite, graphene, carbon nanotubes, etc.) [3-4]. However, significantly increasing the thermal conductivity of composites using traditional methods generally requires high filler concentrations, which may lead to a deterioration in mechanical properties, an increase in density, and the emergence of interfacial thermal resistance due to the increase in the number of interfaces that act as phonon scattering centers.

Nanostructured carbon materials, in particular graphene and its derivatives, have high theoretical thermal conductivity, which is of interest for improving heat transfer in polymer composites. However, the introduction of graphene into polymer matrices causes problems of agglomeration and incompatibility, which reduces the efficiency of heat transfer. Expanded graphite, graphene nanoplatelets and graphene oxide can be used as alternative fillers.

The mechanism of heat transfer in polymer materials differs from that in crystalline structures, where heat is transferred by phonons. In polymers, heat transfer is also primarily phononic, but the chaotic orientation and entanglement of polymer chains lead to significant phonon scattering, which results in low thermal conductivity. Therefore, one of the main tasks is to enhance the thermal conductivity of polymer composites, even at low filler concentrations, by minimizing this scattering effect.

The aim of this study was to investigate the effect of the concentration of a carbon-based filler-graphene oxide on the thermal conductivity of an epoxy resin ED-20-based polymer composite (diglycidyl ether of bisphenol-A, DGEBA).

Experimental results showed that the introduction of small concentrations of graphene oxide leads to a noticeable improvement in heat transfer in the epoxy composite, indicating the promising use of graphene derivatives as efficient thermally conductive fillers in polymer materials.

This work was supported by the National Research Foundation of Ukraine (Project №. 2023.03/0012).

[1] Z. Wang, et al., Adv. Funct. Mater. 33, 2301549 (2023). http://dx.doi.org/10.1002/adfm.202301549.
[2] Y.-C. Li, N. Chu, F.-L. Jin, S.-J. Park, Polymer 313, 127678 (2024). http://dx.doi.org/10.1016/j.polymer.2024.127678.
[3] Z. Ebrahim Nataj, Y. Xu, D. Wright, J. O. Brown, J. Garg, X. Chen, F. Kargar, A. A. Balandin, Nat. Commun. 14, 3190 (2023). http://dx.doi.org/10.1038/s41467-023-38508-3.
[4] H. Yang, Z. Deng, M. Shi, Z. Huang, Polymers 17, 2342 (2025). http://dx.doi.org/10.3390/polym17172342.

Low-temperature mechanical relaxation in commercially pure titanium

Y. Semerenko[1], V. Natsik[1], N. Galtsov[1], D. Hurova[1], T. Bednarchuk[2], P. Zinoviev[1], V. Zoryansky[1], V. Moskalenko[1], R. Smolianets[1], A. Smirnov[1], Y. Pohribnaya[1], N. Aksenova[3]

[1]B.Verkin Institute for Low Temperature Physics and Engineering of NAS of Ukraine, 47 Nauky Ave., Kharkiv, 61103, Ukraine
[2]Institute for Low Temperatures and Structure Research, Polish Academy of Sciences, P.O. Box 1410, 50-950 Wroclaw, Poland
[3]V.N. Karazin Kharkiv National University, 4 Svobody Sq., 61022 Kharkiv, Ukraine
e-mail: semerenko@ilt.kharkov.ua

In the range of 5-325 K, the temperature dependence of acoustic properties – absorption and dynamic Young's modulus – was studied in nanocrystalline and fine-crystalline commercially pure titanium VT1-0. Measurements were performed using resonance mechanical spectroscopy at 2.4-3.7 kHz. The influence of grain size on low-temperature acoustic behavior was examined.

Samples with varying grain sizes were produced by severe plastic deformation through rolling at cryogenic (100 K) and room (290 K) temperature to true strains of 1.20-1.90, followed by annealing at 525 K, 720 K, and 940 K. Their structures were characterized by electron microscopy and X-ray diffraction.

It has been established that severe plastic deformation by rolling leads to pronounced grain fragmentation in the initial titanium material. In the substructure of specimens deformed at 100 K, coherent scattering regions (CSRs) with dimensions of approximately 30-50 nm predominate. In contrast, after deformation at 290 K, the CSRs size ranges from submicron dimensions to several microns

The formation of a nanostructured state during cryogenic deformation is accompanied by a reduction in the dynamic Young's modulus by approximately $\Delta E \approx 0.8\text{-}1.2\%$ across the entire investigated temperature range. Moreover, the magnitude of ΔE increases with the degree of cryodeformation. Recrystallization annealing at 940 K restores the modulus to its original values.

Intense plastic deformation was found to induce an acoustic anomaly namely an absorption peak P_1 observed at 150-230 K. The transition from fine- to nanocrystalline states introduced an additional absorption peak P_2, at 43-78 K. A microscopic dislocation model was proposed to explain these phenomena [1]. The activation parameters of P_1 correspond to thermally activated detachment of dislocation segments from local defects, consistent with the Koiwa-Hasiguti peak. This relaxation mechanism involves the thermally activated detachment of dislocation segments from local structural defects, such as impurity atoms, interstitials, or vacancies, and is a well-established source of internal friction peaks in hexagonal close-packed metals. The identification with this relaxation process underscores the strong role of defect-dislocation interactions in shaping the acoustic and elastic response of cryogenically deformed titanium. The activation parameters of this peak are estimated as an activation energy of 0.38 eV and an attempt period of $2 \cdot 10^{-13}$ s.

In contrast, the activation parameters of P_2 (this peak is associated with an activation energy of approximately 0.03 eV and an attempt period of $2 \cdot 10^{-11}$ s) reflect dislocation motion across a Peierls barrier via thermally activated kink pair formation, analogous to Bordoni peaks observed in fcc crystals.

This study demonstrates that grain refinement and deformation significantly affect the acoustic response of titanium, revealing distinct mechanisms of dislocation dynamics at different temperature ranges.

[1] Y. Semerenko, V. Natsik, E. Tabachnikova, Yi Huang, and Terence G. Langdon. Metals 14, 778 (2024). https://doi.org/10.3390/met14070778.

Microstructure and low temperature mechanical properties of naturally aged micrograined polycrystals of Al-Li alloy

S. Shumilin[1], T. Hryhorova[1], P. Zabrodin[1,2], D. Drozdenko[3]

[1]B.Verkin Institute for Low Temperature Physics and Engineering of NAS of Ukraine, 47 Nauky Ave., Kharkiv, 61103, Ukraine
[2]Institute of Theoretical and Applied Mechanics, Czech Academy of Sciences, Prosecka 809/76, 190 00 Prague, Czech Republic
[3]Faculty of Mathematics and Physics, Department of Physics of Materials, Charles University, Ke Karlovu 5, Prague, 121 16, Czech Republic
e-mail: shumilin@ilt.kharkov.ua

Recently, the extensive use of severe plastic deformation (SPD) methods, including angular hydrostatic extrusion (AHE) and equal-channel angular pressing (ECAP), has allowed the formation of a whole class of metallic materials with an ultrafine-grained (UFG) structure, the strength of which exceeds those of conventional materials [1]. Metals processed by the SPD method have a high dislocation density and high residual stresses. The microstructures of such UGF materials, caused by the storage and dynamic recovery of dislocations, are at most in a metastable non-equilibrium state with limited thermal and mechanical stability [1-3]. That is, such microstructures can be easily changed by dynamic recovery and recrystallization under the action of an applied load even at room temperature, which is a critical problem for their practical engineering applications.

The aim of this work was to analyze the effect of natural aging on the mechanical stability at temperatures of 77 K and 295 K of an aluminum-lithium alloy processed by the AHE method.

The microstructure and low-temperature plasticity of micrograined polycrystals of solid solution Al-Li alloy after long-term natural aging (atmospheric pressure in air at room temperature) were studied. The micrograined state of the samples was obtained by SPD method, namely by AHE of 4 and 6 passes. The influence of the microstructure in the alloy after natural aging on the strain hardening rate of UFG Al-Li alloy was studied.

It is shown that with decreasing temperature, the yield strength of $\sigma_{0.2}$ and the strain hardening coefficient θ of the studied UFG samples increase both in the initial state and after natural aging. The increase in the hardening rate θ can be explained by the higher stress required for the movement of dislocations at low temperatures, which is characteristic of the thermally activated interaction of dislocations with local deformation defects formed at the AHE stage. At a temperature of 295 K, the mechanical characteristics of the samples, both for 4 and for 6 passes of AHE, after natural aging, almost do not change. However, at a temperature of 77 K, the mechanical characteristics of the samples after aging decrease compared to the initial state. At the same time, this decrease in stress is accompanied by an increase in the average strain hardening coefficient θ by approximately 10-12% at 77 K, both for 4 and for 6 passes.

The obtained results are explained by the significant effect of temperature on the rate of accumulation and annihilation of dislocations under conditions of high density of deformation defects in UFG materials processed by the SPD method.

[1] Y. Estrin, A. Vinogradov, Acta Materialia 61, 782-817 (2013). https://doi.org/10.1016/j.actamat.2012.10.038.
[2] Y. H. Zhao, X. Z. Liao, Z. Jin, Acta Materialia 52, 4589-4599 (2004). http://dx.doi.org/10.1016/j.actamat.2004.06.017.
[3] D. Jiang, J. Ning, J. Sun, Z. Min, Yi Hou, Transactions of Nonferrous Metals Society of China 18, 248-254 (2008). https://doi.org/10.1016/S1003-6326(08)60044-8.

Dielectric properties and the pressure-temperature phase diagram of layered $CuInP_2S_6$ crystals

V. S. Shusta, P. P. Guranych, A. G. Slivka, V. Y. Biganych, P. P. Huranych

Uzhhorod National University, 3 Narodna Sq., Uzhhorod, 88000, Ukraine
e-mail: volodymyr.shusta@uzhnu.edu.ua

Crystals of $CuInP_2S_6$ belong to the family of layered van der Waals materials that attract considerable attention due to the combination of ferroelectric ordering and ionic conductivity. Their unique physical properties arise from the fact that ferroelectric ordering occurs at room temperature and is preserved down to thicknesses of only a few nanometers, making these materials highly promising for next-generation electronic, optoelectronic, and sensing devices.

The work presents the results of studies on the hydrostatic pressure effect on the dielectric parameters and specific features of the *p–T* phase diagram of $CuInP_2S_6$ crystals. The investigations were performed on single crystals grown by the Bridgman method. The complex dielectric permittivity was measured in the temperature range of 77–450 K at a frequency of 1 MHz using a high-pressure chamber in the range of p = 0–6000 atm.

Based on baric studies, the *p–T* phase diagram of $CuInP_2S_6$ crystals was constructed. It was established that in the initial pressure region up to p = 2600 atm, the dependence of the PT temperature on pressure is linear, with an exceptionally high positive pressure coefficient of 210 K/GPa. Such a value is atypical for order–disorder type transitions and indicates that even a small applied pressure can push the ferroelectric state far above room temperature. At higher pressures (p > 2600 atm), deviations of the phase boundary from linear behavior are observed. This behavior is evidently related to the anomalous enhancement of polarization in van der Waals $CuInP_2S_6$ under pressure in the range from 0.26 to 1.40 GPa [1, 2].

Above the phase transition temperature, the dielectric permittivity follows the Curie–Weiss law. Increasing pressure leads to a rise in the Curie–Weiss constant, and a distinctive kink is observed near 2600 atm, which correlates with the deviation from linearity in the *p–T* phase diagram.

In the low-temperature region (T < 200 K), relaxation behavior of the dielectric permittivity is detected in $CuInP_2S_6$ crystals. Under pressure, this relaxation anomaly becomes more pronounced and shifts toward lower temperatures, which is associated with changes in the lifetime of relaxators and with a reduction in potential barriers for thermally activated hopping polarization.

The conducted studies confirm the complex nature of the phase transitions in $CuInP_2S_6$ crystals, where the baric evolution of dielectric properties is determined both by structural changes and by the influence of the mobile copper ionic subsystem.

[1] X. Yao, Y. Bai, C. Jin, X. Zhang, Q. Zheng, Z. Xu, L. Chen, S. Wang, Y. Liu, J. Wang, and J. Zhu, Anomalous polarization enhancement in a van der Waals ferroelectric material under pressure, Nature Communications 14, 4301 (2023). http://dx.doi.org/10.1038/s41467-023-40075-6.
[2] Y. Li, Y. Luo, X. Yao, Y. Bai, J. Wang, and J. Zhu, Phase diagram of $CuInP_2S_6$ across wide temperature and pressure ranges. Appl. Phys. Rev. 12, 041425 (2025). https://doi.org/10.1063/5.0299899.

Synergistic effect of the influence of atomic oxygen and ultraviolet radiation on polyimides

V. A. Shuvalov, Yu. P. Kuchugurnyi, I. M. Chumachenko, S. V. Prannik, N. P. Reznichenko, B. V. Yurkov

Institute of Technical Mechanics of NAS of Ukraine and SSA of Ukraine, 15 Leshko-Popel St., Dnipro, 49005, Ukraine
e-mail: vashuvalov@ukr.net

The synergistic effect of accelerated degradation, mass loss, increased sputtering and erosion coefficients of polyimides kapton-H, PM-A, and PM-1E – engineering polymers of rocket and space technology products – was experimentally revealed under the simultaneous action of atomic oxygen (AO) flows and vacuum ultraviolet irradiation (VUV).

It was established that the polyimides are inert to the VUV irradiation effects under stationary conditions in vacuum (at pressure of $\sim 1 \cdot 10^{-5}$ Pa, oil-free pumping).

Irradiation was carried out using three VMF-25 hydrogen lamps with a radiation flux density on the polymer sample surface of $\Phi_v \approx 3.9$ mW/cm^2 at wavelengths of $\lambda_v \approx$ 135-165 nm (VUV) and $\overline{\Phi}_v \approx 0.45$ mW/cm^2 at $\overline{\lambda}_v \approx$ 165-380 nm (UV). A flux of AO ions with a velocity of $U_{AO} \approx 7.6$ km/s and concentrations of $N_{AO} \approx 5\ 10^{13} - 2\ 10^{16}$ m^{-3} (AO fluence from 10^{16} to 10^{21} cm^{-2}) created a gas-discharge accelerator with self-acceleration of plasma.

Studies of the mass loss ΔM_{AO} and the erosion coefficient Y_{AO} in a vacuum chamber with a gas leakage and an operating pressure of $\sim 1 \cdot 10^{-3}$ Pa showed that chemical etching with AO ions being the one among two mechanisms of destruction of polyimides predominates over kinetic sputtering.

Molecular oxygen does not participate in the destruction of polymers. Polymer samples with a thickness of 0.05 mm and a diameter of 45 mm were used. Under VUV irradiation, the sample surface temperature was $T_W \approx 297$ K, while the combined simultaneous action of AO and VUV fluxes (ΣAK+VUV) leads to $T_W \approx 304$ K. The threshold ratio value of the VUV energy flux Φ_v to the AO flux density Φ_{AO} was determined. For kapton-H, PM-A, and PM-1E polymers, the threshold value Φ_v / Φ_{AO} that determines the region of existence of the synergistic effect under the influence of ΣAK+VUV on polyimides is $\geq 7.1 \cdot 10^{-15}$ mJ/atomO. In this case, the dependence holds for the mass loss ΔM_Σ and the erosion coefficient Y_Σ (the index Σ means ΣAK+VUV) is $\Delta M_\Sigma / \Delta M_{AO} = Y_\Sigma / Y_{AO} \approx 9.891 \cdot 10^8 \left(\beta \Phi_v / \Phi_{AO}\right)^{0.635}$, where $\beta = 1$ atomO/mJ. At an average level of solar activity, the region of existence of the synergistic effect of ΣAK+VUV on structural polyimides corresponds to an altitude of 460 km in the Earth's upper atmosphere.

Correlation morphological analysis of secondary phase inclusions in $Ge_{1-x-y}Sn_xMn_yTe$

V. E. Slynko[1], V. I. Ivanov[1], O. A. Sydor[1], V. M. Vodopyanov[1], L. Kilanski[2], S. Piotrowska[2]

[1]Chernivtsi Branch of Frantsevych Institute for Problems of Materials Science, NASU,
5 Iryny Vilde St., Chernivtsi, 58001, Ukraine
[2]Institute of Physics, Polish Academy of Sciences,
Aleja Lotnikow 32/46, PL-02668 Warsaw, Poland
e-mail: slynko.vasily@gmail.com

Introduction. The interpretation of magnetic phenomena in IV-VI diluted magnetic semiconductors (DMS) often rests on the assumption of host-lattice homogeneity. However, thermodynamic instabilities during synthesis can lead to phase separation, creating a nano-micro-composite structure. This work proposes a method to identify and quantify these "hidden" phases to ensure the correct interpretation of low-temperature magnetic responses.

Methodology. We developed a *Correlation Morphological Analysis (CMA)* based on a dataset of 160+ high-resolution SEM images (1280×960 px). By correlating grayscale contrast with localized micro-XRF (EDS) data, we reconstructed the volumetric distribution of secondary phases using Delesse's principle ($\Phi \approx A_{inc}/A_{total}$), which is statistically valid for randomly oriented inclusions [1]. Here Φ – volumetric fraction of the secondary phase inclusions; A_{inc} – total area of inclusions measured on the SEM micrographs; A_{total} – total analyzed area of the sample surface.

Results. Three types of structural anomalies were identified across the $Ge_{1-x-y}Sn_xMn_yTe$ sample series (1292–1295) obtained from ingots grown by the vertical Bridgman method:

1. Stoichiometric ditellurides $(Ge,Sn,Mn)Te_2$ (Te ≈ 65%). These result from *cationic sublattice degradation* – a localized expulsion of Mn and Sn from the NaCl-type lattice to minimize Gibbs free energy $G = H - T \times S$ (where H – enthalpy, T – absolute temperature, S – entropy).

2. Te-rich eutectic enclaves (Te ≈ 75%). These represent residues of the melt (eutectic point ≈ 375 °C [2]), forming non-magnetic "ballast" in inter-dendritic spaces. According to the Ge–Te phase diagram, the eutectic point corresponds to a composition of ≈85 at. % Te and 15 at. % Ge.

3. Defective Matrix (Te ≈ 56÷62%) saturated with cation vacancies (V_{Ge}).

Table. Volumetric and compositional parameters of micro-inclusions

Ingot	Dominant phase	Te (at. %)	Size (μm)	Vol. (%)
1292	$(Ge,Sn,Mn)Te_2$ + Te	65.0÷75.0	5÷15	5÷7
1293	$(Ge,Sn,Mn)Te_2$	≈ 64.0	2÷8	3÷4
1294	V_{Ge}-rich matrix	56.0÷66.0	3÷10	4÷5
1295	Mn-rich ditelluride	≈ 65.5	2÷12	4÷6

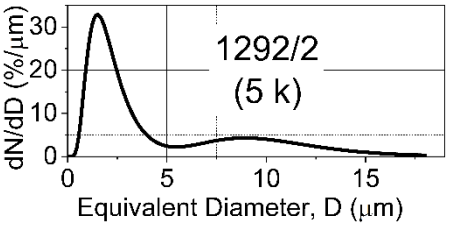

Conclusions. The identified micro-inclusions (3–7% vol.) act as a static antiferromagnetic background *without altering the fundamental magnetic behavior* of the DMS matrix. Identifying this composite nature is a prerequisite for "virtual purification" (deconvolution) of the magnetic signal. This approach effectively eliminates secondary "ballast" effects, thereby enabling a more rigorous validation of advanced dynamic cluster model (0D–3D) in $Ge_{1-x-y}Sn_xMn_yTe$ systems [3].

[1] E. E. Underwood, Quantitative Stereology for Microstructural Analysis, in: Microstructural Analysis, Springer, pp. 35–66 (1970). https://doi.org/10.1007/978-1-4615-8693-7_3.
[2] H. Okamoto, Ge-Te (Germanium-Tellurium), J. Phase Equilib. 21, 496 (2000). https://doi.org/10.1361/105497100770339789.
[3] V. Slynko et al., Dynamic cluster magnetic subsystems in diluted magnetic semiconductor $Ge_{1-x-y}Sn_xMn_yTe$, Fiz. Nizk. Temp. 52, 290 (2026) [Low Temp. Phys. 52, 290 (2026)]. https://doi.org/10.1063/10.0042378.

Refined 0D–3D dynamic cluster model of magnetic susceptibility in $Ge_{1-x-y}Sn_xMn_yTe$: the role of secondary phase microinclusions

V. E. Slynko[1], M. V. Tovarnitskii[1], A. V. Zaslonkin[1], V. V. Netyaga[1], L. Kilanski[2], S. Piotrowska[2]

[1]Chernivtsi Branch of Frantsevych Institute for Problems of Materials Science, NASU, 5 Iryny Vilde St., Chernivtsi, 58001, Ukraine
[2]Institute of Physics, Polish Academy of Sciences, Aleja Lotnikow 32/46, PL-02668 Warsaw, Poland
e-mail: slynko.vasily@gmail.com

The complex nature of the magnetic response in diluted magnetic semiconductors (DMS) $Ge_{1-x-y}Sn_xMn_yTe$, particularly the anomalous double-peaked temperature dependence of the dynamic magnetic susceptibility $\chi_{AC}(T)$, has been previously described within the framework of a dynamic 0D–3D cluster magnetic subsystem model [1]. While the initial theoretical approach successfully parameterized the macroscopic magnetic behavior, the microscopic mechanism driving the inter-cluster interactions requires refinement to avoid overestimating the role of bulk thermal lattice vibrations. Recent comprehensive micro-XRF mapping of DMS $Ge_{1-x-y}Sn_xMn_yTe$ crystals (specifically, samples from ingot 1292) has revealed the physical origin of these magnetic anomalies. The data unambiguously demonstrate the presence of structural micro-inhomogeneities. Instead of an idealized homogeneous matrix, the material contains localized microregions with pronounced deviations from stoichiometry, primarily characterized by an enriched tellurium content (reaching 65.0–75.0 at.% Te, in stark contrast to the nominal ~50 at.% of the host lattice). These secondary phase microinclusions exhibit typical dimensions ranging from 5 to 15 μm and occupy a volumetric fraction of approximately 5–7%.

Typical secondary phase microinclusions (enriched Te) in the $Ge_{1-x-y}Sn_xMn_yTe$ matrix (ingot 1292).

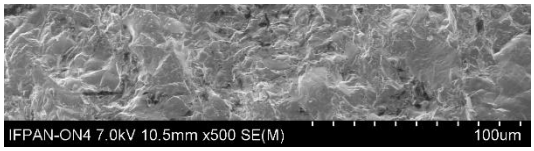

The formation of these Te-enriched microinclusions is an inevitable consequence of the crystal growth thermodynamics. Specifically, they arise due to compositional instabilities and segregation processes in the melt [2], which lead to microscopic fluctuations in the composition and density of *low-temperature eutectics* throughout the entire crystallization process. Therefore, absolute spatial homogeneity in these quaternary solid solutions is thermodynamically unattainable.

Recognizing this intrinsic micro-heterogeneity allows for a critical enhancement of the 0D–3D cluster model. The primary driver of the complex magnetic response $\chi_{AC}(T)$ is not the uniform thermal vibration of an ideal lattice, but rather the interface effects at the boundaries between the Te-enriched microinclusions and the main matrix. These boundaries act as intense centers for phonon scattering. Furthermore, the local lattice strain at these interfaces causes a sharp, exponential dependence of the p-d exchange interaction constant (J_{pd}) on the overlap of wave functions [3]. Even minute displacements of magnetic ions (Mn^{2+}) within these highly strained boundary regions result in significant modulations of the local magnetic order.

Thus, the refined 0D–3D cluster model, grounded in direct micro-XRF evidence, demonstrates that the macroscopic magnetic anomalies in $Ge_{1-x-y}Sn_xMn_yTe$ are governed by the dynamic interplay and boundary scattering effects between structurally distinct, thermodynamically inevitable micro-phases, rather than purely by uniform thermal lattice dynamics.

[1] V. Slynko et al., Low Temp. Phys. 52, 262 (2026). https://doi.org/10.1063/10.0042378.
[2] P. Rudolph, M. Mühlberg, Mater. Sci. Eng. B 16 (1-3), 8-16 (1993). https://doi.org/10.1016/0921-5107(93)90005-8.
[3] A. Abragam, B. Bleaney, Electron Paramagnetic Resonance of Transition Ions, Oxford Univ. Press (1970). ISBN: 978-0198512509.

Synthesis and characterization of iron oxide nanostructures for energy storage devices

O. Smirnov[1,2], R. Savkina[1,2], R. Minikayev[3]

[1]V. Lashkaryov Institute of Semiconductor Physics of NAS of Ukraine, 41 Nauky Ave., Kyiv, 03028, Ukraine
[2]National University "Kyiv-Mohyla Academy", Kyiv, 04070 Ukraine
[3]Institute of Physics, Polish Academy of Sciences, 02-668 Warsaw, Poland
e-mail: alex_tenet@ukr.net

The development of renewable and reliable energy storage devices with features of environmental friendliness and low cost is very relevant. High power density, excellent cycle stability, and fast charge/discharge process make supercapacitors a promising energy device. However, the energy density of supercapacitors is still lower than that of conventional batteries. As is known, the supercapacitors properties largely depend on the materials of the electrodes. The development of inexpensive electrode materials with advantageous electrochemical properties is still a great challenge. To overcome these problems, much attention is paid to the fabrication of metal oxide nanostructures and their modification by various approaches, such as doping, introduction of oxygen vacancies, and hybridization with carbon allotrope nanomaterials and polymers to improve electrochemical properties.

Transition metal oxides are extensively studied in supercapacitor research due to their ability to undergo fast and reversible redox reactions at the electrode–electrolyte interface, resulting in improved energy storage. Among them, α-Fe_2O_3 (hematite) is considered a promising candidate for the negative electrode because of its broad working voltage window (−1.2 V to +0.25 V), strong redox activity ($Fe^{3+} \rightleftharpoons Fe^{2+}$), economic advantages, and natural abundance. Nevertheless, its practical use is hindered by intrinsic limitations such as low electrical conductivity and high recombination rates of charge carriers, which are mainly caused by sluggish transport kinetics. Several techniques have been proposed to address these drawbacks, including doping with conductive elements, morphological optimization, and the creation of composite or hybrid architectures – e.g., TiO_2/α-Fe_2O_3 or Fe_2O_3/WO_3 systems. Our research focuses on the latter approach.

We synthesized TiO_2/α-Fe_2O_3 and Fe_2O_3/WO_3 nanocomposites using an ultrasonic-assisted method, combining commercial WO_3 and TiO_2 nanopowders with Fe_2O_3 nanoparticles derived from $Fe(NO_3)_3 \cdot 9H_2O$ (Aldrich, 98%). The synthesis involved heating a solution of iron nitrate and monohydrated citric acid ($C_6H_8O_7 \cdot H_2O$) under vigorous stirring at 70 °C until gel formation occurred after water evaporation. The obtained gel was then thermally treated at 400 °C to yield Fe_2O_3 nanoparticles. The crystalline structure of synthesized α-Fe_2O_3 nanopowder and iron oxide-based composites were characterized by X-ray diffraction method, SEM microscopy (Tescan Mira 3 LMU) and diffuse reflectance spectroscopy using a two-beam spectrophotometer Shimadzu UV-3600. The optical absorption spectra were calculated from the diffuse reflectance spectra using the Kubelka-Munk theory.

It was observed that Fe_2O_3 nanoparticle morphology and size were strongly influenced by synthesis parameters. Optimal fabrication conditions were identified, particularly the use of ultrasound, which significantly reduced the particle size from approximately 30 nm to ~15 nm. SEM analysis confirmed uniform distribution of Fe_2O_3 particles (15–16 nm) on the surface of WO_3, as well as their deposition into the pores of the TiO_2 matrix. Furthermore, incorporating varying amounts of Fe_2O_3 into the TiO_2 framework led to a noticeable reduction in band gap energy, enabling photocatalytic activity under visible light conditions. The considered dual-absorber photoanode architecture demonstrates significant potential, effectively integrating the complementary advantages of each component to achieve significantly improved performance of the final device.

The role of the Peierls relief in low-temperature plasticity of the Ti-Nb substitutional alpha solid solution

V. A. Moskalenko, R. V. Smolianets

B. Verkin Institute for Low Temperature Physics and Engineering of the NAS of Ukraine,
47 Nauky Ave., Kharkiv, 61103, Ukraine
e-mail: smoljanets@ilt.kharkov.ua

Alloying elements and impurities have a significant impact on the physical mechanisms of plastic deformation of pure metals. It is important to consider not only their concentration but also their type, which can make this impact quite different. In this regard, they can be divided into two classes. Interstitial atoms of the solute, located in the interstitial sites of the crystal lattice, usually create large asymmetric deformations and cause more "rapid strengthening". On the other hand, substitutional atoms, which cause strengthening as a result of distortion of the crystal lattice due to a size mismatch with the matrix atoms, belong to a class with a smaller strengthening effect. Plastic deformation of high-purity Ti at low temperatures is determined by the overcoming of Peierls barriers by dislocations via the mechanism of nucleation, expansion, and annihilation of paired kinks [1, 2], but can vary even with a relatively small content of solute atoms [3-5].

A detailed study of low-temperature plastic deformation of Ti-Nb alpha substitutional solid solutions (with Nb concentrations of 0.25, 1.05, and 2.1 at.%) based on high-purity Ti was conducted. The low concentration of interstitial impurities (O + N) less than 0.1 at.% makes it more possible to more accurately separate the two most probable plasticity mechanisms - overcoming of Peierls barriers and impurity barriers by dislocations. The temperature dependences of the yield strength and its rate sensitivity, as well as the values of the activation volume of the plastic deformation process in the temperature range of 1.7 - 423 K, were determined. The experimental results were analysed in order to determine the controlling mechanisms of substitutional solid solution plasticity under conditions where the role of interstitial impurity atoms is insignificant, and the temperature range of the performed studies is quite wide. It is shown that the plastic flow of Ti-Nb alloys, which are substitution solid solutions with a hexagonal close-packed structure, at moderately low temperatures ($18\ K < T < 150\ K$) occurs as a result of thermally activated overcoming of Peierls barriers by dislocations via the mechanism of generation, expansion and annihilation of paired kinks. Empirical values of the theory parameters for prismatic slip $\{10\bar{1}0\}\langle 11\bar{2}0\rangle$ in Ti-Nb alloys with Nb concentrations of 0.25, 1.05, and 2.1 at.% at low temperatures are obtained: Peierls stress τ_p and characteristic energy of the critical pair kink H_c. At temperatures $T < 18$ K, the plasticity of Ti-Nb alpha solid solutions exhibits a clearly expressed anomaly in the behavior of the plasticity parameters, the probable cause of which may be the transition from the thermally activated dislocation motion regime to the dynamic (thermoinertial) one with decreasing temperature.

[1] E. D. Levine, Trans. Metall. Soc. AIME 236, 1558 (1966).
[2] V. A. Moskalenko, V. D. Natsik and V. N. Kovaleva, Low Temp. Phys. 31, 1190 (2005). https://doi.org/10.1063/1.2126949
[3] A. T. Churchman, Proc R Soc Lond A 226, 216 (1954).
[4] V. A. Moskalenko, V. N. Puptsova, Mater. Sci. Eng. A 16, 269 (1974).
[5] V. N. Kovaleva, V. A. Moskalenko and V. D. Natsik, Phil. Mag. 70, 423 (1994). https://doi.org/10.1080/01418619408242549

Physical-mechanical properties of high entropy alloy $CrMnFeCoNi_2Cu$ in two structural states in the temperature range of 4.2–350 K

O. D. Tabachnikova[1], Yu. O. Shapovalov[1], S. M. Smirnov[1], V. F. Gorban[2], M. O. Krapivka[2], and S. O. Firstov[2]

[1]B. Verkin Institute for Low Temperature Physics and Engineering of the NAS of Ukraine, 47 Nauky Ave., Kharkiv, 61103, Ukraine
[2]I.M. Frantsevich Institute for Problems of Materials Sciences of the NASciences of Ukraine, 3 O. Pritsaka street, Kiev, 03142, Ukraine
e-mail: tabachnikova@ilt.kharkov.ua

The $CrMnFeCoNi_2Cu$ alloy was produced by arc melting of the constituent elements in a purified argon atmosphere. The purity of the initial components exceeded 99.9%. To achieve chemical homogeneity, the ingots were remelted at least 6–7 times, after which the melt was cooled to room temperature (state I). The obtained ingots were subjected to rolling on a rolling mill at room temperature with a deformation degree of 60% (state II). Structural studies showed that two FCC phases with different copper contents are present in the alloy in both states. After rolling, the fraction of the Cu-enriched phase decreases from 36.5 to 12.6 wt.%. Measurements of microhardness, H, and Young's modulus, E, showed that upon transition from state I to state II the microhardness increases from 2.6 to 4.5 GPa, while Young's modulus increases from 122 to 155 GPa. For state II, the regularities of plastic deformation and fracture behavior were investigated in the temperature range of 4.2–300 K under uniaxial tension and compression. The temperature dependences of the yield strength $\sigma_{0.2}$ were obtained, and the stages of the deformation curves were determined. It was established that throughout the studied temperature range, the alloy exhibits a high-strength state while retaining considerable plasticity. At all temperatures, the plasticity of samples in state II under compression exceeds 15%, whereas under tension, it is about 5%. During compression, the value of $\sigma_{0.2}$ increases monotonically from 1.14 to 1.68 GPa (by 47%) as the temperature decreases from 300 to 4.2 K. Under tension, $\sigma_{0.2}$ increases from 1.11 to 1.70 GPa (by 53%). At temperatures below approximately 15 K, an unstable character of plastic deformation is observed, manifested by stress serrations on the deformation curves. These serrations appear immediately after yielding and persist up to fracture of the specimen. The average amplitude of the serrations increases with strain during compression, whereas under tension it changes only slightly at strains ≥ 1–2%. The serrated plastic deformation is associated with slip localization and is governed by the combined action of interrelated dislocation-dynamic and thermal processes. At all investigated temperatures, the fracture mode remains ductile. Based on experimental measurements of the temperature and strain-rate dependences of the flow stress (at ≈ 2% plastic strain) in the temperature range of 25–340 K, a thermoactivation analysis of the processes controlling the deformation behavior of the alloy was performed. Empirical estimates of the microscopic parameters of plasticity as well as internal and effective stresses were obtained. The analysis showed that within the investigated temperature range a single dislocation mechanism governs the thermally activated plasticity of the high-entropy alloy. It was established that the distribution of barriers on dislocations follows Friedel statistics, which is typical for thermally activated motion of dislocations through a network of randomly distributed local obstacles. It was shown that the most probable local barriers controlling the thermally activated motion of dislocations are atomic-scale structural heterogeneities (atom clusters) with an activation energy $H_0 \approx 0.82$ eV. These clusters consist of several identical atoms and are located at distances of several nanometers from each other. The $CrMnFeCoNi_2Cu$ alloy is promising for cryogenic technology, space and energy applications.

Structural peculiarities of cadmium halides and their manifestation in electronic spectrum and opto-luminescent studies: experiment and theoretical justification

N. K. Tovstyuk[1], M. M. Rudka[1], B. O. Seredyuk[2], M. S. Karkulovska[1], M. M. Romanyuk[1]

[1]Institute of Mathematics and Applied Sciences, Lviv Polytechnic National University, 12 Bandera str., Lviv, 79013, Ukraine
[2]Faculty of military engineering, Hetman Petro Sahaidachnyi National Army Academy, 32 Heroes of Maidan street, Lviv, 79032, Ukraine
e-mail: nataliia.k.tovstiuk@lpnu.ua; ntovstyuk@gmail.com

Cadmium halides CdX_2 (X = Cl, Br, I) are wide-bandgap materials in which structured packets (X-Cd-X) form a cubic close-packed ($CdCl_2$, $CdBr_2$) or hexagonal (CdI_2) packing. Cd cations occupy half of the octahedral cavities between the halogens.

Within the layer, the interaction is covalent-ionic (with a predominance of the covalent component), while between the layers, there are weak (an order of magnitude smaller than intra-layer) molecular (van der Waals) forces. In [1], it is shown that in CdI_2, the dominant structural defects are donor-acceptor (DA) complexes – trimers of the (Cd_i^- – V_{Cd} – Cd_i^+) type as well as vacancies of molecules of the V_{CdI2} crystal, as a (V_I – V_{Cd} – V_I) trimer, which are strictly oriented with respect to the main crystallographic axis C_6. When cadmium iodide is activated with impurities, vacancy trimers are "healed": self-impurity and even purely impurity (at high concentrations of the activator) trimers are added to the intrinsic (D_i^0 – A_{Cd}^- – D_i^+) trimers. Such DA complexes play a key role in the luminescent properties of cadmium iodide.

In this work, we investigate the manifestation of the same type of defects in cubic symmetry crystals of $CdCl_2$, $CdBr_2$ in their experimental opto-luminescent studies and theoretical models.

The electronic spectrum and density of states of such crystals were calculated in a model of a highly anisotropic crystal with different types of chemical bonding. The degree of anisotropy was taken into account through the ratio of the parameters of electronic mixing in the layer (α) and between the layers along the C_6 axis (*t*): for CdI_2 $t/\alpha \cong 0.1$ and the disappearance of anisotropy ($t/\alpha \rightarrow 1$) for $CdCl_2$ and $CdBr_2$. The different inclination of the trimers with respect to the plane of the layers was taken into account through the calculated different effective masses and their dependence on the concentration of the donor-acceptor pairs that form the trimers. The structure of the levels in the band gap was also taken into account [2]. The electronic spectrum was written for a 4-band model (conduction band, shallow impurity level band, acceptor band, and valence band). Features in the electronic spectrum during the transition from hexagonal to cubic crystal and their manifestation in luminescence spectra were analyzed.

[1] M. M. Rudka, Low Temp. Phys. 52, 182 (2026). http://dx.doi.org/10.1063/10.0042295.
[2] N. K. Tovstyuk, M. M. Rudka, O. B. Bilenka, F. Ivashchyshyn, M. S. Karkulovska, B. O. Seredyuk, Low Temp. Phys. 52, 113 (2026). https://doi.org/10.1063/10.0042179.

Investigation of donor-type localized charge carrier states in CdZnTe crystals

O. M. Chuhai, Yu. A. Voloshyn, S. M. Kulish, D. S. Zavadskyi, D. O. Omelianchuk

National Aerospace University "Kharkiv Aviation Institute",
17 Chkalova St., Kharkiv, 61070, Ukraine
e-mail y.voloshyn@khai.edu

Crystals of $Cd_{1-x}Zn_xTe$ (x = 0.10-0.20) grown from the melt by the Bridgman method were studied. Experiments were carried out on samples with the highest photosensitivity. The spectra of specular light reflection and the photodielectric effect were measured in the wavelength scanning mode. This mode provides determination of the energy spectrum of localized charge carrier states in crystals by the method of scanning photodielectric spectroscopy (SPDS) [1]. A feature of the implementation of this method is the absence of changes in the sample temperature and the absence of exposure to a strong electric field, which usually leads to changes in the state of some intrinsic structural defects. At the same time, it had not previously been possible to detect donor-type localized states in $Cd_{1-x}Zn_xTe$ (CZT) crystals by the SPDS method. On the other hand, such states always exist in crystals and significantly affect their photoelectric properties [2].

A comparative analysis of the spectra of specular light reflection and the energy spectrum of localized charge carrier states, taking into account the spin- orbit splitting of the energy levels of the valence band as well as the influence of the near-surface electrostatic potential on the photoionization energy of localized states, made it possible to establish a method for calculating the energy position of donor-type localized states in CZT crystals. The method is based on the photoionization energies of localized states determined by the SPDS method. The relationship of these states with acceptor-type states is considered. The influence of donor states on the polarizability in the low-frequency region and on the near-surface electrostatic potential of the crystal is discussed.

[1] O. Chugai, O. Poluboiarov, S. Oliinyk & S. Sulima, "Scanning Photodielectric Spectroscopy of CdZnTe Crystals," in Advances in Fabrication and Investigation of Nanomaterials for Industrial Applications (Springer International Publishing, Cham, 2024), pp. 111–132.
[2] L. Xu, T. Feng, and W. Jie, J. Cryst. Growth 560, 126050 (2021).

The influence of electromagnetic radiation from a spark discharge on localized charge carrier states in CdZnTe crystals

O. M. Chuhai, Yu. A. Voloshyn, S. M. Kulish, D. S. Zavadskyi, D. O. Omelianchuk

National Aerospace University "Kharkiv Aviation Institute",
17 Chkalova St., Kharkiv, 61070, Ukraine
e-mail y.voloshyn@khai.edu

$Cd_{1-x}Zn_xTe$ (CZT) crystals are one of the promising materials for uncooled gamma-radiation spectrometers. At the same time, there are difficulties in obtaining these materials of high quality due to the formation of point defects during their growth. Therefore, the study of localized states (LS) of charge carriers generated by such defects is of both scientific and practical interest. In [1], the influence of electromagnetic radiation of a spark discharge (ERSD) on the dielectric properties of CZT crystals, as well as on acceptor-type localized states of carriers in these materials, was established. In this connection, it is of interest to carry out more detailed studies of the influence of ERSD on localized states, in particular on donor-type states.

The studied $Cd_{1-x}Zn_xTe$ crystals (x = 0.10-0.20) were grown from the melt under high pressure of an inert gas. The resistivity of the samples exceeded 10^{10} Ω·cm, which is important considering their use in gamma-radiation spectrometers. The energy spectrum and relative occupancy of the states were investigated by the method of scanning photodielectric spectroscopy [2]. The corresponding measurements were performed not only under the action of electromagnetic radiation on the sample, but also when the sample was in the initial state. In the analysis of the photodielectric effect spectra, an original computer program was used, which provided increased accuracy in determining the energy position of localized states of carriers of different types.

Refined data on the energy position of acceptor-type localized states were obtained, and for the first time, the position of donor centers was determined in samples that differ in resistivity. The features of changes in the relative occupancy of localized states of carriers of different types under the action of ERSD were established. A difference in the behavior of the occupancy of donor-type localized states under irradiation compared with acceptor-type states was shown. These differences are explained by the peculiarities of the electron–phonon interaction of defects. It is concluded that the study of localized states of charge carriers in CZT-type crystals provides additional information about the nature of point defects in them.

[1] O. Chugai et al., Effect of electromagnetic radiation of spark discharge on dielectric properties of $Cd_{1-x}Zn_xTe$ Crystals in the low-frequency region, Low Temp. Phys. 52, 265–270 (2026).
[2] O. Chugai, O. Poluboiarov, S. Oliinyk & S. Sulima, “Scanning Photodielectric Spectroscopy of CdZnTe Crystals,” in Advances in Fabrication and Investigation of Nanomaterials for Industrial Applications (Springer International Publishing, Cham, 2024), pp. 111–132.

Modeling charge-state evolution of point defects in YAG0 from growth temperature to room temperature

M. Y. Vovsianiker[1], D. V. Fil[1,2]

[1]Institute for Single Crystals of NAS of Ukraine, 60 Nauky Ave., Kharkiv, 61072, Ukraine
[2]V. N. Karazin Kharkiv National University, 4 Svobody Square, Kharkiv, 61022, Ukraine
e-mail: mark.vovsianiker@gmail.com

Density functional theory (DFT) is widely used to determine the formation energies of point defects in crystals. The defect formation energy is given by the equation [1]:

$$E_i = E_{def,i} - E_{ideal} - \sum_X \mu_X p_{X,i} + \mu_e q_i + E_i^{(corr)}, \qquad (1)$$

where $E_{def,i}$ is the energy of a cell containing a defect of type i, E_{ideal} is the energy of a cell without defects, μ_X is the chemical potential of an atom of type X, $p_{X,i}$ is the number of atoms of type X added ($p_{X,i} > 0$) or removed ($p_{X,i} < 0$) from the cell, μ_e is the chemical potential of the electron, q_i is the charge of the defect in units of the elementary positive charge, $E_i^{(corr)}$ is a correction that accounts for the error associated with the finite cell dimensions in DFT calculations. The concentration of the i-th type of defects is determined by the equation [2]:

$$c_i = N_i exp\left(-\frac{E_i}{k_B T}\right), \qquad (2)$$

where N_i is the number of possible sites for the i-th type of defect per unit volume. The chemical potential of the electron μ_e is determined from the condition of electroneutrality [2]:

$$\sum_i q_i c_i + c_h - c_e = 0, \qquad (3)$$

where c_e and c_h are the equilibrium concentrations of electrons and holes. These concentrations depend on μ_e and the electronic density of states, which can be obtained from DFT calculations.

It is assumed that defects form during crystal growth or ceramic synthesis; therefore, the temperature T to be substituted into equation (2) is the crystallization or synthesis temperature. For yttrium aluminum garnet (YAG) this temperature is high enough and concentrations of electrons and holes are comparable to the concentrations of defects and make a significant contribution to the charge neutrality equation (3). At room temperature, the concentration of free carriers in wide-bandgap insulators is low. As the temperature decreases, free charge carriers should be captured by defects, causing, in turn, a change in the relative populations of different charge states of defect species.

We propose a model that describes this process. It is based on the assumption that the total concentration of a given type of defect, summed over all charge states, remains constant during cooling. The temperature dependence of the concentrations of point defects in different charge states, as well the concentrations of electrons and holes are computed for YAG crystal. The SIESTA software package was used for the DFT calculations. It is found that for each type of defect, the concentration of one energetically favorable charge state increases at the expense of other charge states that are thermodynamically accessible at high temperatures.

[1] S. B. Zhang and J. E. Northrup, Chemical potential dependence of defect formation energies in GaAs: Application to Ga self-diffusion, Phys. Rev. Lett. 67, 2339 (1991). https://doi.org/10.1103/PhysRevLett.67.2339
[2] C. Freysoldt, B. Grabowski, T. Hickel, J. Neugebauer, G. Kresse, A. Janotti, and C. G. Van de Walle, First-principles calculations for point defects in solids, Rev. Mod. Phys. 86, 253 (2014). https://doi.org/10.1103/RevModPhys.86.253.

Diffusion of hydrogen in metals with substitutional defects

A. Grib, A. Yaroshenko

Physics Department, V. N. Karazin Kharkiv National University,
Svobody sq. 4, Kharkiv, 61022, Ukraine
e-mail: alexander.grib@karazin.ua

It is known that substitutional defects in metals can create bound states with migrating hydrogen atoms. For example, an increased concentration of electron density near a defect forces hydrogen to move near the defect together with its own electron cloud [1]. This state of the hydrogen atom (a proton) is usually considered as a deep potential well (a trap) in the set of more shallow interstitial positions for protons between matrix atoms. Diffusion in such a lattice with traps was considered in the range of the model of continuous time random walking (CTRW) [2]. Within the model, a function of a "memory" of the quantity of traps visited by a proton is considered, so the dependence of its mean squared displacement $<x^2>$ on time t is not linear. The presence of deep traps leads to a decrease in the diffusion coefficient of a proton. However, a substitutional defect creates also the gradient of elastic deformation. In the present report, we consider defects which expand the matrix lattice and study the influence of this expansion on hydrogen diffusion.

The lattice expansion leads to the flux of protons from a matrix lattice toward the expanded place, i.e. toward the defect. This effect of the flux of impurities toward expanded places is called the Gorsky effect. Since its description using the CTRW model is complicated, we modeled it within a simple quasi-one-dimensional model of random walks of a proton along the line of potential wells. The process of random walks is organized as follows. Randomly chosen wells are deeper than others. A proton jumps between wells. The probability of leaving a trap is smaller than that for other wells. Far from a defect, after a proton leaves the well, it has an equal probability to jump to the neighbor well (rightwards or leftwards). However, if a shallow well is placed near the trap, the jump probability of a proton from this shallow well inside a trap is larger than that in the opposite direction. This difference of probabilities is proportional to the gradient of elastic deformations near structural defects. After some number of jumps, the position of a proton is recorded. The process is repeated from $5 \cdot 10^5$ to 10^7 times, including a choice of positions for traps. Both the distribution of probabilities of being in a given place of a chain of wells in a chosen time (an analog of the concentration distribution) and dependences $<x^2> = f(t)$ were found in calculations.

Results of calculations are as follows. Firstly, we checked the agreement of analytical expressions for dependences $<x^2> = f(t)$ of the CTRW model with random walks without fluxes corresponding to the Gorsky effect. We obtained a very good (with the less than one percent accuracy) coincidence of slopes of dependences $<x^2> = f(t)$ for both models at large times of walking. However, at small concentrations of traps and small times, values of $<x^2>$ for the model of random walks were always larger than those for the CTRW model. This occurred because in the CTRW model, the concentration of traps was rigidly defined, whereas in our model at small concentration of traps, there were long sets of shallow wells without traps, i. e. the condition of the constant concentration of deep wells was violated.

After the described check of models, we "switched on" the mechanism of fluxes of probabilities of jumps toward defects. We obtained decreases of slopes of dependences $<x^2> = f(t)$ that meant the decrease of the effective diffusion coefficient D^*. It was found that D^* decreases linearly with an increase in the gradient of elastic deformations near structural defects.

[1] G. Alefeld and J. Völkl (eds.), Hydrogen in Metals, Vol. 2 (Springer-Verlag, Berlin–Heidelberg–New York, 1978).
[2] V. L. Merisov, O. V. Usatenko, G. Ya. Khadzhai, A. N. Grib, Diffusion of impurity particles in disordered systems, Metallofizika 8, 63-67 (1986). https://mfint.imp.kiev.ua/ru/toc/v08/i01.html

p-Si/SiOx(Si)&AlyOz(Al) nanocomposite structure for IR–THz detection with shifted infrared peak sensitivity

V. V. Zabudsky, N. I. Kukhtaruk, I. O. Lysiuk, Z. F. Tsybrii, O. G. Golenkov, A. V. Shevchik-Shekera, A. Yu. Shekera, O. L. Bratus, K. V. Svezhentsova, M. V. Vuichyk

V. E. Lashkaryov Institute of Semiconductor Physics, NAS of Ukraine,
41, Nauky Ave., Kyiv 03028, Ukraine
e-mail: zvv1968@yahoo.com

The creation of broadband photodetectors capable of operating in both infrared (IR) and terahertz (THz) spectral ranges is an important objective in modern optoelectronic research. Devices that respond to radiation across such an extended spectral region can simultaneously provide information from both the IR and THz domains, which significantly broadens their potential technological and scientific applications. Although a few materials have already demonstrated sensitivity to radiation in these two spectral ranges [1], further improvement of device performance, reduction of fabrication costs, as well as the realization of compact and technologically compatible structures remain challenging tasks. The ~100 nm depth SiOx(Si)&AlyOz(Al) active layers on *p-Si* substrate were integrated with metallic bow-tie antennas by depositing an ~1 μm thick aluminum layer using thermal evaporation, followed by photolithography and subsequent chemical processing steps. It has previously been demonstrated that these structures are sensitive to radiation at a frequency of 140, 270 GHz at room temperature. In that case, the detection mechanism was attributed to the thermoelectric effect.

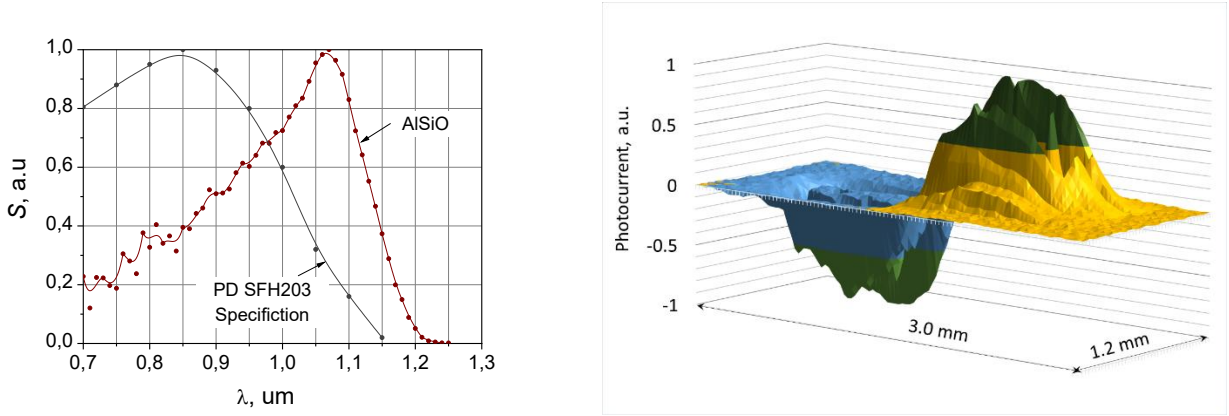

Fig. 1. Spectral sensitivity of the investigated sample compared to the SFH203 photodiode (OSRAM) and its photosensitivity map across the surface.

In the present study, the response of these structures to IR radiation is investigated in more detail. The results of the spectral sensitivity measurements of the sample in the 0.7–5 μm range, as well as the surface uniformity of photosensitivity of the detectors in the infrared range (using an optical probe [2] with a radiation source wavelength of 940 nm and a spot diameter of approximately 60 μm), are shown in Figure 1. The shift of the spectral sensitivity maximum toward longer wavelengths is attributed to the presence of oxide phases, impurities, and structural features of varying sizes in the nanocomposite, which can introduce energy levels within the band gap and enable absorption of photons with lower energy.

The results reported in this article were supported by the National Research Foundation of Ukraine, project No. 2025.06/0089.

[1] S. Wei, W. Zhou, X. Liu, K. Wang, Y. Liao, F. Yan, and X. Ji, Micromachines 15, 427 (2024). https://doi.org/10.3390/mi15040427.
[2] O. G. Golenkov, A. V. Shevchik-Shekera, V. V. Zabudsky, I. O. Lysiuk, Z. F. Tsybrii, A. S. Stanislavskyi, S. V. Korinets, A. Yu. Shekera, Sensor Electronics and Microsystem Technologies 22, 30 (2025). https://doi.org/10.18524/1815-7459.2025.4.343569.

THEORY OF CONDENSED MATTER PHYSICS

$$\hat{H}\psi(r) = E\psi(r)$$

$$\left[-\frac{\hbar^2}{2m}\nabla^2 + V(r)\right]\psi(r) = E\psi(r)$$

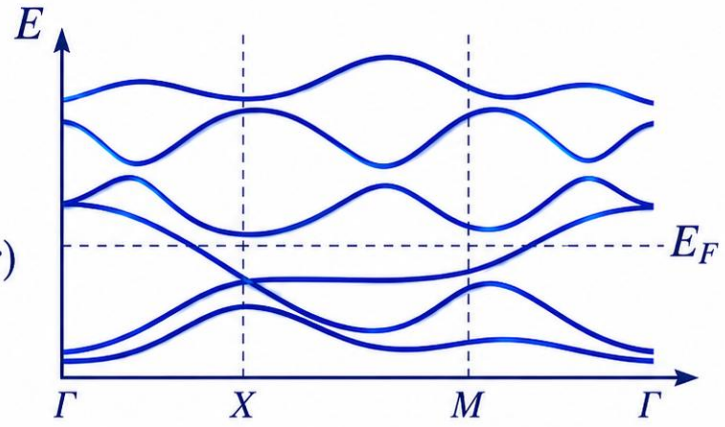

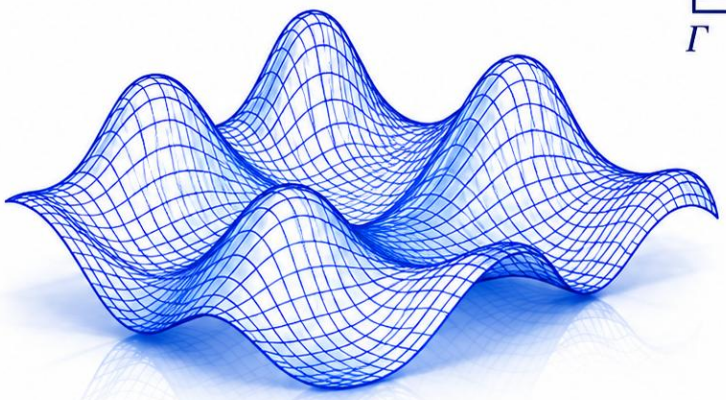

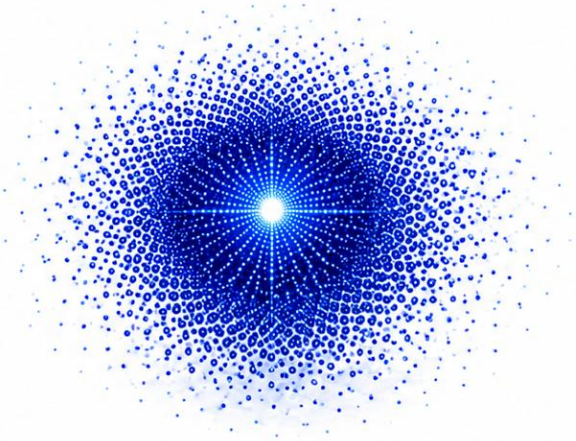

$$V_{\text{eff}}(r) = \sum_q V(q)\, e^{iq\cdot r}$$

Polaron dynamics in external magnetic field

L. S. Brizhik[1], B. M. A. G. Piette[2]

[1]Bogolyubov Institute for Theoretical Physics of the NAS of Ukraine,
14-b, Metrolohichna Str., Kyiv, 03143, Ukraine
[2]Department of Mathematical Sciences, University of Durham,
P.O. Box DH1 3LE, Durham, UK
e-mail: brizhik@bitp.kyiv.ua, b.m.a.g.piette@durham.ac.uk

We study the dynamics of large polarons in quasi-one-dimensional materials, such as polypeptides, (semi)conducting polymers and macromolecules, in the presence of a constant magnetic field. Such systems are described by a system of coupled nonlinear equations which are solved within two approaches: (I) numerically in the discrete representation and (ii) analytically within the continuum approximation, when the system of equations in the absence of the field is reduced to the Cubic Nonlinear Schoedinger Equation which admits soliton solution [1], or to the Modified Nonlinear Schoedinger Equation in the presence of magnetic field. The latter is solved using a nonlinear perturbation method [2]. It is shown that in the presence of the field soliton velocity attains oscillations with the frequency determined by the field. It is shown that the impact of a magnetic field within both approaches depends not only on the field strength, but also on the parameter values of the system which define such properties of polarons like their energy, amplitude, width of localization [3]. We also studied polaron dynamics in a complex system Donor – Molecular Chain.

The obtained results demonstrate that polaron dynamics remains stable even in relatively strong magnetic fields and therefore, that polarons can provide effective long-range electron transport almost without energy dissipation in biological systems and novel low-dimensional functional materials used in modern nano- and bio-technologies.

Acknowledgment

LB acknowledges grant N 2025.07/0335 of the Fundamental Research Foundation of Ukraine and the support of the INI-LMS Rebuild Ukraine Scheme at the Department of Mathematical Sciences of the University of Durham (UK).

[1] A.S. Davydov, Solitons in Molecular Systems. Dordrecht, Reidel, 1985.
[2] L. Brizhik. Chaos, Sol. Fractals **187** (2024) 115459 https://doi.org/10.1016/j.chaos.2024.115459.
[3] L. Brizhik B.M.G. Piette, Submitted to Phys. Rev.E., March 10, 2026.

The Lindblad equation in different bases: application to two- and multilevel systems

O. A. Ilinskaya[1], O. V. Ivakhnenko[1,2], A. I. Ryzhov[1], S. N. Shevchenko[1,3]

[1]B.Verkin Institute for Low Temperature Physics and Engineering of the NAS of Ukraine, 47 Nauky Ave., Kharkiv, 61103, Ukraine
[2]RIKEN Center for Quantum Computing (RQC), RIKEN, Wakoshi, Saitama 351-0198, Japan
[3]Department of Mathematics, Kyiv School of Economics, Kyiv 03113, Ukraine
e-mail: ilinskaya@ilt.kharkov.ua

The Lindblad equation, also known as the Gorini-Kossakowski-Sudarshan-Lindblad (GKSL) equation, is the most common Markovian master equation. There are different approaches to the search of a master equation for a time-dependent system Hamiltonian. If the Hamiltonian changes with time adiabatically, one obtains the master equation in the Lindblad form with time-dependent Lindblad operators written in the instantaneous energy eigenbasis [1]. For the case of strong periodic driving, it is suggested to use the Floquet theory and the Floquet basis for the Lindblad equation [2]. Importantly, the dissipator in the Lindblad form can be used beyond the adiabatic regime [3].

In this report, we revisit description of a driven-dissipative quantum system making accent on the appropriate choice of the system's basis and respective transformations. Approximations used in the derivation of the GKSL equation are separability, the Born-Markov approximation, and rotating-wave approximation. We note that the physical basis (the one in which the initial Hamiltonian is written) is not the correct basis for the Lindblad operators and they should be written in the instantaneous basis. We review different bases for quantum systems (diabatic, instantaneous, dressed-states, Floquet-states, superadiabatic bases) and show the dynamics for a two-level and a multilevel system in different bases as an example.

This work was partially supported by the U.S. National Academy of Sciences (NAS) and the Office of Naval Research (ONR) in the framework of the International Multilateral Partnerships for Resilient Education and Science System in Ukraine IMPRESS-U (Grant No. 7120), National Research Foundation of Ukraine (Grant No. 2025.07/0044), and the scholarship of the National Academy of Sciences of Ukraine.

[1] T. Albash, S. Boixo, D. A. Lidar, and P. Zanardi, New J. Phys. 14, 123016 (2012). doi:10.1088/1367-2630/14/12/123016.
[2] H. P. Breuer and F. Petruccione, The Theory of Open Quantum Systems (OUP Oxford, 2002). DOI: 10.1093/acprof:oso/9780199213900.001.0001.
[3] M. Yamaguchi, T. Yuge, and T. Ogawa, Phys. Rev. E 95, 012136 (2017). DOI: 10.1103/PhysRevE.95.012136.

Fast GPU-based quantum interferometry solver

O. V. Ivakhnenko[1,2], S. N. Shevchenko[1,3], and F. Nori[2,4]

[1]B. Verkin Institute for Low Temperature Physics and Engineering, Kharkiv 61103, Ukraine
[2]RIKEN Center for Quantum Computing, RIKEN, Wakoshi, Saitama 351-0198, Japan
[3]Department of Mathematics, Kyiv School of Economics, Kyiv 03113, Ukraine
[4]Physics Department, University of Michigan, Ann Arbor, MI 48109-1040, USA
e-mail: olegiv333@gmail.com

Quantum interferograms of driven quantum systems are a useful tool for calibrating quantum systems, finding parameters for optimal working regimes, mapping the resonance conditions, etc. [1]. While there are many analytical approaches to deriving interferometry conditions, most of those have quite strict limitations in parameter space where they are applicable, due to the approximations and assumptions made. Numerical solution of the quantum systems dynamics is much more insightfull while sweeping over different parameters values [2] because its area of applicability is usually wider, but numerical solutions require considerable computational power. Also, the are more flexible with respect to the shapes of the driving pulses and specific noise patterns, which can easily be added to the numerical solution, without the need to rederive with different approximations [1], as is required for analytical methods. Moreover, sometimes parameters fall into a grey zone, where neither of the analytical approaches works well. Interferometry is very demanding in terms of computational power because sweeps usually come over several different parameters, so we need to calculate thousands or even millions of quantum systems' dynamics to obtain the evolution of a high-definition interferometry map [2].

The developed framework, well-optimized for parallel computations GPU (graphical processing unit), allows us to numerically calculate the dynamics of the Lindblad equation with the fourth-order Runge-Kutta method several orders of magnitude faster than on a multithread CPU (central processing unit).

This work was supported by the ARO, ONR, IEEE, JST, NAS, NRFU (Grant No. 2025.07/0044).

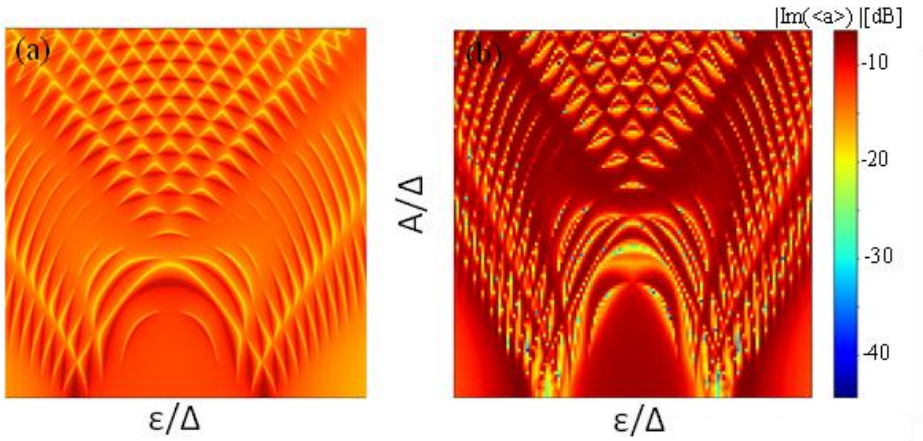

Figure 1: (a) Interferometry pattern of qubit-resonator system [2] calculated on a GPU RTX 3080 with the developed framework 2.2sec (2048x2048) =4.2e+6 points, (b) the same interferometry calculated on a multithread CPU I7 11900K at a much lower resolution 60 sec (1x128x128) =1.63e+4 points. Thus, we can see that GPU calculation can provide higher resolution for fine resonance lines while having much faster calculation times around 7000 times; faster per point.

[1] O. V. Ivakhnenko, S. N. Shevchenko, F. Nori, Phys. Rep. 995, 1 (2023). https://doi.org/10.1016/j.physrep.2022.10.002.
[2] O. V. Ivakhnenko, C. D. Satrya, Yu-C. Chang, R. Upadhyay, J. T. Peltonen, S. N. Shevchenko, F. Nori, J. P. Pekola, arXiv, 2508.03188 (2025). https://doi.org/10.48550/arXiv.2508.03188.

Hydrodynamics of polarons in semiconductors

S. O. Sokolovsky[1,2], A. I. Sokolovsky[3]

[1]Dnipro polylingual lyceum №23 of Dnipro city council,
Dmitro Yavornitskyi Avenue, 14, Dnipro, 49000, Ukraine
[2]Dnipro Academy of Continuing Education,
VolodymyrAntonovych St.,70, Dnipro, 49006, Ukraine
[3]Oles Honchar Dnipro National University, Dnipro, Ukraine
Nauky Avenue, 72, Dnipro, 49000, Ukraine
e-mail: sergeysokolovsky2021@gmail.com, alexander.i.sokolovsly@gmail.com

In this work, we investigate the transport phenomena of a polaron gas in semiconductor structures using a generalization of the Chapman–Enskog method (see for example [1]). The approach is based on the functional hypothesis, where the polaron distribution function $\mathrm{f}_p(x,t)$ at times $t >> \tau_0$ is considered a functional of the basic hydrodynamic variables $\eta_\mu(x,t)$: temperature $T(x,t)$, velocity $u_l(x,t)$ and particle density $n(x,t)$. Kinetic equation for distribution function $\mathrm{f}_p(x,t)$ has the form

$$\frac{\partial \mathrm{f}_p(x,t)}{\partial t} = -\frac{p_n}{m}\frac{\partial \mathrm{f}_p(x,t)}{\partial x_n} + eE_n\frac{\partial \mathrm{f}_p(x,t)}{\partial p_n} + I_p(x,\mathrm{f}(t)),$$

$$I_p(x,\mathrm{f}) = \frac{1}{4\pi^3\hbar^2}\int_{-\infty}^{0} d\tau\int d^3k g_k^2\left\{n_k\,\mathrm{f}_{p-k\hbar}\left(x+\frac{k\hbar}{2m}\tau\right)-(1+n_k)\mathrm{f}_p\left(x-\frac{k\hbar}{2m}\tau\right)\right\}\times$$

$$\times\cos\frac{\tau}{\hbar}\left(\varepsilon_{p-k\hbar}+\hbar\omega_k-\varepsilon_p\right)+$$

$$+\frac{1}{4\pi^3\hbar^2}\int_{-\infty}^{0} d\tau\int d^3k g_k^2\left\{(1+n_k)\mathrm{f}_{p+k\hbar}\left(x-\frac{k\hbar}{2m}\tau\right)-n_k\,\mathrm{f}_p\left(x+\frac{k\hbar}{2m}\tau\right)\right\}\times$$

$$\times\cos\frac{\tau}{\hbar}\left(\varepsilon_p+\hbar\omega_k-\varepsilon_{p+k\hbar}\right)$$

and was derived in our paper [2] (n_k is phonon distribution function).

The solution to the kinetic equation is found using a perturbation theory where key physical factors are considered to be of the **same order of smallness:**

Particle density gradient: The spatial non-uniformity of the system is characterized by the gradient of the number of particles density

Electric field: The system is subjected to a weak external electric field.

This choice of small parameters allows for a consistent modification of the standard transport theory by accounting for the non-locality of the collision integral. In this approximation, the distribution function $\mathrm{f}_p(x,t)$ and the resulting flux densities of energy q_n and momentum t_{nl} include terms that directly describe the combined influence of the electric field and the density gradient.

[1] A.I. Akhiezer and S.V. Peletminsky, Methods of Statistical Physics (Pergamon Press, Oxford 1981). https://doi.org/10.1016/C2013-0-05932-4.
[2] S.A. Sokolovsky, Theor. Math. Phys. 168, 1150 (2011).
https://link.springer.com/article/10.1007/s11232-011-0093-z.

Comprehensive investigation of the structural, mechanical, electronic, phonon, thermodynamic and hydrogen storage properties of the hydride perovskite Mg_2IrH_6

C. Aksu[1], N. Arikan[1], A. İyigör[2] and E. Tel[1]

[1]Department of Physics, Osmaniye Korkut Ata University, Faculty of Engineering and Natural Sciences, 80100 Osmaniye, Türkiye
[2]Department of Machine and Metal Technologies, 40100 Kırşehir Ahi Evran University, Kırşehir, Türkiye
e-mail: cevataksu@hotmail.com.tr, nihatarikan@osmaniye.edu.tr, ahmetiyigor@ahievran.edu.tr, eyuptel@osmaniye.edu.tr

In this work, a comprehensive first-principles investigation of the hydride perovskite Mg_2IrH_6 is presented. Structural optimization, elastic response, electronic characteristics, lattice dynamics, and thermodynamic behavior were systematically examined within the framework of density functional theory (DFT). The optimized equilibrium structure confirms energetic stability, supported by a negative formation enthalpy. Mechanical stability is verified through elastic constants satisfying the Born–Huang stability criteria. Electronic band structure and density of states analyses reveal metallic behavior dominated by Ir–H hybridization near the Fermi level. Phonon dispersion relations show no imaginary frequencies, confirming dynamical stability. Thermodynamic properties evaluated within the quasi-harmonic Debye approximation indicate characteristic low-temperature T^3 heat capacity dependence and convergence toward the Dulong–Petit limit at elevated temperatures. The gravimetric hydrogen density and hydrogen desorption temperature for Mg_2IrH_6 were calculated as 2.45% and 758 K, respectively. The calculated hydrogen storage capacity suggests that Mg_2IrH_6 may be considered a potential hydrogen material for energy-related applications.

Algorithm for unitary evolution of quantum systems with tridiagonal Hamiltonians

D. Bondar[1], R. T. Ovsiannikov[2], K. Jacobs[3, 4], A. G. Sotnikov[2]

[1]Tulane University, New Orleans, Louisiana, United States
[2]NSC «Kharkiv Institute of Physics and Technology», Kharkiv Ukraine
[3]United States Army Research Laboratory, Adelphi, Maryland 20783, USA
[4]Department of Physics, University of Massachusetts at Boston, Boston, Massachusetts 02125, USA
e-mail: roman.ovsiannikov@kipt.kharkov.ua

We present an efficient numerical algorithm for the unitary time evolution of undamped quantum systems whose Hamiltonians can be represented as a sum of tridiagonal and diagonal components in suitable basis orderings. The immediate motivation is the time-dependent Tavis-Cummings model beyond the rotating-wave approximation for a finite collective spin coupled to a cavity mode. In our calculations for resonant parameter regimes with time-dependent NV-center frequencies, standard propagation in QuTiP produced irregular behavior and did not reliably preserve the expected unitary character of the evolution. This motivated the development of a dedicated solver explicitly tailored to the algebraic structure of the Hamiltonian, and that remains efficient for large Hilbert-space dimensions. The system is formulated in the product basis $|n\rangle \otimes |j,m\rangle$, where n labels cavity Fock states and m is the collective spin projection. The Hamiltonian is decomposed as $H(t) = H_0 + V + \Delta(t)Jz$. Here, H_0 contains the cavity term together with the rotating-wave interaction, V contains the counter-rotating contribution, and the modulation term $\Delta(t)Jz$ is diagonal in the same physical basis. The key structural observation is that H_0 and V are both tridiagonal, but in different orderings of the basis states. As a result, the propagation problem can be reformulated as a sequence of operations with tridiagonal matrices combined with simple reindexing of the state vector, rather than dense similarity transformations. This substantially reduces both the arithmetic cost and the memory footprint.

For the temporal discretization we employ a symmetric second-order Trotter-Suzuki splitting of the short-time propagator. The diagonal substeps associated with $\Delta(t)Jz$ are applied exactly as elementwise phase multipliers. The tridiagonal substeps are evaluated in two complementary ways. The first approach identifies zeros on the off-diagonals, separates the Hamiltonian into independent blocks, exponentiates each block spectrally, and then reconstructs the global propagator. The second, more efficient approach uses the Cayley rational approximation, which transforms the exponential action into the solution of a tridiagonal linear system for the next state vector. Because both tridiagonal matrix-vector multiplication and the solution of a tridiagonal system scale linearly with the vector dimension D, the resulting propagation step has approximately O(D) time complexity and O(D) memory usage.

A practical advantage of the method is that it preserves the physically essential unitary structure of the undamped Schrödinger dynamics while remaining simple enough for large-scale simulations. The algorithm is naturally suited for computing observables during propagation, including field quadratures, variances, covariances, and squeezing characteristics derived from the covariance matrix. Since permutations rather than full transition matrices implement the basis changes, the method remains lightweight even when the rotating-wave and counter-rotating parts are treated in different optimal orderings. Although the present construction is motivated by the non-RWA Tavis-Cummings problem, its scope is broader. The same strategy can be applied to other undamped quantum models whenever the Hamiltonian admits a decomposition into a small number of tridiagonal operators in convenient bases. This makes the algorithm attractive for simulations in which direct exponentiation becomes prohibitive, but strict control over numerical stability, computational cost, and memory consumption is required. R.O. and A.G.S. acknowledge support by the National Research Foundation of Ukraine, project No. 2023.03/0073.

Heisenberg model on the face-centered cubic lattice: iPEPS study

I. V. Lukin[1,2], A. G. Sotnikov[2,3]

[1]Haiqu, Inc., 95 Third Street, San Francisco, California 94103, United States
[2]Akhiezer Institute for Theoretical Physics, NSC KIPT, Akademichna 1, 61108 Kharkiv, Ukraine
[3]Karazin Kharkiv National University, Svobody Square 4, 61022 Kharkiv, Ukraine
e-mail: illya.lukin11@gmail.com

Tensor network based methods have proved themselves worthy in both analytics and numerics in the study of one-dimensional quantum systems. Some of the tensor network algorithms, in particular, those dealing with infinite projected entangled pair states (iPEPS), are also extensively used in the investigation of two-dimensional strongly correlated matter on the lattice. Recently, iPEPS tensor networks were successfully extended to the three-dimensional simple cubic lattice [1-2] and were used to investigate ground state properties of the Heisenberg model on this lattice.

Here we report our subsequent progress with development of three dimensional tensor network algorithms. In particular, we generalized iPEPS algorithms to face-centered cubic and diamond lattices with arbitrary unit cells. We have also developed a new version of the boundary PEPS optimization algorithm, that allowed us to circumvent the previous memory bottleneck on the simple cubic lattice.

The iPEPS on the face-centered cubic lattice was successfully employed to investigate the ground state of the Heisenberg model on this lattice. In contrast to simple cubic lattice, the face-centered cubic lattice is highly frustrated, and its ground state does not exhibit simple Neel order. Instead, there is a tight competition between two different magnetic orders, usually denoted as AF1 and AF3 (for more information see [3]). We studied both orders with 3d iPEPS tensor networks with bond dimension D=2, 3 (D=4 is work in progress) and compared the energies of the two orders. Our calculations point towards AF1 order as the true ground state, with its energy being approximately 0.3% lower. This agrees with recent results with other methods [3], but contradicts with some of the older results.

The authors acknowledge support by the National Research Foundation of Ukraine, project No. 2023.03/0073.

[1] P. C. G. Vlaar and P. Corboz, Simulation of three-dimensional quantum systems with projected entangled-pair states, Phys. Rev. B 103, 205137 (2021).
https://doi.org/10.1103/PhysRevB.103.205137.
[2] I. V. Lukin and A. G. Sotnikov, Single-layer tensor network approach for three-dimensional quantum systems, Phys. Rev. B 110, 064422 (2024).
https://doi.org/10.1103/PhysRevB.110.064422.
[3] Schick, R., Götze, O., Ziman, T., Zinke, R., Richter, J., & Zhitomirsky, M. E. (2022). Ground-state selection by magnon interactions in a fcc antiferromagnet. Phys. Rev. B 106.9 (2022): 094431.
https://doi.org/10.1103/PhysRevB.106.094431.

Tensor network study of quasi-one-dimensional Hubbard models

O. R. Hryniv[1,2], I. V. Lukin[1,2], A. G. Sotnikov[2,3]

[1]Haiqu, Inc., 95 Third Street, San Francisco, California 94103, United States
[2]Akhiezer Institute for Theoretical Physics, NSC KIPT, Akademichna 1, 61108 Kharkiv, Ukraine
[3]Karazin Kharkiv National University, Svobody Square 4, 61022 Kharkiv, Ukraine
e-mail: oleksa.hryniv@gmail.com

Tensor network methods have become one of the most powerful numerical approaches for studying strongly correlated quantum many-body systems. In particular, the matrix product state (MPS) formalism and the density matrix renormalization group (DMRG) algorithm provide highly accurate descriptions of ground states of one-dimensional lattice models. These methods are especially effective for systems with strong correlations, where conventional numerical techniques often encounter severe limitations.

In this work we report our recent progress in the development and application of tensor network algorithms for fermionic lattice models. In particular, we have implemented the infinite-size density matrix renormalization group (iDMRG) algorithm with support for arbitrary unit cells and internal symmetries. The method was tested on several benchmark models, including the one-dimensional Heisenberg and Hubbard models, where the obtained ground-state energies demonstrate excellent agreement with exact solutions and known results.

Using this framework, we study quasi-one-dimensional Hubbard systems that interpolate between strictly one-dimensional and two-dimensional geometries. In particular, we investigate the two-leg Hubbard ladder and the frustrated zigzag Hubbard chain, where next-nearest-neighbor hopping introduces kinetic frustration and leads to rich phase diagrams with competing magnetic and charge orders [1,2]. Such quasi-one-dimensional systems are known to exhibit diverse quantum phases and serve as important models for strongly correlated materials [3].

In addition, we explore the role of non-Abelian symmetries in tensor network simulations. The implemented algorithms incorporate SU(2) symmetry and are being generalized to higher symmetries such as SU(3) and SU(N). This significantly improves the computational efficiency and allows for the investigation of more complex fermionic systems.

As a further extension of this work, we develop tensor-network approaches for two-dimensional lattice models, including the two-dimensional Hubbard model. These studies aim to bridge the gap between quasi-one-dimensional systems and fully two-dimensional strongly correlated materials.

The authors acknowledge support by the National Research Foundation of Ukraine under the call “Excellence science in Ukraine” (2024-2026), project No. 2023.03/0073.

[1] E. Dagotto and T. M. Rice, “Surprises on the Way from One- to Two-Dimensional Quantum Magnets: The Ladder Materials,” Science 271, 618 (1996).
[2] S. Daul and R. M. Noack, “Ferromagnetic transition and phase diagram of the one-dimensional Hubbard model with next-nearest-neighbor hopping,” Phys. Rev. B 58, 2635 (1998).
[3] N. B. Ivanov, “Spin models of quasi-1D quantum ferrimagnets with competing interactions,” Condensed Matter Physics 12, 435 (2009).

Spin-dependent atomtronic current induced by asymmetric potential barriers in the Fermi-Hubbard lattice model

S. S. Litvinova[1], A. G. Sotnikov[1,2]

[1]V.N. Karazin Kharkiv National University, Svobody Square 4, 61022 Kharkiv, Ukraine
[2]Akhiezer Institute for Theoretical Physics, NSC KIPT, Akademichna 1, 61108 Kharkiv, Ukraine
e-mail: litvinova2022tya11@student.karazin.ua

Using numerical modeling, we investigate the emergence and evolution of directed spin currents in a one-dimensional interacting fermionic ring with static, spin-independent asymmetric potential barriers.

Spin transport is usually controlled by directly influencing the spin—using magnetic fields, spin–orbit coupling, or artificially created spin-dependent potentials. In our work, we demonstrate an alternative mechanism: by introducing spatial asymmetry in the potential barrier in a closed ring, finite spin-separated circulating currents arise even for initially spin-symmetric configurations. This effect can be enhanced or reversed in direction by appropriately preparing the initial state and adjusting the barrier asymmetry, with the resonant state of the barrier leading to the emergence of opposite spin currents. This opens up the possibility of controlling spin transport without direct spin selectivity of the potential.

Spin-flow control is a central goal of spintronics and is important for the development of energy-efficient information-processing devices with low dissipation. The results demonstrate the fundamental possibility of realizing controllable spin currents in minimal models, which may be useful for the development of new quantum memory elements, logic gates, and spin-current circuits in nanostructures.

The authors acknowledge support by the National Research Foundation of Ukraine under the call "Excellence science in Ukraine" (2024-2026), project No. 2023.03/0073.

Inhomogeneous equilibrium structures in s=3/2 magnets under spontaneously broken SO(3)×U(1) symmetry

M. Yu. Kovalevsky, M. G. Shatnev

National Science Center "Kharkiv Institute of Physics and Technology" of NAS of Ukraine,
1, Akademicheskaya St., Kharkiv, 61108, Ukraine
e-mail: mik@kipt.kharkov.ua, mshatnev@yahoo.com

This work is motivated by the development of spintronics and the recognition of the role of inhomogeneous magnetic structures in their practical applications. The origin of such structures is diverse and can be attributed to the chirality properties of the magnet, competition of magnetic interactions, or spontaneous symmetry breaking. Spin-orbit coupling enables the transfer of spatial anisotropy of the material into the space of magnetic degrees of freedom. Interest in spiral magnetic structures is motivated by the demand for high-density memory devices, reduced energy consumption, and the possibility of tuning the magnetization of the layers [1, 2].

We examine equilibrium states of a medium in which both magnetic and spatial symmetries are simultaneously broken, with particles having spin s=3/2 and exchange Hamiltonian symmetry SO(3)×U(1). Our study is based on the approach developed in [3]. Inhomogeneous solutions for the magnetic degrees of freedom are presented and analyzed. Graphical materials of the corresponding three-dimensional structures are obtained. We note that, alongside the emergence of well-known inhomogeneous structures, the possibility arises for realizing alternative inhomogeneous states driven by the influence of additional magnetic degrees of freedom associated with the spontaneously broken symmetry of the equilibrium state. In particular, for the vector fields, the possibility emerges for modulation of longitudinal and transverse components characterized by two periods.

[1] See-Hun Yang, Ron Naaman, Yossi Paltiel, Stuart S.P. Parkin Nature reviews physics, 3, pp. 328–343 (2021).
[2] Tao Yu, Zhaochu Luo, Gerrit E.W. Bauer, Physics Reports 1009 pp. 1-115 (2023).
[3] M.Y. Kovalevsky, Low Temp. Phys. 52 43-49 (2026). http://doi.org/10.1063/10.0042161.

Statistical ensembles for non-Boltzmann-Gibbs distributions of Ising-Markov sequences

O. V. Usatenko[1,2]

[1]A.Ya. Usikov Institute for Radiophysics and Electronics Ukrainian Academy of Science, 12 Proskura Street, 61805 Kharkiv, Ukraine
[2]Center for Theoretical Physics, Polish Academy of Sciences, Al. Lotnikow 32/46, 02-668 Warsaw, Poland
e-mail: usatenkoleg@gmail.com

Temperature is one of the fundamental quantities in statistical physics and thermodynamics. In the classical Boltzmann-Gibbs framework, temperature emerges as the parameter conjugate to energy and governs the exponential weighting of configurations. However, in many information-theoretic and stochastic systems, where the concept of interaction energy of subsystems is absent, its introduction is rather non-obvious, since the absence of energy precludes the formulation of the concept of a system's statistical ensemble and the introduction of its statistical weight. The main result of the present work is the construction of a statistical ensemble for binary Markov sequences based on auxiliary interaction energies and the introduction of an information temperature defined through entropy and energy of short fragments. Considered as a binary, a $\epsilon \{0,1\}$, the step-wise Markov chain [1] is characterized by the correlation parameter μ, satisfying $|\mu|<1/2$.

The first, natural method is based on an association of a Markov chain and a two-sided random chain [2], as well as relating the latter with the Boltzmann distribution. Despite the apparent simplicity of the method, it turns out that the statistics of Markov and Ising chains not only do not coincide but also cannot always be reduced to a one-to-one correspondence.

The second approach [3] to introducing temperature uses its standard definition in terms of entropy and energy. However, unlike the first approach, here we are not interested in whether the chain of symbols-spins obeys the Boltzmann distribution at a given temperature. By introducing fictitious auxiliary energies of spin, s=2a-1, interaction with nearest neighbors 1and next to them 2energies, using the Chapmen-Kolmogorov equation, we calculate the entropy and average auxiliary energy of binary two-step Markov sequence of 3-symbol fragments and introduce the information temperature, $-\infty < \tau < \infty$, as the derivative of the entropy with respect to energy, 1/T=dS/dE,

$$\frac{1}{\tau} = \frac{1}{4}\ln\frac{1+2\mu}{1-2\mu}, \qquad \tau = \frac{T}{\langle\varepsilon\rangle}, \qquad \langle\varepsilon\rangle = \frac{2\varepsilon_1+\varepsilon_2}{3}$$

Here the positive and negative values of μ and τ describe ferromagnetic persistent and anti-ferromagnetic anti-persistent correlations, respectively. The ratio for 1/τ can be viewed in different ways. Either, we can equate 1and 2 to one, in which case the resulting value of τ can be considered an absolute temperature. Another approach is to consider $\langle\varepsilon\rangle$ as a scale for measuring the temperature of the Markov chain. Third, the most important observation is that the two introduced auxiliary energy effectively determine the state of the statistical ensemble. Its important property is related to the rapid growth of the number of configurations with energy, which makes the entropy weakly sensitive to the specific definition of statistical weights.

These results demonstrate that a consistent thermodynamic description of correlated symbolic sequences can be constructed even in the absence of a genuine Boltzmann distribution.

[1] O. V. Usatenko and V. A. Yampolskii, Phys. Rev. Lett. 90, 11060 (2003). https://doi.org/10.1103/PhysRevLett.90.11060.
[2] S. S. Apostolov, Z. A. Mayzelis, O. V. Usatenko, and V. A. Yampol'skii. Europhys. Lett. 76, 1015 (2006). DOI 10.1209/epl/i2006-10410-4.
[3] O. V. Usatenko, S. S. Melnyk, G. M. Pritula, and V. A. Yampol'skii, Phys. Rev. E 106, 034127 (2022). https://doi/10.1103/PhysRevE.106.034127.

Resonant transmission of nonlinear terahertz waves through layered superconductors

T. Rokhmanova[1], Z. Maizelis[1,2], V. Yampol'skii[2]

[1]O.Ya. Usikov Institute for Radiophysics and Electronics, NAS of Ukraine, 61085 Kharkiv, Ukraine
[2]V.N. Karazin Kharkiv National University, 61022 Kharkiv, Ukraine
e-mail: tetiana.rokhmanova@karazin.ua

Layered superconductors are periodic structures, in which thin superconducting layers are coupled through comparatively thicker dielectric layers via the intrinsic Josephson effect (see e.g., [1]). They exhibit unusual electromagnetic properties caused by strong anisotropy of their structure. This anisotropy leads to a decrease of the effective plasma frequency to the terahertz range and makes layered superconductors promising materials for terahertz applications [2]. A remarkable feature of these systems is the intrinsic nonlinearity of their electrodynamics, originating from the nonlinear dependence of the interlayer Josephson current on the phase difference between superconducting layers. It enables researchers to predict a wide range of striking phenomena such as self-induced transparency, hysteretic response, specific superposition rules, and laser focusing (see e.g. [3]). There are also many recent experiments that observed amplification of Josephson plasmons, enhanced coherent terahertz emission, anomalous emission, and selective phase excitation (see e.g. [4]).

In this work, we theoretically study the transmission of terahertz electromagnetic waves through a layered superconductor placed between two dielectric media in the bilateral Otto configuration in the nonlinear regime. A mathematical model describing wave propagation in the system is developed on the basis of the coupled sine-Gordon equations in the continuous limit. The dependence of the transmission coefficient on the amplitude of the incident wave, the angle of incidence, the thickness of dielectric gaps, and the thickness of the layered superconductor is analyzed.

We demonstrate that nonlinear Josephson plasma waves can be excited in this configuration and that localized modes may arise in the layered superconducting plate. For certain values of system parameters, the excitation of such localized nonlinear modes leads to resonant transmission, potentially reaching total transmittance. The obtained results show hysteretic behavior and nontrivial amplitude-dependent transmission effects and indicate the possibility of controlling terahertz wave propagation using nonlinear properties of layered superconductors.

The research was conducted under the support of National Research Foundation of Ukraine, Project No. 2025.07/0256 "Electrodynamic linear and nonlinear phenomena in layered superconductors".

[1] R. Kleiner and P. Müller, "Intrinsic Josephson effects in high-Tc superconductors," Phys. Rev. B, vol. 49, no. 2, pp. 1327–1341, 1994. https://doi.org/10.1103/PhysRevB.49.1327.
[2] T. Kashiwagi, H. Kubo, K. Sakamoto, et al, "The present status of high-Tc superconducting terahertz emitters," Supercond. Sci. Technol, vol. 30, no. 7, p. 074008, 2017. https://doi.org/10.1088/1361-6668/aa6dd7.
[3] N. Kvitka, H. V. Ovcharenko, Z. A. Maizelis, S. S. Apostolov, and V. A. Yampol'skii, "Layered superconductors as nonlinear lenses for laser beams tunable by dc magnetic field," Phys. Rev. B, vol. 110, p. 174517, Nov 2024. https://doi.org/10.1103/PhysRevB.110.174517.
[4] N. Taherian, M. Först, A. Liu, et al, "Probing amplified josephson plasmons in YBa2Cu3O6+x by multidimensional spectroscopy," npj Quantum Materials, vol. 10, 2025. https://doi.org/10.1038/s41535-025-00776-1.

Impact of frequency noise statistics on measurement-assisted entanglement

A. O. Guzenko[1], O. M. Konovalenko[1] and Z. A. Maizelis[1,2]

[1]O. Ya. Usikov Institute for Radiophysics and Electronics of the NASU,
12, Ac. Proskura st., Kharkiv, 61085, Ukraine
[2]V. N. Karazin Kharkiv National University,
4 Svobody Sq., Kharkiv, 61022, Ukraine
e-mail: guzenko.anastasiya@gmail.com

Low-frequency fluctuations in qubit transition frequencies represent a major source of decoherence in solid-state quantum devices. In superconducting and mesoscopic systems, these fluctuations are typically attributed to microscopic fluctuators and exhibit long correlation times as well as non-Gaussian statistics [1,2]. Since this noise cannot be described by simple Markovian dephasing, it affects the dynamics of entangled states in complex ways [3].

We investigate the dynamics of an entangled two-qubit register exposed to frequency noise with varying statistical characteristics. The system evolution is modeled using the Lindblad master equation, which incorporates both relaxation and thermal excitation, while classical longitudinal noise modulates the transition frequencies [4]. We implement a protocol that involves repeated rank-1 projections onto a target Bell state to preserve entanglement, using a mechanism similar to the Quantum Zeno effect. [5].

Analytic asymptotic expressions for the noise-averaged dynamics and entanglement concurrence are derived for three representative models: Gaussian Ornstein-Uhlenbeck noise, random-telegraph noise from bistable fluctuators, and Poissonian phase jumps [3]. The influence of frequency noise is incorporated through phase-memory factors that describe the decay of the relevant two-qubit coherence. In the dephasing-dominated regime, these factors determine the short-time behavior of the concurrence and reveal distinct signatures of Gaussian and non-Gaussian noise statistics. To quantify the protocol's effectiveness, we introduce a survival-gain metric comparing measurement-assisted evolution to free decay.

Our results demonstrate that repeated projections can significantly extend entanglement lifetimes. Crucially, the protocol's performance is sensitive to higher-order noise statistics, even when the integrated noise power is matched across models.

We identify regimes in which non-Gaussian features either enhance or limit the effectiveness of Zeno-based stabilization. These findings provide guidelines for selecting measurement intervals based on the characteristic noise timescales of solid-state qubit registers.

[1] M. Spiecker, A. Pavlov, S. N. Filippov, and A. Pechen, Solomon equations for qubit and two-level systems: Insights into non-Poissonian and non-Markovian fluctuations, Phys. Rev. A 109, 052218 (2024). https://doi.org/10.1103/PhysRevA.109.052218.
[2] S. Sung, Non-gaussian noise spectroscopy with a superconducting qubit sensor, Nature Communications 10 (2019). https://doi.org/10.1038/s41467-019-11699-4.
[3] E. Paladino, Y. M. Galperin, G. Falci, and B. L. Altshuler, 1/f noise: Implications for solid-state quantum information, Rev. Mod. Phys. 86, 361418 (2014). https://doi.org/10.1103/RevModPhys.86.361.
[4] H.-P. Breuer and F. Petruccione, The Theory of Open Quantum Systems (2006). https://doi.org/10.1093/acprof:oso/9780199213900.001.0001.
[5] S. Maniscalco, F. Francica, R. L. Zano, N. Lo Gullo, and F. Plastina, Protecting entanglement via the quantum zeno effect, Physical Review Letters 100, 090503 (2008). https://doi.org/10.1103/PhysRevLett.100.090503.

Sensitivity of two qubit Werner state entanglement preservation to decoherence parameters in measurement based protocol

O. Konovalenko[1], Z. Maizelis[1,2]

[1]O. Ya. Usikov Institute for Radiophysics and Electronics of the NAS of Ukraine, 12 Ac. Proskura st., Kharkiv, 61085, Ukraine
[2]V. N. Karazin Kharkiv National University, 4 Svobody Sq., Kharkiv, 61022, Ukraine
e-mail: o.konovalenko34@gmail.com

We study how the effectiveness of a measurement-assisted entanglement-protection scheme depends on the parameters that describe environmental decoherence in a system of two qubits prepared in a Werner state [1,2]. The considered protocol is based on periodically repeated joint measurements and is aimed at extending the lifetime of coherence responsible for bipartite quantum correlations [1,3-5]. Each qubit is assumed to interact with its own dissipative reservoir through linear channels with rates γ_1 and γ_2, while both qubits are also subject to identical dispersive couplings, $\gamma_{\perp 1} = \gamma_{\perp 2} = \gamma_\perp$. To characterize the action of the protocol, we use an efficiency parameter η, which measures the degree to which the measurement sequence reduces coherence decay and, consequently, supports entanglement retention [1].

For the initially maximally entangled case, corresponding to the Werner parameter $p = 1$, the behavior of η is strongly determined by the competition between linear and dispersive decoherence channels. In the region where the linear couplings dominate and $\gamma_\perp$ remains much smaller than γ_1 and γ_2, the efficiency follows a hyperbolic trend as a function of $\gamma_\perp$. By contrast, when the dispersive interaction becomes the leading mechanism, that is, for $\gamma_1, \gamma_2 \ll \gamma_\perp$, the value of η tends to unity, which signals that the measurements no longer provide noticeable suppression of decoherence [1].

The influence of the thermal occupation parameter n and the qubit frequency ω_1 on the dependencies $\eta(\gamma_1), \eta(\gamma_\perp)$ has also been investigated. An increase in n is found to improve the efficiency of the suppression procedure. The role of ω_1 is more intricate: the corresponding maps contain side regions with neutral or enhanced efficiency and a central domain of reduced performance. For $p = 0.9$, in comparison with $p = 1$, the overall efficiency decreases and the structure of the parameter-space patterns becomes simpler. The obtained results indicate that properly adjusted measurement strategies, especially for strongly entangled initial states, can noticeably weaken environmental degradation and may be useful for quantum communication and quantum-computing applications relying on stable two-qubit correlations.

[1] O. M. Konovalenko and Z. A. Maizelis, J. V. N. Karazin Kharkiv Natl. Univ. Ser. Phys. 42, 22--26 (2025).
http://dx.doi.org/10.26565/2222-5617-2025-42-02.
[2] R. F. Werner, Phys. Rev. A 40, 4277--4281 (1989).
http://dx.doi.org/10.1103/PhysRevA.40.4277.
[3] P. Facchi and S. Pascazio, J. Phys. A: Math. Theor. 41, 493001 (2008).
http://dx.doi.org/10.1088/1751-8113/41/49/493001.
[4] K. Koshino and A. Shimizu, Phys. Rep. 412, 191--275 (2005).
http://dx.doi.org/10.1016/j.physrep.2005.03.001.
[5] S. Maniscalco, F. Francica, R. L. Zaffino, N. Lo Gullo, and F. Plastina, Phys. Rev. Lett. 100, 090503 (2008). http://dx.doi.org/10.1103/PhysRevLett.100.090503.

Exceptional-point control of reset-induced quantum Zeno and anti-Zeno transport

J. Kumar

Department of Applied Physics, Aalto University,
P.O. Box 15600, FI-00076 Aalto, Espoo, Finland
e-mail: kumar.jishad@gmail.com

Frequent interventions on an open quantum system can suppress or enhance decay, giving rise to quantum Zeno and anti-Zeno effects, but their impact on coherent transport in extended systems remains less explored. Motivated by continuous resetting protocols in quadratic open systems, we develop a microscopic theory of reset-controlled transport through a tight-binding chain with a bright/dark lossy region coupled to a structured reservoir. Starting from a repeated-interaction model, we derive a Kofman-Kurizki-type decay rate whose dependence on the reset interval is governed by a sinc-squared filter. For smooth Ohmic baths this produces a purely Zeno-like suppression of transport, whereas for Lorentzian structured baths it yields a pronounced Zeno–anti-Zeno crossover that is reflected in the transmission of a single bright/dark dimer and in the exponential attenuation of chains of many dimers. We map out energy- and length-resolved transport phase diagrams, extend the resetting protocol to finite-temperature reservoirs, and analyze charge and heat currents within a Landauer framework. Finally, by periodically repeating the bright/dark cell we construct a reset-controlled non-Hermitian lattice whose complex Bloch bands host exceptional points (EP) tuned by the reset interval; the corresponding EP time coincides with the strongest suppression of transport, establishing a direct link between resetting protocols, Kofman-Kurizki dynamical control, and non-Hermitian band engineering in mesoscopic quantum transport.

[1] Jishad Kumar, Exceptional-point control of reset-induced quantum Zeno and anti-Zeno transport, Physical Review B (accepted 2026).

First-principles investigation of Mg_3XH_4 (X = Sc, Ti) hydrides: structural, electronic, elastic, thermodynamic, and hydrogen storage properties

C. Aksu[1], N. Arikan[1], A. İyigör[2] and E. Tel[1]

[1]Department of Physics, Osmaniye Korkut Ata University, Faculty of Engineering and Natural Sciences, 80100 Osmaniye, Türkiye
[2]Department of Machine and Metal Technologies, 40100 Kırşehir Ahi Evran University, Kırşehir, Türkiye
e-mail: cevataksu@hotmail.com.tr, nihatarikan@osmaniye.edu.tr, ahmetiyigor@ahievran.edu.tr, eyuptel@osmaniye.edu.tr

This study employs first-principles calculations to comprehensively examine the physical properties of cubic Mg_3XH_4 (X = Sc, Ti) alloys, with particular emphasis on their potential applications in hydrogen storage. The structural, electronic, elastic, and thermodynamic characteristics of both materials are systematically analyzed. The two alloys exhibit moderate efficiency in hydrogen storage applications. The calculated formation energies of Mg_3XH_4 (X = Sc, Ti) are negative, supporting the possibility of experimental synthesis of the investigated compounds. The electronic band structures of Mg_3ScH_4 and Mg_3TiH_4 reveal metallic behavior, as energy bands intersect the Fermi level in both systems. The evolution of elastic constants indicates mechanical stability according to the Born stability criteria for both materials; Mg_3TiH_4, having higher bulk and shear moduli, demonstrates greater resistance to compression. In addition, thermodynamic parameters including free energy, entropy, specific heat capacity, Debye temperature, and melting temperature have been predicted and discussed. Although Mg_3ScH_4 and Mg_3TiH_4 display comparable gravimetric hydrogen capacities (3.31% and 3.23%, respectively), their relatively high desorption temperatures (711 K and 658 K) indicate that further thermodynamic or structural tuning would be required to achieve practical hydrogen storage performance.

Predicting magnetic properties of one-dimensional Ising systems with arbitrary lattice geometry

O. O. Kryvchikov, D. V. Laptiev

B.Verkin Institute for Low Temperature Physics and Engineering of the NAS of Ukraine,
47 Nauky Ave., Kharkiv, 61103, Ukraine
e-mail: Kryvchikov@ilt.kharkov.ua

We present a graph-based deep learning framework for predicting magnetization curves in one-dimensional antiferromagnetic Ising systems. The Hamiltonian is reformulated in terms of repeating structural units. It can be represented as repeating blocks defined by intra- and inter-block coupling matrices that uniquely determine the interaction graph. In this case the lattice is represented as a graph with spins as nodes and non-zero couplings as edges. This graph used as input to a graph neural network (GNN).

The model is trained on Monte Carlo data generated for interaction graphs with different levels of frustration and symmetry. Once trained, it enables immediate prediction of magnetization curves for new graphs without performing additional Monte Carlo simulations. Given an interaction graph, the GNN outputs the magnetization as a function of the external magnetic field.

The use of a unified graph representation ensures applicability across systems with different sizes and geometries, including irregular unit cells, without retraining or modification of the model architecture. Evaluation on previously unseen graphs shows accurate reproduction of key features of the magnetization curve, including plateaus, transition fields, and frustration-induced behavior.

The model was tested on systems with different lattice geometries. In favorable cases, the mean prediction error reaches 0.045, with the largest deviations observed for highly regular geometries such as two-leg ladder structures. The model exhibits sensitivity to both local structural motifs and global symmetries.

By eliminating the need for repeated Monte Carlo simulations, the proposed approach offers a computationally efficient alternative for estimating magnetic response functions in low-dimensional systems. The results support the broader applicability of graph-based models in statistical physics and indicate potential extensions to higher-dimensional systems and other spin models such as the Potts or Heisenberg variants.

[1] M. Withnall, et al., J. Cheminform. 12, 1 (2020).
[2] L. A. Pastur and V. Y. Slavin, arXiv preprint arXiv:2302.14382 (2023).
[3] D. V. Laptiev, et al., Low Temp. Phys. 50, 158 (2024). Originally published in Fiz. Nizk. Temp., pp. 158–166.

Zero-temperature phase diagrams and thermodynamic properties of the armchair-type and zigzag-type decorated honeycomb Ising spin chains

D. V. Laptiev, O. O. Kryvchikov

B.Verkin Institute for Low Temperature Physics and Engineering of the NAS of Ukraine,
47 Nauky Ave., Kharkiv, 61103, Ukraine
e-mail: laptev@ilt.kharkov.ua

Decorated spin lattices constitute an important class of exactly solvable models in statistical physics and the theory of magnetism [1]. In such systems additional magnetic ions are inserted between the sites of an underlying lattice, leading to competing exchange interactions and geometric frustration. Frustrated magnetic systems [2] exhibit unusual thermodynamic phenomena such as magnetization plateaux, macroscopic ground-state degeneracy and nonzero residual entropy at zero temperature, which are of fundamental interest for the theory of phase transitions and for the interpretation of experimental data in low-dimensional magnetic compounds.

In the present work we investigate frustrated decorated honeycomb Ising chains obtained as quasi-one-dimensional cuts of a decorated honeycomb lattice. The honeycomb lattice has the same topology as the graphene lattice, and two natural directions of cuts generate chains of armchair-type and zigzag-type geometries. Each chain consists of triangular spin units formed by three classical Ising spins $S = \pm 1$ coupled by identical intra-triangle exchange interactions, while additional exchange bonds connect neighboring triangles along the chain. The models are analyzed using the Kramers–Wannier transfer-matrix method [3], which allows one to obtain exact expressions for the partition function and calculate thermodynamic quantities. To construct the transfer matrices we employ a graph-theoretical representation of the spin lattice in which the elementary blocks of the chain are treated as finite graphs whose boundary vertices define the spin variables entering the transfer matrix. An important difference between the two geometries is the number of boundary spins of the elementary block. In the armchair-type chain the block contains more boundary spins than in the zigzag-type chain, which leads to different transfer-matrix dimensions and different sets of possible ground states and magnetization plateaux. The zero-temperature phase diagrams are obtained by comparing the energies of block configurations in an external magnetic field. Since the exchange interactions repeat periodically along the chain, the ground states are also periodic and can be described in terms of a magnetic unit cell. Due to the frustrated character of the triangular units, the systems exhibit highly degenerate ground states in certain parameter regions, resulting in nonzero residual entropy in the thermodynamic limit. A remarkable feature of the frustrated decorated chains is that the number of degenerate ground states follows well-known integer sequences. In particular, in some parameter regimes the degeneracy obeys Fibonacci-type recurrence relations, so that the residual entropy per spin can be expressed through logarithms of algebraic constants related to these sequences, including the golden ratio. The magnetization curves exhibit fractional plateaux corresponding to different arrangements of triangular spin units. The plateau structure depends on the chain geometry and interaction parameters. Within the transfer-matrix framework we also calculate the temperature dependences of entropy, magnetic susceptibility and heat capacity.

The obtained results demonstrate that decorated honeycomb Ising chains provide a convenient exactly solvable model for studying geometric frustration in low-dimensional magnetic systems. The combination of transfer-matrix techniques with graph-theoretical analysis reveals the combinatorial structure of the ground states and the associated thermodynamic anomalies.

[1] D. V. Laptiev, O.O. Kryvchikov, Yu. V. Savin and V. V. Slavin, Low Temperature Physics/Fizika Nizkikh Temperatur. vol. 50, No. 2, pp. 168–176 (2024).
[2] I. Syozi and H. Nakano, Progress of Theoretical Physics. 13, 69 (1955).
[3] A. V. Zarubin, F. A. Kassan-Ogly, A. I. Proshkin, J. Phys.: Conf. Ser. 1389 012009 (2019).

Influence of magnetic quantization and exchange interaction on the seebeck coefficient in diluted magnetic semiconductor superlattices

M. M. Mahmudov, R. Y. Damirov

Baku State University, 23 Street Z. Khalilov, AZ1148, Baku, Azerbaijan
e-mail: damirovraghib@gmail.com

Enhancing the thermoelectric figure of merit ZT beyond unity remains a central challenge in modern solid-state physics. Low-dimensional heterostructures provide a promising route toward improving thermoelectric efficiency, since quantum confinement modifies the electronic density of states. Interface scattering further suppresses phonon heat transport, reducing thermal conductivity. Diluted magnetic semiconductors (DMS), particularly II–VI compounds such as *CdTe* partially substituted by Mn^{2+} ions, introduce an additional degree of freedom through the exchange interaction between itinerant carriers and localized manganese spins [1]. Because this interaction strongly depends on temperature and magnetic field, DMS superlattices placed in quantizing magnetic fields represent an attractive platform for studying magnetothermoelectric effects [2]. We consider a superlattice consisting of a periodic stack of quantum wells with period *a* along the growth direction z. A magnetic field ***B*** is applied perpendicular to the layers. The Seebeck coefficient is derived using a thermodynamic approach rather than the Boltzmann transport equation. Starting from the relation:

$$\alpha = -\frac{1}{e}\left(\frac{\partial \zeta}{\partial T}\right)_{n,B} \tag{1}$$

and applying the Maxwell identity, the thermopower can be written as

$$\alpha = \frac{S}{Ne} = \frac{S}{neV} \tag{2}$$

where *S* is the electronic entropy. In the degenerate limit the entropy is evaluated using the Sommerfeld expansion. For a two-dimensional electron gas with N_{max} occupied Landau levels, the Seebeck coefficient takes the analytical form

$$\alpha = \frac{\pi k_B^2 TB}{6\hbar^2 an} \tag{3}$$

This expression leads to several characteristic scaling relations:

$$\alpha = \frac{\pi k_B^2 T}{6\hbar e}\frac{1}{N_{max}+1} = \frac{k_B^2 T m^*}{3\hbar en} \tag{4}$$

Thus, the thermopower increases linearly with temperature and magnetic field, while it is inversely proportional to the two-dimensional carrier density. In strong magnetic fields the discrete Landau level structure leads to oscillatory behavior similar to de Haas–van Alphen oscillations.

The exchange interaction between conduction electrons and Mn^{2+} spins introduce an additional contribution to the thermopower,

$$\alpha_{ex} = \frac{25\alpha x g_J \mu_B B}{e k_B T^2} \exp\left(\frac{5 g_J \mu_B B}{2 k_B T}\right) \tag{5}$$

which depends strongly on temperature and magnetic field. At moderate fields this term can enhance the thermoelectric response, whereas in the strong-field limit the saturation of Mn spins suppresses the exchange contribution. The obtained results provide experimentally testable predictions for magneto-Seebeck measurements in *CdMnTe* and *ZnMnSe* superlattices. Diluted magnetic semiconductor heterostructures thus offer a magnetically tunable platform for thermoelectric transport, with potential applications in low-dimensional spintronic devices.

[1] Kossut, J., Gaj, J.A. (2010). Introduction to the physics of diluted magnetic semiconductors. Springer Berlin, Heidelberg. https://doi.org/10.1007/978-3-642-15856-8
[2] Figarova S.R., Mahmudov M.M., Damirov R.Y. Magnetization of diluted magnetic semiconductor II type superlattices with impurities Mn (manganese) ions. Journal of Baku Engineering University, Physics. 2024, 8 (1), 9-15. 10.30546/09081.2024.101.5002.

Current-Voltage & Current ? Phase of superconducting order parameter scattering matrix for semiconducting & superconducting structures

K. Pomorski[1,2], D. Khadka[1], M. Osinski[1]

[1]University of New Mexico, Center for High Technology Materials, Albuquerque, USA
[2]Quantum Hardware Systems, Lodz, Poland
e-mail: kdvpomorski@gmail.com

The methodology of scattering matrices for input/output state vector describing current-voltage (I,V) or current-phase of superconducting order parameter (I,Θ) is employed to describe transport properties of normal and superconducting state systems in 1, 2 and 3 dimensions. It allows for justification of various measurement methodologies as van der Pauw measurement scheme. It has also potential in bringing new modeling methodologies in study of supercondncuting-semiconductor hybrid systems in the framework of analytical, semi-analytical and numerical view.

Temperature-dependent dopant ionization and electrostatic behavior in n-β-Ga_2O_3/p-Si heterostructures

J. Abdullayev[1], M. Ibragimova[2]

[1]National Research University TIIAME, Department of Physics and Chemistry, Tashkent, Uzbekistan
[2]Urgench State University, Hamid Olimjon street 14, Urgench, 220100 Uzbekistan
e-mail: j.sh.abdullayev6@gmail.com

Incomplete dopant ionization plays a fundamental role in governing the electrostatics and capacitance response of n-type β-Ga_2O_3/p-type Si heterojunctions. Using a physics-based theoretical framework incorporating temperature- and doping-dependent ionization, band alignment, and mobility degradation, we analyze shallow and deep donors/acceptors' impact on depletion width, junction capacitance, and peak electric field over 77–300 K. Modeling shows that carrier freeze-out in moderate-doping junctions ($N_A = N_D = 4\times10^{17}$ cm^{-3}) reduces forward capacitance by ~17%, widens the depletion region by ~0.10 μm, and lowers the peak electric field by ~0.5 MV/cm, while high-doping devices ($N_A = N_D = 1\times10^{18}$ cm^{-3}) exhibit smaller variations (<5%). Progressive dopant activation between 150–250 K and near-complete ionization above 300 K confirm convergence with full-ionization predictions. These results provide a quantitative theoretical framework for understanding freeze-out effects in wide-bandgap oxide/Si heterojunctions, guiding future device design.

Inverse problem of electron scattering on the potential of the multilayer semiconductor resonance-tunneling structure

I. V. Boyko[1], Yu. O. Seti[2]

[1]Ternopil Ivan Puluj National Technical University,
56 Ruska Str., Ternopil, 46001, Ukraine
[2]Lviv Polytechnic National University,
12 Stepan Bandera Str., Lviv, 79013, Ukraine
e-mail: boyko.i.v.theory@gmail.com

Electron tunneling in multilayer semiconductor quantum cascade lasers and detectors [1, 2] is physically equivalent to electron scattering by the effective potential of nanostructures in the presence of static and time-dependent fields. At the same time, the geometric configuration of the potential profile in multilayer structures determines the spectral characteristics of electronic quasi-stationary states and their scattering properties, such as the lifetime and scattering cross section. Solving the direct problem of quantum scattering theory for the effective potential of a nanostructure makes it possible to determine and analyze the spectral characteristics of electron quasi-stationary states, including their resonance energies and widths, as well as to calculate the electrical conductivity or tunneling current. In the general case, the direct problem of electron scattering theory in multilayer nanostructures consists in solving the full Schrödinger equation given below

$$i\hbar\frac{\partial\Psi(x,t)}{\partial t}=\left[-\frac{\hbar^2}{2}\frac{\partial}{\partial x}\frac{1}{m(x)}\frac{\partial}{\partial x}+U_{eff}(x)+H(x,t)\right]\Psi(x,t), \qquad (1)$$

where $U_{eff}(x)$ is the effective potential of the nanostructure for an electron, $H(x,t)$ is its time-dependent component, $m(x)$ - is the time-dependent effective mass of an electron in a nanostructure. Solving the full Schrödinger equation (1) makes it possible to determine the spectral parameters of electronic stationary states and to analyze their dependence on the geometric configuration of the structure.

A completely different class of problems arises when experimental or computational data are available that provide information about the electronic wave function of a nanostructure and its behavior at the heterointerfaces. This represents a fundamentally different class of problems in quantum scattering theory, namely the reconstruction of the spatial profile of the potential in nanostructures from spectral and wave-function data. For multilayer nanostructures, this class of problems is still in its early stages of development; however, its importance stems from the need to efficiently process experimental data in order to reconstruct potential profiles for subsequent theoretical calculations and modeling of electron transport. In the present work, we solve the non-stationary inverse problem of quantum scattering theory, aimed at reconstructing the potential of a multilayer nanostructure from complete time-dependent scattering data. The restored effective potential of the nanostructure as the sum of the stationary and time-dependent components is obtained in the form of Marchenko's functional equation with scattering function $F(x,t)$:

$$\begin{aligned}&U_{eff}(\xi,t)=H_0\left[x(\xi)\right]+H\left[x(\xi),t\right]+V_m(\xi);\ V_m(\xi)=\left(\hbar^2/2m_0\right)\left[5\left(m'\right)^2/16m^3-m''/4m^2\right]\Big|_{x=x(\xi)};\\&U_{eff}(\xi,t)=-2\frac{K(\xi,\xi,t)}{\partial\xi};\ K(\xi,y,y)+F(\xi+y,t)+\int_{\xi}^{+\infty}K(\xi,s,t)F(s+y,t)ds=0,\ y\geq\xi.\end{aligned} \qquad (2)$$

[1] Y. Hu, S. Suri, J. Kirch, B. Knipfer, S. Jacobs, S. K. Nair, Z. Zhou, Z. Yu, D. Botez, and L. J. Mawst, Appl. Phys. Lett. 124, 241103 (2024). http://dx.doi.org/10.1063/5.0209613.
[2] B. Chomet, D. Gacemi, O. Lopez, L. Del Balzo, A. Vasanelli, Yanko Todorov, Benoît Darquié, and C. Sirtori, Appl. Phys. Lett. 122, 231103 (2023). http://dx.doi.org/10.1063/5.0152013.

Multipolar exchange in many-body homonuclear mixture of atoms in different internal states

M. Bulakhov[1], A. S. Peletminskii[1], and Yu. V. Slyusarenko[1,2,3]

[1]Akhiezer Institute for Theoretical Physics, National Science Center "Kharkiv Institute of Physics and Technology", NAS of Ukraine, 1 Akademichna Str., 61108 Kharkiv, Ukraine
[2]V.N. Karazin Kharkiv National University, 4 Svobody Sq., 61022 Kharkiv, Ukraine
[3]Lviv Polytechnic National University, 79000 Lviv, Ukraine
e-mail: bulakh@kipt.kharkov.ua

We develop a general method to construct the many-body Hamiltonian of pairwise interaction for homonuclear mixtures with atoms occupying states of different total angular momentum or other quantum numbers. The advantage of the irreducible spherical tensor operator formalism is demonstrated: these operators give the Hamiltonian an explicit physical structure, account for all scattering channels, and include multipolar exchange interactions [1]. The latter are associated with the exchange of both angular-momentum projections and the total angular momentum. Particular realizations of the general Hamiltonian, widely used in the physics of ultracold gases, are also analyzed. The resulting Hamiltonian provides a universal framework for investigating a broad range of quantum many-body phenomena in bosonic and fermionic atomic gases.

The authors acknowledge support by the National Research Foundation of Ukraine under the call “Excellence science in Ukraine” (2024-2026), project No. 2023.03/0073.

[1] Bulakhov M., Peletminskii A.S., Slyusarenko Yu.V. General collisionless kinetic approach to studying excitations in arbitrary-spin quantum atomic gases. Annals of Physics 2025, Vol. 474. P. 169920. DOI: 10.1016/j.aop.2025.169920.

Domain walls and breathers in metamaterials constructed of magnetic molecules

O. V. Charkina, M. M. Bogdan

B.Verkin Institute for Low Temperature Physics and Engineering of NAS of Ukraine,
47 Nauky Ave., Kharkiv, 61103, Ukraine
e-mail: charkina@ilt.kharkov.ua

The idea of creating a low-dimensional magnetic metamaterial in the form of a molecular crystal, in which molecular nanoclusters, are regularly arranged in the form of chains, separated by non-magnetic organic structures, has been proposed in [1]. Such molecular nanomagnets, so-called "magnetic molecules", consist of alternating magnetic ions and radicals whose spins are not the same. In the ground state, they are the ring ferrimagnets with a large total spin [2]. Due to the special molecule arrangement, one may obtain a quasi-one-dimensional metamaterial with a given structure period and, accordingly, with a given interaction parameter between classical spins, which can be either of the same order or much less than the single-ion anisotropy constant.

In the present contribution the theoretical study of the structure of topological and non-topological excitations and their nonlinear dynamics in such artificial ferromagnetic spin chains has been carried out. In particular, domain walls and their internal modes, as well as magnetic breathers are studied, starting from the Landau-Lifshitz equation for the chain magnetization. In the case of biaxial anisotropy with a predominant "easy plane" anisotropy, the equation is reduced to the discrete Takeno-Homma equation [3] for the variables of the azimuthal angle of the total spin of magnetic molecules.

In the framework of the Takeno-Homma equation, numerical solutions have been found, which correspond to domain walls and magnetic breathers, provided that the exchange integral is greater than the constant of the easy-axis anisotropy in the "easy plane". The analytical study of the effects of strong dispersion, caused by the discreteness of the metamaterial, has been carried out within the framework of the generalized Kosevich-Kovalev equation, to which the Takeno-Homma equation is reduced in the long-wavelength limit. The analytical expression for the domain wall of the Kosevich-Kovalev equation is constructed using perturbation theory in terms of the dispersion parameter, which is in good quantitative agreement with the numerical solution of the Taken-Homma equation for a discrete kink. Based on this expression, the ansatz for the discrete domain wall of an anisotropic ferromagnetic chain with the time-dependent parameters is proposed. It is shown that small oscillations of the parameters near the equilibrium values well reproduce the internal oscillations of the discrete domain boundary, in particular their frequency dependences, which have been previously found numerically. Besides, the asymptotic expression for the magnetic breather of the Kosevich-Kovalev equation has been constructed, using the proximity of this equation to the integrable Konno-Kameyama-Sanuki equation. The comparison of numerical and analytical results for breathers has shown their good agreement. The obtained results can be used to create new artificial materials with predefined structural and predicted here nonlinear magnetic properties that make these structures very attractive from the point of view of their use as basic memory elements in new computer technologies.

The work was supported by the F-26-5 program of the National Academy of Sciences of Ukraine.

[1] O. V. Charkina and M. M. Bogdan, Low Temp. Phys. 44, 644 (2018). https://doi.org/10.1063/1.5041429.
[2] D. Gatteschi, R. Sessoli, and J. Villain, Molecular Nanomagnets (Oxford University Press, New York 2006. https://doi.org/10.1093/acprof:oso/9780198567530.001.0001.
[3] S. Takeno and S. Homma, J. Phys. Soc. Jpn. 55, 2547 (1986). https://doi.org/10.1143/JPSJ.55.2547.

Electronic structure of GaAs doped with rare-earth elements (La, Ce, Pr and Nd)

H. A. Ilchuk[1], I. V. Semkiv[1], S. I. Krukovskyi[2,3], B. Andriyevsky[4], A. I. Kashuba[1]

[1]Department of General Physics, Lviv Polytechnic National University, 12 Bandera Street, 79013 Lviv, Ukraine
[2]Scientific Research Company 'Electron-Carat', 202 Stryiska Street, 79031 Lviv Ukraine
[3]Department of Semiconductor Electronics, Lviv Polytechnic National University, 12 Bandera Street, 79013 Lviv, Ukraine
[4]Faculty of Electronics and Computer Sciences, Koszalin University of Technology, 2 Śniadeckich Street, 75453 Koszalin, Poland
e-mail: andrii.i.kashuba@lpnu.ua

Gallium arsenide (GaAs) ionizing radiation detectors exhibit significant advantages over silicon-based (Si) counterparts for X-ray and electron beam registration, owing to their high electron mobility, sensitivity, and material density. Their low X-ray fluorescence photon detection threshold, coupled with superior radiation hardness, renders them highly suitable for a diverse range of applications.

GaAs-based sensors effectively detect and quantify X-ray radiation up to energy levels of 60–80 keV, depending on the thickness of the sensor's active region. These devices find application in various fields, including medical physics, industrial engineering, scientific research, and environmental monitoring. However, GaAs exhibits a low infrared absorption coefficient and poor photoelectric conversion efficiency, which imposes significant constraints on its range of practical applications. Doping represents a one of primary method for extending the functional capabilities and achieving controlled modification of GaAs properties.

The electronic energy spectra of the GaAs doped with rare-earth elements (La, Ce, Pr and Nd) have been calculated within the framework of the density functional theory (DFT). To describe the exchange-correlation energy of the electronic subsystem, we used a functional taken in the approximation of generalized gradient (GGA) and Perdew –Burke–Ernzerhof (PBEsol) parameterization [1]. In our calculations, the value $E_{\text{cut-off}}$= 880 eV was taken for the cutting-off energy of the plane waves (this energy corresponded to the minimum value of the total energy). The convergence of the total energy was about 5×10^{-6} eV/atom. Integration over the Brillouin zone was performed on a 2×2×2 grid of *k* points, using a Monkhorst–Pack scheme. At the initial stage of our calculations, we optimized a starting GaAs structure for the case of 2×2×2 supercell. The atomic coordinates and the unit-cell parameters were optimized following a Broyden–Fletcher–Goldfarb–Shanno technique. Optimization was continued until the forces acting on atoms became less than 0.01 eV/Å, the maximum displacement less than 5.0×10^{-4} Å, and the mechanical stresses in the cell less than 0.02 GPa. Formation energy is calculated based on the results of the total energy of the study samples. A complex dielectric function ε(ħω) was used to study the optical properties. The spectral behavior of the refractive index was calculated based on the dielectric function.

ACKNOWLEDGMENTS

This research was supported by the National research foundation of Ukraine (project "Development of novel *p*+/*i*/*n*+ structures based on gallium arsenide thin films", No 2025.07/0258).

[1] J.P. Perdew, A. Ruzsinszky, G.I. Csonka, O.A. Vydrov, G.E. Scuseria, L.A. Constantin, X. Zhou, and K. Burke, Physical Review Letters. 100, 136406 (2008). https://doi.org/10.1103/physrevlett.100.136406.

Modeling strengthening kinetics in metals under extreme plastic straining

O. V. Khomenko, A. P. Chopov, K. P. Khomenko, A. Yu. Badalian, I. A. Chelnokov

Sumy State University, 116, Kharkivska st., Sumy, 40007, Ukraine
e-mail: o.khomenko@mss.sumdu.edu.ua

This study utilizes the formalism of nonequilibrium evolutionary thermodynamics (NET) to describe structural evolution [1, 2]. The variation in internal energy is formulated through a fundamental thermodynamic identity, which balances energy flux from external sources with its dissipation through internal degrees of freedom during relaxation. We specifically model the system's response to external work and thermal driving forces. Relaxation is bifurcated into two simultaneous channels: the kinetic accumulation of lattice defects and entropy production via heat dissipation. It is established that the primary energy storage mode in the early stages is the rapid escalation of internal energy, governed by the synergetic increase in both the density and the specific energy of the defect population.

Furthermore, we evaluate the synthesis of nanostructured materials by contrasting severe plastic deformation (SPD) techniques with NET-based predictive models. Implementing a dual-defect approximation, we elucidate the constitutive relations of internal energy and the hierarchical stages of substructure fragmentation. The analysis focuses on the coupled nonlinear dynamics of dislocation ensembles and grain boundary networks. Our results indicate a sharp transition in dislocation density at the inception of SPD, characteristic of a structural phase transition. While the dislocation subsystem reaches a dynamic equilibrium (steady state) relatively early, the grain boundary density exhibits a delayed saturation, constrained by the underlying dislocation kinetics.

In conclusion, the work characterizes the functional dependence of yield stress on grain boundary density, accounting for nonlinear feedback loops. This relationship manifests as a monotonic decay lacking stochastic oscillations or discontinuities. However, a significant inflection point is identified within the phase transition regime, suggesting a fundamental shift in the strain hardening exponent and the overall constitutive behaviour of the material.

[1] A. V. Khomenko, J. Phys. Stud. 24, No. 2, 2001 (20 p.) (2020).
https://doi.org/10.30970/jps.24.2001.
[2] A. V. Khomenko, D. S. Troshchenko, L. S. Metlov, Phys. Rev. E, 100, 022110 (2019).
https://doi.org/10.1103/PhysRevE.100.022110.

Longitudinal and transverse oscillations of hydrogen bonds in water

O. D. Stoliaryk[1], O. V. Khorolskyi[2]

[1]Odesa I. I. Mechnikov National University,
2 Dvoryanska Str., Odesa, 65082, Ukraine
[2]Poltava V. G. Korolenko National Pedagogical University,
2 Ostrogradskogo Str., Poltava, 36003, Ukraine
e-mail: khorolskiy.alexey@gmail.com

The elucidation of hydrogen bonding's role in determining water's properties remains among the principal scientific questions that have not yet been comprehensively resolved [1]. Recent experimental studies using inelastic neutron scattering [2] and hyper-Raman spectroscopy [3] have revealed complex collective dynamics with distinct longitudinal and transverse modes in water.

Zanatta and colleagues in [2] present an inelastic neutron scattering investigation of water's atomic dynamics, employing an innovative methodology that permits the direct experimental determination of the nature of dynamic structure factors in aqueous systems. Their findings reveal intricate collective dynamics characterized by two distinct propagating excitations, which are interpreted within the theoretical framework of an interacting-modes model. The initial high-energy excitation is typically interpreted as a continuation of the longitudinal acoustic phonon and exhibits enhanced sound velocity, which is ascribed to its coupling with the secondary low-energy mode. This analytical framework substantiates the predominantly longitudinal character of the primary mode while definitively establishing the transverse nature of the secondary mode. The relaxation times of the modes point toward a unified physical mechanism underlying the secondary mode, plausibly originating from the structural organization of the hydrogen-bonded network.

Shelton in [3] reports measurements of the hyper-Raman light scattering (HRS) spectrum for liquid heavy water, decomposed into contributions from transverse and longitudinal dipolar modes and octupolar modes on the basis of HRS polarization dependence analysis. Transverse HRS is observed for orientational and stretching modes, whereas longitudinal HRS is detected for translational, librational, and bending modes. The rocking/wagging, twisting, and translation modes of D_2O molecules incorporated in the hydrogen-bonded network are distinctly resolved. The long-range correlation observed for orientational and stretching modes is rationalized as a manifestation of dipole-dipole orientational correlations within the liquid medium. It is noted that the long-range correlation of longitudinally polarized librational and bending modes requires further investigation.

Our theoretical approach rests upon the modeling of hydrogen bonding in intimate connection with the molecular structure of water, incorporating the characteristic distribution of electronic density originating from the oxygen atom [1]. Specifically, the formation of hydrogen bonds in water is naturally linked to the development of dimeric aggregates. It has been demonstrated that the structural parameters of water dimers, derived through geometric arguments from isolated water molecules, are in satisfactory accord with experimental observations. Furthermore, it has been established that transverse oscillations of hydrogen bonds in water exhibit substantially reduced stability in comparison with their longitudinal counterparts: the amplitude of transverse oscillations is 4 to 5 times greater than that of longitudinal oscillations. These observations yield the following conclusions: (1) hydrogen bonds formed in water exhibit short lifetimes, and (2) the magnitude of shear viscosity in water is comparable in order of magnitude to the viscosity of argon and other low-molecular-weight liquids.

[1] O. Khorolskyi and N. P. Malomuzh, Chem. Phys. Lett. 828, 140713 (2023). https://doi.org/10.1016/j.cplett.2023.140713.
[2] M. Zanatta, A. Orecchini, F. Sacchetti, and C. Petrillo, J. Mol. Liq. 393, 123550 (2024). https://doi.org/10.1016/j.molliq.2023.123550.
[3] D. P. Shelton, Phys. Rev. B 108, 174203 (2023). https://doi.org/10.1103/PhysRevB.108.174203.

The dynamics of vortex pairs in magnetic nanodots

M. V. Brusenceva[1], A. S. Kovalev[1,2]

[1]V.N.Karazin Kharkiv National University of the MES of Ukraine,
4 Svobody Sq., Kharkiv, 61022, Ukraine
[2]B.Verkin Institute for Low Temperature Physics and Engineering of the NAS of Ukraine,
47 Nauky Ave., Kharkiv, 61103, Ukraine
e-mail: kovalev@ilt.kharkov.ua

Magnetic vortices represent new topological excitations in magnetically ordered media with easy-plane magnetic anisotropy that hold great promise for technical applications in microelectronics [1]. Possessing four combinations of topological characteristics (polarization and chirality signs), vortices can play an important role in the problem of recording information in artificial lattices of magnetic nanodots in a vortex state. Vortex transitions between nanodots enable the latter to exist in states with vortex pairs. The dynamics of vortex pairs in a nanodot depends on their topological characteristics and the magnetic properties of the nanodot and the surrounding magnetic matrix. In particular, it differs for nanodots (a cylindrical region with a thickness greater than the thickness of the magnetic background) and "nanoholes"—cylindrical regions with a thickness less than the thickness of the surrounding magnetic matrix). In the first case, the dynamics of the vortex pair are similar to those of similar excitations in a BEC droplet, but are characterized by greater diversity due to the polarization of the magnetic vortices and the influence of the magnetic matrix surrounding the nanodot.

The theoretical study of the problem was done using the method of collective variables for the coordinates of vortices in a pair, in which the initial Landau-Lifshitz dynamic equations without damping lead to ordinary differential Thiele equations and Nikiforov-Sonin equations. The nanodot is considered as a finite-radius defect in which the exchange interaction differs from the exchange in the surrounding matrix. A methodologically similar problem was previously considered for the scattering of vortex pairs on a nanodot [2]. The Nikiforov-Sonin equations were solved numerically in the MAPLE program for a wide range of excitation energies and their angular momenta for vortex/antivortex and vortex/vortex pairs. It is shown that in the case of a magnetic dot, these dynamics are stable, i.e., steady states of rotation of two vortices exist. However, in the case of a magnetic cavity, the vortex/antivortex pair exhibits a tendency toward mutual annihilation and annihilation on the cavity surface.

Using the Hamiltonian approach for the vortex system and the Thiele equations, the integrals of motion were calculated: the field angular momentum and the total energy, including the interaction of the vortices with each other and with the interface between the magnetic media. Knowledge of these integrals leads to the complete integrability of the dynamic system for two vortices and the possibility of a complete analysis of the corresponding dynamics using methods of the qualitative theory of dynamic systems analysis. An analysis of the vortex dynamics on the phase plane and a complete classification of all possible scenarios for the dynamics of two-vortex excitations of magnetic dots and magnetic cavities were performed.

The work was supported by the F-26-5 program of the National Academy of Sciences of Ukraine.

[1] A. M. Kosevich, B. A. Ivanov and A. S. Kovalev, Magnetic solitons, Phys. Rep., 194, 117 (1990). https://doi.org/10.1016/0370-1573(90)90130-T.
[2] A. S. Kovalev and J. E. Prilepskii, Low Temp. Phys. 44, 663 (2018). https://doi.org/10.1063/1.5041432.

Resonance in a two-level system caused by time-dependent coupling with the phonon bath

V. O. Leonov, Ye. V. Shevchenko, E. G. Petrov

Bogolyubov Institute for Theoretical Physics, National Academy of Sciences of Ukraine, 03143, Kyiv, Ukraine
e-mail: leogluck@gmail.com

The main features of the temporal behavior of an open quantum dynamical system are determined by the relations between the matrix elements of transitions between the electronic states of the system and the couplings of each electronic state to vibrational states of the environment. For weak coupling, the kinetics can be described by the Redfield equations for the elements of the density matrix of the system. With strong coupling, a noticeable change in the rates of transition between system states occurs, and the Pauli equations for the probabilities of population of system states are used to describe the kinetics. When the relationship between the specified degrees of freedom is independent of time, the kinetic equations contain transition rates that are independent of time. The influence of external dc and ac fields is taken into account, as a rule, in the electronic energies of the system and interior transition matrix elements. In this case, in a system controlled by high-frequency regular or stochastic fields, time-independent rates of transitions between states can be formed if the equilibrium position of the nuclei of the system and/or the environment does not change with time, and only small displacements of the nuclei from the equilibrium position occur. If the coupling between the electronic and nuclear degrees of freedom becomes time-dependent, the kinetics of the time evolution of the probabilities of occupation the states of the system become significantly more complicated. It has been shown that with weak coupling between the system and the environment this leads to Redfield-type kinetic equations with time-dependent transition rates. For two-level system (TLS), these issues are analyzed in detail in [1].

We have considered a situation in which the interaction of a system with its environment depends on time. We investigated the situation where the coupling between the electronic states of the system and the phonons of the environment is strong. It was shown that, due to the time dependence of the coupling, the electronic states of the system manifest themselves as polarons with a non-stationary "phonon coat" [2]. A unitary transformation was proposed that made it possible to take into account the non-stationary coupling directly in the operator responsible for transitions between system states. As an example of the application of non-stationary polaron transformation, the kinetics of establishing the probabilities of occupation the electron states of a TLS is considered. Based on the spin-boson version of the TLS, the corresponding kinetic equations for the occupation probabilities were obtained, as well as the corresponding expressions for the transition rates. The analysis showed the presence of three different time scales for the development of kinetics. Physically, these scales are associated with the stationary interaction of the TLS with the environment, the influence of the non-stationary interaction of electronic and vibronic states inside the TLS, and the transitions between the electronic states of the TLS. Thus, we show how a time-dependent interaction (in our case periodic) between electronic and vibrational degrees of freedom can control a kinetic process in an open dynamic quantum system.

[1] I. Goychuk and P. Hanggi, Adv. Phys. 54, 525 (2005). dx.doi.org/10.1080/00018730500429701
[2] E. G. Petrov, Ye. V. Shevchenko, V. O. Leonov, and V. I. Teslenko, Ukr. J. Phys., 69, 552 (2024). dx.doi.org/10.15407/ujpe69.8.552.

Self-induced topological interface and non-Hermitian localization of fluctuations in an asymmetric exclusion process

S. P. Lukyanets, O. V. Kliushnichenko

Institute of Physics of NAS of Ukraine, 46 Nauky Ave., Kyiv, 03028, Ukraine
e-mail: lukyan@iop.kiev.ua, kliushnychenko@iop.kiev.ua

We consider the kinetics of gas-density fluctuations at a nonequilibrium phase transition arising from the scattering of a gas flow at a partially penetrable obstacle (impurity) in a quasi-one-dimensional lattice [1,2]. The transition manifests as the formation of a two-domain gas structure with a dense domain ahead of the impurity at certain critical system parameters. We show that the kinetics is governed by non-Hermitian stochastic equations. In this regard, the behavior of fluctuations demonstrates properties inherent to non-Hermitian quantum systems such as the PT-breaking transition, skin effect induced by a domain wall, the closing of the Liouvillian gap, which serves as an indicator of dissipative phase transition [3-5]. In particular, we show that this transition is accompanied by the opening of a finite spectral gap for fluctuations in the thermodynamic limit — corresponding to the minimal relaxation rate in the system or Liouvillian gap. The spatial behavior of fluctuation eigenstates demonstrates the emergence of strong skin effect induced by the domain wall between the dense and rarefied gas phases. This leads to a pinning effect of the induced gas-density fluctuations near the domain wall in the long-time limit, accompanied by their suppression at the impurity site. In contrast, below the transition the Liouvillian gap vanishes, resulting in the accumulation of induced fluctuations over time that can be associated with linear instability.

[1] S. P. Lukyanets, O. V. Kliushnichenko, Phys. Rev. E 109, 054103 (2024). https://doi.org/10.1103/PhysRevE.109.054103.
[2] O. V. Kliushnychenko, S. P. Lukyanets, Phys. Rev. E 98, 020101(R) (2018). https://doi.org/10.1103/PhysRevE.98.020101.
[3] F. Minganti, A. Biella, N. Bartolo, and C. Ciuti, Phys. Rev. A 98, 042118 (2018). https://doi.org/10.1103/PhysRevA.98.042118.
[4] T. Haga, Phys. Rev. B 110, 104303 (2024). https://doi.org/10.1103/PhysRevB.110.104303
[5] M. Matsumoto, Z. Cai, and M. Baggioli, Phys. Rev. A 112, 012226 (2025). https://doi.org/10.1103/2fw8-bsjy.

Implementation and features of nodal points in phonon spectra of crystals of the A15 family

I. I. Nebola, D. I. Kayntz, A. V. Korneychuk, M. V. Pino, R. I. Zosimov

Uzhhorod National University, Faculty of Physics, 3, Narodna Sq., 88000 Uzhhorod, Ukraine
e-mail: ivan.nebola@uzhnu.edu.ua

In crystals of the A15 family, a stable set of phonon mode degeneracies at the R point of the Brillouin zone was discovered [1]. The family of crystals with the A15 structure (Pm-3n (No. 223)) covers the class of the most practically used A3B superconductors (among them (A-Nb, V, Mo, Ti, Cr, Ta. B-Sn, Al, Ge, Ga, Sb. Au, Pt, Rh, Re, C, Si) and is distinguished by the specificity of the six-fold and four-fold degeneracy of the phonon spectrum at the highly symmetrical point R (Pi/a, Pi/a, Pi/a). The discovered [1] and determined degenerate nodal phonons [2,3] in a number of crystals with space group symmetry (with numbers 218, 220, 222, 223, and 230) contributed to the growth of interest in the detailed analysis of their phonon spectra. Using the method proposed by us, the calculation of model curves of the phonon spectrum in the concept of superspatial symmetry [4] allowed us to conduct a detailed analysis of representatives of this family using the example of a V3Si crystal in the vicinity of a nodal point.

V3Si	V3V	X3Si
6.0197321949788 4	5.9303327846141 6	13.251820527 6
6.0933892270528 6	6.0296628391192 4	
6.5051434522217 6	6.3218472816906 6	
6.9796723267041 2	6.9625073945346 2	
10.499021522126 6	8.2428584913213 6	

In this case, all calculations were performed with the same sets of force constants for the crystal (V3Si), in the modified fragment of which the positions of Si atoms are occupied by V atoms (V3V), in the second case the positions of Si atoms are vacant (V3X) and in the third case only the positions of Si atoms are occupied (X3Si). From the presented data it follows that the highest energy six-fold degenerate mode is unambiguously associated with vibrations of Si atoms, and two other - four- and two-fold degenerate - modes are mainly associated with the V3 construction.

[1] W. Weber, "Phonons and electron–phonon interaction in A15 compounds" (1973) *Phys. Rev. B* 8, 5082.
[2] J. Harada & S. Axe, "Lattice dynamics of V_3Si" (1973) *Phys. Rev. B* 8, 1653.
[3] Chengwu Xie et al., "Sixfold degenerate nodal-point phonons: Symmetry analysis and materials realization", (2021).*Phys. Rev. B* 104, 045148.
[4] I.I. Nebola, A.F. Katanytsia, I.M. Shkyrta, Yu.O. Pal, I.P. Studenyak, M. Timko, P. Kopčanský. Comparison of features arising in phonon spectra of crystals belonging to the argyrodite family for various combinations of orbits filled with Ag(Cu) atoms. Semiconductor Physics, Quantum Electronics & Optoelectronics, (2022). V. 25, No 1. P. 043–048.

Generalized modeling of incomplete dopant ionization with constant and temperature-dependent activation energy in semiconductors (10–300 K)

M. Ibragimova[1], D. Qalandarova[1], J. Abdullayev[2]

[1]Urgench State University, Hamid Olimjon street 14, Urgench, 220100 Uzbekistan
[2]National Research University TIIAME, Department of Physics and Chemistry, Tashkent, Uzbekistan
e-mail: dildora.qalandarova.90@gmail.com

Incomplete dopant ionization fundamentally limits the accuracy of carrier concentration modeling in semiconductors operating at cryogenic and intermediate temperatures. In this work, a generalized theoretical framework is developed to quantify incomplete ionization over the temperature range 10–300 K by comparing two physically distinct approaches: (i) constant activation energy $E_a = E_{a0}$and (ii) temperature-dependent activation energy $E_a(T)$. Carrier concentrations are obtained self-consistently from Fermi–Dirac statistics and charge neutrality equations for a representative donor density $N_D = 1 \times 10^{16}\ cm^{-3}$. For a constant activation energy $E_{a0} = 40\ meV$, the ionization fraction remains below 1% at 10 K, yielding $n \approx 4–6 \times 10^{13}\ cm^{-3}$. At 77 K, the ionization degree increases to ~15%, while at 300 K it exceeds 98%, marking the transition from freeze-out to extrinsic conduction near 130–150 K. To account for bandgap narrowing and screening effects, the temperature-dependent activation energy is modeled as $E_a(T) = E_{a0} - \alpha T$, with $E_{a0} = 45\ meV$ and $\alpha = 0.02\ meV/K$. This reduces the effective activation energy by ~6 meV at 300 K and shifts the freeze-out transition toward lower temperatures by approximately 20–30 K. The resulting carrier concentration deviates by up to 30–35% below 150 K compared to the constant-energy approximation. The analysis demonstrates that neglecting the temperature dependence of activation energy leads to substantial underestimation of free carrier density and conductivity in the cryogenic regime. The proposed generalized approach provides a physically consistent framework for accurate modeling of semiconductor materials and devices operating from deep cryogenic to room temperature conditions.

Renormalization of electron states by interaction with confined phonons in a wurtzite-type nanostructure

Yu. O. Seti[1], I. V. Boyko[2]

[1]Lviv Polytechnic National University,12 Stepan Bandera Str., Lviv, 79013, Ukraine
[2]Ternopil Ivan Puluj National Technical University, 56 Ruska Str., Ternopil, 46001 Ukraine
e-mail: jseti18@gmail.com, yuliia.o.seti@lpnu.ua

It is well known that anisotropic nitride-based nanostructures with a wurtzite crystal lattice are characterized by strong internal fields of spontaneous and piezoelectric polarization [1]. These fields significantly modify the properties of electrons and phonons, making their characteristics fundamentally different from those of quasiparticles in isotropic semiconductor nanostructures with a zinc-blende cubic lattice [2-4]. Furthermore, the high optical phonon energies in nitride compounds lead to a stronger electron-phonon coupling compared to isotropic structures. This substantially affects the optical properties of such structures, which is particularly important given their application as active elements in optoelectronic nanodevices.

The anisotropy of wurtzite nanostructures gives rise to four types of optical phonons: interface, confined, half-confined, and propagating [2]. Unlike isotropic nanostructures, which feature three types of optical phonons (interface, confined, and half-confined) where only the interface phonon energies depend on the wave vector, all optical phonon branches in wurtzite structures exhibit dispersion. Given the strong localization of electron states in the inner layers of quantum well structures, the strongest coupling is expected to occur with interface and confined phonons, whose potentials peak at the interfaces and within the inner layers of the nanostructure, respectively. Such interaction leads to the renormalization of the spectral characteristics of electron states [5] and, consequently, may affects the optical properties of wurtzite nanostructures.

In this work, we investigate the effect of confined phonons on electron states in a wurtzite-type AlGaN/GaN/AlGaN nanostructure. The theoretical description is performed within the dielectric continuum model for phonons and the effective mass approximation for electrons. Based on the derived electron-phonon interaction Hamiltonian in the second quantization representation for all system variables, the mass operator is calculated analytically. This calculation takes into account the full configuration interaction, which includes intra-level and inter-level processes with phonon emission and absorption at a finite temperature. This approach allowed us to determine the contributions of different types of configuration interactions and individual confined phonon branches to the renormalization of electron states. It is shown that the dominant contribution to the energy shifts and damping of electron levels is driven by intra-level interaction processes with several branches of confined phonons from the high-energy subband.

This work was supported by the Ministry of Education and Science of Ukraine (Grant No. 0126U001246).

[1] M. Beeler, E. Trichas, E. Monroy, Semicond. Sci. Technol. 28, 074022 (2013). https://doi.org/10.1088/0268-1242/28/7/074022.
[2] M.A. Stroscio, M. Dutta, Phonons in Nanostructures (Cambridge University Press, Cambridge, 2001), https://doi.org/10.1017/CBO9780511534898.
[3] J. Seti, O. Voitsekhivska, E. Vereshko, M. Tkach, Appl. Nanosci. 12, 533 (2022). https://doi.org/10.1007/s13204-021-01708-8.
[4] I.V. Boyko, Phys. Rev. B 108, 075403 (2023). https://doi.org/10.1103/PhysRevB.108.075403.
[5] Ju.O. Seti, I.V. Boyko, Low Temp. Phys. 52, 1 90 (2026). https://doi.org/10.1063/10.0042172.

Combined effect of Fermi liquid and spin-orbit interactions on electron transport

D. I. Stepanenko

B.Verkin Institute for Low Temperature Physics and Engineering of NAS of Ukraine,
47 Nauky Ave., Kharkiv, 61103, Ukraine
e-mail: stepanenko@ilt.kharkov.ua

In recent decade considerable attention has been devoted to the study of transport phenomena arising from combined effect of electron correlation and spin-orbit interaction (SOI) in novel quantum materials such as topological insulators, Dirac and Weyl semimetals, iridates and related materials containing 4d and 5d transition metal elements, heterojunctions, in which strong spin-orbit interaction leads to the appearance of non-trivial topology of electron band structure and surface states. In contrast to usual metals, the single-particle Hamiltonian of conduction electron in these systems represents a matrix operator and, at calculating kinetic coefficients it is necessary to take into account the off-diagonal elements of the density matrix with respect to spin polarization or pseudospin quantum numbers. The SOI forms a connection between orbital and spin dynamics of conduction electrons and spin direction becomes dependent on electron momentum. This leads to phenomena which are absent in system where SOI can be neglected. At present, a significant number of works devoted to electron and spin transport in SOI systems are based on the Boltzmann kinetic equation for the diagonal in spin polarization *s* components of the density matrix. However, if the SOI energy is comparable of the Fermi energy, the diagonal and off-diagonal in *s* components can give the same order of magnitude contribution to the kinetic coefficients. Taking into account the Fermi liquid interaction can lead to new physical effects, even in the case of weak SOI. A proven method for describing systems of interacting electrons in usual metals is the Landau-Silin Fermi liquid theory. In the Landau-Silin theory SOI is neglected and in the absence of an external magnetic field, the Landau function enters into the kinetic equations only in the gradient terms, which vanish when high-frequency electromagnetic field is uniform. In this case the kinetic coefficients do not depend explicitly on the parameters of Fermi liquid interaction. We present the gradient-invariant kinetic equations for the single-particle density matrix of a system of correlated electrons with SOI, which generalize the Landau-Silin equations, and show that when SOI is taken into account, the conductivity of 2D interacting electrons system includes constants of the Fermi liquid interaction even in a uniform alternating electromagnetic field [1]. This is a result of the contribution to the conductivity of the density matrix components that are off-diagonal in spin polarization quantum number. Other kinetic coefficients have the same property.

[1] D.I. Stepanenko, EPL, 151 46005 (2025), https://doi.org/10.1209/0295-5075/adfc94.

TECHNOLOGIES AND INSTRUMENTATION FOR PHYSICAL EXPERIMENTS

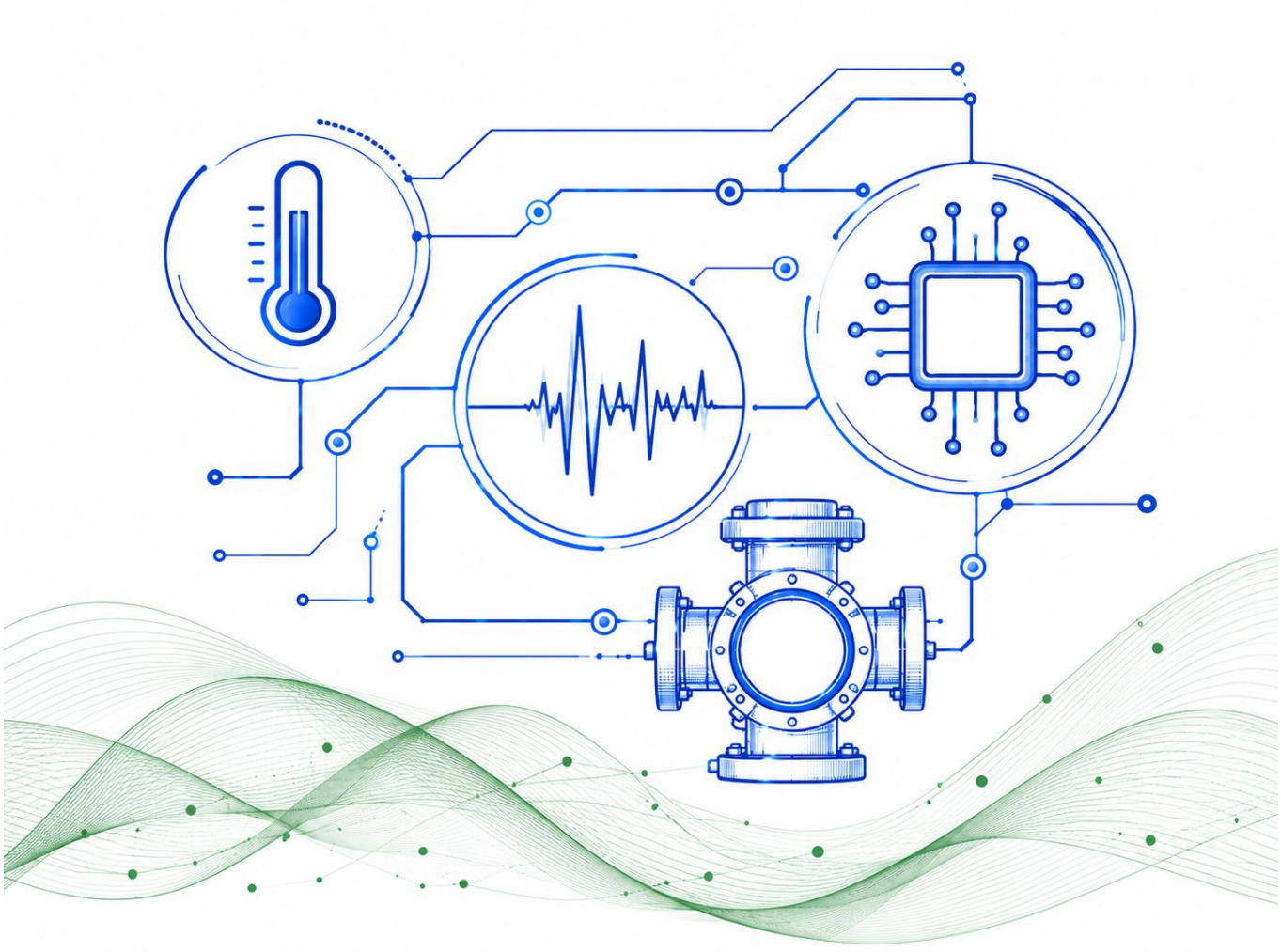

Ultrasonic monitoring of ice ball formation in biological tissues under low-temperature exposure

V. Yu. Globa, G. O. Kovalov, M. O. Chyzh, A. O. Manchenko

Institute for Problems of Cryobiology and Cryomedicine of the NAS of Ukraine,
23 Pereyaslavska str., Kharkiv, 61016, Ukraine
e-mail: globa.1978@gmail.com

Low temperatures down to –195 °C are used in cryosurgery for the complete destruction of pathological tissue while maximally preserving adjacent healthy tissue. To obtain the required results of cryogenic exposure, it is necessary to control the volume of the freezing zone, consider the cooling rate, final tissue temperature, exposure time, and rate of thawing. In clinical settings, the primary method of intraoperative monitoring of the freezing zone size and shape dynamics of the freezing zone is ultrasound examination (US). US provides insight into the outer edges of the freezing zone with a typical ultrasound imaging resolution of about 1 mm in real time.

However, there are errors that can lead to an incorrect assessment of the dynamics of the freezing zone size and, consequently, to incomplete destruction of pathological tissue [1]. These errors may be due to violation of methodological principles of positioning the ultrasonic sensor and inconsistency of technical characteristics of the ultrasonic equipment (sensor frequency, actual dimensions and inappropriate software) [2, 3].

A technology has been developed to use the US for exploring the ice ball during low-temperature exposure, which is capable of constructing the 3D- volumetric models of an ice ball under low-temperature exposure for the analysis of its boundaries and the freezing-thawing front movement.

The technology consists of a special laboratory facility for ultrasonic research and an appropriate methodology for monitoring in vitro / in vivo cryogenic exposure on this complex.

The laboratory facility for ultrasonic research of the development of ice balls in biological tissues during low-temperature exposure includes a positioning device, a cryoinstrument mounted on a tripod, an ultrasonic echotomoscope with a linear sensor, the scanning surface of which is flush with the outer surface of the device, on top of which is a latex container filled with ultrasound gel, on which the object of study is placed. The placement of the linear sensor in the positioning device allows for reducing the number of errors and artifacts due to its rigid fixation, which prevents violations of the methodological principles of positioning the ultrasound sensor. Such fixation of the linear sensor enables controlling the volume of the freezing zone, as well as the state of cryogenic influence objects regardless of the operator's experience and skills, which allows for obtaining reliable data from experimental studies.

The methodology contains requirements for equipment and facilities as well as a step-by-step description of testing and preparing equipment, measuring using all components of the set-up, quantitative analysis of the results obtained, etc.

This work was supported by the NAS of Ukraine (State registration number of scientific research work 0121U113328).

[1] J. Tacke, R. Speetzen, I. Heschel, D. W. Hunter, G. Rau and R. W. Günther. Imaging of interstitial cryotherapy-an in vitro comparison of ultrasound, computed tomography, and magnetic resonance imaging. Cryobiology 38(3), 250-259 (1999). https://doi.org/10.1006/cryo.1999.2168.
[2] P. B. Bertrand, R. A. Levine, E. M. Isselbacher and P. M. Vandervoort. Fact or artifact in two-dimensional echocardiography: avoiding misdiagnosis and missed diagnosis. Journal of the American Society of Echocardiography 29(5), 381-391, (2016). http://doi.org/10.1016/j.echo.2016.01.009.
[3] M. M. Quien and M. Saric. Ultrasound imaging artifacts: How to recognize them and how to avoid them. Echocardiography 35(9), 1388-1401 (2018). https://doi.org/10.1111/echo.14116.

Visualization of a photosensitive area of infrared photodiodes using two-dimension scanning method

O. G. Golenkov, A. V. Shevchik-Shekera, V. V. Zabudsky, I. O. Lysiuk, Z. F. Tsybrii, A. S. Stanislavskyi, M. V. Vuichyk, S. V. Korinets

V. Lashkaryov Institute of semiconductor physics of NAS of Ukraine,
41 Nauky Ave., Kyiv, 03028, Ukraine
e-mail: golenkov@isp.kiev.ua

Accurate characterization of the spatial uniformity of photosensitivity is an important step in the development and optimization of infrared photodetectors. Non-uniformity of the photoresponse can significantly influence the performance of detectors in imaging systems, spectroscopy, and precision optical measurements. Therefore, investigation of the spatial distribution of sensitivity provides valuable information about material quality, device fabrication processes, and the presence of local defects affecting detector performance.

The non-uniformity of photosensitivity (Fig. 1) of an *InSb* infrared photodiode developed and fabricated at the V. Lashkaryov Institute of Semiconductor Physics of the NAS of Ukraine [1] was investigated. The photodiode has performance characteristics comparable with commercially available ones. Its topology dimensions are 230×40 um^2.

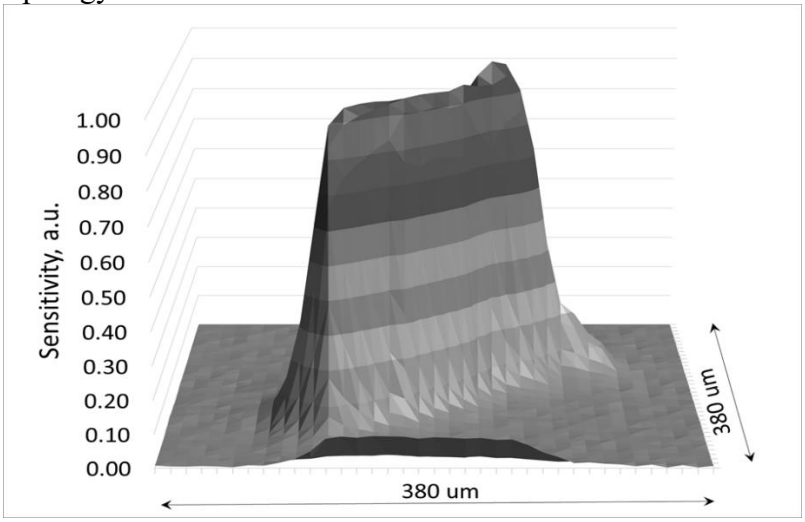

Fig. 1. 3D mapping of the *InSb* photodiode photosensitivity at liquid nitrogen temperature.

There is increased (up to 5%) photosensitivity near the contact area (Fig. 1). This can be explained by a combination of reasons: both the increased width of the photodiode on the contact side and not small enough the size of the optical probe.

The surface distribution of photosensitivity was investigated with the assistance of an optical probe [2] at 4.3 um radiation source wavelength. A spot diameter of a focused radiation was <30 μm.

Visualization of photosensitivity allows determining the effective sensitive area of the detector, sensitivity uniformity, and crosstalk coefficient between neighboring detectors.

Results reported in this article were supported by the National Research Foundation of Ukraine, project No. 2025.06/0089.

[1] S.V. Sapon, M.S. Boltovets, O.A. Kulbachynskyi, V.V. Zabudsky, O.G. Golenkov, V.V. Korotyeyev, A.A. Efremov, SPQEO 27(3), 356-365 (2024). https://doi.org/10.15407/spqeo27.03.
[2] O. G. Golenkov, A. V. Shevchik-Shekera, V. V. Zabudsky, I. O. Lysiuk, Z. F. Tsybrii, A. S. Stanislavskyi, S. V. Korinets, A. Yu. Shekera, Sensor Electronics and Microsystem Technologies 22(4), 30-39 (2025). https://semst.onu.edu.ua/article/view/343569/336882.

Application of ourselves-developed infrared thermal imagers in laboratory experiments

E. Gordiyenko[1], Yu. Fomenko[1], G. Shustakova[1], G. Kovalov[2]

[1]B.Verkin Institute for Low Temperature Physics and Engineering of NAS of Ukraine, 47 Nauky Ave., Kharkiv, 61103, Ukraine
[2]Institute for Problems of Cryobiology and Cryomedicine of NAS of Ukraine, 23, Pereyaslavska Str., Kharkiv, 61016, Ukraine
e-mail: gordiyenko@ilt.kharkov.ua

Standard parameters and software of commercial thermal imagers may not be sufficient for solving specific scientific problems. Therefore, two basic thermal imaging models with an open architecture and modular hardware and software design have been developed at the B. Verkin Institute for Low Temperature Physics and Engineering of the NAS of Ukraine. This design enables targeted adaptation of the devices to address non-standard thermal analysis tasks. Here, we present two of the laboratory experiments in which the results were obtained using the advanced capabilities of our ourselves -developed thermal imagers.

To study the dynamics of thermal fields arising from cryo-impact *in vitro* (on the surface of a model system) and *in vivo* (on the skin of experimental animals), a basic thermal imager model equipped with a single-element CdHgTe cooled detector and a mechanical IR scanner was used. Its main parameters are as follows: temperature sensitivity of 0.1°C in the spectral range of 7–14 μm, frame rate of 0.5 Hz, field of view of 22°H × 22°V, and spatial resolution of 1.5 mrad. To extend the measurable negative temperature range down to −150°C, as required for these experiments, a special shutter with combined emissivity was integrated into the device. The software was supplemented with additional functions, including automatic recording of thermographic video sequences up to 30 minutes in duration (continuous image acquisition at 0.5 Hz) directly to the hard drive [1,2]. For simultaneous monitoring of thermal field dynamics and other processes, thermal images were displayed on a PC via a USB interface.

To develop a method for optimal detection of internal defects in composite materials and determination of their parameters (depth, size, defect material, etc.), experimental studies of surface thermal processes in carbon fiber and fiberglass samples were conducted under thermal stimulation (active thermography). For this purpose, another self-developed thermal imager was employed. It is based on an uncooled microbolometric 384 × 288 FPA matrix and has the following basic parameters: temperature sensitivity of 0.07°C in the 7–14 μm spectral range, spatial resolution of 1 mrad, frame rate of 20 Hz, and field of view of 22.5°H × 18°V. In this case, images were displayed on the built-in LCD screen and recorded on an SD memory card. The software was enhanced with a function for automatic recording of thermographic sequences at 2 Hz for up to 1 minute, which was sufficient to monitor the evolution of the surface thermal field during thermal wave propagation. Additional software tools were implemented to improve post-processing efficiency and enhance thermogram quality [3].

It should be noted that after each hardware and software modification, and prior to the experiments, the devices were calibrated and tested using the Infrared Calibrator 9133 metrology stand (Fluke Corporation, USA).

[1] E. Gordiyenko, Yu. Fomenko, G. Shustakova, G. Kovalov, S. Shevchenko, Rev. Sci. Instrum. 95, 035116 (2024). https://doi.org/10.1063/5.0188276.
[2] G. O. Kovalov, M.O. Chyzh, V.Yu. Globa, et al, Cryobiology, 120, 105259 (2025). https://doi.org/10.1016/j.cryobiol.2025.105259.
[3] E.Yu. Gordiyenko, N.I. Glushchuk, Yu.V. Fomenko, et al, Sci. innov., 14, 37 (2018). https://doi.org/10.15407/scine14.02.037.

Purification of starting materials as a key element in the technology of synthesis of quantum point-contact sensors

M. Romanov[1], D. Harbuz[1], V. Gudimenko[1], O. Pospelov[2], D. Chudak[3], I. Zinchenko[4], G. Kamarchuk[1]

[1]B.Verkin Institute for Low Temperature Physics and Engineering of NAS of Ukraine, 47 Nauky Ave., Kharkiv, 61103, Ukraine
[2]National Technical University "Kharkiv Polytechnic Institute", 2 Kyrpychov Str., Kharkiv, 61002, Ukraine
[3]V. Karazin Kharkiv National University, 4 Svobody Sq., Kharkiv, 61077, Ukraine
[4]State Scientific Institution "Institute for Single Crystals" of NAS of Ukraine, Nauky ave. 60, Kharkiv, 61072, Ukraine
e-mail: m.d.romanov.1997@gmail.com

Breath analysis is a rapidly advancing field, as human exhaled breath contains a wealth of biomarkers indicative of physiological and psychological states. While various detection techniques exist, conductometric sensors offer a practical route for daily monitoring. Recent breakthroughs utilizing quantum point-contact (QPC) sensors have demonstrated selective detection of the complex gas medium components through quantum mechanisms [1]. Tetracyanoquinodimethane (TCNQ)-based salts are promising materials for the sensitive layers of such devices due to their semiconductive nature and tendency to form high-surface-area nanostructures [2]. However, the realization of quantum detection mechanisms in QPC sensors is critically dependent on the purity of the starting material, and commercially available TCNQ compounds often fail to meet these stringent requirements [3].

This study focuses on the development and optimization of technology and purification equipment for synthetic conductors applied to the fabrication of quantum point-contact breath sensors. Commercial TCNQ substance with a starting purity of 98% does not provide the necessary conditions for the synthesis of highly perfect Yanson point contacts used to create quantum sensors [2]. Therefore, we developed a technology and device for fine purification of organic conductors. The purification device was designed to implement vacuum zone sublimation, utilizing ability of solids to sublimate under reduced pressure. The raw material was placed within a quartz tube under vacuum. A resistive heater, shifting along the tube by a stepper motor, created a moving sublimation zone confined by a teflon piston. Temperature was precisely controlled via a microchip-regulated heating element and monitored by an integrated thermocouple, allowing for programmable sublimation parameters through a connected personal computer.

After just one purification cycle, the TCNQ substance was analyzed by spectrophotometry, which showed a purity of up to 99.8. The purified material was subsequently used to synthesize a relevant TCNQ compound and fabricate quantum point-contact sensors. Electrical characterization confirmed that these sensitive elements meet the criteria for Yanson point contacts [2], thereby enabling the quantum-based selective detection mechanisms essential for advanced breath analysis [1].

[1] G. Kamarchuk, A. Pospelov, L. Kamarchuk et al. Sci Rep. 13, 21432 (2023). https://doi.org/10.1038/s41598-023-48207-0.
[2] D.A. Harbuz, A.P. Pospelov, V.A. Gudimenko, et al. Molecular Crystals and Liquid Crystals, 718(1), 25 (2021). https://doi.org/10.1080/15421406.2020.1861518.
[3] O. Pyshkin, G. Kamarchuk, A. Yeremenko, A. Kravchenko, A. Pospelov, Yu. Alexandrov, E. Faulques, Journal of Breath Research, 5(1), 016005. (2011). https://doi.org/10.1088/1752-7155/5/1/016005.

Experimental investigation and mathematical modeling of film thickness in channels of centrifugal sprayer

O. V. Khomenko, M. V. Naida, K. P. Khomenko

Sumy State University, 116 Kharkivska St., Sumy, 40007, Ukraine
e-mail: maks.nai@ukr.net

The study of the behavior of liquid films on the surfaces of centrifugal atomizer is an important direction for many industrial and technological processes. The formation, distribution and transformation of liquid films play a key role in such industries as agriculture, the chemical industry, pharmaceutical production and materials science. In these areas, precise control of liquid atomizer parameters directly affects the efficiency of technological operations, the quality of the final product and the economic feasibility of the process. For example, in agriculture, centrifugal atomizers are used for uniform application of fertilizers and plant protection products, which helps to increase yield and reduce environmental load. At the same time, in the chemical and pharmaceutical industries, control of the dispersion of the liquid phase affects the processes of drying, emulsification, encapsulation of active substances and other critically important operations.

Centrifugal atomizer, which are widely used in industry, are designed to disperse liquids into small droplets using centrifugal forces. The basic principle of their operation is the formation of a thin liquid film on the surface of a rotating disk or other atomizing element. However, the distribution of the thickness of this film is uneven, which significantly affects the parameters of the final atomization: droplet size, their speed and homogeneity of the atomized mixture. The influence of the geometric parameters of the atomizer channels, rotation speed (from 1000 rpm to 6000 rpm), physicochemical properties of the liquid (density, viscosity, surface tension) and liquid flow rate is a critically important aspect that determines the efficiency of such devices. Previous studies have mostly focused either on purely theoretical approaches or on limited experimental observations that do not allow for a complete description of the mechanisms of interaction of the liquid with the atomizer surface. At the same time, modern methods of experimental analysis, such as optical interferometry, laser Doppler anemometry and high-speed video recording, allow obtaining more accurate data on the dynamics of the liquid film and the process of its disintegration on the droplet. An integrated approach that combines experimental data with theoretical modeling can provide a deeper understanding of the physical mechanisms that determine the behavior of the liquid film.

This study is aimed at filling existing scientific gaps by detailed analysis of the distribution of the thickness of the liquid film in the channels of the centrifugal atomizer. For this purpose, a specially developed experimental method was used, which includes the use of a local liquid receiver, which allows for measurements of film parameters under controlled conditions [1]. The conducted experiments allow us to obtain quantitative characteristics of the film formation process, which are important for the validation and further improvement of existing theoretical models. Comparison of the obtained experimental data with the predictions of mathematical models allows us to assess their accuracy, identify key patterns and identify factors affecting the behavior of the liquid film. The proposed approach to theoretical modeling can be adapted to study other types of film systems, which makes it a universal tool for further scientific research. In conclusion, this article provides a comprehensive analysis of the dynamics of thin liquid films in centrifugal systems, combining modern methods of experimental analysis with analytical modeling to achieve a deeper understanding of the mechanisms of liquid atomizer.

[1] P. E. Trofimenko, M. V. Naida, O. V. Khomenko, A. M. Litzman, Method and device for experimental determination of film formation parameters on static film formers, Nanosystems, nanomaterials, nanotechnologies 20(1), 81 – 90 (2022).

AUTHOR INDEX

E

F

G

H

I

J

K

L

M

N

O

P

Q

R

S

T

U

V

W

Y

Z

VI International Conference
Condensed Matter and Low Temperature Physics
CM&LTP 2026

Book of abstracts

Kharkiv, B. Verkin ILTPE of NASU, 2026

Електронне видання, ум. друк. арк. 5.2.
Свідоцтво про внесення суб'єкта видавничої справи
до Державного реєстру видавців, виготівників
і розповсюджувачів видавничої продукції
від 07.06.2002 р., серія ДК № 941.
Видавництво ФТІНТ ім. Б. І. Вєркіна НАН України
просп. Науки, 47, Харків, 61103, Україна
https://www.ilt.kharkiv.ua